

ORGANOCATALYTIC ENANTIOSELECTIVE SYNTHESIS OF
DIHYDRONAPHTHOFURANS AND DIHYDROBENZOFURANS:
REACTION DEVELOPMENT AND INSIGHTS INTO STEREOSELECTIVITY
&
DESIGN AND SYNTHESIS OF HETEROGENEOUS RECYCLABLE
ORGANOCATALYSTS

A THESIS SUBMITTED TO
THE GRADUATE SCHOOL OF NATURAL AND APPLIED SCIENCES
OF
MIDDLE EAST TECHNICAL UNIVERSITY

BY

ZEYNEP DİLŞAD SUSAM

IN PARTIAL FULFILLMENT OF THE REQUIREMENTS
FOR
THE DEGREE OF DOCTOR OF PHILOSOPHY
IN
CHEMISTRY

NOVEMBER 2022

Approval of the thesis:

**ORGANOCATALYTIC ENANTIOSELECTIVE SYNTHESIS OF
DIHYDRONAPHTHOFURANS AND DIHYDROBENZOFURANS:
REACTION DEVELOPMENT AND INSIGHTS INTO
STEREOSELECTIVITY
&
DESIGN AND SYNTHESIS OF HETEROGENEOUS RECYCLABLE
ORGANOCATALYSTS**

submitted by **ZEYNEP DİLŞAD SUSAM** in partial fulfillment of the requirements
for the degree of **Doctor of Philosophy in Chemistry, Middle East Technical
University** by,

Prof. Dr. Halil Kalıpçılar
Dean, Graduate School of **Natural and Applied Sciences**

Prof. Dr. Özdemir Doğan
Head of the Department, **Chemistry**

Prof. Dr. Cihangir Tanyeli
Supervisor, **Chemistry, METU**

Examining Committee Members:

Prof. Dr. Özdemir Doğan
Chemistry, METU

Prof. Dr. Cihangir Tanyeli
Chemistry, METU

Prof. Dr. Adnan Bulut
Chemistry, Kırıkkale University

Assoc. Prof. Dr. Salih Özçubukçu
Chemistry, METU

Assoc. Prof. Dr. Yunus Emre Türkmen
Chemistry, Bilkent University

Date: 18.11.2022

I hereby declare that all information in this document has been obtained and presented in accordance with academic rules and ethical conduct. I also declare that, as required by these rules and conduct, I have fully cited and referenced all material and results that are not original to this work.

Name Last name : Zeynep Dilşad Susam

Signature :

ABSTRACT

**ORGANOCATALYTIC ENANTIOSELECTIVE SYNTHESIS OF
DIHYDRONAPHTHOFURANS AND DIHYDROBENZOFURANS:
REACTION DEVELOPMENT AND INSIGHTS INTO
STEREOSELECTIVITY
&
DESIGN AND SYNTHESIS OF HETEROGENEOUS RECYCLABLE
ORGANOCATALYSTS**

Susam, Zeynep Dilşad
Doctor of Philosophy, Chemistry
Supervisor: Prof. Dr. Cihangir Tanyeli

November 2022, 323 pages

The first part of thesis comprises Friedel-Crafts/substitution, which is the most common and widely used C-C bond forming reaction in synthetic organic chemistry. Applications of these reactions in domino type reactions are trending topic in organocatalytic studies in the recent years. These types of reactions are used to perform dihydrobenzofuran (DHB) and dihydronaphthofuran (DHN) skeletons, which are very important pharmaceutical precursors. In this study, it was chosen as the key step in domino reaction to afford disubstituted dihydronaphthofuran derivatives possessing two chiral centers in enantiomerically enriched form. For this purpose, (*Z*)-(2-bromo-2-nitrovinyl) benzene and β -naphthol was used to perform model organocatalytic Friedel-Crafts/substitution domino type reaction. In this part, 65 different chiral DHN and DHB derivatives were synthesized with quinine based novel bifunctional organocatalyst, which has been developed in our group, in up to >99% ee under the optimized condition with 5 mol% catalyst loading.

In the second part of the study, a similar Friedel-Crafts domino approach was also applied to synthesize 2,3-dihydrofuran derivatives. 11 different DHF derivatives were synthesized in up to 95% ee with complete conversion.

In the third part of the study, novel heterogeneous catalysts are constructed from our homogeneous catalysts. For this purpose, initial trials with the small amount of catalyst have started to generate the active site for the attachment to gold nanoparticles. The attachment of the catalysts to the gold surfaces were also performed. After other characterization studies of these catalysts will be completed and they will be ready to be tested in different type of asymmetric reactions.

Keywords: Organocatalyst, Enantioselectivity, Friedel-Crafts, Domino, Recyclable Heterogeneous Catalyst

ÖZ

DİHİDRONAFTOFURANLARIN VE DİHİDROBENZOFURANLARIN ORGANOKATALİTİK ENANTİYOSELEKTİF SENTEZİ: REAKSİYON GELİŞTİRİLMESİ VE STEREOSELEKTİF İÇERİKLERİ & HETEROJEN GERİ DÖNÜŞÜMLÜ ORGANOKATALİZÖRLERİN DİZAYN VE SENTEZİ

Susam, Zeynep Dilşad
Doktora, Kimya
Tez Yöneticisi: Prof. Dr. Cihangir Tanyeli

Kasım 2022, 323 sayfa

Tezin ilk bölümü, sentetik organik kimyada en yaygın ve yaygın olarak kullanılan C-C bağı oluşturma reaksiyonu olan Friedel-Crafts/sübstitüsyon işlemini içermektedir. Bu reaksiyonların domino tipi reaksiyonlardaki uygulamaları son yıllarda organokatalitik çalışmalarda trend olan bir konudur. Bu tür reaksiyonlar, çok önemli farmasötik öncüller olan dihidrobenzofuran (DHB) ve dihidronaftofuran (DHN) iskeletlerini gerçekleştirmek için kullanılır. Bu çalışmada, enantiyomerik olarak zenginleştirilmiş formda iki kiral merkeze sahip iki ikameli dihidronaftofuran türevlerini elde etmek için, domino reaksiyonunda anahtar adım olarak seçilmiştir. Bu amaçla, model organokatalitik Friedel-Crafts/sübstitüsyon domino tipi reaksiyonu gerçekleştirmek için (Z)-(2-bromo-2-nitrovinil)benzen ve β -naftol kullanıldı. Bu bölümde, grubumuzda geliştirilen kinin bazlı özgün bifonksiyonel organokatalizör ile optimize koşul altında %5 mol katalizör yüklemesi ile >%99 ee'ye kadar 65 farklı kiral DHN ve DHB türevi sentezlendi.

Çalışmanın ikinci bölümünde, 2,3-dihidrofuran türevlerini sentezlemek için benzer bir Friedel-Crafts domino yaklaşımı da uygulandı. Tam dönüşüm ile %95 ee'ye kadar 11 farklı DHF türevi sentezlendi.

Çalışmanın üçüncü bölümünde, homojen katalizörlerimizden yeni heterojen katalizörler oluşturulmuştur. Bu amaçla, az miktarda katalizörle yapılan ilk denemeler, altın nanoparçacıklara bağlanma için aktif bölge oluşturmaya başlanmıştır. Katalizörlerin altın yüzeylere bağlanması da gerçekleştirilmiştir. Bu katalizörlerin diğer karakterizasyon çalışmaları tamamlandıktan sonra farklı asimetric reaksiyonlarda test edilmeye hazır hale gelecektir.

Anahtar Kelimeler: Organokatalizör, Enantioselektiflik, Friedel-Crafts, Domino, Geri Dönüştürülebilir Heterojen Katalizör

Sevinç'ciğime...

ACKNOWLEDGMENTS

This is the story of a 7-year adventure of a thesis that was very difficult and very demanding and this is a thesis that not only involves repeated experiments but has even experienced a pandemic. It may have been full of tears and stress, but I am happy that it has come to an end, for better or worse. Many people have contributed in big and small ways, it is impossible to mention them all here, but I am grateful to all of you and you are always in my heart.

Before anyone else, I would like to express my deepest gratitude to my doctor father *Cihangir Tanyeli*. Thank you for giving me a chance in your laboratory even though I don't seem like a very bright student when I was an undergraduate. But he believed in me, and now I've been in his group for nearly the past 11 years and I am grateful for his academic guidance, wisdom, and moral support. Thank you, for your endless patience every time I cry. ☺

I would like to thank *Salih Özçubukçu* for his guidance, help, and support through my research. Especially for helping me to build up a UV light system and providing me lots of chemicals from his inventory that helped me initiate the third-chapter experiments. But I didn't forget that you took away my chiller back. I know it wasn't my personal property, but gifts should not be taken back. ☹ And thank you for being my court witness, it was a really fun process, even though all the scripts we wrote went down the drain.

I am also grateful to my thesis monitoring committee, *Özdemir Doğan*, and *Yunus Emre Türkmen*, for their insightful comments for synthesis and encouragement.

I also thank *Erol Yıldırım* for the computational calculations of the first chapter studies.

I also would like to thank *İrem Tanyeli*, I am glad that all the contributions and her ideas through heterogeneous support studies, especially for providing us the GNP fused silica plates.

This work is partially funded by the Scientific and Technological Research Council of Turkey under grant number TUBITAK 217Z035. I also would like to thank *Ferdi Karadaş* and *Gülsüm Gündoğdu* (Bilkent University) for X-ray analysis, *Zeynep Erdoğan* (UNAM) for HRMS analyses, *Ömür Çelikbıçak* and *Melis Şardan Ekiz* (HÜNİTEK) for MALDI-MS experiments.

Many people helped me throughout my work, but one of the most important people was *Esra Kanberoğlu*. She has been a great lab partner and roommate for me. Thank you so much for her help at every point I needed, for the days and nights we spent together in the lab.

My other little precious was *Deniz Tözendemir*. She has been the most amusing person this lab has brought into my life. Maybe we parted early, but knowing that she is always just a phone call away whenever I needed her always gives me strength.

Special thanks to great moral supporters *Melis Kesik* and *Selin Ceyhan* for supporting me without any hesitation or judging whenever I need it. Thank you very much for being with me since our undergraduate years.

I had the chance to share this laboratory with many people. Former lab members *Ezgi Bayer* and *Seda Okumuş*, thank you for being amazing lab partners for me. I am thankful to all old and new *Tanyeli Research Group members* because they somehow contributed to this work. For that, a special credit of course goes to my current lab members *Bilge Deniz Özcan* and *Enis Kurtkaya*, thanks for the great afford you performed for the first chapter of this study. *Begüm Nemutlu* and *Üstün Utkan Acar*, your partial help in that study were also very valuable to me.

A special thanks with sprinkles on top goes to long-lasting friends *Irmak Sancar*, *Okan Şeker*, and *Merve Yurtcan* for every time being there for me. I feel so lucky to have found you, the most wonderful people this school has given me. I love you so much for being my wonderful companions for almost 15 years together, for the good and the bad, and for making me laugh in every situation. I would like to write more

beautiful things but *Okancım* used all the cool phrases and killed my creativity just because he graduated before me, pihh.

One of the most important people I met during the most challenging times of my PhD when I was feeling the worst, and who has been with me ever since and encouraged me to continue on this path was *Neşe Nizamettinođlu*. I am glad we met; you have been one of my biggest supporters for a long time.

Tabi ki her zaman beni destekleyen big sis *Dilüşüm*, anecim *Serpilcim* ve babik *Ertancım*, iyi ki varsınız, sonsuz teşekkürler! Sizi çok seviyorum!

And my final thanks go to my little stress relievers, *Odin*, *Çakıl*, and *Lucy*. I love them so much for creating a wonderful home for me. *Balkızım*, you were with me for a very long time while I was writing this thesis but sadly you couldn't see the end of it. May all good things be with you wherever you go. You will always be in my heart *Çakılıcım*. ♡

TABLE OF CONTENTS

ABSTRACT.....	v
ÖZ.....	vii
ACKNOWLEDGMENTS.....	x
TABLE OF CONTENTS.....	xiii
LIST OF TABLES.....	xxiii
LIST OF FIGURES.....	xxiv
LIST OF ABBREVIATIONS.....	xxxix
CHAPTERS	
1 INTRODUCTION.....	1
1.1 Asymmetric Organocatalysis.....	1
1.1.1 Cinchona Alkaloids.....	3
1.1.2 Squaramides.....	5
1.1.3 Asymmetric Reactions with Cinchona Alkaloids/Squaramides.....	6
1.2 Dihydronaphthofurans and Dihydrobenzofurans.....	10
1.2.1 Asymmetric Synthesis of DHN and DHB.....	12
1.3 Recyclable Organocatalysis.....	13
1.3.1 Gold Nanoparticle Supported Organocatalysts.....	14
1.3.2 Fluorous Supported Organocatalyst.....	17
1.4 Aim of the Study.....	20
2 RESULTS AND DISCUSSION.....	23
2.1 Synthesis of Quinine and 2-AminoDMAP Based Bifunctional Organocatalysts.....	23

2.2	Evaluation of the Bifunctional Organocatalysts in Friedel-Crafts Domino Type Reactions	24
2.2.1	Optimization Studies.....	24
2.2.2	Substrate Scope.....	29
2.2.3	Computational Methods.....	36
2.3	Evaluation of the Bifunctional Organocatalysts in Michael Addition/S _N 2 Type Reactions	40
2.4	Design and Synthesis of Recyclable Organocatalysts.....	43
2.4.1	Gold Nanoparticle Anchored Bifunctional Organocatalysts	43
2.4.2	Synthesis of Fluorous Supported Organocatalysts	52
3	EXPERIMENTAL	53
3.1	Materials and Methods	53
3.2	General Procedure for the synthesis of α -bromonitroalkenes (20a-t)	54
3.2.1	(<i>Z</i>)-(2-bromo-2-nitrovinyl)benzene (20a).....	54
3.2.2	(<i>Z</i>)-1-bromo-2-(2-bromo-2-nitrovinyl)benzene (20b)	55
3.2.3	(<i>Z</i>)-1-(2-bromo-2-nitrovinyl)-2-chlorobenzene (20c).....	55
3.2.4	(<i>Z</i>)-1-(2-bromo-2-nitrovinyl)-2-fluorobenzene (20d).....	55
3.2.5	(<i>Z</i>)-1-bromo-3-(2-bromo-2-nitrovinyl)benzene (20e)	56
3.2.6	(<i>Z</i>)-1-(2-bromo-2-nitrovinyl)-3-chlorobenzene (20f).....	56
3.2.7	(<i>Z</i>)-1-(2-bromo-2-nitrovinyl)-4-methoxybenzene (20g).....	56
3.2.8	(<i>Z</i>)-1-(2-bromo-2-nitrovinyl)-2,4-dichlorobenzene (20h)	56
3.2.9	(<i>Z</i>)-2-(2-bromo-2-nitrovinyl)-1,4-dimethoxybenzene (20i)	57
3.2.10	(<i>Z</i>)-1-(2-bromo-2-nitrovinyl)-4-fluorobenzene (20j).....	57
3.2.11	(<i>Z</i>)-1-bromo-4-(2-bromo-2-nitrovinyl)benzene (20k)	57

3.2.12	(<i>Z</i>)-1-(2-bromo-2-nitrovinyl)-4-methylbenzene (20l).....	58
3.2.13	(<i>Z</i>)-1-(benzyloxy)-4-(2-bromo-2-nitrovinyl)benzene (20m).....	58
3.2.14	(<i>Z</i>)-1-(2-bromo-2-nitrovinyl)-2-(trifluoromethyl)benzene (20n).....	58
3.2.15	(<i>Z</i>)-1-(2-bromo-2-nitrovinyl)-4-chlorobenzene (20o).....	59
3.2.16	(<i>Z</i>)-1-(2-bromo-2-nitrovinyl)-4-(trifluoromethyl)benzene (20p).....	59
3.2.17	(<i>Z</i>)-1-(benzyloxy)-2-(2-bromo-2-nitrovinyl)benzene (20q).....	59
3.2.18	(<i>Z</i>)-1-(2-bromo-2-nitrovinyl)-2-nitrobenzene (20r).....	60
3.2.19	(<i>Z</i>)-2-bromo-5-(2-bromo-2-nitrovinyl)furan (20s).....	60
3.2.20	(<i>Z</i>)-2-(2-bromo-2-nitrovinyl)thiophene (20t).....	60
3.3	General Procedure for Friedel-Crafts Domino Substitution Reaction.....	60
3.3.1	(1 <i>R</i> ,2 <i>R</i>)-2-nitro-1-phenyl-1,2-dihydronaphtho[2,1- <i>b</i>]furan (23aa).....	62
3.3.2	(1 <i>S</i> ,2 <i>R</i>)-1-(2-bromophenyl)-2-nitro-1,2-dihydronaphtho[2,1- <i>b</i>]furan (23ab)	62
3.3.3	(1 <i>S</i> ,2 <i>R</i>)-1-(2-chlorophenyl)-2-nitro-1,2-dihydronaphtho[2,1- <i>b</i>]furan (23ac)	63
3.3.4	(1 <i>S</i> ,2 <i>R</i>)-1-(2-fluorophenyl)-2-nitro-1,2-dihydronaphtho[2,1- <i>b</i>]furan (23ad)	63
3.3.5	(1 <i>R</i> ,2 <i>R</i>)-1-(3-bromophenyl)-2-nitro-1,2-dihydronaphtho[2,1- <i>b</i>]furan (23ae)	64
3.3.6	(1 <i>R</i> ,2 <i>R</i>)-1-(3-chlorophenyl)-2-nitro-1,2-dihydronaphtho[2,1- <i>b</i>]furan (23af)	65
3.3.7	(1 <i>R</i> ,2 <i>R</i>)-1-(4-methoxyphenyl)-2-nitro-1,2-dihydronaphtho[2,1- <i>b</i>]furan (23ag).....	65
3.3.8	(1 <i>S</i> ,2 <i>R</i>)-1-(2,4-dichlorophenyl)-2-nitro-1,2-dihydronaphtho[2,1- <i>b</i>]furan (23ah).....	66

3.3.9 (1 <i>R</i> ,2 <i>R</i>)-1-(2,5-dimethoxyphenyl)-2-nitro-1,2-dihydronaphtho[2,1- <i>b</i>]furan (23ai).....	67
3.3.10 (1 <i>R</i> ,2 <i>R</i>)-1-(4-fluorophenyl)-2-nitro-1,2-dihydronaphtho[2,1- <i>b</i>]furan (23aj)	67
3.3.11 (1 <i>R</i> ,2 <i>R</i>)-1-(4-bromophenyl)-2-nitro-1,2-dihydronaphtho[2,1- <i>b</i>]furan (23ak)	68
3.3.12 (1 <i>R</i> ,2 <i>R</i>)-2-nitro-1-(<i>p</i> -tolyl)-1,2-dihydronaphtho[2,1- <i>b</i>]furan (23al).....	68
3.3.13 (1 <i>R</i> ,2 <i>R</i>)-1-(4-(benzyloxy)phenyl)-2-nitro-1,2-dihydronaphtho[2,1- <i>b</i>]furan (23am).....	69
3.3.14 (1 <i>R</i> ,2 <i>R</i>)-2-nitro-1-(2-(trifluoromethyl)phenyl)-1,2-dihydronaphtho[2,1- <i>b</i>]furan (23an)	70
3.3.15 (1 <i>R</i> ,2 <i>R</i>)-1-(4-chlorophenyl)-2-nitro-1,2-dihydronaphtho[2,1- <i>b</i>]furan (23ao)	70
3.3.16 (1 <i>R</i> ,2 <i>R</i>)-2-nitro-1-(4-(trifluoromethyl)phenyl)-1,2-dihydronaphtho[2,1- <i>b</i>]furan (23ap)	71
3.3.17 (1 <i>R</i> ,2 <i>R</i>)-1-(2-(benzyloxy)phenyl)-2-nitro-1,2-dihydronaphtho[2,1- <i>b</i>]furan (23aq).....	72
3.3.18 (1 <i>R</i> ,2 <i>R</i>)-7-bromo-2-nitro-1-phenyl-1,2-dihydronaphtho[2,1- <i>b</i>]furan (23ba)	72
3.3.19 (1 <i>S</i> ,2 <i>S</i>)-7-methoxy-2-nitro-1-phenyl-1,2-dihydronaphtho[2,1- <i>b</i>]furan (23ca)	73
3.3.20 (1 <i>R</i> ,2 <i>R</i>)-4-bromo-2-nitro-1-phenyl-1,2-dihydronaphtho[2,1- <i>b</i>]furan (23da)	74
3.3.21 (1 <i>R</i> ,2 <i>R</i>)-8-methoxy-2-nitro-1-phenyl-1,2-dihydronaphtho[2,1- <i>b</i>]furan (23ea)	74

3.3.22	(1 <i>S</i> ,2 <i>R</i>)-1-(5-bromofuran-2-yl)-2-nitro-1,2-dihydronaphtho[2,1- <i>b</i>]furan (23as).....	75
3.3.23	(1 <i>R</i> ,2 <i>R</i>)-2-nitro-1-(thiophen-2-yl)-1,2-dihydronaphtho[2,1- <i>b</i>]furan (23at)	75
3.3.24	(2 <i>R</i> ,3 <i>R</i>)-2-nitro-3-phenyl-2,3-dihydronaphtho[1,2- <i>b</i>]furan (60aa).....	76
3.3.25	(2 <i>R</i> ,3 <i>S</i>)-3-(2-bromophenyl)-2-nitro-2,3-dihydronaphtho[1,2- <i>b</i>]furan (60ab)	77
3.3.26	(2 <i>R</i> ,3 <i>S</i>)-3-(2-bromophenyl)-2-nitro-2,3-dihydronaphtho[1,2- <i>b</i>]furan (60ac)	77
3.3.27	(2 <i>R</i> ,3 <i>S</i>)-3-(2-fluorophenyl)-2-nitro-2,3-dihydronaphtho[1,2- <i>b</i>]furan (60ad)	78
3.3.28	(2 <i>R</i> ,3 <i>R</i>)-3-(3-bromophenyl)-2-nitro-2,3-dihydronaphtho[1,2- <i>b</i>]furan (60ae)	79
3.3.29	(2 <i>R</i> ,3 <i>R</i>)-3-(3-chlorophenyl)-2-nitro-2,3-dihydronaphtho[1,2- <i>b</i>]furan (60af)	79
3.3.30	(2 <i>S</i> ,3 <i>S</i>)-3-(4-methoxyphenyl)-2-nitro-2,3-dihydronaphtho[1,2- <i>b</i>]furan (60ag)	80
3.3.31	(2 <i>R</i> ,3 <i>S</i>)-3-(2,4-dichlorophenyl)-2-nitro-2,3-dihydronaphtho[1,2- <i>b</i>]furan (60ah)	81
3.3.32	(2 <i>R</i> ,3 <i>R</i>)-3-(2,5-dimethoxyphenyl)-2-nitro-2,3-dihydronaphtho[1,2- <i>b</i>]furan (60ai)	81
3.3.33	(2 <i>R</i> ,3 <i>R</i>)-3-(4-fluorophenyl)-2-nitro-2,3-dihydronaphtho[1,2- <i>b</i>]furan (60aj)	82
3.3.34	(2 <i>R</i> ,3 <i>R</i>)-3-(4-bromophenyl)-2-nitro-2,3-dihydronaphtho[1,2- <i>b</i>]furan (60ak)	83
3.3.35	(2 <i>R</i> ,3 <i>R</i>)-2-nitro-3-(<i>p</i> -tolyl)-2,3-dihydronaphtho[1,2- <i>b</i>]furan (60al)	83

3.3.36	(2 <i>R</i> ,3 <i>R</i>)-2-nitro-3-(2-(trifluoromethyl)phenyl)-2,3-dihydronaphtho[1,2- <i>b</i>]furan (60an)	84
3.3.37	(2 <i>R</i> ,3 <i>R</i>)-3-(4-chlorophenyl)-2-nitro-2,3-dihydronaphtho[1,2- <i>b</i>]furan (60ao)	85
3.3.38	(2 <i>R</i> ,3 <i>R</i>)-2-nitro-3-(4-(trifluoromethyl)phenyl)-2,3-dihydronaphtho[1,2- <i>b</i>]furan (60ap)	85
3.3.39	(2 <i>R</i> ,3 <i>R</i>)-3-(2-(benzyloxy)phenyl)-2-nitro-2,3-dihydronaphtho[1,2- <i>b</i>]furan (60aq)	86
3.3.40	(2 <i>R</i> ,3 <i>R</i>)-2-nitro-3-(thiophen-2-yl)-2,3-dihydronaphtho[1,2- <i>b</i>]furan (60at)	87
3.3.41	(2 <i>R</i> ,3 <i>R</i>)-5-methoxy-2-nitro-3-phenyl-2,3-dihydronaphtho[1,2- <i>b</i>]furan (60ba)	87
3.3.42	(2 <i>R</i> ,3 <i>R</i>)-5-chloro-2-nitro-3-phenyl-2,3-dihydronaphtho[1,2- <i>b</i>]furan (60ca)	88
3.3.43	(2 <i>R</i> ,3 <i>S</i>)-3-(2-fluorophenyl)-5-methoxy-2-nitro-2,3-dihydronaphtho[1,2- <i>b</i>]furan (60bd)	89
3.3.44	(2 <i>R</i> ,3 <i>R</i>)-3-(4-chlorophenyl)-5-methoxy-2-nitro-2,3-dihydronaphtho[1,2- <i>b</i>]furan (60bo)	89
3.3.45	(2 <i>R</i> ,3 <i>R</i>)-5-methoxy-2-nitro-3-(4-(trifluoromethyl)phenyl)-2,3-dihydronaphtho[1,2- <i>b</i>]furan (60bp)	90
3.3.46	(2 <i>R</i> ,3 <i>R</i>)-4,6-dimethoxy-2-nitro-3-phenyl-2,3-dihydrobenzofuran (60ba)	91
3.3.47	(2 <i>R</i> ,3 <i>S</i>)-3-(2-bromophenyl)-4,6-dimethoxy-2-nitro-2,3-dihydrobenzofuran (62bb)	91
3.3.48	(2 <i>R</i> ,3 <i>S</i>)-3-(2-chlorophenyl)-4,6-dimethoxy-2-nitro-2,3-dihydrobenzofuran (62bc)	92

3.3.49 (2 <i>R</i> ,3 <i>S</i>)-3-(2-fluorophenyl)-4,6-dimethoxy-2-nitro-2,3-dihydrobenzofuran (62bd)	93
3.3.50 (2 <i>R</i> ,3 <i>R</i>)-3-(3-bromophenyl)-4,6-dimethoxy-2-nitro-2,3-dihydrobenzofuran (62be)	93
3.3.51 (2 <i>R</i> ,3 <i>S</i>)-3-(2,4-dichlorophenyl)-4,6-dimethoxy-2-nitro-2,3- dihydrobenzofuran (62bh).....	94
3.3.52 (2 <i>R</i> ,3 <i>R</i>)-3-(4-fluorophenyl)-4,6-dimethoxy-2-nitro-2,3-dihydrobenzofuran (62bj).....	95
3.3.53 (2 <i>R</i> ,3 <i>R</i>)-3-(4-bromophenyl)-4,6-dimethoxy-2-nitro-2,3-dihydrobenzofuran (62bk)	96
3.3.54 (2 <i>R</i> ,3 <i>R</i>)-4,6-dimethoxy-2-nitro-3-(<i>p</i> -tolyl)-2,3-dihydrobenzofuran (62bl)	96
3.3.55 (2 <i>R</i> ,3 <i>R</i>)-4,6-dimethoxy-2-nitro-3-(2-(trifluoromethyl)phenyl)-2,3- dihydrobenzofuran (62bn).....	97
3.3.56 (2 <i>R</i> ,3 <i>R</i>)-3-(4-chlorophenyl)-4,6-dimethoxy-2-nitro-2,3-dihydrobenzofuran (62bo)	98
3.3.57 (2 <i>R</i> ,3 <i>R</i>)-4,6-dimethoxy-2-nitro-3-(4-(trifluoromethyl)phenyl)-2,3- dihydrobenzofuran (62bp).....	98
3.3.58 (2 <i>R</i> ,3 <i>R</i>)-3-(2-(benzyloxy)phenyl)-4,6-dimethoxy-2-nitro-2,3- dihydrobenzofuran (62bq).....	99
3.3.59 (2 <i>R</i> ,3 <i>R</i>)-4,5,6-trimethoxy-2-nitro-3-phenyl-2,3-dihydrobenzofuran (62ca)	100
3.3.60 (2 <i>R</i> ,3 <i>S</i>)-3-(2-bromophenyl)-4,5,6-trimethoxy-2-nitro-2,3- dihydrobenzofuran (62cb).....	100
3.3.61 (2 <i>R</i> ,3 <i>S</i>)-3-(2-fluorophenyl)-4,5,6-trimethoxy-2-nitro-2,3-dihydrobenzofuran (62cd)	101

3.3.62	(2 <i>R</i> ,3 <i>R</i>)-4,5,6-trimethoxy-2-nitro-3-(<i>p</i> -tolyl)-2,3-dihydrobenzofuran (62cl)	102
3.3.63	(2 <i>R</i> ,3 <i>R</i>)-4,5,6-trimethoxy-2-nitro-3-(2-(trifluoromethyl)phenyl)-2,3-dihydrobenzofuran (62cn)	103
3.4	General Procedure for Michael/S _N 2 Type Domino Substitution Reaction	103
3.4.1	1-((4 <i>S</i> ,5 <i>S</i>)-2-methyl-5-nitro-4-phenyl-4,5-dihydrofuran-3-yl)ethan-1-one (64aa)	104
3.4.2	1-((4 <i>R</i> ,5 <i>S</i>)-4-(2-bromophenyl)-2-methyl-5-nitro-4,5-dihydrofuran-3-yl)ethan-1-one (64ab)	104
3.4.3	1-((4 <i>R</i> ,5 <i>S</i>)-4-(2-chlorophenyl)-2-methyl-5-nitro-4,5-dihydrofuran-3-yl)ethan-1-one (64ac)	105
3.4.4	1-((4 <i>R</i> ,5 <i>S</i>)-4-(2,4-dichlorophenyl)-2-methyl-5-nitro-4,5-dihydrofuran-3-yl)ethan-1-one (64ah)	106
3.4.5	1-((4 <i>S</i> ,5 <i>S</i>)-4-(2,5-dimethoxyphenyl)-2-methyl-5-nitro-4,5-dihydrofuran-3-yl)ethan-1-one (64ai)	106
3.4.6	1-((4 <i>S</i> ,5 <i>S</i>)-4-(4-bromophenyl)-2-methyl-5-nitro-4,5-dihydrofuran-3-yl)ethan-1-one (64ak)	107
3.4.7	1-((4 <i>S</i> ,5 <i>S</i>)-2-methyl-5-nitro-4-(<i>p</i> -tolyl)-4,5-dihydrofuran-3-yl)ethan-1-one (64al)	107
3.4.8	1-((4 <i>S</i> ,5 <i>S</i>)-2-methyl-5-nitro-4-(2-(trifluoromethyl)phenyl)-4,5-dihydrofuran-3-yl)ethan-1-one (64an)	108
3.4.9	1-((4 <i>S</i> ,5 <i>S</i>)-4-(4-chlorophenyl)-2-methyl-5-nitro-4,5-dihydrofuran-3-yl)ethan-1-one (64ao)	109
3.4.10	Methyl (4 <i>R</i> ,5 <i>S</i>)-4-(2-fluorophenyl)-2-methyl-5-nitro-4,5-dihydrofuran-3-carboxylate (64bd)	109

3.4.11	Methyl (4 <i>S</i> ,5 <i>S</i>)-4-(4-methoxyphenyl)-2-methyl-5-nitro-4,5-dihydrofuran-3-carboxylate (64bg)	110
3.5	Synthesis of Acetylation of Quinine: (<i>R</i>)-(6-methoxyquinolin-4-yl)((1 <i>S</i> ,2 <i>S</i> ,4 <i>S</i> ,5 <i>R</i>)-5-vinylquinuclidin-2-yl)methyl acetate (65).....	110
3.6	General Procedure for the Thiol-Ene Reaction.....	111
3.6.1	Thiol-Ene Reaction with Thermal Initiator	111
3.6.2	Thiol-Ene Reaction with Photoinitiator	111
3.6.3	<i>S</i> -(2-((2-((1 <i>S</i> ,3 <i>R</i> ,4 <i>S</i> ,6 <i>S</i>)-6-((<i>S</i>)-((2-(<i>tert</i> -butylamino)-3,4-dioxocyclobut-1-en-1-yl)amino)(6-methoxyquinolin-4-yl)methyl)quinuclidin-3-yl)ethyl)thio)ethyl) ethanethioate (69)	112
3.6.4	3-(<i>tert</i> -butylamino)-4-(((<i>S</i>)-((1 <i>S</i> ,2 <i>S</i> ,4 <i>S</i> ,5 <i>R</i>)-5-(2-((2-mercaptoethyl)thio)ethyl)quinuclidin-2-yl)(6-methoxyquinolin-4-yl)methyl)amino)cyclobut-3-ene-1,2-dione (70)	113
3.6.5	3-(<i>tert</i> -butylamino)-4-(((<i>S</i>)-((1 <i>S</i> ,2 <i>S</i> ,4 <i>S</i> ,5 <i>R</i>)-5-(2-((9-mercaptononyl)thio)ethyl)quinuclidin-2-yl)(6-methoxyquinolin-4-yl)methyl)amino)cyclobut-3-ene-1,2-dione (71)	114
3.6.6	(2 <i>S</i> ,4 <i>R</i>)-1-(<i>tert</i> -butoxycarbonyl)-4-(3-((2-mercaptoethyl)thio)propoxy)pyrrolidine-2-carboxylic acid (77).....	114
3.6.7	(2 <i>S</i> ,4 <i>R</i>)-1-(<i>tert</i> -butoxycarbonyl)-4-(3-((6-mercaptohexyl)thio)propoxy)pyrrolidine-2-carboxylic acid (78).....	115
3.6.8	(2 <i>S</i> ,4 <i>R</i>)-1-(<i>tert</i> -butoxycarbonyl)-4-(3-((9-mercaptononyl)thio)propoxy)pyrrolidine-2-carboxylic acid (79).....	115
3.7	General Procedure for the Cleavage of Acetyl Groups.....	116
3.7.1	(<i>R</i>)-((1 <i>S</i> ,2 <i>S</i> ,4 <i>S</i> ,5 <i>R</i>)-5-(2-((2-mercaptoethyl)thio)ethyl)quinuclidin-2-yl)(6-methoxyquinolin-4-yl)methyl acetate (68).....	116
3.8	Synthesis of Thiol Stabilized GNPs 73.....	117

3.9	Place Exchange Reaction for the Synthesis of GNP Supported Organocatalysts 74, 80	117
3.10.	Synthesis of Monosquarate 82.....	118
4	CONCLUSION	119
	REFERENCES	121
	APPENDICES	
A.	NMR SPECTRA	131
B.	HPLC CHROMATOGRAMS.....	235
C.	COMPUTATIONAL DATA.....	305
D.	X-RAY CRYSTALLOGRAPHY	319
	CURRICULUM VITAE	323

LIST OF TABLES

TABLES

Table 1. Optimization studies; organocatalyst screening ^a	25
Table 2. Optimization studies; base screening ^a	26
Table 3. Optimization studies; solvent screening ^a	27
Table 4. Optimization studies; catalyst loading, base eq, substituent ratio, and concentration ^a	28
Table 5. Substrate scope of FC domino reaction between α -bromonitroalkenes and β -naphthols ^a	29
Table 6. Substrate scope of FC domino reaction between α -bromonitroalkenes and α -naphthols ^a	31
Table 7. Optimization studies for DHB cycles	33
Table 8. Substrate scope of FC domino reaction between α -bromonitroalkenes and phenols ^a	34

LIST OF FIGURES

FIGURES

Figure 1. Press release of the Nobel prize in chemistry 2021	1
Figure 2. Some bifunctional organocatalysts literature examples	3
Figure 3. Most commonly used natural Cinchona Alkaloids	4
Figure 4. Squarate derivatives	5
Figure 5. Duality in ditopic- and hydrogen-bonding of squaramides.....	6
Figure 6. Calculated computational data on thiourea and squaramide.....	6
Figure 7. DHN and DHB containing pharmaceuticals	11
Figure 8. Bifunctional organocatalysts tried in organocatalyst screening.....	24
Figure 9. a) cis and b) trans conformations for the lowest energy structures of two reactants. c-d) Two transition state geometries of the initial step of the reaction mechanism in the presence of catalyst 19b	37
Figure 10. Reactant, transition state, and product of the reaction between α -bromonitroalkene derivative and β -naphthol coordinated with the active site of the catalyst where a) two amine groups of the catalyst coordinated by single oxygen of the nitro group, b) by two oxygens of the nitro group.....	39
Figure 11. X-Ray crystal structure of 64aa	42
Figure 12. Plausible transition state for the reaction of α -bromonitroalkene 20 and acetylacetone 63a	42
Figure 13. Active sites and the vinylic group of the catalysts 19a-c	44
Figure 14. ^1H NMR spectra of organocatalysts 19c , 70 and 71	47
Figure 15. a) The SEM images of the empty support, b) solid-supported organocatalyst covered	49
Figure A. 1. ^1H NMR spectrum of 20a	131
Figure A. 2. ^{13}C NMR spectrum of 20a	131
Figure A. 3. ^1H NMR spectrum of 20b	132
Figure A. 4. ^{13}C NMR spectrum of 20b	132
Figure A. 5. ^1H NMR spectrum of 20c	133

Figure A. 6. ^{13}C NMR spectrum of 20c	133
Figure A. 7. ^1H NMR spectrum of 20d	134
Figure A. 8. ^{13}C NMR spectrum of 20d	134
Figure A. 9. ^1H NMR spectrum of 20e	135
Figure A. 10. ^{13}C NMR spectrum of 20e	135
Figure A. 11. ^1H NMR spectrum of 20f	136
Figure A. 12. ^{13}C NMR spectrum of 20f	136
Figure A. 13. ^1H NMR spectrum of 20g	137
Figure A. 14. ^{13}C NMR spectrum of 20g	137
Figure A. 15. ^1H NMR spectrum of 20h	138
Figure A. 16. ^{13}C NMR spectrum of 20h	138
Figure A. 17. ^1H NMR spectrum of 20i	139
Figure A. 18. ^{13}C NMR spectrum of 20i	139
Figure A. 19. ^1H NMR spectrum of 20j	140
Figure A. 20. ^{13}C NMR spectrum of 20j	140
Figure A. 21. ^1H NMR spectrum of 20k	141
Figure A. 22. ^{13}C NMR spectrum of 20k	141
Figure A. 23. ^1H NMR spectrum of 20l	142
Figure A. 24. ^{13}C NMR spectrum of 20l	142
Figure A. 25. ^1H NMR spectrum of 20m	143
Figure A. 26. ^{13}C NMR spectrum of 20m	143
Figure A. 27. ^1H NMR spectrum of 20n	144
Figure A. 28. ^{13}C NMR spectrum of 20n	144
Figure A. 29. ^1H NMR spectrum of 20o	145
Figure A. 30. ^{13}C NMR spectrum of 20o	145
Figure A. 31. ^1H NMR spectrum of 20p	146
Figure A. 32. ^{13}C NMR spectrum of 20p	146
Figure A. 33. ^1H NMR spectrum of 20q	147
Figure A. 34. ^{13}C NMR spectrum of 20q	147
Figure A. 35. ^1H NMR spectrum of 20r	148

Figure A. 36. ^{13}C NMR spectrum of 20r	148
Figure A. 37. ^1H NMR spectrum of 20s	149
Figure A. 38. ^{13}C NMR spectrum of 20s	149
Figure A. 39. ^1H NMR spectrum of 20t	150
Figure A. 40. ^{13}C NMR spectrum of 20t	150
Figure A. 41. ^1H NMR spectrum of 23aa	151
Figure A. 42. ^{13}C NMR spectrum of 23aa	151
Figure A. 43. ^1H NMR spectrum of 23ab	152
Figure A. 44. ^{13}C NMR spectrum of 23ab	152
Figure A. 45. ^1H NMR spectrum of 23ac	153
Figure A. 46. ^{13}C NMR spectrum of 23ac	153
Figure A. 47. ^1H NMR spectrum of 23ad	154
Figure A. 48. ^{13}C NMR spectrum of 23ad	154
Figure A. 49. ^1H NMR spectrum of 23ae	155
Figure A. 50. ^{13}C NMR spectrum of 23ae	155
Figure A. 51. ^1H NMR spectrum of 23af	156
Figure A. 52. ^{13}C NMR spectrum of 23af	156
Figure A. 53. ^1H NMR spectrum of 23ag	157
Figure A. 54. ^{13}C NMR spectrum of 23ag	157
Figure A. 55. ^1H NMR spectrum of 23ah	158
Figure A. 56. ^{13}C NMR spectrum of 23ah	158
Figure A. 57. ^1H NMR spectrum of 23ai	159
Figure A. 58. ^{13}C NMR spectrum of 23ai	159
Figure A. 59. ^1H NMR spectrum of 23aj	160
Figure A. 60. ^{13}C NMR spectrum of 23aj	160
Figure A. 61. ^1H NMR spectrum of 23ak	161
Figure A. 62. ^{13}C NMR spectrum of 23ak	161
Figure A. 63. ^1H NMR spectrum of 23al	162
Figure A. 64. ^{13}C NMR spectrum of 23al	162
Figure A. 65. ^1H NMR spectrum of 23am	163

Figure A. 66. ^{13}C NMR spectrum of 23am	163
Figure A. 67. ^1H NMR spectrum of 23an	164
Figure A. 68. ^{13}C NMR spectrum of 23an	164
Figure A. 69. ^1H NMR spectrum of 23ao	165
Figure A. 70. ^{13}C NMR spectrum of 23ao	165
Figure A. 71. ^1H NMR spectrum of 23ap	166
Figure A. 72. ^{13}C NMR spectrum of 23ap	166
Figure A. 73. ^1H NMR spectrum of 23aq	167
Figure A. 74. ^{13}C NMR spectrum of 23aq	167
Figure A. 75. ^1H NMR spectrum of 23ba	168
Figure A. 76. ^{13}C NMR spectrum of 23ba	168
Figure A. 77. ^1H NMR spectrum of 23ca	169
Figure A. 78. ^{13}C NMR spectrum of 23ca	169
Figure A. 79. ^1H NMR spectrum of 23da	170
Figure A. 80. ^{13}C NMR spectrum of 23da	170
Figure A. 81. ^1H NMR spectrum of 23ea	171
Figure A. 82. ^{13}C NMR spectrum of 23ea	171
Figure A. 83. ^1H NMR spectrum of 23as	172
Figure A. 84. ^{13}C NMR spectrum of 23as	172
Figure A. 85. ^1H NMR spectrum of 23at	173
Figure A. 86. ^{13}C NMR spectrum of 23at	173
Figure A. 87. ^1H NMR spectrum of 60aa	174
Figure A. 88. ^{13}C NMR spectrum of 60aa	174
Figure A. 89. ^1H NMR spectrum of 60ab	175
Figure A. 90. ^{13}C NMR spectrum of 60ab	175
Figure A. 91. ^1H NMR spectrum of 60ac	176
Figure A. 92. ^{13}C NMR spectrum of 60ac	176
Figure A. 93. ^1H NMR spectrum of 60ad	177
Figure A. 94. ^{13}C NMR spectrum of 60ad	177
Figure A. 95. ^1H NMR spectrum of 60ae	178

Figure A. 96. ^{13}C NMR spectrum of 60ae	178
Figure A. 97. ^1H NMR spectrum of 60af	179
Figure A. 98. ^{13}C NMR spectrum of 60af	179
Figure A. 99. ^1H NMR spectrum of 60ag	180
Figure A. 100. ^{13}C NMR spectrum of 60ag	180
Figure A. 101. ^1H NMR spectrum of 60ah	181
Figure A. 102. ^{13}C NMR spectrum of 60ah	181
Figure A. 103. ^1H NMR spectrum of 60ai	182
Figure A. 104. ^{13}C NMR spectrum of 60ai	182
Figure A. 105. ^1H NMR spectrum of 60aj	183
Figure A. 106. ^{13}C NMR spectrum of 60aj	183
Figure A. 107. ^1H NMR spectrum of 60ak	184
Figure A. 108. ^{13}C NMR spectrum of 60ak	184
Figure A. 109. ^1H NMR spectrum of 60al	185
Figure A. 110. ^{13}C NMR spectrum of 60al	185
Figure A. 111. ^1H NMR spectrum of 60an	186
Figure A. 112. ^{13}C NMR spectrum of 60an	186
Figure A. 113. ^1H NMR spectrum of 60ao	187
Figure A. 114. ^{13}C NMR spectrum of 60ao	187
Figure A. 115. ^1H NMR spectrum of 60ap	188
Figure A. 116. ^{13}C NMR spectrum of 60ap	188
Figure A. 117. ^1H NMR spectrum of 60aq	189
Figure A. 118. ^{13}C NMR spectrum of 60aq	189
Figure A. 119. ^1H NMR spectrum of 60at	190
Figure A. 120. ^{13}C NMR spectrum of 60at	190
Figure A. 121. ^1H NMR spectrum of 60ba	191
Figure A. 122. ^{13}C NMR spectrum of 60ba	191
Figure A. 123. ^1H NMR spectrum of 60ca	192
Figure A. 124. ^{13}C NMR spectrum of 60ca	192
Figure A. 125. ^1H NMR spectrum of 60bd	193

Figure A. 126. ^{13}C NMR spectrum of 60bd	193
Figure A. 127. ^1H NMR spectrum of 60bo	194
Figure A. 128. ^{13}C NMR spectrum of 60bo	194
Figure A. 129. ^1H NMR spectrum of 60bp	195
Figure A. 130. ^{13}C NMR spectrum of 60bp	195
Figure A. 131. ^1H NMR spectrum of 62ba	196
Figure A. 132. ^{13}C NMR spectrum of 62ba	196
Figure A. 133. ^1H NMR spectrum of 62bb	197
Figure A. 134. ^{13}C NMR spectrum of 62bb	197
Figure A. 135. ^1H NMR spectrum of 62bc	198
Figure A. 136. ^{13}C NMR spectrum of 62bc	198
Figure A. 137. ^1H NMR spectrum of 62bd	199
Figure A. 138. ^{13}C NMR spectrum of 62bd	199
Figure A. 139. ^1H NMR spectrum of 62be	200
Figure A. 140. ^{13}C NMR spectrum of 62be	200
Figure A. 141. ^1H NMR spectrum of 62bh	201
Figure A. 142. ^{13}C NMR spectrum of 62bh	201
Figure A. 143. ^1H NMR spectrum of 62bj	202
Figure A. 144. ^{13}C NMR spectrum of 62bj	202
Figure A. 145. ^1H NMR spectrum of 62bk	203
Figure A. 146. ^{13}C NMR spectrum of 62bk	203
Figure A. 147. ^1H NMR spectrum of 62bl	204
Figure A. 148. ^{13}C NMR spectrum of 62bl	204
Figure A. 149. ^1H NMR spectrum of 62bn	205
Figure A. 150. ^{13}C NMR spectrum of 62bn	205
Figure A. 151. ^1H NMR spectrum of 62bo	206
Figure A. 152. ^{13}C NMR spectrum of 62bo	206
Figure A. 153. ^1H NMR spectrum of 62bp	207
Figure A. 154. ^{13}C NMR spectrum of 62bp	207
Figure A. 155. ^1H NMR spectrum of 62bq	208

Figure A. 156. ^{13}C NMR spectrum of 62bq	208
Figure A. 157. ^1H NMR spectrum of 62ca	209
Figure A. 158. ^{13}C NMR spectrum of 62ca	209
Figure A. 159. ^1H NMR spectrum of 62cb	210
Figure A. 160. ^{13}C NMR spectrum of 62cb	210
Figure A. 161. ^1H NMR spectrum of 62cd	211
Figure A. 162. ^{13}C NMR spectrum of 62cd	211
Figure A. 163. ^1H NMR spectrum of 62cl	212
Figure A. 164. ^{13}C NMR spectrum of 62cl	212
Figure A. 165. ^1H NMR spectrum of 62cn	213
Figure A. 166. ^{13}C NMR spectrum of 62cn	213
Figure A. 167. ^1H NMR spectrum of 64aa	214
Figure A. 168. ^{13}C NMR spectrum of 64aa	214
Figure A. 169. ^1H NMR spectrum of 64ab	215
Figure A. 170. ^{13}C NMR spectrum of 64ab	215
Figure A. 171. ^1H NMR spectrum of 64ac	216
Figure A. 172. ^{13}C NMR spectrum of 64ac	216
Figure A. 173. ^1H NMR spectrum of 64ah	217
Figure A. 174. ^{13}C NMR spectrum of 64ah	217
Figure A. 175. ^1H NMR spectrum of 64ai	218
Figure A. 176. ^{13}C NMR spectrum of 64ai	218
Figure A. 177. ^1H NMR spectrum of 64ak	219
Figure A. 178. ^{13}C NMR spectrum of 64ak	219
Figure A. 179. ^1H NMR spectrum of 64al	220
Figure A. 180. ^{13}C NMR spectrum of 64al	220
Figure A. 181. ^1H NMR spectrum of 64an	221
Figure A. 182. ^{13}C NMR spectrum of 64an	221
Figure A. 183. ^1H NMR spectrum of 64ao	222
Figure A. 184. ^{13}C NMR spectrum of 64ao	222
Figure A. 185. ^1H NMR spectrum of 64bd	223

Figure A. 186. ^{13}C NMR spectrum of 64bd	223
Figure A. 187. ^1H NMR spectrum of 64bg	224
Figure A. 188. ^{13}C NMR spectrum of 64bg	224
Figure A. 189. ^1H NMR spectrum of 65	225
Figure A. 190. ^{13}C NMR spectrum of 65	225
Figure A. 191. ^1H NMR spectrum of 67	226
Figure A. 192. ^{13}C NMR spectrum of 67	226
Figure A. 193. ^1H NMR spectrum of 68	227
Figure A. 194. ^{13}C NMR spectrum of 68	227
Figure A. 195. ^1H NMR spectrum of crude 69	229
Figure A. 196. ^1H NMR spectrum of 70	229
Figure A. 197. ^{13}C NMR spectrum of 70	230
Figure A. 198. ^1H NMR spectrum of 71	230
Figure A. 199. ^{13}C NMR spectrum of 71	231
Figure A. 200. ^1H NMR spectrum of 77	231
Figure A. 201. ^{13}C NMR spectrum of 77	232
Figure A. 202. ^1H NMR spectrum of 78	232
Figure A. 203. ^{13}C NMR spectrum of 78	233
Figure A. 204. ^1H NMR spectrum of 79	233
Figure A. 205. ^{13}C NMR spectrum of 79	234
Figure A. 206. ^1H NMR spectrum of crude 82	234
Figure B. 1. HPLC Chromatogram of <i>rac</i> - 23aa	235
Figure B. 2. HPLC Chromatogram of enantiomerically enriched 23aa	235
Figure B. 3. HPLC Chromatogram of <i>rac</i> - 23ab	236
Figure B. 4. HPLC Chromatogram of enantiomerically enriched 23ab	236
Figure B. 5. HPLC Chromatogram of <i>rac</i> - 23ac	237
Figure B. 6. HPLC Chromatogram of enantiomerically enriched 23ac	237
Figure B. 7. HPLC Chromatogram of <i>rac</i> - 23ad	238
Figure B. 8. HPLC Chromatogram of enantiomerically enriched 23ad	238
Figure B. 9. HPLC Chromatogram of <i>rac</i> - 23ae	239

Figure B. 10. HPLC Chromatogram of enantiomerically enriched 23ae	239
Figure B. 11. HPLC Chromatogram of <i>rac</i> - 23af	240
Figure B. 12. HPLC Chromatogram of enantiomerically enriched 23af	240
Figure B. 13. HPLC Chromatogram of <i>rac</i> - 23ag	241
Figure B. 14. HPLC Chromatogram of enantiomerically enriched 23ag	241
Figure B. 15. HPLC Chromatogram of <i>rac</i> - 23ah	242
Figure B. 16. HPLC Chromatogram of enantiomerically enriched 23ah	242
Figure B. 17. HPLC Chromatogram of <i>rac</i> - 23ai	243
Figure B. 18. HPLC Chromatogram of enantiomerically enriched 23ai	243
Figure B. 19. HPLC Chromatogram of <i>rac</i> - 23aj	244
Figure B. 20. HPLC Chromatogram of enantiomerically enriched 23aj	244
Figure B. 21. HPLC Chromatogram of <i>rac</i> - 23ak	245
Figure B. 22. HPLC Chromatogram of enantiomerically enriched 23ak	245
Figure B. 23. HPLC Chromatogram of <i>rac</i> - 23al	246
Figure B. 24. HPLC Chromatogram of enantiomerically enriched 23al	246
Figure B. 25. HPLC Chromatogram of <i>rac</i> - 23am	247
Figure B. 26. HPLC Chromatogram of enantiomerically enriched 23am	247
Figure B. 27. HPLC Chromatogram of <i>rac</i> - 23an	248
Figure B. 28. HPLC Chromatogram of enantiomerically enriched 23an	248
Figure B. 29. HPLC Chromatogram of <i>rac</i> - 23ao	249
Figure B. 30. HPLC Chromatogram of enantiomerically enriched 23ao	249
Figure B. 31. HPLC Chromatogram of <i>rac</i> - 23ap	250
Figure B. 32. HPLC Chromatogram of enantiomerically enriched 23ap	250
Figure B. 33. HPLC Chromatogram of <i>rac</i> - 23aq	251
Figure B. 34. HPLC Chromatogram of enantiomerically enriched 23aq	251
Figure B. 35. HPLC Chromatogram of <i>rac</i> - 23ba	252
Figure B. 36. HPLC Chromatogram of enantiomerically enriched 23ba	252
Figure B. 37. HPLC Chromatogram of <i>rac</i> - 23ca	253
Figure B. 38. HPLC Chromatogram of enantiomerically enriched 23ca	253
Figure B. 39. HPLC Chromatogram of <i>rac</i> - 23da	254

Figure B. 40. HPLC Chromatogram of enantiomerically enriched 23da	254
Figure B. 41. HPLC Chromatogram of <i>rac</i> - 23ea	255
Figure B. 42. HPLC Chromatogram of enantiomerically enriched 23ea	255
Figure B. 43. HPLC Chromatogram of <i>rac</i> - 23as	256
Figure B. 44. HPLC Chromatogram of enantiomerically enriched 23as	256
Figure B. 45. HPLC Chromatogram of <i>rac</i> - 23at	257
Figure B. 46. HPLC Chromatogram of enantiomerically enriched 23at	257
Figure B. 47. HPLC Chromatogram of <i>rac</i> - 60aa	258
Figure B. 48. HPLC Chromatogram of enantiomerically enriched 60aa	258
Figure B. 49. HPLC Chromatogram of <i>rac</i> - 60ab	259
Figure B. 50. HPLC Chromatogram of enantiomerically enriched 60ab	259
Figure B. 51. HPLC Chromatogram of <i>rac</i> - 60ac	260
Figure B. 52. HPLC Chromatogram of enantiomerically enriched 60ac	260
Figure B. 53. HPLC Chromatogram of <i>rac</i> - 60ad	261
Figure B. 54. HPLC Chromatogram of enantiomerically enriched 60ad	261
Figure B. 55. HPLC Chromatogram of <i>rac</i> - 60ae	262
Figure B. 56. HPLC Chromatogram of enantiomerically enriched 60ae	262
Figure B. 57. HPLC Chromatogram of <i>rac</i> - 60af	263
Figure B. 58. HPLC Chromatogram of enantiomerically enriched 60af	263
Figure B. 59. HPLC Chromatogram of <i>rac</i> - 60ag	264
Figure B. 60. HPLC Chromatogram of enantiomerically enriched 60ag	264
Figure B. 61. HPLC Chromatogram of <i>rac</i> - 60ai	265
Figure B. 62. HPLC Chromatogram of enantiomerically enriched 60ai	265
Figure B. 63. HPLC Chromatogram of <i>rac</i> - 60aj	266
Figure B. 64. HPLC Chromatogram of enantiomerically enriched 60aj	266
Figure B. 65. HPLC Chromatogram of <i>rac</i> - 60ak	267
Figure B. 66. HPLC Chromatogram of enantiomerically enriched 60ak	267
Figure B. 67. HPLC Chromatogram of <i>rac</i> - 60al	268
Figure B. 68. HPLC Chromatogram of enantiomerically enriched 60al	268
Figure B. 69. HPLC Chromatogram of <i>rac</i> - 60an	269

Figure B. 70. HPLC Chromatogram of enantiomerically enriched 60an	269
Figure B. 71. HPLC Chromatogram of <i>rac-60ao</i>	270
Figure B. 72. HPLC Chromatogram of enantiomerically enriched 60ao	270
Figure B. 73. HPLC Chromatogram of <i>rac-60ap</i>	271
Figure B. 74. HPLC Chromatogram of enantiomerically enriched 60ap	271
Figure B. 75. HPLC Chromatogram of <i>rac-60aq</i>	272
Figure B. 76. HPLC Chromatogram of enantiomerically enriched 60aq	272
Figure B. 77. HPLC Chromatogram of <i>rac-60at</i>	273
Figure B. 78. HPLC Chromatogram of enantiomerically enriched 60at	273
Figure B. 79. HPLC Chromatogram of <i>rac-60ba</i>	274
Figure B. 80. HPLC Chromatogram of enantiomerically enriched 60ba	274
Figure B. 81. HPLC Chromatogram of <i>rac-60ca</i>	275
Figure B. 82. HPLC Chromatogram of enantiomerically enriched 60ca	275
Figure B. 83. HPLC Chromatogram of <i>rac-60bd</i>	276
Figure B. 84. HPLC Chromatogram of enantiomerically enriched 60bd	276
Figure B. 85. HPLC Chromatogram of <i>rac-60bo</i>	277
Figure B. 86. HPLC Chromatogram of enantiomerically enriched 60bo	277
Figure B. 87. HPLC Chromatogram of <i>rac-60bp</i>	278
Figure B. 88. HPLC Chromatogram of enantiomerically enriched 60bp	278
Figure B. 89. HPLC Chromatogram of <i>rac-62ba</i>	279
Figure B. 90. HPLC Chromatogram of enantiomerically enriched 62ba	279
Figure B. 91. HPLC Chromatogram of <i>rac-62bb</i>	280
Figure B. 92. HPLC Chromatogram of enantiomerically enriched 62bb	280
Figure B. 93. HPLC Chromatogram of <i>rac-62bc</i>	281
Figure B. 94. HPLC Chromatogram of enantiomerically enriched 62bc	281
Figure B. 95. HPLC Chromatogram of <i>rac-62be</i>	282
Figure B. 96. HPLC Chromatogram of enantiomerically enriched 62be	282
Figure B. 97. HPLC Chromatogram of <i>rac-62bj</i>	283
Figure B. 98. HPLC Chromatogram of enantiomerically enriched 62bj	283
Figure B. 99. HPLC Chromatogram of <i>rac-62bk</i>	284

Figure B. 100. HPLC Chromatogram of enantiomerically enriched 62bk	284
Figure B. 101. HPLC Chromatogram of <i>rac-62bl</i>	285
Figure B. 102. HPLC Chromatogram of enantiomerically enriched 62bl	285
Figure B. 103. HPLC Chromatogram of <i>rac-62bn</i>	286
Figure B. 104. HPLC Chromatogram of enantiomerically enriched 62bn	286
Figure B. 105. HPLC Chromatogram of <i>rac-62bo</i>	287
Figure B. 106. HPLC Chromatogram of enantiomerically enriched 62bo	287
Figure B. 107. HPLC Chromatogram of <i>rac-62bp</i>	288
Figure B. 108. HPLC Chromatogram of enantiomerically enriched 62bp	288
Figure B. 109. HPLC Chromatogram of <i>rac-62bq</i>	289
Figure B. 110. HPLC Chromatogram of enantiomerically enriched 62bq	289
Figure B. 111. HPLC Chromatogram of <i>rac-62ca</i>	290
Figure B. 112. HPLC Chromatogram of enantiomerically enriched 62ca	290
Figure B. 113. HPLC Chromatogram of <i>rac-62cb</i>	291
Figure B. 114. HPLC Chromatogram of enantiomerically enriched 62cb	291
Figure B. 115. HPLC Chromatogram of <i>rac-62cd</i>	292
Figure B. 116. HPLC Chromatogram of enantiomerically enriched 62cd	292
Figure B. 117. HPLC Chromatogram of <i>rac-62cl</i>	293
Figure B. 118. HPLC Chromatogram of enantiomerically enriched 62cl	293
Figure B. 119. HPLC Chromatogram of <i>rac-64aa</i>	294
Figure B. 120. HPLC Chromatogram of enantiomerically enriched 64aa	294
Figure B. 121. HPLC Chromatogram of <i>rac-64ab</i>	295
Figure B. 122. HPLC Chromatogram of enantiomerically enriched 64ab	295
Figure B. 123. HPLC Chromatogram of <i>rac-64ac</i>	296
Figure B. 124. HPLC Chromatogram of enantiomerically enriched 64ac	296
Figure B. 125. HPLC Chromatogram of <i>rac-64ah</i>	297
Figure B. 126. HPLC Chromatogram of enantiomerically enriched 64ah	297
Figure B. 127. HPLC Chromatogram of <i>rac-64ai</i>	298
Figure B. 128. HPLC Chromatogram of enantiomerically enriched 64ai	298
Figure B. 129. HPLC Chromatogram of <i>rac-64ak</i>	299

Figure B. 130. HPLC Chromatogram of enantiomerically enriched 64ak	299
Figure B. 131. HPLC Chromatogram of <i>rac</i> - 64al	300
Figure B. 132. HPLC Chromatogram of enantiomerically enriched 64al	300
Figure B. 133. HPLC Chromatogram of <i>rac</i> - 64an	301
Figure B. 134. HPLC Chromatogram of enantiomerically enriched 64an	301
Figure B. 135. HPLC Chromatogram of <i>rac</i> - 64ao	302
Figure B. 136. HPLC Chromatogram of enantiomerically enriched 64ao	302
Figure B. 137. HPLC Chromatogram of <i>rac</i> - 64bd	303
Figure B. 138. HPLC Chromatogram of enantiomerically enriched 64bd	303
Figure B. 139. HPLC Chromatogram of <i>rac</i> - 64bg	304
Figure B. 140. HPLC Chromatogram of enantiomerically enriched 64bg	304
Figure C. 1. Reactant, transition state (TS1) and product of the reaction between bromonitroalkene derivative and β -naphthol coordinated with the active site of the catalyst 19c where two amine groups of the catalyst coordinated by two oxygens of the nitro group	305
Figure C. 2. Reactant, transition state (TS2) and product of the reaction between bromonitroalkene derivative and β -naphthol coordinated with the active site of the catalyst where two amine groups of the catalyst coordinated by single oxygen of the nitro group	311
Figure C. 3. Transition State 1	318
Figure C. 4. Transition State 2	318
Figure D. 1. Ortep diagram of 64aa , thermal ellipsoids are shown at the 50% probability level.....	319
Figure D. 2. Crystal packing of 64aa projected onto the <i>ab</i> plane.....	320

LIST OF SCHEMES

SCHEMES

Scheme 1. Inversion of C-9 at quinine	5
Scheme 2. Synthesis of organocatalyst 5	7
Scheme 3. Conjugate addition of acetylacetone to β -nitrostyrenes with organocatalyst 5	7
Scheme 4. Catalytic DKR of the racemic valine-derived azlactone with allyl alcohol.....	8
Scheme 5. Michael addition reaction with organocatalyst 12	8
Scheme 6. Michael reaction of 1,3-dicarbonyl compounds and nitroalkenes with catalyst 14	9
Scheme 7. Tamura cycloaddition with organocatalyst 17	9
Scheme 8. Michael addition of 1-nitropropane to nitroalkenes with catalyst 19 ...	10
Scheme 9. Friedel-Crafts Domino type reaction with organocatalyst 22	12
Scheme 10. Friedel-Crafts Domino type reaction with organocatalysts 24 & 25 ..	13
Scheme 11. Asymmetric reduction of ketimines 26 with trichlorosilane 28 with catalyst 27	15
Scheme 12. Asymmetric α -amination of β -ketoesters with organocatalyst 32	16
Scheme 13. Synthesis of GNP-supported and <i>o</i> -lauroyl- <i>trans</i> -4-hydroxy-L-proline catalysts 39	17
Scheme 14. Direct asymmetric aldol reaction of cyclohexanone and aryl aldehydes with organocatalyst 39c	17
Scheme 15. Diels-Alder reaction of acrolein and cyclohexadiene with organocatalyst 40	18
Scheme 16. Conjugate addition of isobutyl aldehyde 42 to <i>N</i> -phenyl maleimide 41 with organocatalyst 43	18
Scheme 17. Synthesis of dihydrofuranone spirooxindoles 48 and tetrahydropyranone spirooxindoles 49 with catalyst 46	19

Scheme 18. Friedel/Crafts domino-type reaction of α -bromonitroalkenes and naphthols/phenols	20
Scheme 19. Michael addition and S _N 2 type reaction of α -bromonitroalkenes and active methylene nucleophiles.....	21
Scheme 20. Gold nanoparticle supported organocatalysts.....	21
Scheme 21. Solid supported organocatalyst	21
Scheme 22. Fluorous supported organocatalyst.....	22
Scheme 23. Synthetic route for 2-aminoDMAP and quinine based organocatalysts	23
Scheme 24. The synthetic route for the generation of free -SH unit on quinine	44
Scheme 25. The synthetic route for the generation of free -SH unit on organocatalyst 19c by thermal initiator	45
Scheme 26. The synthetic routes for the generation of free -SH unit on organocatalyst 19c by the photoinitiator	45
Scheme 27. The synthetic routes for the generation of longer chain free -SH unit on organocatalyst 19c by the photoinitiator	46
Scheme 28. Representative synthesis of the solid-supported organocatalyst 72	48
Scheme 29. Generation of thiol-stabilized gold nanoparticles	50
Scheme 30. Ligand exchange reaction to generate organocatalyst 74	50
Scheme 31. a) Generation of free thiol unit on 4-hydroxy-L-proline 36 b) Synthesis of GNP-supported L-proline derived organocatalyst 80	51
Scheme 32. Synthetic route for fluororous organocatalyst 83	52

LIST OF ABBREVIATIONS

AIBN	: Azobisisobutyronitrile
BINOL	: 1,1'-Bi-2-naphthol
BOC	: Butoxycarbonyl
DCE	: Dichloroethane
DHB	: Dihydrobenzofuran
DHF	: Dihydrofuran
DHN	: Dihydronaphthofuran
DKR	: Dynamic kinetic resolution
DMPA	: 2,2-Dimethoxy-2-phenylacetophenone
DPPA	: Diphenyl phosphoryl azide
PMP	: <i>p</i> -Methoxyphenyl
SEM	: Scanning Electron Microscopy

CHAPTER 1

INTRODUCTION

1.1 Asymmetric Organocatalysis

“An ingenious tool for building molecules”

“Building molecules is a difficult art. Benjamin List and David MacMillan are awarded the Nobel Prize in Chemistry 2021 for their development of a precise new tool for molecular construction: organocatalysis. This has had a great impact on pharmaceutical research, and has made chemistry greener.”^{1,2}

THE NOBEL PRIZE
IN CHEMISTRY 2021



Figure 1. Press release of the Nobel prize in chemistry 2021

Chiral organic molecules, organocatalysts, have been widely used in substoichiometric amount to catalyze asymmetric transformations. These metal-free, easily accessible, robust, environmentally friendly skeletons provide an extensive range of research area for scientists. David MacMillan and Benjamin List, who were the pioneer scientists for the development of this concept, were awarded with Nobel prize in Chemistry.

Although the organocatalysis term frequently used in literature by MacMillan and List in 2000,^{3,4} Wolfgang Longenback wrote a book covering “organic catalysis” in 1935.⁵ Even the very known example of asymmetric organocatalysis was applied by the work belonging to Bredig and Fiske in 1912.⁶ No matter who discovered the area, many developments have been done over the years on the concept of asymmetric organocatalysis. Especially in the last two decades, excellent examples of studies have been published.

Different classifications on this concept have been done according to their interactions during the course of a reaction. List and Seayad,⁷ categorized them to their acidity or basicity as Lewis acid, Lewis base, Brønsted acid, and Brønsted base. On the other hand, Buckley et al. classified them as iminium catalysis, SOMO catalysis, hydrogen catalysis, counter-ion catalysis, and *N*-heterocyclic carbon (NHC) catalysis.⁸

A special concept became to the top of the agenda as “bifunctional organocatalysis” in 2003 by Takemoto contexts both acidic and basic units together.⁹ Using different Lewis/Brønsted basic units such as cyclohexanediamines,^{10,11} Cinchona alkaloids,¹² binaphthylamines,¹³ and DMAPs,¹⁴ causes nucleophilic activation by increasing HOMO level which is provided by partial deprotonation. On the other hand, different acidic parts used in the activation of electrophile by decreasing the LUMO level can be differentiated by ureas,¹⁵ thioureas,^{15,16} phosphoric acids,¹⁷ sulfonamides,¹⁸ and squaramides¹⁹. The common property of these type of organocatalysts has a chiral spacer to induce enantioselectivity between the acidic and basic parts (Figure 2).

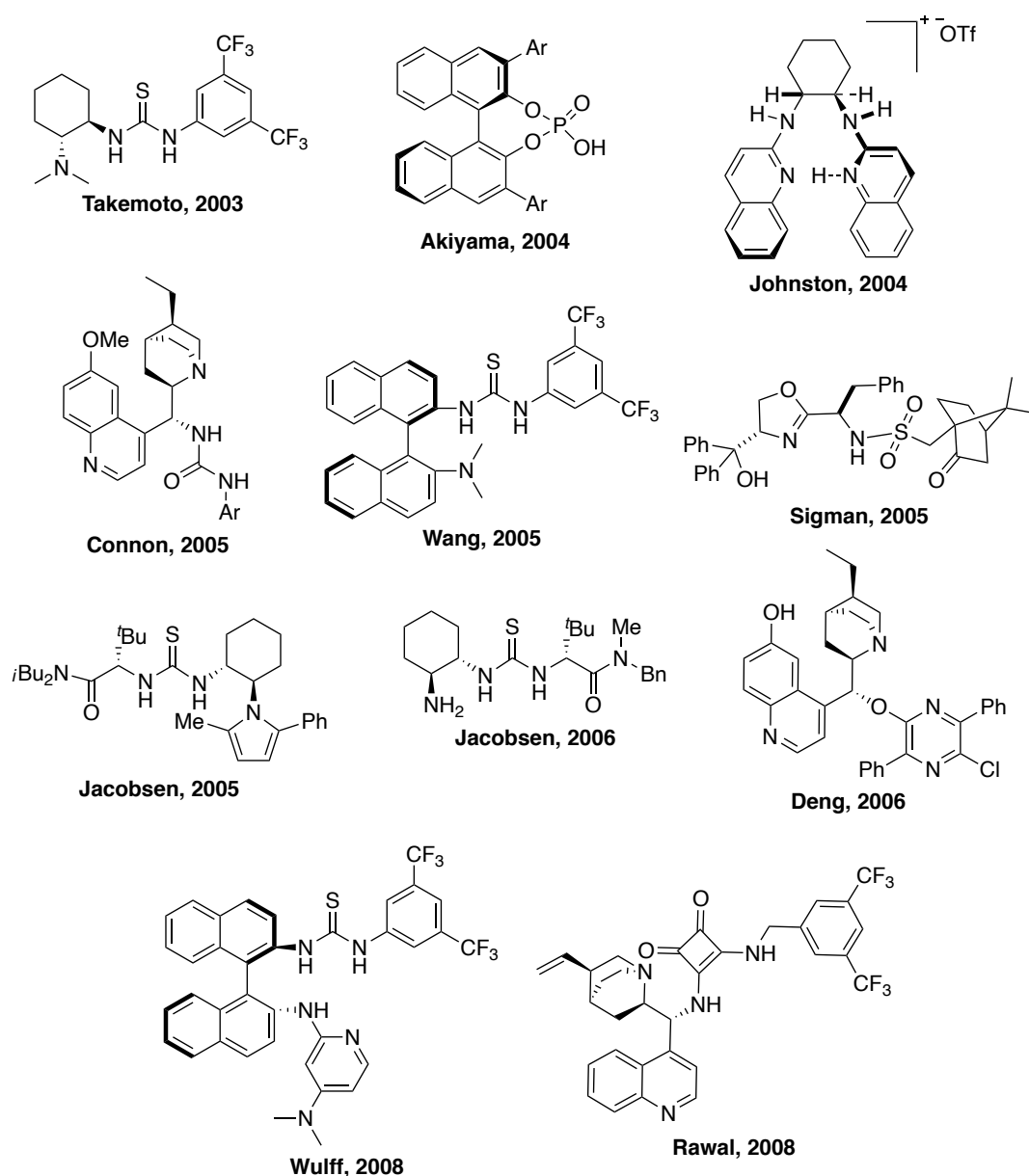


Figure 2. Some bifunctional organocatalysts literature examples

1.1.1 Cinchona Alkaloids

Cinchona alkaloids (Figure 3), especially quinine derivative, hold a unique place in human civilization among the thousands of natural compounds isolated, characterized and classified thus far, from cinchona tree family *Rubiaceae*, including *Cinchona succirubra*, *Cinchona ledgeriana*, *Cinchona calisaya*.^{20,21}

Rumor has it, Cinchona tree bark was first discovered as an anti-fever agent by South American Indians, and it was transported to Europe around 1640. Until 1820, when pure quinine was discovered and mainly replaced the natural substance, the bark prevailed in malaria medicine in Europe. Quinine could be considered the first, pure, and genuinely active chemotherapeutic in this context.²²

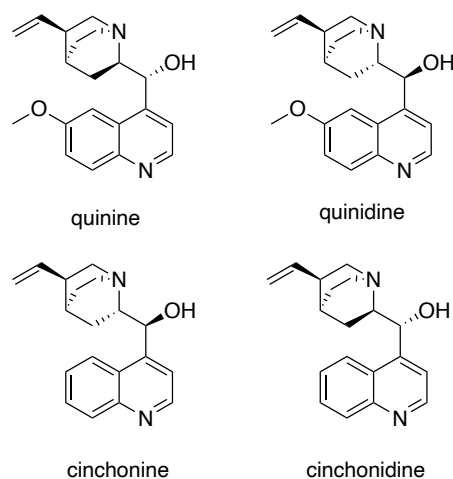
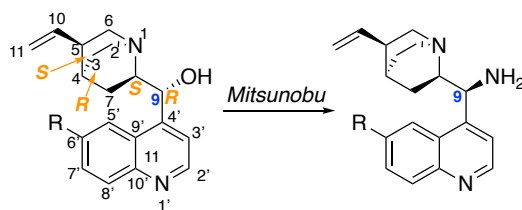


Figure 3. Most commonly used natural Cinchona Alkaloids

Despite the relative simplicity of the Cinchona alkaloid structure, the first total synthesis of quinine was not performed until 2001, 150 years after quinine isolation, when Stork revealed the first stereoselective version.²³

The science behind quinine has a huge influence on the rapid development of natural product pharmaceutical and organic chemistry.^{6,24} Many of these compounds are often utilized as chiral agents or catalysts in asymmetric synthesis either directly or converting to any of the derivatives by a substitution reaction. Substitution of the 9-hydroxyl group, as in the Mitsunobu reaction leads to a variety of useful derivatives, most of which have a complete inversion of the configuration at C-9 such as their corresponding amines (Scheme 1).²⁵



Scheme 1. Inversion of C-9 at quinine

1.1.2 Squaramides

Squaramides are important four-membered ring structures that could generate up to four hydrogen bonds and are synthesized from squaric acid. An increase in aromaticity of the ring drives a strong affinity for hydrogen bonding. Many of the uses of squaramides have taken advantage of hydrogen bonding and aromatic switching in combination with structural stiffness. Several derivatives of squaric acid have been widely used in different areas of catalysis (Figure 4). Substituted squaramides are attractive units for bioconjugation and supramolecular chemistry because they could be synthesized in a modular fashion under moderate or aqueous conditions.

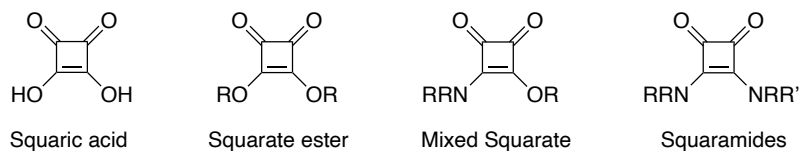


Figure 4. Squarate derivatives

In the organocatalysis field, Rawal was the pioneer of the transition of acidic parts from ureas/thioureas to squaramides.¹⁹ The first major distinction between squaramides and their urea/thiourea counterparts is the ion- and H-bonding duality. While ureas and thioureas have high anion binding affinity, their capacity to detect cations is substantially lower. The squaramide functionality, on the other hand, exhibits duality and readily participates in ditopic binding (Figure 5, left). Additionally, there are three binding sites for the H-bonding in squaramides as shown in Figure 5, right.^{26,27}

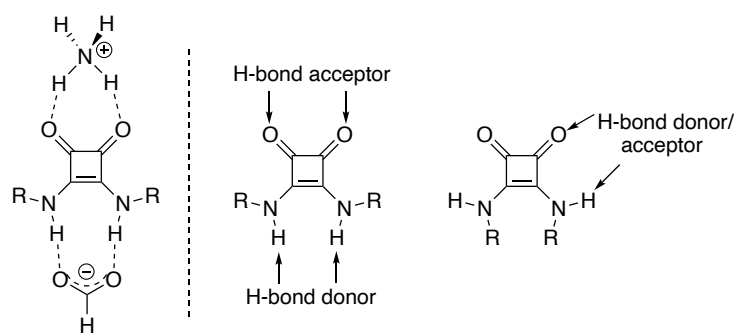


Figure 5. Duality in ditopic- and hydrogen-bonding of squaramides

Another proof for the dual activation of squaramide is shown in the calculation of crystallographic and computational data on both thiourea and squaramide (Figure 6).¹⁹ The distance between two H atoms on the thiourea is calculated 2.13 Å, whereas the distance between bisamides is calculated 2.72 Å. This approximate 6° activates the dual H-bonding.

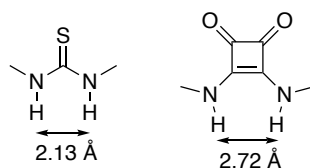
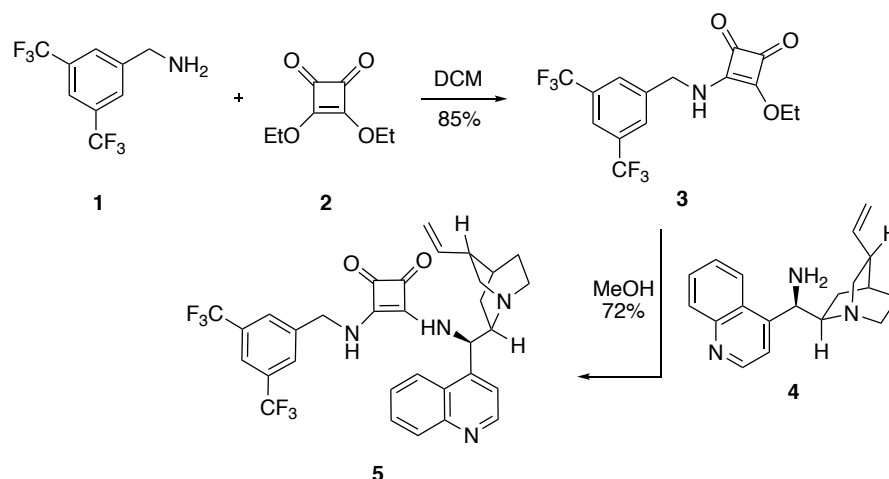


Figure 6. Calculated computational data on thiourea and squaramide

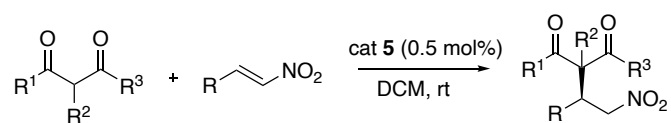
1.1.3 Asymmetric Reactions with Cinchona Alkaloids/Squaramides

Although the first example of the squaramide ligand motif in asymmetric synthesis was applied by Xie et al. in 2005,²⁸ the potential and variety of applications of squaramide organocatalysts were not realized until the Rawal group's pioneering work on the development of Cinchona-squaramide organocatalysts in 2008.¹⁹ Merging cinchona alkaloids with squaramides are relatively easy as shown in Scheme 2.



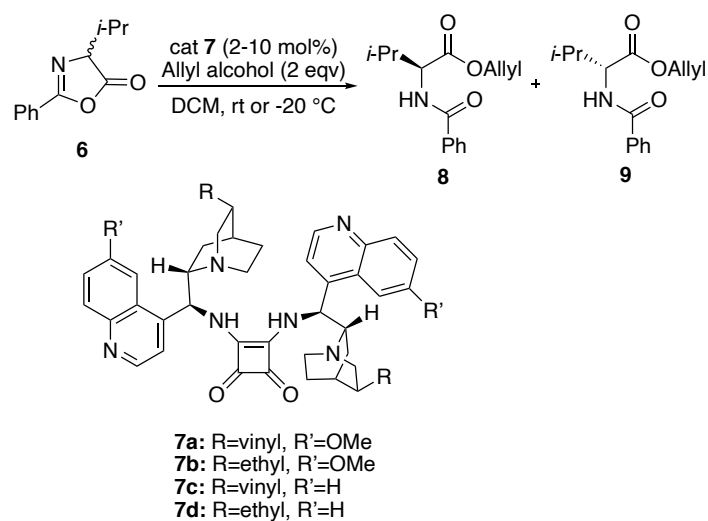
Scheme 2. Synthesis of organocatalyst **5**

The synthesized organocatalysts were tested in the conjugate addition of acetylacetone to β -nitrostyrene. Using 0.5 mol% organocatalysts led to excellent chemical yields up to 99% and enantioselectivities up to 98% in 24 hours maximum in different derivatives (Scheme 3).



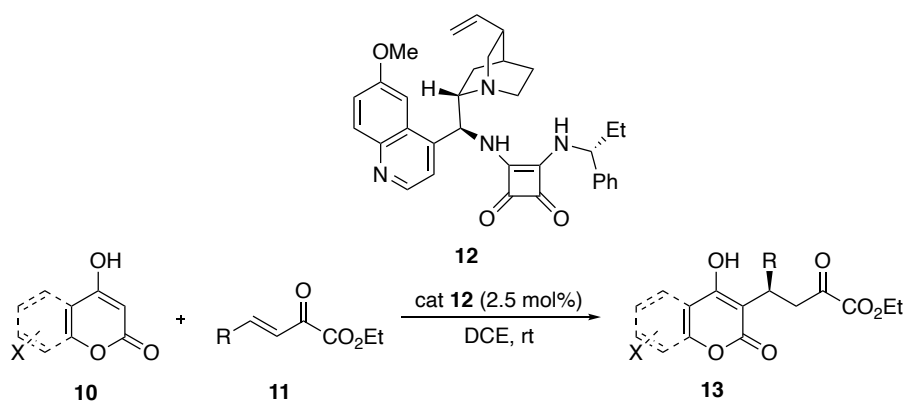
Scheme 3. Conjugate addition of acetylacetone to β -nitrostyrenes with organocatalyst **5**

One year later, Song and co-workers presented a dynamic kinetic resolution (DKR) of racemic azlactones **6** utilizing dimeric squaramides produced from cinchona alkaloid **7**, which were easily synthesized by combining the chiral amine with dimethyl squarate.²⁹ DKR of azlactones **6** afford a variety of natural and non-natural α -amino acid derivatives **8**, **9** in high yields and enantioselectivities (up to 99% and 97% ee, respectively). Additionally, due to low solubility of these organocatalysts in organic solvents, they could be easily recovered using a simple precipitation process, allowing for repeated recycling with no loss in turnover time or enantioselectivity (Scheme 4).



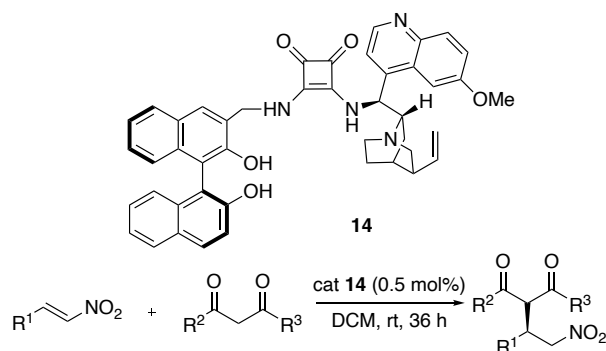
Scheme 4. Catalytic DKR of the racemic valine-derived azlactone with allyl alcohol

Another example of cinchona/squaramide type organocatalysts was published by Xu et al.³⁰ and evaluated on the Michael addition reactions of 4-hydroxycoumarins and 4-hydroxypyron **10** to β,γ -unsaturated α -keto esters **11**. With the usage of 2.5 mol% of catalyst **12** was used in DCE and resulted that most of the derivatives were synthesized in very good yields (73-95%) with excellent enantioselectivities (91- <99% ee). Most of the 18 derivative reactions were completed in 10-12 h (Scheme 5).



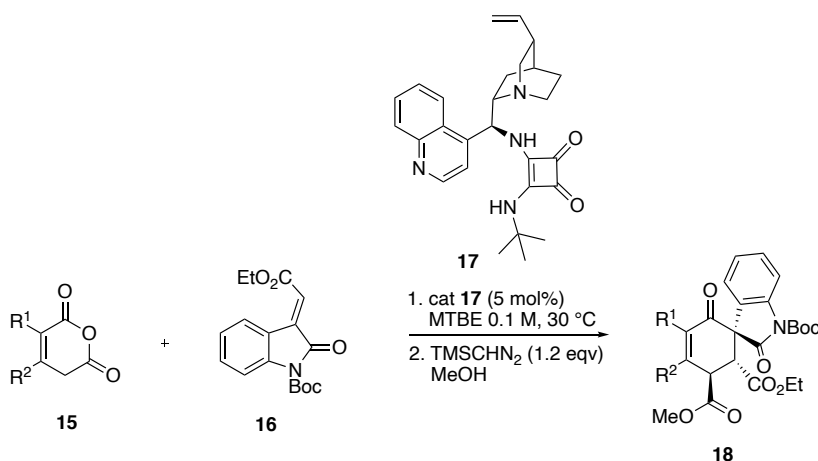
Scheme 5. Michael addition reaction with organocatalyst **12**

An interesting example of cinchona/squaramide type organocatalysts was designed by Dong et al. as BINOL-quinine-squaramide **14** for the Michael reaction between 1,3-dicarbonyl compounds and nitroalkenes (Scheme 6).³¹ Using 0.5 mol% **14** caused long duration hours (36 h) with good yields (70-92%); however, led to excellent stereoselectivities (91 - <99% ee).



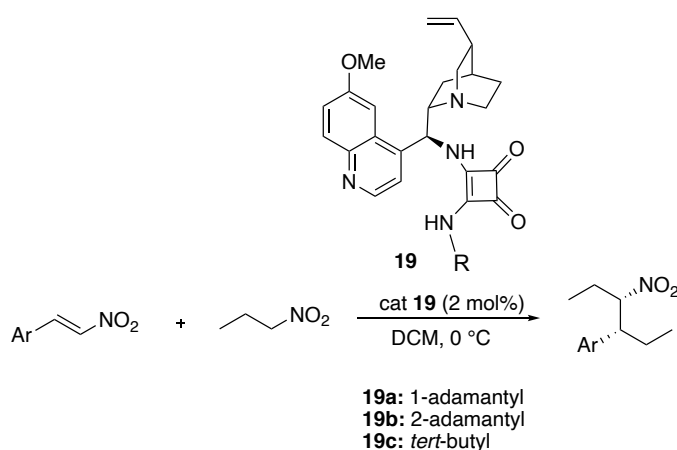
Scheme 6. Michael reaction of 1,3-dicarbonyl compounds and nitroalkenes with catalyst **14**

A novel *tert*-butyl squaramide organocatalyst was published by Connon et al. in 2014 to induce the stereoselectivity of the Tamura cycloaddition to generate spirooxindoles.³² The homophthalic anhydride **15** and *N*-Boc oxindole **16** was subjected to reaction with organocatalyst **17** and achieved up to excellent enantioselectivities (92->99%) in very high yields (82-96%) and stereocontrol (Scheme 7).



Scheme 7. Tamura cycloaddition with organocatalyst **17**

Quinine-derived sterically encumbered squaramides were published by Tanyeli et al. in 2016.³³ Three novel bifunctional organocatalysts were used in the conjugate Michael addition of 1-nitropropane to various *trans*- β -nitroalkenes (Scheme 8). Among the organocatalysts, quinine/*tert*-butyl squaramide **19c** gave the best result in terms of both chemical yield and stereoselectivity, so that, the derivatization study was completed with organocatalyst **19c**. The best result was achieved with *p*-OMe derivate, 95% ee (*syn*), 96:4 dr, 73% yield.



Scheme 8. Michael addition of 1-nitropropane to nitroalkenes with catalyst **19**

1.2 Dihydronaphthofurans and Dihydrobenzofurans

Dihydronaphthofurans (DHN) and dihydrobenzofurans (DHB) are biologically active molecules found in many natural products, so they can be considered as the fundamental motifs within pharmaceutical and agrochemical chemistry.^{34–43} Drugs used in the treatment of many diseases like hernia, arthritis, or carcinoma have DHN and DHB skeletons. These structures may also possess anti-viral, anti-tumor, anti-fungal properties as in the case of (\pm)- ϵ -viniferin,^{34,41} (-)-ephedradines,^{35,36} *o*-methylorantine,³⁶ obsutafuran,^{37,43} conocarpan,^{38,43} bicunningines A & B,³⁹ (-)-glycinol,⁴⁰ caraciphenol C, amphelopsin H, nepalensinol B,⁴¹ toxol, (\pm)-lawsonicin, furaquinocins,⁴² megapodiol,⁴³ PPAR α agonist (Figure 7).⁴⁴

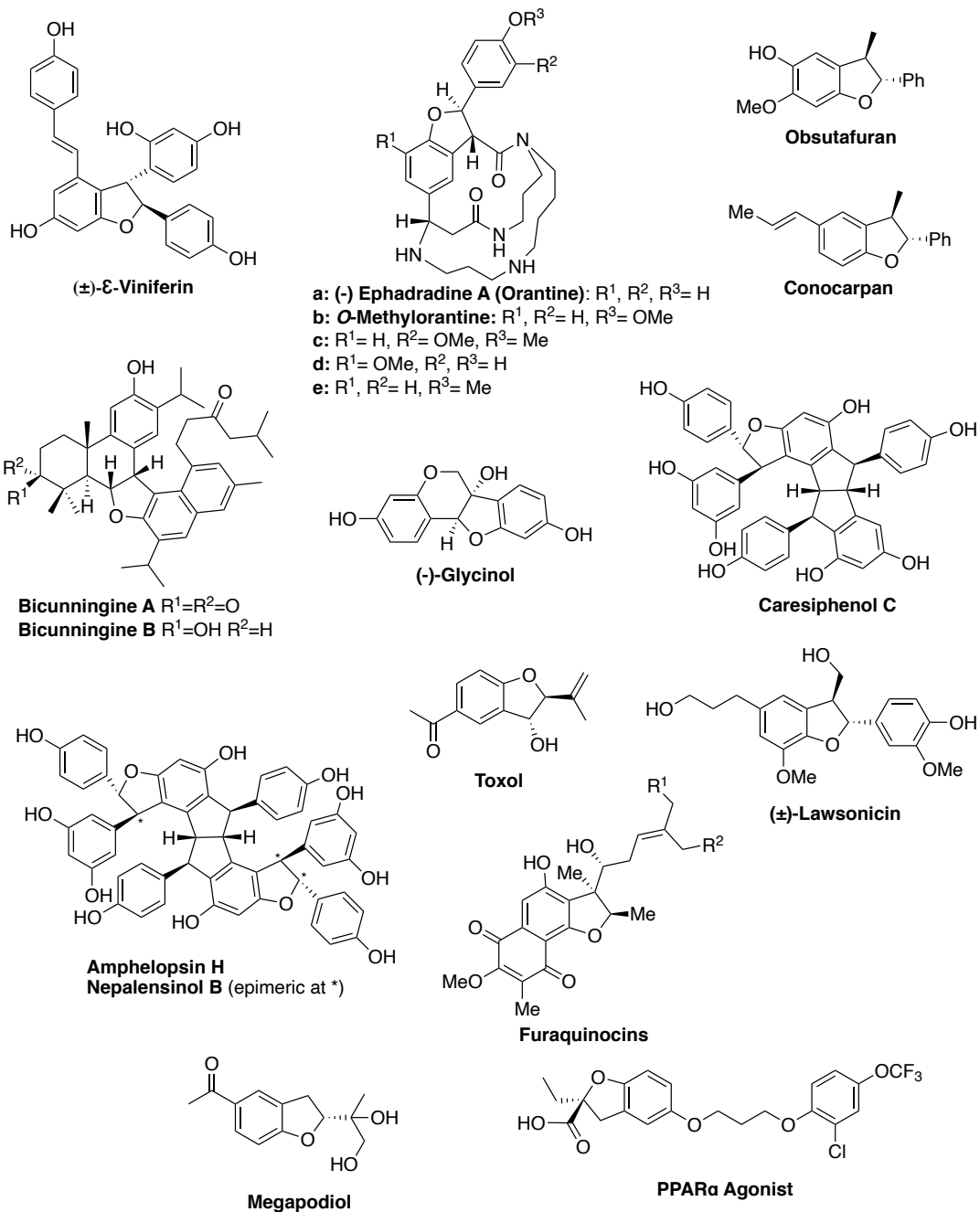
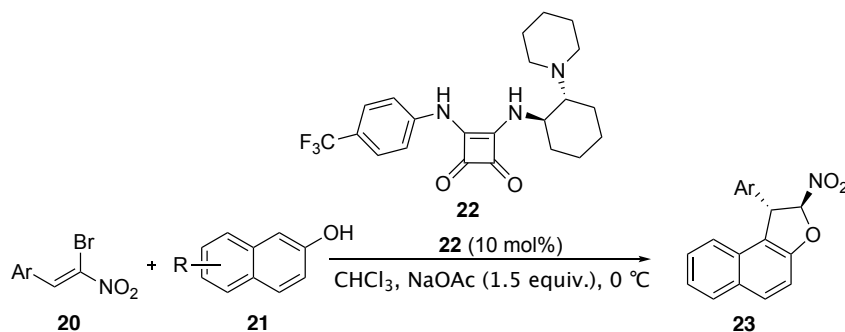


Figure 7. DHN and DHB containing pharmaceuticals

1.2.1 Asymmetric Synthesis of DHN and DHB

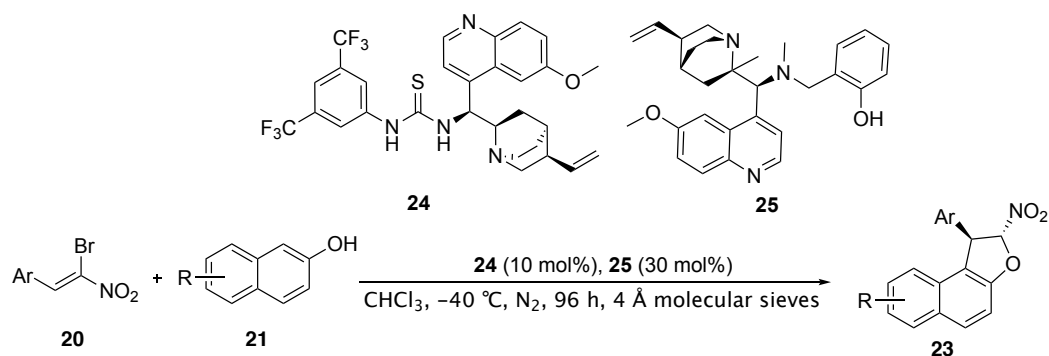
Although there are some transition metal catalysts available in the synthesis of those DHN and DHB moieties, their asymmetric synthesis is quite unexplored.^{45–52} While it is known that the synthesis of asymmetric DHB cycles requires relatively less effort, the DHN case is limited to naphthol unit containing compounds as expected. To our knowledge, only two asymmetric approaches are available to construct DHNs using bielelectrophilic *Z*-(α)-bromonitroalkenes which were reacted with β -naphthols in both studies.^{53,54} The major drawback for the use of *Z*-(α)-bromonitroalkenes is the generation of HBr during the product occurrence, which inhibits the active site of the catalyst, thereby decreasing the rate of the reaction. In order to overcome this problem, basic-character additives must be used.

In 2013, Alemán and co-workers applied an asymmetric domino reaction catalyzed by a squaramide, analogous to Takemoto's catalyst (Scheme 9).⁵³ They used an inorganic base and achieved moderate to excellent ee values in the presence of 10 mol% organocatalyst with reaction durations ranging from 16 h to 7 days.



Scheme 9. Friedel-Crafts Domino type reaction with organocatalyst **22**

The work done by Pan et al., which was published in the same year, focuses on the same reaction (Scheme 10).⁵⁴ Even though their results are good enough in terms of chemical yield and enantioselectivities, their reaction conditions (10 mol% quinine derived thiourea with a 30 mol% secondary Cinchona alkaloid derivative under $-40\text{ }^\circ\text{C}$ in 96 h) were more severe than Alemán's. Due to quite harsh reaction conditions in both cases, the subject is required to be explored.



Scheme 10. Friedel-Crafts Domino type reaction with organocatalysts **24** & **25**

1.3 Recyclable Organocatalysis

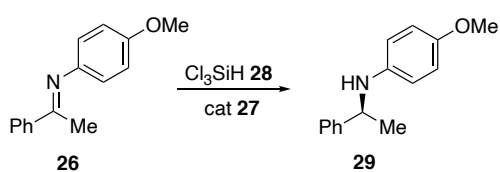
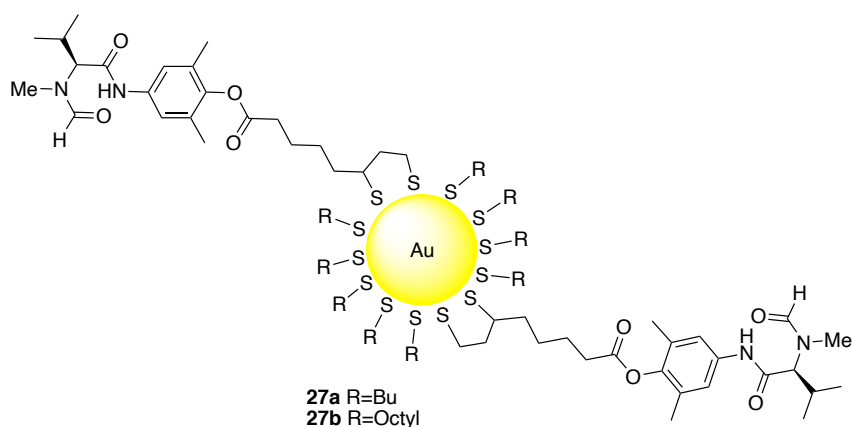
Among the asymmetric synthesis methods, organocatalysis has been used as a powerful tool for the last couple of decades, preferably due to its cheap, non-toxic, robust, metal-free, environmentally-friendly, inert, easily available nature. Besides that, they are also simple in terms of handling and storage. A great interest has been arisen to enhance these precious chiral structures to achieve remarkable results in asymmetric synthesis.^{55–59} Countless studies have been done in many different types of reactions such as Michael,^{9,60–62} aldol,^{63–69} Diels-Alder,^{3,70–73} Henry,^{74–79} aza-Henry,^{80–85} Friedel-Crafts,^{42,86–89} Povarov,^{90–93} decarboxylative Doebner-Knoevenagel^{94,95} reactions and many others. Although asymmetric organocatalysis could be considered as the most successful and easy way to synthesize enantioenriched compounds,⁹⁶ one of the most debated drawbacks is the possibility of agglomeration and aggregation due to high catalyst loading in the reactions. In some cases, up to 20-30 mol% catalyst loading^{97,98} is required; so that it draws attention to the recyclization of the catalyst for many researchers in addition to developing new catalysts for stereoselective synthesis. For this purpose, immobilized and reusable catalyst studies have been pursued to recycle these significant structures. By using solid support, alongside the promoted activity and selectivity, recovery and recycling were achieved in many applications with either cheap and easily accessible organocatalysts like L-proline or relatively expensive and synthetic complex organocatalysts. In principle, insoluble support causes a heterogeneous

catalyst, which is easy to recover from the reaction medium by simple filtration; however slower reaction rate can occur. On the contrary, soluble support for example like polymer supports needs an additional step to be recovered (precipitation by addition of a solvent) may fasten the reaction rate. In addition to the aforementioned advancements, reusable immobilized organocatalysts can be adopted to flow chemistry.^{99,100} Herein this thesis, I would like to combine and survey the studies only on different types of anchored materials such as; gold nanoparticle and fluororous supports for immobilized organocatalysts in asymmetric transformations.

1.3.1 Gold Nanoparticle Supported Organocatalysts

Working with nanoparticles offers a better way to control the number and the accessibility of the catalyst molecules attached to the surface with the place-exchange reactions. Besides that, nanoparticles have a great advantage over the encapsulated catalysts by polymer-supported ones, since the catalysts are immersed in the nanoparticle surface.

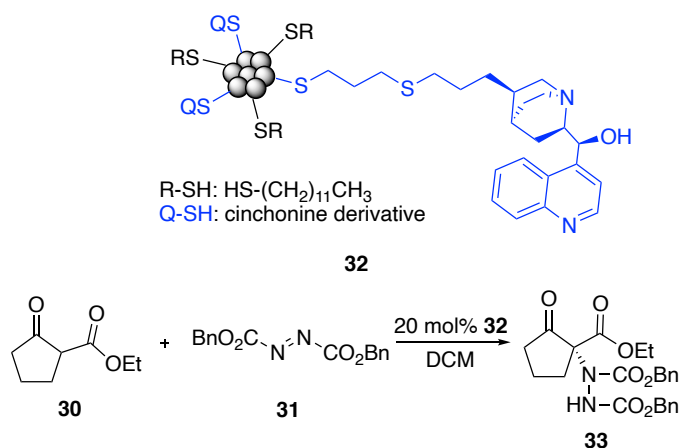
A valine-derived formamide was anchored onto the surface of gold nanoparticles (GNP) **27** by Malkov et al. to be used in the asymmetric reduction of PMP-protected ketimines **26** with trichlorosilane **28** (Scheme 11).¹⁰¹ The gold nanoparticles were prepared from auric acid with Brust-Schiffrin synthesis and covered up with long-chain thiols. The subsequent place-exchanged reaction took place to prepare the gold nanoparticle immobilized organocatalyst with a lipoic acid linker.



Scheme 11. Asymmetric reduction of ketimines **26** with trichlorosilane **28** with catalyst **27**

The catalyst **27a** gave the best result as 84% ee with 90% isolated yield. The recovered catalyst was used up to 4th run, which was obtained with the same yield but with a decrease in the enantioselectivity to 68% ee.

Vallribera and co-workers described the first example of a thiol functionalized alkaloid attached to gold nanoparticles (Scheme 12).¹⁰² Cinchonine was chosen to be the organocatalyst and functionalized with a thiol linker via thiol-ene reaction. Subsequent facile ligand exchange reaction yielded the desired gold nanoparticle-supported organocatalyst **32**.

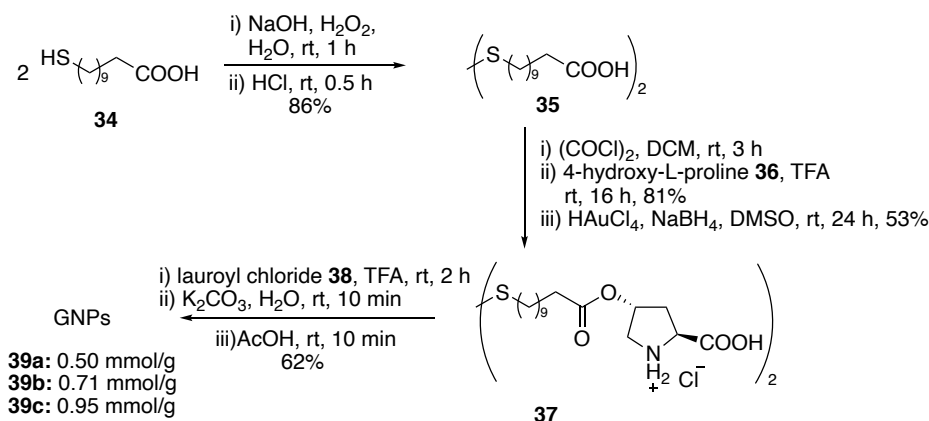


Scheme 12. Asymmetric α -amination of β -ketoesters with organocatalyst **32**

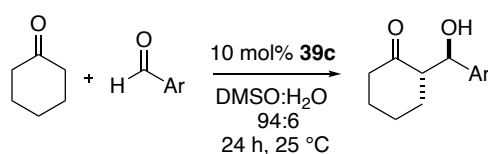
Organocatalyst **32** was evaluated in the asymmetric α -amination of β -ketoesters (Scheme 12). The model reaction was performed between ethyl 2-oxocyclopentanecarboxylate **30** and dibenzyl azodicarboxylate **31**. The best result was 90% ee, in the presence of 20 mol% catalyst **32** in DCM at -78°C in 2 h.

Another gold nanoparticle-supported organocatalyst was prepared by S3ti et al. starting from 4-hydroxy-L-proline **52** and chloroauric acid in four steps (Scheme 13).¹⁰³ The efficiency of these catalysts were tested on the direct asymmetric aldol reaction of cyclohexanone and aryl aldehydes (Scheme 14). In most cases, high enantioselectivities and chemical yields were obtained (77-89% ee, 65-99% yield, respectively).

The recyclability was tested in the aldol reaction between cyclohexanone and *p*-nitrobenzaldehyde. The supported organocatalyst was recovered by centrifugation and decantation. The results remained unchanged in terms of enantio- and diastereoselectivity with isolated yield.



Scheme 13. Synthesis of GNP-supported and *o*-lauroyl-*trans*-4-hydroxy-L-proline catalysts **39**

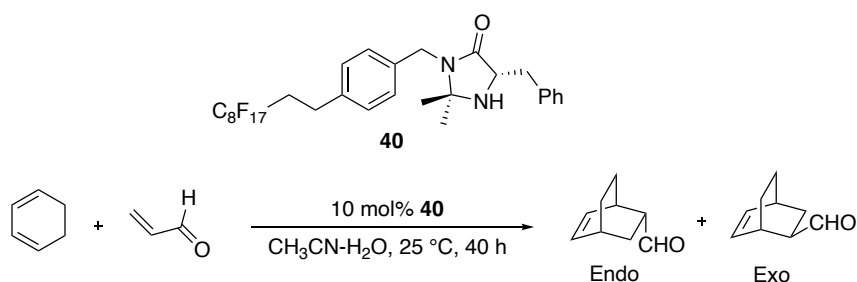


Scheme 14. Direct asymmetric aldol reaction of cyclohexanone and aryl aldehydes with organocatalyst **39c**

1.3.2 Fluorous Supported Organocatalyst

Fluorous supported organocatalysts are recently preferred because they are soluble in common solvents and they are also easily recovered by fluorous solid-phase extraction method or fluorous-organic solvent extraction.

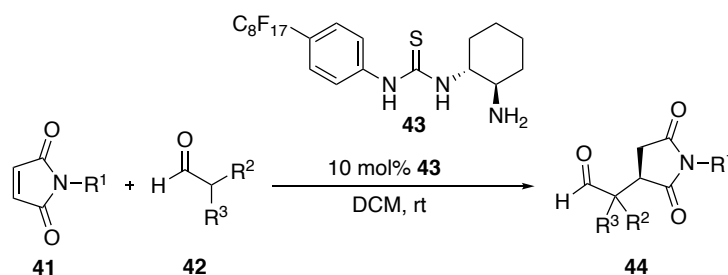
Curran and co-workers used chiral imidazolidinone catalyst **40** in the asymmetric Diels-Alder reaction of acrolein and cyclohexadiene (Scheme 15).¹⁰⁴ The reaction was performed with 10 mol% **40** in CH₃CN-H₂O mixture at room temperature for 40 h. The products were obtained with 86% isolated yield, 93:7/endo:exo ratio and 93% ee (endo). The recovery of the catalyst from this reaction was 84% with 99% purity.



Scheme 15. Diels-Alder reaction of acrolein and cyclohexadiene with organocatalyst **40**

In the optimized condition a variety of dienes and α,β -unsaturated aldehydes were used. Good enantioselectivities (88-93% ee) and isolated yields (78-89%) were obtained with a high recovery of the catalyst (80-86%).

Itoh and co-workers synthesized a catalyst derived from Takemoto's thiourea with perfluorooctyl group.¹⁰⁵ Conjugate addition of isobutyl aldehyde to *N*-phenyl maleimide was chosen as the model reaction in the presence of 10 mol% of **43** (Scheme 16). As a result of the solvent screening study, DCM was chosen as the best one affording 99% ee with 86% yield in 24 h at room temperature.

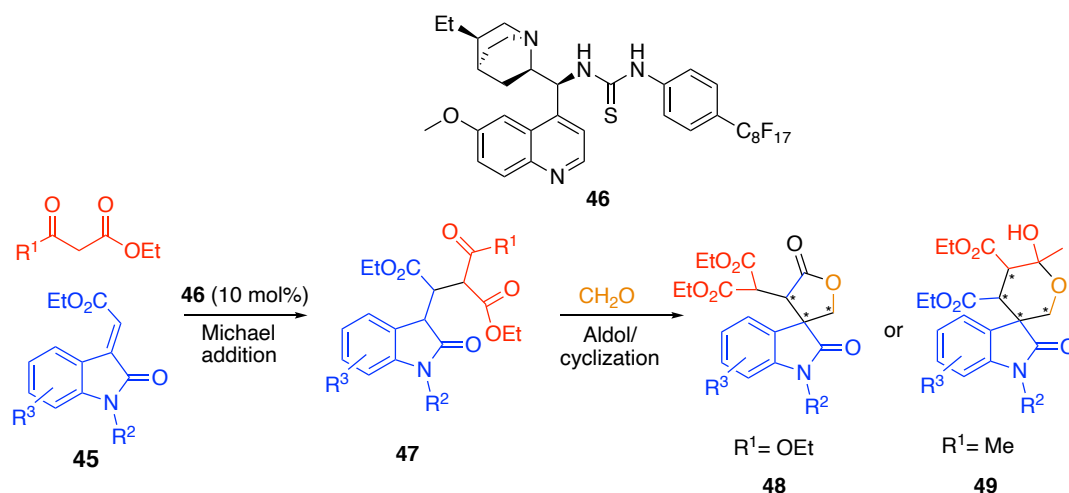


Scheme 16. Conjugate addition of isobutyl aldehyde **42** to *N*-phenyl maleimide **41** with organocatalyst **43**

Further trials were done with different maleimides and aldehydes. The enantioselectivities were excellent (91-99% ee) with good yields (43-99%). The

catalyst **43** was easily recovered from the reaction medium by simple filtration. The catalytic activity and the stereoselectivity did not change for three subsequent reactions.

A fluororous anchored thiourea-based bifunctional cinchona alkaloid organocatalyst **46** was synthesized by Liu et al. and its efficiency was tested in a domino reaction involving Michael/aldol/cyclization for the synthesis of dihydrofuranone spirooxindoles **48** and tetrahydropyranone spirooxindoles **49**.¹⁰⁶ For the dihydrofuranone derivatives, diethyl malonate, olefinic oxindole **45**, and formaldehyde were chosen as the starting materials (Scheme 17). Toluene was the proper Michael reaction solvent, whereas DCM was the best co-solvent for the aldol/cyclization process. Lowering the temperature during the Michael addition step causes a decrease in the isolated yields and a drastic increase in the enantioselectivity. Therefore, the optimized condition was found as -25 °C for the Michael addition, 25 °C for the aldol/cyclization process in the presence of 10 mol% catalyst **46** resulted in 93% ee and 6:1 dr with 82% yields. Different olefinic oxindoles were used in the derivatization study, and the products were synthesized in 39-82% yields with >3:1 dr and up to 99% ee.

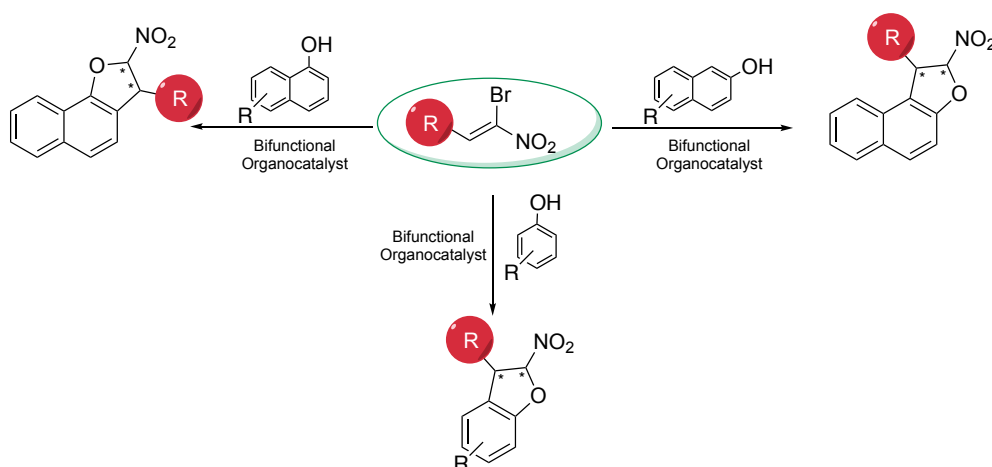


Scheme 17. Synthesis of dihydrofuranone spirooxindoles **48** and tetrahydropyranone spirooxindoles **49** with catalyst **46**

The same condition was applied for the synthesis of tetrahydropyranone spirooxindoles with ethyl acetoacetate which afforded six-membered cyclic hemiketals. The results were obtained in the range of 81-93% ee, 4:1 dr and 70-91% yields.

1.4 Aim of the Study

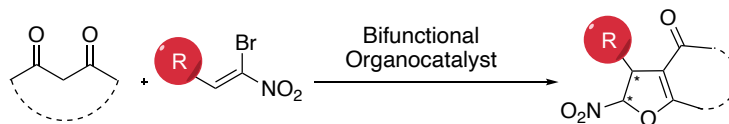
In the first part of the thesis, the main objective is to evaluate our group's bifunctional organocatalysts in the Friedel/Crafts domino-type reaction of α -bromonitroalkenes and naphthols/phenols (Scheme 18). We wanted to test if our sterically encumbered squaramide-type organocatalysts could fill the deficiency in this field. For this purpose, an optimization study will be initiated with catalyst screening by using 2-aminoDMAP and quinine-based organocatalysts. Further optimization studies such as catalyst loading, base screening, solvent screening, etc. will be performed in order to find the optimized condition. Once the optimization studies will be done, the derivatization study is going to be applied with this condition by using different α -bromonitroalkenes and naphthols/phenols.



Scheme 18. Friedel/Crafts domino-type reaction of α -bromonitroalkenes and naphthols/phenols

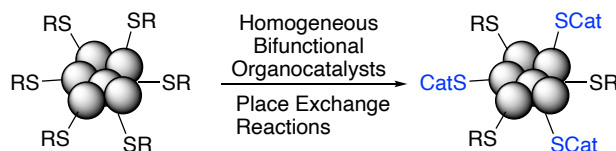
In the second part of the thesis, dihydrofuran (DHF) derivatives will be synthesized with a similar approach to the first part. We would like to start with α -

bromonitroalkenes and acetylacetone to generate the desired DHF cycles with a Michael addition followed by S_N2 type reaction. Various types of active methylene nucleophiles will also be tested (Scheme 19).

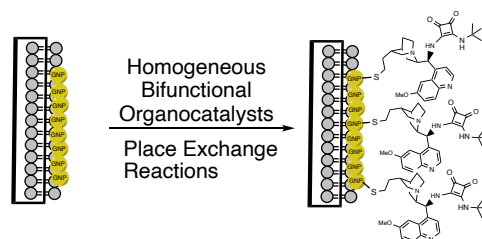


Scheme 19. Michael addition and S_N2 type reaction of α -bromonitroalkenes and active methylene nucleophiles

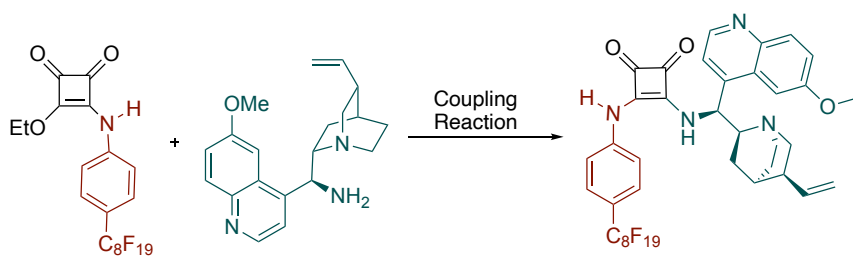
In the third part of the thesis, recyclable heterogeneous organocatalysts will be designed and synthesized from homogeneous organocatalyst in order to increase the reusability and to get an advantage from the atom economy. L-proline and quinine derived homogenous organocatalysts will be anchored to a solid support to increase the heterogeneous property of the catalyst (Scheme 20 and 21). An additional fluororous supported catalyst will also be synthesized (Scheme 22).



Scheme 20. Gold nanoparticle supported organocatalysts



Scheme 21. Solid supported organocatalyst



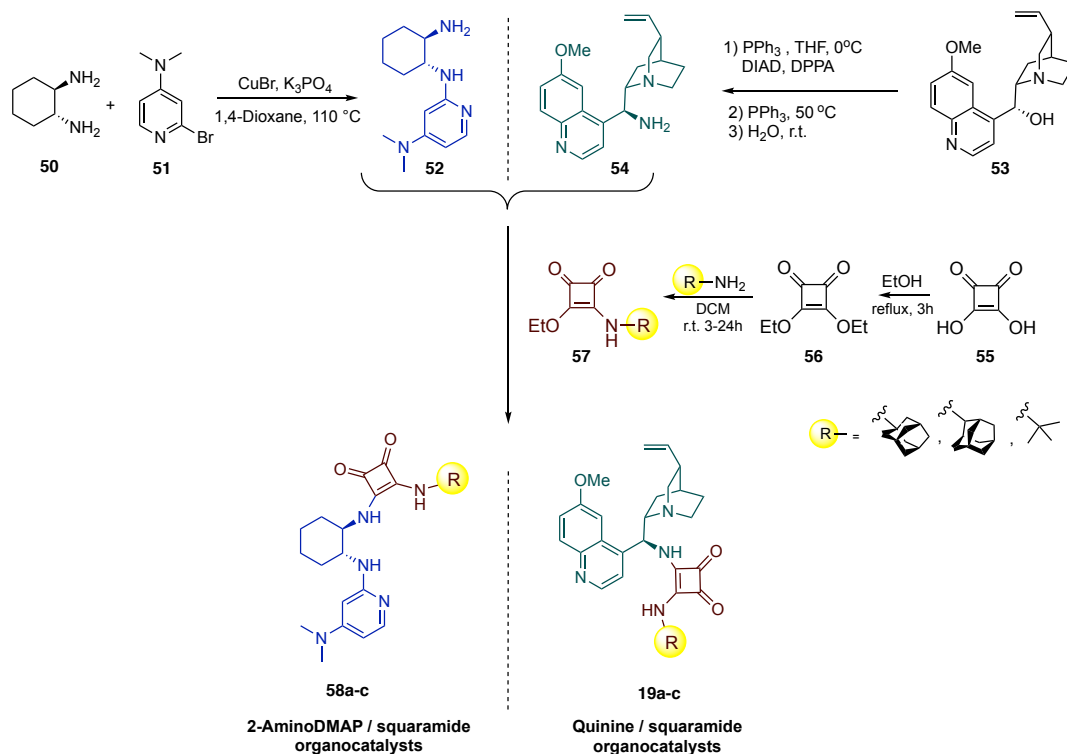
Scheme 22. Fluorous supported organocatalyst

CHAPTER 2

RESULTS AND DISCUSSION

2.1 Synthesis of Quinine and 2-AminoDMAP Based Bifunctional Organocatalysts

In our research group, we have been developing bifunctional organocatalysts. These organocatalysts can be classified into two different groups according to their basic units; 2-aminoDMAP **52** and quinine amine **54**. By changing the acidic units of the catalyst, we can differentiate the acidity, H-bonding spacer and sterical effects. General route for the synthesis both 2-aminoDMAP and quinine type organocatalysts are used in this thesis depicted in Scheme 23.



Scheme 23. Synthetic route for 2-aminoDMAP and quinine based organocatalysts

2.2 Evaluation of the Bifunctional Organocatalysts in Friedel-Crafts Domino Type Reactions

2.2.1 Optimization Studies

Friedel-Crafts domino reaction's optimization study was initiated with the benzaldehyde derived α -bromonitroalkene and β -naphthol. The studies were initiated by organocatalyst screening using our library (Figure 8). Throughout this study, all of the experiments were repeated at least two times to check the reproducibility.

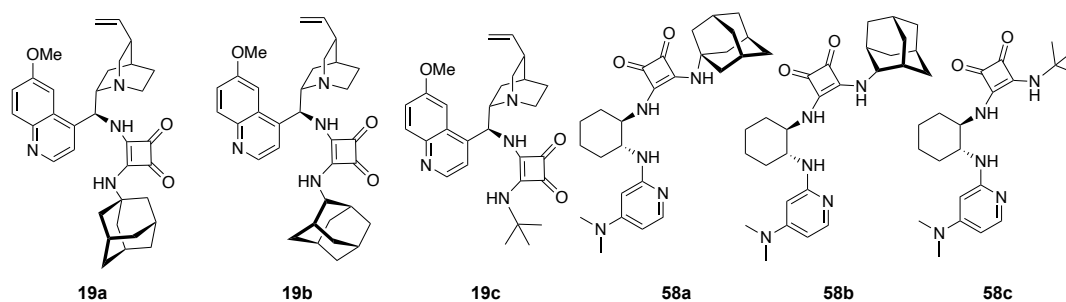
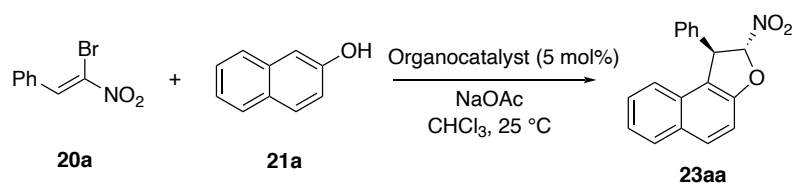


Figure 8. Bifunctional organocatalysts tried in organocatalyst screening

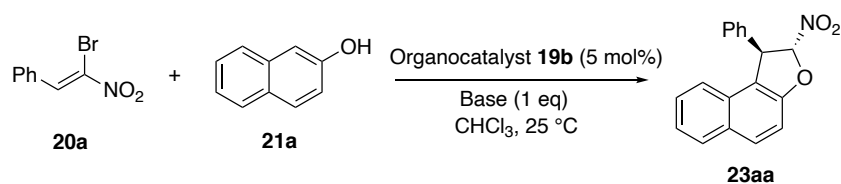
We conducted these asymmetric reactions in the presence of a base, NaOAc in chloroform at room temperature with 5 mol% organocatalyst (Table 1). We used an additional base (NaOAc) to inhibit the HBr formation during the course of the reaction because it affects the active site of the catalyst. When the results were examined, it was observed that the catalysts **19a-c** gave higher enantioselectivity in the range of 68-74% (entries 1-3). Although organocatalyst **19c** showed 3% more ee value (entry 3), it was decided to test other parameters with organocatalyst **19b**, since the isolated yield was much better than the previous case (entry 2).

Table 1. Optimization studies; organocatalyst screening^a

Entry	Organocatalyst	Time (h)	Yield ^b (%)	ee ^c (%)
1	19a	12	63	44
2	19b	14.5	65	68
3	19c	14.5	50	71
4	58a	19.5	64	9
5	58b	21.5	49	rac
6	58c	19.5	72	6

^a Unless stated otherwise, all reactions were performed with 0.15 mmol **20a** and 0.30 mmol **21a** in 0.3 mL of solvent, in the presence of 5 mol% organocatalyst at 25 °C. ^b Isolated yields. ^c Determined by chiral HPLC analysis, OD-H column, 90:10 Hexane/isopropanol, 1.0 mL/min, 230 nm.

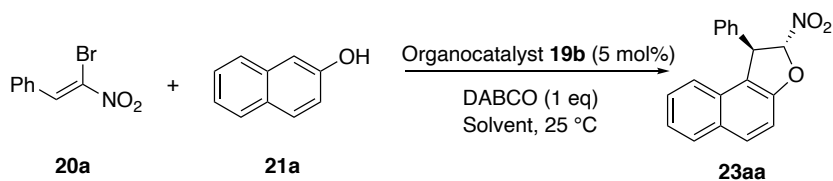
Some inorganic and organic bases were tested to scavenge HBr evolved during the reaction (Table 2). Among the inorganic bases tested, K₂CO₃ and Cs₂CO₃ enhanced the rate, whereas the enantioselectivity decreased drastically (60 min with 40% ee and 10 min with 26 ee%, entries 3-4, respectively). All organic bases accelerated the rate of 40 min to 4 h with the enantioselectivities varied racemic to 65 ee% (entries 5-8). DABCO afforded the best result, with a high chemical yield and good enantioselectivity. It is presumably due to no background reaction, which would occur as in the case of most of the bases (entry 6).

Table 2. Optimization studies; base screening^a

Entry	Base	Time (h/m)	Yield ^b (%)	ee ^c (%)
1	NaOAc	14.5 h	65	68
2	NaHCO ₃	24 h	84	32
3	K ₂ CO ₃	60 min	96	40
4	Cs ₂ CO ₃	10 min	94	26
5	DMAP	4 h	93	12
6	DABCO	2 h	92	65
7	Et ₃ N	2 h	90	12
8	DBU	40 min	75	rac

^aUnless stated otherwise, all reactions were performed with 0.15 mmol **20a** and 0.30 mmol **21a** in 0.3 mL of solvent, in the presence of 5 mol% **19b** at 25 °C. ^bIsolated yields. ^cDetermined by chiral HPLC analysis, OD-H column, 90:10 Hexane/isopropanol, 1.0 mL/min, 230 nm.

In the solvent screening studies, DHN formation reaction was carried out with 5 mol% organocatalyst **19b** with one equivalent of base DABCO (Table 3). Fortunately, toluene and mix-xylene gave excellent results in both chemical yield and enantioselectivities (quantitative yield with 95% ee and 95% yield with >99% ee, entries 16 and 22, respectively). Since the reaction was completed in 90 min in xylene with >99% ee, we further screened catalyst loading, base equivalency, substrate ratio, and concentration parameters with this solvent (Table 4).

Table 3. Optimization studies; solvent screening^a

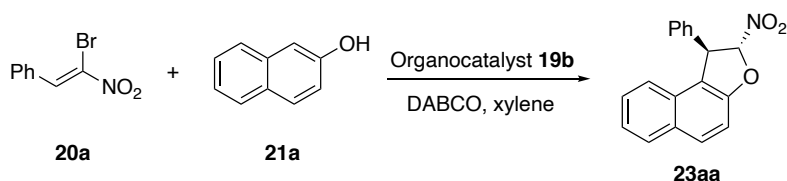
Entry	Solvent	Time (h)	Yield ^b (%)	ee ^c (%)
1	DCM	2.5 h	86	60
2	Hexane	2.5 h	97	47
3	Toluene	5.5 h	quant.	95
4	THF	5.5 h	nd.	20
5	1,4-Dioxane	6 h	nd.	60
6	TBME	6 h	59	75
7	MeCN	6 h	73	16
8	Et ₂ O	6 h	95	60
9	Xylene	1.5 h	95	>99
10	1,2-DCE	6 h	97	43

^a Unless stated otherwise, all reactions were performed with 0.15 mmol **20a** and 0.30 mmol **21a** in 0.3 mL of solvent, in the presence of 5 mol% **19b** at 25 °C. ^b Isolated yields. ^c Determined by chiral HPLC analysis, OD-H column, 90:10 Hexane/isopropanol, 1.0 mL/min, 230 nm.

We tested the catalyst loading with 1, 2, and 10 mol% (Table 4, entries 1-3). Lowering the catalyst loading increased the reaction duration with a slight decrease in enantioselectivities. On the contrary, we obtained the best result with a 10 mol% catalyst (entry 3), choosing that would not change the previous outcome in enantioselectivity, chemical yield, and reaction duration. Thus, we decided to continue our optimal condition as 5 mol%, which would be wiser in terms of atom economy. The effect of the base stoichiometry was also tested by decreasing the amounts 0.5 and 0.25 equivalent (entries 4 and 5, respectively). Both cases caused the blocking of the organocatalyst's active site with HBr as elongation of reaction duration up to 24-36 h with a loss in the enantiomeric excess values. Changing the

substrate ratio to 1:1 and 1:3 decreased the enantioselectivity drastically (entries 6 and 7). In the final optimization attempt, we changed the concentration of the reaction medium; however, none of these gave a better result (entries 8 and 9).

Table 4. Optimization studies; catalyst loading, base eq, substituent ratio, and concentration^a



Entry	Cat. Loading (mol %)	Base Eq.	20a:21a Ratio	Conc. (M)	Time (h/m)	Yield ^b (%)	ee ^c (%)
1	1	1	1:2	0.5	3 h	95	93
2	2	1	1:2	0.5	2 h	75	92
3	10	1	1:2	0.5	70 min	quant.	98
4	5	0.5	1:2	0.5	24 h	43	68
5	5	0.25	1:2	0.5	36 h	42	77
6	5	1	1:1	0.5	160 min	81	48
7	5	1	1:3	0.5	80 min	90	58
8	5	1	1:2	1	120 min	92	81
9	5	1	1:2	0.25	50 min	91	70

^a Unless stated otherwise, all reactions were performed with 0.15 mmol **20a** and 0.30 mmol **21a** in the presence of 5 mol% **19b**, 0.3 mL of solvent at 25 °C. ^b Isolated yields. ^c Determined by chiral HPLC analysis, OD-H column, 90:10 Hexane/isopropanol, 1.0 mL/min, 230 nm.

All the optimization results in our hands, we see that using 2-adamantyl amine squaramide substituted organocatalyst **19b** helps to increase the reaction rate and enantioselectivity, even though using 5 mol% catalyst loading, one equivalent of the base at the ambient temperature.

2.2.2 Substrate Scope

After completing the optimization study, we studied the scope of the reaction with different derivatives of α -bromonitroalkenes and β -naphthols (Table 5). All of the reactions were performed in xylene at ambient temperature in 0.5 M concentration. Among α -bromonitroalkenes, the unsubstituted, *o*-F, *p*-F, and *o*-Bn substituted derivatives yielded the best results as >99%, 95, 98, and >99% ee, respectively. There is no obvious indication of the electron-donating or withdrawing group on the ring affecting the enantioselectivity; however, we observed that all the groups on the *para*-positions gave similar enantioselectivities and isolated yields, except the *p*-F substituted one.

Table 5. Substrate scope of FC domino reaction between α -bromonitroalkenes and β -naphthols^a

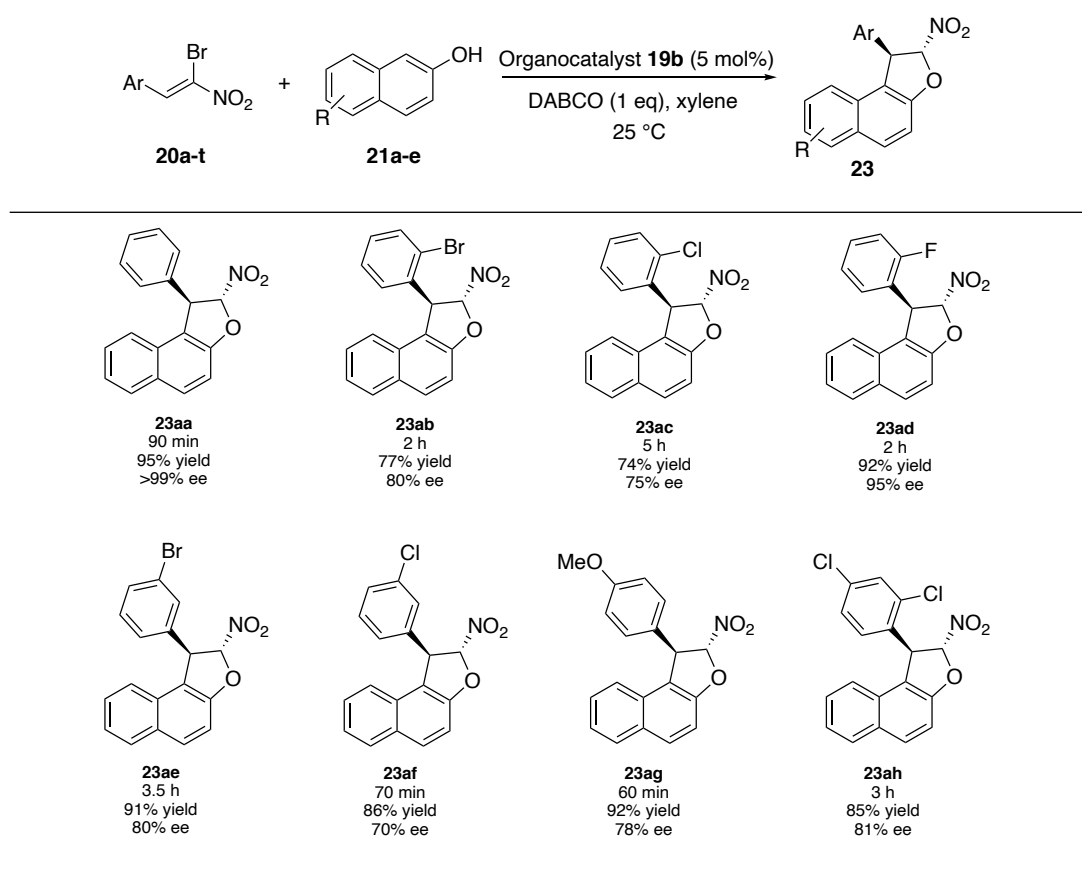
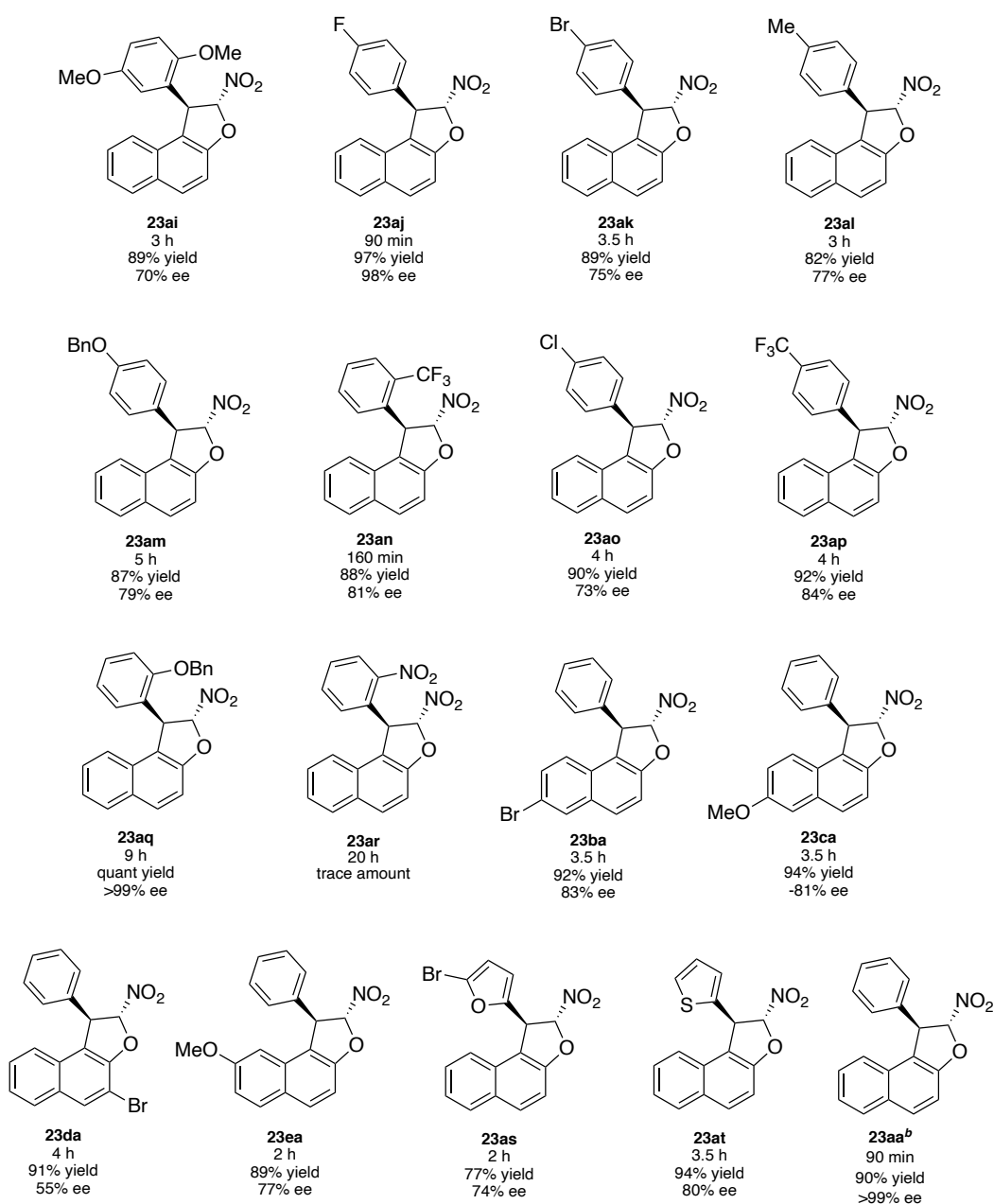


Table 5. continued^a



^a Unless stated otherwise, all reactions were performed with 0.15 mmol **20** and 0.30 mmol **21** in the presence of 5 mol % organocatalyst **19b**, 0.3 mL of solvent at 25 °C. ^b Performed with 1.5 mmol of **20a** with 3.0 mmol of **21a**.

o-Br, *m*-Br, 2,4-Cl, *o*-CF₃, *p*-OBn substituted ones were also well tolerated (79-81% ee), and the *o*-Cl, *p*-OMe, *p*-Br, *p*-Me substituted derivatives affording good enantioselectivities between 75-77%. The lowest ee values were obtained with *m*-

Cl, 2,5-OMe, and *o*-Br substituted furyl as 70% ee. *o*-NO₂ substituted derivative did not give any reaction with β -naphthol.

To demonstrate the efficiency of the asymmetric induction, a scale-up experiment was performed by using 1.5 mmol of **20a** with 3.0 mmol of **21a**. Fortunately, the scale-up synthesis yielded **23aa** without loss of enantioselectivity as >99% ee and 90% chemical yield (Table 5).

We extended the scope of the construction of DHN units with α -naphthols (Table 6). Compared with the β -naphthol results, they mostly showed lower chemical yields and enantioselectivities. No drastic improvement was obtained with the organocatalyst screening. Among the 25 α -DHN derivatives, *p*-Me, *o*-OBn, and thienyl substituted bromonitroalkenes gave the best results as 92, 91, and 89% ee, respectively. The other derivatives showed intermediate results between 29-71% ee and afforded the products in the range of 33 to quantitative yields in 80 min to 21 h. No better results were observed by using *p*-OMe and *p*-Cl substituted α -naphthol derivatives. We obtained the best result with *p*-OMe substituted α -naphthol and *o*-F substituted bromonitroalkene as 55% ee with 74% isolated yield in 50 min.

Table 6. Substrate scope of FC domino reaction between α -bromonitroalkenes and α -naphthols^a

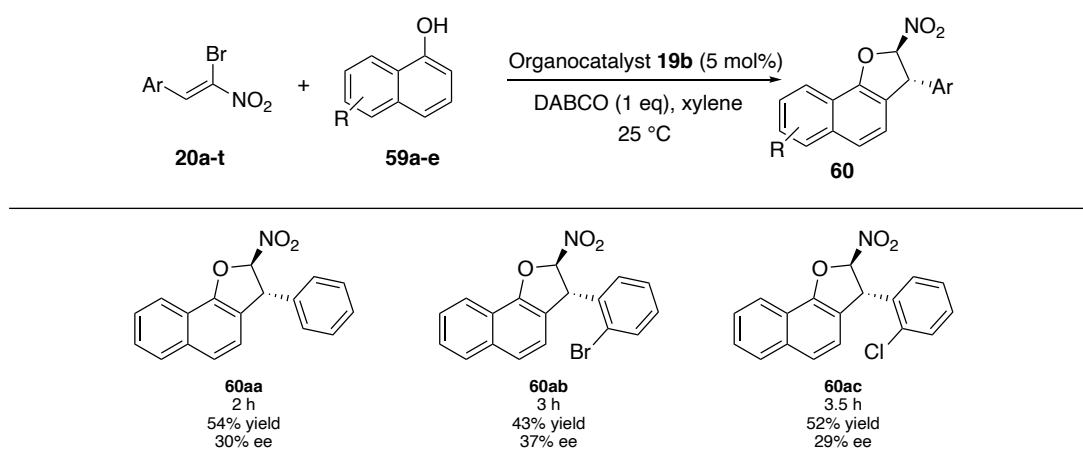


Table 6. continued^a

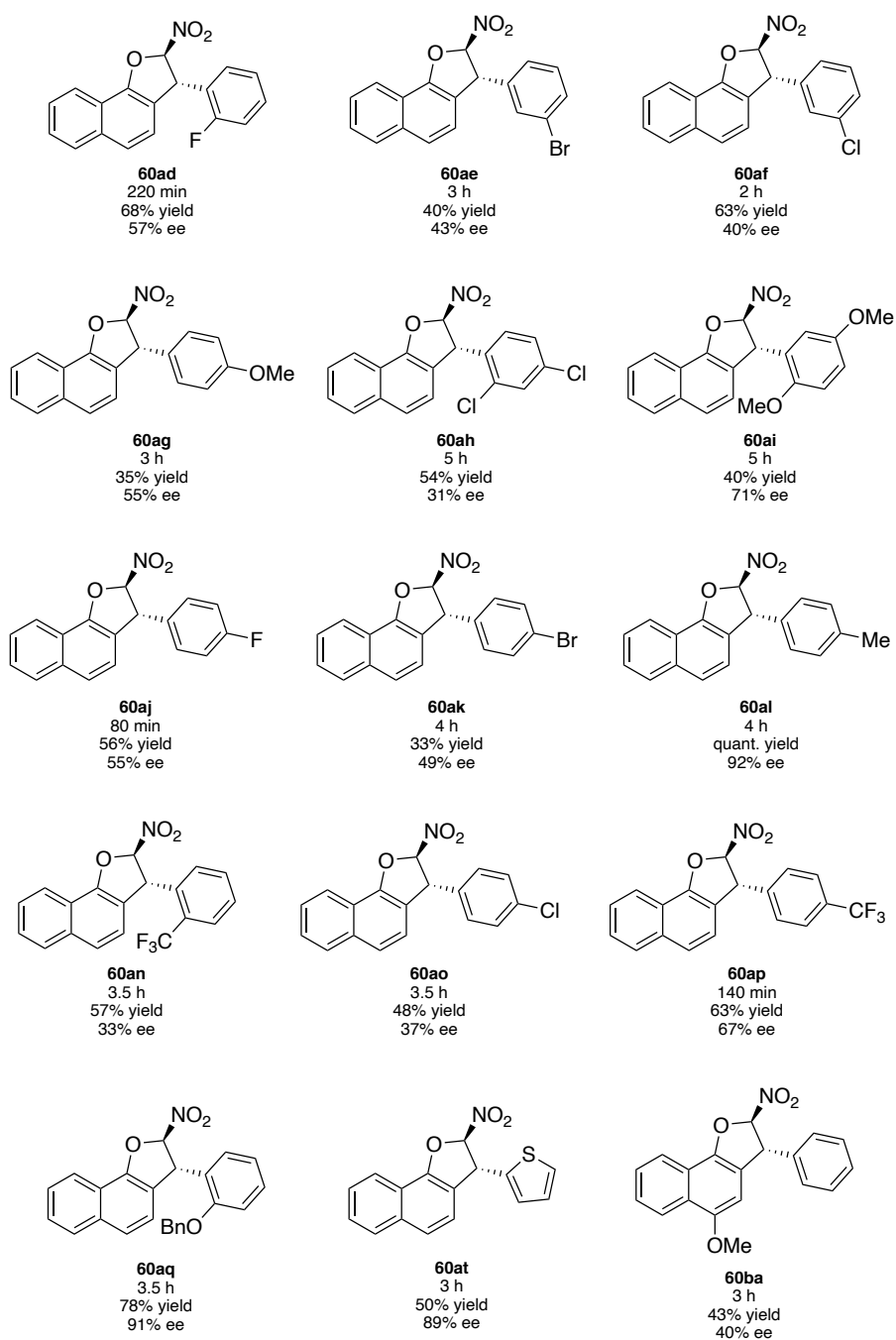
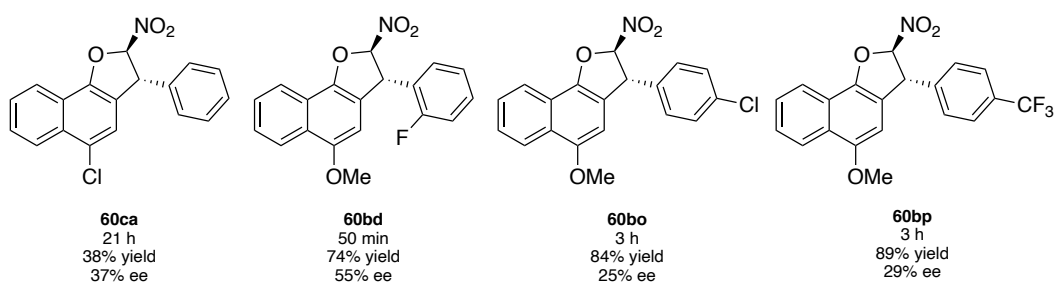
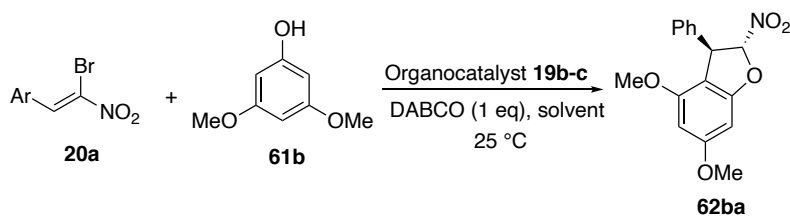


Table 6. continued^a

^a Unless stated otherwise, all reactions were performed with 0.15 mmol **20** and 0.30 mmol **59** in the presence of 5 mol % organocatalyst **19b**, 0.3 mL of solvent at 25 °C.

We attempted to use phenol-type nucleophiles to synthesize DHB cycles in dihydrofuran motif construction. Optimization studies were initiated with *Z*-(α)-bromonitroalkene **20** and phenol **61a**. Even after 56 h, no product formation was observed. Due to the insufficient nucleophilic nature of the phenol, in this regard, we attempted to use electronically enriched phenolic unit 3,5-dimethoxyphenol **61b**. Fortunately, with the organocatalyst **19b** used in the previous part, we obtained 82% ee in 3 h with 68% chemical yield. To improve the result, a short screening was performed once again (Table 7). Using 5 mol% organocatalyst **19c**, the DHB cycle formation was accomplished with 85% ee and 94% isolated yield in 1 h. We did subsequent trials by using organocatalyst **19c**.

Table 7. Optimization studies for DHB cycles

Entry	Organocatalyst	Cat. Loading (%)	Solvent	Time (h/m)	Yield ^b (%)	ee ^c (%)
1	19c	5	Xylene	2 h	86	82

2	19b	5	DCM	1 h	94	85
3	19c	10	DCM	30 min	89	82

^a Unless stated otherwise, all reactions were performed with 0.15 mmol **20a** and 0.30 mmol **61b** in the presence organocatalyst and 0.3 mL of solvent at 25 °C. ^b Isolated yields. ^c Determined by chiral HPLC analysis, OD-H column, 90:10 Hexane/isopropanol, 1.0 mL/min, 230 nm.

Among other derivatives, we obtained the best result with *o*-CF₃ substituted in **4 h** with 98% ee in quantitative yield. *p*-Cl and *p*-CF₃ substituted substrates resulted in very good results as 89% ee, 80% yield in 100 min and 83% ee, 70% yield in 155 min, respectively. The other 11 DHB derivatives were synthesized with moderate to good enantioselectivities ranging between 47-77% ee in 2.5-9 h. Nevertheless, we observed no apparent effect of the electron-donating or withdrawing group attached to bromonitroalkene on enantioselectivity.

Table 8. Substrate scope of FC domino reaction between α -bromonitroalkenes and phenols^a

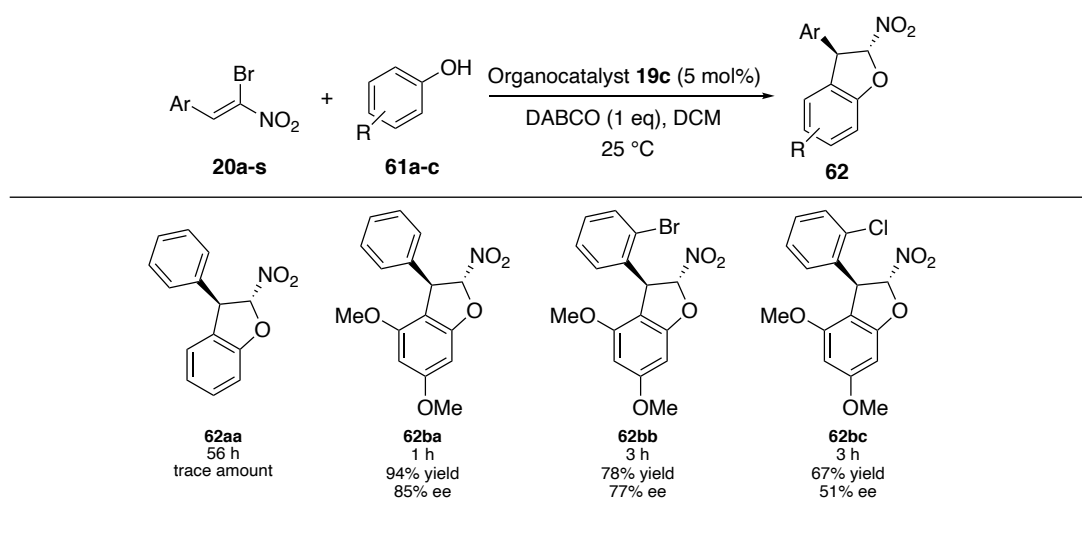
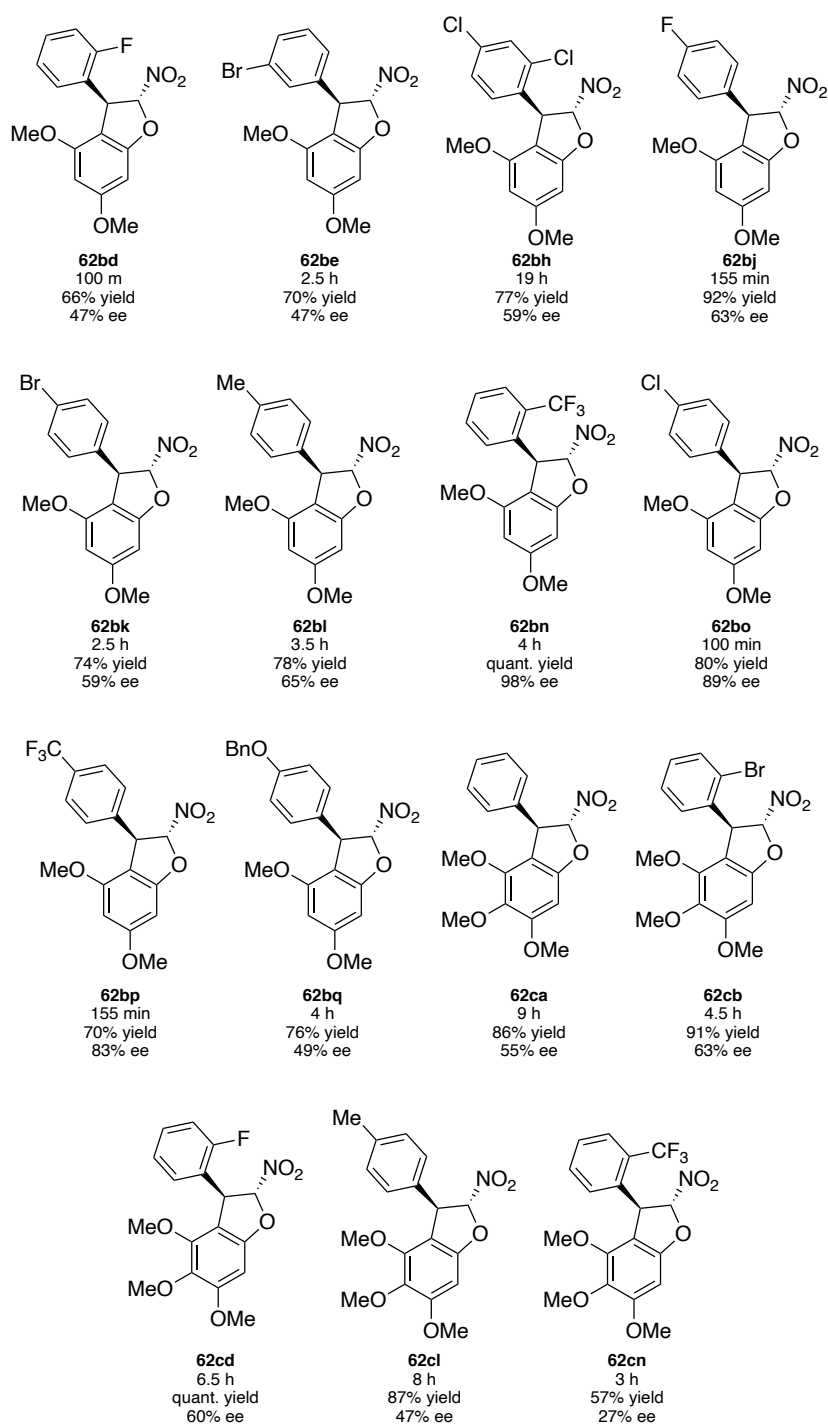


Table 8. continued^a



^a Unless stated otherwise, all reactions were performed with 0.15 mmol **20** and 0.30 mmol **61** in the presence of 5 mol % organocatalyst **19c**, 0.3 mL of solvent at 25 °C.

The absolute configuration of chiral adduct **23da** was assigned as (*R,R*) by the literature comparison of its specific rotation, and HPLC analysis, but those of the rest were assigned in analogy.^{53,54} To enlighten the chiral induction transferred from sterically encumbered squaramide type bifunctional organocatalyst in the transition state, we attempted to do computational calculations. The studies gave further information on the reaction mechanism for converting **20a** with **21a**. They gained insight into the observed enantioselectivity in the Friedel-Crafts C-C bond step.

2.2.3 Computational Methods

Density functional theory (DFT) calculations were performed in the Gaussian 09 Revision A.02 software with tight SCF convergence criteria at the B3LYP hybrid functional and 6-31(d) basis set.¹⁰⁷⁻¹¹⁰ All calculations were performed in *p*-xylene to mimic the experimental solvent conditions by integral equation formalism polarizable continuum model.¹¹¹ Long-range non-covalent interactions were corrected by Grimme's D3 methods by the addition of a pairwise additive, and anisotropic dispersive term for the long-range attraction which diminishes with R^{-6} and Becke-Johnson damping (D3BJ).^{112,113} Geometry optimizations were initiated from different initial conformations to obtain the lowest energy geometry. We selected the reactants as unsubstituted α -bromonitroalkene **20a** and β -naphthol **21a** given in Table 1, where reactants were optimized in the absence, and the presence of 2-adamantyl amine squaramide substituted organocatalyst **19b**.

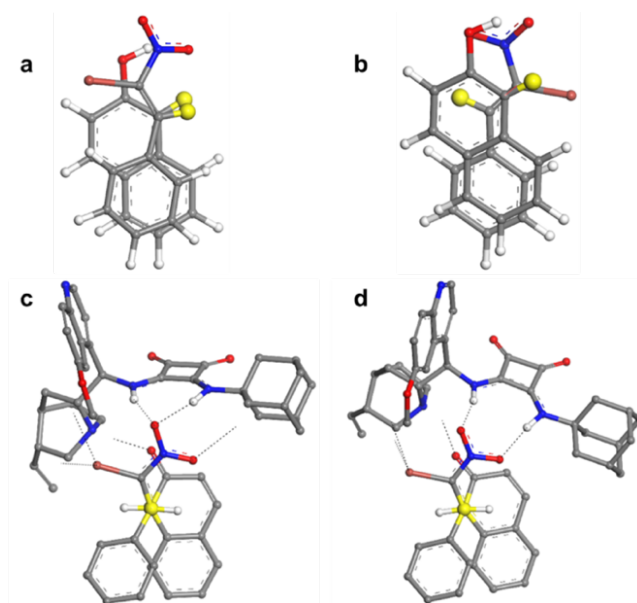


Figure 9. a) cis and b) trans conformations for the lowest energy structures of two reactants. c-d) Two transition state geometries of the initial step of the reaction mechanism in the presence of catalyst **19b**

The geometry of a transition structure and activation barriers is essential in describing the reaction mechanism and enantioselectivity. The free energy profile for the reaction barrier was calculated at room temperature.

The reaction barrier for the first step of the reaction that determines the enantioselectivity of the DHN and DHB products was presented after transition state confirmation. The stationary states were calculated by vibrational frequencies, where transition states were confirmed as saddle points by only one imaginary frequency given in Appendix Section C.

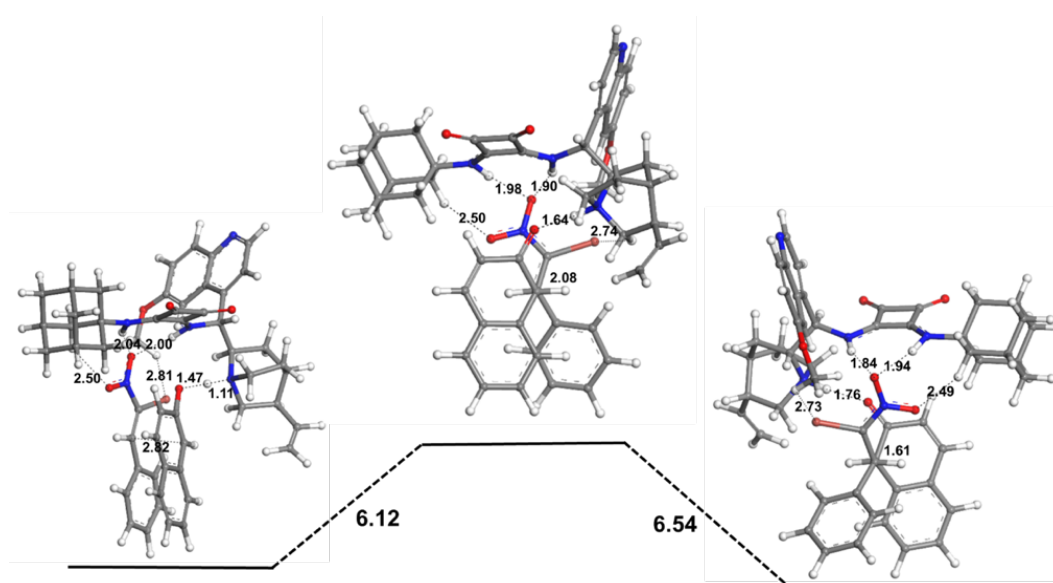
2.2.3.1 Computational Results

α -Bromonitroalkene derivative **20a** and β -naphthol **21a** reactants were optimized in the absence of organocatalyst. The two lowest energy structures were determined with close energy value, where both have π -stacked structures and interaction

between the hydroxyl and nitro groups (Figure 9a-b). *Trans*-conformation concerning the two possibly reacting -CH groups of the reactants is 0.79 kcal/mol more stable, close to the thermal energy provided by room temperature. *Cis*-conformation has a better overlap of these carbon atoms and a closer distance between reactants.

The two lowest energy structures were determined in the presence of catalyst **19b** after more than 20 trials at different positions, constructed pockets, and conformations of the organocatalyst. These structures are *trans* conformations positioned in the catalyst active pocket with a perfect overlap of the reactants and decreased intermolecular distance compared with their pristine states (Figure 9c-d). The only difference between these structures is the single oxygen and double oxygen of nitro groups hydrogen-bonded with the two amine groups of the catalyst. Strong hydrogen bonding with proton transfer was observed between the β -naphthol and tertiary amine group of the catalyst. In addition to these two main interactions with the catalyst, bromine atoms were coordinated by the -CH and methoxy groups. One of the nitro group oxygens has weak interactions with the 2-adamantyl group that contributed to the interactions of catalyst and reactant in the active site.

a



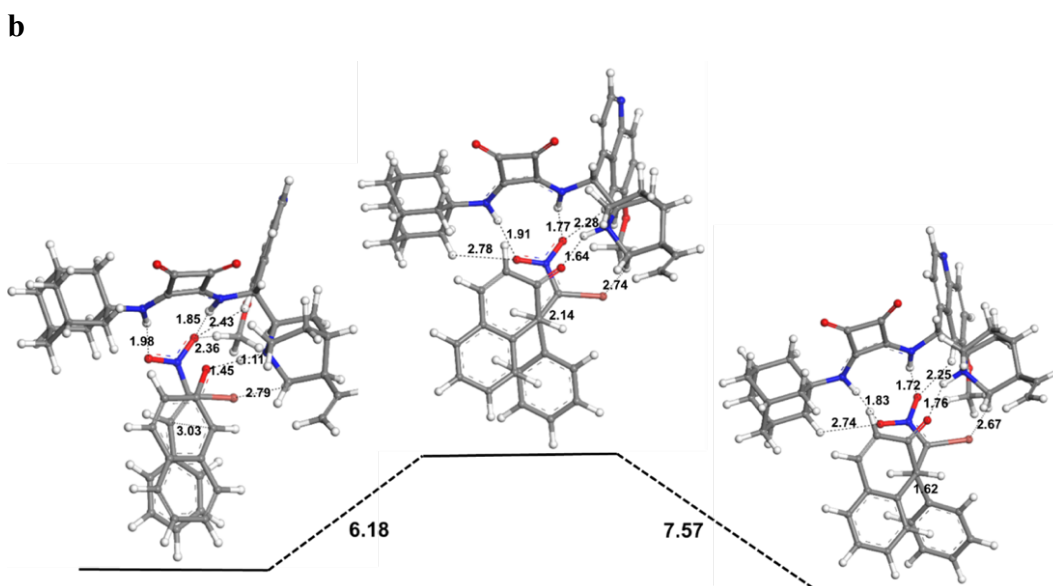


Figure 10. Reactant, transition state, and product of the reaction between α -bromonitroalkene derivative and β -naphthol coordinated with the active site of the catalyst where a) two amine groups of the catalyst coordinated by single oxygen of the nitro group, b) by two oxygens of the nitro group.

Transition state calculations that gave a single imaginary frequency show that the reaction barrier is 6.12 and 6.18 kcal/mol for two transition states that indicate these reactions are highly probable at room temperature with catalyst **19b** (Figure 10a-b). The structural and energetic difference is not significant between the two transition states. Only low-energy trans conformers in the catalyst's active site show the catalyst's enantioselectivity and explain the chiral synthesis with this catalysis. Organocatalyst not only imposed chirality but also decreased the barrier energy in the active site. Alternative visuals of the two transition states from a different point of view, atomic coordinates, and movies for the imaginary vibrations corresponding to these transition states are given in Appendix Section C. Our calculations could not locate any transition state for the *cis* conformations for the same position of the organocatalyst VI which points out the stereoselectivity of the reaction for only one of the stereoisomers that explain experimental observations.

2.3 Evaluation of the Bifunctional Organocatalysts in Michael Addition/S_N2 Type Reactions

Depending on the results obtained from the first part, we would like to extend the application to synthesize another important motif as, dihydrofurans (DHF). A similar synthetic route was followed for the synthesis of different DHF derivatives in the Michael addition, followed by an intramolecular S_N2 type reaction starting from α -bromonitroalkenes **20** and various types of active methylene nucleophiles **63**. The optimization study was completed with using acetylacetone **63a**, and some derivatives were synthesized in a previous study.¹¹⁴ Additional derivatives were also studied during this thesis (Table 9). Besides the previously synthesized derivatives, 10 additional derivatives were obtained in the optimized condition. The acetylacetone derivatives were ranged between 71-82% ee in 3.5-6.5h at room temperature. The additional two derivatives were synthesized with another β -dicarbonyl compound, methyl acetoacetate **63b**. It was chosen, since the unsubstituted α -bromonitroalkene **20a** and methyl acetoacetate **63b** gave the best result among other β -dicarbonyl compounds, 80% ee in 5 h with full conversion. *o*-F and *p*-OMe derivatives (**64bd**, **64bg**) were obtained in 3 h with 79% ee and 98% yield, 89% ee and 95% yield, respectively. These results were published in early 2022.¹¹⁵

Table 9. Substrate scope of Michael addition/S_N2 type reaction

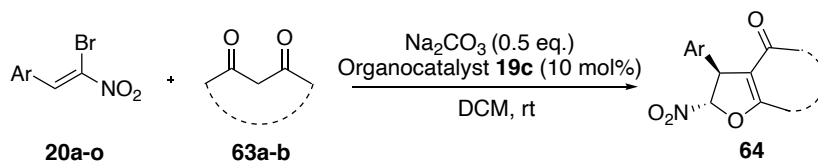
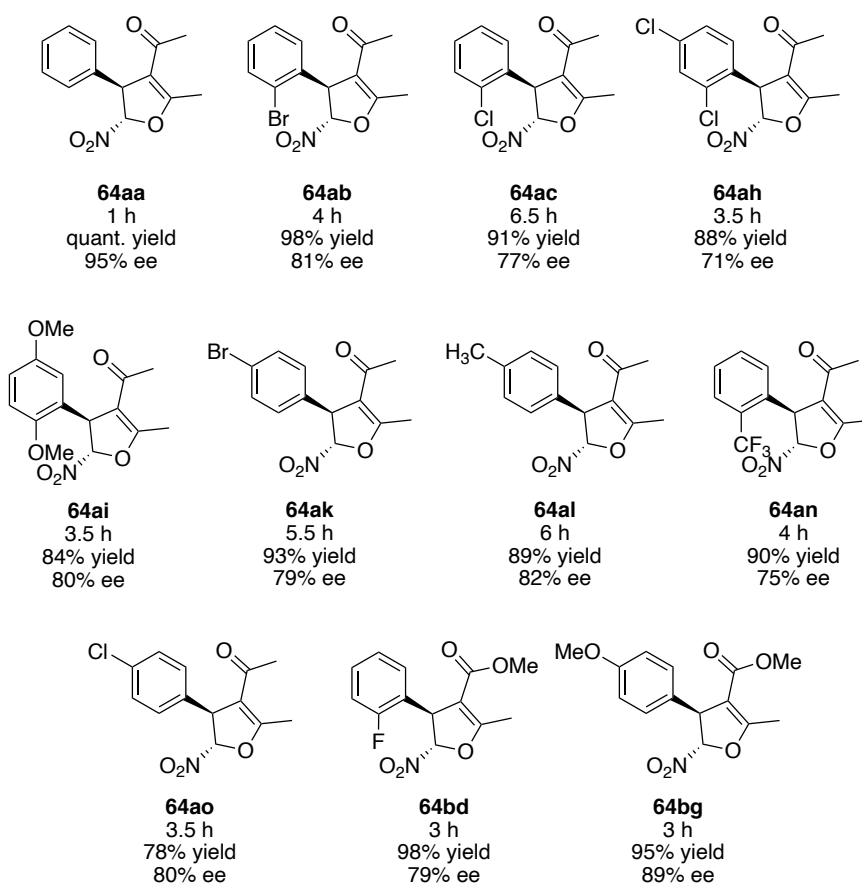


Table 9. continued^a

^a Unless stated otherwise, all reactions were performed with 0.1 mmol **20** and 0.18 mmol **63** in the presence of 10 mol % organocatalyst **19c**, 0.5 mL of solvent at 25 °C.

The absolute configuration of **64aa** was determined as *S,S* by X-ray analysis (Figure 11). The other derivatives were assigned by analogy. A plausible transition state was suggested to explain the determined absolute configuration. According to the proposed model, the nucleophile is activated by a quinuclidine moiety of the organocatalyst **19c**. Simultaneously, the electrophile is activated by double H-bonding with the squaramide hydrogens, allowing the nucleophile to attack from the *Si*-face (Figure 12).

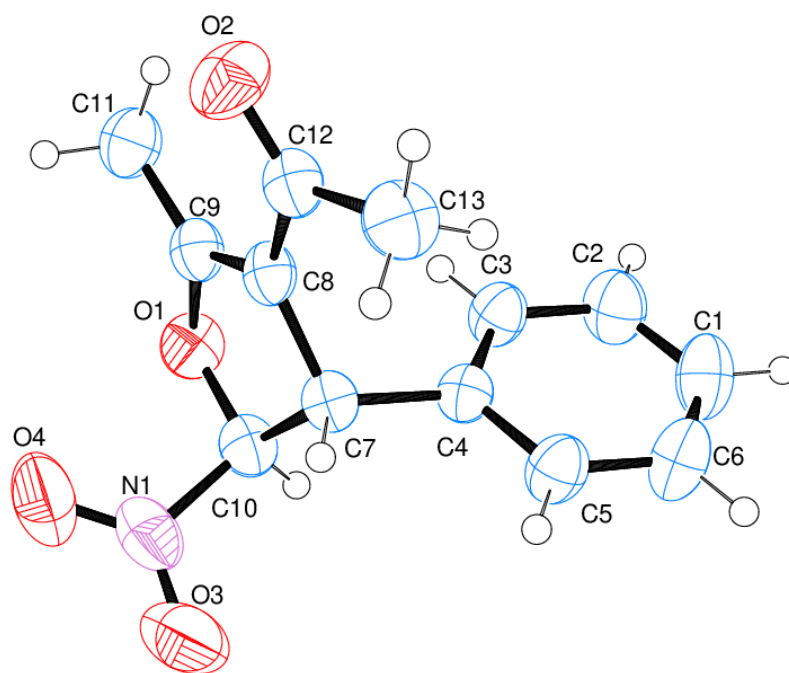


Figure 11. X-Ray crystal structure of **64aa**

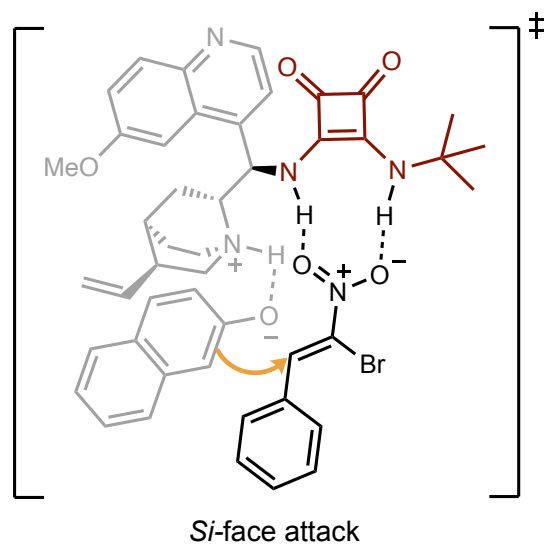


Figure 12. Plausible transition state for the reaction of α -bromonitroalkene **20** and acetylacetone **63a**.

2.4 Design and Synthesis of Recyclable Organocatalysts

The third part of the study involves the attempts that would provide an added value to sterically encumbered organocatalyst systems possessing recyclable character. To this end, we designed some transformation models that would make conversion designs from homogeneous catalyst characters to heterogeneous characters. Thus, we will ensure the recyclable feature of quinine-based organocatalysts.

For this purpose, we chose the approaches given below as gold nanoparticles, gold nanoparticles fused silica as the support units, and fluororous-supported organocatalyst.

2.4.1 Gold Nanoparticle Anchored Bifunctional Organocatalysts

In the first attempt, we wanted to generate anchored organocatalysts by using gold-nanoparticles and gold-nanoparticle fused silica plates as the matrix unit. The best method was the metal complexes' grafting (tethering) method.¹¹⁶⁻¹¹⁸ We decided to go further with this method since it involves a spacer between the solid support and the catalyst, which provides an open, active site for the organocatalyst to work. Another advantage of this method is that the catalysts show similar activity in their homogeneous state.

The strong affinity of sulfur to gold has been utilized in generating metal complexes or clusters.¹¹⁹ In the light of this information, we wanted to introduce free -SH units to our catalysts. Without touching the catalyst's active sites depicted with arrows in Figure 13-left, the most available position would be the vinyl unit circled in Figure 13-right. In addition, we can provide the spacer for the grafting method.

Before studying with our catalyst directly, we wanted to test our synthetic methods with quinine **53**. To be sure that the active -OH group does not involve in any of the reactions, we decided to protect it with an acetyl unit. An overnight reaction yielded the quantitative yield of product **65** (Scheme 24). We added *S*-(2-mercaptoethyl)

ethanethioate **66** with a thermal radical reaction with AIBN and afforded to product **67**, we hydrolyzed the acetyl unit with HCl or hydrazine hydride and got the free -SH unit on the quinine motif **68**.

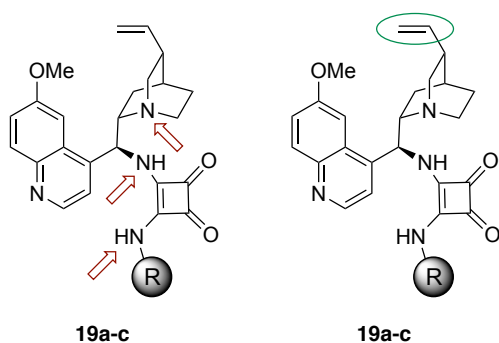
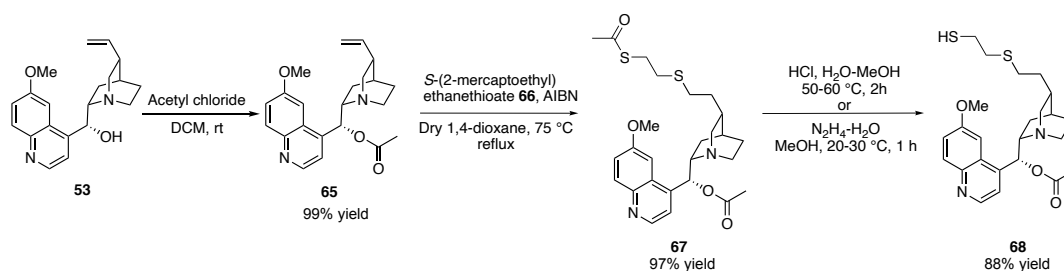
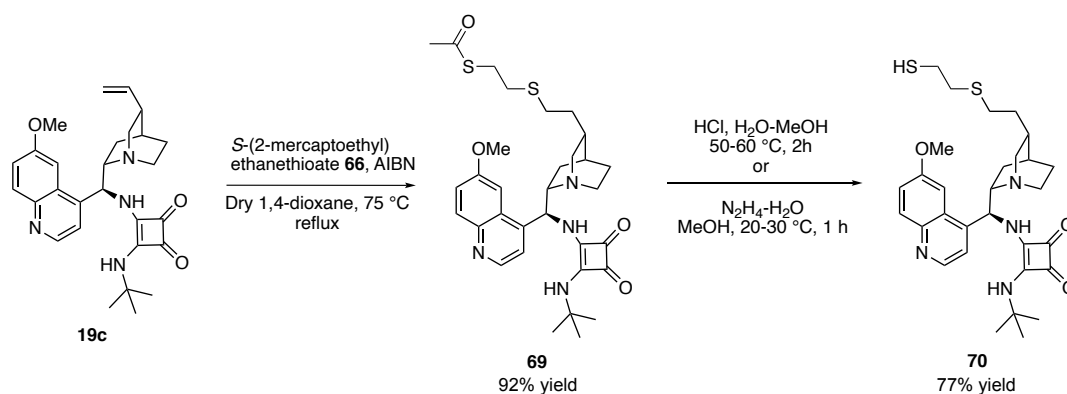


Figure 13. Active sites and the vinylic group of the catalysts **19a-c**



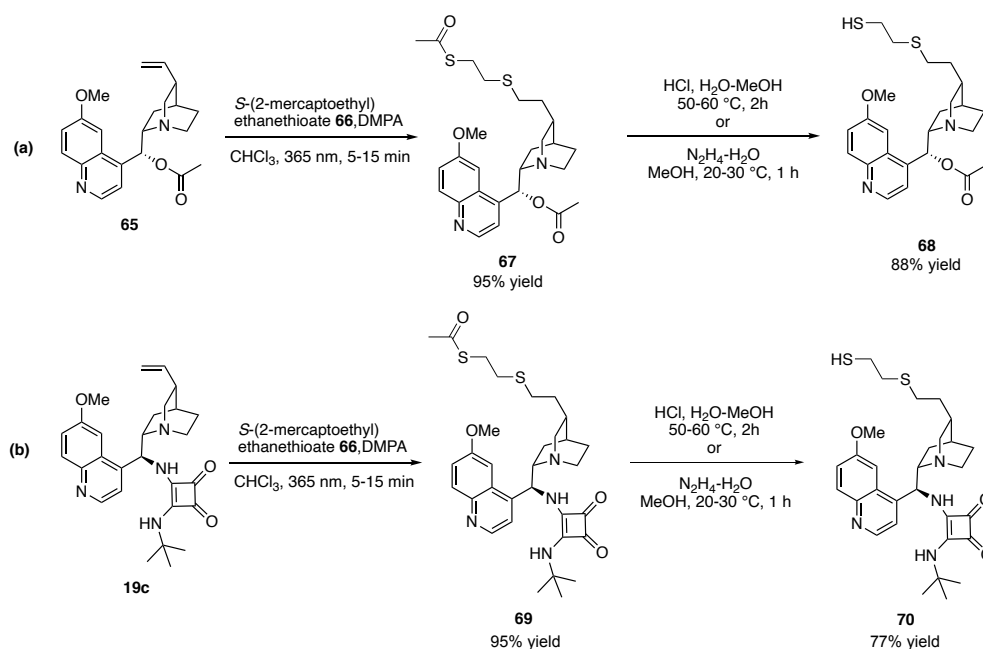
Scheme 24. The synthetic route for the generation of free -SH unit on quinine

After using the same synthetic route, we were able to generate the free -SH unit onto *tert*-butyl squaramide quinine bifunctional organocatalyst **19c** (Scheme 25). Although there is a slight decrease in the hydrolysis step's yield to 77%, it was a success in synthesizing the desired -SH unit bonded to our bifunctional organocatalyst.



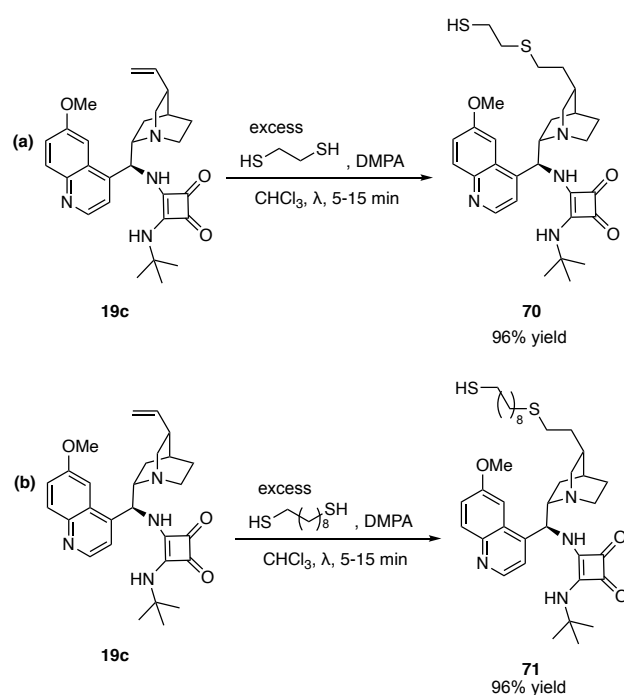
Scheme 25. The synthetic route for the generation of free -SH unit on organocatalyst **19c** by thermal initiator

Although yields were excellent in these reactions, the reaction durations were too long (up to 24-48 hours). Therefore, we wanted to test the thiol-ene reaction under a photochemical reaction. When we tried the same reactions using DMPA as the photoinitiator and under UV light (365 nm), the reactions were usually completed in 5 to 15 mins tops with again excellent chemical yields (Scheme 26).



Scheme 26. The synthetic routes for the generation of free -SH unit on organocatalyst **19c** by the photoinitiator

In order to shorten the reaction mechanism excess amount of 1,2-ethanedithiol was used in the photoreaction so that we don't have to use *S*-(2-mercaptoethyl) ethanethioate **66** and try to hydrolyze to get the free -SH unit. We successfully synthesized the product **70** in one step and also with this method our chemical yield increased up to 96%. However with 1,2-ethanedithiol, the spacer would be very short. It may cause a steric hindrance; therefore, we decided to increase the chain. Applying the same procedure with a longer chain of 1,9-nonanedithiol, we obtained the desired product **71** with complete conversion (Scheme 27).



Scheme 27. The synthetic routes for the generation of longer chain free -SH unit on organocatalyst **19c** by the photoinitiator

In the ¹H NMR spectrum of **19c** shown in Figure 14, the proton resonates at 5.68 ppm, and two protons that resonate at 4.89 ppm belong to vinylic protons at the top of the quinuclidine part. Crude ¹H NMR spectra of products **70** and **71** show that the double bond proton signals disappeared, proving that the substitution reactions occurred successfully (Figure 14).

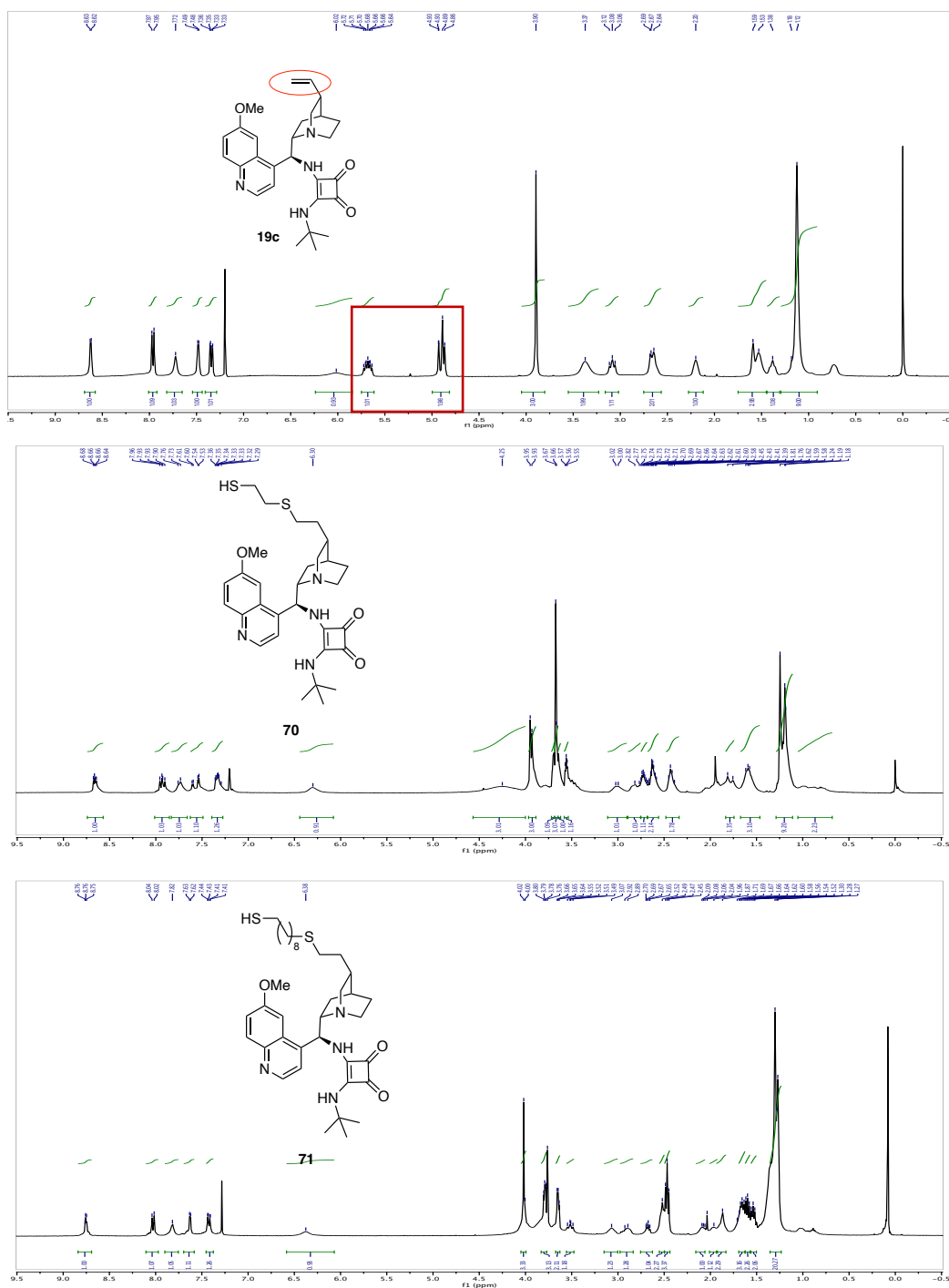
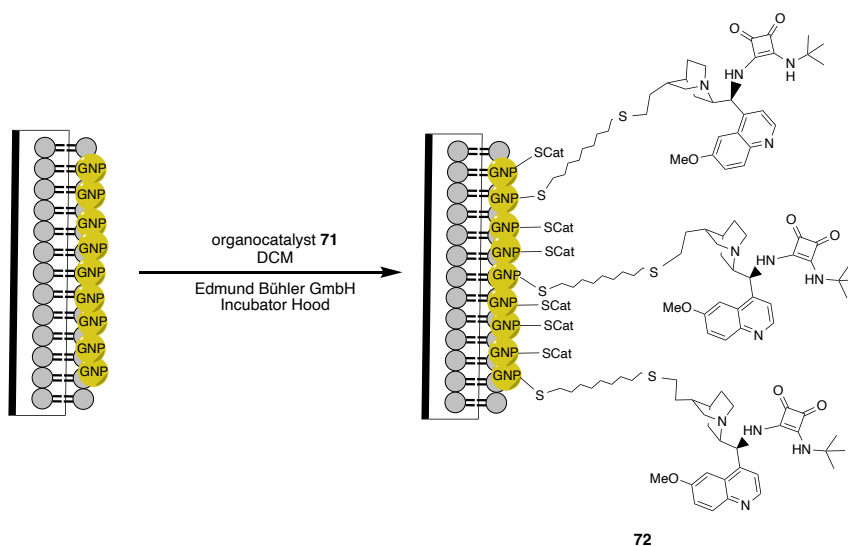


Figure 14. ¹H NMR spectra of organocatalysts **19c**, **70** and **71**

After synthesizing the desired products, we aimed to prepare the solid-supported organocatalysts with gold nanoparticles immersed in fused silica solid.

Product **71** was dissolved in DCM to prepare that organocatalyst, and solid support was introduced into the solution. That solution was shaken in Edmund Bühler GmbH incubator hood for a couple of days (Scheme 28). Then, the solid-supported organocatalyst **72** was removed from the solution and washed with DCM a few times.



Scheme 28. Representative synthesis of the solid-supported organocatalyst **72**

After completion of the synthesis, The SEM images were recorded (Figure 15). The SEM images show dispersion and cloudiness caused by the applied organocatalyst (Figure 15, b). Small aggregation parts over some gold nanoparticles are also observed.

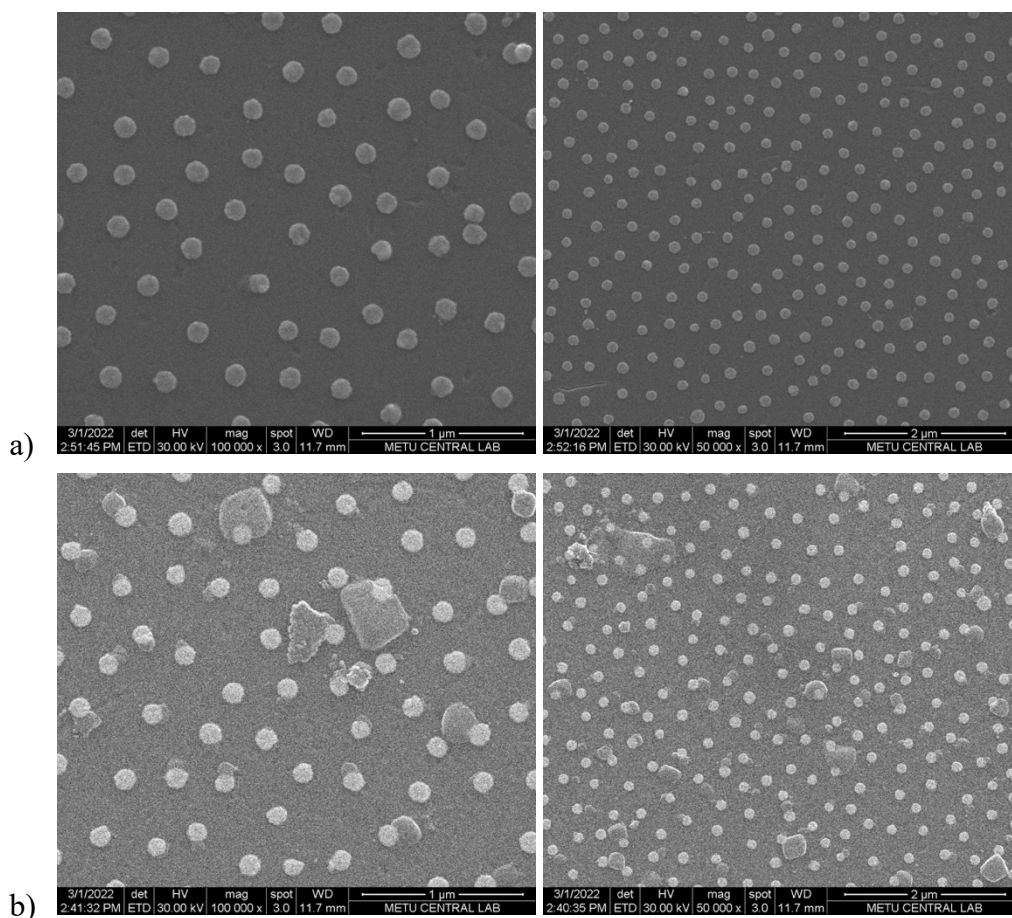
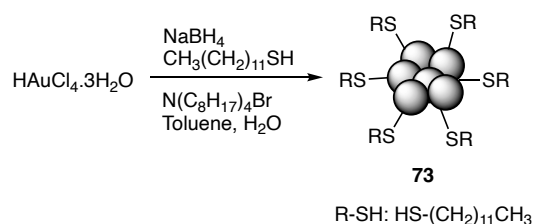


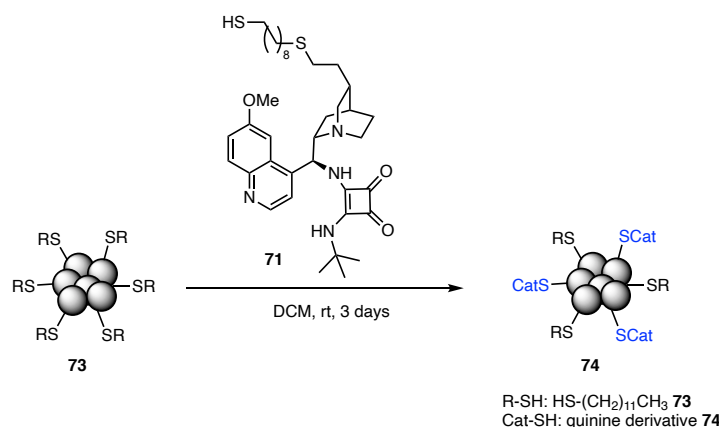
Figure 15. a) The SEM images of the empty support, b) solid-supported organocatalyst covered

Our other plan is to use gold nanoparticles as the support unit. We were encouraged by the stability of the gold clusters that would prevent the metal core from interfering with the reaction and make it easier to functionalize gold surfaces. In this case, we wanted to use our thiol functionalized bifunctional organocatalysts again, and to generate the gold nanoparticles, we preferred a known Brust–Schiffrin method starting from auric acid (Scheme 29). This method could perform a facile ligand exchange reaction at the surface because the particles were already thiol-stabilized with 1-dodecanethiol.



Scheme 29. Generation of thiol-stabilized gold nanoparticles

With these functionalized nanoparticles **73** in hand, the subsequent place-exchange reaction between **73** and the thiol group chain introduced organocatalyst **74** was carried out in DCM at room temperature for 3 days (Scheme 30). The elemental analysis also indicates that the presence of a “nitrogen” atom proves that the exchange reaction occurred.

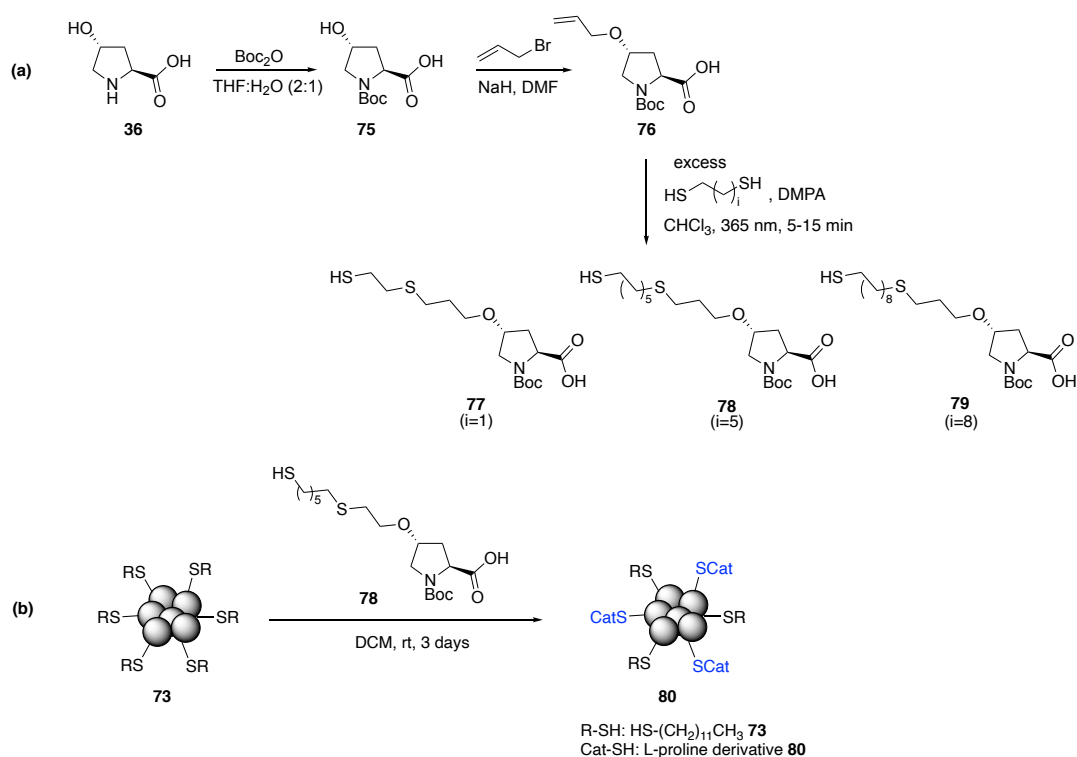


Scheme 30. Ligand exchange reaction to generate organocatalyst **74**

After the characterization studies of GNP-supported organocatalyst **74** is completed, its efficiency on different asymmetric reactions and its recycling efficiency will be tested beyond this thesis.

Another approach for the GNP-supported organocatalyst was derived from L-proline. To avoid touching the active basic NH and acidic COOH group, we started with 4-hydroxy-L-proline **36**. Similar synthetic routes were applied for synthesizing

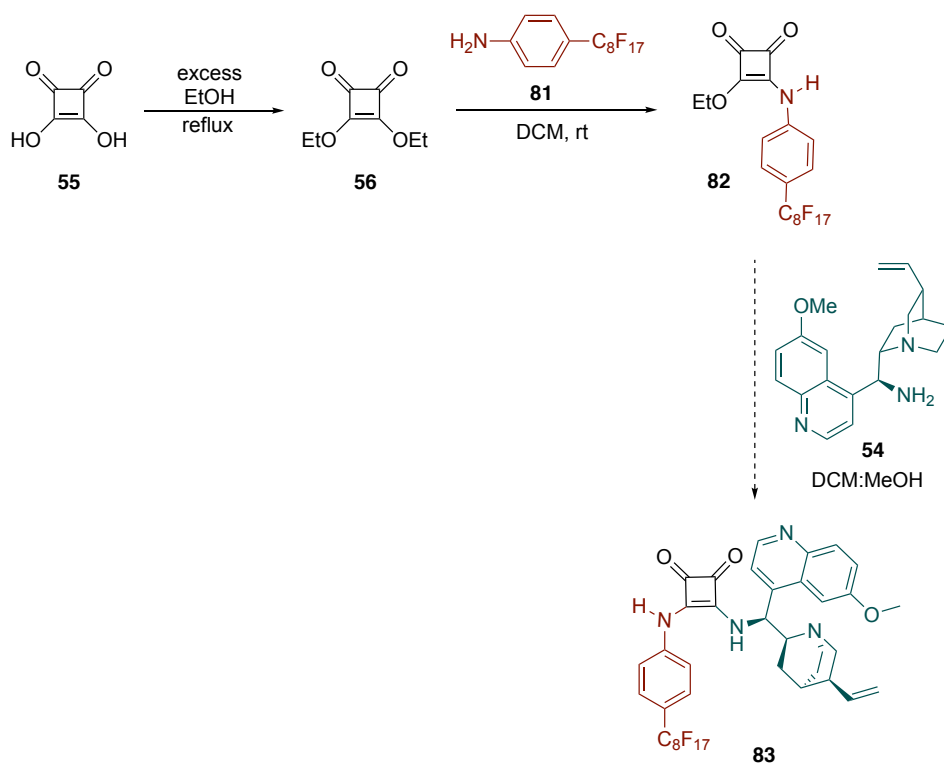
GNP-supported L-proline catalyst depicted in Scheme 31,a. Starting from 4-hydroxy-L-proline **36**, the basic NH group was protected with di-*tert*-butyl dicarbonate, and product **75** was obtained. After that, using allyl bromide, the 4-hydroxy group was allylated, and the product **76** was synthesized with 94% isolated yield. Thiol-ene reaction was performed with 1,2-ethanedithiol, 1,6-hexanedithiol and 1,9-nonanedithiol under photochemical reaction. Products **77**, **78**, and **79** was obtained with full conversions. To synthesize the GNP-supported catalysts, the place-exchange reaction was used again between **73** and **78** for 3 days in DCM (Scheme 32, b). As the final step, deprotection will applied with TFA to regenerate the activate the proline's basic character and again after the characterization studies of GNP-supported organocatalysts are completed, its efficiency on different asymmetric reactions and its recycling efficiency and the effect of chain length will be tested beyond this thesis.



Scheme 31. a) Generation of free thiol unit on 4-hydroxy-L-proline **36** b) Synthesis of GNP-supported L-proline derived organocatalyst **80**

2.4.2 Synthesis of Fluorous Supported Organocatalysts

The last heterogeneous organocatalyst system was synthesized with fluorous support. Fluorous supported organocatalysts are recently preferred because they are well-known soluble in common solvents and are easily recovered by the fluorous solid-phase extraction method. Rather than known fluorous type catalysts, we designed a squaramide type bifunctional organocatalyst. Starting from squaric acid **55**, it was converted into diethyl squarate **56**; after that fluorous group was attached, and mono squarate **82** was synthesized in 50% yield. Merging with quinine amine **54**, the desired organocatalyst **83** will also be synthesized (Scheme 32).



Scheme 32. Synthetic route for fluorous organocatalyst **83**

CHAPTER 3

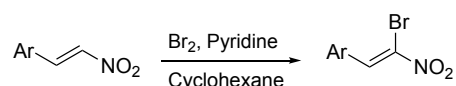
EXPERIMENTAL

3.1 Materials and Methods

¹H NMR and ¹³C NMR spectra were recorded in CDCl₃ on Bruker Spectrospin Avance DPX-400 spectrometer. The chemical shifts were reported in ppm relative to CDCl₃ (δ 7.26 and 77.0 for ¹H and ¹³C NMR, respectively) as the internal standard, and the data are specified as s (singlet), d (doublet), bs (broad singlet), bd (broad doublet), dd (doublet of doublets), ddd (doublet of doublet of doublets), t (triplet), td (triplet of doublets), dt (doublet of triplets), tdd (triplet of doublet of doublets) tt (triplet of triplets), m (multiplet) and coupling constants (*J*) in Hertz (Hz). HPLC chromatograms were recorded on Agilent Technologies & Thermo-Finnigan HPLC systems. Daicel ODH, ASH, OJH chiral columns were used with different solvent systems. Infrared measurements were done on Thermo Nicolet IS10 ATR / FT-IR spectrophotometer. HRMS data were collected on Agilent 6224 TOF LC/MS at UNAM, Bilkent University, and Thermo Scientific Dionex UltiMate 3000 LC-Quantiva Triple Quadrupole (QQQ) at HUNITEK, Hacettepe University. MALDI/TOF data were detected on Bruker Daltonics UltrafleXtreme MALDI-TOF/TOF Mass Spectrometer at HUNITEK, Hacettepe University. The elemental analyses were recorded on LECO, CHNS-932, at METU Central Laboratory. Optical rotations were recorded with Rudolph Scientific Autopol III polarimeter and reported as follows $[\alpha]_D^T$ (*c* is in gram per 100 mL solvent). The melting points of solid products were measured with MEL-TEMP 1002D. Using Merck Silica Gel 60 with mesh size 230-400 was used for flash column chromatography. Reactions were monitored by TLC using precoated silica gel plates (Merck Silica Gel PF-254), visualized by UV-light and polymolybden phosphoric acid, potassium permanganate, ninhydrin, and *p*-anisaldehyde stains as appropriate. All extracts were

dried over anhydrous sodium sulphate and solutions were concentrated under vacuum by using rotary evaporator. Characterization data of novel compounds are given in experimental section and related literature is cited. Compounds names were written with ChemBioDraw 16.0.

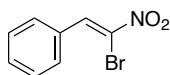
3.2 General Procedure for the synthesis of α -bromonitroalkenes (20a-t)



The following slightly modified literature procedure is performed:¹²⁰

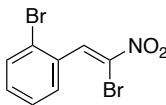
In a Schlenk tube, *trans*- β -nitrostyrene (5.0 mmol), pyridine (8.0 mmol) and cyclohexane (20 mL) were added and stirred for 10 min. Then, neat Br₂ (7.5 mmol) was added dropwise over 5 min at room temperature. After that, the cloudy yellow reaction was then heated to reflux and stirred for 4-12 h. The reaction mixture was monitored by TLC and after completion, the mixture was transferred to a single-neck round-bottom flask with ethyl acetate. The solvent was removed under *vacuo*, and the resulting residue was dissolved in ethyl acetate (50 mL). The organic layer was washed with aqueous Na₂S₂O₃ (1.0 M, 2 × 20 mL), H₂O (20 mL), and brine (20 mL) and then dried over Na₂SO₄. The solvent was removed under *vacuo*, and crude product that was purified by column chromatography (EtOAc/Hexane gradient). If needed recrystallization performed in DCM/Hexane mixture.

3.2.1 (Z)-(2-bromo-2-nitrovinyl)benzene (20a)



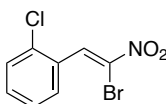
Yellow needles. 74% yield. ¹H NMR (400 MHz, CDCl₃) δ 8.64 (s, 1H), 7.89 (dd, *J* = 7.8, 1.8 Hz, 2H), 7.60 – 7.45 (m, 3H). ¹³C NMR (101 MHz, CDCl₃) δ 136.6, 132.0, 131.1, 130.3, 129.1, 128.3.

3.2.2 (Z)-1-bromo-2-(2-bromo-2-nitrovinyl)benzene (20b)



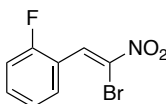
Orange solid. 43% yield. ^1H NMR (400 MHz, CDCl_3) δ 8.70 (s, 1H), 7.79 (dd, $J = 7.9, 1.7$ Hz, 1H), 7.62 (dd, $J = 8.0, 1.3$ Hz, 1H), 7.37 (td, $J = 7.6, 1.3$ Hz, 1H), 7.28 (td, $J = 7.8, 1.7$ Hz, 1H). ^{13}C NMR (101 MHz, CDCl_3) δ 136.0, 133.3, 132.2, 131.4, 131.0, 130.4, 127.5, 125.5.

3.2.3 (Z)-1-(2-bromo-2-nitrovinyl)-2-chlorobenzene (20c)



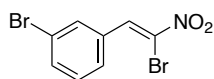
Yellow solid. 48% yield. ^1H NMR (400 MHz, CDCl_3) δ 8.84 (s, 1H), 7.94 (dd, $J = 7.6, 1.8$ Hz, 1H), 7.51 (dd, $J = 7.8, 1.6$ Hz, 1H), 7.42 (dtd, $J = 17.9, 7.4, 1.7$ Hz, 2H). ^{13}C NMR (101 MHz, CDCl_3) δ 135.7, 133.7, 132.3, 131.1, 130.3, 130.2, 129.6, 127.0.

3.2.4 (Z)-1-(2-bromo-2-nitrovinyl)-2-fluorobenzene (20d)



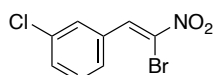
Light yellow needles. 54% yield. ^1H NMR (400 MHz, CDCl_3) δ 8.83 (s, 1H), 8.15 (td, $J = 7.7, 1.8$ Hz, 1H), 7.57 – 7.45 (m, 1H), 7.29 (td, $J = 7.7, 1.2$ Hz, 1H), 7.19 (ddd, $J = 9.8, 8.3, 1.2$ Hz, 1H). ^{13}C NMR (101 MHz, CDCl_3) δ 161.4 (d, $^1J_{\text{CF}} = 255.6$ Hz), 133.7 (d, $^3J_{\text{CF}} = 8.7$ Hz), 130.0, 129.4 (d, $^4J_{\text{CF}} = 0.7$ Hz), 128.9 (d, $^3J_{\text{CF}} = 7.3$ Hz), 124.4 (d, $^4J_{\text{CF}} = 3.8$ Hz), 118.8 (d, $^2J_{\text{CF}} = 11.8$ Hz), 116.1 (d, $^2J_{\text{CF}} = 21.6$ Hz).

3.2.5 (Z)-1-bromo-3-(2-bromo-2-nitrovinyl)benzene (20e)



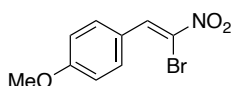
Yellow solid. 55% yield. ^1H NMR (400 MHz, CDCl_3) δ 8.47 (s, 1H), 7.95 (d, $J = 1.9$ Hz, 1H), 7.73 – 7.68 (m, 1H), 7.59 – 7.55 (m, 1H), 7.30 (t, $J = 7.9$ Hz, 1H). ^{13}C NMR (101 MHz, CDCl_3) δ 134.9, 134.7, 133.3, 132.3, 130.5, 129.5, 128.6, 123.1.

3.2.6 (Z)-1-(2-bromo-2-nitrovinyl)-3-chlorobenzene (20f)



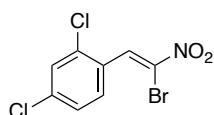
Yellow solid. 56% yield. ^1H NMR (400 MHz, CDCl_3) δ 8.57 (s, 1H), 7.89 (t, $J = 1.9$ Hz, 1H), 7.73 (dt, $J = 7.6, 1.6$ Hz, 1H), 7.52 – 7.38 (m, 2H). ^{13}C NMR (101 MHz, CDCl_3) δ 135.1, 135.0, 132.0, 131.8, 130.4, 130.3, 129.5, 129.1.

3.2.7 (Z)-1-(2-bromo-2-nitrovinyl)-4-methoxybenzene (20g)



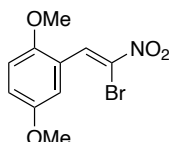
Yellow solid. 63% yield. ^1H NMR (400 MHz, CDCl_3) δ 8.55 (s, 1H), 8.02 – 7.73 (m, 2H), 7.07 – 6.68 (m, 2H), 3.81 (s, 3H). ^{13}C NMR (101 MHz, CDCl_3) δ 162.8, 136.4, 133.5, 122.4, 114.6, 55.6.

3.2.8 (Z)-1-(2-bromo-2-nitrovinyl)-2,4-dichlorobenzene (20h)



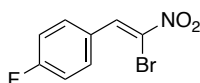
Yellow solid. 65% yield. ^1H NMR (400 MHz, CDCl_3) δ 8.78 (s, 1H), 7.91 (d, $J = 8.5$ Hz, 1H), 7.53 (d, $J = 2.1$ Hz, 1H), 7.39 (dd, $J = 8.5, 2.1$ Hz, 1H). ^{13}C NMR (101 MHz, CDCl_3) δ 135.6, 134.2, 130.1, 129.1, 128.6, 127.9, 125.7, 125.2.

3.2.9 (Z)-2-(2-bromo-2-nitrovinyl)-1,4-dimethoxybenzene (20i)



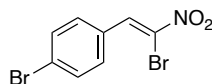
Yellow solid. 60% yield. ^1H NMR (400 MHz, CDCl_3) δ 8.97 (s, 1H), 7.67 (d, $J = 3.1$ Hz, 1H), 7.04 (dd, $J = 9.1, 3.1$ Hz, 1H), 6.88 (d, $J = 9.1$ Hz, 1H), 3.86 (s, 3H), 3.81 (s, 3H). ^{13}C NMR (101 MHz, CDCl_3) δ 153.5, 153.1, 131.8, 128.2, 119.7, 119.3, 114.3, 112.0, 56.3, 56.0.

3.2.10 (Z)-1-(2-bromo-2-nitrovinyl)-4-fluorobenzene (20j)



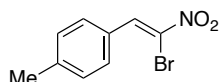
Light yellow needles. 73% yield. ^1H NMR (400 MHz, CDCl_3) δ 8.62 (s, 1H), 7.93 (dd, $J = 8.8, 5.4$ Hz, 2H), 7.19 (t, $J = 8.6$ Hz, 2H). ^{13}C NMR (101 MHz, CDCl_3) δ 164.7 (d, $^1J_{\text{CF}} = 255.9$ Hz), 135.4, 133.4 (d, $^3J_{\text{CF}} = 8.9$ Hz), 128.0, 126.5 (d, $^4J_{\text{CF}} = 3.2$ Hz), 116.5 (d, $^2J_{\text{CF}} = 21.9$ Hz).

3.2.11 (Z)-1-bromo-4-(2-bromo-2-nitrovinyl)benzene (20k)



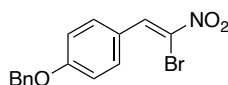
Yellow solid. 68% yield. ^1H NMR (400 MHz, CDCl_3) δ 8.50 (s, 1H), 7.71 – 7.65 (m, 2H), 7.56 (d, $J = 8.6$ Hz, 2H). ^{13}C NMR (101 MHz, CDCl_3) δ 135.3, 132.3, 132.2, 129.2, 129.1, 126.7.

3.2.12 (Z)-1-(2-bromo-2-nitrovinyl)-4-methylbenzene (20l)



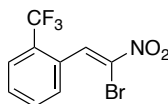
Yellow needles. 72% yield. ^1H NMR (400 MHz, CDCl_3) δ 8.62 (s, 1H), 7.81 (d, $J = 8.3$ Hz, 2H), 7.30 (d, $J = 8.0$ Hz, 2H), 2.42 (s, 3H). ^{13}C NMR (101 MHz, CDCl_3) δ 143.0, 136.6, 131.1, 129.7, 127.3, 127.0, 21.7.

3.2.13 (Z)-1-(benzyloxy)-4-(2-bromo-2-nitrovinyl)benzene (20m)



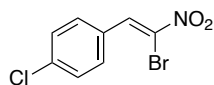
Yellow solid. 57% yield. ^1H NMR (400 MHz, CDCl_3) δ 8.63 (s, 1H), 7.93 (d, $J = 8.9$ Hz, 2H), 7.52 – 7.28 (m, 5H), 7.08 (d, $J = 8.9$ Hz, 2H), 5.15 (s, 2H). ^{13}C NMR (101 MHz, CDCl_3) δ 136.8, 136.0, 133.4, 128.8, 128.4, 127.5, 122.7, 115.4, 70.3.

3.2.14 (Z)-1-(2-bromo-2-nitrovinyl)-2-(trifluoromethyl)benzene (20n)



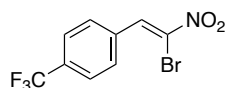
Yellow solid. 54% yield. ^1H NMR (400 MHz, CDCl_3) δ 8.70 (t, $J = 2.2$ Hz, 1H), 7.76 – 7.66 (m, 2H), 7.66 – 7.57 (m, 1H), 7.52 (t, $J = 7.7$ Hz, 1H). ^{13}C NMR (101 MHz, CDCl_3) δ 139.8, 134.8 (q, $^4J_{\text{CF}} = 1.7$ Hz), 132.5, 131.4, 129.9, (q, $^2J_{\text{CF}} = 30.7$ Hz), 128.6, 128.5, 126.9 (q, $^3J_{\text{CF}} = 5.6$ Hz), 123.6 (q, $^1J_{\text{CF}} = 274.1$ Hz).

3.2.15 (Z)-1-(2-bromo-2-nitrovinyl)-4-chlorobenzene (20o)



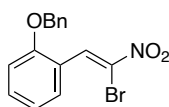
Light yellow needles. 73% yield. ^1H NMR (400 MHz, CDCl_3) δ 8.58 (s, 1H), 7.83 (d, $J = 8.6$ Hz, 2H), 7.46 (d, $J = 8.6$ Hz, 1H). ^{13}C NMR (101 MHz, CDCl_3) δ 138.1, 135.2, 132.1, 129.3, 128.6.

3.2.16 (Z)-1-(2-bromo-2-nitrovinyl)-4-(trifluoromethyl)benzene (20p)



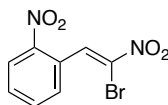
Yellow solid. 63% yield. ^1H NMR (400 MHz, CDCl_3) δ 8.57 (s, 1H), 7.89 (d, $J = 8.2$ Hz, 1H), 7.68 (d, $J = 8.3$ Hz, 1H). ^{13}C NMR (101 MHz, CDCl_3) δ 133.7, 132.7 (q, $^4J_{\text{CF}} = 1.1$ Hz), 132.0 (q, $^2J_{\text{CF}} = 33.0$ Hz), 129.8, 129.4, 124.8 (q, $^3J_{\text{CF}} = 3.8$ Hz), 122.5 (q, $^1J_{\text{CF}} = 272.4$ Hz).

3.2.17 (Z)-1-(benzyloxy)-2-(2-bromo-2-nitrovinyl)benzene (20q)



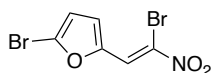
Yellow solid. 46% yield. ^1H NMR (400 MHz, CDCl_3) δ 8.95 (s, 1H), 8.01 (dd, $J = 1.3$ Hz, 1H), 7.37 – 7.19 (m, 6H), 6.96 (t, $J = 7.7$ Hz, 1H), 6.90 (d, $J = 8.4$ Hz, 1H), 5.05 (s, 2H). ^{13}C NMR (101 MHz, CDCl_3) δ 158.0, 136.1, 133.4, 132.0, 129.7, 128.8, 128.4, 128.3, 127.1, 120.9, 120.0, 112.7, 70.8.

3.2.18 (Z)-1-(2-bromo-2-nitrovinyl)-2-nitrobenzene (20r)



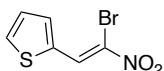
Light Brown solid. 33% yield. ^1H NMR (400 MHz, CDCl_3) δ 10.43 (s, 1H), 8.13 (dd, $J = 7.8, 1.4$ Hz, 1H), 7.96 (dd, $J = 7.5, 1.7$ Hz, 1H), 7.83 – 7.74 (m, 2H). ^{13}C NMR (101 MHz, CDCl_3) δ 188.1, 149.6, 134.1, 133.7, 133.3, 131.4, 129.6, 124.5.

3.2.19 (Z)-2-bromo-5-(2-bromo-2-nitrovinyl)furan (20s)



Yellow solid. 41% yield. ^1H NMR (400 MHz, CDCl_3) δ 8.50 (s, 1H), 7.38 (d, $J = 3.7$ Hz, 1H), 6.61 (d, $J = 3.7$ Hz, 1H). ^{13}C NMR (101 MHz, CDCl_3) δ 148.4, 129.4, 124.9, 123.7, 121.9, 115.5.

3.2.20 (Z)-2-(2-bromo-2-nitrovinyl)thiophene (20t)



Yellow solid. 53% yield. ^1H NMR (400 MHz, CDCl_3) δ 8.15 (dd, $J = 13.3, 6.6$ Hz, 1H), 7.56 (d, $J = 5.0$ Hz, 1H), 7.51 – 7.43 (m, 2H), 7.15 (dd, $J = 5.0, 3.7$ Hz, 1H). ^{13}C NMR (101 MHz, CDCl_3) δ 135.4, 134.6, 133.8, 132.1, 131.6, 128.9.

3.3 General Procedure for Friedel-Crafts Domino Substitution Reaction

Racemic synthesis (α - and β -naphthols):

(Z)- α -bromoalkenes **20a-t** (0.10 mmol), naphthol **21a-e** or **59a-c** (0.20 mmol) and DABCO (11.2 mg, 0.10 mmol) were in DCM (0.5 mL) and stirred at room

temperature. The reaction was monitored with TLC upon the consumption of limiting reactant, directly loaded into column chromatography. EtOAc:Hexane mixtures were used as eluent to purify the products.

Racemic synthesis (phenols);

(*Z*)- α -bromoalkenes **20a-t** (0.10 mmol), phenol **61a-c** (0.20 mmol) and DABCO (11.2 mg, 0.10 mmol) were in DCM (0.5 mL) and stirred at room temperature. The reaction was monitored with TLC upon the consumption of limiting reactant, directly loaded into column chromatography. EtOAc:Hexane mixtures were used as eluent to purify the products.

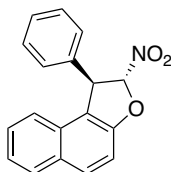
Asymmetric synthesis (α - and β -naphthols);

(*Z*)- α -bromoalkenes **20a-t** (0.15 mmol), naphthol **21a-e**, **59a-c** (0.30 mmol), organocatalyst **19b** (4.2 mg, 0.0075 mmol) and DABCO (16.8 mg, 0.15 mmol) were in xylene (0.3 mL) and stirred at room temperature. The reaction was monitored with TLC upon the consumption of limiting reactant, directly loaded into column chromatography. EtOAc:Hexane mixtures were used as eluent to purify the products.

Asymmetric synthesis (phenols);

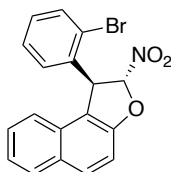
(*Z*)- α -bromoalkenes **20a-t** (0.15 mmol), phenol **61a-c** (0.30 mmol), organocatalyst **19c** (3.6 mg, 0.0075 mmol) and DABCO (16.8 mg, 0.15 mmol) were in DCM (0.3 mL) and stirred at room temperature. The reaction was monitored with TLC upon the consumption of limiting reactant, directly loaded into column chromatography. EtOAc:Hexane mixtures were used as eluent to purify the products.

3.3.1 (1*R*,2*R*)-2-nitro-1-phenyl-1,2-dihydronaphtho[2,1-*b*]furan (23aa)



General procedure starting from **20a** and **21a** afforded to desired chiral product with 95% isolated yield and 98% ee in 90 min as a white solid. M.p.= 110 °C Optical rotation was determined as $[\alpha]_D^{25} = -5.50^\circ$ (c 2.0, CH₂Cl₂). ¹H NMR (400 MHz, CDCl₃) δ 7.93 (d, J = 8.9 Hz, 1H), 7.92 – 7.86 (m, 1H), 7.47 (d, J = 8.9 Hz, 1H), 7.41 – 7.30 (m, 6H), 7.25 – 7.14 (m, 2H), 6.12 (d, J = 2.0 Hz, 1H), 5.34 (d, J = 1.8 Hz, 1H). ¹³C NMR (101 MHz, CDCl₃) δ 156.2, 138.0, 131.5, 130.9, 129.6, 129.4, 129.1, 128.4, 127.7, 127.6, 124.5, 123.0, 118.3, 112.3, 111.9, 55.4. Chiralpak ODH column, 90:10 (n-hexane/*i*-PrOH), flow rate 1.0 mL/min, 230 nm, temp=25 °C, t_{minor} = 6.743 min, t_{major} = 11.062 min.

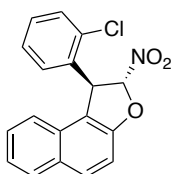
3.3.2 (1*S*,2*R*)-1-(2-bromophenyl)-2-nitro-1,2-dihydronaphtho[2,1-*b*]furan (23ab)



General procedure starting from **20b** and **21a** afforded to desired chiral product with 77% isolated yield and 80% ee in 2h as a yellow solid. M.p.= 135 °C Optical rotation was determined as $[\alpha]_D^{25} = -52.96^\circ$ (c 1.0, CH₂Cl₂). ¹H NMR (400 MHz, CDCl₃) δ 7.94 (d, J = 8.9 Hz, 1H), 7.92 – 7.85 (m, 1H), 7.73 (dd, J = 7.9, 1.4 Hz, 1H), 7.46 (d, J = 8.9 Hz, 1H), 7.45 – 7.32 (m, 3H), 7.17 (td, J = 7.6, 1.8 Hz, 1H), 7.11 (td, J = 7.5, 1.4 Hz, 1H), 6.62 (d, J = 7.5 Hz, 1H), 6.11 (d, J = 1.7 Hz, 1H), 5.91 (s, 1H). ¹³C NMR (101 MHz, CDCl₃) δ 159.7, 158.6, 136.4, 135.9, 133.9, 133.5, 131.9, 131.3,

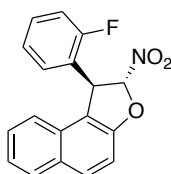
130., 128.3, 123.8, 118.4, 117.8, 116.0, 115.8, 115.6, 55.7, 55.4. Chiralpak ODH column, 90:10 (n-hexane/i-PrOH), flow rate 1.0 mL/min, 220 nm, temp=25 °C, $t_{\text{minor}}=7.791$ min, $t_{\text{major}}=12.106$ min.

3.3.3 (1*S*,2*R*)-1-(2-chlorophenyl)-2-nitro-1,2-dihydronaphtho[2,1-*b*]furan (23ac)



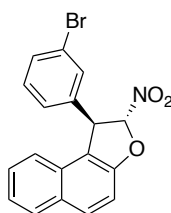
General procedure starting from **20c** and **21a** afforded to desired chiral product with 74% isolated yield and 75% ee in 5h as a pink-white solid. M.p.= 117 °C Optical rotation was determined as $[\alpha]_D^{25} = -96.08^\circ$ (c 1.7, CH₂Cl₂). ¹H NMR (400 MHz, CDCl₃) δ 7.85 (d, $J = 8.9$ Hz, 1H), 7.85 – 7.77 (m, 1H), 7.46 (dd, $J = 8.0, 1.3$ Hz, 1H), 7.37 (d, $J = 8.9$ Hz, 1H), 7.35 – 7.23 (m, 2H), 7.21 – 7.12 (m, 1H), 6.99 (td, $J = 7.6, 1.3$ Hz, 1H), 6.55 (d, $J = 7.9$ Hz, 1H), 6.04 (d, $J = 1.6$ Hz, 1H), 5.79 (s, 1H). ¹³C NMR (101 MHz, CDCl₃) δ 156.5, 136.8, 133.6, 131.7, 130.9, 130.0, 129.4, 129.2, 129.1, 128.4, 127.9, 124.7, 123.9, 123.1, 118.7, 111.9, 111.8, 53.6. Chiralpak ODH column, 90:10 (n-hexane/i-PrOH), flow rate 1.0 mL/min, 230 nm, temp=25 °C, $t_{\text{minor}}=7.725$ min, $t_{\text{major}}=10.022$ min.

3.3.4 (1*S*,2*R*)-1-(2-fluorophenyl)-2-nitro-1,2-dihydronaphtho[2,1-*b*]furan (23ad)



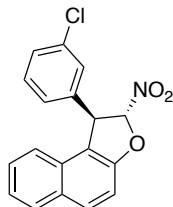
General procedure starting from **20d** and **21a** afforded to desired chiral product with 92% isolated yield and 95% ee in 2h as a white solid. M.p.= 87 °C Optical rotation was determined as $[\alpha]_D^{25} = -4.73^\circ$ (*c* 2.0, CH₂Cl₂). ¹H NMR (400 MHz, CDCl₃) δ 7.82 (d, *J* = 8.9 Hz, 1H), 7.79 – 7.73 (m, 1H), 7.35 (d, *J* = 8.9 Hz, 1H), 7.31 – 7.24 (m, 3H), 7.20 (dtd, *J* = 7.4, 5.7, 2.6 Hz, 1H), 7.15 – 7.05 (m, 1H), 6.88 (t, *J* = 7.6 Hz, 1H), 6.65 (td, *J* = 7.7, 1.7 Hz, 1H), 6.07 (d, *J* = 1.7 Hz, 1H), 5.56 (d, *J* = 1.6 Hz, 1H). ¹³C NMR (101 MHz, CDCl₃) δ 160.2 (d, ¹*J*_{CF} = 248.2 Hz), 156.3, 131.6, 130.9, 130.3 (d, ³*J*_{CF} = 8.2 Hz), 129.5, 129.0 (d, ⁴*J*_{CF} = 3.2 Hz), 127.9, 125.0 (d, ⁴*J*_{CF} = 4.0 Hz), 124.9, 124.8, 124.6, 122.7, 117.5, 116.1 (d, ²*J*_{CF} = 21.4 Hz), 111.9, 111.7, 48.0 (d, ⁴*J*_{CF} = 3.8 Hz). Chiralpak ODH column, 90:10 (n-hexane/*i*-PrOH), flow rate 1.0 mL/min, 220 nm, temp=25 °C, *t*_{minor}= 8.293 min, *t*_{major}= 11.345 min.

3.3.4.1 (1*R*,2*R*)-1-(3-bromophenyl)-2-nitro-1,2-dihydronaphtho[2,1-*b*]furan (23ae)



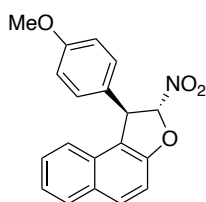
General procedure starting from **20e** and **21a** afforded to desired chiral product with 91% isolated yield and 80% ee in 3.5 h as a yellow semi-solid. Optical rotation was determined as $[\alpha]_D^{25} = -3.74^\circ$ (*c* 2.0, CH₂Cl₂). ¹H NMR (400 MHz, CDCl₃) δ 7.94 (d, *J* = 8.9 Hz, 1H), 7.93 – 7.86 (m, 1H), 7.46 (dd, *J* = 8.6, 2.4 Hz, 2H), 7.44 – 7.30 (m, 4H), 7.21 (t, *J* = 7.8 Hz, 1H), 7.11 (d, *J* = 7.8 Hz, 1H), 6.07 (d, *J* = 1.8 Hz, 1H), 5.28 (d, *J* = 1.7 Hz, 1H). ¹³C NMR (101 MHz, CDCl₃) δ 156.3, 140.1, 131.9, 131.8, 131.0, 130.9, 130.6, 129.4, 129.2, 127.9, 126.3, 124.7, 123.5, 122.8, 117.6, 112.0, 111.9, 54.9. Chiralpak ODH column, 90:10 (n-hexane/*i*-PrOH), flow rate 1.0 mL/min, 220 nm, temp=25 °C, *t*_{minor}= 7.791 min, *t*_{major}= 12.106 min. IR(neat): 2923, 1626, 1518, 1495, 1446, 1361, 1265, 1235, 1198, 1156, 1080, 1061, 1001 cm⁻¹. HRMS (ESI-TOF) *m/z*: [M+H]⁺ Calcd. for C₁₈H₁₂BrNO₃ 370.0079; Found 369.9767.

3.3.5 (1*R*,2*R*)-1-(3-chlorophenyl)-2-nitro-1,2-dihydronaphtho[2,1-*b*]furan (23af)



General procedure starting from **20f** and **21a** afforded to desired chiral product with 86% isolated yield and 70% ee in 70 min as a white solid. M.p.= 128 °C Optical rotation was determined as $[\alpha]_D^{25} = -42.17^\circ$ (c 2.0, CH₂Cl₂). ¹H NMR (400 MHz, CDCl₃) δ 7.93 (d, J = 8.9 Hz, 1H), 7.88 (dd, J = 7.4, 2.1 Hz, 1H), 7.45 (d, J = 8.9 Hz, 1H), 7.42 – 7.34 (m, 2H), 7.35 – 7.30 (m, 1H), 7.30 – 7.22 (m, 2H), 7.18 (d, J = 2.0 Hz, 1H), 7.07 (dt, J = 7.1, 1.7 Hz, 1H), 6.06 (d, J = 1.8 Hz, 1H), 5.28 (d, J = 1.8 Hz, 1H). ¹³C NMR (101 MHz, CDCl₃) δ 156.3, 139.9, 135.4, 131.8, 130.9, 130.7, 129.4, 129.2, 128.8, 127.9, 127.7, 125.8, 124.7, 122.8, 117.6, 112.0, 111.9, 54.9. Chiralpak ODH column, 90:10 (n-hexane/*i*-PrOH), flow rate 1.0 mL/min, 220 nm, temp=25 °C, t_{minor} = 7.039 min, t_{major} = 11.337 min.

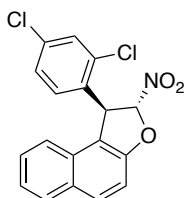
3.3.6 (1*R*,2*R*)-1-(4-methoxyphenyl)-2-nitro-1,2-dihydronaphtho[2,1-*b*]furan (23ag)



General procedure starting from **20g** and **21a** afforded to desired chiral product with 92% isolated yield and 77% ee in 1 h as a yellow solid. M.p.= 109 °C Optical rotation was determined as $[\alpha]_D^{25} = -12.31^\circ$ (c 1.0, CH₂Cl₂). ¹H NMR (400 MHz, CDCl₃) δ 7.92 (d, J = 8.9 Hz, 1H), 7.89 (d, J = 4.6 Hz, 1H), 7.45 (d, J = 8.9 Hz, 1H), 7.38 (d,

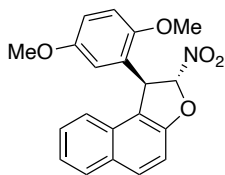
$J = 2.3$ Hz, 3H), 7.14 – 7.08 (m, 2H), 6.88 – 6.83 (m, 2H), 6.08 (d, $J = 1.8$ Hz, 1H), 5.29 (s, 1H), 3.77 (s, 3H). ^{13}C NMR (101 MHz, CDCl_3) δ 159.6, 156.1, 131.4, 130.9, 130.0, 129.6, 129.1, 128.7, 127.6, 124.5, 123.0, 118.5, 114.7, 112.7, 111.8, 55.3, 54.8. Chiralpak ODH column, 90:10 (n-hexane/*i*-PrOH), flow rate 1.0 mL/min, 230 nm, temp=25 °C, $t_{\text{minor}} = 8.880$ min, $t_{\text{major}} = 11.767$ min.

3.3.7 (1*S*,2*R*)-1-(2,4-dichlorophenyl)-2-nitro-1,2-dihydronaphtho[2,1-*b*]furan (23ah)



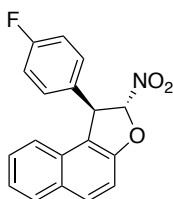
General procedure starting from **20h** and **21a** afforded to desired chiral product with 85% isolated yield and 81% ee in 3 h as a white solid. M.p.= 135 °C Optical rotation was determined as $[\alpha]_D^{25} = -68.22$ (c 2.0, CH_2Cl_2). ^1H NMR (400 MHz, CDCl_3) δ 7.95 (d, $J = 8.9$ Hz, 1H), 7.93 – 7.86 (m, 1H), 7.57 (d, $J = 2.2$ Hz, 1H), 7.45 (d, $J = 8.9$ Hz, 1H), 7.41 (ddd, $J = 7.1, 4.5, 1.8$ Hz, 2H), 7.34 – 7.28 (m, 1H), 7.05 (dd, $J = 8.5, 2.1$ Hz, 1H), 6.54 (d, $J = 8.5$ Hz, 1H), 6.08 (d, $J = 1.6$ Hz, 1H), 5.81 (s, 1H). ^{13}C NMR (101 MHz, CDCl_3) δ 156.5, 135.0, 134.2, 133.5, 131.8, 130.8, 129.9, 129.9, 129.1, 129.1, 128.0, 127.9, 124.7, 122.6, 117.6, 111.8, 111.3, 50.6. Chiralpak ODH column, 90:10 (n-hexane/*i*-PrOH), flow rate 1.0 mL/min, 230 nm, temp=25 °C, $t_{\text{minor}} = 7.625$ min, $t_{\text{major}} = 8.556$ min. IR(neat): 3032, 2923, 1634, 1599, 1562, 1522, 1490, 1453, 1366, 1269, 1232, 1155, 1104, 1061, 1052, 1006 cm^{-1} . MS (MALDI-TOF) m/z : $[\text{M}-\text{NO}_2]^+$ Calcd. for $\text{C}_{18}\text{H}_{11}\text{Cl}_2\text{O}$ 313.019; Found 313.282.

3.3.8 (1*R*,2*R*)-1-(2,5-dimethoxyphenyl)-2-nitro-1,2-dihydronaphtho[2,1-*b*]furan (23ai)



General procedure starting from **20i** and **21a** afforded to desired chiral product with 89% isolated yield and 70% ee in 3 h as a yellow semi-solid. Optical rotation was determined as $[\alpha]_D^{25} = -48.05$ (*c* 2.0, CH₂Cl₂). ¹H NMR (400 MHz, CDCl₃) δ 7.91 (t, *J* = 7.5 Hz, 2H), 7.42 (m, 4H), 6.95 (d, *J* = 8.9 Hz, 1H), 6.82 (dd, *J* = 8.9, 3.1 Hz, 1H), 6.23 (d, *J* = 3.1 Hz, 1H), 6.16 (d, *J* = 1.9 Hz, 1H), 5.71 (d, *J* = 1.8 Hz, 1H), 3.98 (s, 3H), 3.58 (d, *J* = 0.8 Hz, 3H). ¹³C NMR (101 MHz, CDCl₃) δ 156.3, 153.6, 150.8, 131.0, 130.6, 129.7, 128.9, 127.4, 126.9, 124.2, 123.1, 118.1, 115.2, 113.0, 112.6, 111.7, 56.1, 55.4, 48.5. Chiralpak ODH column, 90:10 (n-hexane/*i*-PrOH), flow rate 1.0 mL/min, 230 nm, temp=25 °C, *t*_{minor} = 8.423 min, *t*_{major} = 10.113 min.

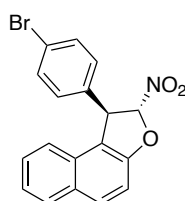
3.3.9 (1*R*,2*R*)-1-(4-fluorophenyl)-2-nitro-1,2-dihydronaphtho[2,1-*b*]furan (23aj)



General procedure starting from **20j** and **21a** afforded to desired chiral product with 97% isolated yield and 98% ee in 90 min as a white solid. M.p.= 115 °C Optical rotation was determined as $[\alpha]_D^{25} = -97.92$ (*c* 1.0, CH₂Cl₂). ¹H NMR (400 MHz, CDCl₃) δ 7.93 (d, *J* = 8.8 Hz, 1H), 7.92 – 7.87 (m, 1H), 7.46 (d, *J* = 8.9 Hz, 1H), 7.42 – 7.36 (m, 2H), 7.37 – 7.30 (m, 1H), 7.18 (ddd, *J* = 8.6, 5.2, 2.7 Hz, 2H), 7.11 – 6.96 (m, 2H), 6.07 (d, *J* = 1.8 Hz, 1H), 5.32 (d, *J* = 1.7 Hz, 1H). ¹³C NMR (101

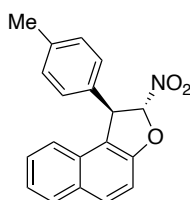
MHz, CDCl₃) δ 162.6 (d, $^1J_{CF} = 248.0$ Hz), 156.2, 133.7 (d, $^4J_{CF} = 3.1$ Hz), 131.7, 130.9, 129.3, 129.3(d, $^2J_{CF} = 31.2$ Hz), 129.3, 127.8, 124.6, 122.9, 118.0, 116.4 (d, $^2J_{CF} = 21.7$ Hz), 112.3, 111.9, 54.6. Chiralpak ODH column, 90:10 (n-hexane/i-PrOH), flow rate 1.0 mL/min, 220 nm, temp=25 °C, $t_{\text{minor}} = 7.060$ min, $t_{\text{major}} = 10.396$ min.

3.3.10 (1*R*,2*R*)-1-(4-bromophenyl)-2-nitro-1,2-dihydronaphtho[2,1-*b*]furan (23ak)



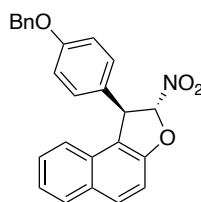
General procedure starting from **20k** and **21a** afforded to desired chiral product with 89% isolated yield and 75% ee in 3.5 h as a pink-white solid. M.p.= 91 °C Optical rotation was determined as $[\alpha]_D^{25} = -34.47$ (c 2.0, CH₂Cl₂). ¹H NMR (400 MHz, CDCl₃) δ 7.93 (d, $J = 8.9$ Hz, 1H), 7.91 – 7.86 (m, 1H), 7.46 (dd, $J = 8.8, 7.6$ Hz, 3H), 7.41 – 7.36 (m, 2H), 7.35 – 7.29 (m, 1H), 7.12 – 7.02 (m, 2H), 6.06 (d, $J = 1.8$ Hz, 1H), 5.29 (d, $J = 1.8$ Hz, 1H). ¹³C NMR (101 MHz, CDCl₃) δ 154.9, 135.2, 131.9, 130.1, 129.3, 128.4, 127.4, 126.8, 126.3, 123.1, 121.4, 117.1, 110.3, 110.2, 110.2, 52.1. Chiralpak ODH column, 90:10 (n-hexane/i-PrOH), flow rate 1.0 mL/min, 220 nm, temp=25 °C, $t_{\text{minor}} = 8.510$ min, $t_{\text{major}} = 11.935$ min.

3.3.11 (1*R*,2*R*)-2-nitro-1-(*p*-tolyl)-1,2-dihydronaphtho[2,1-*b*]furan (23al)



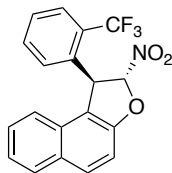
General procedure starting from **20l** and **21a** afforded to desired chiral product with 82% isolated yield and 77% ee in 3 h as a white solid. M.p.= 86 °C Optical rotation was determined as $[\alpha]_D^{25} = -69.35$ (*c* 2.0, CH₂Cl₂). ¹H NMR (400 MHz, CDCl₃) δ 7.81 (d, *J* = 8.9 Hz, 1H), 7.77 (d, *J* = 4.0 Hz, 1H), 7.35 (d, *J* = 8.9 Hz, 1H), 7.27 (m, *J* = 3.8, 3.3 Hz, 1H), 7.04 (d, *J* = 7.9 Hz, 1H), 6.98 (d, *J* = 8.2 Hz, 1H), 5.98 (d, *J* = 1.8 Hz, H), 5.19 (d, *J* = 1.8 Hz, 1H), 2.22 (s, 3H). ¹³C NMR (101 MHz, CDCl₃) δ 156.16, 138.27, 135.01, 131.37, 130.87, 130.05, 129.65, 129.04, 127.61, 127.42, 124.47, 123.04, 118.48, 112.71, 111.84, 55.12, 21.12. Chiralpak ODH column, 90:10 (n-hexane/*i*-PrOH), flow rate 1.0 mL/min, 220 nm, temp=25 °C, *t*_{minor}= 6.330 min, *t*_{major}= 9.037 min.

3.3.12 (1*R*,2*R*)-1-(4-(benzyloxy)phenyl)-2-nitro-1,2-dihydronaphtho[2,1-*b*]furan (**23am**)



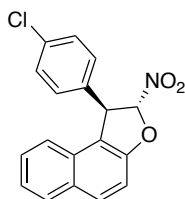
General procedure starting from **20m** and **21a** afforded to desired chiral product with 87% isolated yield and 79% ee in 5 h as a white solid. M.p.= 153 °C Optical rotation was determined as $[\alpha]_D^{25} = -28.74$ (*c* 1.0, CH₂Cl₂). ¹H NMR (400 MHz, CDCl₃) δ 7.96 – 7.88 (m, 3H), 7.90 – 7.86 (m, 1H), 7.45 (d, *J* = 8.9 Hz, 1H), 7.43 – 7.32 (m, 6H), 7.11 (d, *J* = 8.0 Hz, 2H), 6.99 – 6.87 (m, 2H), 6.08 (d, *J* = 1.8 Hz, 1H), 5.28 (d, *J* = 1.8 Hz, 1H), 5.03 (s, 2H). ¹³C NMR (101 MHz, CDCl₃) δ 158.8, 156.1, 136.7, 131.4, 130.9, 130.3, 129.6, 129.1, 128.7, 128.7, 128.1, 127.6, 127.5, 124.5, 123.1, 118.5, 115.6, 112.7, 111.9, 70.1, 54.8. Chiralpak ODH column, 90:10 (n-hexane/*i*-PrOH), flow rate 1.0 mL/min, 220 nm, temp=25 °C, *t*_{minor}= 14.981 min, *t*_{major}= 13.549 min.

3.3.13 (1*R*,2*R*)-2-nitro-1-(2-(trifluoromethyl)phenyl)-1,2-dihydronaphtho[2,1-*b*]furan (23an)



General procedure starting from **20n** and **21a** afforded to desired chiral product with 88% isolated yield and 81% ee in 160 m as a white semi-solid. Optical rotation was determined as $[\alpha]_D^{25} = -140.23$ (*c* 1.0, CH₂Cl₂). ¹H NMR (400 MHz, CDCl₃) δ 7.96 (d, *J* = 8.9 Hz, 1H), 7.92 – 7.85 (m, 1H), 7.83 (dd, *J* = 7.9, 1.4 Hz, 1H), 7.47 (d, *J* = 8.9 Hz, 1H), 7.41 (d, *J* = 7.0 Hz, 1H), 7.39 – 7.36 (m, 2H), 7.33 (td, *J* = 6.4, 3.4 Hz, 2H), 6.75 (d, *J* = 7.8 Hz, 1H), 6.07 (d, *J* = 1.5 Hz, 1H), 5.78 (s, 1H). ¹³C NMR (101 MHz, CDCl₃) δ 156.6, 135.9, 133.0, 131.9, 131.1, 129.3 (q, ²*J*_{CF} = 23.1 Hz), 129.1, 128.6, 128.0, 126.6, 126.5 (q, ³*J*_{CF} = 5.8 Hz), 125.7, 124.7, 124.3 (q, ¹*J*_{CF} = 273.9 Hz), 122.9, 118.9, 112.1, 111.7, 49.8. Chiralpak ODH column, 90:10 (n-hexane/i-PrOH), flow rate 1.0 mL/min, 220 nm, temp=25 °C, *t*_{minor}= 6.263 min, *t*_{major}= 7.419 min.

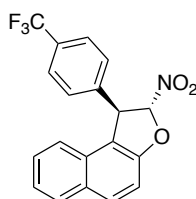
3.3.14 (1*R*,2*R*)-1-(4-chlorophenyl)-2-nitro-1,2-dihydronaphtho[2,1-*b*]furan (23ao)



General procedure starting from **20o** and **21a** afforded to desired chiral product with 90% isolated yield and 73% ee in 4 h as a white solid. M.p.= 120 °C. Optical rotation was determined as $[\alpha]_D^{24} = -27.27$ (*c* 0.9, CH₂Cl₂). ¹H NMR (400 MHz, CDCl₃) δ 7.84 (d, *J* = 8.9 Hz, 1H), 7.82 – 7.73 (m, 1H), 7.36 (d, *J* = 8.9 Hz, 1H), 7.33 – 7.27

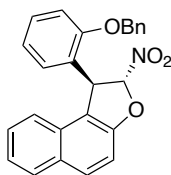
(m, 2H), 7.26 – 7.19 (m, 3H), 7.07 – 7.00 (m, 2H), 5.97 (d, $J = 1.7$ Hz, 1H), 5.21 (d, $J = 1.7$ Hz, 1H). ^{13}C NMR (101 MHz, CDCl_3) δ 155.2, 135.3, 133.4, 130.7, 129.9, 128.6, 128.4, 128.1, 127.9, 126.8, 123.6, 121.8, 116.7, 111.1, 110.8, 53.7. Chiralpak ODH column, 90:10 (n-hexane/*i*-PrOH), flow rate 1.0 mL/min, 220 nm, temp=25 °C, $t_{\text{minor}} = 7.645$ min, $t_{\text{major}} = 11.094$ min.

3.3.15 (1*R*,2*R*)-2-nitro-1-(4-(trifluoromethyl)phenyl)-1,2-dihydronaphtho[2,1-*b*]furan (23ap)



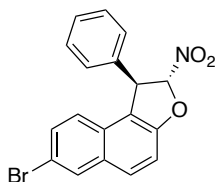
General procedure starting from **20p** and **21a** afforded to desired chiral product with 92% isolated yield and 84% ee in 4 h as a yellow oil. Optical rotation was determined as $[\alpha]_D^{21} = -46.48$ (c 1.0, CH_2Cl_2). ^1H NMR (400 MHz, CDCl_3) δ 7.96 (d, $J = 8.9$ Hz, 1H), 7.94 – 7.86 (m, 1H), 7.61 (d, $J = 8.0$ Hz, 2H), 7.48 (d, $J = 8.9$ Hz, 1H), 7.42 – 7.38 (m, 2H), 7.35 – 7.30 (m, 3H), 6.08 (d, $J = 1.8$ Hz, 1H), 5.39 (d, $J = 1.7$ Hz, 1H). ^{13}C NMR (101 MHz, CDCl_3) δ 156.4, 141.8, 132.0, 131.0, 130.8 (q, $^2J_{\text{CF}} = 32.7$ Hz), 129.3, 129.2, 128.1, 128.0, 126.5 (q, $^4J_{\text{CF}} = 3.7$ Hz), 126.4, 124.8, 123.8 (q, $^1J_{\text{CF}} = 272.3$ Hz), 122.7, 117.4, 111.9 (q, $^3J_{\text{CF}} = 7.9$ Hz), 54.9. Chiralpak ODH column, 90:10 (n-hexane/*i*-PrOH), flow rate 1.0 mL/min, 220 nm, temp=25 °C, $t_{\text{minor}} = 7.620$ min, $t_{\text{major}} = 9.274$ min. IR(neat): 2924, 1813, 1710, 1620, 1588, 1523, 1462, 1412, 1323, 1236, 1167, 1125, 1088, 1017 cm^{-1} . MS (MALDI-TOF) m/z : $[\text{M}-\text{NO}_2]^+$ Calcd. for $\text{C}_{19}\text{H}_{12}\text{F}_3\text{O}$ 313.084; Found 313.195.

3.3.16 (1*R*,2*R*)-1-(2-(benzyloxy)phenyl)-2-nitro-1,2-dihydronaphtho[2,1-*b*]furan (23aq)



General procedure starting from **20q** and **21a** afforded to desired chiral product with quantitative yield and >99% ee in 8 h as a pink oil. Optical rotation was determined as $[\alpha]_D^{21} = -120.66$ (*c* 0.5, CH₂Cl₂). ¹H NMR (400 MHz, CDCl₃) δ 7.83 – 7.67 (m, 2H), 7.38 – 7.33 (m, 2H), 7.33 – 7.29 (m, 2H), 7.29 – 7.23 (m, 5H), 7.16 – 7.08 (m, 1H), 6.95 (dd, *J* = 8.3, 1.1 Hz, 1H), 6.69 (td, *J* = 7.5, 1.1 Hz, 1H), 6.60 (dd, *J* = 7.7, 1.7 Hz, 1H), 6.08 (d, *J* = 1.9 Hz, 1H), 5.66 (d, *J* = 1.9 Hz, 1H), 5.12 (d, *J* = 1.8 Hz, 2H). ¹³C NMR (101 MHz, CDCl₃) δ 156.5, 155.8, 136.4, 131.0, 130.8, 129.8, 129.6, 129.0, 128.9, 128.7, 128.3, 127.7, 127.5, 126.2, 124.3, 123.2, 121.3, 118.5, 112.6, 112.4, 111.8, 70.6, 49.1. Chiralpak ODH column, 90:10 (n-hexane/*i*-PrOH), flow rate 1.0 mL/min, 230 nm, temp=25 °C, *t*_{minor}= 9.756 min, *t*_{major}= 13.521 min. IR(neat): 3033, 2923, 1634, 1598, 1562, 1523, 1489, 1452, 1375, 1304, 1243, 1163, 1105, 1052, 1006 cm⁻¹. MS (MALDI-TOF) *m/z*: [M-HNO₂]⁺ Calcd. for C₂₅H₁₈O₂ 350.131; Found 350.253.

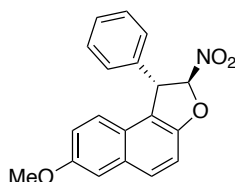
3.3.17 (1*R*,2*R*)-7-bromo-2-nitro-1-phenyl-1,2-dihydronaphtho[2,1-*b*]furan (23ba)



General procedure starting from **20a** and **21b** afforded to desired chiral product with 92% isolated yield and 83% ee in 3.5 h as a white solid. M.p.= 99 °C Optical rotation

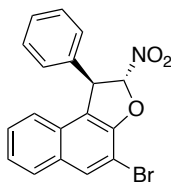
was determined as $[\alpha]_D^{24} = -51.72$ (c 1.0, CH_2Cl_2). ^1H NMR (400 MHz, CDCl_3) δ 8.03 (d, $J = 2.0$ Hz, 1H), 7.82 (d, $J = 8.9$ Hz, 1H), 7.47 (d, $J = 8.9$ Hz, 1H), 7.43 (dd, $J = 8.9, 2.0$ Hz, 1H), 7.39 – 7.30 (m, 3H), 7.23 (d, $J = 8.9$ Hz, 1H), 7.20 – 7.13 (m, 2H), 6.11 (d, $J = 1.8$ Hz, 1H), 5.30 (d, $J = 1.9$ Hz, 1H). ^{13}C NMR (101 MHz, CDCl_3) δ 156.4, 137.5, 131.8, 130.9, 130.9, 130.5, 129.4, 128.5, 128.0, 127.4, 124.5, 118.6, 118.1, 112.8, 112.2, 55.1. Chiralpak ODH column, 90:10 (n-hexane/i-PrOH), flow rate 1.0 mL/min, 220 nm, temp=25 °C, $t_{\text{minor}} = 6.771$ min, $t_{\text{major}} = 10.093$ min.

3.3.18 (1*S*,2*S*)-7-methoxy-2-nitro-1-phenyl-1,2-dihydro-*naphtho*[2,1-*b*]furan (23ca)



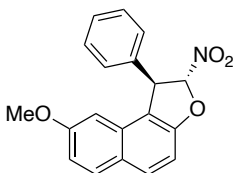
General procedure starting from **20a** and **21c** afforded to desired chiral product with 89% isolated yield and -81% ee in 3.5 h as a white solid. M.p.= 111 °C Optical rotation was determined as $[\alpha]_D^{24} = +1.84$ (c 1.0, CH_2Cl_2). ^1H NMR (400 MHz, CDCl_3) δ 7.83 (d, $J = 8.9$ Hz, 1H), 7.44 (d, $J = 8.9$ Hz, 1H), 7.42 – 7.33 (m, 3H), 7.30 (d, $J = 9.1$ Hz, 1H), 7.21 (dd, $J = 7.5, 2.1$ Hz, 3H), 7.09 (dd, $J = 9.0, 2.5$ Hz, 1H), 6.11 (d, $J = 1.8$ Hz, 1H), 5.33 (d, $J = 1.8$ Hz, 1H), 3.90 (s, 3H). ^{13}C NMR (101 MHz, CDCl_3) δ 156.5, 154.6, 137.9, 131.9, 129.8, 129.3, 128.3, 127.4, 124.8, 124.3, 120.4, 118.4, 112.4, 112.0, 107.1, 55.4, 55.2. Chiralpak ODH column, 90:10 (n-hexane/i-PrOH), flow rate 1.0 mL/min, 230 nm, temp=25 °C, $t_{\text{minor}} = 7.412$ min, $t_{\text{major}} = 9.183$ min. IR(neat): 2933, 2834, 2375, 2321, 1609, 1562, 1518, 1494, 1472, 1452, 1364, 1264, 1235, 1211, 1181, 1145, 1133, 1085, 1052, 1024 cm^{-1} . MS (MALDI-TOF) m/z : $[\text{M}-\text{H}_2\text{NO}_2]^+$ Calcd. for $\text{C}_{19}\text{H}_{13}\text{O}_2$ 273.092; Found 273.418.

3.3.19 (1*R*,2*R*)-4-bromo-2-nitro-1-phenyl-1,2-dihydronaphtho[2,1-*b*]furan (23da)



General procedure starting from **20a** and **21d** afforded to desired chiral product with 83% isolated yield and 55% ee in 4 h as a white solid. M.p.= 148 °C Optical rotation was determined as $[\alpha]_D^{24} = -23.18$ (*c* 0.5, CH₂Cl₂). ¹H NMR (400 MHz, CDCl₃) δ 8.14 (s, 1H), 7.91 – 7.74 (m, 1H), 7.49 – 7.32 (m, 6H), 7.27 – 7.09 (m, 2H), 6.19 (d, *J* = 1.9 Hz, 1H), 5.42 (d, *J* = 1.9 Hz, 1H). ¹³C NMR (101 MHz, CDCl₃) δ 153.2, 137.1, 133.2, 131.8, 129.4, 128.6, 128.4, 128.1, 127.8, 127.4, 125.4, 123.0, 119.7, 111.6, 104.1, 56.2. Chiralpak ODH column, 90:10 (n-hexane/*i*-PrOH), flow rate 1.0 mL/min, 220 nm, temp=25 °C, *t*_{minor}= 7.804 min, *t*_{major}= 12.983 min.

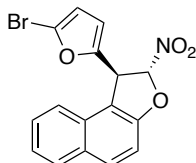
3.3.20 (1*R*,2*R*)-8-methoxy-2-nitro-1-phenyl-1,2-dihydronaphtho[2,1-*b*]furan (23ea)



General procedure starting from **20a** and **21e** afforded to desired chiral product with 90% isolated yield and 77% ee in 2 h as a white solid. M.p.= 94 °C Optical rotation was determined as $[\alpha]_D^{24} = -36.88$ (*c* 0.25, CH₂Cl₂). ¹H NMR (400 MHz, CDCl₃) δ 7.82 (dd, *J* = 25.0, 8.9 Hz, 2H), 7.43 – 7.29 (m, 4H), 7.27 – 7.20 (m, 2H), 7.04 (dd, *J* = 9.1, 2.5 Hz, 1H), 6.62 (d, *J* = 2.5 Hz, 1H), 6.15 (t, *J* = 1.5 Hz, 1H), 5.29 (s, 1H), 3.71 (s, 3H). ¹³C NMR (101 MHz, CDCl₃) δ 158.8, 156.6, 137.6, 131.0, 130.9, 130.5, 129.3, 128.3, 127.4, 126.1, 117.3, 116.9, 112.4, 109.0, 101.4, 55.2, 55.1. Chiralpak

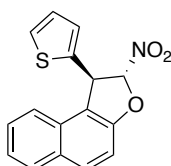
ODH column, 90:10 (n-hexane/i-PrOH), flow rate 1.0 mL/min, 220 nm, temp=25 °C, $t_{\text{minor}}=7.001$ min, $t_{\text{major}}=10.125$ min.

3.3.21 (1*S*,2*R*)-1-(5-bromofuran-2-yl)-2-nitro-1,2-dihydronaphtho[2,1-*b*]furan (23as)



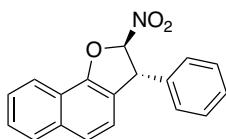
General procedure starting from **20s** and **21a** afforded to desired chiral product with 74% isolated yield and 70% ee in 2 h as a yellow semi-solid. Optical rotation was determined as $[\alpha]_D^{25} = -92.39^\circ$ (c 2.0, CH_2Cl_2). ^1H NMR (400 MHz, CDCl_3) δ 8.00 – 7.79 (m, 1H), 7.58 – 7.46 (m, 1H), 7.46 – 7.34 (m, 1H), 6.28 (d, $J = 1.6$ Hz, 1H), 6.22 (d, $J = 3.4$ Hz, 1H), 5.92 (dd, $J = 3.4, 0.9$ Hz, 1H), 5.40 (s, 1H). ^{13}C NMR (101 MHz, CDCl_3) δ 154.6, 150.0, 130.4, 129.2, 127.9, 127.5, 126.3, 123.1, 121.3, 121.1, 113.2, 110.9, 110.4, 109.9, 107.7, 47.2. Chiralpak ODH column, 90:10 (n-hexane/i-PrOH), flow rate 1.0 mL/min, 230 nm, temp=25 °C, $t_{\text{minor}}=7.864$ min, $t_{\text{major}}=10.378$ min. IR(neat): 2921, 2850, 1767, 1714, 1627, 1572, 1523, 1461, 1353, 1264 cm^{-1} . HRMS (ESI-TOF) m/z : $[\text{M}+\text{H}_2]^+$ Calcd. for $\text{C}_{16}\text{H}_{12}\text{BrNO}_4$ 360.9950; Found 360.9680.

3.3.22 (1*R*,2*R*)-2-nitro-1-(thiophen-2-yl)-1,2-dihydronaphtho[2,1-*b*]furan (23at)



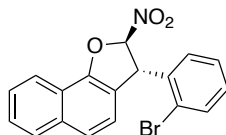
General procedure starting from **20t** and **21a** afforded to desired chiral product with 94% isolated yield and 80% ee in 4.5 h as a white solid. M.p.= 123 °C Optical rotation was determined as $[\alpha]_D^{25} = -52.02^\circ$ (c 1.0, CH_2Cl_2). ^1H NMR (400 MHz, CDCl_3) δ 7.96 (d, $J = 8.9$ Hz, 1H), 7.92 (dd, $J = 7.4, 1.7$ Hz, 1H), 7.57 – 7.49 (m, 1H), 7.49 – 7.37 (m, 3H), 7.32 – 7.25 (m, 1H), 6.99 (dd, $J = 5.1, 3.5$ Hz, 1H), 6.92 (dd, $J = 3.6, 1.1$ Hz, 1H), 6.19 (d, $J = 1.7$ Hz, 1H), 5.64 (d, $J = 1.7$ Hz, 1H). ^{13}C NMR (101 MHz, CDCl_3) δ 155.7, 140.6, 131.8, 130.8, 129.4, 129.0, 127.7, 127.4, 126.2, 126.1, 124.5, 122.8, 117.9, 112.0, 111.8, 50.2. Chiralpak ODH column, 90:10 (n-hexane/*i*-PrOH), flow rate 1.0 mL/min, 230 nm, temp=25 °C, $t_{\text{minor}} = 8.274$ min, $t_{\text{major}} = 10.390$ min. IR(neat): 2922, 2852, 1816, 1633, 1565, 1522, 1460, 1434, 1410, 1351, 1238, 1155, 1128, 1086, 1051 cm^{-1} . MS (MALDI-TOF) m/z : $[\text{M}-\text{HNO}_2]^+$ Calcd. for $\text{C}_{16}\text{H}_{10}\text{OS}$ 250.045; Found 250.457.

3.3.23 (2*R*,3*R*)-2-nitro-3-phenyl-2,3-dihydronaphtho[1,2-*b*]furan (60aa)



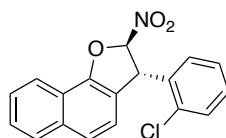
General procedure starting from **20a** and **59a** afforded to desired chiral product with 54% isolated yield and 30% ee in 2 h as a white solid. M.p.= 89-92 °C. Optical rotation was determined as $[\alpha]_D^{22} = -88.50$ (c 1.0, CH_2Cl_2). ^1H NMR (400 MHz, CDCl_3) δ 8.13 – 8.06 (m, 1H), 7.87 – 7.79 (m, 1H), 7.58 – 7.45 (m, 3H), 7.35 – 7.21 (m, 8H), 7.21 – 7.13 (m, 1H), 7.10 (dd, $J = 7.6, 1.9$ Hz, 2H), 6.13 (d, $J = 2.0$ Hz, 1H), 5.04 (d, $J = 1.9$ Hz, 1H). ^{13}C NMR (101 MHz, CDCl_3) δ 153.8, 138.7, 134.7, 129.3, 128.4, 128.1, 127.6, 127.0, 126.7, 124.0, 121.8, 121.4, 120.4, 119.9, 112.2, 56.6. Chiralpak ODH column, 90:10 (n-hexane/*i*-PrOH), flow rate 1.0 mL/min, 220 nm, temp=25 °C, $t_{\text{minor}} = 7.754$ min, $t_{\text{major}} = 8.846$ min.

3.3.24 (2*R*,3*S*)-3-(2-bromophenyl)-2-nitro-2,3-dihydronaphtho[1,2-*b*]furan (60ab)



General procedure starting from **59a** and **20b** afforded to desired chiral product with 43% isolated yield and 37% ee in 3 h as a white solid. M.p.= 104-108 °C Optical rotation was determined as $[\alpha]_D^{25} = -43.26$ (*c* 1.0, CH₂Cl₂). ¹H NMR (400 MHz, CDCl₃) δ 8.20 – 8.11 (m, 1H), 7.95 – 7.87 (m, 1H), 7.74 – 7.65 (m, 1H), 7.66 – 7.53 (m, 3H), 7.28 (d, *J* = 8.4 Hz, 1H), 7.22 – 7.13 (m, 2H), 6.71 (dd, *J* = 5.8, 3.7 Hz, 1H), 6.23 (d, *J* = 1.7 Hz, 1H), 5.68 (d, *J* = 1.4 Hz, 1H). ¹³C NMR (101 MHz, CDCl₃) δ 153.9, 137.8, 134.7, 133.4, 129.8, 129.1, 128.1, 128.0, 126.9, 126.6, 124.0, 123.8, 121.4, 121.2, 120.2, 119.8, 111.6, 54.8. Chiralpak ODH column, 90:10 (n-hexane/*i*-PrOH), flow rate 1.0 mL/min, 220 nm, temp=25 °C, *t*_{minor}= 8.218 min, *t*_{major}= 9.393 min. IR(neat): 3058, 2917, 2849, 1666, 1553, 1465, 1440, 1361, 1263, 1156, 1066, 1024 cm⁻¹. MS (MALDI-TOF) *m/z*: [M-HNO₂]⁺ Calcd. for C₁₈H₁₁BrO 321.999; Found 321.878.

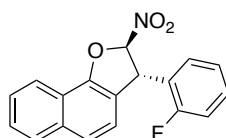
3.3.25 (2*R*,3*S*)-3-(2-bromophenyl)-2-nitro-2,3-dihydronaphtho[1,2-*b*]furan (60ac)



General procedure starting from **59a** and **20c** afforded to desired chiral product with 52% isolated yield and 29% ee in 3.5 h as a yellow solid. M.p.= 84 °C. Optical rotation was determined as $[\alpha]_D^{21} = -2.66$ (*c* 2.0, CH₂Cl₂). ¹H NMR (400 MHz, CDCl₃) δ 8.29 – 8.10 (m, 1H), 8.02 – 7.90 (m, 1H), 7.72 – 7.56 (m, 3H), 7.54 (dd, *J* = 8.0, 1.3 Hz, 1H), 7.35 – 7.25 (m, 2H), 7.16 (td, *J* = 7.6, 1.4 Hz, 1H), 6.75 (dd, *J* =

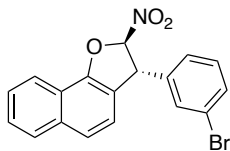
7.8, 1.7 Hz, 1H), 6.27 (d, $J = 1.7$ Hz, 1H), 5.69 (d, $J = 1.8$ Hz, 1H). ^{13}C NMR (101 MHz, CDCl_3) δ 154.0, 135.9, 134.7, 133.5, 130.1, 129.6, 129.0, 128.0, 127.5, 127.0, 126.7, 124.0, 121.5, 121.2, 120.2, 119.4, 111.4, 52.5. Chiralpak OJH column, 90:10 (n-hexane/*i*-PrOH), flow rate 1.0 mL/min, 230 nm, temp=25 °C, $t_{\text{minor}} = 17.516$ min, $t_{\text{major}} = 13.211$ min. IR(neat): 3059, 2961, 1666, 1563, 1468, 1442, 1381, 1259, 1157, 1088, 1054, 1020 cm^{-1} . MS (MALDI-TOF) m/z : $[\text{M}-\text{HNO}_2]^+$ Calcd. for $\text{C}_{18}\text{H}_{11}\text{ClO}$ 278.050; Found 278.243.

3.3.26 (2*R*,3*S*)-3-(2-fluorophenyl)-2-nitro-2,3-dihydronaphtho[1,2-*b*]furan (60ad)



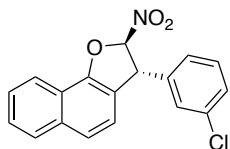
General procedure starting from **59a** and **20d** afforded to desired chiral product with 68% isolated yield and 57% ee in 220 min as a white solid. M.p.= 135.5 °C Optical rotation was determined as $[\alpha]_D^{25} = -32.38$ (c 0.5, CH_2Cl_2). ^1H NMR (400 MHz, CDCl_3) δ 8.08 (dd, $J = 8.0, 1.4$ Hz, 1H), 7.85 – 7.79 (m, 1H), 7.57 – 7.49 (m, 3H), 7.24 (tdd, $J = 7.3, 5.3, 1.7$ Hz, 1H), 7.20 – 7.14 (m, 1H), 7.10 (ddd, $J = 9.8, 8.3, 1.3$ Hz, 1H), 6.97 (td, $J = 7.6, 1.3$ Hz, 1H), 6.75 (td, $J = 7.6, 1.8$ Hz, 1H), 6.20 (d, $J = 1.9$ Hz, 1H), 5.36 (d, $J = 1.9$ Hz, 1H). ^{13}C NMR (101 MHz, CDCl_3) δ 160.3 (d, $^1J_{\text{CF}} = 248.3$ Hz), 153.9, 134.8, 130.2 (d, $^3J_{\text{CF}} = 8.1$ Hz), 128.9 (d, $^4J_{\text{CF}} = 3.2$ Hz), 128.1, 126.9 (d, $^2J_{\text{CF}} = 32.0$ Hz), 125.7 (d, $^2J_{\text{CF}} = 14.2$ Hz), 124.8 (d, $^4J_{\text{CF}} = 3.7$ Hz), 123.5, 121.5 (d, $^2J_{\text{CF}} = 16.1$ Hz), 121.4, 120.4, 118.9, 116.1 (d, $^2J_{\text{CF}} = 21.3$ Hz), 111.4, 109.7, 49.5 (d, $^4J_{\text{CF}} = 3.4$ Hz). Chiralpak ODH column, 90:10 (n-hexane/*i*-PrOH), flow rate 1.0 mL/min, 220 nm, temp=25 °C, $t_{\text{minor}} = 7.735$ min, $t_{\text{major}} = 8.392$ min. IR(neat): 3058, 2914, 1667, 1568, 1490, 1457, 1364, 1264, 1230, 1090, 1054, 1020 cm^{-1} . MS (MALDI-TOF) m/z : $[\text{M}-\text{HNO}_2]^+$ Calcd. for $\text{C}_{18}\text{H}_{11}\text{FO}$ 262.079; Found 262.349.

3.3.27 (2*R*,3*R*)-3-(3-bromophenyl)-2-nitro-2,3-dihydronaphtho[1,2-*b*]furan (60ae)



General procedure starting from **59a** and **20e** afforded to desired chiral product with 40% isolated yield and 43% ee in 3 h as a white solid. M.p.= 89 °C. Optical rotation was determined as $[\alpha]_D^{25} = -24.46$ (*c* 0.5, CH₂Cl₂). ¹H NMR (400 MHz, CDCl₃) δ 8.25 – 8.15 (m, 1H), 7.94 (dd, *J* = 7.4, 1.7 Hz, 1H), 7.70 – 7.60 (m, 3H), 7.50 (dt, *J* = 7.9, 1.4 Hz, 1H), 7.34 (t, *J* = 1.9 Hz, 1H), 7.26 (td, *J* = 7.9, 7.3, 2.1 Hz, 2H), 7.18 – 7.12 (m, 1H), 6.20 (d, *J* = 1.9 Hz, 1H), 5.11 (d, *J* = 2.0 Hz, 1H). ¹³C NMR (101 MHz, CDCl₃) δ 153.8, 140.7, 134.7, 131.6, 130.8, 130.5, 128.0, 127.1, 126.7, 126.2, 124.1, 123.3, 121.4, 121.3, 120.2, 119.0, 111.6, 55.9. Chiralpak ODH column, 90:10 (n-hexane/*i*-PrOH), flow rate 1.0 mL/min, 230 nm, temp=25 °C, *t*_{minor}= 9.717 min, *t*_{major}= 11.692 min. IR(neat): 3059, 2918, 2850, 1809, 1667, 1565, 1472, 1363, 1259, 1090, 1055 cm⁻¹. MS (MALDI-TOF) *m/z*: [M-HNO₂]⁺ Calcd. for C₁₈H₁₁BrO 321.999; Found 321.756.

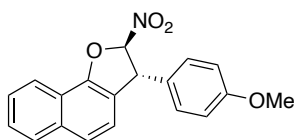
3.3.28 (2*R*,3*R*)-3-(3-chlorophenyl)-2-nitro-2,3-dihydronaphtho[1,2-*b*]furan (60af)



General procedure starting from **59a** and **20f** afforded to desired chiral product with 64% isolated yield and 40% ee in 2 h as a yellow semi-solid. Optical rotation was determined as $[\alpha]_D^{22} = -12.16$ (*c* 1.0, CH₂Cl₂). ¹H NMR (400 MHz, CDCl₃) δ 8.21 (dd, *J* = 8.0, 1.6 Hz, 1H), 8.00 – 7.89 (m, 1H), 7.70 – 7.55 (m, 3H), 7.40 – 7.31 (m,

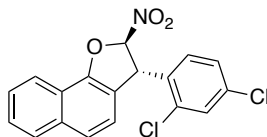
2H), 7.29 (d, $J = 6.0$ Hz, 1H), 7.17 (d, $J = 2.1$ Hz, 1H), 7.13 (dt, $J = 6.2, 2.1$ Hz, 1H), 6.21 (d, $J = 1.9$ Hz, 1H), 5.13 (d, $J = 1.9$ Hz, 1H). ^{13}C NMR (101 MHz, CDCl_3) δ 153.8, 140.4, 135.2, 134.7, 130.5, 128.6, 128.0, 127.6, 127.1, 126.7, 125.7, 124.1, 121.4, 121.3, 120.2, 119.0, 111.6, 55.9. Chiralpak ODH column, 90:10 (n-hexane/*i*-PrOH), flow rate 1.0 mL/min, 230 nm, temp=25 °C, $t_{\text{minor}} = 9.309$ min, $t_{\text{major}} = 10.768$ min. IR(neat): 3059, 2915, 1812, 1743, 1667, 1596, 1564, 1518, 1475, 1432, 1363, 1318, 1263, 1156, 1090, 1054, 1020 cm^{-1} . MS (MALDI-TOF) m/z : $[\text{M}-\text{HNO}_2]^+$ Calcd. for $\text{C}_{18}\text{H}_{11}\text{ClO}$ 278.050; Found 278.312.

3.3.29 (2*S*,3*S*)-3-(4-methoxyphenyl)-2-nitro-2,3-dihydronaphtho[1,2-*b*]furan (60ag)



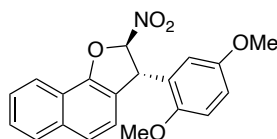
General procedure starting from **59a** and **20g** afforded to desired chiral product with 35% isolated yield and 55% ee in 3 h as a yellow oil. Optical rotation was determined as $[\alpha]_D^{21} = -55.94$ (c 1.0, CH_2Cl_2). ^1H NMR (400 MHz, CDCl_3) δ 8.17 (d, $J = 8.1$ Hz, 1H), 7.90 (d, $J = 8.5$ Hz, 1H), 7.66 – 7.46 (m, 3H), 7.23 (d, $J = 8.2$ Hz, 1H), 7.08 (d, $J = 8.7$ Hz, 2H), 6.87 (d, $J = 8.7$ Hz, 2H), 6.16 (d, $J = 2.0$ Hz, 1H), 5.07 (d, $J = 2.0$ Hz, 1H), 3.79 (s, 3H). ^{13}C NMR (101 MHz, CDCl_3) δ 159.5, 153.5, 134.5, 130.7, 128.6, 128.0, 126.8, 126.5, 123.8, 121.6, 121.2, 120.2, 120.1, 114.5, 112.3, 55.8, 55.2. Chiralpak ODH column, 90:10 (n-hexane/*i*-PrOH), flow rate 1.0 mL/min, 220 nm, temp=25 °C, $t_{\text{minor}} = 13.427$ min, $t_{\text{major}} = 12.335$ min. IR(neat): 2922, 2838, 1810, 1600, 1564, 1511, 1461, 1367, 1252, 1176, 1088, 1054, 1031 cm^{-1} . MS (MALDI-TOF) m/z : $[\text{M}-\text{HNO}_2]^+$ Calcd. for $\text{C}_{19}\text{H}_{14}\text{O}_2$ 274.099; Found 274.449.

3.3.30 (2*R*,3*S*)-3-(2,4-dichlorophenyl)-2-nitro-2,3-dihydronaphtho[1,2-*b*]furan (60ah)



General procedure starting from **59a** and **20h** afforded to desired chiral product with 54% isolated yield and 31% ee in 5 h as a white solid. M.p.= 104 °C. Optical rotation was determined as $[\alpha]_D^{21} = -49.21$ (*c* 1.5, CH₂Cl₂). ¹H NMR (400 MHz, CDCl₃) δ 8.18 (dd, *J* = 7.5, 1.9 Hz, 1H), 8.01 – 7.85 (m, 1H), 7.70 – 7.59 (m, 3H), 7.56 (d, *J* = 2.2 Hz, 1H), 7.26 (d, *J* = 8.4 Hz, 1H), 7.14 (dd, *J* = 8.4, 2.2 Hz, 1H), 6.67 (d, *J* = 8.4 Hz, 1H), 6.21 (d, *J* = 1.8 Hz, 1H), 5.63 (d, *J* = 1.7 Hz, 1H). ¹³C NMR (101 MHz, CDCl₃) δ 154.0, 134.9, 134.7, 134.5, 134.2, 129.9, 129.9, 128.0, 127.8, 127.1, 126.8, 124.2, 121.3, 121.3, 120.2, 118.8, 111.1, 52.0. Chiralpak ODH column, 90:10 (n-hexane/*i*-PrOH), flow rate 1.0 mL/min, 230 nm, temp=25 °C, *t*_{minor}= 6.159 min, *t*_{major}= 7.933 min. IR(neat): 2923, 2854, 1567, 1511, 1469, 1382, 1259, 1088 cm⁻¹. MS (MALDI-TOF) *m/z*: [M-NO₂]⁺ Calcd. for C₁₈H₁₁Cl₂O 313.019; Found 313.282.

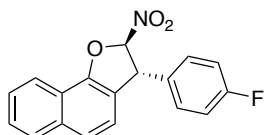
3.3.31 (2*R*,3*R*)-3-(2,5-dimethoxyphenyl)-2-nitro-2,3-dihydronaphtho[1,2-*b*]furan (60ai)



General procedure starting from **59a** and **20i** afforded to desired chiral product with 40% isolated yield and 71% ee in 5 h as a yellow semi-solid. Optical rotation was determined as $[\alpha]_D^{22} = -10.20$ (*c* 1.0, CH₂Cl₂). ¹H NMR (400 MHz, CDCl₃) δ 8.18 – 8.11 (m, 1H), 7.96 – 7.90 (m, 1H), 7.53 (t, *J* = 2.8 Hz, 2H), 7.47 (d, *J* = 8.2 Hz, 1H), 7.36 – 7.32 (m, 2H), 6.89 – 6.83 (m, 2H), 6.29 (d, *J* = 2.0 Hz, 1H), 5.50 (d, *J* = 2.1 Hz, 1H), 3.90 (d, *J* = 1.4 Hz, 3H), 3.67 (d, *J* = 1.4 Hz, 3H). ¹³C NMR (101 MHz,

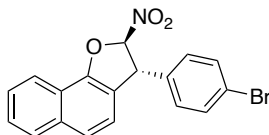
CDCl₃) δ 151.4, 134.6, 128.0, 127.6, 126.7, 126.4, 126.3, 125.8, 125.1, 124.3, 123.5, 122.0, 121.5, 121.2, 120.5, 115.1, 112.3, 108.5, 56.0, 55.6, 50.2. Chiralpak ODH column, 90:10 (n-hexane/*i*-PrOH), flow rate 1.0 mL/min, 230 nm, temp=25 °C, t_{minor} = 6.669 min, t_{major} = 5.788 min. IR(neat): 3059, 2924, 2835, 1664, 1609, 1591, 1564, 1498, 1462, 1378, 1331, 1299, 1270, 1223, 1179, 1156, 1116, 1048, 1024 cm⁻¹. MS (MALDI-TOF) m/z : [M-HNO₂]⁺ Calcd. for C₂₀H₁₆O₃ 304.110; Found 304.400.

3.3.32 (2*R*,3*R*)-3-(4-fluorophenyl)-2-nitro-2,3-dihydronaphtho[1,2-*b*]furan (60aj)



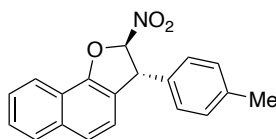
General procedure starting from **59a** and **20j** afforded to desired chiral product with 56% isolated yield and 55% ee in 80 min as a white solid. M.p.= 80 °C. Optical rotation was determined as $[\alpha]_D^{22} = -18.74$ (c 1.0, CH₂Cl₂). ¹H NMR (400 MHz, CDCl₃) δ 8.09 (d, J = 8.0 Hz, 1H), 7.84 (d, J = 7.7 Hz, 1H), 7.58 – 7.45 (m, 3H), 7.41 (dd, J = 8.6, 2.5 Hz, 2H), 7.14 (d, J = 8.4 Hz, 1H), 6.97 (dd, J = 8.5, 2.5 Hz, 2H), 6.07 (d, J = 2.1 Hz, 1H), 5.00 (d, J = 2.2 Hz, 1H). ¹³C NMR (101 MHz, CDCl₃) (3 overlapped signals) δ 153.8, 136.2 (d, $^1J_{CF}$ = 291.5 Hz), 132.5, 129.3, 128.1, 127.0 (d, $^2J_{CF}$ = 33.0 Hz), 124.2, 122.6, 121.5 (d, $^3J_{CF}$ = 10.3 Hz), 120.3, 119.3, 111.8, 56.0. Chiralpak ODH column, 90:10 (n-hexane/*i*-PrOH), flow rate 1.0 mL/min, 230 nm, temp=25 °C, t_{minor} = 7.617 min, t_{major} = 10.055 min. IR(neat): 2922, 2845, 1635, 1603, 1565, 1506, 1456, 1427, 1354, 1297, 1219, 1201, 1171, 1142, 1077, 1042 cm⁻¹. MS (MALDI-TOF) m/z : [M-H₂NO₂]⁺ Calcd. for C₁₈H₁₀OF 261.072; Found 261.439.

3.3.33 (2*R*,3*R*)-3-(4-bromophenyl)-2-nitro-2,3-dihydronaphtho[1,2-*b*]furan (60ak)



General procedure starting from **59a** and **20k** afforded to desired chiral product with 33% isolated yield and 49% ee in 4 h as a white solid. M.p.= 94 °C. Optical rotation was determined as $[\alpha]_D^{22} = -86.0$ (*c* 0.9, CH₂Cl₂). ¹H NMR (400 MHz, CDCl₃) δ 8.12 – 8.05 (m, 1H), 7.85 – 7.76 (m, 1H), 7.59 – 7.46 (m, 3H), 7.21 – 7.12 (m, 2H), 7.10 – 7.02 (m, 2H), 6.97 (d, *J* = 8.5 Hz, 1H), 6.07 (d, *J* = 1.9 Hz, 1H), 5.02 (d, *J* = 1.9 Hz, 1H). ¹³C NMR (101 MHz, CDCl₃) δ 153.8, 134.7, 129.4, 129.3, 128.1, 127.1, 126.8, 124.1, 121.6, 121.4, 120.3, 119.7, 116.4, 116.2, 112.0, 55.8. Chiralpak ODH column, 90:10 (n-hexane/*i*-PrOH), flow rate 1.0 mL/min, 230 nm, temp=25 °C, *t*_{minor}= 8.774 min, *t*_{major}= 10.618 min. IR(neat): 3058, 2921, 1738, 1564, 1518, 1487, 1363, 1260, 1156, 1090, 1071, 1056, 1011 cm⁻¹. MS (MALDI-TOF) *m/z*: [M-HNO₂]⁺ Calcd. for C₁₈H₁₁BrO 321.999; Found 322.071.

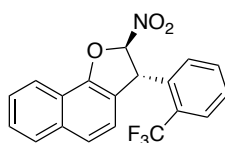
3.3.34 (2*R*,3*R*)-2-nitro-3-(*p*-tolyl)-2,3-dihydronaphtho[1,2-*b*]furan (60al)



General procedure starting from **59a** and **20l** afforded to desired chiral product with quantitative yield and 92% ee in 4 h as a white solid. M.p.= 80 °C. Optical rotation was determined as $[\alpha]_D^{21} = -55.55$ (*c* 0.7, CH₂Cl₂). ¹H NMR (400 MHz, CDCl₃) δ 8.20 (d, *J* = 8.0 Hz, 1H), 8.04 – 7.87 (m, 1H), 7.71 – 7.52 (m, 3H), 7.28 (d, *J* = 5.5 Hz, 1H), 7.22 – 7.16 (m, 2H), 7.08 (d, *J* = 7.8 Hz, 2H), 6.21 (d, *J* = 2.0 Hz, 1H), 5.10 (d, *J* = 2.0 Hz, 1H), 2.37 (s, 3H). ¹³C NMR (101 MHz, CDCl₃) δ 153.6, 138.2, 135.7, 134.5, 129.8, 128.0, 127.3, 126.8, 126.5, 123.8, 121.7, 121.3, 120.2, 120.0, 112.3,

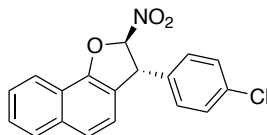
56.1, 21.0. Chiralpak ODH column, 90:10 (n-hexane/*i*-PrOH), flow rate 1.0 mL/min, 230 nm, temp=25 °C, $t_{\text{minor}}=7.656$ min, $t_{\text{major}}=8.818$ min. IR(neat): 2922, 2856, 1599, 1564, 1514, 1444, 1365, 1319, 1267, 1177, 1089, 1055, 1020 cm^{-1} . MS (MALDI-TOF) m/z : $[\text{M}-\text{NO}_2]^+$ Calcd. for $\text{C}_{19}\text{H}_{15}\text{O}$ 259.112; Found 259.490.

3.3.35 (2*R*,3*R*)-2-nitro-3-(2-(trifluoromethyl)phenyl)-2,3-dihydronaphtho[1,2-*b*]furan (60an)



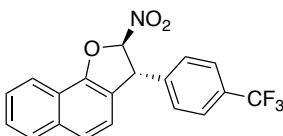
General procedure starting from **59a** and **20n** afforded to desired chiral product with 57% isolated yield and 33% ee in 3.5 h as a white solid. M.p.= 103-107 °C. Optical rotation was determined as $[\alpha]_D^{21} = -79.06$ (c 1.9, CH_2Cl_2). ^1H NMR (400 MHz, CDCl_3) δ 8.10 (d, $J = 8.0$ Hz, 1H), 7.81 (d, $J = 8.1$ Hz, 1H), 7.69 (td, $J = 6.6, 5.8, 2.5$ Hz, 2H), 7.60 (d, $J = 7.5$ Hz, 1H), 7.56 – 7.50 (m, 2H), 7.48 (d, $J = 8.2$ Hz, 1H), 7.37 – 7.32 (m, 2H), 7.10 (d, $J = 8.3$ Hz, 1H), 7.00 – 6.76 (m, 1H), 6.18 (d, $J = 1.7$ Hz, 1H), 5.45 (s, 1H). ^{13}C NMR (101 MHz, CDCl_3) δ 153.6, 134.8, 133.9, 133.1, 132.1, 130.5, 130.1, 129.4, 128.3 (q, $^2J_{\text{CF}} = 23.4$ Hz), 127.0 (q, $^2J_{\text{CF}} = 32.1$ Hz), 126.9, 126.4 (q, $^3J_{\text{CF}} = 7.1$ Hz), 126.2 (q, $^3J_{\text{CF}} = 5.2$ Hz), 122.9 (q, $^1J_{\text{CF}} = 296.7$ Hz), 121.3, 121.3 (q, $^2J_{\text{CF}} = 13.8$ Hz), 120.3, 111.9, 51.4. Chiralpak ODH column, 90:10 (n-hexane/*i*-PrOH), flow rate 1.0 mL/min, 220 nm, temp=25 °C, $t_{\text{minor}}=5.451$ min, $t_{\text{major}}=6.868$ min. IR(neat): 3070, 1739, 1566, 1518, 1497, 1453, 1365, 1312, 1261, 1159, 1109, 1087, 1062, 1036 cm^{-1} . MS (MALDI-TOF) m/z : $[\text{M}-\text{NO}_2]^+$ Calcd. for $\text{C}_{19}\text{H}_{11}\text{F}_3\text{O}$ 312.076; Found 312.313.

3.3.36 (2*R*,3*R*)-3-(4-chlorophenyl)-2-nitro-2,3-dihydronaphtho[1,2-*b*]furan (60ao)



General procedure starting from **59a** and **20o** afforded to desired chiral product with 48% isolated yield and 37% ee in 3.5 h as a white solid. M.p.= 98 °C. Optical rotation was determined as $[\alpha]_D^{22} = -99.24$ (*c* 0.9, CH₂Cl₂). ¹H NMR (400 MHz, CDCl₃) δ 8.17 (d, *J* = 7.9 Hz, 1H), 7.91 (d, *J* = 7.5 Hz, 1H), 7.75 – 7.49 (m, 3H), 7.33 (d, *J* = 8.2 Hz, 2H), 7.22 (d, *J* = 8.3 Hz, 1H), 7.11 (d, *J* = 8.2 Hz, 2H), 6.15 (d, *J* = 1.9 Hz, 1H), 5.10 (d, *J* = 2.0 Hz, 1H). ¹³C NMR (101 MHz, CDCl₃) δ 153.7, 137.0, 134.6, 134.4, 129.4, 128.8, 128.0, 127.0, 126.7, 124.0, 121.4, 121.3, 120.2, 119.3, 111.8, 55.8. Chiralpak ODH column, 90:10 (n-hexane/*i*-PrOH), flow rate 1.0 mL/min, 220 nm, temp=25 °C, *t*_{minor}= 7.089 min, *t*_{major}= 8.381 min. IR(neat): 3058, 2919, 1597, 1565, 1518, 1489, 1443, 1363, 1265, 1089, 1055, 1015 cm⁻¹. MS (MALDI-TOF) *m/z*: [M-HNO₂]⁺ Calcd. for C₁₈H₁₁ClO 278.050; Found 278.334.

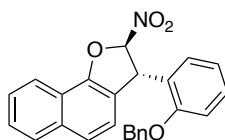
3.3.37 (2*R*,3*R*)-2-nitro-3-(4-(trifluoromethyl)phenyl)-2,3-dihydronaphtho[1,2-*b*]furan (60ap)



General procedure starting from **59a** and **20p** afforded to desired chiral product with 63% isolated yield and 67% ee in 140 min as a white solid. M.p.= 80 °C. Optical rotation was determined as $[\alpha]_D^{22} = -30.80$ (*c* 2.0, CH₂Cl₂). ¹H NMR (400 MHz, CDCl₃) δ 8.10 (d, *J* = 7.4 Hz, 1H), 7.84 (d, *J* = 7.4 Hz, 1H), 7.62 – 7.50 (m, 5H), 7.24 (m, 2H), 7.20 – 7.09 (m, 1H), 6.10 (d, *J* = 2.0 Hz, 1H), 5.10 (d, *J* = 1.9 Hz, 1H). ¹³C NMR (101 MHz, CDCl₃) δ 153.8, 142.4, 134.7, 131.9, 130.7 (q, ²*J*_{CF} = 30.1 Hz),

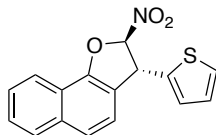
130.2, 128.0 (q, $^3J_{CF} = 6.9$ Hz), 127.1, 126.8, 126.2 (q, $^4J_{CF} = 3.4$ Hz), 124.2, 122.7 (q, $^1J_{CF} = 289.8$ Hz), 121.3 (q, $^4J_{CF} = 2.7$ Hz), 120.2, 118.9, 111.4, 56.0. Chiralpak ODH column, 90:10 (n-hexane/i-PrOH), flow rate 1.0 mL/min, 220 nm, temp=25 °C, $t_{\text{minor}} = 7.844$ min, $t_{\text{major}} = 9.517$ min. IR(neat): 2957, 2927, 2858, 1719, 1577, 1516, 1459, 1384, 1324, 1275, 1166, 1126, 1070, 1042, 1016 cm^{-1} . MS (MALDI-TOF) m/z: $[\text{M}-\text{NO}_2]^+$ Calcd. for $\text{C}_{19}\text{H}_{12}\text{OF}_3$ 313.084; Found 313.312.

3.3.38 (2*R*,3*R*)-3-(2-(benzyloxy)phenyl)-2-nitro-2,3-dihydronaphtho[1,2-*b*]furan (60aq)



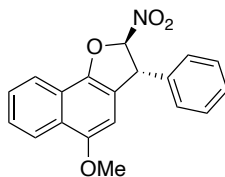
General procedure starting from **59a** and **20q** afforded to desired chiral product with 78% isolated yield and 92% ee in 3.5 h as a white solid. M.p.= 96 °C. Optical rotation was determined as $[\alpha]_D^{25} = -31.52$ (c 0.25, CH_2Cl_2). ^1H NMR (400 MHz, CDCl_3) δ 8.12 – 8.04 (m, 1H), 7.95 – 7.89 (m, 1H), 7.63 – 7.58 (m, 2H), 7.57 (dd, $J = 4.2, 2.4$ Hz, 1H), 7.46 (d, $J = 4.0$ Hz, 1H), 7.35 – 7.33 (m, 4H), 7.26 (d, $J = 8.3$ Hz, 1H), 7.08 (d, $J = 7.9$ Hz, 1H), 7.05 (d, $J = 8.0$ Hz, 1H), 6.89 (t, $J = 7.4$ Hz, 1H), 6.84 (dd, $J = 7.6, 1.8$ Hz, 1H), 6.33 (d, $J = 2.3$ Hz, 1H), 5.52 (d, $J = 2.3$ Hz, 1H), 5.17 (s, 2H). ^{13}C NMR (101 MHz, CDCl_3) δ 155.7, 134.0, 133.8, 131.1, 129.8, 129.4, 127.4, 127.1, 126.8, 126.6, 126.5, 126.4, 126.0, 126.0, 125.3, 125.1, 124.9, 118.9, 118.6, 117.7, 110.4, 68.5, 48.7. Chiralpak ODH column, 90:10 (n-hexane/i-PrOH), flow rate 1.0 mL/min, 230 nm, temp=25 °C, $t_{\text{minor}} = 7.838$ min, $t_{\text{major}} = 10.110$ min. IR(neat): 3034, 2921, 2853, 1598, 1565, 1533, 1481, 1451, 1380, 1302, 1245, 1164, 1113, 1051, 1020 cm^{-1} . MS (MALDI-TOF) m/z: $[\text{M}-\text{NO}_2]^+$ Calcd. for $\text{C}_{25}\text{H}_{18}\text{O}_2$ 350.131; Found 350.312.

3.3.39 (2R,3R)-2-nitro-3-(thiophen-2-yl)-2,3-dihydronaphtho[1,2-*b*]furan (60at)



General procedure starting from **59a** and **20t** afforded to desired chiral product with 50% isolated yield and 89% ee in 3 h as a yellow semi-solid. Optical rotation was determined as $[\alpha]_D^{25} = -39.60$ (*c* 0.1, CH₂Cl₂). ¹H NMR (400 MHz, CDCl₃) δ 8.18 (dd, *J* = 7.6, 1.8 Hz, 1H), 8.05 – 7.89 (m, 1H), 7.67 – 7.63 (m, 1H), 7.61 (dd, *J* = 7.2, 1.8 Hz, 1H), 7.37 (d, *J* = 8.3 Hz, 1H), 7.31 (dd, *J* = 5.1, 1.3 Hz, 1H), 7.30 – 7.27 (m, 1H), 7.02 (dd, *J* = 5.1, 3.5 Hz, 1H), 6.93 (dd, *J* = 3.6, 1.1 Hz, 1H), 6.28 (d, *J* = 1.9 Hz, 1H), 5.42 (d, *J* = 1.9 Hz, 1H). ¹³C NMR (101 MHz, CDCl₃) δ 153.5, 141.5, 134.7, 134.1, 128.0, 127.4, 127.0, 126.6, 126.0, 123.9, 121.4, 121.3, 120.2, 119.3, 111.8, 51.5. Chiralpak ODH column, 90:10 (n-hexane/*i*-PrOH), flow rate 1.0 mL/min, 230 nm, temp = 25 °C, *t*_{minor} = 8.502 min, *t*_{major} = 9.024 min. IR (neat): 2923, 2853, 1712, 1598, 1567, 1524, 1459, 1414, 1356, 1307, 1279, 1213, 1061, 1056 cm⁻¹. MS (MALDI-TOF) *m/z*: [M-NO₂]⁺ Calcd. for C₁₆H₁₁OS 251.053; Found 251.422.

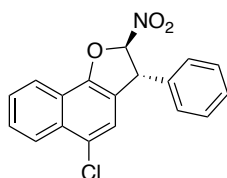
3.3.40 (2R,3R)-5-methoxy-2-nitro-3-phenyl-2,3-dihydronaphtho[1,2-*b*]furan (60ba)



General procedure starting from **59b** and **20a** afforded to desired chiral product with 43% isolated yield and 40% ee in 3 h as a blue solid. M.p. = 100-104 °C. Optical rotation was determined as $[\alpha]_D^{25} = -18.02$ (*c* 0.1, CH₂Cl₂). ¹H NMR (400 MHz, CDCl₃) δ 8.31 (d, *J* = 8.5 Hz, 1H), 8.13 (d, *J* = 8.1 Hz, 1H), 7.66 (ddd, *J* = 8.2, 6.8,

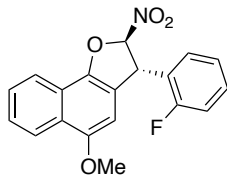
1.3 Hz, 1H), 7.59 (ddd, $J = 8.3, 6.9, 1.4$ Hz, 1H), 7.45 – 7.34 (m, 3H), 7.22 (dd, $J = 7.6, 1.9$ Hz, 2H), 6.59 (s, 1H), 6.16 (d, $J = 1.8$ Hz, 1H), 5.11 (d, $J = 1.8$ Hz, 1H), 3.93 (s, 3H). ^{13}C NMR (101 MHz, CDCl_3) δ 152.5, 147.2, 138.5, 135.0, 129.2, 128.3, 127.5, 127.2, 126.1, 122.8, 121.0, 120.7, 118.9, 112.2, 99.4, 57.1, 55.8. Chiralpak ODH column, 90:10 (n-hexane/i-PrOH), flow rate 1.0 mL/min, 230 nm, temp=25 °C, $t_{\text{minor}} = 7.332$ min, $t_{\text{major}} = 16.230$ min. IR(neat): 2924, 2854, 1667, 1563, 1495, 1460, 1430, 1403, 1379, 1366, 1257, 1222, 1161, 1115, 1091, 1026 cm^{-1} . MS (MALDI-TOF) m/z : $[\text{M}-\text{HNO}_2]^+$ Calcd. for $\text{C}_{16}\text{H}_{11}\text{OS}$ 274.099; Found 274.126.

3.3.41 (2*R*,3*R*)-5-chloro-2-nitro-3-phenyl-2,3-dihydronaphtho[1,2-*b*]furan (60ca)



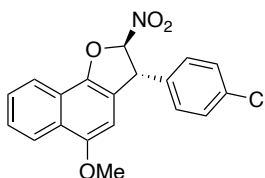
General procedure starting from **59c** and **20a** afforded to desired chiral product with 38% isolated yield and 37% ee in 21 h as a white solid. M.p.= 80 °C. Optical rotation was determined as $[\alpha]_D^{22} = -62.67$ (c 1.2, CH_2Cl_2). ^1H NMR (400 MHz, CDCl_3) δ 8.36 – 8.29 (m, 1H), 8.29 – 8.17 (m, 1H), 7.72 (qd, $J = 7.4, 3.6$ Hz, 2H), 7.47 – 7.34 (m, 4H), 7.20 (dd, $J = 7.4, 2.2$ Hz, 2H), 6.24 (d, $J = 2.0$ Hz, 1H), 5.12 (d, $J = 1.9$ Hz, 1H). ^{13}C NMR (101 MHz, CDCl_3) δ 152.7, 137.9, 131.4, 129.3, 128.6, 128.0, 127.4, 126.8, 125.0, 121.8, 120.9, 120.0, 111.9, 56.3 (overlapped peaks). Chiralpak ODH column, 90:10 (n-hexane/i-PrOH), flow rate 1.0 mL/min, 220 nm, temp=25 °C, $t_{\text{minor}} = 7.774$ min, $t_{\text{major}} = 12.874$ min. IR(neat): 3064, 3031, 1814, 1666, 1598, 1565, 1495, 1451, 1427, 1362, 1257, 1204, 1180, 1157, 1089, 1028 cm^{-1} . MS (MALDI-TOF) m/z : $[\text{M}-\text{NO}_2]^+$ Calcd. for $\text{C}_{18}\text{H}_{12}\text{OCl}$ 279.058; Found 279.121.

3.3.42 (2*R*,3*S*)-3-(2-fluorophenyl)-5-methoxy-2-nitro-2,3-dihydronaphtho[1,2-*b*]furan (60bd)



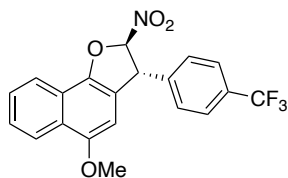
General procedure starting from **59b** and **20d** afforded to desired chiral product with 74% isolated yield and 55% ee in 50 min as a blue solid. M.p.= 106 °C. Optical rotation was determined as $[\alpha]_D^{25} = -12.54$ (*c* 0.1, CH₂Cl₂). ¹H NMR (400 MHz, CDCl₃) δ 8.30 (dd, *J* = 8.4, 1.2 Hz, 1H), 8.18 – 8.05 (m, 1H), 7.69 – 7.63 (m, 1H), 7.59 (ddd, *J* = 8.4, 6.9, 1.5 Hz, 1H), 7.35 (dt, *J* = 7.4, 1.6 Hz, 1H), 7.22 (ddd, *J* = 9.8, 8.3, 1.3 Hz, 1H), 7.08 (td, *J* = 7.6, 1.3 Hz, 1H), 6.87 (td, *J* = 7.6, 1.7 Hz, 1H), 6.59 (s, 1H), 6.23 (d, *J* = 1.7 Hz, 1H), 5.46 (d, *J* = 1.8 Hz, 1H), 3.94 (d, *J* = 1.3 Hz, 3H). ¹³C NMR (101 MHz, CDCl₃) δ 160.1 (d, ¹*J*_{CF} = 248.3 Hz), 152.6, 147.3, 130.1 (d, ³*J*_{CF} = 8.1 Hz), 128.8 (d, ⁴*J*_{CF} = 3.2 Hz), 127.2, 126.2, 125.5, 125.4, 124.7 (d, *J* = 3.7 Hz), 122.8, 121.0, 120.7, 117.9, 115.9 (d, ²*J*_{CF} = 21.3 Hz), 111.3, 99.2, 55.8, 49.8 (d, ⁴*J*_{CF} = 3.6 Hz). Chiralpak ODH column, 90:10 (n-hexane/*i*-PrOH), flow rate 1.0 mL/min, 230 nm, temp=25 °C, *t*_{minor}= 7.484 min, *t*_{major}= 17.418 min. IR(neat): 2937, 1665, 1564, 1489, 1459, 1430, 1403, 1379, 1364, 1256, 1220, 1161, 1115, 1069, 1026 cm⁻¹. MS (MALDI-TOF) *m/z*: [M-NO₂]⁺ Calcd. for C₁₉H₁₃O₂F 292.090; Found 292.363.

3.3.43 (2*R*,3*R*)-3-(4-chlorophenyl)-5-methoxy-2-nitro-2,3-dihydronaphtho[1,2-*b*]furan (60bo)



General procedure starting from **59b** and **20o** afforded to desired chiral product 84% isolated yield and 29% ee in **3** has a green solid. M.p.= 108-110 °C. Optical rotation was determined as $[\alpha]_D^{22} = -3.16$ (*c* 0.1, CH₂Cl₂). ¹H NMR (400 MHz, CDCl₃) δ 8.31 (d, *J* = 8.4 Hz, 1H), 8.13 (d, *J* = 8.1 Hz, 1H), 7.67 (ddd, *J* = 8.2, 6.9, 1.3 Hz, 1H), 7.60 (ddd, *J* = 8.3, 6.9, 1.3 Hz, 1H), 7.36 (d, *J* = 8.5 Hz, 2H), 7.15 (d, *J* = 8.5 Hz, 2H), 6.54 (s, 1H), 6.10 (d, *J* = 1.8 Hz, 1H), 5.08 (d, *J* = 1.8 Hz, 1H), 3.92 (s, 3H). ¹³C NMR (101 MHz, CDCl₃) δ 152.7, 147.2, 136.9, 134.3, 129.4, 128.9, 127.3, 126.3, 126.3, 122.8, 121.0, 120.7, 118.4, 111.8, 99.0, 56.5, 55.8. Chiralpak ODH column, 90:10 (n-hexane/*i*-PrOH), flow rate 1.0 mL/min, 230 nm, temp=25 °C, *t*_{minor}= 8.278 min, *t*_{major}= 17.198 min. IR(neat): 2921, 2853, 1666, 1565, 1490, 1460, 1403, 1378, 1365, 1340, 1256, 1222, 1115, 1090, 1014 cm⁻¹. MS (MALDI-TOF) *m/z*: [M-NO₂]⁺ Calcd. for C₁₉H₁₃O₂Cl 308.060; Found 308.069.

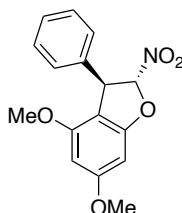
3.3.44 (2*R*,3*R*)-5-methoxy-2-nitro-3-(4-(trifluoromethyl)phenyl)-2,3-dihydronaphtho[1,2-*b*]furan (60bp)



General procedure starting from **59b** and **20p** afforded to desired chiral product 89% isolated yield and 25% ee in **3** has a blue solid. M.p.= 106-108 °C. Optical rotation was determined as $[\alpha]_D^{22} = -24.62$ (*c* 0.1, CH₂Cl₂). ¹H NMR (400 MHz, CDCl₃) δ 8.35 – 8.29 (m, 1H), 8.18 – 8.11 (m, 1H), 7.67 (ddd, *J* = 8.5, 7.1, 5.7 Hz, 4H), 7.35 (d, *J* = 8.0 Hz, 2H), 6.55 (s, 1H), 6.13 (d, *J* = 1.7 Hz, 1H), 5.17 (d, *J* = 1.8 Hz, 1H), 3.93 (s, 3H). ¹³C NMR (101 MHz, CDCl₃) δ 152.8, 147.4, 142.3, 130.7 (q, ²*J*_{CF} = 32.2 Hz), 128.0, 127.4, 126.4, 126.3, 126.2 (q, ⁴*J*_{CF} = 3.6 Hz), 125.1, 122.8 (q, ¹*J*_{CF} = 272.4 Hz), 121.0, 120.7, 118.1, 111.5, 98.9, 56.7, 55.8. Chiralpak ODH column, 90:10 (n-hexane/*i*-PrOH), flow rate 1.0 mL/min, 220 nm, temp=25 °C, *t*_{minor}= 7.830 min, *t*_{major}= 14.816 min. IR(neat): 2940, 2838, 1620, 1566, 1461, 1404, 1366, 1323,

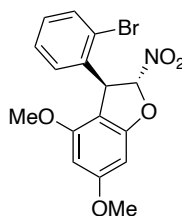
1259, 1223, 1164, 1112, 1092, 1067, 1018 cm^{-1} . MS (MALDI-TOF) m/z : $[\text{M}-\text{NO}_2]^+$
Calcd. for $\text{C}_{20}\text{H}_{14}\text{O}_2\text{F}_3$ 343.095; Found 343.090.

3.3.45 (2*R*,3*R*)-4,6-dimethoxy-2-nitro-3-phenyl-2,3-dihydrobenzofuran (60ba)



General procedure starting from **59b** and **20a** afforded to desired chiral product with 94% isolated yield and 85% ee in 1 h as a white solid. M.p.= 110-115 °C. Optical rotation was determined as $[\alpha]_D^{19} = -42.48$ (c 0.5, CH_2Cl_2). ^1H NMR (400 MHz, CDCl_3) δ 7.32 – 7.19 (m, 3H), 7.12 – 7.02 (m, 2H), 6.32 (d, $J = 2.0$ Hz, 1H), 6.09 (d, $J = 2.0$ Hz, 1H), 5.87 (d, $J = 1.5$ Hz, 1H), 4.82 (d, $J = 1.5$ Hz, 1H), 3.75 (s, 3H), 3.58 (s, 3H). ^{13}C NMR (101 MHz, CDCl_3) δ 163.1, 160.2, 156.9, 138.3, 129.0, 128.0, 127.2, 112.6, 105.2, 94.1, 89.0, 55.8, 55.5, 53.5. Chiralpak ODH column, 90:10 (n-hexane/*i*-PrOH), flow rate 1.0 mL/min, 220 nm, temp=25 °C, $t_{\text{minor}} = 6.803$ min, $t_{\text{major}} = 11.567$ min.

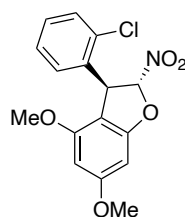
3.3.46 (2*R*,3*S*)-3-(2-bromophenyl)-4,6-dimethoxy-2-nitro-2,3-dihydrobenzofuran (62bb)



General procedure starting from **61b** and **20b** afforded to desired chiral product with 78% isolated yield and 77% ee in 3 h as a white solid. M.p.= 116-118 °C. Optical

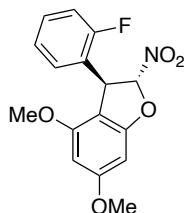
rotation was determined as $[\alpha]_D^{21} = -48.44$ (c 1.0, CH_2Cl_2). ^1H NMR (400 MHz, CDCl_3) δ 7.72 – 7.64 (m, 1H), 7.27 – 7.11 (m, 2H), 6.70 (dd, $J = 7.3, 2.2$ Hz, 1H), 6.42 (d, $J = 1.9$ Hz, 1H), 6.20 (d, $J = 1.9$ Hz, 1H), 5.96 (d, $J = 1.3$ Hz, 1H), 5.42 (d, $J = 1.4$ Hz, 1H), 3.87 (s, 3H), 3.69 (s, 3H). ^{13}C NMR (101 MHz, CDCl_3) δ 163.2, 160.6, 156.7, 136.8, 133.3, 129.6, 128.6, 127.9, 124.0, 111.9, 104.7, 94.0, 88.9, 55.7, 55.4, 51.9. Chiralpak ODH column, 90:10 (n-hexane/*i*-PrOH), flow rate 1.0 mL/min, 230 nm, temp=25 °C, $t_{\text{minor}} = 7.669$ min, $t_{\text{major}} = 12.703$ min. IR(neat): 2938, 2842, 1634, 1603, 1564, 1505, 1454, 1427, 1218, 1201, 1171, 1141, 1076, 1041 cm^{-1} . HRMS (ESI-TOF) m/z : $[\text{M}+\text{H}]^+$ Calcd. for $\text{C}_{16}\text{H}_{15}\text{BrNO}_5$ 380.0134; Found 380.0122.

3.3.47 (2*R*,3*S*)-3-(2-chlorophenyl)-4,6-dimethoxy-2-nitro-2,3-dihydrobenzofuran (62bc)



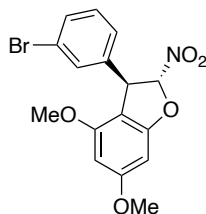
General procedure starting from **61b** and **20c** afforded to desired chiral product with 67% isolated yield and 51% ee in 3 h as a white solid. M.p.= 120 °C. Optical rotation was determined as $[\alpha]_D^{19} = -11.76$ (c 0.5, CH_2Cl_2). ^1H NMR (400 MHz, CDCl_3) δ 7.50 (d, $J = 8.0$ Hz, 1H), 7.31 – 7.27 (m, 1H), 7.22 – 7.13 (m, 1H), 6.77 – 6.68 (m, 1H), 6.42 (t, $J = 1.6$ Hz, 1H), 6.21 (t, $J = 1.6$ Hz, 1H), 5.98 (d, $J = 1.3$ Hz, 1H), 5.41 (s, 1H), 3.88 (s, 3H), 3.70 (s, 3H). ^{13}C NMR (101 MHz, CDCl_3) δ 163.2, 160.6, 156.7, 135.0, 133.7, 129.9, 129.3, 128.5, 127.2, 111.7, 104.2, 93.9, 89.0, 55.7, 55.4, 49.6. Chiralpak ODH column, 90:10 (n-hexane/*i*-PrOH), flow rate 1.0 mL/min, 220 nm, temp=25 °C, $t_{\text{minor}} = 7.088$ min, $t_{\text{major}} = 11.561$ min. IR(neat): 2971, 2940, 2843, 1634, 1600, 1561, 1467, 1441, 1427, 1363, 1266, 1222, 1199, 1184, 1139, 1073, 1036 cm^{-1} . HRMS (ESI-TOF) m/z : $[\text{M}+\text{H}]^+$ Calcd. for $\text{C}_{16}\text{H}_{15}\text{ClNO}_5$ 336.0639; Found 336.0629.

3.3.48 (2*R*,3*S*)-3-(2-fluorophenyl)-4,6-dimethoxy-2-nitro-2,3-dihydrobenzofuran (62bd)



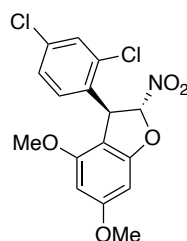
General procedure starting from **61b** and **20d** afforded to desired chiral product with 66% isolated yield and 47% ee in 100 m as a white solid. M.p.= 130-134 °C. Optical rotation was determined as $[\alpha]_D^{18} = -32.66$ (c 1.0, CH_2Cl_2). ^1H NMR (400 MHz, CDCl_3) δ 7.44 – 7.29 (m, 1H), 7.22 – 7.12 (m, 1H), 7.08 (dd, $J = 7.6, 1.3$ Hz, 1H), 6.83 (dd, $J = 7.7, 1.8$ Hz, 1H), 6.42 (d, $J = 2.0$ Hz, 1H), 6.20 (d, $J = 2.0$ Hz, 1H), 6.10 – 5.96 (m, 1H), 5.21 (d, $J = 1.4$ Hz, 1H), 3.87 (s, 3H), 3.70 (s, 3H). ^{13}C NMR (101 MHz, CDCl_3) δ 161.7 (d, $^1J_{\text{CF}} = 287.8$ Hz), 159.0, 156.7, 146.4, 143.4, 129.8 (d, $^3J_{\text{CF}} = 8.1$ Hz), 128.6 (d, $^4J_{\text{CF}} = 3.5$ Hz), 124.4 (d, $^3J_{\text{CF}} = 5.2$ Hz), 115.7 (d, $^2J_{\text{CF}} = 20.7$ Hz), 111.6, 103.7, 93.9, 88.9, 55.7, 55.4, 46.6. Chiralpak ODH column, 90:10 (n-hexane/*i*-PrOH), flow rate 1.0 mL/min, 230 nm, temp=25 °C, $t_{\text{minor}} = 5.460$ min, $t_{\text{major}} = 6.896$ min. IR(neat): 2923, 2845, 1633, 1604, 1566, 1505, 1487, 1457, 1428, 1353, 1216, 1199, 1136, 1074 cm^{-1} . HRMS (ESI-TOF) m/z : $[\text{M}+\text{H}]^+$ Calcd. for $\text{C}_{16}\text{H}_{14}\text{FNO}_5$ 320.0934; Found 320.0930.

3.3.49 (2*R*,3*R*)-3-(3-bromophenyl)-4,6-dimethoxy-2-nitro-2,3-dihydrobenzofuran (62be)



General procedure starting from **61b** and **20e** afforded to desired chiral product with 40% isolated yield and 47% ee in 2.5 h as a white solid. M.p.= 135 °C. Optical rotation was determined as $[\alpha]_D^{22} = -14.82$ (*c* 1.0, CH₂Cl₂). ¹H NMR (400 MHz, CDCl₃) δ 7.41 (ddd, *J* = 8.0, 2.1, 1.0 Hz, 1H), 7.26 – 7.23 (m, 1H), 7.19 (t, *J* = 7.8 Hz, 1H), 7.08 (dt, *J* = 7.6, 1.4 Hz, 1H), 6.37 (d, *J* = 1.9 Hz, 1H), 6.14 (d, *J* = 2.0 Hz, 1H), 5.90 (d, *J* = 1.5 Hz, 1H), 4.83 (d, *J* = 1.5 Hz, 1H), 3.82 (s, 3H), 3.65 (s, 3H). ¹³C NMR (101 MHz, CDCl₃) δ 163.3, 160.2, 156.8, 140.5, 131.3, 130.6, 130.2, 128.8, 126.0, 123.1, 112.1, 94.2, 89.1, 55.8, 55.6, 53.0. Chiralpak ODH column, 90:10 (n-hexane/*i*-PrOH), flow rate 1.0 mL/min, 230 nm, temp=25 °C, *t*_{minor}= 7.630 min, *t*_{major}= 11.854 min. IR(neat): 2923, 2841, 1633, 1601, 1566, 1504, 1463, 1424, 1354, 1304, 1266, 1218, 1200, 1173, 1073, 1040 cm⁻¹. HRMS (ESI-TOF) *m/z*: [M+H]⁺ Calcd. for C₁₆H₁₅BrNO₅ 380.0134; Found 380.0130.

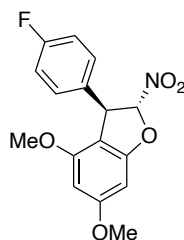
3.3.50 (2*R*,3*S*)-3-(2,4-dichlorophenyl)-4,6-dimethoxy-2-nitro-2,3-dihydrobenzofuran (**62bh**)



General procedure starting from **61b** and **20h** afforded to desired chiral product with 77% isolated yield and 59% ee in 19 h as a white solid. M.p.= 154 °C. Optical rotation was determined as $[\alpha]_D^{19} = -24.12$ (*c* 1.0, CH₂Cl₂). ¹H NMR (400 MHz, CDCl₃) δ 7.52 (d, *J* = 2.0 Hz, 1H), 7.15 (dd, *J* = 8.5, 2.1 Hz, 1H), 6.65 (d, *J* = 8.3 Hz, 1H), 6.42 (d, *J* = 2.0 Hz, 1H), 6.21 (d, *J* = 2.0 Hz, 1H), 5.93 (d, *J* = 1.5 Hz, 1H), 5.44 – 5.24 (m, 1H), 3.87 (s, 3H), 3.70 (s, 3H). ¹³C NMR (101 MHz, CDCl₃) δ 163.4, 160.5, 156.6, 134.5, 134.4, 133.7, 129.8, 129.4, 127.5, 111.3, 103.8, 94.0, 89.0, 55.7, 55.4, 49.2. Chiralpak ODH column, 90:10 (n-hexane/*i*-PrOH), flow rate 1.0 mL/min, 230 nm, temp=25 °C, *t*_{minor}= 7.470 min, *t*_{major}= 12.462 min. IR(neat): 2923, 2850, 1633,

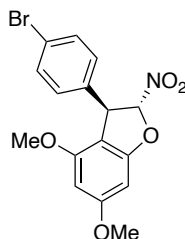
1604, 1566, 1505, 1468, 1354, 1218, 1201, 1143, 1078 cm^{-1} . HRMS (ESI-TOF) m/z : $[\text{M}+\text{H}]^+$ Calcd. for $\text{C}_{16}\text{H}_{13}\text{Cl}_2\text{NO}_5$ 370.0249; Found 380.0925.

3.3.51 (2*R*,3*R*)-3-(4-fluorophenyl)-4,6-dimethoxy-2-nitro-2,3-dihydrobenzofuran (62bj)



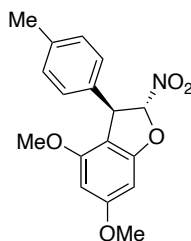
General procedure starting from **61b** and **20j** afforded to desired chiral product with 92% isolated yield and 63% ee in 155 m as a white solid. M.p.= 130-134 °C. Optical rotation was determined as $[\alpha]_D^{21} = -12.14$ (c 1.0, CH_2Cl_2). ^1H NMR (400 MHz, CDCl_3) δ 7.15 (dd, $J = 8.6, 5.4$ Hz, 2H), 7.05 (t, $J = 8.6$ Hz, 2H), 6.42 (d, $J = 2.0$ Hz, 1H), 6.19 (d, $J = 1.9$ Hz, 1H), 5.94 (d, $J = 1.5$ Hz, 1H), 4.91 (d, $J = 1.5$ Hz, 1H), 3.87 (s, 3H), 3.70 (s, 3H). ^{13}C NMR (101 MHz, CDCl_3) δ 163.1, 162.3 (d, $^1J_{\text{CF}} = 246.4$ Hz), 160.0, 156.7, 133.9 (d, $^3J_{\text{CF}} = 3.1$ Hz), 128.7 (d, $^3J_{\text{CF}} = 8.3$ Hz), 115.9 (d, $^2J_{\text{CF}} = 21.6$ Hz), 112.3, 104.9, 94.0, 88.9, 55.7, 55.4, 52.6. Chiralpak ODH column, 90:10 (n-hexane/*i*-PrOH), flow rate 1.0 mL/min, 230 nm, temp=25 °C, $t_{\text{minor}} = 7.110$ min, $t_{\text{major}} = 12.428$ min. IR(neat): 2940, 2845, 1635, 1602, 1563, 1506, 1467, 1428, 1355, 1282, 1220, 1201, 1173, 1142, 1075, 1041, 1017 cm^{-1} . HRMS (ESI-TOF) m/z : $[\text{M}+\text{H}]^+$ Calcd. for $\text{C}_{16}\text{H}_{15}\text{FNO}_5$ 320.0934; Found 320.0925.

3.3.52 (2*R*,3*R*)-3-(4-bromophenyl)-4,6-dimethoxy-2-nitro-2,3-dihydrobenzofuran (62bk)



General procedure starting from **61b** and **20k** afforded to desired chiral product with 74% isolated yield and 59% ee in 2.5 h as a white solid. M.p.= 96 °C. Optical rotation was determined as $[\alpha]_D^{17} = -37.84$ (*c* 1.0, CH₂Cl₂). ¹H NMR (400 MHz, CDCl₃) δ 7.49 (d, *J* = 8.4 Hz, 2H), 7.06 (d, *J* = 8.4 Hz, 2H), 6.42 (d, *J* = 2.0 Hz, 1H), 6.19 (d, *J* = 2.0 Hz, 1H), 5.93 (d, *J* = 1.5 Hz, 1H), 4.88 (d, *J* = 1.5 Hz, 1H), 3.86 (s, 3H), 3.69 (s, 3H). ¹³C NMR (101 MHz, CDCl₃) δ 163.1, 160.0, 156.6, 137.2, 132.1, 128.8, 122.0, 112.0, 104.5, 94.0, 88.9, 55.7, 55.4, 52.8. Chiralpak ODH column, 90:10 (n-hexane/*i*-PrOH), flow rate 1.0 mL/min, 230 nm, temp=25 °C, *t*_{minor}= 8.656 min, *t*_{major}= 13.612 min. IR(neat): 2963, 2936, 2842, 1636, 1566, 1505, 1487, 1454, 1426, 1354, 1265, 1218, 1200, 1171, 1142, 1078, 1039, 1011 cm⁻¹. HRMS (ESI-TOF) *m/z*: [M+H]⁺ Calcd. for C₁₆H₁₅BrNO₅ 380.0134; Found 380.0132.

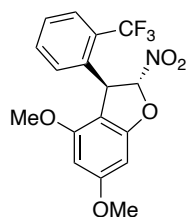
3.3.53 (2*R*,3*R*)-4,6-dimethoxy-2-nitro-3-(*p*-tolyl)-2,3-dihydrobenzofuran (62bl)



General procedure starting from **61b** and **20l** afforded to desired chiral product with 78% isolated yield and 65% ee in 3.5 h as a white solid. M.p.= 94-100 °C. Optical

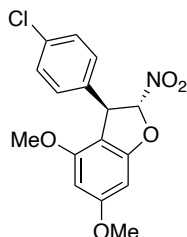
rotation was determined as $[\alpha]_D^{19} = -38.92$ (c 1.0, CH_2Cl_2). ^1H NMR (400 MHz, CDCl_3) δ 7.17 (d, $J = 7.8$ Hz, 2H), 7.07 (d, $J = 7.9$ Hz, 2H), 6.43 (d, $J = 1.9$ Hz, 1H), 6.19 (d, $J = 1.9$ Hz, 1H), 5.96 (d, $J = 1.5$ Hz, 1H), 4.90 (d, $J = 1.5$ Hz, 1H), 3.87 (s, 3H), 3.69 (s, 3H), 2.36 (s, 3H). ^{13}C NMR (101 MHz, CDCl_3) δ 162.9, 160.1, 156.7, 137.7, 135.2, 129.6, 126.9, 112.6, 105.2, 93.9, 88.8, 55.6, 55.4, 53.0, 21.0. Chiralpak ODH column, 90:10 (n-hexane/*i*-PrOH), flow rate 1.0 mL/min, 230 nm, temp=25 °C, $t_{\text{minor}} = 6.696$ min, $t_{\text{major}} = 9.331$ min. IR(neat): 2939, 2842, 1635, 1604, 1565, 1505, 1455, 1427, 1354, 1300, 1218, 1201, 1170, 1142, 1079 1042 cm^{-1} . HRMS (ESI-TOF) m/z : $[\text{M}+\text{H}]^+$ Calcd. for $\text{C}_{17}\text{H}_{18}\text{NO}_5$ 316.1185; Found 316.1176.

3.3.54 (2*R*,3*R*)-4,6-dimethoxy-2-nitro-3-(2-(trifluoromethyl)phenyl)-2,3-dihydrobenzofuran (62bn)



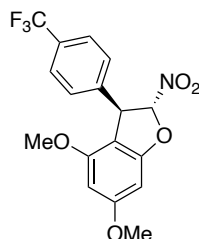
General procedure starting from **61b** and **20n** afforded to desired chiral product with quantitative isolated yield and 98% ee in 4 h as a white solid. M.p.= 90 °C. Optical rotation was determined as $[\alpha]_D^{21} = -49.46$ (c 1.0, CH_2Cl_2). ^1H NMR (400 MHz, CDCl_3) δ 7.83 – 7.66 (m, 1H), 7.51 – 7.38 (m, 2H), 6.89 (d, $J = 7.0$ Hz, 1H), 6.43 (d, $J = 2.0$ Hz, 1H), 6.17 (d, $J = 2.0$ Hz, 1H), 5.93 (d, $J = 1.5$ Hz, 1H), 5.36 (s, 1H), 3.87 (s, 3H), 3.65 (s, 3H). ^{13}C NMR (101 MHz, CDCl_3) δ 163.2, 160.4, 156.4, 136.6, 133.0, 132.5, 128.7, 128.0, 126.2 (q, $^3J_{\text{CF}} = 5.6$ Hz), 124.3 (q, $^1J_{\text{CF}} = 257.5$ Hz), 112.0, 105.9, 94.0, 88.7, 55.7, 55.4, 48.0. Chiralpak ODH column, 90:10 (n-hexane/*i*-PrOH), flow rate 1.0 mL/min, 230 nm, temp=25 °C, $t_{\text{minor}} = 7.271$ min, $t_{\text{major}} = 10.377$ min. IR(neat): 2932, 2852, 1727, 1637, 1604, 1569, 1506, 1455, 1361, 1314, 1218, 1202, 1145, 1079, 1038 cm^{-1} . HRMS (ESI-TOF) m/z : $[\text{M}+\text{H}]^+$ Calcd. for $\text{C}_{17}\text{H}_{15}\text{F}_3\text{NO}_5$ 370.0902; Found 370.0898.

3.3.55 (2*R*,3*R*)-3-(4-chlorophenyl)-4,6-dimethoxy-2-nitro-2,3-dihydrobenzofuran (62bo)



General procedure starting from **61b** and **20o** afforded to desired chiral product with 80% isolated yield and 89% ee in 100 m as a white solid. M.p.= 89-91 °C. Optical rotation was determined as $[\alpha]_D^{18} = -44.86$ (c 1.0, CH_2Cl_2). ^1H NMR (400 MHz, CDCl_3) δ 7.15 (dd, $J = 8.5, 5.4$ Hz, 2H), 7.05 (t, $J = 8.6$ Hz, 2H), 6.42 (d, $J = 1.9$ Hz, 1H), 6.19 (d, $J = 1.9$ Hz, 1H), 5.94 (d, $J = 1.5$ Hz, 1H), 4.91 (d, $J = 1.5$ Hz, 1H), 3.87 (s, 3H), 3.70 (s, 3H). ^{13}C NMR (101 MHz, CDCl_3) δ 163.1, 160.0, 156.6, 136.6, 133.8, 129.1, 128.5, 112.1, 104.6, 94.0, 88.9, 55.7, 55.4, 52.7. Chiralpak ODH column, 90:10 (n-hexane/*i*-PrOH), flow rate 1.0 mL/min, 230 nm, temp=25 °C, $t_{\text{minor}} = 7.696$ min, $t_{\text{major}} = 12.275$ min. IR(neat): 2938, 2842, 1633, 1603, 1564, 1505, 1491, 1465, 1427, 1354, 1218, 1201, 1171, 1141, 1077, 1042, 1015 cm^{-1} . HRMS (ESI-TOF) m/z : $[\text{M}+\text{H}]^+$ Calcd. for $\text{C}_{16}\text{H}_{15}\text{ClNO}_5$ 336.0639; Found 336.0641.

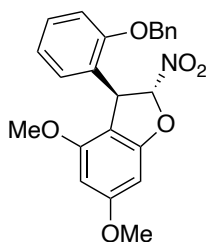
3.3.56 (2*R*,3*R*)-4,6-dimethoxy-2-nitro-3-(4-(trifluoromethyl)phenyl)-2,3-dihydrobenzofuran (62bp)



General procedure starting from **61b** and **20p** afforded to desired chiral product with 70% isolated yield and 83% ee in 155 m as a white solid. M.p.= 89-92 °C. Optical

rotation was determined as $[\alpha]_D^{18} = -23.08$ (c 1.0, CH_2Cl_2). ^1H NMR (400 MHz, CDCl_3) δ 7.63 (d, $J = 8.1$ Hz, 2H), 7.32 (d, $J = 8.0$ Hz, 2H), 6.44 (d, $J = 1.9$ Hz, 1H), 6.20 (d, $J = 1.9$ Hz, 1H), 5.96 (d, $J = 1.5$ Hz, 1H), 4.98 (d, $J = 1.6$ Hz, 1H), 3.87 (s, 3H), 3.70 (s, 3H). ^{13}C NMR (101 MHz, CDCl_3) δ 163.3, 160.1, 156.6, 142.0, 130.2 (q, $^2J_{\text{CF}} = 32.9$ Hz), 127.6, 125.9 (q, $^4J_{\text{CF}} = 3.6$ Hz), 123.8 (q, $^1J_{\text{CF}} = 272.2$ Hz), 111.8, 104.3, 94.0, 89.0, 55.7, 55.4, 53.0. Chiralpak ODH column, 90:10 (n-hexane/i-PrOH), flow rate 1.0 mL/min, 230 nm, temp=25 °C, $t_{\text{minor}} = 7.730$ min, $t_{\text{major}} = 11.099$ min. IR(neat): 2942, 2845, 1638, 1605, 1567, 1506, 1465, 1417, 1355, 1325, 1262, 1219, 1201, 1179, 1160, 1143, 1109, 1067, 1035, 1017 cm^{-1} . HRMS (ESI-TOF) m/z : $[\text{M}+\text{H}]^+$ Calcd. for $\text{C}_{17}\text{H}_{15}\text{F}_3\text{NO}_5$ 370.0902; Found 370.0904.

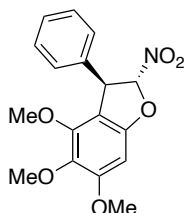
3.3.57 (2*R*,3*R*)-3-(2-(benzyloxy)phenyl)-4,6-dimethoxy-2-nitro-2,3-dihydrobenzofuran (62bq)



General procedure starting from **61b** and **20q** afforded to desired chiral product with 76% isolated yield and 49% ee in 4 h as a white solid. M.p.= 82-84 °C. Optical rotation was determined as $[\alpha]_D^{25} = -31.52$ (c 0.25, CH_2Cl_2). ^1H NMR (400 MHz, CDCl_3) δ 7.38 (dt, $J = 5.9, 1.5$ Hz, 2H), 7.32 (dt, $J = 6.8, 1.6$ Hz, 2H), 7.28 – 7.25 (m, 1H), 7.22 – 7.15 (m, 1H), 6.91 (dd, $J = 8.3, 1.1$ Hz, 1H), 6.78 (dd, $J = 7.5, 1.1$ Hz, 1H), 6.65 (d, $J = 1.8$ Hz, 1H), 6.25 (d, $J = 2.0$ Hz, 1H), 6.10 (d, $J = 2.0$ Hz, 1H), 5.92 (d, $J = 1.6$ Hz, 1H), 5.23 (d, $J = 1.6$ Hz, 1H), 5.11 (d, $J = 1.9$ Hz, 2H), 3.75 (s, 3H), 3.59 (s, 3H). ^{13}C NMR (101 MHz, CDCl_3) δ 162.9, 160.7, 156.9, 155.9, 136.5, 129.3, 128.6, 128.4, 128.1, 127.5, 126.1, 120.9, 112.6, 112.0, 104.6, 93.9, 89.0, 70.3, 55.7, 55.5, 47.6. Chiralpak ODH column, 90:10 (n-hexane/i-PrOH), flow rate 1.0 mL/min, 230 nm, temp=25 °C, $t_{\text{minor}} = 10.373$ min, $t_{\text{major}} = 16.597$ min. IR(neat): 2938,

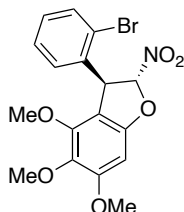
2841, 1600, 1562, 1503, 1453, 1352, 1325, 1289, 1199, 1142, 1076, 1018 cm^{-1} .
HRMS (ESI-TOF) m/z : $[M+H]^+$ Calcd. for $\text{C}_{23}\text{H}_{22}\text{NO}_6$ 408.1447; Found 408.1086.

3.3.58 (2*R*,3*R*)-4,5,6-trimethoxy-2-nitro-3-phenyl-2,3-dihydrobenzofuran (62ca)



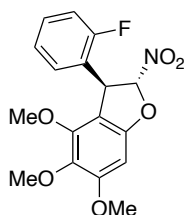
General procedure starting from **61c** and **20a** afforded to desired chiral product with 86% isolated yield and 55% ee in 9 h as a yellow semi-solid. Optical rotation was determined as $[\alpha]_D^{23} = -44.56$ (c 1.0, CH_2Cl_2). ^1H NMR (400 MHz, CDCl_3) δ 7.37 – 7.22 (m, 3H), 7.15 – 7.06 (m, 2H), 6.49 (s, 1H), 5.87 (d, $J = 1.5$ Hz, 1H), 4.92 (d, $J = 1.6$ Hz, 1H), 3.84 (s, 3H), 3.70 (s, 3H), 3.54 (s, 3H). ^{13}C NMR (101 MHz, CDCl_3) δ 155.6, 154.5, 150.1, 138.6, 129.2, 128.3, 127.2, 112.3, 90.7, 61.1, 60.1, 56.3, 54.5. Chiralpak ODH column, 90:10 (n-hexane/*i*-PrOH), flow rate 1.0 mL/min, 230 nm, temp=25 °C, $t_{\text{minor}} = 7.492$ min, $t_{\text{major}} = 17.479$ min. IR(neat): 2937, 2847, 1625, 1603, 1565, 1474, 1415, 1361, 1303, 1199, 1120, 1066, 1034 cm^{-1} . HRMS (ESI-TOF) m/z : $[M-\text{NO}_2]^+$ Calcd. for $\text{C}_{17}\text{H}_{17}\text{O}_4$ 285.1121; Found 285.1127.

3.3.59 (2*R*,3*S*)-3-(2-bromophenyl)-4,5,6-trimethoxy-2-nitro-2,3-dihydrobenzofuran (62cb)



General procedure starting from **61c** and **20b** afforded to desired chiral product with 91% isolated yield and 63% ee in 4.5 h as a white semi-solid. Optical rotation was determined as $[\alpha]_D^{25} = -16.64$ (c 1.0, CH_2Cl_2). NMR (400 MHz, CDCl_3) δ 7.60 (dd, $J = 7.7, 1.5$ Hz, 1H), 7.13 (ddd, $J = 11.8, 7.5, 1.7$ Hz, 2H), 6.64 (dd, $J = 7.6, 1.9$ Hz, 1H), 6.48 (s, 1H), 5.86 (d, $J = 1.3$ Hz, 1H), 5.47 (d, $J = 1.4$ Hz, 1H), 3.84 (s, 3H), 3.71 (s, 3H), 3.58 (s, 3H). ^{13}C NMR (101 MHz, CDCl_3) δ 155.8, 154.9, 150.0, 137.4, 133.5, 129.9, 128.9, 128.2, 125.4, 123.7, 111.7, 108.7, 90.7, 61.2, 60.0, 56.3, 53.0. Chiralpak ODH column, 90:10 (n-hexane/*i*-PrOH), flow rate 1.0 mL/min, 230 nm, temp=25 °C, $t_{\text{minor}} = 7.680$ min, $t_{\text{major}} = 21.607$ min. IR(neat): 2930, 2849, 1625, 1565, 1474, 1416, 1359, 1266, 1242, 1198, 1122, 1069, 1034 cm^{-1} . HRMS (ESI-TOF) m/z : $[\text{M}+\text{H}]^+$ Calcd. for $\text{C}_{17}\text{H}_{17}\text{BrNO}_6$ 410.0239; Found 410.0240.

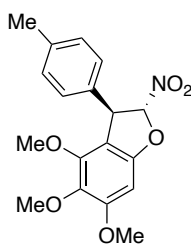
3.3.60 (2*R*,3*S*)-3-(2-fluorophenyl)-4,5,6-trimethoxy-2-nitro-2,3-dihydrobenzofuran (**62cd**)



General procedure starting from **61c** and **20d** afforded to desired chiral product with quantitative isolated yield and 60% ee in 6.5 h as a yellow semi-solid. Optical rotation was determined as $[\alpha]_D^{18} = -22.40$ (c 1.0, CH_2Cl_2). ^1H NMR (400 MHz, CDCl_3) δ 7.25 (tdd, $J = 7.3, 5.3, 2.6$ Hz, 1H), 7.12 – 7.05 (m, 1H), 7.01 (td, $J = 7.5, 1.2$ Hz, 1H), 6.77 (td, $J = 7.6, 1.7$ Hz, 1H), 6.48 (s, 1H), 5.93 (d, $J = 1.5$ Hz, 1H), 5.22 (d, $J = 1.5$ Hz, 1H), 3.83 (s, 3H), 3.71 (s, 3H), 3.58 (s, 3H). ^{13}C NMR (101 MHz, CDCl_3) δ 160.1 (d, $^1J_{\text{CF}} = 248.2$ Hz), 155.8, 154.6, 150.0, 137.4 (d, $^4J_{\text{CF}} = 2.6$ Hz), 130.2 (d, $^3J_{\text{CF}} = 8.2$ Hz), 128.8 (d, $^4J_{\text{CF}} = 3.3$ Hz), 125.3 (d, $^2J_{\text{CF}} = 14.1$ Hz), 124.7 (d, $^4J_{\text{CF}} = 3.7$ Hz), 116.0 (d, $^2J_{\text{CF}} = 21.3$ Hz), 111.4, 107.9, 90.8, 61.2, 60.1, 47.6 (d, $^4J_{\text{CF}} = 3.3$ Hz), 29.7. Chiralpak ODH column, 90:10 (n-hexane/*i*-PrOH), flow rate 1.0 mL/min, 230 nm, temp=25 °C, $t_{\text{minor}} = 6.567$ min, $t_{\text{major}} = 16.824$ min. IR(neat):

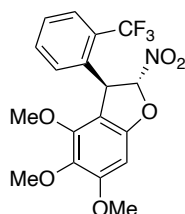
2939, 2848, 1626, 1565, 1475, 1417, 1362, 1299, 1196, 1121, 1068, 1035 cm^{-1} . HRMS (ESI-TOF) m/z : $[\text{M}+\text{H}_2]^+$ Calcd. for $\text{C}_{17}\text{H}_{18}\text{FNO}_6$ 351.1118; Found 351.1105.

3.3.61 (2*R*,3*R*)-4,5,6-trimethoxy-2-nitro-3-(*p*-tolyl)-2,3-dihydrobenzofuran (62cl)



General procedure starting from **61c** and **20l** afforded to desired chiral product with 87% isolated yield and 47% ee in 8 h as a yellow semi-solid. Optical rotation was determined as $[\alpha]_D^{21} = -44.32$ (c 0.5, CH_2Cl_2). ^1H NMR (400 MHz, CDCl_3) δ 7.08 (d, $J = 7.9$ Hz, 2H), 6.97 (d, $J = 8.1$ Hz, 1H), 6.48 (s, 1H), 5.84 (d, $J = 1.5$ Hz, 1H), 4.88 (d, $J = 1.5$ Hz, 1H), 3.83 (s, 3H), 3.70 (s, 3H), 3.55 (s, 3H), 2.26 (s, 3H). ^{13}C NMR (101 MHz, CDCl_3) δ 155.5, 154.5, 153.7, 150.1, 138.1, 135.6, 132.5, 129.9, 127.0, 112.5, 90.7, 61.1, 60.1, 56.3, 54.2, 21.1. Chiralpak ODH column, 90:10 (n-hexane/*i*-PrOH), flow rate 1.0 mL/min, 230 nm, temp=25 $^\circ\text{C}$, $t_{\text{minor}} = 7.492$ min, $t_{\text{major}} = 17.479$ min. IR(neat): 2933, 2851, 1625, 1565, 1513, 1474, 1416, 1363, 1304, 1199, 1172, 1129, 1068, 1036 cm^{-1} . HRMS (ESI-TOF) m/z : $[\text{M}+\text{H}]^+$ Calcd. for $\text{C}_{18}\text{H}_{20}\text{NO}_6$ 346.1291; Found 346.1290.

3.3.62 (2*R*,3*R*)-4,5,6-trimethoxy-2-nitro-3-(2-(trifluoromethyl)phenyl)-2,3-dihydrobenzofuran (62cn)



General procedure starting from **61c** and **20e** afforded to desired chiral product with 57% isolated yield and 27% ee in 3 h as a white solid. M.p.= 102-106 °C. Optical rotation was determined as $[\alpha]_D^{25} = -24.50$ (*c* 0.5, CH₂Cl₂). ¹H NMR (400 MHz, CDCl₃) δ 7.88 – 7.65 (m, 1H), 7.56 – 7.39 (m, 2H), 6.88 (d, *J* = 7.6 Hz, 1H), 6.60 (s, 1H), 5.93 (d, *J* = 1.4 Hz, 1H), 5.45 (s, 1H), 3.94 (s, 3H), 3.78 (s, 3H), 3.59 (s, 3H). ¹³C NMR (101 MHz, CDCl₃) δ 155.8, 154.6, 149.7, 137.7, 136.8, 132.6, 128.9, 128.3, 128.0 (q, ³*J*_{CF} = 6.8 Hz), 126.3 (q, ³*J*_{CF} = 5.8 Hz), 123.9 (q, ¹*J*_{CF} = 274.5 Hz), 111.7, 110.0, 90.6, 61.0, 60.0, 56.2, 48.9. Chiralpak ODH column, 90:10 (n-hexane/*i*-PrOH), flow rate 1.0 mL/min, 220 nm, temp=25 °C, *t*_{minor}= 6.314 min, *t*_{major}= 17.410 min. IR(neat): 2936, 2850, 1626, 1568, 1476, 1417, 1361, 1313, 1202, 1159, 1122, 1069, 1037 cm⁻¹. HRMS (ESI-TOF) *m/z*: [M+H]⁺ Calcd. for C₁₈H₁₆F₃NO₆ 400.1008; Found 400.0989.

3.4 General Procedure for Michael/S_N2 Type Domino Substitution Reaction

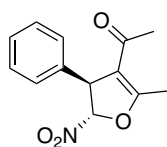
Racemic synthesis;

(*Z*)-α-bromoalkene **20** (0.10 mmol), β-dicarbonyl compound **63** (0.18 mmol), and Na₂CO₃ (0.05 mmol) were in DCM (0.5 mL) and stirred at room temperature. The reaction was monitored with TLC upon the consumption of limiting reactant, directly loaded into column chromatography. EtOAc:Hexane mixtures were used as eluent to purify the products.

Asymmetric synthesis;

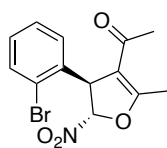
(*Z*)- α -bromoalkene **20** (0.10 mmol), β -dicarbonyl compound **63** (0.18 mmol), organocatalyst **19c** (0.01 mmol), and Na₂CO₃ (0.05 mmol) were in DCM (0.2 mL) and stirred at room temperature. The reaction was monitored with TLC upon the consumption of limiting reactant, directly loaded into column chromatography. EtOAc:Hexane mixtures were used as eluent to purify the products.

3.4.1 1-((4*S*,5*S*)-2-methyl-5-nitro-4-phenyl-4,5-dihydrofuran-3-yl)ethan-1-one (64aa)



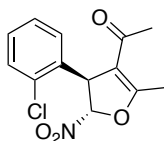
General procedure starting from **63a** and **20a** afforded to desired chiral product with quantitative yield and 95% ee in 1 h as a white solid. M.p.= 95 °C. Optical rotation was determined as $[\alpha]_D^{25} = -182.49$ (*c* 0.5, CH₂Cl₂). ¹H NMR (400 MHz, CDCl₃) δ 7.36–7.25 (m, 3H), 7.19–7.14 (m, 2H), 5.67 (d, *J* = 1.8 Hz, 1H), 4.58 (d, *J* = 2.7 Hz, 1H), 2.48 (d, *J* = 1.4 Hz, 3H), 1.97 (s, 3H). ¹³C NMR (101 MHz, CDCl₃) δ 192.1, 165.9, 136.4, 128.5, 127.7, 126.1, 114.6, 108.4, 55.3, 28.8, 13.5. Chiralpak ODH column, 95:5 (n-hexane/*i*-PrOH), flow rate 1.0 mL/min, 254 nm, temp=25 °C, *t*_{minor}= 10.983 min, *t*_{major}= 13.008 min. IR(neat): 2919, 1678, 1608, 1561, 1420, 1365, 1216, 1186 cm⁻¹. See Appendix D for crystallographic data.

3.4.2 1-((4*R*,5*S*)-4-(2-bromophenyl)-2-methyl-5-nitro-4,5-dihydrofuran-3-yl)ethan-1-one (64ab)



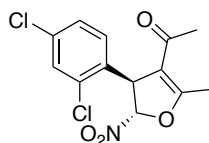
General procedure starting from **63a** and **20b** afforded to desired chiral product with 98% isolated yield and 79% ee in 4.5 h as a colorless oil. Optical rotation was determined as $[\alpha]_D^{23} = -77.08$ (c 1.0, CH_2Cl_2). ^1H NMR (400 MHz, CDCl_3) δ 7.71 (dd, $J=7.9, 1.3$ Hz, 1H), 7.36 (td, $J=7.6, 1.3$ Hz, 1H), 7.25(td, $J=7.7, 1.7$ Hz, 1H), 7.07–6.99 (m, 1H), 5.75 (d, $J=1.8$ Hz, 1H), 5.28 (s, 1H), 2.58 (s, 3H), 2.04 (s, 3H). ^{13}C NMR (101 MHz, CDCl_3) δ 192.9, 167.7, 136.0, 133.8, 130.2, 128.4, 128.1, 124.2, 115.1, 108.9, 54.5, 29.6, 14.4. Chiralpak ODH column, 80:20 (n-hexane/i-PrOH), flow rate 1.0 mL/min, 230 nm, temp=25 °C, $t_{\text{minor}}=6.923$ min, $t_{\text{major}}=7.374$ min. IR(neat): 2923, 1687, 1643, 1621, 1569, 1366, 1210, 1184 cm^{-1} . HRMS (ESI-TOF) m/z: $[\text{M}+\text{H}]^+$ Calcd. for $\text{C}_{13}\text{H}_{13}\text{BrNO}_4$ 326.0028; Found 326.0077.

3.4.3 1-((4*R*,5*S*)-4-(2-chlorophenyl)-2-methyl-5-nitro-4,5-dihydrofuran-3-yl)ethan-1-one (**64ac**)



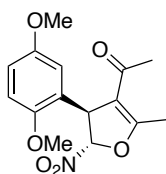
General procedure starting from **63a** and **20c** afforded to desired chiral product with 91% isolated yield and 77% ee in 6.5 h as a white solid. M.p.= 74-78 °C. Optical rotation was determined as $[\alpha]_D^{32} = -89.96$ (c 0.5, CH_2Cl_2). ^1H NMR (400 MHz, CDCl_3) δ 7.40 (m, 1H), 7.28–7.20 (m, 2H), 7.00–6.94 (m, 1H), 5.67(d, $J=1.8$ Hz, 1H), 5.23–5.07 (m, 1H), 2.49 (s, 3H), 1.96 (s, 3H). ^{13}C NMR (101 MHz, CDCl_3) δ 192.8, 168.0, 135.2, 133.1, 129.0, 128.2, 127.0, 127.0, 115.5, 109.4, 50.8, 29.7, 14.4. Chiralpak ODH column, 90:10 (n-hexane/i-PrOH), flow rate 1.0 mL/min, 230 nm, temp=25 °C, $t_{\text{minor}}=7.907$ min, $t_{\text{major}}=8.340$ min. IR(neat): 2924, 2156, 1687, 1643, 1620, 1568, 1436, 1367, 1210, 1089 cm^{-1} . HRMS (ESI-TOF) m/z: $[\text{M}+\text{H}]^+$ Calcd. for $\text{C}_{13}\text{H}_{13}\text{ClNO}_4$ 282.0533; Found 282.0274.

3.4.4 1-((4*R*,5*S*)-4-(2,4-dichlorophenyl)-2-methyl-5-nitro-4,5-dihydrofuran-3-yl)ethan-1-one (64ah)



General procedure starting from **63a** and **20h** afforded to desired chiral product with 88% isolated yield and 71% ee in 3.5 h as a white solid. M.p.= 174 °C. Optical rotation was determined as $[\alpha]_D^{33} = -115.58$ (*c* 1.0, CH₂Cl₂). ¹H NMR (400 MHz, CDCl₃) δ 7.45 (d, *J*= 2.2 Hz, 1H), 7.19 (dd, *J*=8.4,2.2 Hz, 1H),6.89 (d, *J*= 8.4 Hz, 1H), 5.63 (d, *J*= 1.8 Hz, 1H), 5.17–5.06 (m, 1H), 2.48 (s, 3H), 2.00 (s, 3H). ¹³C NMR (101 MHz, CDCl₃) δ 192.4, 167.8, 135.4, 134.7, 133.2, 130.4, 129.1, 128.1, 115.0, 108.5, 52.0, 29.5, 14.6. Chiralpak ODH column, 95:5 (n-hexane/*i*-PrOH), flow rate 1.0 mL/min, 230 nm, temp=25 °C, *t*_{minor}= 9.656 min, *t*_{major}= 11.035 min. IR(neat): 2926, 1687, 1643, 1570, 1471, 1366, 1210, 1183, 1091 cm⁻¹. HRMS (ESI-TOF) *m/z*: [M]⁺ Calcd. for C₁₃H₁₁Cl₂NO₄ 315.0065; Found 314.9922.

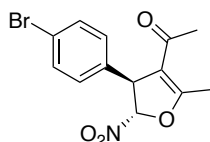
3.4.5 1-((4*S*,5*S*)-4-(2,5-dimethoxyphenyl)-2-methyl-5-nitro-4,5-dihydrofuran-3-yl)ethan-1-one (64ai)



General procedure starting from **63a** and **20i** afforded to desired chiral product with 78% isolated yield and 80% ee in 3.5 h as a white solid. M.p.= 73 °C. Optical rotation was determined as $[\alpha]_D^{32} = -119.60$ (*c* 1.0, CH₂Cl₂). ¹H NMR (400 MHz, CDCl₃) δ 6.82 (d, *J*= 8.9 Hz, 1H), 6.76 (dd, *J*= 8.9, 3.0 Hz, 1H), 6.47 (d, *J*= 2.9 Hz, 1H), 5.66 (d, *J*= 2.0 Hz, 1H), 4.98 (t, *J*= 1.7 Hz, 1H), 3.80 (s, 3H), 3.67 (s, 3H), 2.44 (s, 3H), 1.96 (s, 3H). ¹³C NMR (101 MHz, CDCl₃) δ 193.5, 167.4, 153.9, 151.1, 126.6, 114.6,

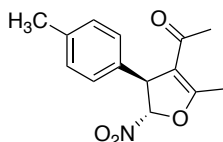
114.4, 113.3, 112.1, 109.8, 56.1, 55.7, 49.6, 29.5, 14.5. Chiralpak ODH column, 95:5 (n-hexane/*i*-PrOH), flow rate 1.0 mL/min, 230 nm, temp=25 °C, t_{minor} = 12.300 min, t_{major} = 13.746 min. IR(neat): 2924, 1685, 1642, 1618, 1566, 1500, 1464, 1366, 1210, 1090 cm^{-1} . HRMS (ESI-TOF) m/z : $[M+H]^+$ Calcd. for $\text{C}_{15}\text{H}_{18}\text{NO}_6$ 308.1134; Found 308.0783.

3.4.6 1-((4*S*,5*S*)-4-(4-bromophenyl)-2-methyl-5-nitro-4,5-dihydrofuran-3-yl)ethan-1-one (64ak)



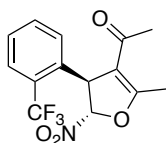
General procedure starting from **63a** and **20k** afforded to desired chiral product with 93% isolated yield and 79% ee in 5.5 h as a dark yellow solid. M.p.= 131 °C. Optical rotation was determined as $[\alpha]_D^{25} = -100.58$ (c 0.5, CH_2Cl_2). ^1H NMR (400 MHz, CDCl_3) δ 7.66–7.60 (m, 2H), 7.48–7.44 (m, 2H), 5.63 (d, $J=1.8\text{Hz}$, 1H), 4.55 (d, $J=5.7\text{Hz}$, 1H), 2.48 (d, $J=1.4\text{Hz}$, 3H), 2.01 (s, 3H). ^{13}C NMR (101 MHz, CDCl_3) δ 191.6, 166.0, 135.5, 131.7, 129.9, 127.8, 107.9, 67.1, 54.8, 13.1. Chiralpak ASH column, 95:5 (n-hexane/*i*-PrOH), flow rate 1.0 mL/min, 254 nm, temp=25 °C, t_{minor} = 11.959 min, t_{major} = 15.438 min. IR(neat): 2992, 1734, 1677, 1609, 1562, 1362, 1210, 1180 cm^{-1} . HRMS (ESI-TOF) m/z : $[M+H]^+$ Calcd. for $\text{C}_{13}\text{H}_{13}\text{BrNO}_4$ 326.0029; Found 326.0023.

3.4.7 1-((4*S*,5*S*)-2-methyl-5-nitro-4-(*p*-tolyl)-4,5-dihydrofuran-3-yl)ethan-1-one (64al)



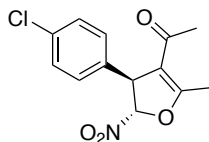
General procedure starting from **63a** and **20l** afforded to desired chiral product with 89% isolated yield and 82% ee in 6 h as a white solid. M.p.= 95 °C. Optical rotation was determined as $[\alpha]_D^{25} = -140.50$ (*c* 1.0, CH₂Cl₂). ¹H NMR (400 MHz, CDCl₃) δ 7.16–7.09 (m, 2H), 7.07–7.03 (m, 2H), 5.65 (d, *J*= 1.8 Hz, 1H), 4.54 (s, 1H), 2.47 (d, *J*= 1.4 Hz, 3H), 2.29 (s, 3H), 1.95 (s, 3H). ¹³C NMR (101 MHz, CDCl₃) δ 193.3, 166.9, 138.6, 134.5, 130.2, 128.8, 127.0, 115.6, 109.7, 55.9, 29.9, 21.1, 14.5. Chiralpak ODH column, 98:2 (n-hexane/*i*-PrOH), flow rate 1.0 mL/min, 254 nm, temp=25 °C, *t*_{minor}= 12.7 min, *t*_{major}= 13.7 min. IR(neat): 2918, 1734, 1680, 1613, 1565, 1369, 1215, 1185 cm⁻¹.

3.4.8 1-((4*S*,5*S*)-2-methyl-5-nitro-4-(2-(trifluoromethyl)phenyl)-4,5-dihydrofuran-3-yl)ethan-1-one (**64an**)



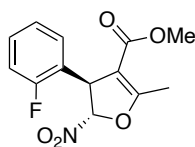
General procedure starting from **63a** and **20n** afforded to desired chiral product with 90% isolated yield and 75% ee in 4 h as a colorless oil. Optical rotation was determined as $[\alpha]_D^{25} = -193.01$ (*c* 1.0, CH₂Cl₂). ¹H NMR (400 MHz, CDCl₃) δ 7.73 (d, *J*= 7.8 Hz, 1H), 7.52 (t, *J*= 7.6 Hz, 1H), 7.43 (t, *J*= 7.7 Hz, 1H), 7.10 (d, *J*= 7.8 Hz, 1H), 5.64 (d, *J*= 1.7 Hz, 1H), 5.09 (s, 1H), 2.51 (s, 3H), 1.91 (s, 3H). ¹³C NMR (101 MHz, CDCl₃) δ 192.8, 168.0, 135.2, 133.1, 129.0, 128.6, 128.2, 127.0 (q, *J*= 5.7 Hz), 125.3, 115.5, 109.4, 50.8, 29.7, 14.4 (Other CF₃ coupling could not be identified). Chiralpak IA column, 98:2 (n-hexane/*i*-PrOH), flow rate 0.7 mL/min, 230 nm, temp=25 °C, *t*_{minor}= 10.529 min, *t*_{major}= 11.403 min. IR(neat): 2960, 2923, 1687, 1644, 1571, 1336, 1205, 1160 cm⁻¹. HRMS (ESI-TOF) *m/z*: [M]⁺ Calcd. for C₁₄H₁₂F₃NO₄ 315.0718; Found 315.0623.

3.4.9 1-((4*S*,5*S*)-4-(4-chlorophenyl)-2-methyl-5-nitro-4,5-dihydrofuran-3-yl)ethan-1-one (64ao)



General procedure starting from **63a** and **20o** afforded to desired chiral product with 78% isolated yield and 81% ee in 4 h as a colorless oil. Optical rotation was determined as $[\alpha]_D^{33} = -128.18$ (c 1.0, CH_2Cl_2). ^1H NMR (400 MHz, CDCl_3) δ 7.30 (d, $J = 8.4$ Hz, 2H), 7.11 (d, $J = 8.4$ Hz, 2H), 5.63 (d, $J = 1.8$ Hz, 1H), 4.57 (d, $J = 1.7$ Hz, 1H), 2.47 (s, 3H), 2.00 (s, 3H). ^{13}C NMR (101 MHz, CDCl_3) δ 192.6, 167.0, 136.0, 134.7, 129.7, 128.5, 115.8, 109.1, 55.7, 29.7, 14.6. Chiralpak ASH column, 90:10 (n-hexane/*i*-PrOH), flow rate 1.0 mL/min, 230 nm, temp=25 °C, $t_{\text{minor}} = 8.626$ min, $t_{\text{major}} = 10.512$ min. IR(neat): 2923, 1686, 1641, 1619, 1566, 1365, 1211, 1178 cm^{-1} . HRMS (ESI-TOF) m/z : $[\text{M} + \text{H}]^+$ Calcd. for $\text{C}_{13}\text{H}_{13}\text{ClNO}_4$ 282.0533; Found 282.0262.

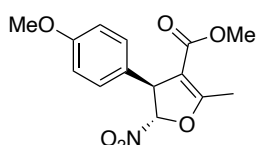
3.4.10 Methyl (4*R*,5*S*)-4-(2-fluorophenyl)-2-methyl-5-nitro-4,5-dihydrofuran-3-carboxylate (64bd)



General procedure starting from **63b** and **20d** afforded to desired chiral product with 98% isolated yield and 79% ee in 3 h as a colorless oil. Optical rotation was determined as $[\alpha]_D^{23} = -108.04$ (c 1.0, CH_2Cl_2). ^1H NMR (400 MHz, CDCl_3) δ 7.29–7.21 (m, 1H), 7.05 (dddd, $J = 9.3, 7.2, 4.4, 2.6$ Hz, 3H), 5.77 (d, $J = 2.0$ Hz, 1H), 4.83 (s, 1H), 3.55 (s, 3H), 2.44 (s, 3H). ^{13}C NMR (101 MHz, CDCl_3) δ 167.9, 163.6, 160.3 (d, $J = 248.4$ Hz), 130.0 (d, $J = 8.3$ Hz), 128.5 (d, $J = 3.4$ Hz), 124.5 (d, $J = 3.6$ Hz),

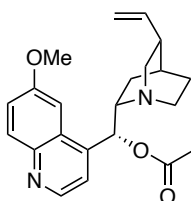
116.0 (d, $J=21.5$ Hz), 108.8, 105.9, 51.4, 49.2, 49.2, 13.7. Chiralpak ASH column, 90:10 (n-hexane/*i*-PrOH), flow rate 1.0 mL/min, 230 nm, temp=25 °C, $t_{\text{minor}}=5.359$ min, $t_{\text{major}}=6.412$ min. IR(neat): 3320, 2953, 2194, 2157, 2042, 2003, 1710, 1667, 1569, 1492, 1439, 1362, 1322, 1226, 1205, 1104, 1063 cm^{-1} . HRMS (ESI-TOF) m/z : $[M]^+$ Calcd. for $\text{C}_{13}\text{H}_{12}\text{FNO}_5$ 281.0700; Found 281.2479.

3.4.11 Methyl (4*S*,5*S*)-4-(4-methoxyphenyl)-2-methyl-5-nitro-4,5-dihydrofuran-3-carboxylate (**64bg**)



General procedure starting from **63b** and **20g** afforded to desired chiral product with 95% isolated yield and 89% ee in 3 h as a yellow oil. Optical rotation was determined as $[\alpha]_D^{23} = -116.40$ (c 1.0, CH_2Cl_2). ^1H NMR (400 MHz, CDCl_3) δ 7.16 (d, $J=8.7$ Hz, 2H), 6.92 (d, $J=8.7$ Hz, 2H), 5.76 (d, $J=1.8$ Hz, 1H), 4.67–4.41 (m, 1H), 3.83 (s, 3H), 3.64 (s, 3H), 2.53 (s, 3H). ^{13}C NMR (101 MHz, CDCl_3) δ 167.1, 163.8, 159.5, 129.7, 128.0, 114.4, 109.7, 107.5, 55.2, 55.0, 51.3, 13.7, 0.9. Chiralpak ASH column, 90:10 (n-hexane/*i*-PrOH), flow rate 1.0 mL/min, 230 nm, temp=25 °C, $t_{\text{minor}}=6.651$ min, $t_{\text{major}}=7.925$ min. IR(neat): 2952, 2839, 2176, 1708, 1666, 1610, 1569, 1512, 1438, 1359, 1255, 1182, 1062, 1032 cm^{-1} . HRMS (ESI-TOF) m/z : $[M]^+$ Calcd. for $\text{C}_{14}\text{H}_{15}\text{NO}_6$ 293.0899; Found 293.1771.

3.5 Synthesis of Acetylation of Quinine: (*R*)-(6-methoxyquinolin-4-yl)((1*S*,2*S*,4*S*,5*R*)-5-vinylquinuclidin-2-yl)methyl acetate (**65**)



According to literature procedure,¹²¹ 0.30 mmol quinine was dissolved in DCM (10 mL) and 0.46 mmol acetyl chloride was added slowly into the solution. The reaction was stirred for 24 h at room temperature and it was quenched with 15 mL NaHCO₃ solution. After that the solution was extracted with DCM (x3), washed with brine solution. Organic phases was dried over Na₂SO₄, filtered and concentrated with rotary evaporator to give cloudy yellowish oil in 99% yield. Analytical data matched previously reported value.

3.6 General Procedure for the Thiol-Ene Reaction

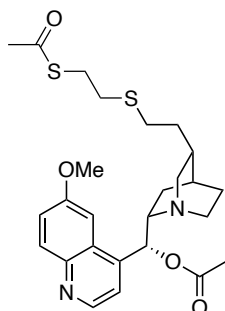
3.6.1 Thiol-Ene Reaction with Thermal Initiator

According to slightly modified literature procedure,¹⁰² a screw-capped reaction vial was charged with 0.34 mmol cinchonine derivative, 0.09 mmol AIBN and 3.4 mmol thioacetic acid was dissolved in chloroform (4 mL) under argon atmosphere. The reaction was stirred under reflux for 48 h. Then, chloroform was evaporated and the residue was directly loaded to column chromatography.

3.6.2 Thiol-Ene Reaction with Photoinitiator

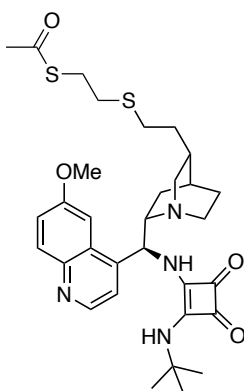
According to slightly modified literature procedure,¹²² a screw-capped reaction vial was charged with 0.76 mmol cinchonine derivative, 0.253 mmol DMPA and 7.6 mmol *S*-(2-mercaptoethyl) ethanethioate **66** (or 1,2-ethanedithiol, 1,6-hexanedithiol, 1,9-nonanedithiol) was dissolved in chloroform or dry THF (7.3 mL) under argon atmosphere. The reaction was stirred 5-15 mins. Then the residue was directly loaded to column chromatography.

3.6.2.1 (R)-((1S,2S,4S,5R)-5-(2-((2-(acetylthio)ethyl)thio)ethyl)quinuclidin-2-yl)(6-methoxyquinolin-4-yl)methyl acetate (67)



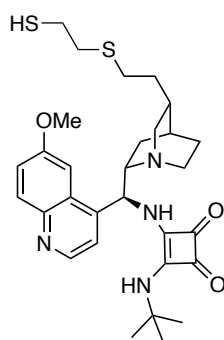
Yellow semi-solid. 95% yield. ^1H NMR (400 MHz, CDCl_3) δ 8.7 (d, $J = 4.5$ Hz, 1H), 7.9 (d, $J = 9.2$ Hz, 1H), 7.4 (d, $J = 2.7$ Hz, 1H), 7.3 – 7.2 (m, 2H), 6.5 (d, $J = 7.1$ Hz, 1H), 3.9 (s, 3H), 3.3 (q, $J = 7.8$ Hz, 1H), 3.1 – 2.9 (m, 4H), 2.6 – 2.5 (m, 3H), 2.5 (t, $J = 7.3$ Hz, 2H), 2.3 (d, $J = 14.7$ Hz, 1H), 2.2 (s, 3H), 2.1 (s, 3H), 1.8 (bs, 2H), 1.7 – 1.4 (m, 6H). ^{13}C NMR (101 MHz, CDCl_3) δ 195.2, 169.9, 157.9, 147.4, 144.7, 143.6, 131.8, 127.0, 121.8, 118.8, 101.5, 73.6, 58.9, 57.8, 55.7, 42.4, 34.7, 34.6, 31.8, 30.5, 29.9, 29.2, 28.2, 25.5, 23.9, 21.0. HRMS (ESI-TOF) m/z : $[\text{M}+\text{H}]^+$ Calcd. for $\text{C}_{26}\text{H}_{35}\text{N}_2\text{O}_4\text{S}_2$ 503.2038; Found 503.2047.

3.6.3 S-(2-((2-((1S,3R,4S,6S)-6-((S)-((2-(tert-butylamino)-3,4-dioxocyclobut-1-en-1-yl)amino)(6-methoxyquinolin-4-yl)methyl)quinuclidin-3-yl)ethyl)thio)ethyl) ethanethioate (69)



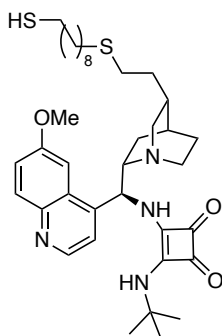
Yellowish semi-solid. 92-95% yield. ^1H NMR (400 MHz, CDCl_3) δ 8.7 (d, $J = 4.5$ Hz, 1H), 8.0 (d, $J = 9.1$ Hz, 1H), 7.7 – 7.6 (m, 2H), 7.4 (dd, $J = 9.2, 2.5$ Hz, 1H), 6.3 (bs, 1H), 4.3 (bs, 1H), 4.1 (q, $J = 7.2$ Hz, 1H), 3.9 (s, 3H), 3.5 (bs, 1H), 3.2 – 3.0 (m, 3H), 3.0 – 2.9 (m, 2H), 2.7 (td, $J = 8.1, 7.4, 4.9$ Hz, 2H), 2.6 – 2.4 (m, 4H), 2.3 (s, 3H), 2.0 (s, 2H), 1.8 (dd, $J = 13.0, 7.2$ Hz, 2H), 1.7 – 1.6 (m, 1H), 1.4 (s, 2H), 1.3 (s, 6H), 1.2 (t, $J = 7.1$ Hz, 3H). HRMS (ESI-TOF) m/z : $[\text{M}+\text{H}]^+$ Calcd. for $\text{C}_{32}\text{H}_{43}\text{N}_4\text{O}_4\text{S}_2$ 611.2726; Found 611.2735.

3.6.4 3-(*tert*-butylamino)-4-(((*S*)-((1*S*,2*S*,4*S*,5*R*)-5-(2-((2-mercaptoethyl)thio)ethyl)quinuclidin-2-yl)(6-methoxyquinolin-4-yl)methyl)amino)cyclobut-3-ene-1,2-dione (70)



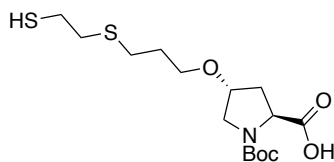
Yellowish viscous. 77% yield. ^1H NMR (400 MHz, CDCl_3) δ 8.7 (dd, $J = 8.2, 4.6$ Hz, 1H), 7.9 (dd, $J = 12.5, 9.1$ Hz, 1H), 7.7 (d, $J = 10.7$ Hz, 1H), 7.6 (dd, $J = 24.9, 4.7$ Hz, 1H), 7.4 – 7.3 (m, 1H), 6.3 (bs, 1H), 4.3 (bs, 3H), 3.9 (d, $J = 7.4$ Hz, 3H), 3.7 – 3.7 (m, 1H), 3.7 (s, 3H), 3.6 – 3.6 (m, 1H), 3.6 (t, $J = 4.4$ Hz, 1H), 3.0 (d, $J = 10.7$ Hz, 1H), 2.8 (bs, 1H), 2.7 (dd, $J = 7.5, 4.2$ Hz, 1H), 2.6 (dt, $J = 10.8, 5.7$ Hz, 2H), 2.4 (q, $J = 9.9, 8.7$ Hz, 2H), 1.8 (bs, 1H), 1.6 – 1.5 (m, 3H), 1.2 (s, 9H), 1.1 – 0.6 (m, 2H). ^{13}C NMR (101 MHz, CDCl_3) δ 182.8, 181.2, 181.1, 180.1, 169.5, 166.6, 159.2, 147.6, 131.8, 123.1, 100.7, 72.4, 63.7, 61.7, 56.2, 53.4, 41.5, 38.7, 36.2, 33.5, 33.1, 32.5, 31.6, 30.5, 29.7, 29.4, 25.6, 24.9, 24.6, 24.4. HRMS (ESI-TOF) m/z : $[\text{M}+\text{H}]^+$ Calcd. for $\text{C}_{30}\text{H}_{41}\text{N}_4\text{O}_3\text{S}_2$ 569.2620; Found 569.2644.

3.6.5 3-(*tert*-butylamino)-4-(((*S*)-((1*S*,2*S*,4*S*,5*R*)-5-(2-((9-mercaptononyl)thio)ethyl)quinuclidin-2-yl)(6-methoxyquinolin-4-yl)methyl)amino)cyclobut-3-ene-1,2-dione (71)



Yellow solid. 96% yield. Mp. = 75-78°C. ¹H NMR (400 MHz, CDCl₃) δ 8.8 (t, *J* = 3.2 Hz, 1H), 8.0 (d, *J* = 9.2 Hz, 1H), 7.8 (bs, 1H), 7.6 (d, *J* = 4.7 Hz, 1H), 7.4 (dd, *J* = 9.2, 2.6 Hz, 1H), 6.4 (bs, 1H), 4.0 (s, 3H), 3.8 – 3.8 (m, 3H), 3.8 (s, 1H), 3.7 – 3.6 (m, 2H), 3.6 – 3.4 (m, 1H), 3.1 (bs, 1H), 2.9 (bs, 1H), 2.7 (t, *J* = 7.0 Hz, 1H), 2.5 – 2.4 (m, 2H), 2.5 (t, *J* = 7.4 Hz, 3H), 2.1 (bs, 1H), 1.9 (bs, 2H), 1.7 (dd, *J* = 14.0, 7.0 Hz, 3H), 1.6 – 1.6 (m, 2H), 1.6 – 1.5 (m, 2H), 1.4 – 1.3 (m, 20H). ¹³C NMR (101 MHz, CDCl₃) δ 182.6, 181.1, 169.3, 166.5, 159.0, 147.5, 144.7, 131.7, 122.9, 100.7, 72.2, 63.5, 61.5, 56.2, 56.1, 53.4, 41.2, 39.1, 33.8, 33.0, 32.5, 32.2, 30.3, 29.6, 29.4, 29.4, 29.2, 29.0, 28.8, 28.7, 28.7, 28.2, 28.1, 25.7, 24.7, 24.5, 24.4. HRMS (ESI-TOF) *m/z*: [M+H]⁺ Calcd. for C₃₇H₅₅N₄O₃S₂ 667.3716; Found 667.3745.

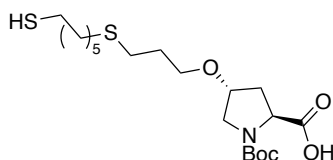
3.6.6 (2*S*,4*R*)-1-(*tert*-butoxycarbonyl)-4-(3-((2-mercaptoethyl)thio)propoxy)pyrrolidine-2-carboxylic acid (77)



Yellow semi-solid. 86% yield. ¹H NMR (400 MHz, CDCl₃) δ 4.5 – 4.4 (m, 1H), 4.4 – 4.3 (m, 1H), 4.2 (q, *J* = 6.1 Hz, 2H), 3.7 – 3.3 (m, 2H), 3.0 – 2.8 (m, 2H), 2.7 (qt,

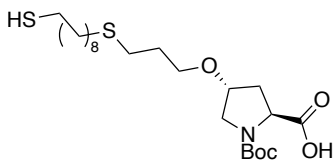
$J = 6.8, 3.8$ Hz, 3H), 2.6 (t, $J = 7.3$ Hz, 2H), 2.3 – 2.2 (m, 1H), 2.0 (td, $J = 8.3, 4.1$ Hz, 1H), 1.9 (t, $J = 6.9$ Hz, 2H), 1.7 (t, $J = 7.7$ Hz, 1H), 1.4 (d, $J = 18.5$ Hz, 9H). ^{13}C NMR (101 MHz, CDCl_3) δ 173.0, 153.9, 80.4, 69.9, 69.1, 63.4, 57.8, 57.5, 54.6, 39.0, 38.3, 36.0, 28.3, 28.2, 24.5. HRMS (ESI-TOF) m/z : $[\text{M}+\text{Na}]^+$ Calcd. for $\text{C}_{15}\text{H}_{27}\text{NO}_5\text{S}_2+\text{Na}$ 388.1228; Found 388.1245.

3.6.7 (2S,4R)-1-(tert-butoxycarbonyl)-4-(3-((6-mercaptohexyl)thio)propoxy)pyrrolidine-2-carboxylic acid (78)



Colourless viscous oil. 88% yield. ^1H NMR (400 MHz, CDCl_3) δ 4.4 (q, $J = 3.8$ Hz, 1H), 4.4 (q, $J = 7.8$ Hz, 1H), 4.2 (h, $J = 6.2$ Hz, 2H), 3.6 – 3.4 (m, 2H), 2.9 – 2.8 (m, 1H), 2.6 – 2.4 (m, 6H), 2.3 – 2.2 (m, 1H), 2.0 (ddd, $J = 13.0, 8.0, 4.8$ Hz, 1H), 1.9 (t, $J = 6.9$ Hz, 2H), 1.6 (dt, $J = 14.0, 7.1$ Hz, 4H), 1.5 – 1.2 (m, 14H). ^{13}C NMR (101 MHz, CDCl_3) δ 173.0, 153.9, 80.3, 69.9, 69.1, 63.6, 57.8, 57.5, 54.6, 39.0, 38.3, 33.7, 31.9, 29.2, 28.4, 28.2, 28.2, 28.1, 27.7. HRMS (ESI-TOF) m/z : $[\text{M}+\text{H}]^+$ Calcd. for $\text{C}_{19}\text{H}_{35}\text{NO}_5\text{S}_2+\text{Na}$ 444.1854; Found 444.1860.

3.6.8 (2S,4R)-1-(tert-butoxycarbonyl)-4-(3-((9-mercaptononyl)thio)propoxy)pyrrolidine-2-carboxylic acid (79)



Colourless viscous oil. 83% yield. ^1H NMR (400 MHz, CDCl_3) δ 4.4 – 4.4 (m, 1H), 4.3 (q, $J = 8.0, 7.3$ Hz, 1H), 4.3 – 4.1 (m, 2H), 3.6 – 3.4 (m, 2H), 3.2 (s, 2H), 2.7 – 2.4 (m, 8H), 2.3 – 2.2 (m, 1H), 2.0 (dd, $J = 8.0, 5.0$ Hz, 2H), 1.9 (q, $J = 6.8$ Hz, 2H),

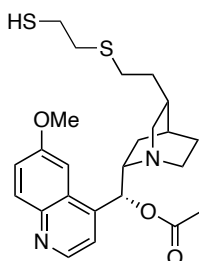
1.6 (dd, $J = 14.6, 7.3$ Hz, 6H), 1.4 (d, $J = 18.8$ Hz, 12H), 1.2 (s, 2H). ^{13}C NMR (101 MHz, CDCl_3) δ 173.0, 154.0, 80.3, 69.7, 69.0, 63.6, 57.9, 54.5, 38.9, 38.3, 33.8, 32.0, 29.4, 29.2, 29.0, 28.8, 28.7, 28.4, 28.2, 28.2, 28.1, 24.5. HRMS (ESI-TOF) m/z : $[\text{M}+\text{H}]^+$ Calcd. for $\text{C}_{22}\text{H}_{41}\text{NO}_5\text{S}_2+\text{Na}$ 486.2324; Found 486.2356.

3.7 General Procedure for the Cleavage of Acetyl Groups

First path: According to literature procedure,¹²³ a 50-mL flask was charged with 9.3 mmol **67** or **68**, 10.2 mmol hydrazine monohydrate and 10 mL methanol, and the reaction was stirred at from 20°C - 30°C for 1 hour. After the completion of the reaction, methanol was removed from the mixture, 3 mL distilled water was added and the resulting mixture was extracted with chloroform (5 mL x 3). The organic phase was dried over with anhydrous magnesium sulfate, and chloroform was removed with rotary evaporator to obtain a crude product. Then the residue was directly loaded to column chromatography.

Second path: According to literature procedure,¹²³ a 50-mL flask was charged with 9.4 mmol **67** or **68**, 0.94 mmol 35% aqueous hydrochloric acid solution, and 12 mL methanol, and the reaction was stirred at from 50°C - 60°C for 2 hours. After the completion of the reaction, methanol and hydrochloric acid were removed from the mixture. Then the residue was directly loaded to column chromatography.

3.7.1 (*R*)-((1*S*,2*S*,4*S*,5*R*)-5-(2-((2-mercaptoethyl)thio)ethyl)quinuclidin-2-yl)(6-methoxyquinolin-4-yl)methyl acetate (**68**)



Yellowish semi-solid. 88% yield. ^1H NMR (400 MHz, CDCl_3) δ 8.7 (d, $J = 4.6$ Hz, 1H), 7.9 (dd, $J = 9.2, 1.4$ Hz, 1H), 7.4 (t, $J = 2.7$ Hz, 1H), 7.3 – 7.2 (m, 2H), 6.4 (dd, $J = 7.1, 4.4$ Hz, 1H), 3.9 (s, 3H), 3.3 – 3.2 (m, 1H), 3.1 – 2.9 (m, 2H), 2.7 – 2.5 (m, 4H), 2.4 (dt, $J = 23.5, 7.2$ Hz, 2H), 2.2 (s, 1H), 2.0 (s, 3H), 1.7 (td, $J = 9.3, 5.0$ Hz, 3H), 1.6 (t, $J = 7.5$ Hz, 2H), 1.6 – 1.5 (m, 2H), 1.5 – 1.3 (m, 3H). ^{13}C NMR (101 MHz, CDCl_3) δ 170.0, 157.9, 147.4, 144.7, 143.6, 131.8, 127.0, 121.8, 118.8, 101.5, 73.6, 59.0, 57.9, 55.7, 42.4, 36.2, 34.7, 30.1, 29.2, 28.2, 25.5, 24.7, 24.0, 21.1. HRMS (ESI-TOF) m/z : $[\text{M}+\text{H}]^+$ Calcd. for $\text{C}_{24}\text{H}_{33}\text{N}_2\text{O}_3\text{S}_2$ 461.1933; Found 461.1965.

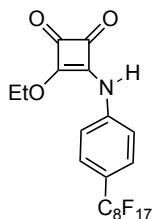
3.8 Synthesis of Thiol Stabilized GNPs 73

According to literature procedure,¹⁰² 4 mmol of tetraoctylammonium bromide was suspended in 80 mL toluene and a solution of 0.91 mmol HAuCl_4 in 30 mL deionized water was added. The mixture was stirred until the tetrachloroauric acid was transferred to the organic phase. Then, 0.84 mmol dodecanethiol was added. An aqueous solution of sodium borohydride (10.07 mmol) was slowly added over one hour. After stirring for another 3 h, the organic phase was separated, evaporated to nearly 10 mL and 400 mL of EtOH was added. The solution was kept overnight at -18 °C. A dark brown/black precipitate was filtered off and washed with EtOH. The precipitation procedure was followed once again. Elemental Analysis. found: 76.18% Au; 17.39% C; 2.84% H; 3.56% S.

3.9 Place Exchange Reaction for the Synthesis of GNP Supported Organocatalysts 74, 80

According to literature procedure,¹⁰² a mixture of gold nanoparticles **73** (80 mg) and free thiol containing catalyst (80 mg) in 20 mL anhydrous DCM under argon atmosphere in a Schlenk tube was stirred at room temperature for three days. Then, the solvent was evaporated and the excess thiol was extracted with ether.

3.10 Synthesis of Monosquarate **82**



4.3 mmol squaric acid **55** was refluxed during 3 h with 10 mL absolute ethanol. Then the solvent was evaporated under vacuum, and this procedure is repeated for three times for 30 minutes reflux. The last evaporation affords diethyl squarate as very light-yellow oil. In order to synthesis the monosquaramide, the diethyl squarate is added to 1 eq. 4-(heptadecafluorooctyl) aniline **81** solution in 4 mL DCM and stirred for 24 hours at room temperature. Then the solvent is removed by rotary evaporator and the crude product was purified with fluorosolid-phase extraction method. The crude product's ^1H NMR proves that 50% of product occurred. ^1H NMR (400 MHz, CDCl_3) δ 7.3 (d, $J = 8.2$ Hz, 2H), 6.7 (d, $J = 8.3$ Hz, 2H), 4.8 (q, $J = 7.1$ Hz, 2H), 4.0 (s, 1H), 1.5 (t, $J = 7.1$ Hz, 3H). HRMS (ESI-TOF) m/z : $[\text{M}]^+$ Calcd. for $\text{C}_{20}\text{H}_{10}\text{F}_{17}\text{NO}_3$ 635.0389; Found 635.0347.

CHAPTER 4

CONCLUSION

In the first part of the study, the enantioselective organocatalytic construction of dihydronaphthofuran (DHN) and dihydrobenzofuran (DHB) motifs via Friedel-Crafts followed by S_N2 domino-type reactions in the presence of bifunctional quinine derived squaramide organocatalyst was surveyed. As a result of this part, we synthesized 24 different DHN derivatives with β -naphthol in the range of 1-9 h reaction durations, up to >99% ee with complete conversion. 22 different DHN derivatives with α -naphthol units were synthesized in the range of 50 min-21 h reaction durations, up to 92% ee with complete conversion. In the end, 19 different DHB derivatives with phenol derivatives were synthesized in the range of 1-9 h reaction durations, up to 98% ee with complete conversion. DFT calculations showed that *trans*-conformation involving the two possibly reacting -CH groups of the reactants having π -stacked interactions in the Friedel-Crafts step are 0.79 kcal/mol more stable than the *cis*-conformation. Additionally, the two lowest energy structures with organocatalyst **19b** possessing *trans*-conformations could satisfy the perfect overlap of the reactants and intermolecular distance to give high *si*-face selectivity over *re*-face.

In the second part of the study, a similar domino approach was also applied for the synthesis of 2,3-dihydrofuran derivatives. 9 different DHF derivatives with acetylacetone were synthesized in the range of 1-6.5 h reaction durations, up to 95% ee with complete conversion, and 2 different DHF derivatives with methyl acetoacetate were synthesized in 3 h reaction durations, up to 89% ee with 96% isolated yield.

In the third part of the study, recyclable different heterogeneous organocatalysts were synthesized starting from homogeneous organocatalysts developed in our group. Gold nanoparticle immersed to fused silica solid-supported *tert*-butyl quinine amine bifunctional organocatalyst **74** was synthesized. Some modifications will be applied to improve that catalyst. Additional methods were generated successfully for synthesizing GNP stabilized organocatalysts **76** and **81**. Finally, a novel fluoros supported squaramide type organocatalyst **84** was designed, and the acidic part of the catalyst **83** was successfully synthesized.

REFERENCES

1. Swedish Academy of Sciences, R. Press release: The Nobel Prize in Chemistry 2021 <https://www.nobelprize.org/uploads/2021/10/press-chemistryprize2021.pdf> (accessed Nov 11, 2021).
2. Press release: The Nobel Prize in Chemistry 2021 - NobelPrize.org <https://www.nobelprize.org/prizes/chemistry/2021/press-release/> (accessed Mar 9, 2022).
3. Ahrendt, K. A.; Borths, C. J.; MacMillan, D. W. C. New Strategies for Organic Catalysis: The First Highly Enantioselective Organocatalytic Diels - Alder Reaction. *J. Am. Chem. Soc.* **2000**, 4243–4244.
4. List, B.; Lerner, R. A.; Barbas, C. F. Proline-Catalyzed Direct Asymmetric Aldol Reactions. *J. Am. Chem. Soc.* **2000**, 2395–2396.
5. Langenbeck, W. Die Organischen Katalysatoren Und Ihre Beziehungen Zu Den Fermenten. *Die Org. Katalysatoren und ihre Beziehungen zu den Fermenten* **1935**.
6. Bredig, G.; Fiske, P. S. *Biochem. Z.* **1912**, 46, 7.
7. Seayad, I.; List, B. Asymmetric Organocatalysis. *Org. Biomol. Chem.* **2005**, 3 (5), 719–724.
8. Buckley, B. R. Organocatalysis. *Annu. Reports Prog. Chem. - Sect. B* **2009**, 105, 113–128.
9. Okino, T.; Hoashi, Y.; Takemoto, Y. Enantioselective Michael Reaction of Malonates to Nitroolefins Catalyzed by Bifunctional Organocatalysts. *J. Am. Chem. Soc.* **2003**, 125 (42), 12672–12673.
10. Huang, H.; Jacobsen, E. N. Highly Enantioselective Direct Conjugate Addition of Ketones to Nitroalkenes Promoted by a Chiral Primary Amine-Thiourea Catalyst. *J. Am. Chem. Soc.* **2006**, 128 (22), 7170–7171.
11. Nugent, B. M.; Yoder, R. A.; Johnston, J. N. Chiral Proton Catalysis: A Catalytic Enantioselective Direct Aza-Henry Reaction. *J. Am. Chem. Soc.* **2004**, 126 (11), 3418–3419.
12. Wu, F.; Hong, R.; Khan, J.; Liu, X.; Deng, L. Asymmetric Synthesis of Chiral Aldehydes by Conjugate Additions with Bifunctional Organocatalysis by Cinchona Alkaloids. *Angew. Chemie - Int. Ed.* **2006**, 45 (26), 4301–4305.
13. Wang, J.; Li, H.; Yu, X.; Zu, L.; Wang, W. Chiral Binaphthyl-Derived Amine-Thiourea Organocatalyst-Promoted Asymmetric Morita–Baylis–Hillman Reaction. *Org. Lett.* **2005**, 7 (19), 4293–4296.
14. Rabalakos, C.; Wulff, W. D. Enantioselective Organocatalytic Direct Michael Addition of Nitroalkanes to Nitroalkenes Promoted by a Unique Bifunctional DMAP-Thiourea. *J. Am. Chem. Soc.* **2008**, 130 (41), 13524–13525.
15. McCooney, S. H.; Connon, S. J. Urea- and Thiourea-Substituted Cinchona Alkaloid Derivatives as Highly Efficient Bifunctional Organocatalysts for the Asymmetric Addition of Malonate to Nitroalkenes: Inversion of Configuration at C9 Dramatically Improves Catalyst Performance. *Angew. Chemie - Int. Ed.* **2005**, 44 (39), 6367–6370.
16. Taylor, M. S.; Tokunaga, N.; Jacobsen, E. N. Enantioselective Thiourea-

- Catalyzed Acyl-Mannich Reactions of Isoquinolines. *Angew. Chemie - Int. Ed.* **2005**, *44* (41), 6700–6704.
17. Akiyama, T.; Itoh, J.; Yokota, K.; Fuchibe, K. Enantioselective Mannich-Type Reaction Catalyzed by a Chiral Brønsted Acid. *Angew. Chemie - Int. Ed.* **2004**, *43* (12), 1566–1568.
 18. Rajaram, S.; Sigman, M. S. Design of Hydrogen Bond Catalysts Based on a Modular Oxazoline Template: Application to an Enantioselective Hetero Diels-Alder Reaction. *Org. Lett.* **2005**, *7* (24), 5473–5475.
 19. Malerich, J. P.; Hagihara, K.; Rawal, V. H. Chiral Squaramide Derivatives Are Excellent Hydrogen Bond Donor Catalysts. *J. Am. Chem. Soc.* **2008**, *130* (44), 14416–14417.
 20. Kacprzak, K. M. Chemistry and Biology of Cinchona Alkaloids. In *Natural Products: Phytochemistry, Botany and Metabolism of Alkaloids, Phenolics and Terpenes*; **2013**, 605–641.
 21. Bharadwaj, K. C.; Gupta, T.; Singh, R. M. Alkaloid Group of Cinchona Officinalis : Structural, Synthetic, and Medicinal Aspects. In *Synthesis of Medicinal Agents from Plants*, **2018**, 205–227.
 22. Abraham, D. J.; Rotella, D. P.; Burger, A. *Burger's Medicinal Chemistry, Drug Discovery and Development*; Wiley, **1997**.
 23. Stork, G.; Niu, D.; Fujimoto, A.; Koft, E. R.; Balkovec, J. M.; Tata, J. R.; Dake, G. R. The First Stereoselective Total Synthesis of Quinine. *J. Am. Chem. Soc.* **2001**, *123* (14), 3239–3242.
 24. Yoon, T. P.; Jacobsen, E. N. Privileged Chiral Catalysts. *Science*. **2003**, 1691–1693.
 25. Brunner, H.; Bügler, J.; Nuber, B. Enantioselective Catalysis 98. Preparation of 9-Amino(9-Deoxy)Cinchona Alkaloids. *Tetrahedron: Asymmetry* **1995**, *6* (7), 1699–1702.
 26. Alemán, J.; Cabrera, S. Applications of Asymmetric Organocatalysis in Medicinal Chemistry. *Chem. Soc. Rev.* **2013**, *42* (2), 774–793.
 27. Storer, R. I.; Aciro, C.; Jones, L. H. Squaramides: Physical Properties, Synthesis and Applications. *Chem. Soc. Rev.* **2011**, *40* (5), 2330–2346.
 28. Zou, H. H.; Hu, J.; Zhang, J.; You, J. S.; Ma, D.; Lü, D.; Xie, R. G. Asymmetric Reduction of Prochiral Ketones with Borane Using Chiral Squaric Amino Alcohols Derived from Camphor as Catalysts. *J. Mol. Catal. A Chem.* **2005**, *242* (1–2), 57–61.
 29. Woong Lee, J.; Hi Ryu, T.; Suk Oh, J.; Yong Bae, H.; Bin Jang, H.; Eui Song, C. Self-Association-Free Dimeric Cinchona Alkaloid Organocatalysts: Unprecedented Catalytic Activity, Enantioselectivity and Catalyst Recyclability in Dynamic Kinetic Resolution of Racemic Azlactones. *Chem. Commun.* **2009**, *46*, 7224–7226.
 30. Xu, D. Q.; Wang, Y. F.; Zhang, W.; Luo, S. P.; Zhong, A. G.; Xia, A. B.; Xu, Z. Y. Chiral Squaramides as Highly Enantioselective Catalysts for Michael Addition Reactions of 4-Hydroxycoumarins and 4-Hydroxypyronone to β , γ -unsaturated α -Keto Esters. *Chem. - A Eur. J.* **2010**, *16* (14), 4177–4180.
 31. Liu, B.; Han, X.; Dong, Z.; Lv, H.; Zhou, H. B.; Dong, C. Highly

- Enantioselective Michael Addition of 1,3-Dicarbonyl Compounds to Nitroalkenes Catalyzed by Designer Chiral BINOL-Quinine-Squaramide: Efficient Access to Optically Active Nitro-Alkanes and Their Isoxazole Derivatives. *Tetrahedron Asymmetry* **2013**, *24* (20), 1276–1280.
32. Manoni, F.; Connon, S. J. Catalytic Asymmetric Tamura Cycloadditions. *Angew. Chemie - Int. Ed.* **2014**, *53* (10), 2628–2632.
 33. Kanberoğlu, E.; Tanyeli, C. Enantioselective Michael Addition of Nitroalkanes to Nitroalkenes Catalyzed by Chiral Bifunctional Quinine-Based Squaramides. *Asian J. Org. Chem.* **2016**, *5* (1), 114–119.
 34. Sultanbawa, M. U. S.; Surendrakumar, S.; Wazeer, M. I. M.; Bladon, P. Novel Resveratrol Tetramer, Vaticaffinol, from *Vatica Affinis* Thw. (Dipterocarpaceae). *J. Chem. Soc. Chem. Commun.* **1981**, *23*, 1204–1206.
 35. Baker, R.; Cooke, N. G.; Humphrey, G. R.; Wright, S. H. B.; Hirshfield, J. Stereoselective Synthesis of the Dihydrobenzo[b]Furan Segments of the Ephedradine Alkaloids. *J. Chem. Soc. Chem. Commun.* **1987**, *14*, 1102–1104.
 36. Kurosawa, W.; Kobayashi, H.; Kan, T.; Fukuyama, T. Total Synthesis of (-)-Ephedradine A: An Efficient Construction of Optically Active Dihydrobenzofuran-Ring via C-H Insertion Reaction. In *Tetrahedron* **2004**, *60*, 9615–9628.
 37. Yin, H. Q.; Lee, B. W.; Kim, Y. C.; Sohn, D. H.; Lee, B. H. Induction of the Anticarcinogenic Marker Enzyme, Quinone Reductase, by *Dalbergiae Lignum*. *Arch. Pharm. Res.* **2004**, *27* (9), 919–922.
 38. Natori, Y.; Tsutsui, H.; Sato, N.; Nakamura, S.; Nambu, H.; Shiro, M.; Hashimoto, S. Asymmetric Synthesis of Neolignans (-)-Epi-Conocarpan and (+)-Conocarpan via Rh(II)-Catalyzed C-H Insertion Process and Revision of the Absolute Configuration of (-)-Epi-Conocarpan. *J. Org. Chem.* **2009**, *74* (11), 4418–4421.
 39. Hou, X. F.; Yao, S.; Mándi, A.; Kurtán, T.; Tang, C. P.; Ke, C. Q.; Li, X. Q.; Ye, Y. Bicinginines A and B, Two New Dimeric Diterpenes from *Cunninghamia Lanceolata*. *Org. Lett.* **2012**, *14* (2), 460–463.
 40. Calter, M. A.; Li, N. Asymmetric Total Syntheses of (-)-Variabilin and (-)-Glycinol. *Org. Lett.* **2011**, *13* (14), 3686–3689.
 41. Snyder, S. A.; Gollner, A.; Chiriac, M. I. Regioselective Reactions for Programmable Resveratrol Oligomer Synthesis. *Nature* **2011**, *474* (7352), 461–466.
 42. Albrecht, L.; Ransborg, L. K.; Lauridsen, V.; Overgaard, M.; Zweifel, T.; Jørgensen, K. A. Taming the Friedel-Crafts Reaction: Organocatalytic Approach to Optically Active 2,3-Dihydrobenzofurans. *Angew. Chemie - Int. Ed.* **2011**, *50* (52), 12496–12500.
 43. Lu, A.; Hu, K.; Wang, Y.; Song, H.; Zhou, Z.; Fang, J.; Tang, C. Enantioselective Synthesis of Trans -Dihydrobenzofurans via Primary Amine-Thiourea Organocatalyzed Intramolecular Michael Addition. *J. Org. Chem.* **2012**, *77* (14), 6208–6214.
 44. Shi, G. Q.; Dropinski, J. F.; Zhang, Y.; Santini, C.; Sahoo, S. P.; Berger, J. P.; MacNaul, K. L.; Zhou, G.; Agrawal, A.; Alvaro, R.; Cai, T. Q.; Hernandez, M.;

- Wright, S. D.; Moller, D. E.; Heck, J. V.; Meinke, P. T. Novel 2,3-Dihydrobenzofuran-2-Carboxylic Acids: Highly Potent and Subtype-Selective PPAR α Agonists with Potent Hypolipidemic Activity. *J. Med. Chem.* **2005**, *48* (17), 5589–5599.
45. Monte, A. P.; Marona-Lewicka, D.; Parker, M. A.; Wainscott, D. B.; Nelson, D. L.; Nichols, D. E. Dihydrobenzofuran Analogues of Hallucinogens. 3. Models of 4-Substituted (2,5-Dimethoxyphenyl)Alkylamine Derivatives with Rigidified Methoxy Groups. *J. Med. Chem.* **1996**, *39* (15), 2953–2961.
46. Pieters, L.; Van Dyck, S.; Gao, M.; Bai, R.; Hamel, E.; Vlietinck, A.; Lemière, G. Synthesis and Biological Evaluation of Dihydrobenzofuran Lignans and Related Compounds as Potential Antitumor Agents That Inhibit Tubulin Polymerization. *J. Med. Chem.* **1999**, *42* (26), 5475–5481.
47. Chiba, K.; Fukuda, M.; Kim, S.; Kitano, Y.; Tada, M. Dihydrobenzofuran Synthesis by an Anodic [3 + 2] Cycloaddition of Phenols and Unactivated Alkenes. *J. Org. Chem.* **1999**, *64* (20), 7654–7656.
48. Stephen, A.; Hashmi, K.; Rudolph, M.; Bats, J. W.; Frey, W.; Rominger, F.; Oeser, T. Gold-Catalyzed Synthesis of Chroman, Dihydrobenzofuran, Dihydroindole, and Tetrahydroquinoline Derivatives. *Chem. - A Eur. J.* **2008**, *14* (22), 6672–6678.
49. Tsui, G. C.; Tsoung, J.; Dougan, P.; Lautens, M. One-Pot Synthesis of Chiral Dihydrobenzofuran Framework via Rh/Pd Catalysis. *Org. Lett.* **2012**, *14* (21), 5542–5545.
50. Blum, T. R.; Zhu, Y.; Nordeen, S. A.; Yoon, T. P. Photocatalytic Synthesis of Dihydrobenzofurans by Oxidative [3+2] Cycloaddition of Phenols. *Angew. Chemie* **2014**, *126* (41), 11236–11239.
51. Xiong, Y. J.; Shi, S. Q.; Hao, W. J.; Tu, S. J.; Jiang, B. A New Dehydrogenative [4 + 1] Annulation between: Para -Quinone Methides (p - QMs) and Iodonium Ylides for the Synthesis of 2,3-Dihydrobenzofurans. *Org. Chem. Front.* **2018**, *5* (23), 3483–3487.
52. Zhang, Z.-M.; Xu, B.; Qian, Y.; Wu, L.; Wu, Y.; Zhou, L.; Liu, Y.; Zhang, J. Palladium-Catalyzed Enantioselective Reductive Heck Reactions: Convenient Access to 3,3-Disubstituted 2,3-Dihydrobenzofuran. *Angew. Chemie* **2018**, *130* (32), 10530–10534.
53. Jarava-Barrera, C.; Esteban, F.; Navarro-Ranninger, C.; Parra, A.; Alemán, J. Asymmetric Synthesis of Trans-Dihydroarylfurans in a Friedel–Crafts/Substitution Domino Reaction under Squaramide Catalysis. *Chem. Commun.* **2013**, *49* (20), 2001.
54. Pan, J.; Li, A. X.; Xu, A. D.; Xie, J.-W. Synthesis of Chiral 1,2-Dihydronaphtho[2,1-b]Furans by Organocatalytic Domino Reactions Catalyzed with Multiple Catalysis. *Aust. J. Chem* **2013**, *66* (11), 1415–1421.
55. Tian, S. K.; Chen, Y.; Hang, J.; Tang, L.; McDaid, P.; Deng, L. Asymmetric Organic Catalysis with Modified Cinchona Alkaloids. *Acc. Chem. Res.* **2004**, *37* (8), 621–631.
56. List, B. Introduction: Organocatalysis. *Chem. Rev.* **2007**, *107* (12), 5413–5415.
57. Dalco, P. I. *Enantioselective Organocatalysis: Reactions and Experimental*

- Procedures*; John Wiley and Sons, **2007**.
58. MacMillan, D. W. C. The Advent and Development of Organocatalysis. *Nature*. **2008**, 304–308.
 59. Pellissier, H. Recent Developments in Enantioselective Organocatalytic Michael Reactions in Aqueous Media. *Curr. Org. Chem.* **2017**, 21.
 60. Işık, M.; Unver, M. Y.; Tanyeli, C. Modularly Evolved 2-Aminodmap/Squaramides as Highly Active Bifunctional Organocatalysts in Michael Addition. *J. Org. Chem.* **2015**, 80 (2), 828–835.
 61. Świderek, K.; Nödling, A. R.; Tsai, Y. H.; Luk, L. Y. P.; Moliner, V. Reaction Mechanism of Organocatalytic Michael Addition of Nitromethane to Cinnamaldehyde: A Case Study on Catalyst Regeneration and Solvent Effects. *J. Phys. Chem. A* **2018**, 122 (1), 451–459.
 62. Shim, J. H.; Lee, M. J.; Lee, M. H.; Kim, B. S.; Ha, D. C. Enantioselective Organocatalytic Michael Reactions Using Chiral (*R,R*)-1,2-Diphenylethylenediamine-Derived Thioureas. *RSC Adv.* **2020**, 10 (53), 31808–31814.
 63. Gryko, D.; Saletta, W. J. Organocatalytic Asymmetric Aldol Reaction in the Presence of Water. *Org. Biomol. Chem.* **2007**, 5 (13), 2148–215.
 64. Mase, N.; Nakai, Y.; Ohara, N.; Yoda, H.; Takabe, K.; Tanaka, F.; Barbas, C. F. Organocatalytic Direct Asymmetric Aldol Reactions in Water. *J. Am. Chem. Soc.* **2006**, 128 (3), 734–735.
 65. Tanaka, F.; Barbas, C. F. Enamine Catalysis: Aldol and Mannich-Type Reactions. In *Enantioselective Organocatalysis: Reactions and Experimental Procedures*; John Wiley & Sons, Ltd, **2007**; 19–55.
 66. Zhao, B. L.; Du, D. M. Chiral-Squaramide-Catalyzed Sulfa-Michael/Aldol Cascade Reactions for Asymmetric Synthesis of Spirothiochromanones. *Asian J. Org. Chem.* **2015**, 4 (8), 778–787.
 67. Heravi, M. M.; Zadsirjan, V.; Dehghani, M.; Hosseintash, N. Current Applications of Organocatalysts in Asymmetric Aldol Reactions: An Update. *Tetrahedron Asymmetry*. Elsevier Ltd **2017**, 587–707.
 68. Zhou, Y. H.; Zhang, Y. Z.; Wu, Z. L.; Cai, T.; Wen, W.; Guo, Q. X. Organocatalytic Asymmetric Aldol Reaction of Arylglyoxals and Hydroxyacetone: Enantioselective Synthesis of 2,3-Dihydroxy-1,4-Diones. *Molecules* **2020**, 25 (3).
 69. Jacoby, C. G.; Vontobel, P. H. V.; Bach, M. F.; Schneider, P. H. Highly Efficient Organocatalysts for the Asymmetric Aldol Reaction. *New J. Chem.* **2018**, 42 (9), 7416–7421.
 70. Merino, P.; Marqués-López, E.; Tejero, T.; Herrera, R. P. Enantioselective Organocatalytic Diels-Alder Reactions. *Synthesis*. **2010**, 1–26.
 71. Suzuki, I.; Ando, M.; Shimabara, R.; Hirata, A.; Takeda, K. A Novel Hydrazone Type Organocatalyst for Enantioselective Diels-Alder Reactions. *Org. Biomol. Chem.* **2011**, 9 (8), 3033–3040.
 72. Gatzenmeier, T.; Van Gemmeren, M.; Xie, Y.; Höfler, D.; Leutzsch, M.; List, B. Asymmetric Lewis Acid Organocatalysis of the Diels-Alder Reaction by a Silylated C-H Acid. *Science*. **2016**, 351 (6276), 949–952.

73. Dell'amico, L.; Vega-Peñaloza, A.; Cuadros, S.; Melchiorre, P. Enantioselective Organocatalytic Diels-Alder Trapping of Photochemically Generated Hydroxy-o-Quinodimethanes. *Angew. Chemie - Int. Ed.* **2016**, *55* (10), 3313–3317.
74. Marcelli, T.; Van Der Haas, R. N. S.; Van Maarseveen, J. H.; Hiemstra, H. Asymmetric Organocatalytic Henry Reaction. *Angew. Chemie - Int. Ed.* **2006**, *45* (6), 929–931.
75. Tan, B.; Chua, P. J.; Li, Y.; Zhong, G. Organocatalytic Asymmetric Tandem Michael-Henry Reactions: A Highly Stereoselective Synthesis of Multifunctionalized Cyclohexanes with Two Quaternary Stereocenters. *Org. Lett.* **2008**, *10* (12), 2437–2440.
76. Uehara, H.; Imashiro, R.; Hernández-Torres, G.; Barbas, C. F. Organocatalytic Asymmetric Assembly Reactions for the Syntheses of Carbohydrate Derivatives by Intermolecular Michael-Henry Reactions. *Proc. Natl. Acad. Sci. U. S. A.* **2010**, *107* (48), 20672–20677.
77. Alvarez-Casao, Y.; Marques-Lopez, E.; Herrera, R. P. Organocatalytic Enantioselective Henry Reactions. *Symmetry*. 2011, pp 220–245.
78. Mahajan, S.; Chauhan, P.; Loh, C. C. J.; Uzungelis, S.; Raabe, G.; Enders, D. Organocatalytic Asymmetric Domino Michael/Henry Reaction of Indolin-3-Ones with o-Formyl- β -Nitrostyrenes. *Synth.* **2015**, *47* (7), 1024–1031.
79. Raja, A.; Hong, B. C.; Liao, J. H.; Lee, G. H. Organocatalytic Enantioselective Michael-Michael-Henry Reaction Cascade. An Entry to Highly Functionalized Hajos-Parrish-Type Ketones with Five to Six Contiguous Stereogenic Centers and Two Quaternary Carbons. *Org. Lett.* **2016**, *18* (8), 1760–1763.
80. Okino, T.; Nakamura, S.; Furukawa, T.; Takemoto, Y. Enantioselective Aza-Henry Reaction Catalyzed by a Bifunctional Organocatalyst. *Org. Lett.* **2004**, *6* (4), 625–627.
81. M.F. Phillips, A. Recent Advances on the Organocatalytic Asymmetric Aza-Henry Reaction. *Curr. Organocatalysis* **2015**, *3* (3), 222–242.
82. Maity, R.; Pan, S. C. Organocatalytic Asymmetric Intramolecular Aza-Henry Reaction: Facile Synthesis of Trans-2,3-Disubstituted Tetrahydroquinolines. *Org. Biomol. Chem.* **2015**, *13* (24), 6825–6831.
83. Susam, D.; Tanyeli, C. Enantioselective Aza-Henry Reaction of *t*-Boc Protected Imines and Nitroalkanes with Bifunctional Squaramide Organocatalysts. *New J. Chem.* **2017**, *41* (9), 3555–3561.
84. Zalte, R. R.; Festa, A. A.; Golantsov, N. E.; Subramani, K.; Rybakov, V. B.; Varlamov, A. V.; Luque, R.; Luque, R.; Voskressensky, L. G. Aza-Henry and Aza-Knoevenagel Reactions of Nitriles for the Synthesis of Pyrido[1,2-a]Indoles. *Chem. Commun.* **2020**, *56* (48), 6527–6530.
85. Sonsona, I. G.; Alegre-Requena, J. V.; Marqués-López, E.; Gimeno, M. C.; Herrera, R. P. Asymmetric Organocatalyzed Aza-Henry Reaction of Hydrazones: Experimental and Computational Studies. *Chem. - A Eur. J.* **2020**, *26* (24), 5469–5478.
86. Bandini, M.; Melloni, A.; Umani-Ronchi, A. New Catalytic Approaches in the Stereoselective Friedel-Crafts Alkylation Reaction. *Angew. Chemie - Int. Ed.*

- 2004, 550–556.
87. Giardinetti, M.; Marrot, J.; Greck, C.; Moreau, X.; Coeffard, V. Aminocatalyzed Synthesis of Enantioenriched Phenalene Skeletons through a Friedel-Crafts/Cyclization Strategy. *J. Org. Chem.* **2018**, *83* (2), 1019–1025.
 88. Heravi, M. M.; Zadsirjan, V.; Heydari, M.; Masoumi, B. Organocatalyzed Asymmetric Friedel-Crafts Reactions: An Update. *Chemical Record.* **2019**, 2236–2340.
 89. Gerosa, G. G.; Marcarino, M. O.; Spanevello, R. A.; Suárez, A. G.; Sarotti, A. M. Re-Engineering Organocatalysts for Asymmetric Friedel-Crafts Alkylation of Indoles through Computational Studies. *J. Org. Chem.* **2020**, *85* (15), 9969–9978.
 90. Bergonzini, G.; Gramigna, L.; Mazzanti, A.; Fochi, M.; Bernardi, L.; Ricci, A. Organocatalytic Asymmetric Povarov Reactions with 2- and 3-Vinylindoles. *Chem. Commun.* **2010**, *46* (2), 327–329.
 91. Shi, F.; Xing, G. J.; Tao, Z. L.; Luo, S. W.; Tu, S. J.; Gong, L. Z. An Asymmetric Organocatalytic Povarov Reaction with 2-Hydroxystyrenes. *J. Org. Chem.* **2012**, *77* (16), 6970–6979.
 92. Simões, J. B.; De Fátima, Â.; Sabino, A. A.; De Aquino, F. J. T.; Da Silva, D. L.; Barbosa, L. C. A.; Fernandes, S. A. Organocatalysis in the Three-Component Povarov Reaction and Investigation by Mass Spectrometry. *Org. Biomol. Chem.* **2013**, *11* (31), 5069–5073.
 93. Huang, J. X.; Hou, K. Q.; Hu, Q. L.; Chen, X. P.; Li, J.; Chan, A. S. C.; Xiong, X. F. Organocatalytic Asymmetric Three-Component Povarov Reactions of Anilines and Aldehydes. *Org. Lett.* **2020**, *22* (5), 1858–1862.
 94. Bermúdez, E.; Ventura, O. N.; Méndez, P. S. Mechanism of the Organocatalyzed Decarboxylative Knoevenagel-Doebner Reaction. A Theoretical Study. *J. Phys. Chem. A* **2010**, *114* (50), 13086–13092.
 95. Lu, J.; Toy, P. H. Organocatalytic Decarboxylative Doebner-Knoevenagel Reactions between Arylaldehydes and Monoethyl Malonate Mediated by a Bifunctional Polymeric Catalyst. *Synlett* **2011**, No. 12, 1723–1726.
 96. Dalko, P. I.; Moisan, L. In the Golden Age of Organocatalysis. *Angew. Chemie - Int. Ed.* **2004**, 5138–5175.
 97. Synthesis of Lophotoxin - New Methodologies and Synthetic Strategies. *Can. J. Chem.* **2006**, *84* (10), 1226–1241.
 98. Kumar, T. P.; Shekhar, R. C.; Sunder, K. S.; Vadaparthi, R. Myrtanyl-Prolinamide: A New Chiral Organocatalyst for Stereoselective Aldol Reactions. *Tetrahedron Asymmetry* **2015**, *26* (10–11), 543–547.
 99. Rueping, M.; Nachtsheim, B. J. A Review of New Developments in the Friedel-Crafts Alkylation - From Green Chemistry to Asymmetric Catalysis. *Beilstein J. Org. Chem.* **2010**, *6*, No. 6.
 100. Finelli, F. G.; Miranda, L. S. M.; De Souza, R. O. M. A. Expanding the Toolbox of Asymmetric Organocatalysis by Continuous-Flow Process. *Chem. Commun.* **2015**, *51* (18), 3708–3722.
 101. Malkov, A. V.; Figlus, M.; Cooke, G.; Caldwell, S. T.; Rabani, G.; Prestly, M. R.; Kočovský, P. Organocatalysts Immobilised onto Gold Nanoparticles:

- Application in the Asymmetric Reduction of Imines with Trichlorosilane. *Org. Biomol. Chem.* **2009**, 7 (9), 1878–1883.
102. Santacruz, L.; Niembro, S.; Santillana, A.; Shafir, A.; Vallribera, A. Gold Nanoparticles Decorated with a Cinchonine Organocatalyst: Application in the Asymmetric α -Amination of β -Ketoesters. *New J. Chem.* **2014**, 38 (2), 636–640.
 103. S3ti, P. L.; Yamashita, H.; Sato, K.; Narumi, T.; Toda, M.; Watanabe, N.; Marosi, G.; Mase, N. Synthesis of a Self-Assembling Gold Nanoparticle-Supported Organocatalyst for Enamine-Based Asymmetric Aldol Reactions. *Tetrahedron* **2016**, 72 (16), 1984–1990.
 104. Chu, Q.; Zhang, W.; Curran, D. P. A Recyclable Fluorous Organocatalyst for Diels-Alder Reactions. *Tetrahedron Lett.* **2006**, 47 (52), 9287–9290.
 105. Miura, T.; Nishida, S.; Masuda, A.; Tada, N.; Itoh, A. Asymmetric Michael Additions of Aldehydes to Maleimides Using a Recyclable Fluorous Thiourea Organocatalyst. *Tetrahedron Lett.* **2011**, 52 (32), 4158–4160.
 106. Liu, M.; Zhang, X.; Huang, X.; Dhawan, G.; Evans, J.; Kaur, M.; Jasinski, J. P.; Zhang, W. Recyclable Organocatalyst for One-Pot Asymmetric Synthesis of Dihydrofuranone and Tetrahydropyranone Spirooxindoles. *Eur. J. Org. Chem.* **2019**, 2019 (1), 150–155.
 107. Stephens, P. J.; Devlin, F. J.; Chabalowski, C. F.; Frisch, M. J. Ab Initio Calculation of Vibrational Absorption and Circular Dichroism Spectra Using Density Functional Force Fields. *J. Phys. Chem.* **1994**, 98 (45), 11623–11627.
 108. Becke, A. D. Density-Functional Thermochemistry. III. The Role of Exact Exchange. *J. Chem. Phys.* **1993**, 98 (7), 5648–5652.
 109. Lee, C.; Yang, W.; Parr, R. G. Development of the Colle-Salvetti Correlation-Energy Formula into a Functional of the Electron Density. *Phys. Rev. B* **1988**, 37 (2), 785–789.
 110. Gaussian 09, Revision A.02, M. J. Frisch, G. W. Trucks, H. B. Schlegel, G. E. Scuseria, M. A. Robb, J. R. Cheeseman, G. Scalmani, V. Barone, G. A. Petersson, H. Nakatsuji, X. Li, M. Caricato, A. Marenich, J. Bloino, B. G. Janesko, R. Gomperts, B. Mennucci, H. P. Hratchian, J. V. Ortiz, A. F. Izmaylov, J. L. Sonnenberg, D. Williams-Young, F. Ding, F. Lipparini, F. Egidi, J. Goings, B. Peng, A. Petrone, T. Henderson, D. Ranasinghe, V. G. Zakrzewski, J. Gao, N. Rega, G. Zheng, W. Liang, M. Hada, M. Ehara, K. Toyota, R. Fukuda, J. Hasegawa, M. Ishida, T. Nakajima, Y. Honda, O. Kitao, H. Nakai, T. Vreven, K. Throssell, J. A. Montgomery, Jr., J. E. Peralta, F. Ogliaro, M. Bearpark, J. J. Heyd, E. Brothers, K. N. Kudin, V. N. Staroverov, T. Keith, R. Kobayashi, J. Normand, K. Raghavachari, A. Rendell, J. C. Burant, S. S. Iyengar, J. Tomasi, M. Cossi, J. M. Millam, M. Klene, C. Adamo, R. Cammi, J. W. Ochterski, R. L. Martin, K. Morokuma, O. Farkas, J. B. Foresman, and D. J. Fox, Gaussian, Inc., Wallingford CT, **2016**.
 111. Tomasi, J.; Mennucci, B.; Cancès, E. The IEF Version of the PCM Solvation Method: An Overview of a New Method Addressed to Study Molecular Solutes at the QM Ab Initio Level. In *Journal of Molecular Structure: Theochem.* **1999**, 464, 211–226.

112. Grimme, S.; Antony, J.; Ehrlich, S.; Krieg, H. A Consistent and Accurate Ab Initio Parametrization of Density Functional Dispersion Correction (DFT-D) for the 94 Elements H-Pu. *J. Chem. Phys.* **2010**, *132* (15).
113. Becke, A. D.; Johnson, E. R. A Density-Functional Model of the Dispersion Interaction. *J. Chem. Phys.* **2005**, *123* (15).
114. Bozdemir, M. Asymmetric Synthesis of 2,3-Dihydrofurans with Bifunctional Quinine / Squaramide Organocatalysts METU, **2019**.
115. Susam, Z. D.; Bozdemir, M.; Gündoğdu, G.; Tanyeli, C. Enantioselective Synthesis of 2,3-Dihydrofurans Using a Bifunctional Quinine/Squaramide Organocatalyst. *New J. Chem.* **2022**, *46* (2), 599–606.
116. Khan, S. A.; Vandervelden, C. A.; Scott, S. L.; Peters, B. Grafting Metal Complexes onto Amorphous Supports: From Elementary Steps to Catalyst Site Populations: Via Kernel Regression. *React. Chem. Eng.* **2020**, *5* (1), 66–76.
117. Zaera, F. Molecular Approaches to Heterogeneous Catalysis. *Coordination Chemistry Reviews.* **2021**.
118. Meyer, N.; de Coster, Y.; Devillers, M.; Hermans, S. Grafting and Anchoring of Molecular Complexes as Metal Precursors for Alumina-Supported Pd Catalysts. *J. Coord. Chem.* **2018**, *71* (15), 2304–2321.
119. Kokkin, D. L.; Zhang, R.; Steimle, T. C.; Wyse, I. A.; Pearlman, B. W.; Varberg, T. D. Au-S Bonding Revealed from the Characterization of Diatomic Gold Sulfide, AuS. *J. Phys. Chem. A* **2015**, *119* (48), 11659–11667.
120. Greger, J. G.; Yoon-Miller, S. J. P.; Bechtold, N. R.; Flewelling, S. A.; MacDonald, J. P.; Downey, C. R.; Cohen, E. A.; Pelkey, E. T. Synthesis of Unsymmetrical 3,4-Diaryl-3-Pyrrolin-2-Ones Utilizing Pyrrole Weinreb Amides. *J. Org. Chem.* **2011**, *76* (20), 8203–8214.
121. Belmessieri, D.; De La Houpliere, A.; Calder, E. D. D.; Taylor, J. E.; Smith, A. D. Stereodivergent Organocatalytic Intramolecular Michael Addition/Lactonization for the Asymmetric Synthesis of Substituted Dihydrobenzofurans and Tetrahydrofurans. *Chem. - A Eur. J.* **2014**, *20* (31), 9762–9769.
122. Martínez-Montero, I.; Bruña, S.; González-Vadillo, A. M.; Cuadrado, I. Thiol-Ene Chemistry of Vinylferrocene: A Simple and Versatile Access Route to Novel Electroactive Sulfur- and Ferrocene-Containing Model Compounds and Polysiloxanes. *Macromolecules* **2014**, *47* (4), 1301–1315.
123. Kazutake Hagiya, M. H. WO1993025544A1 - Process for Producing Amine-Boranes, **2011**.

APPENDICES

A. NMR SPECTRA

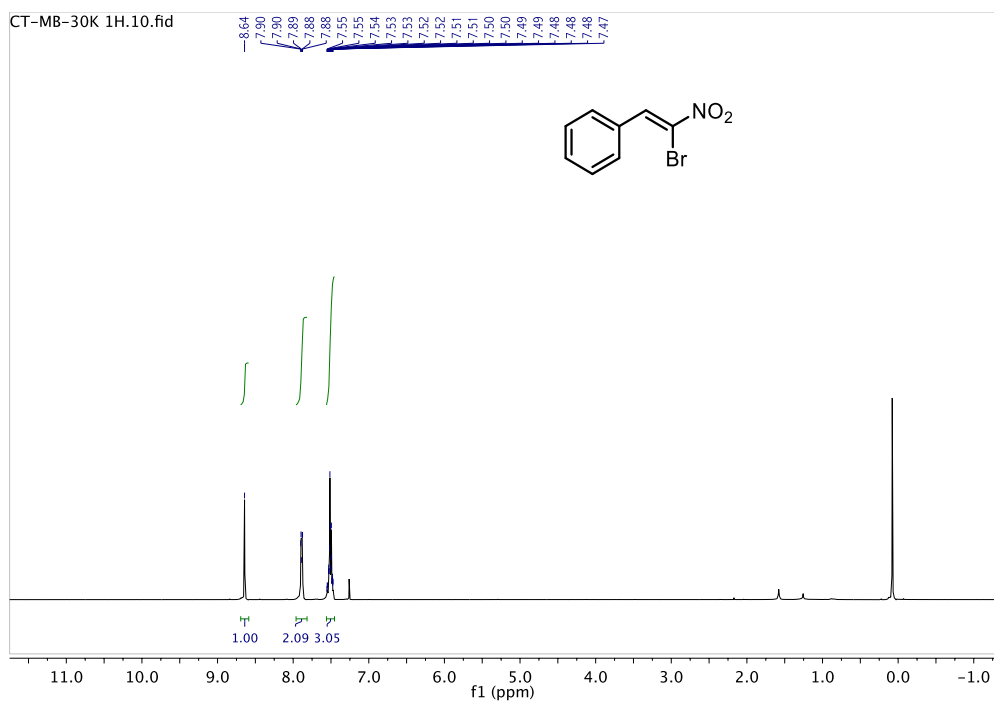


Figure A. 1. ¹H NMR spectrum of 20a

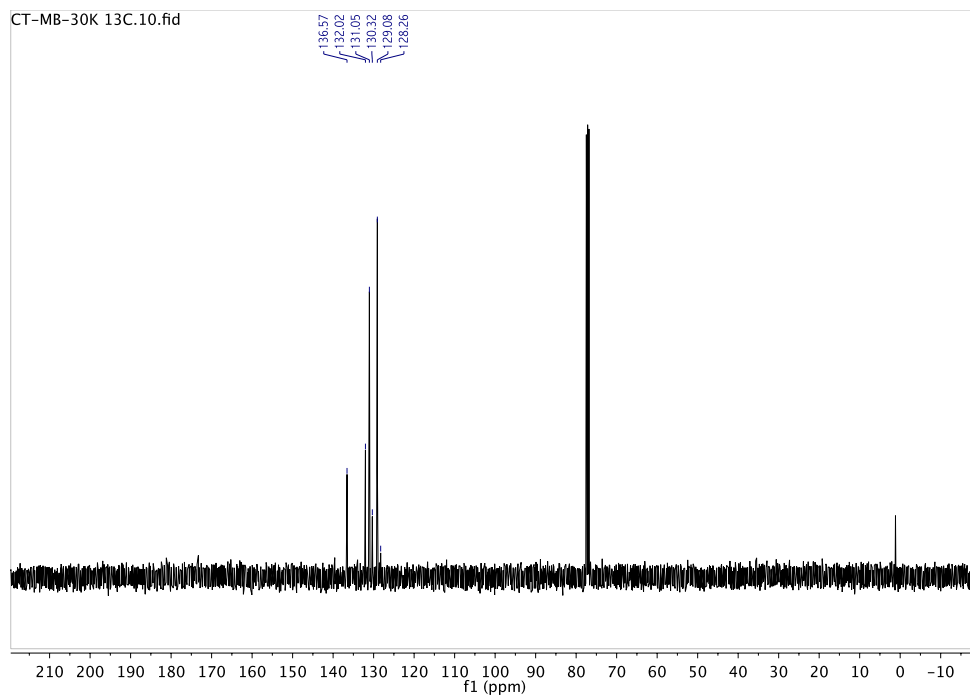


Figure A. 2. ¹³C NMR spectrum of 20a

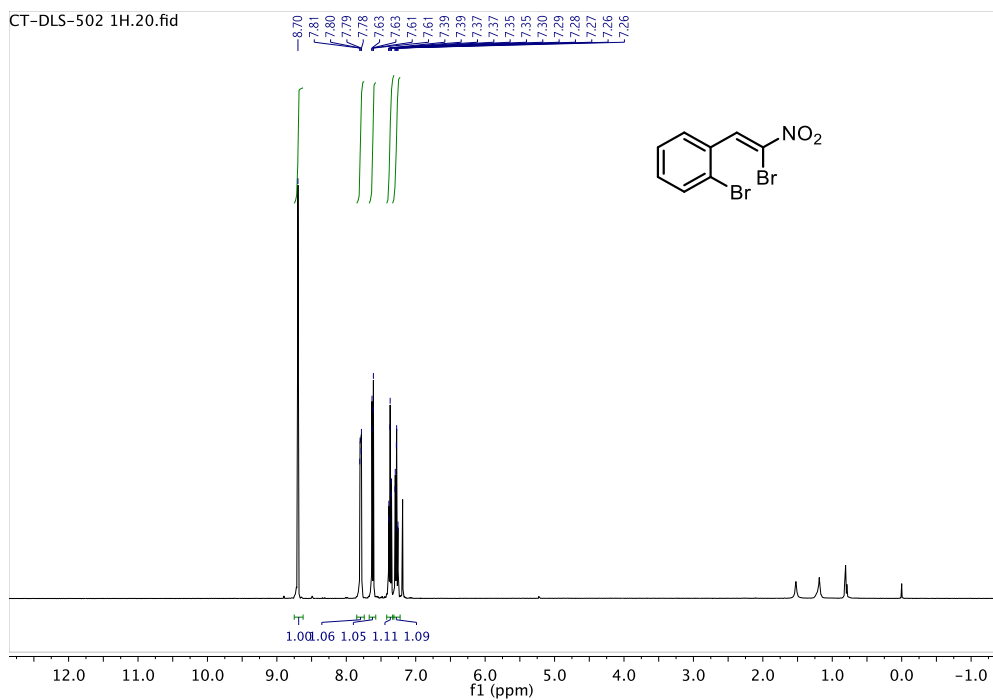


Figure A. 3. ^1H NMR spectrum of **20b**

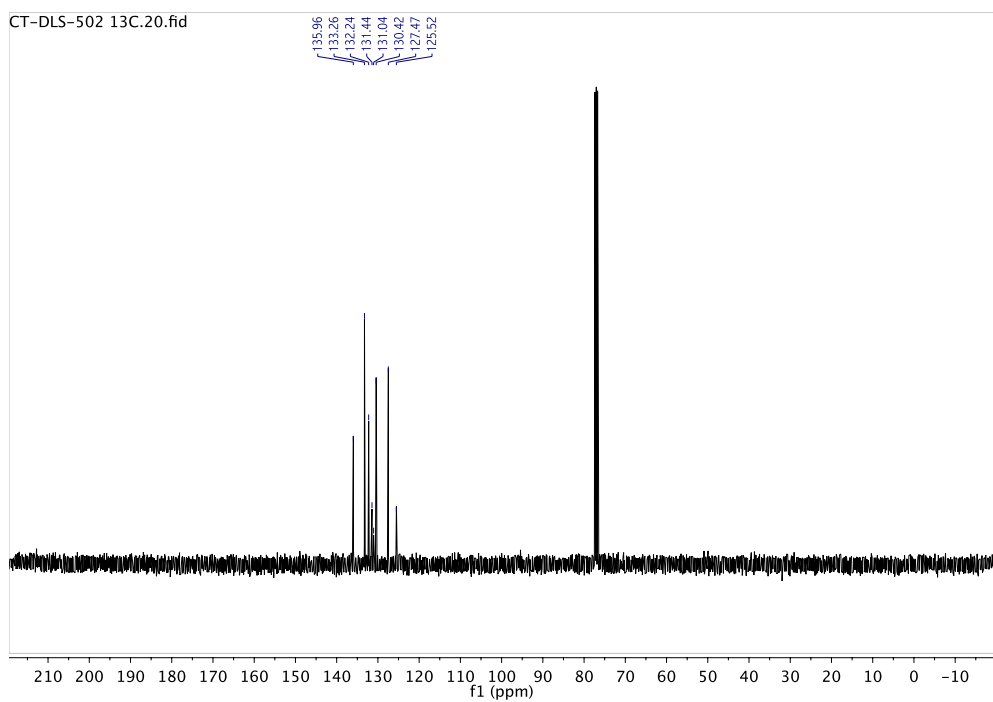


Figure A. 4. ^{13}C NMR spectrum of **20b**

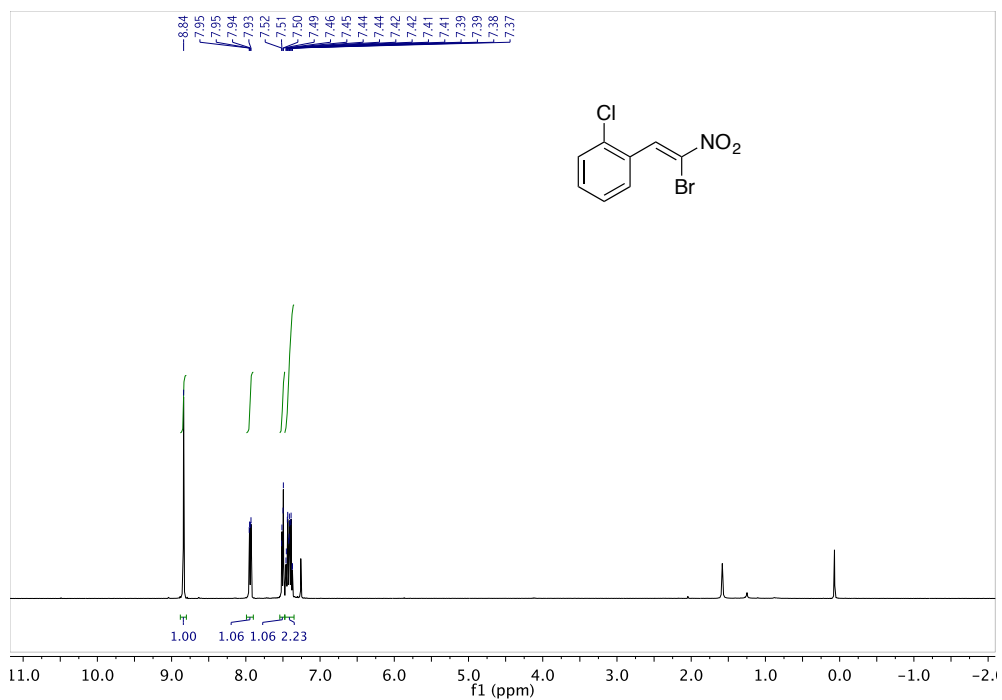


Figure A. 5. ^1H NMR spectrum of 20c

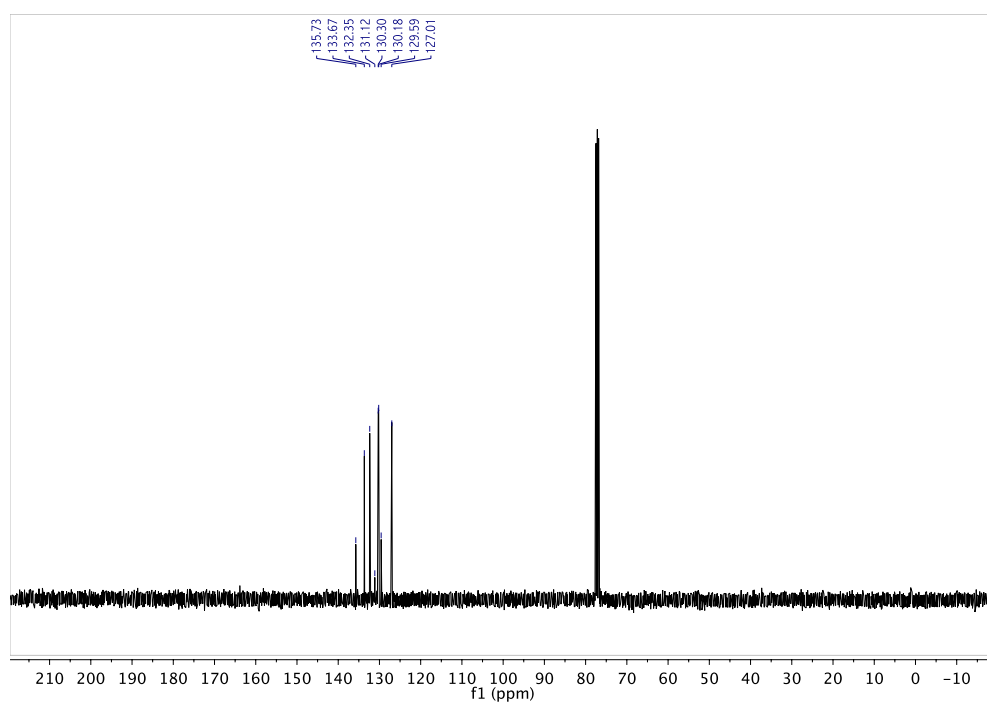


Figure A. 6. ^{13}C NMR spectrum of 20c

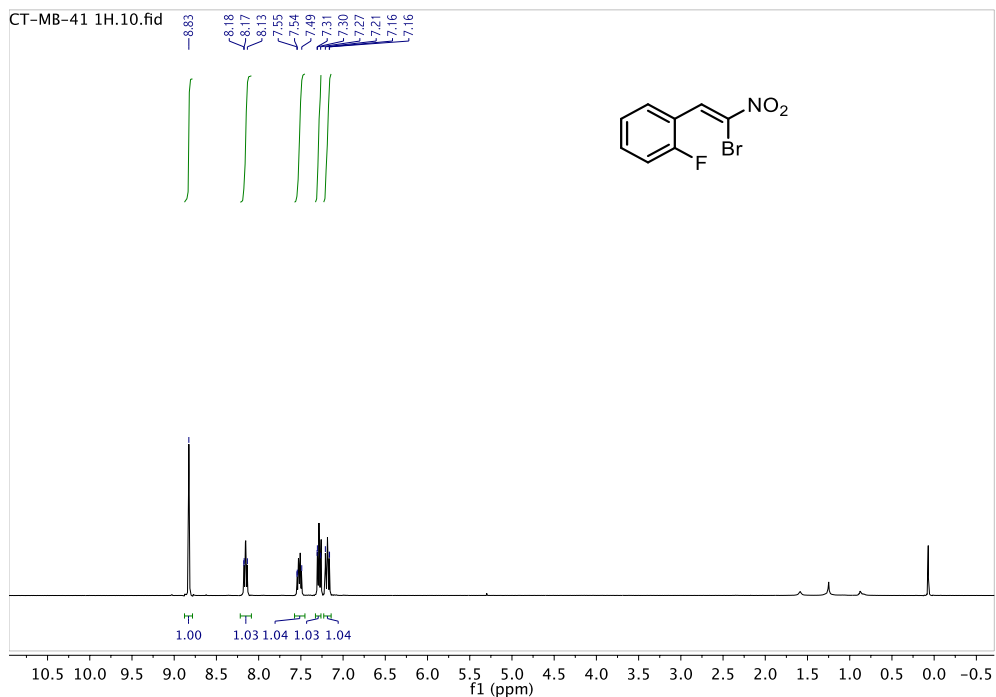


Figure A. 7. ^1H NMR spectrum of **20d**

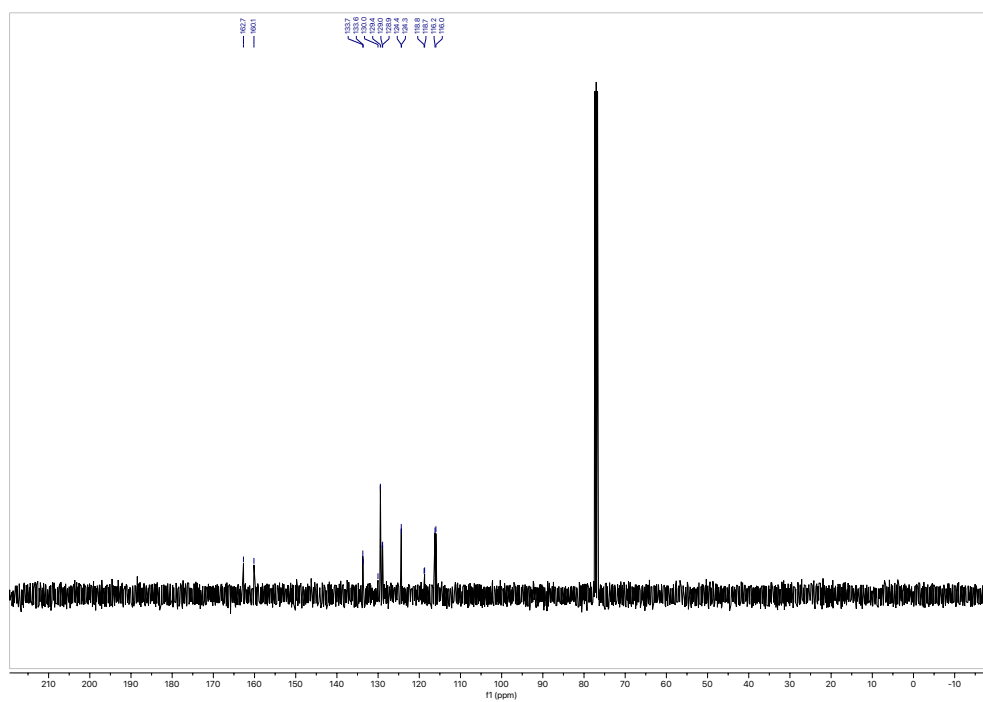


Figure A. 8. ^{13}C NMR spectrum of **20d**

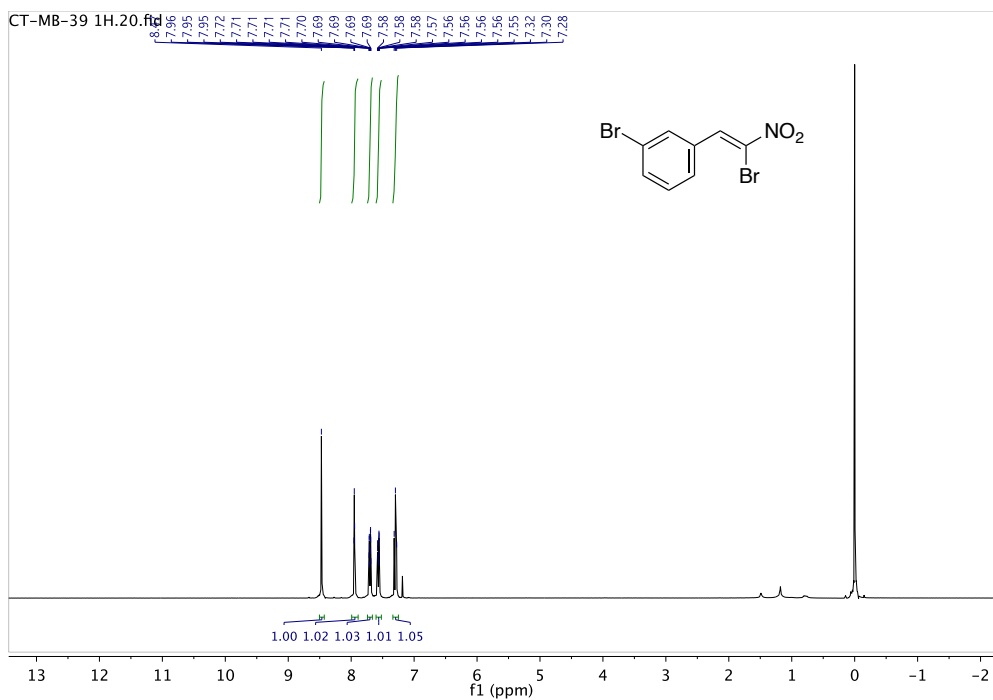


Figure A. 9. ^1H NMR spectrum of 20e

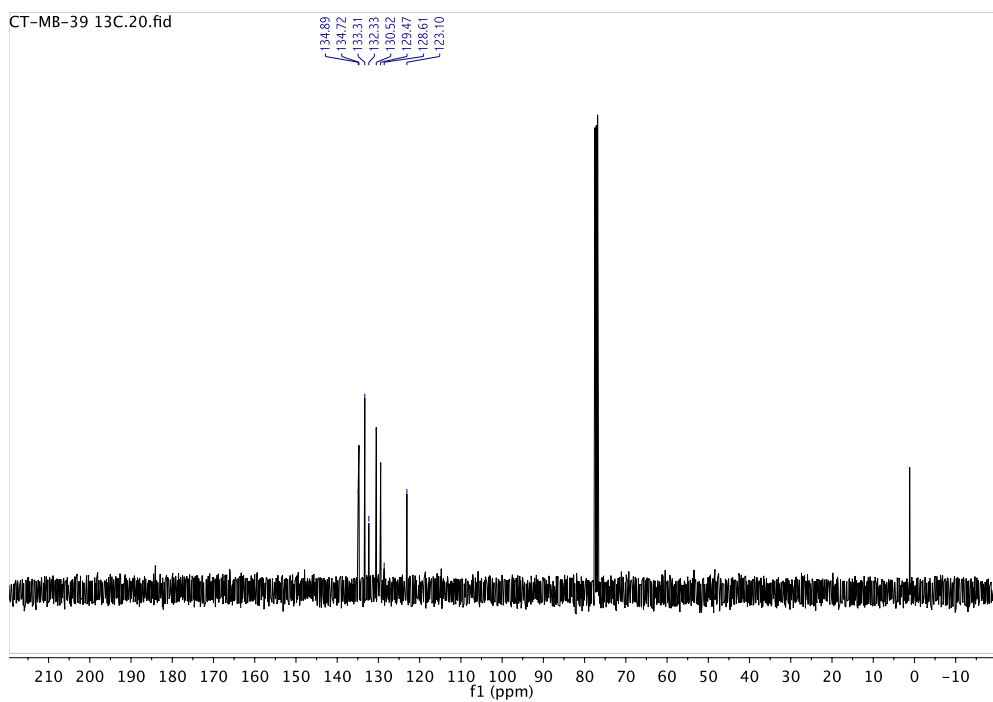


Figure A. 10. ^{13}C NMR spectrum of 20e

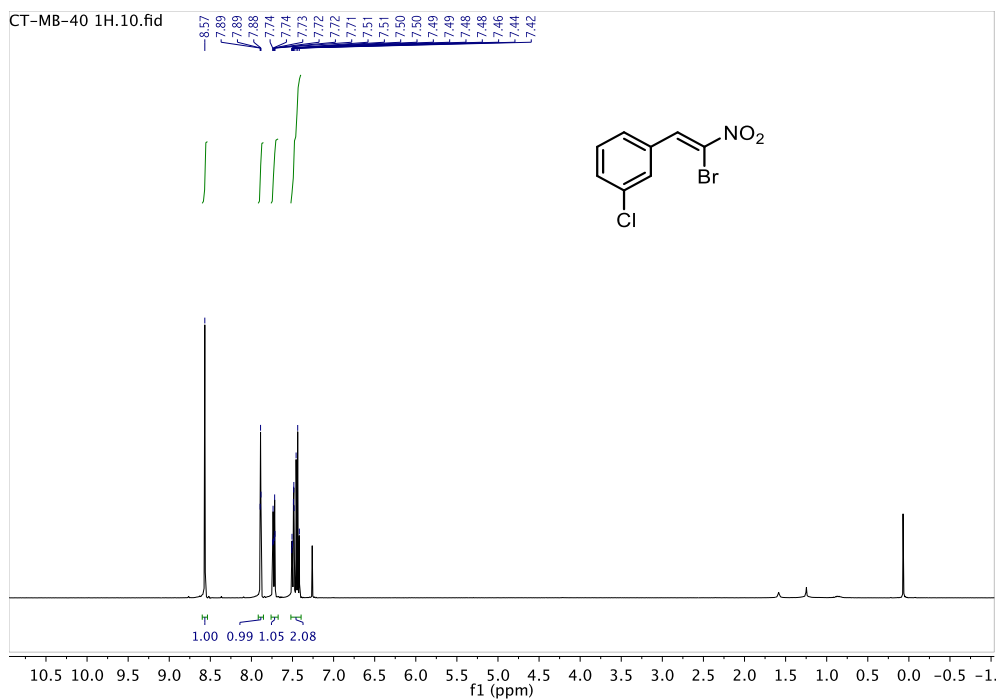


Figure A. 11. ^1H NMR spectrum of 20f

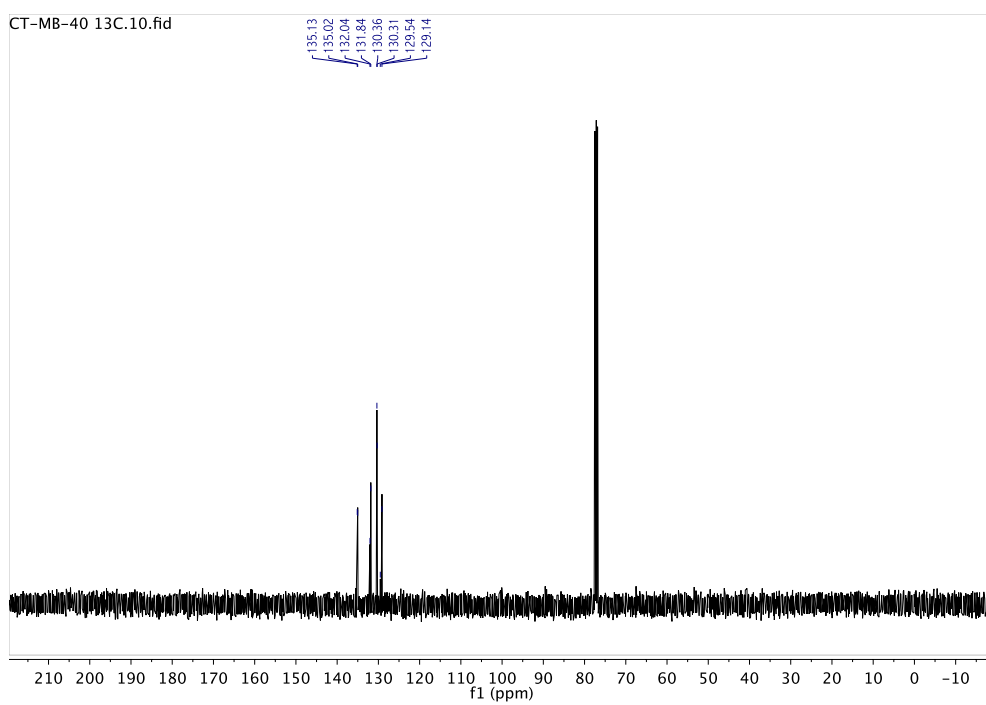


Figure A. 12. ^{13}C NMR spectrum of 20f

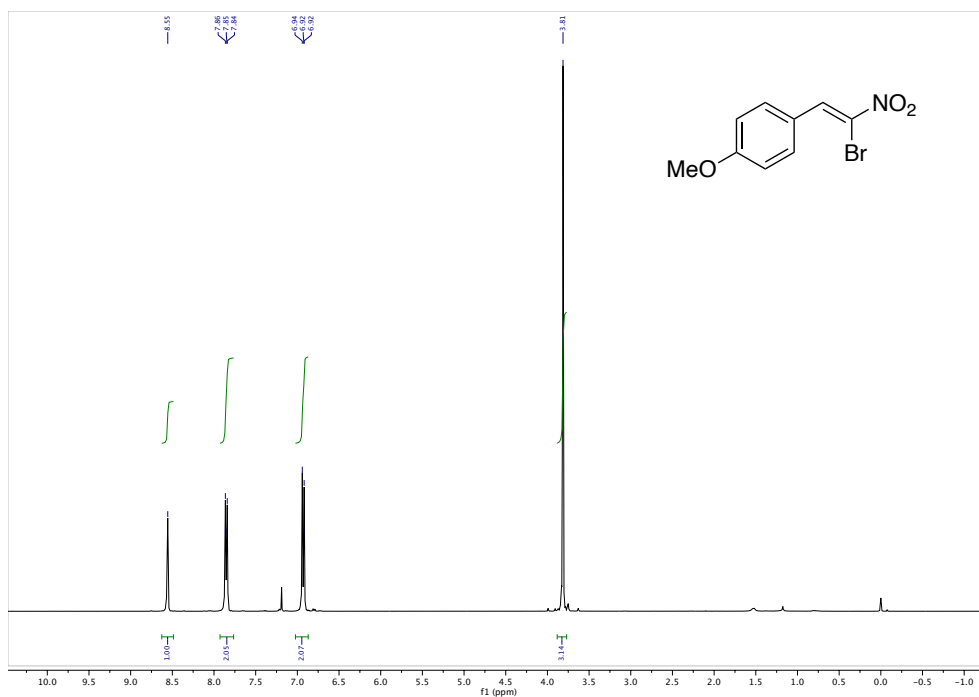


Figure A. 13. ^1H NMR spectrum of **20g**

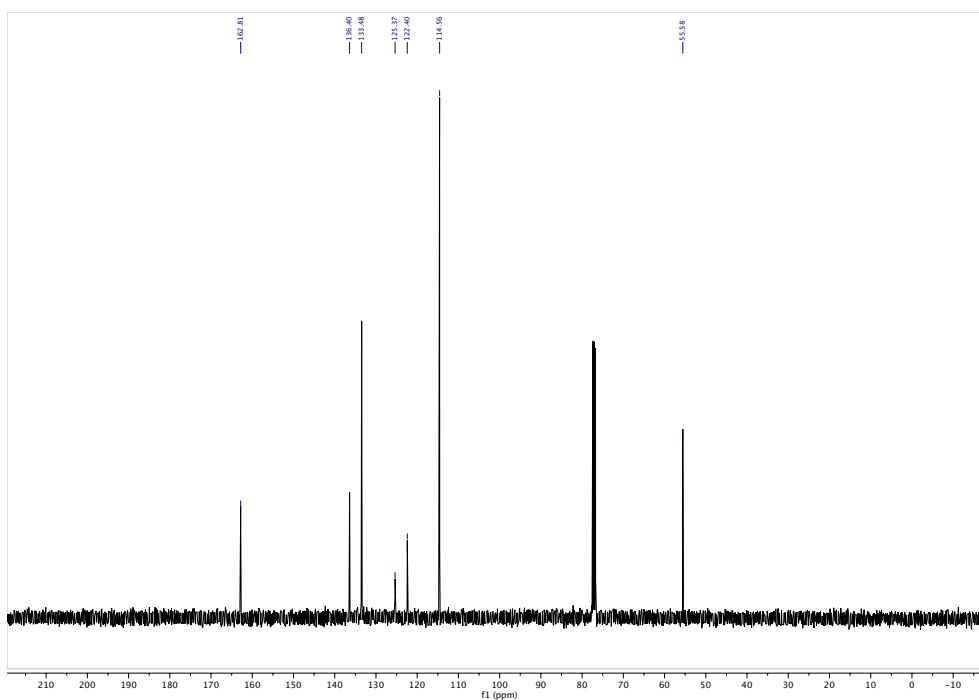


Figure A. 14. ^{13}C NMR spectrum of **20g**

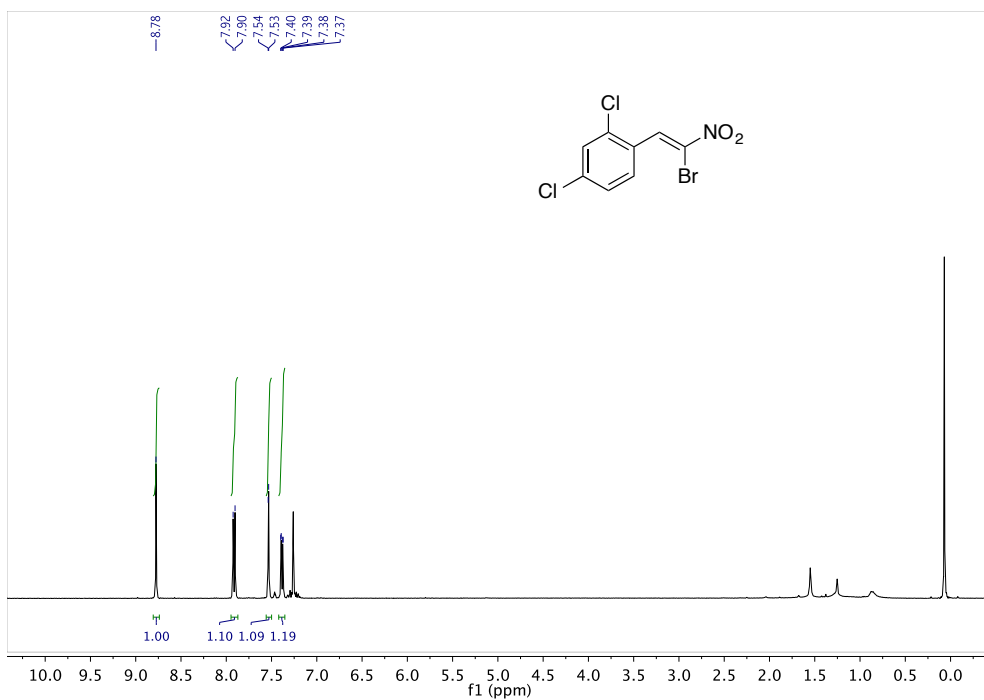


Figure A. 15. ^1H NMR spectrum of 20h

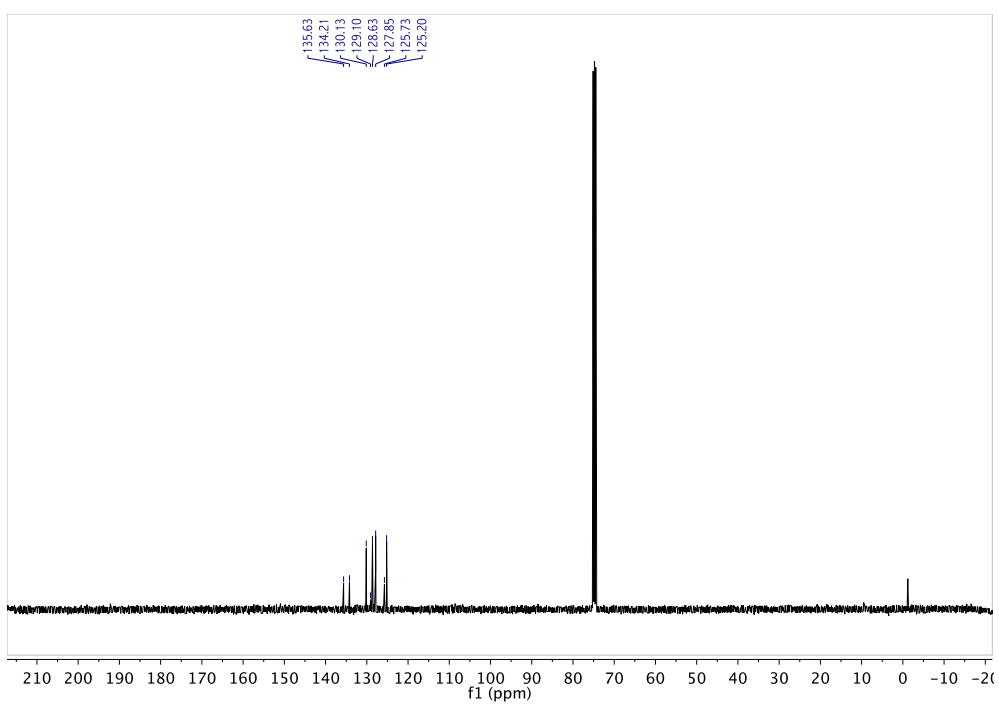
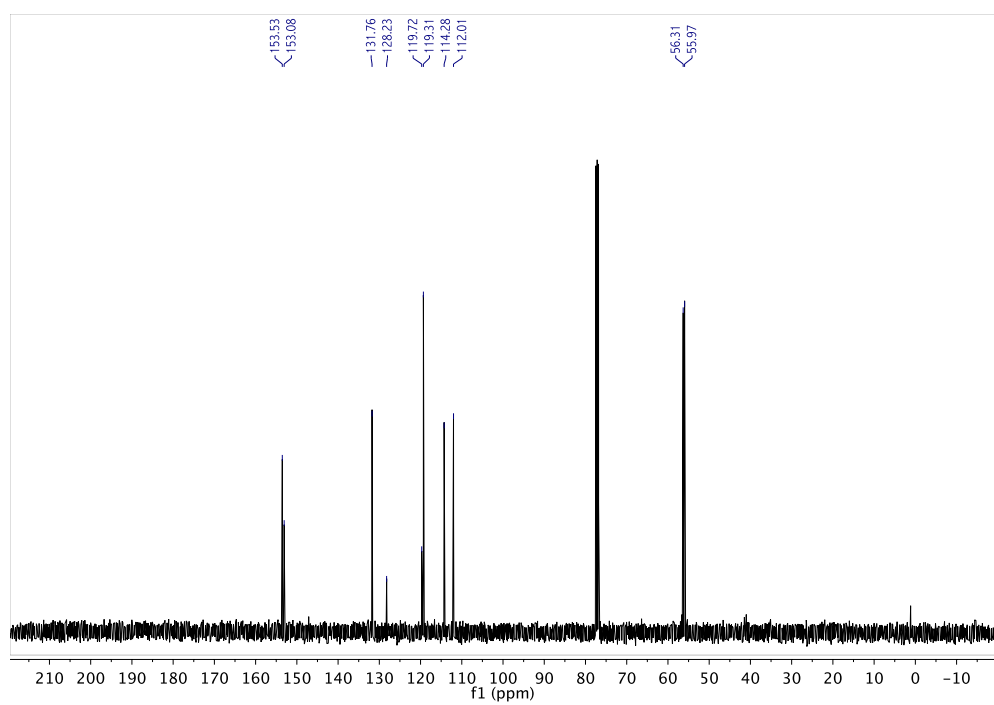
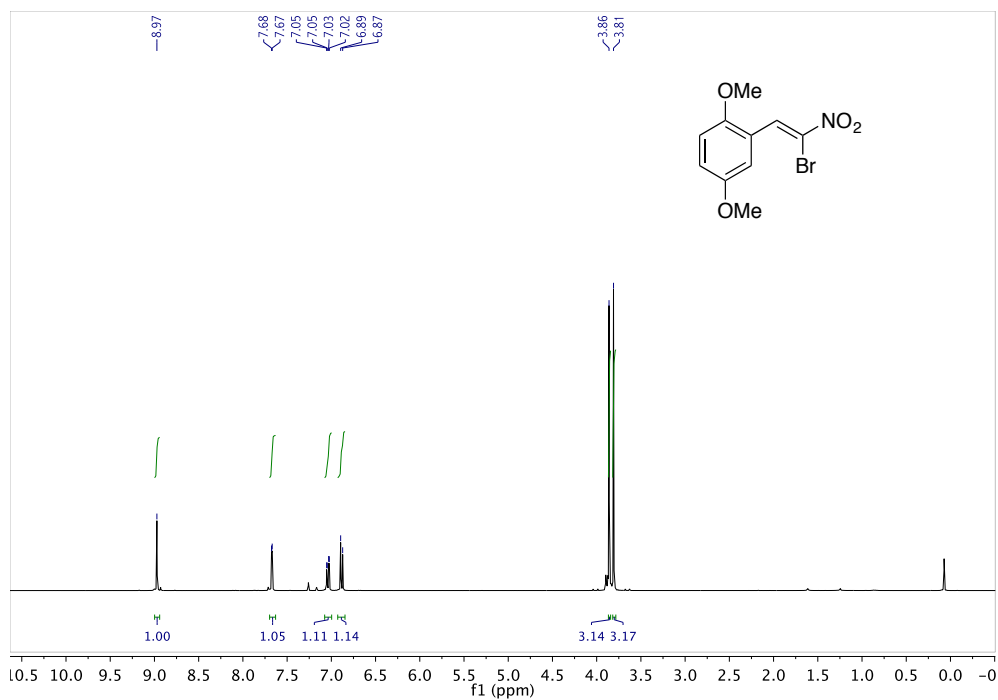


Figure A. 16. ^{13}C NMR spectrum of 20h



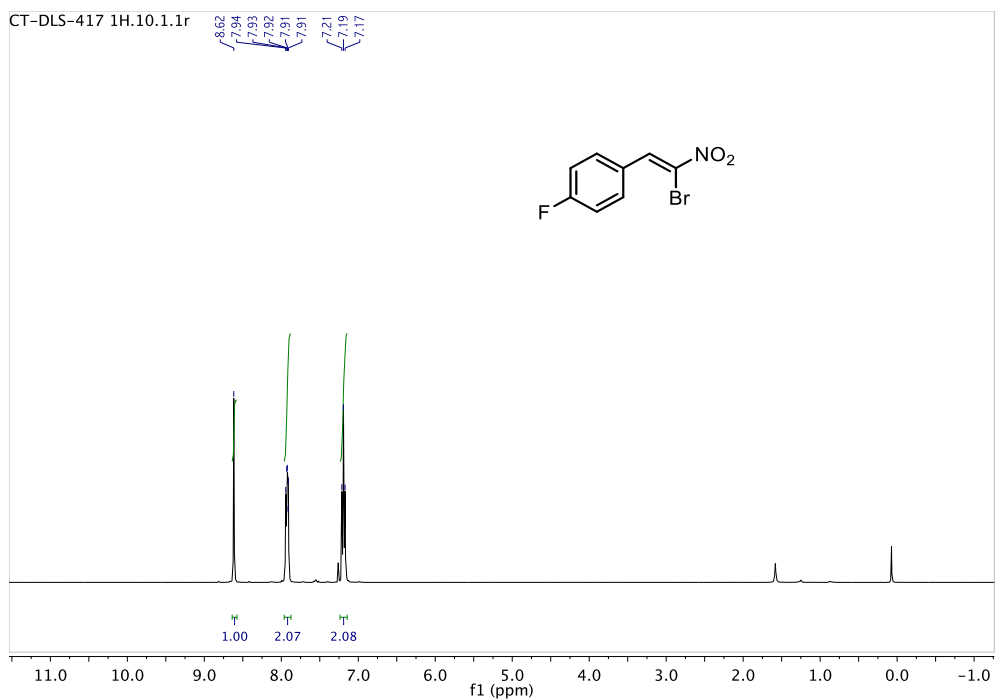


Figure A. 19. ^1H NMR spectrum of **20j**

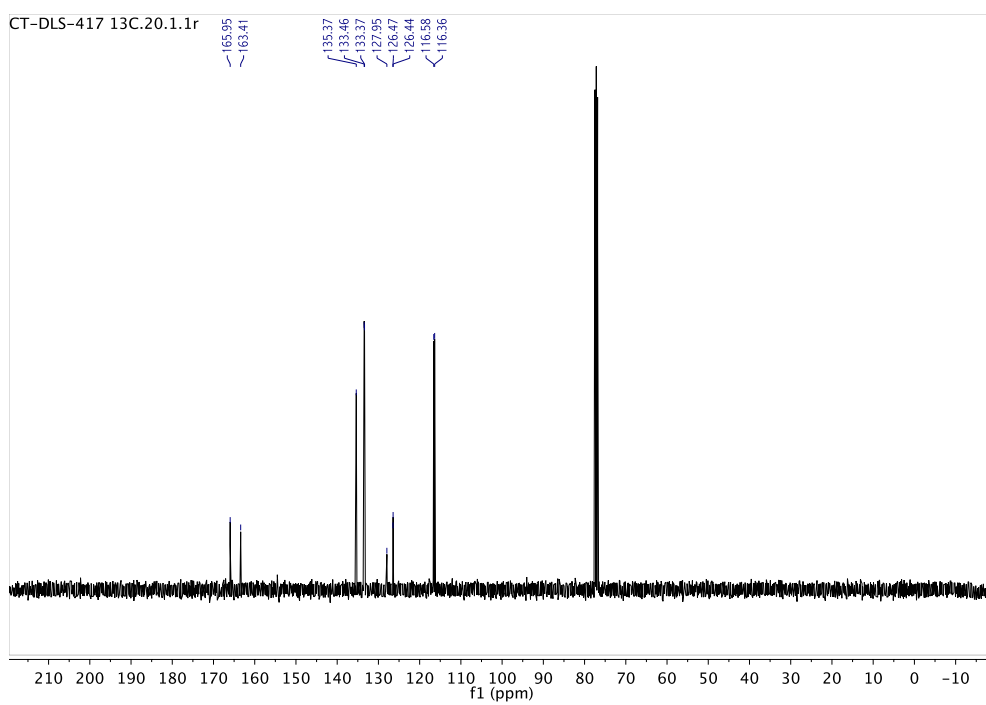


Figure A. 20. ^{13}C NMR spectrum of **20j**

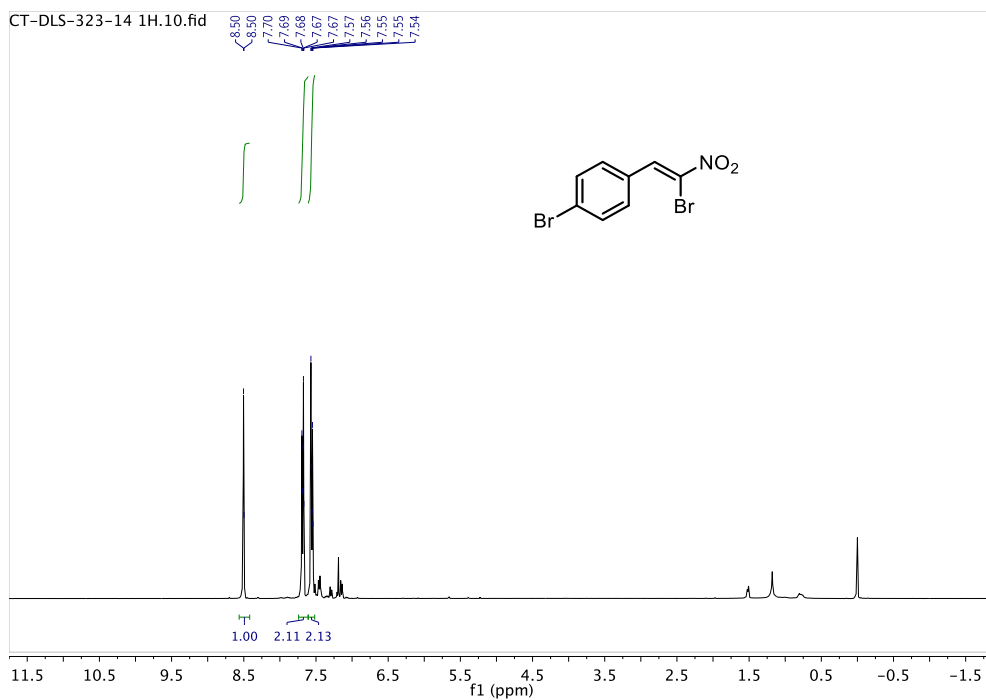


Figure A. 21. ^1H NMR spectrum of **20k**

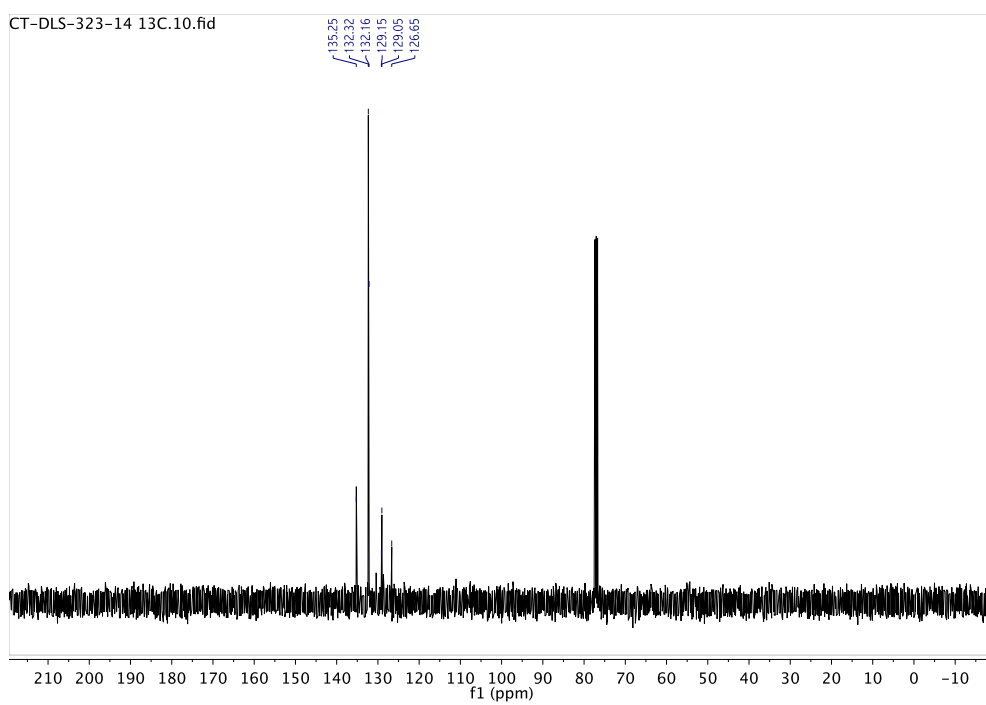


Figure A. 22. ^{13}C NMR spectrum of **20k**

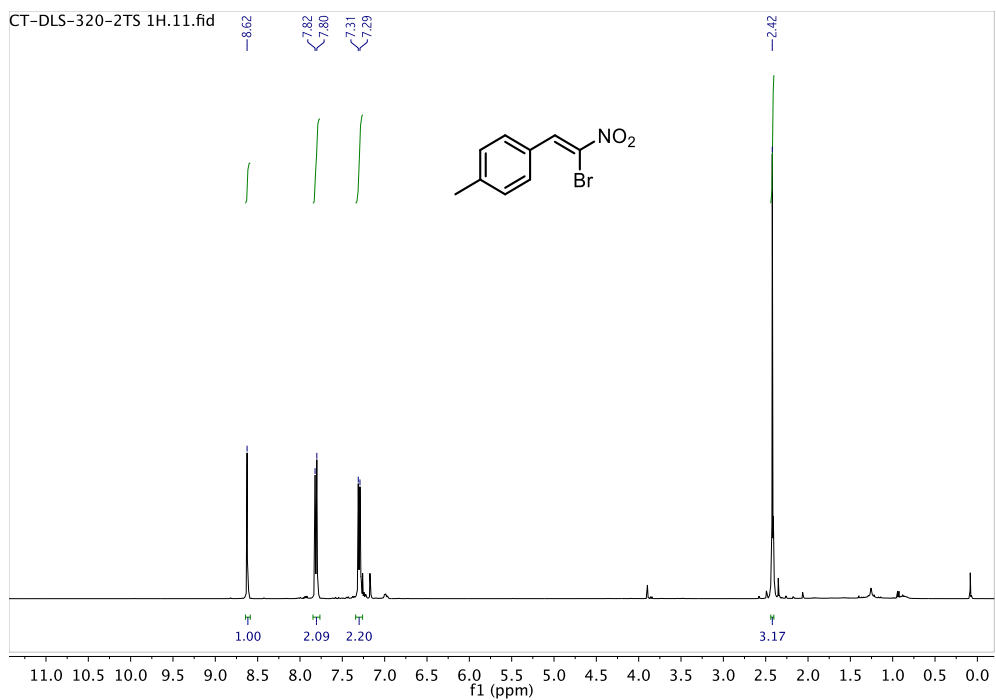


Figure A. 23. ^1H NMR spectrum of 201

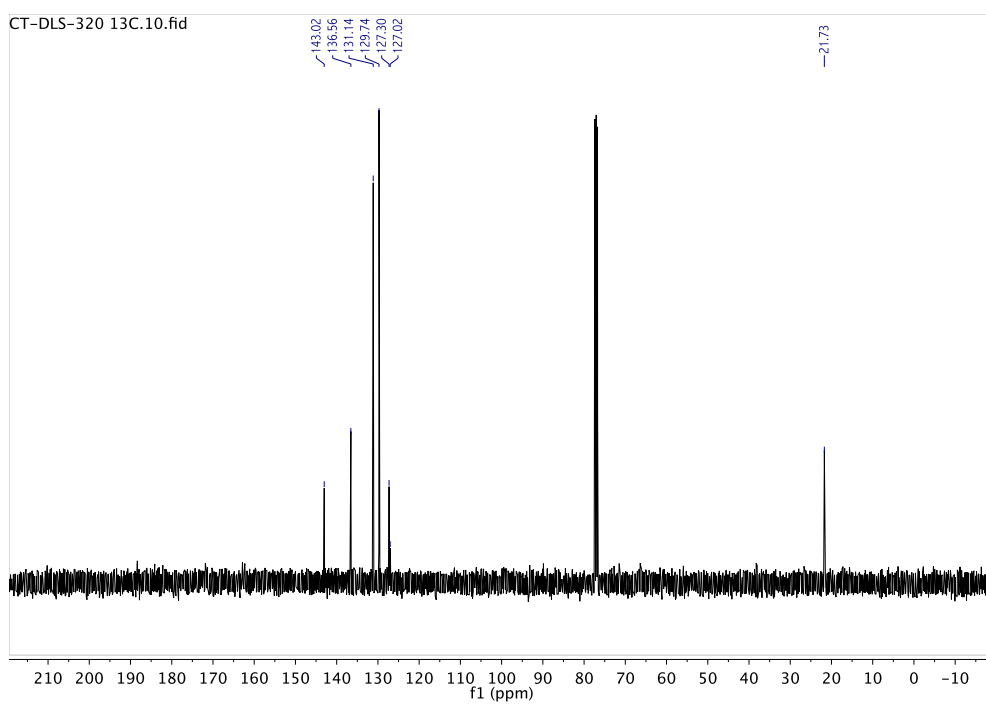


Figure A. 24. ^{13}C NMR spectrum of 201

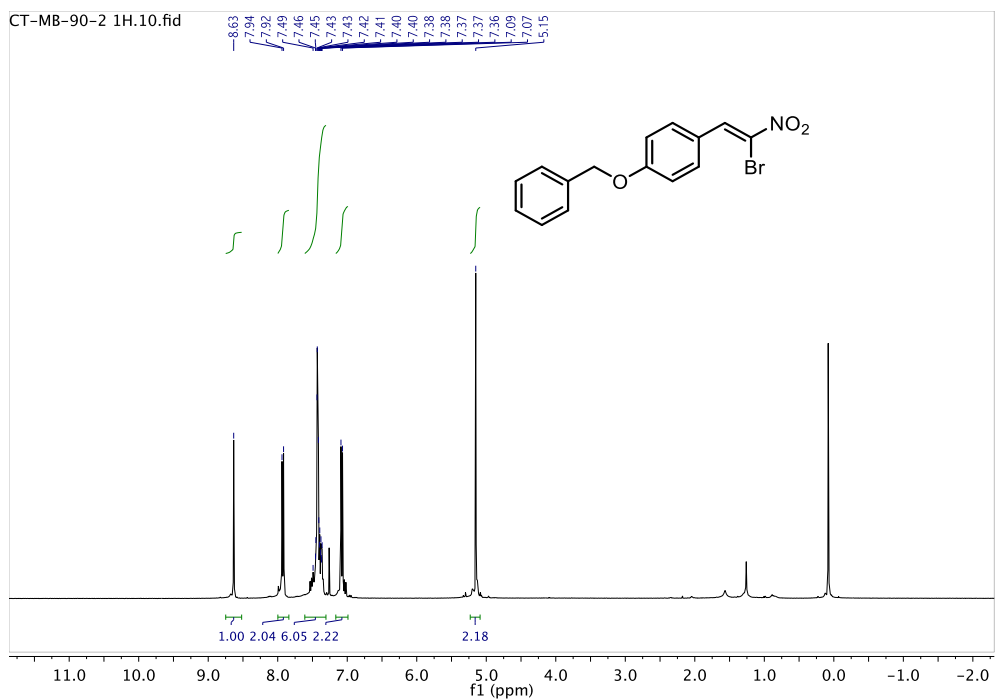


Figure A. 25. ^1H NMR spectrum of **20m**

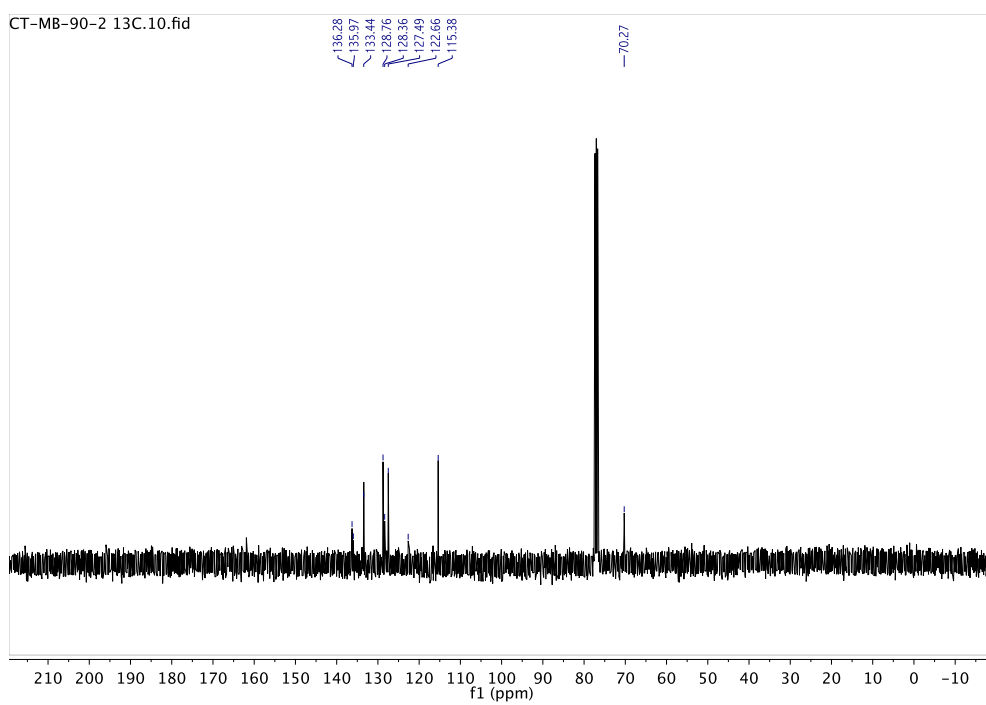


Figure A. 26. ^{13}C NMR spectrum of **20m**

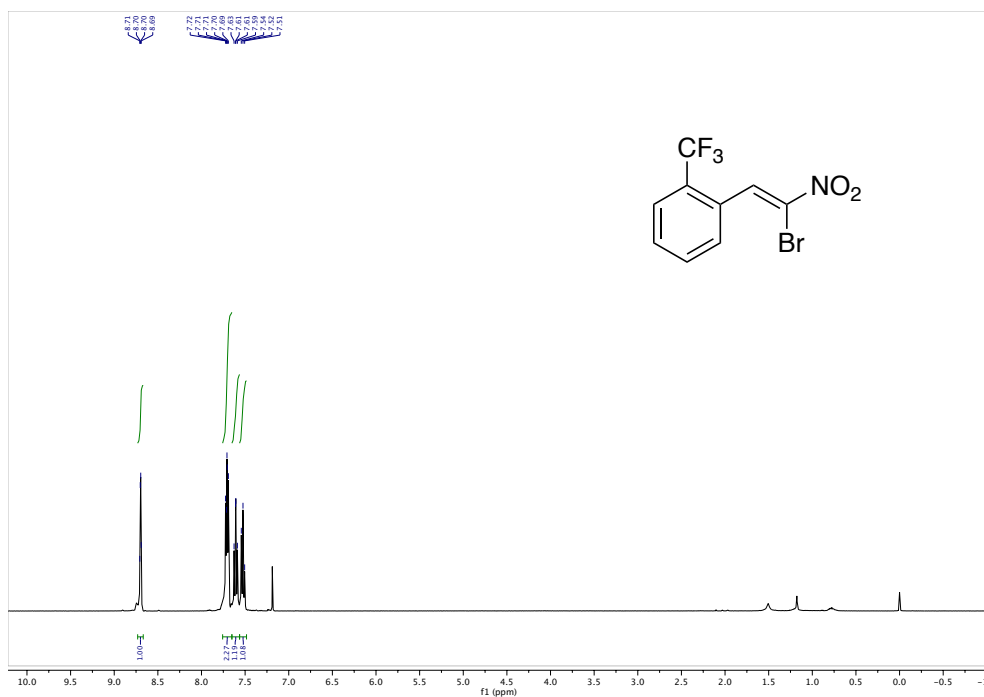


Figure A. 27. ¹H NMR spectrum of 20n

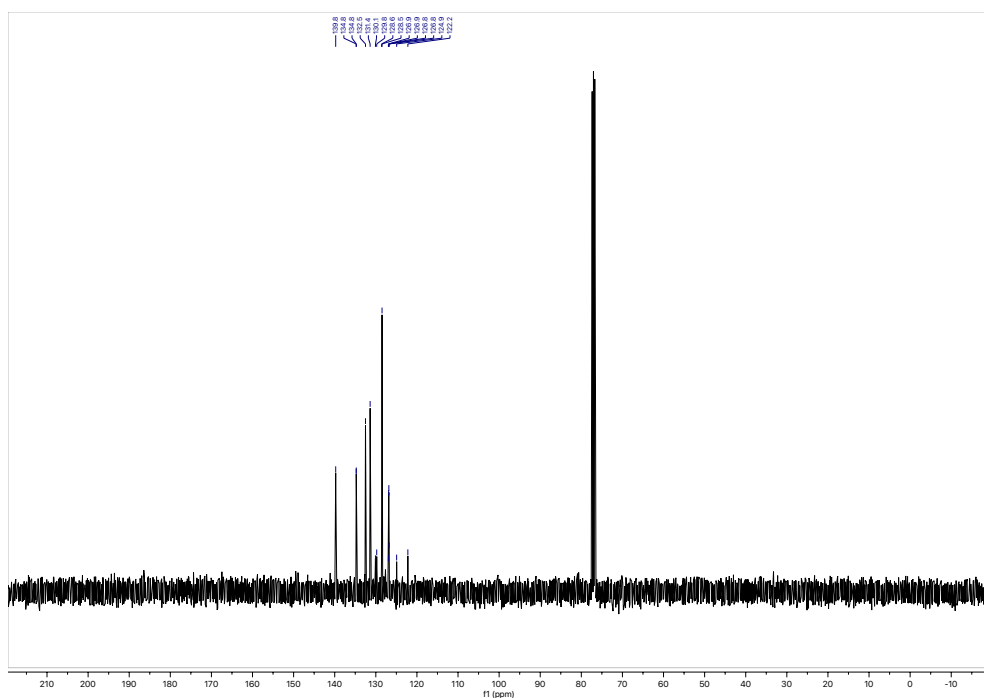


Figure A. 28. ¹³C NMR spectrum of 20n

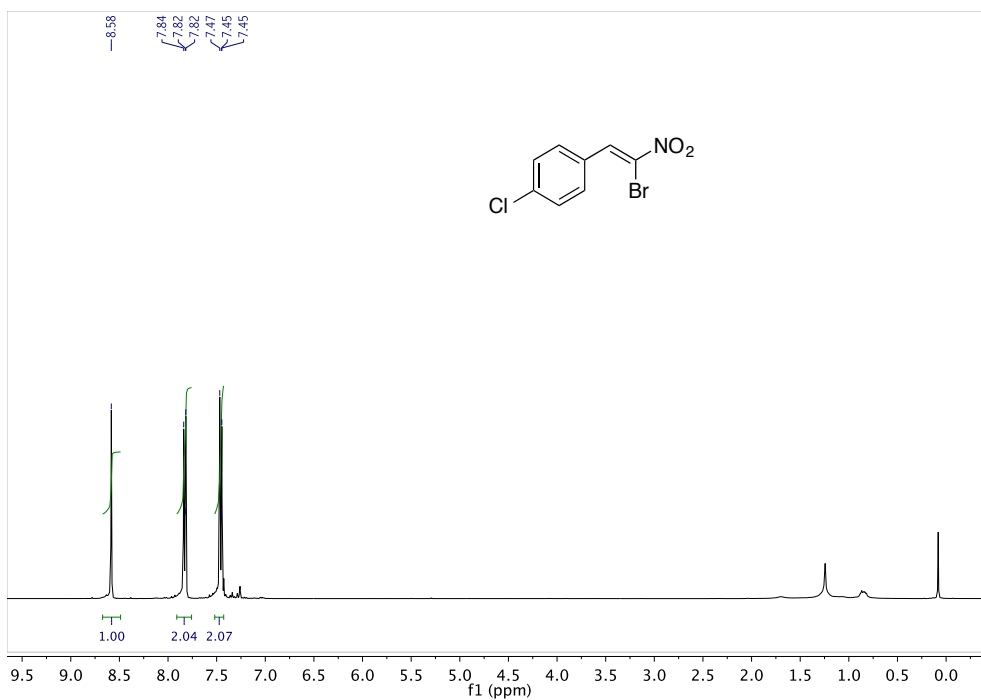


Figure A. 29. ¹H NMR spectrum of **20o**

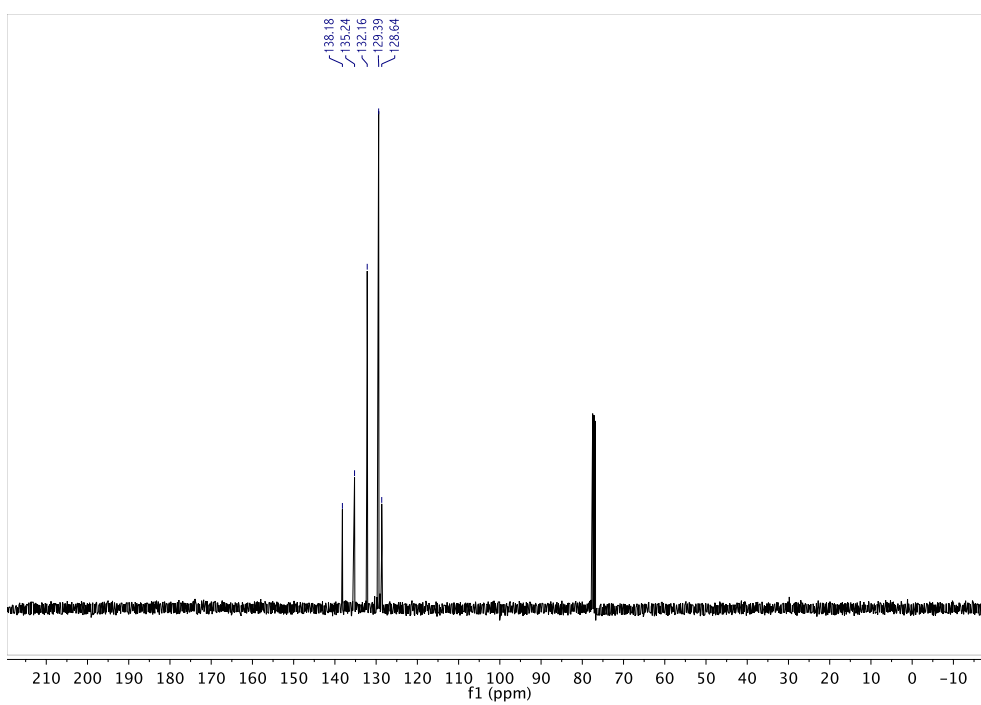


Figure A. 30. ¹³C NMR spectrum of **20o**

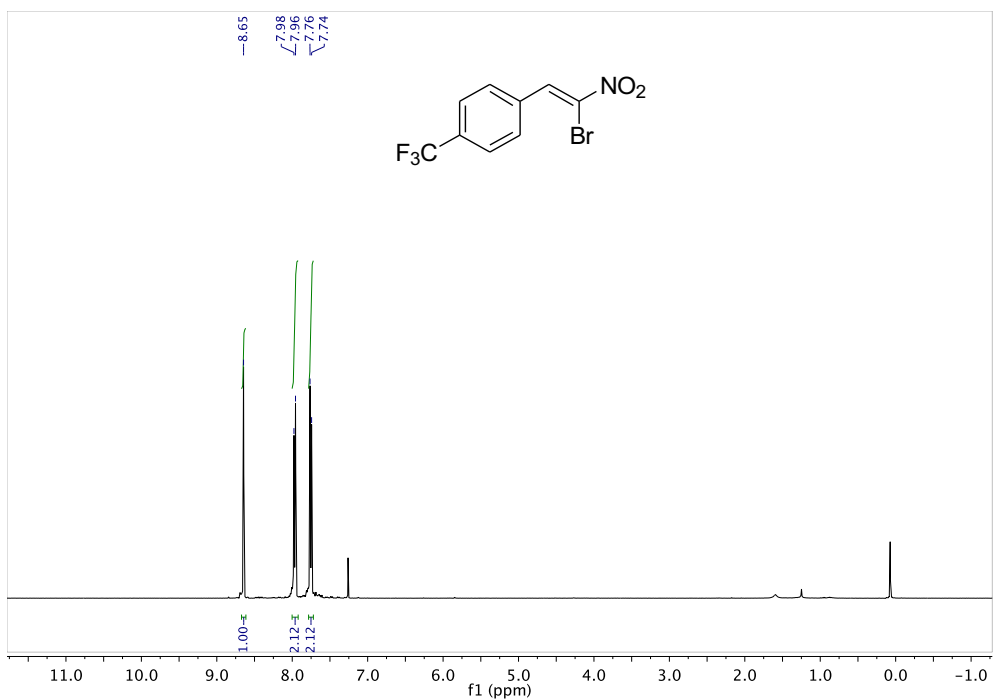


Figure A. 31. ¹H NMR spectrum of **20p**

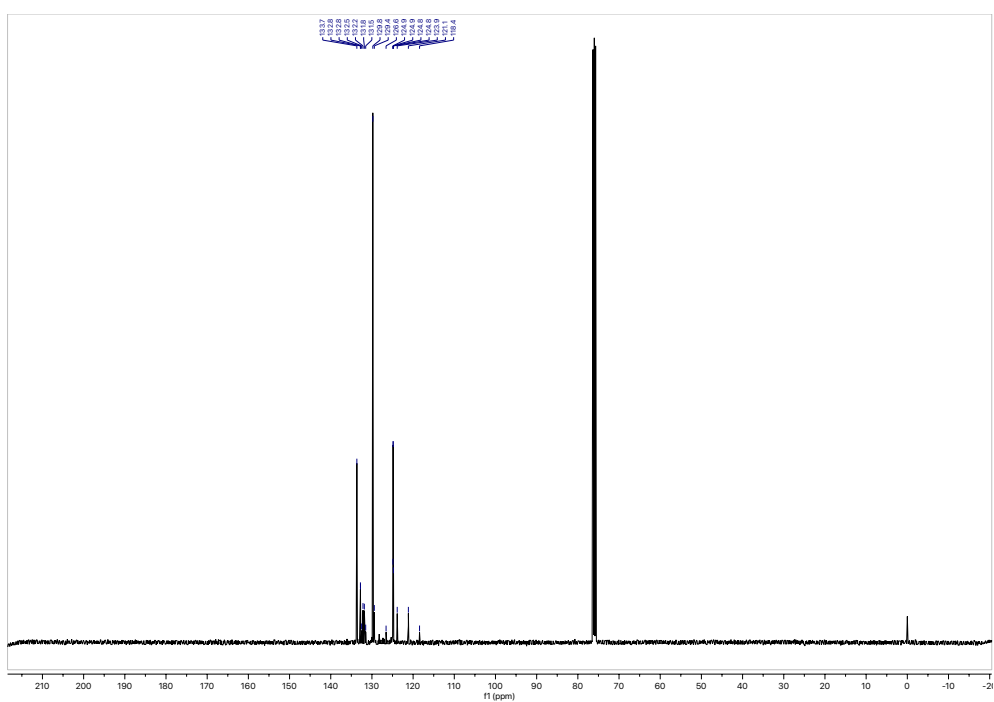


Figure A. 32. ¹³C NMR spectrum of **20p**

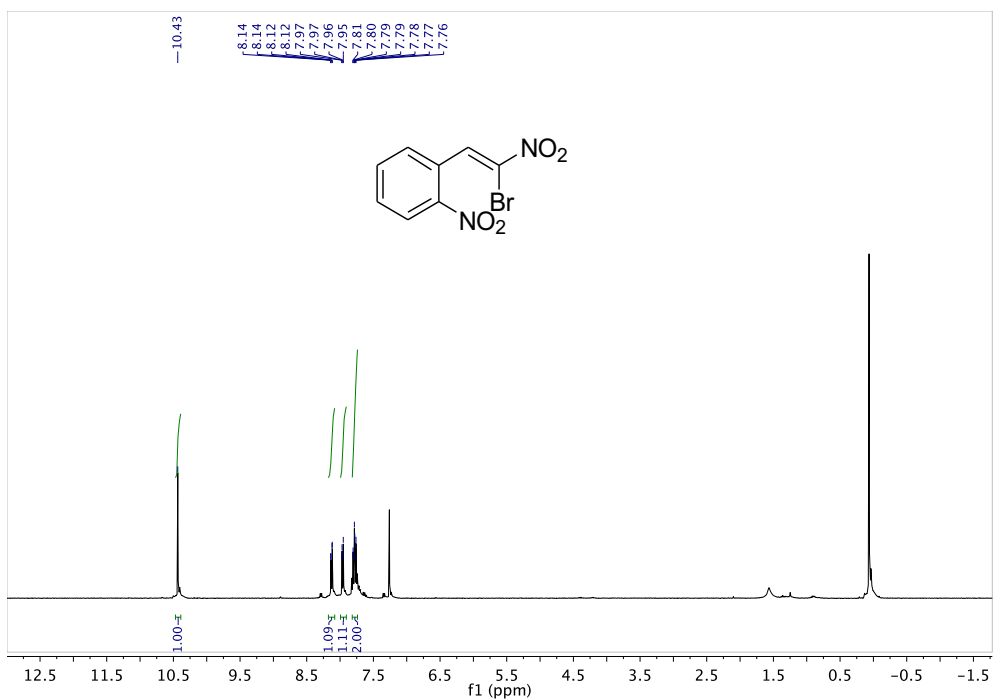


Figure A. 35. ^1H NMR spectrum of **20r**

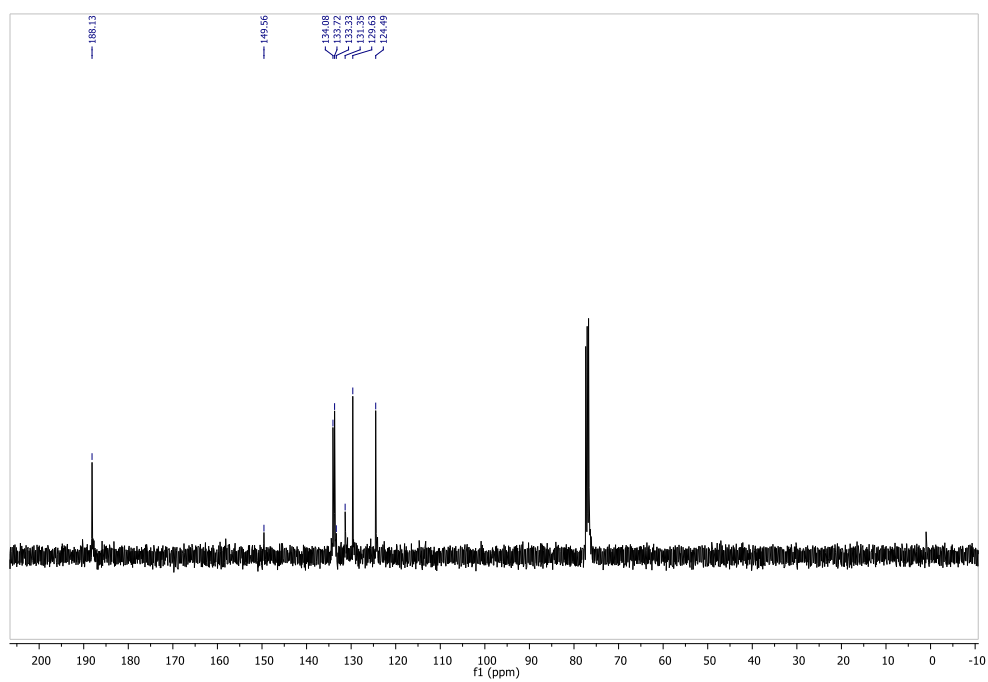


Figure A. 36. ^{13}C NMR spectrum of **20r**

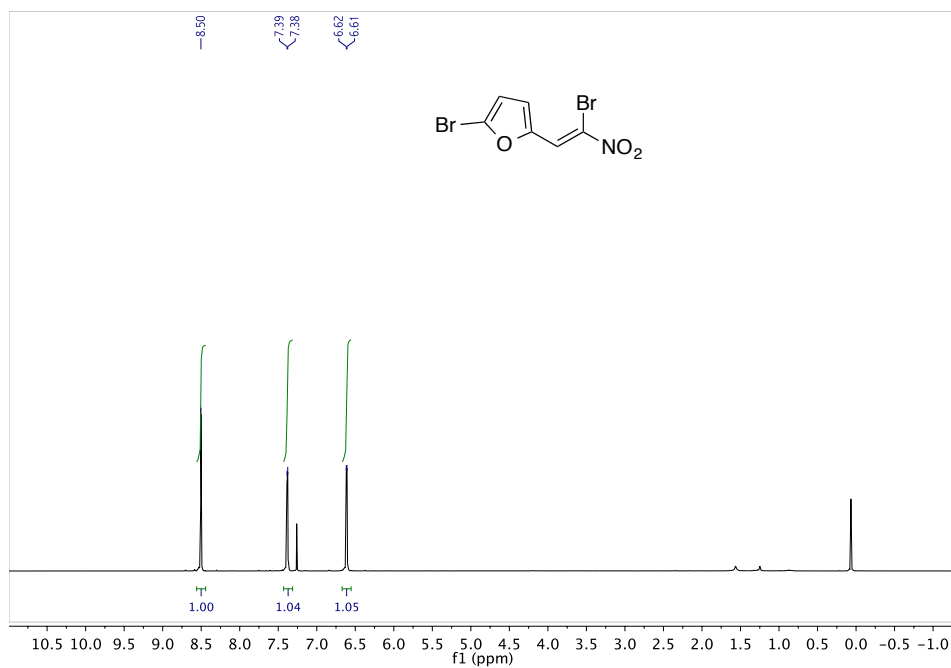


Figure A. 37. ^1H NMR spectrum of 20s

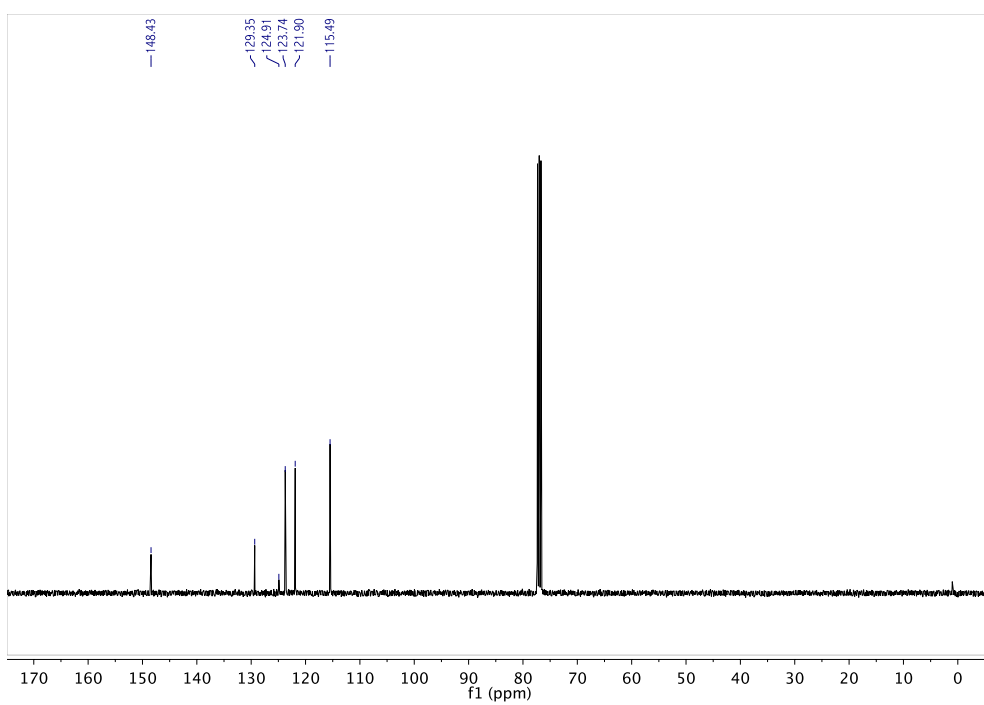


Figure A. 38. ^{13}C NMR spectrum of 20s

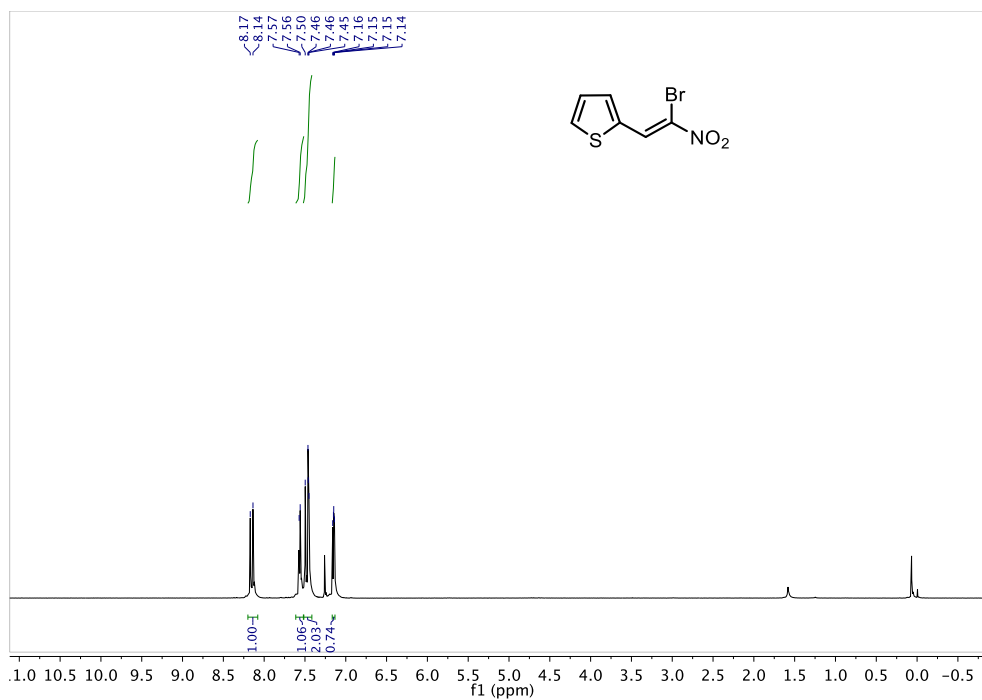


Figure A. 39. ^1H NMR spectrum of 20t

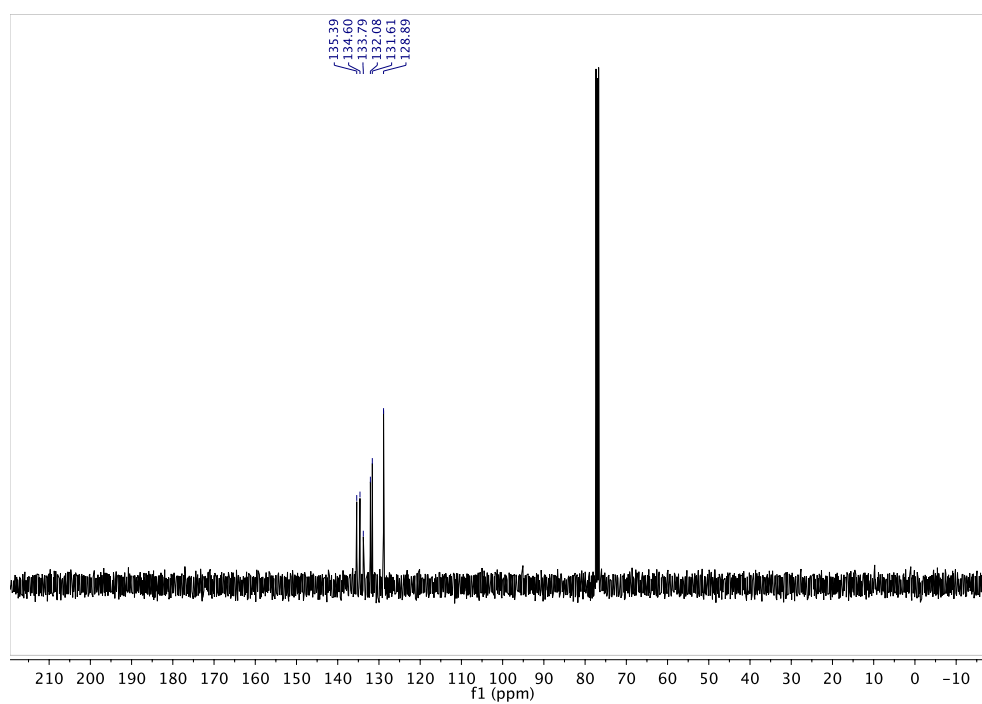


Figure A. 40. ^{13}C NMR spectrum of 20t

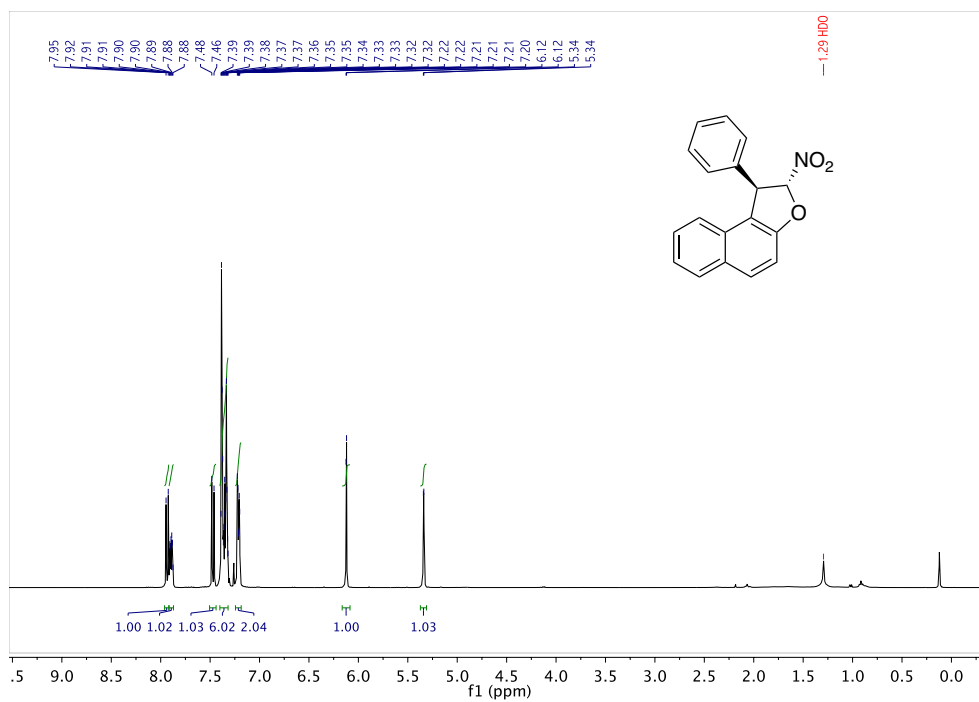


Figure A. 41. ¹H NMR spectrum of 23aa

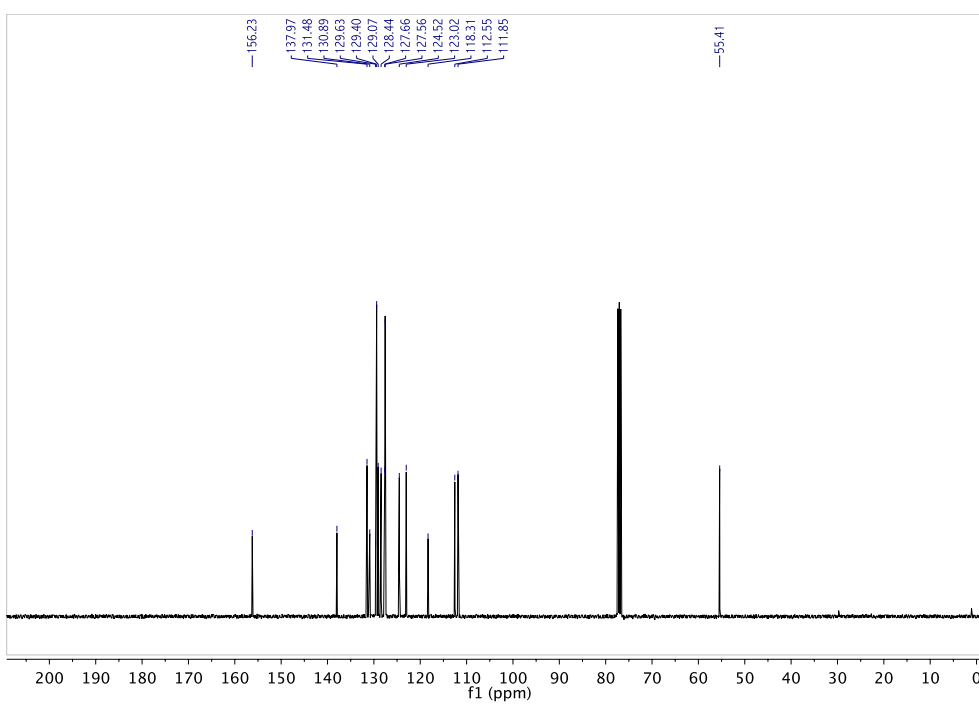


Figure A. 42. ¹³C NMR spectrum of 23aa

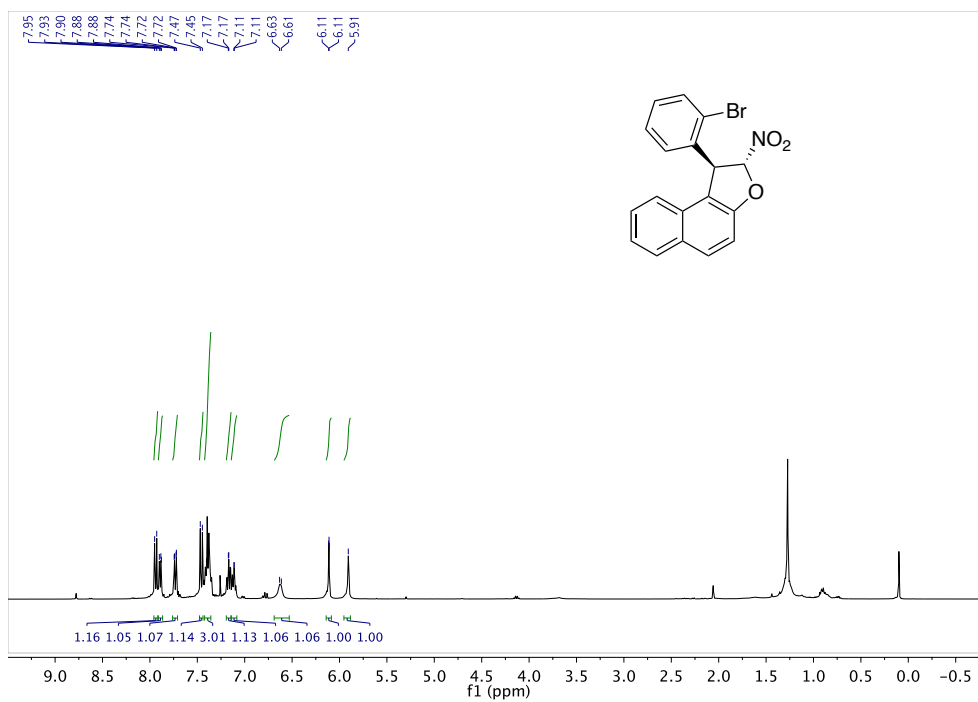


Figure A. 43. ^1H NMR spectrum of **23ab**

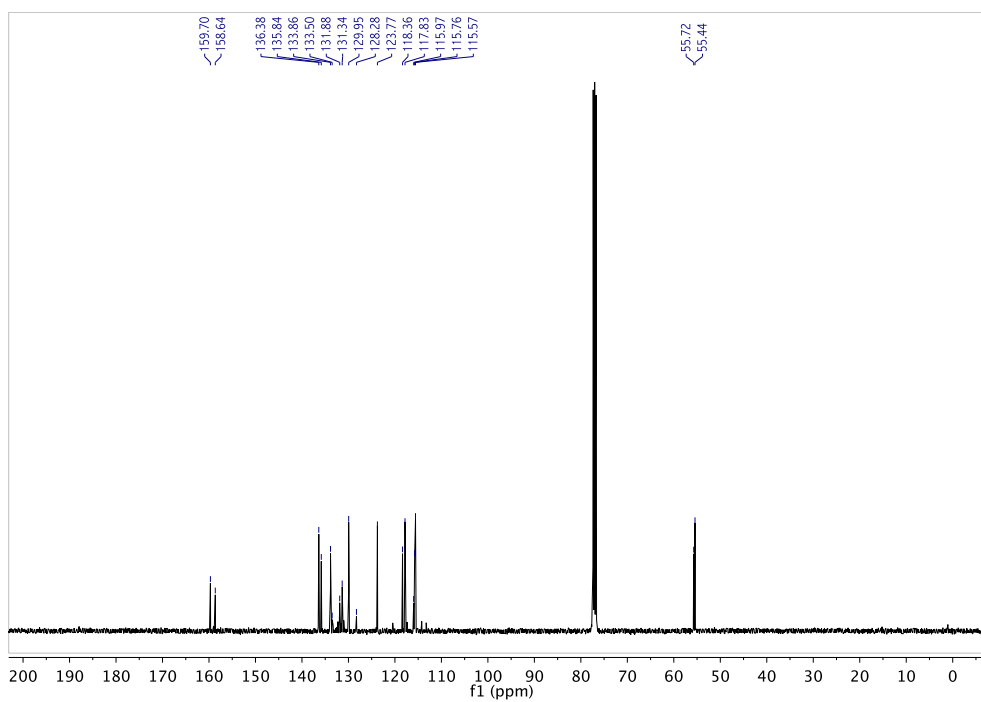


Figure A. 44. ^{13}C NMR spectrum of **23ab**

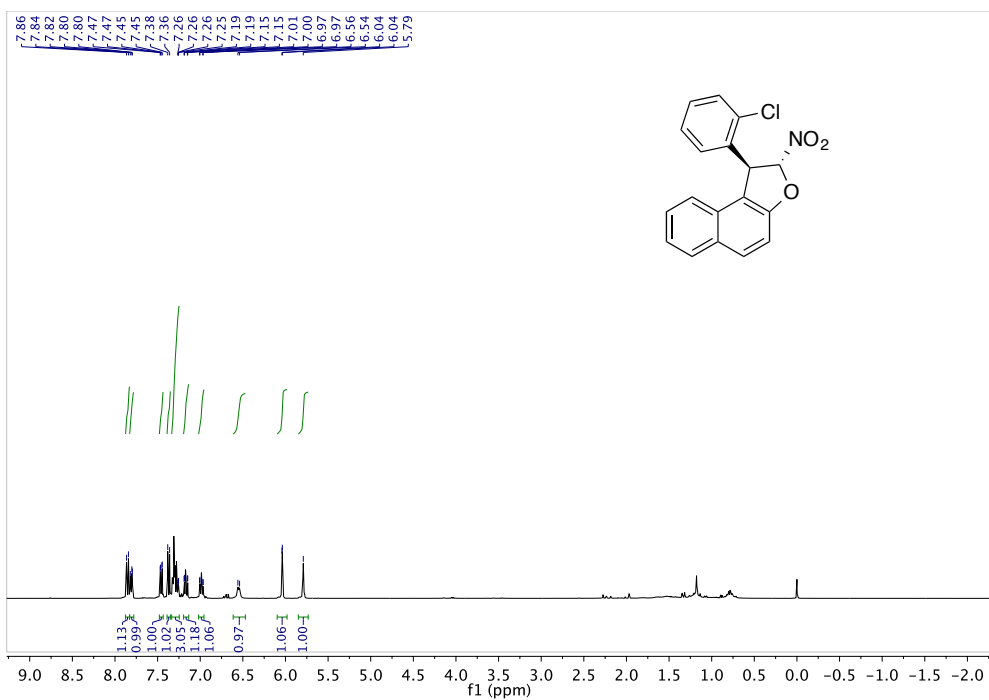


Figure A. 45. ^1H NMR spectrum of **23ac**

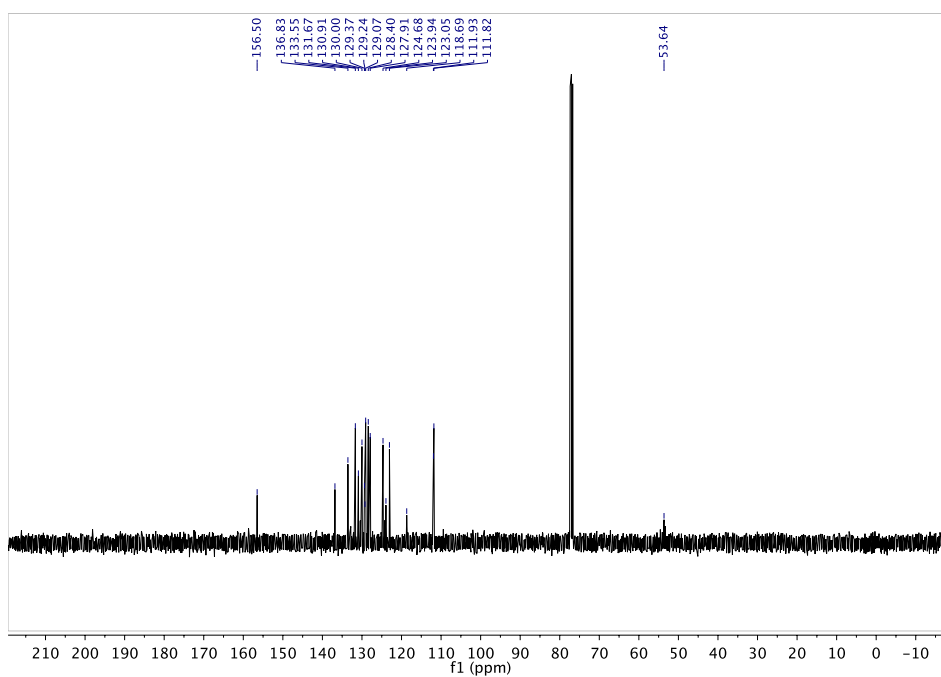


Figure A. 46. ^{13}C NMR spectrum of **23ac**

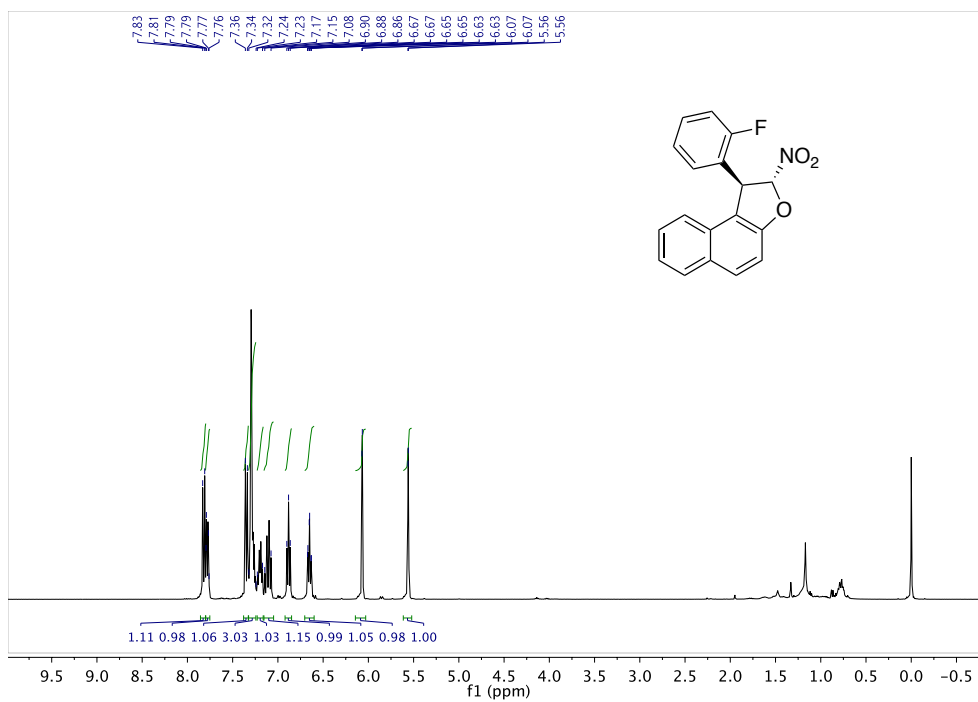
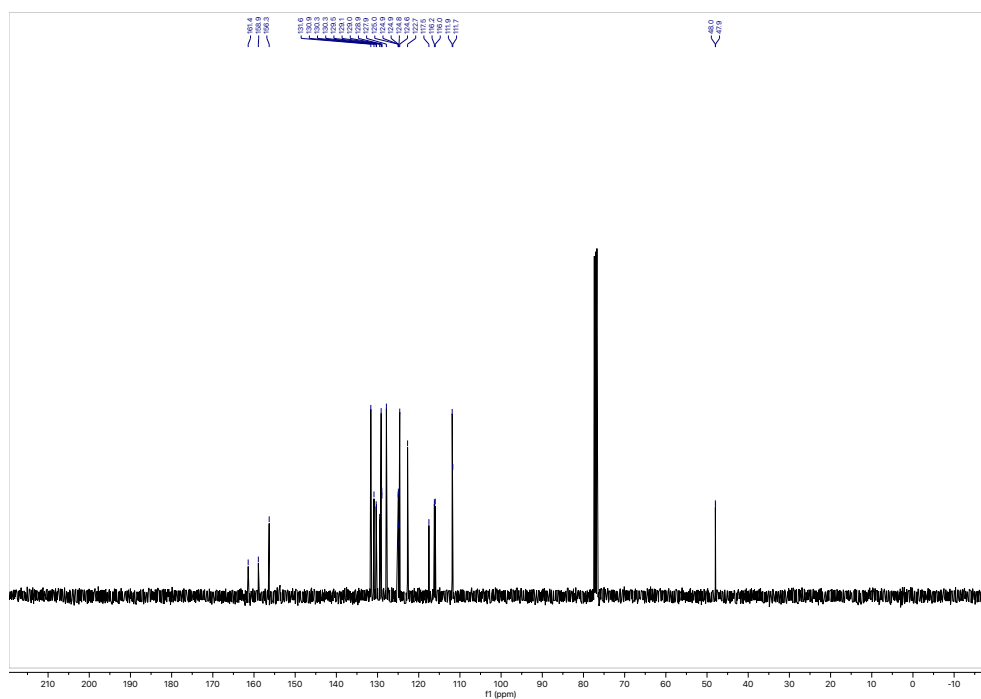


Figure A. 47. ^1H NMR spectrum of 23ad



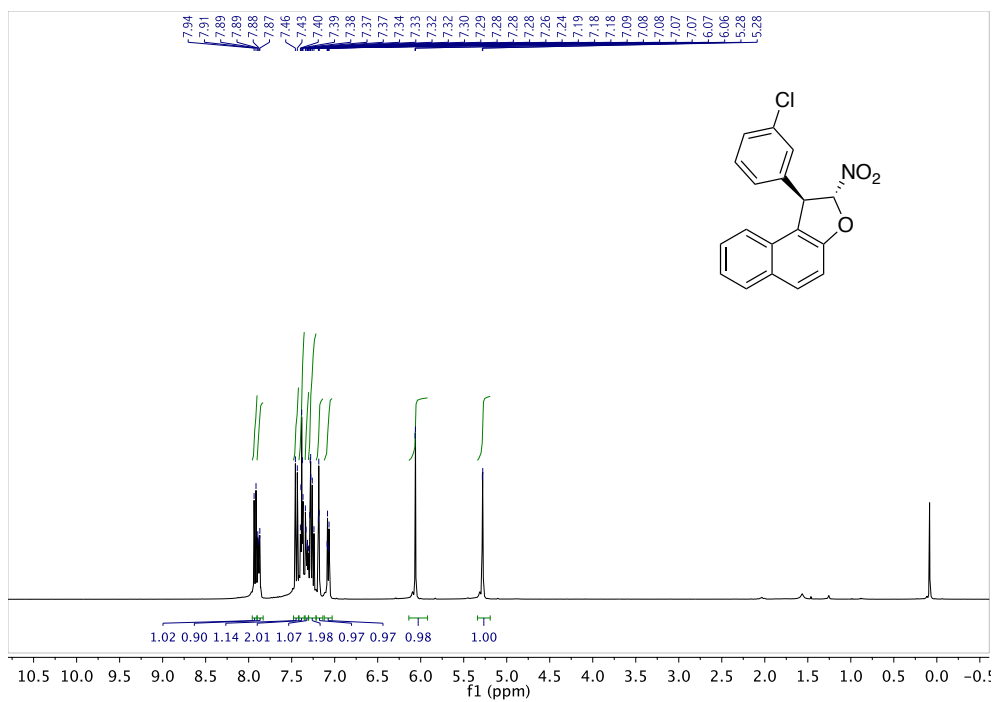


Figure A. 51. ^1H NMR spectrum of 23af

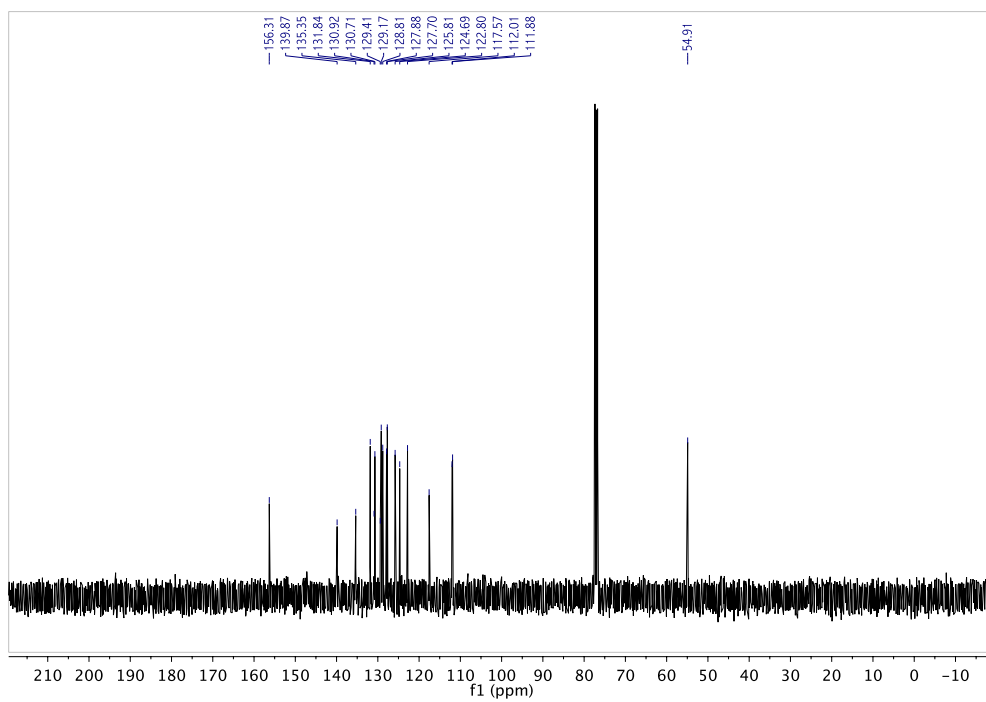
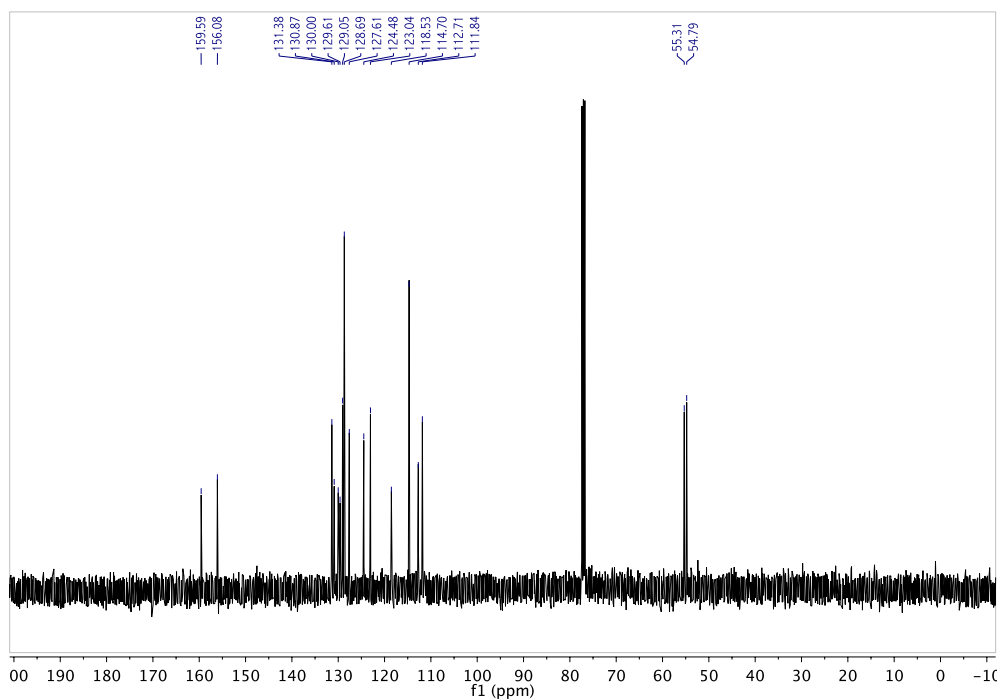
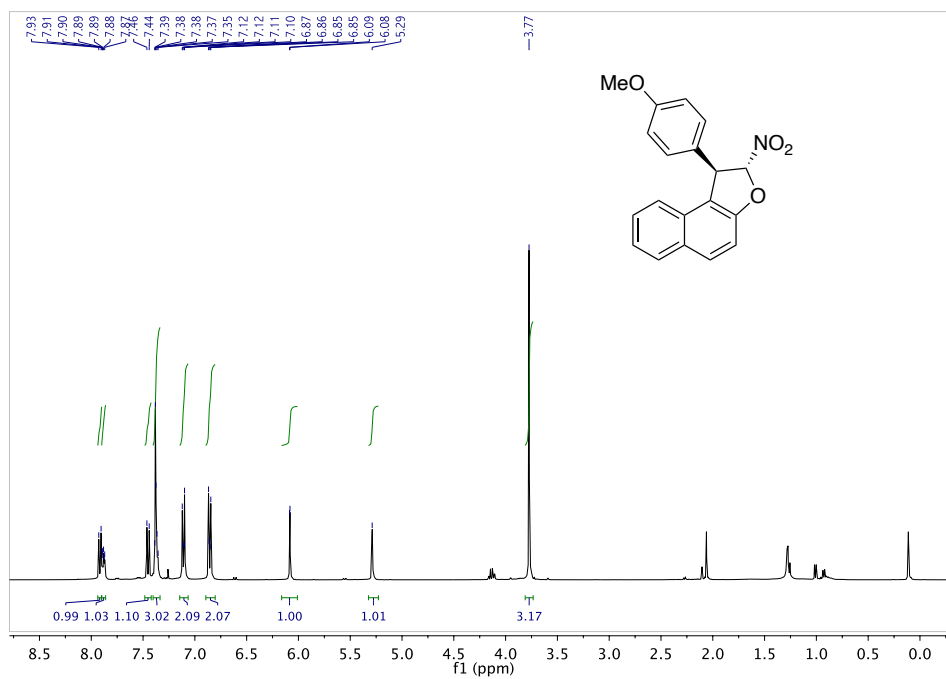
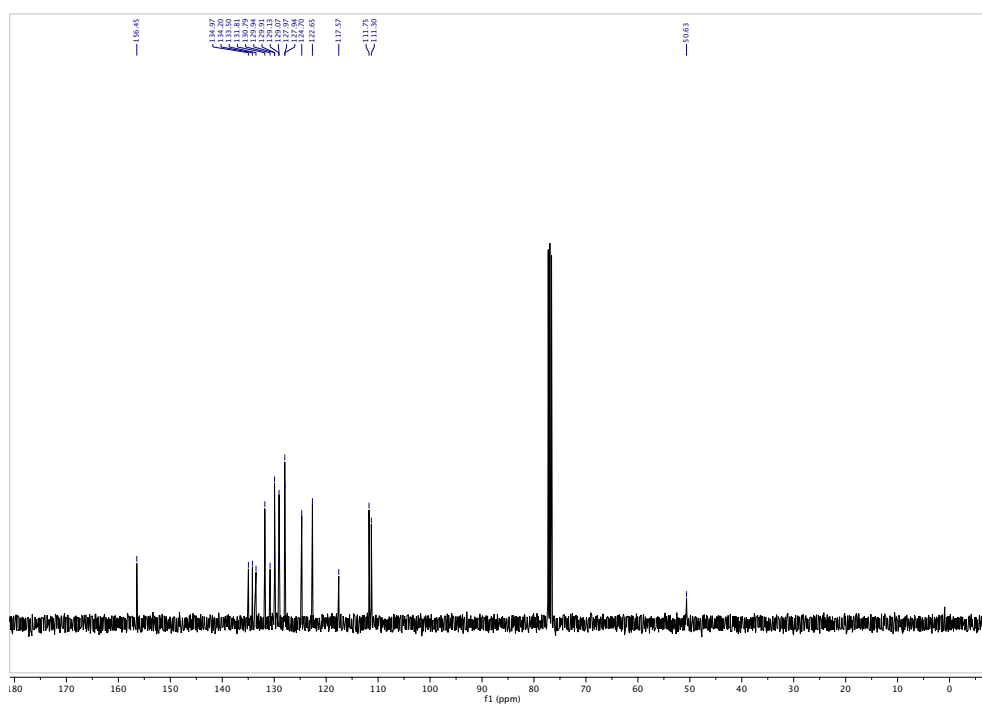
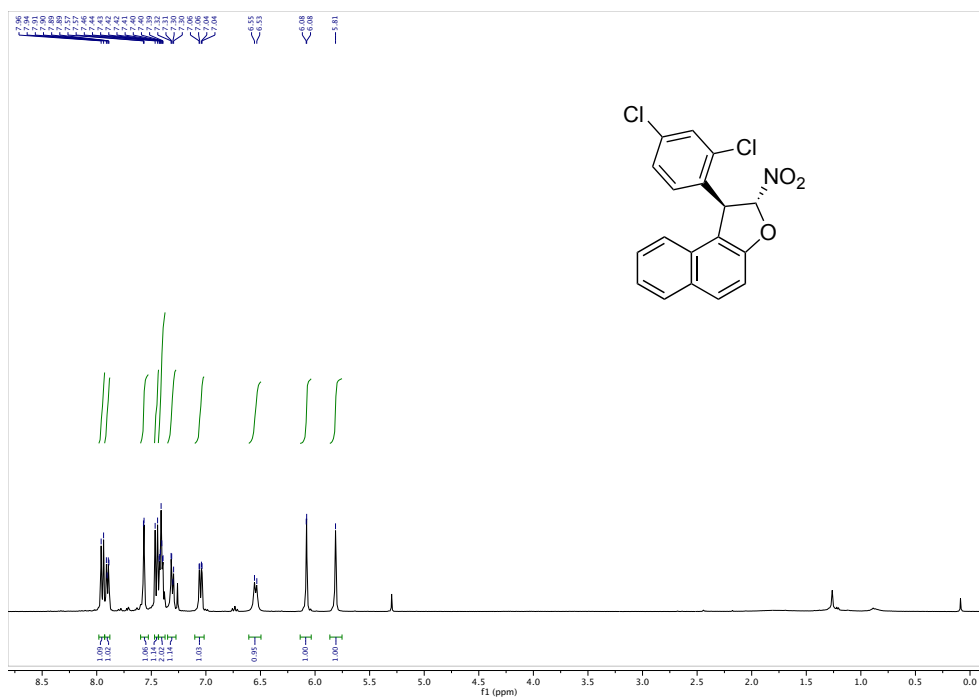


Figure A. 52. ^{13}C NMR spectrum of 23af





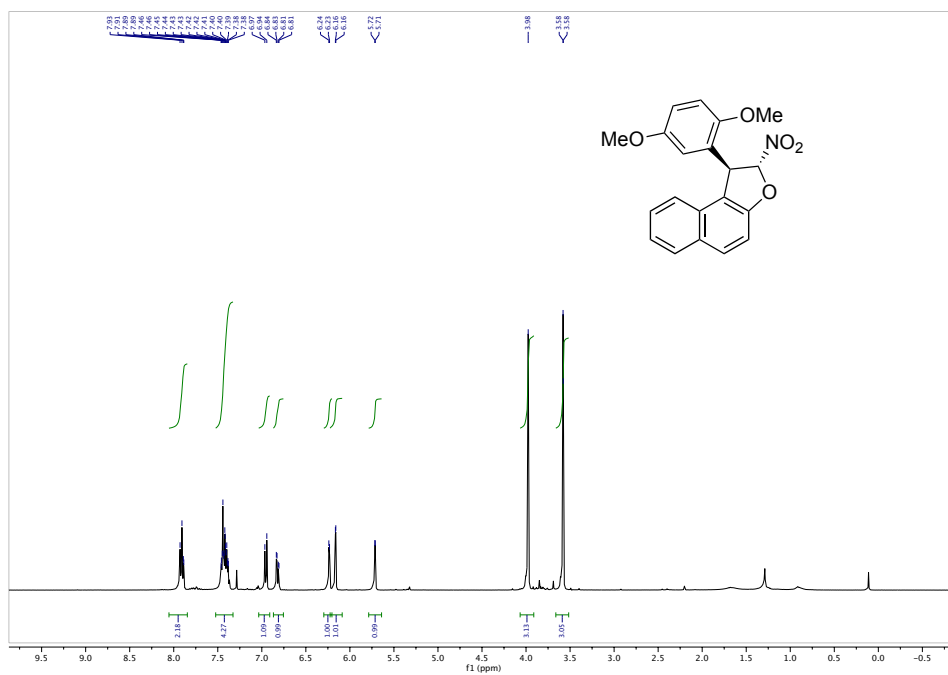


Figure A. 57. ^1H NMR spectrum of 23ai

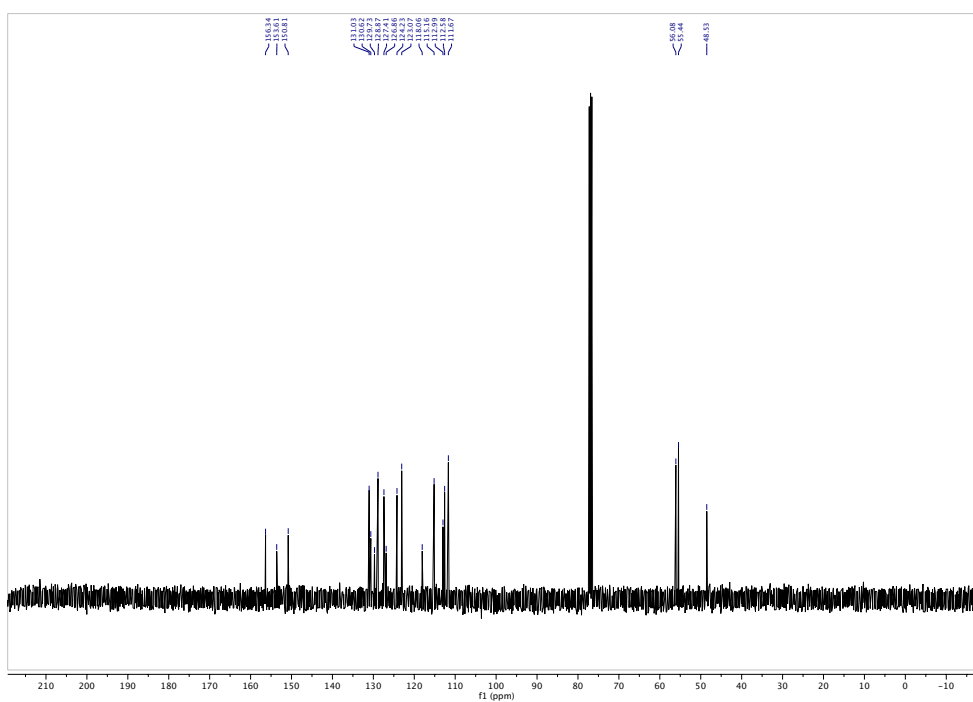


Figure A. 58. ^{13}C NMR spectrum of 23ai

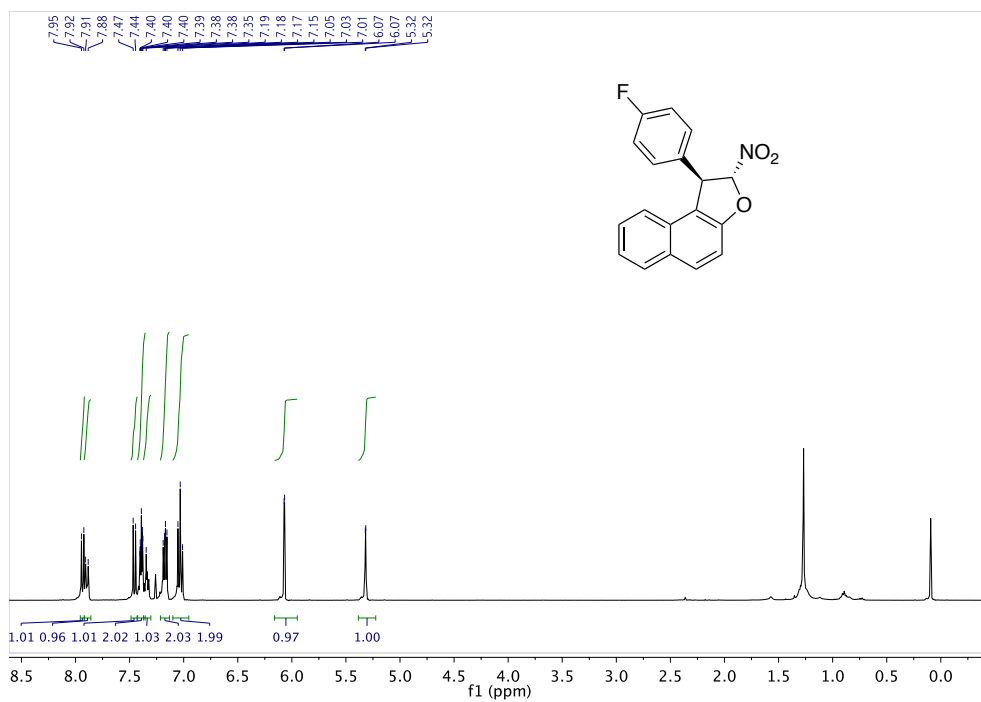


Figure A. 59. ¹H NMR spectrum of **23aj**

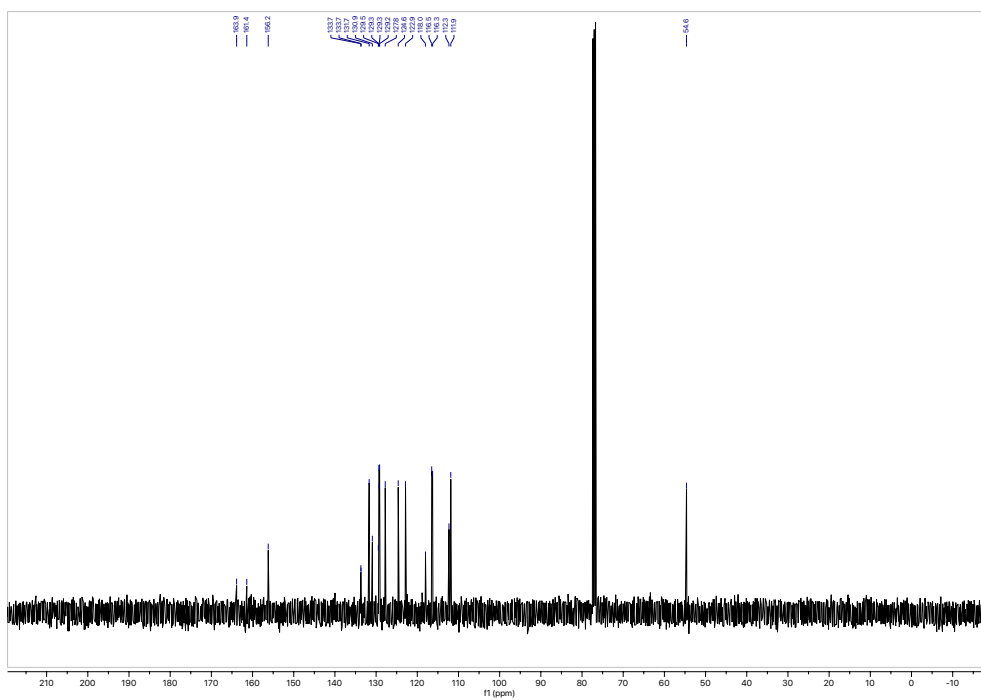


Figure A. 60. ¹³C NMR spectrum of **23aj**

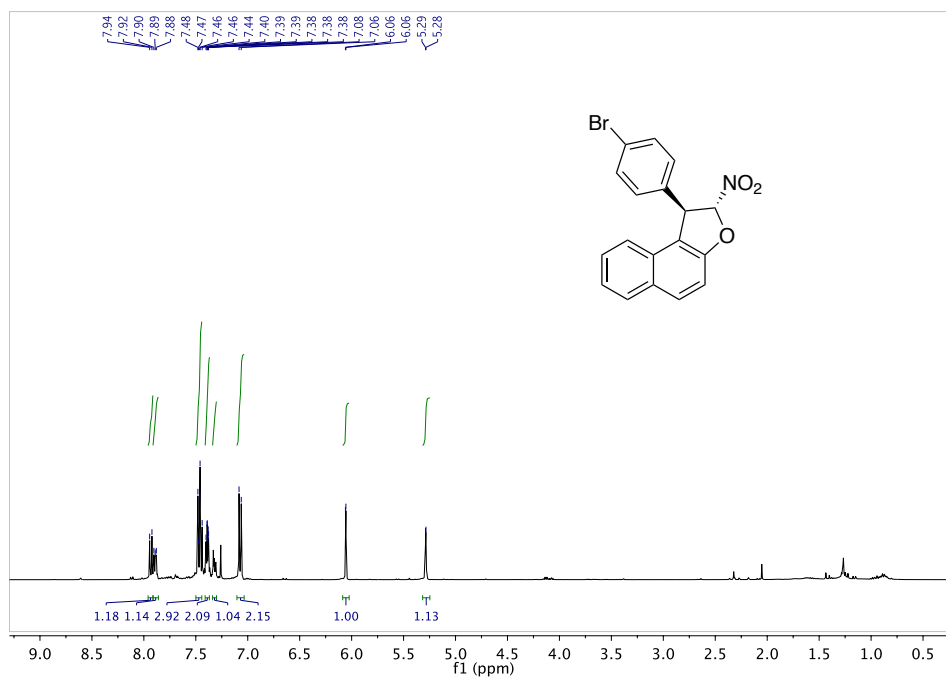


Figure A. 61. ^1H NMR spectrum of 23ak

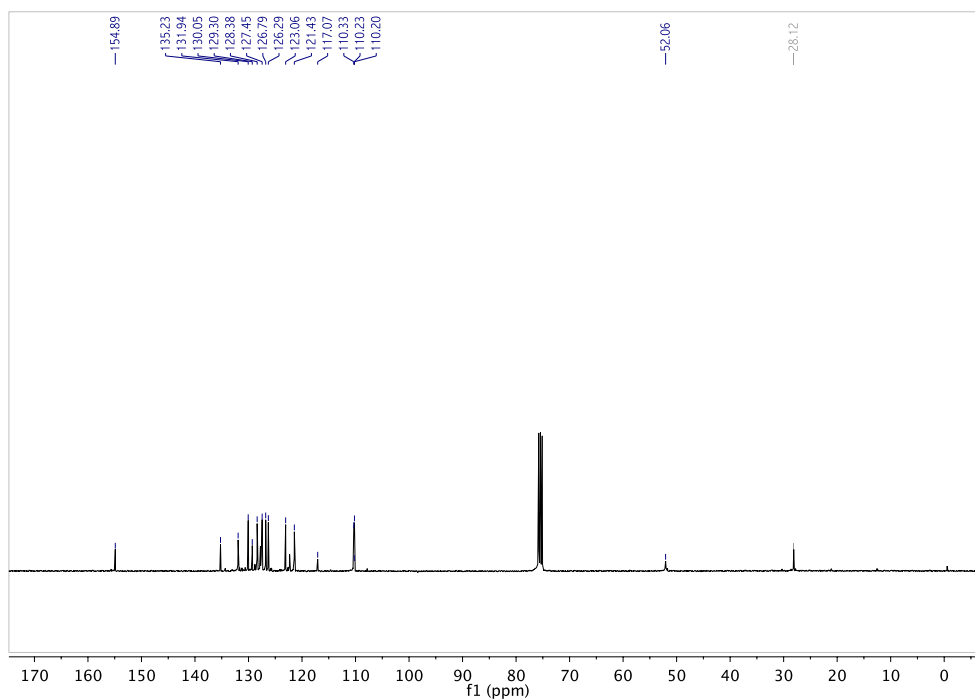


Figure A. 62. ^{13}C NMR spectrum of 23ak

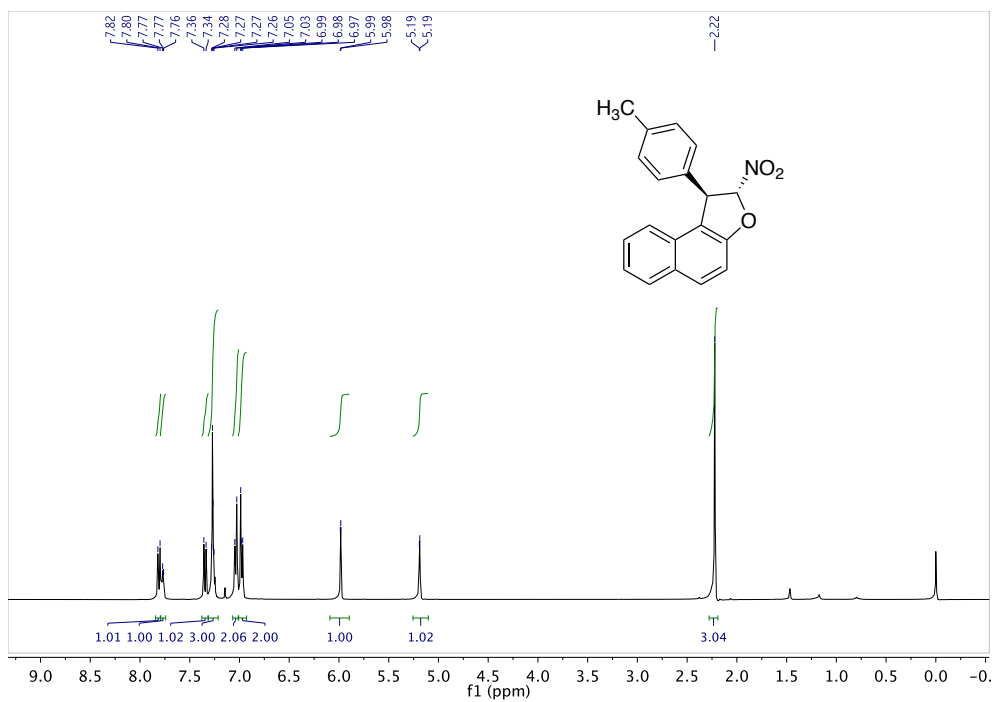


Figure A. 63. ¹H NMR spectrum of **23al**

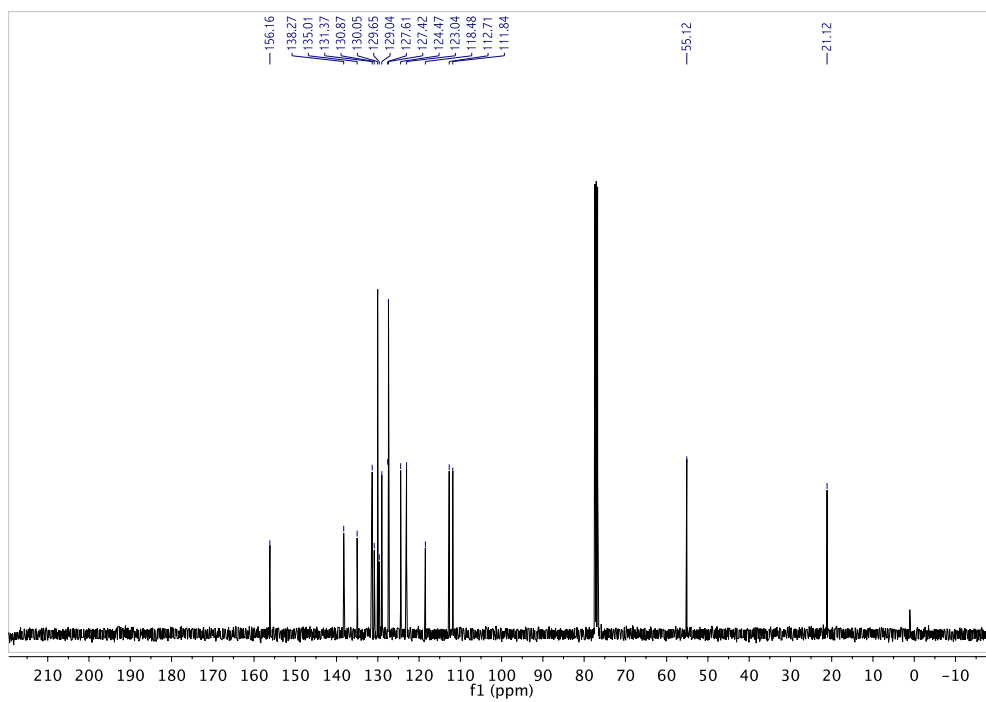


Figure A. 64. ¹³C NMR spectrum of **23al**

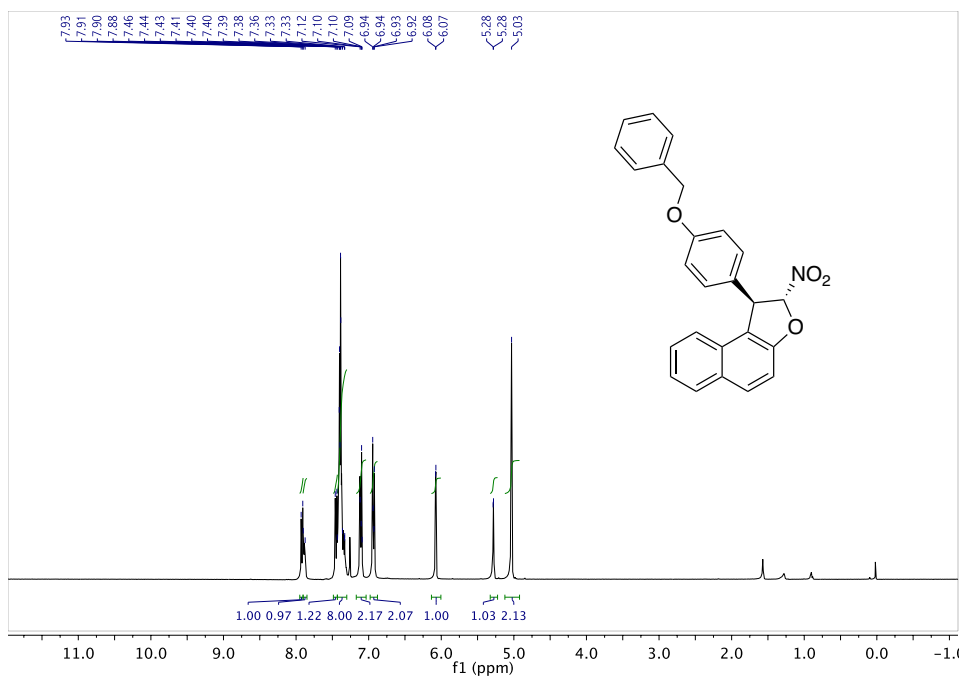


Figure A. 65. ^1H NMR spectrum of 23am

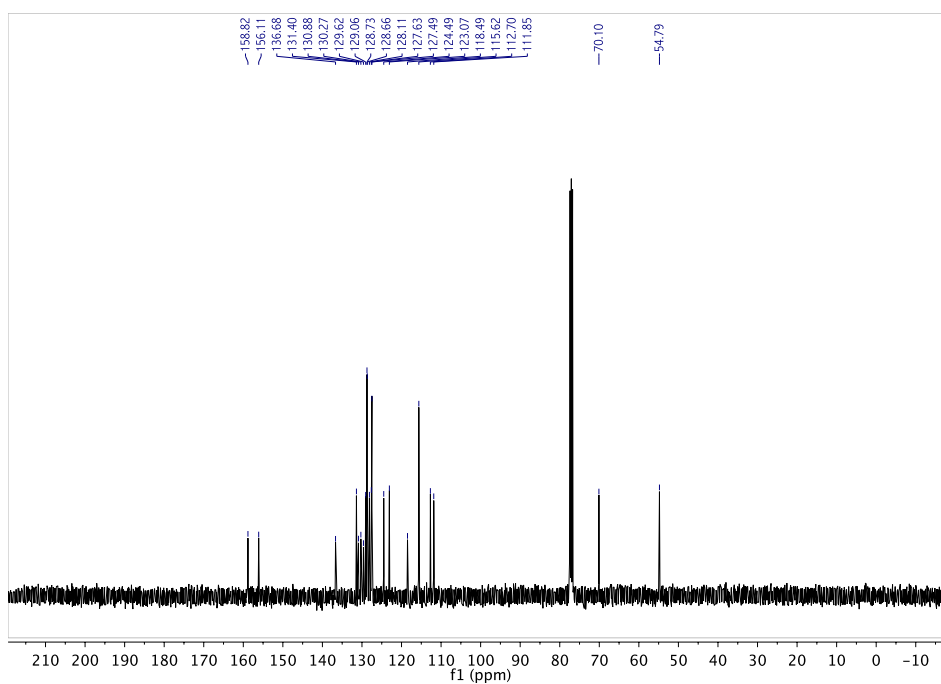


Figure A. 66. ^{13}C NMR spectrum of 23am

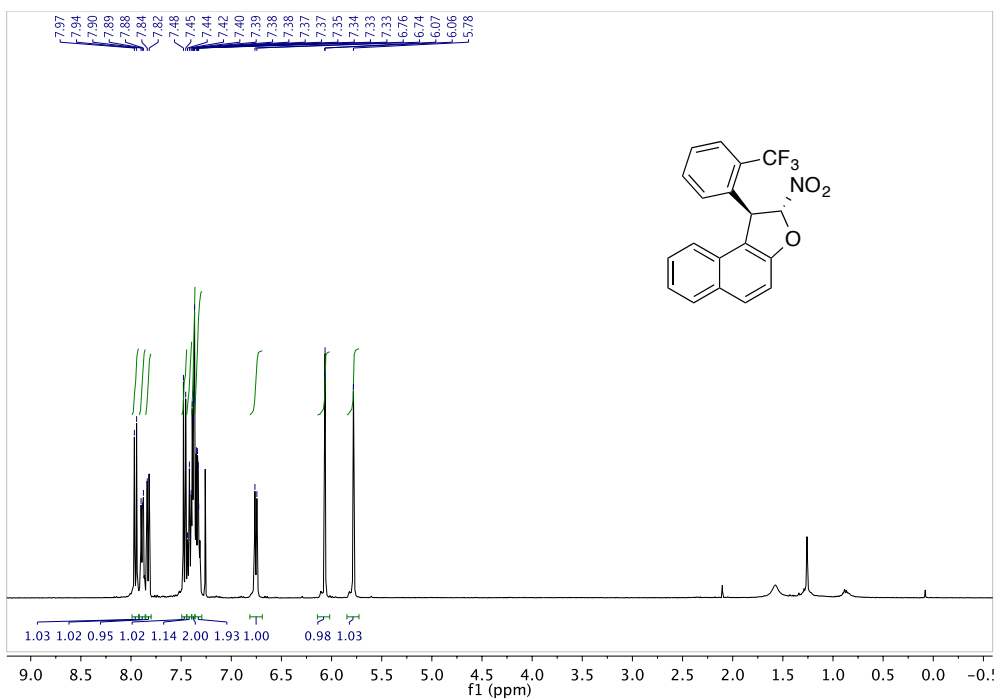


Figure A. 67. ^1H NMR spectrum of 23an

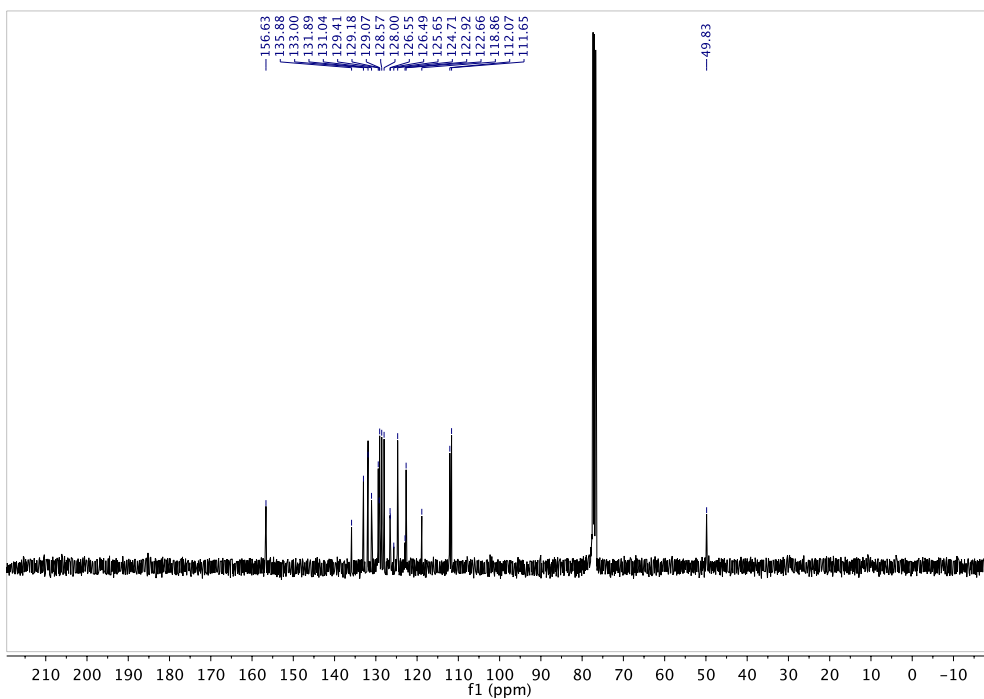


Figure A. 68. ^{13}C NMR spectrum of 23an

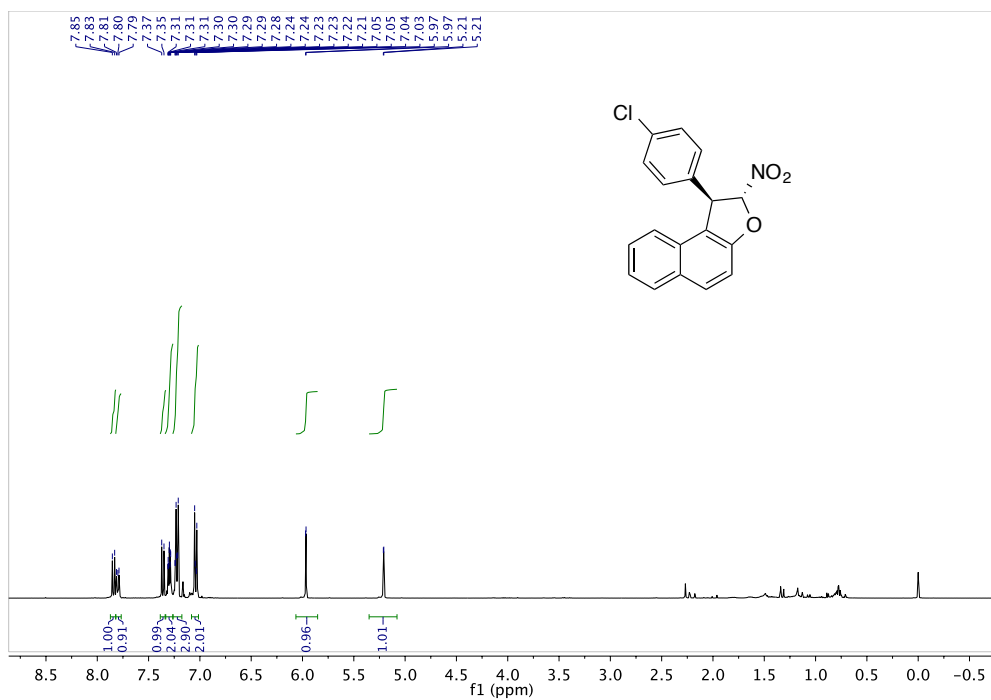


Figure A. 69. ^1H NMR spectrum of **23ao**

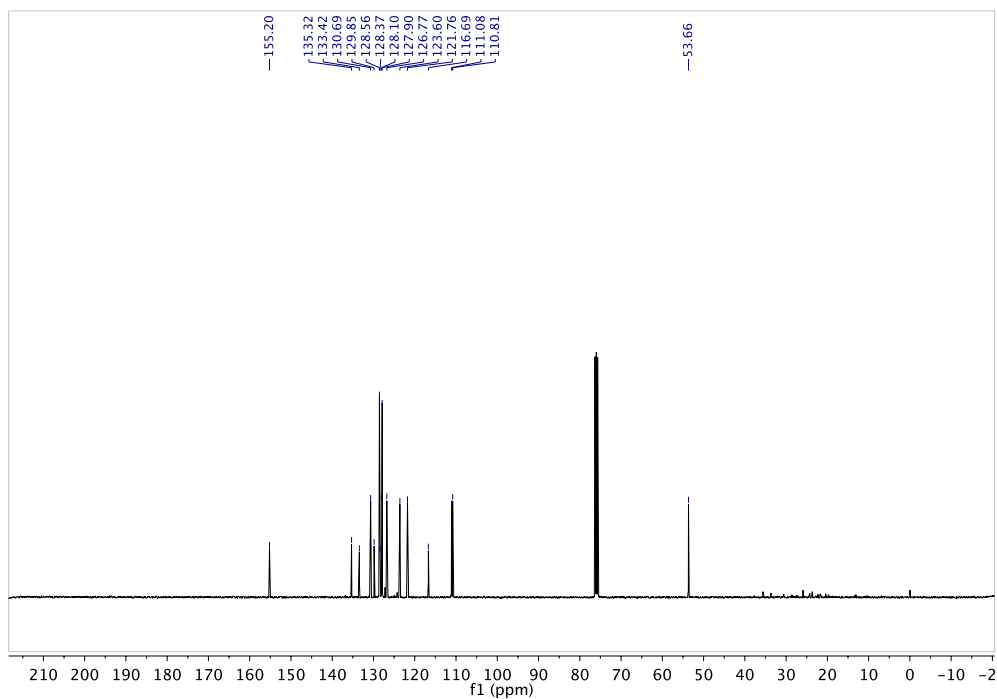
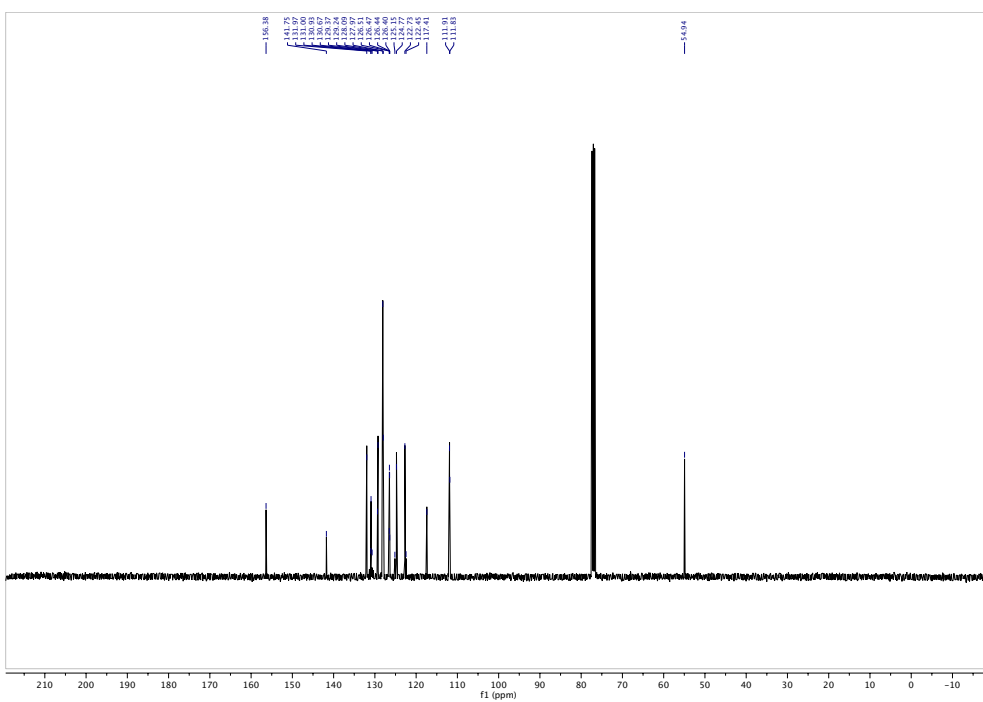
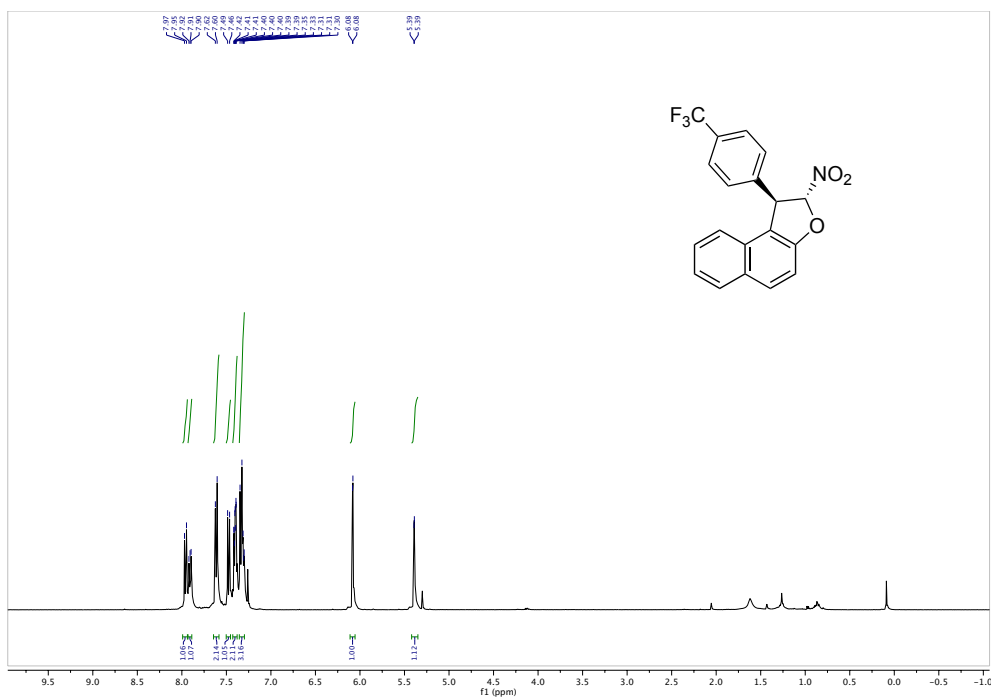
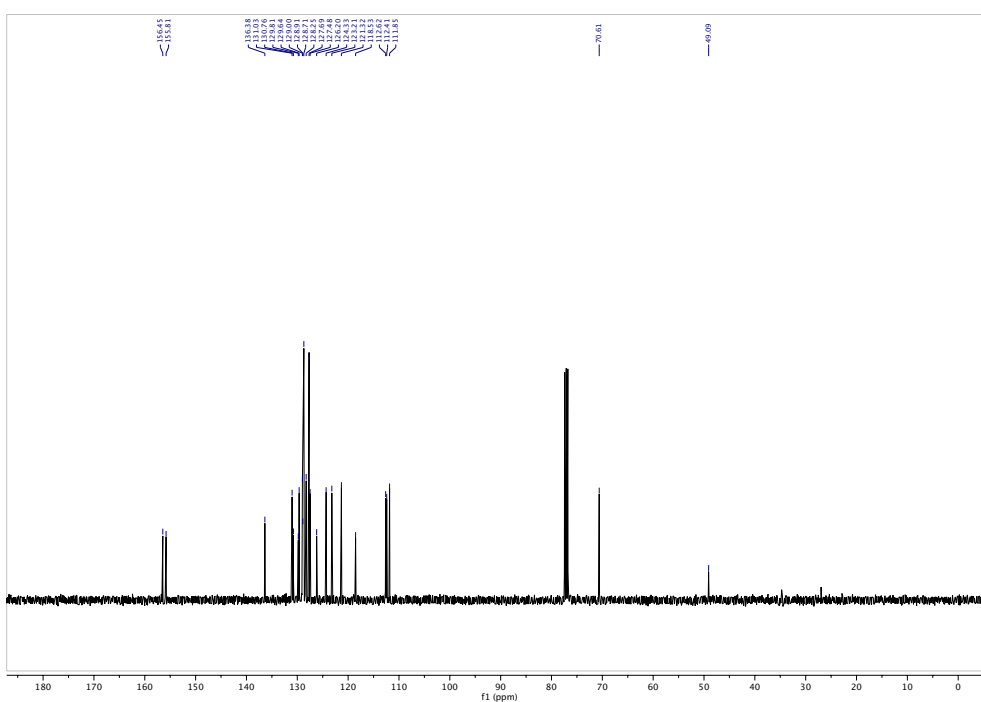
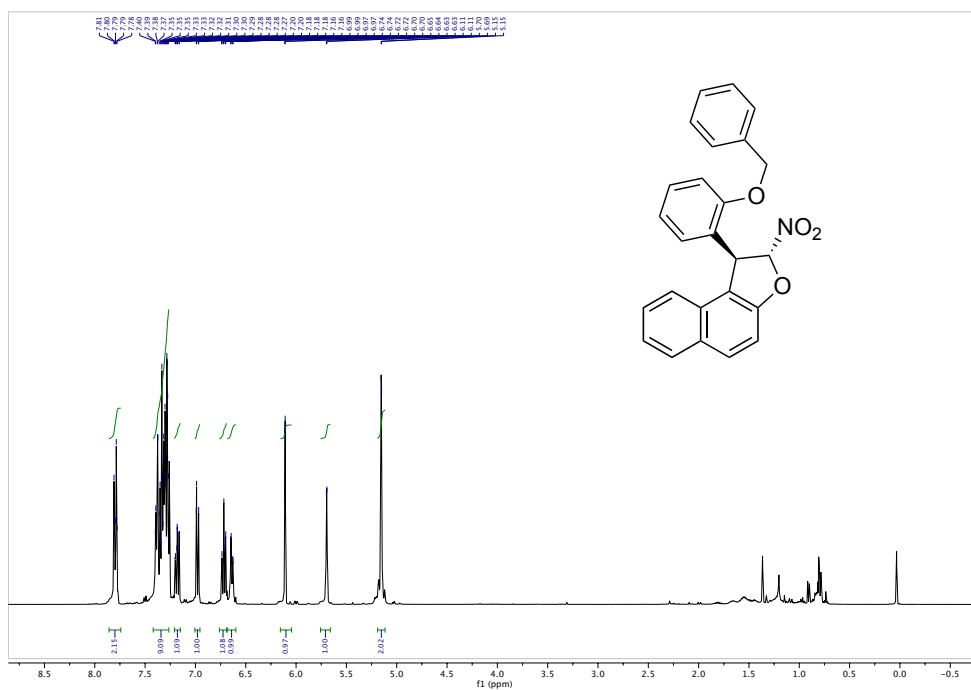


Figure A. 70. ^{13}C NMR spectrum of **23ao**





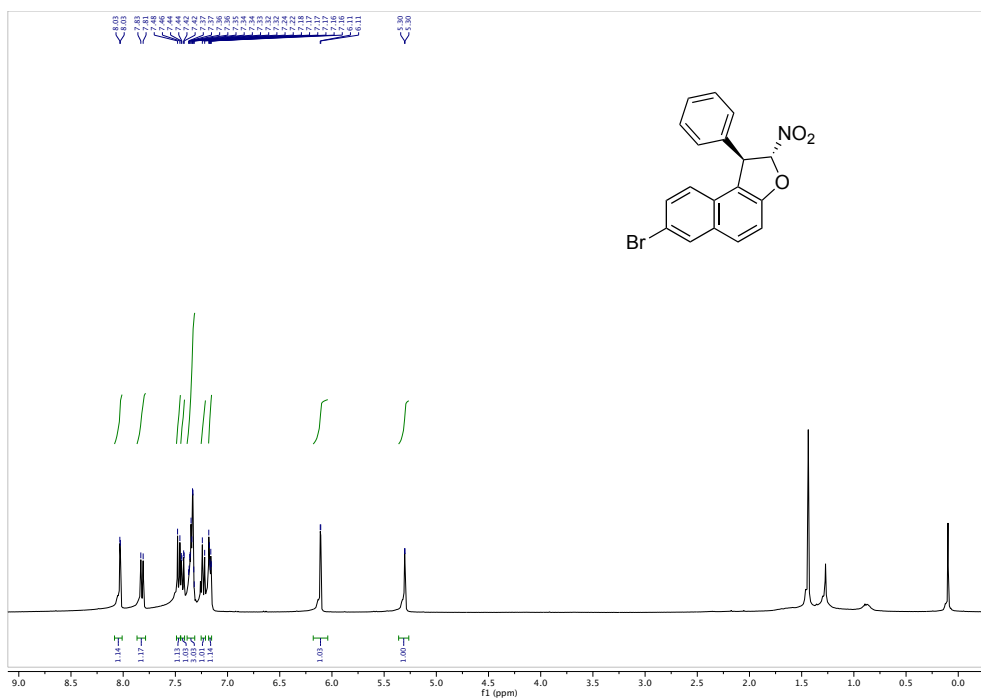


Figure A. 75. ¹H NMR spectrum of **23ba**

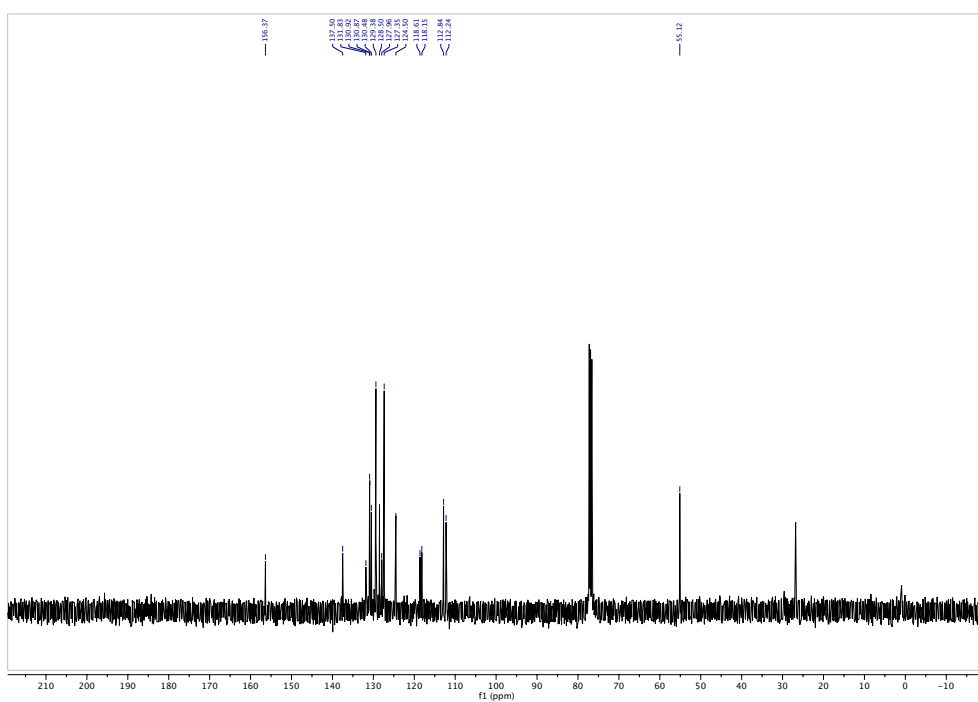


Figure A. 76. ¹³C NMR spectrum of **23ba**

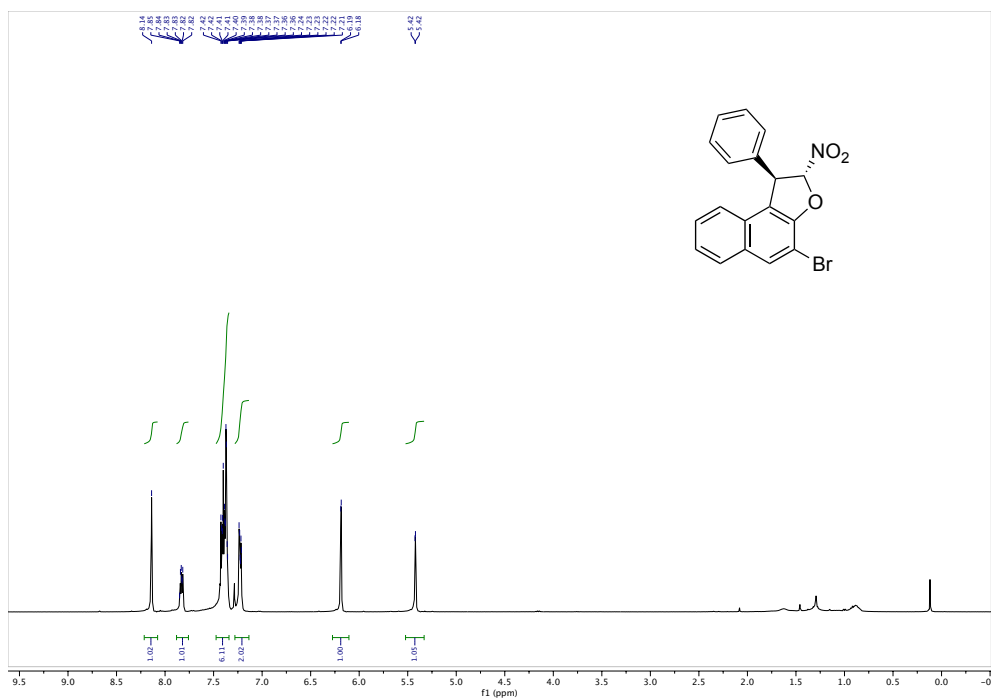


Figure A. 79. ¹H NMR spectrum of 23da

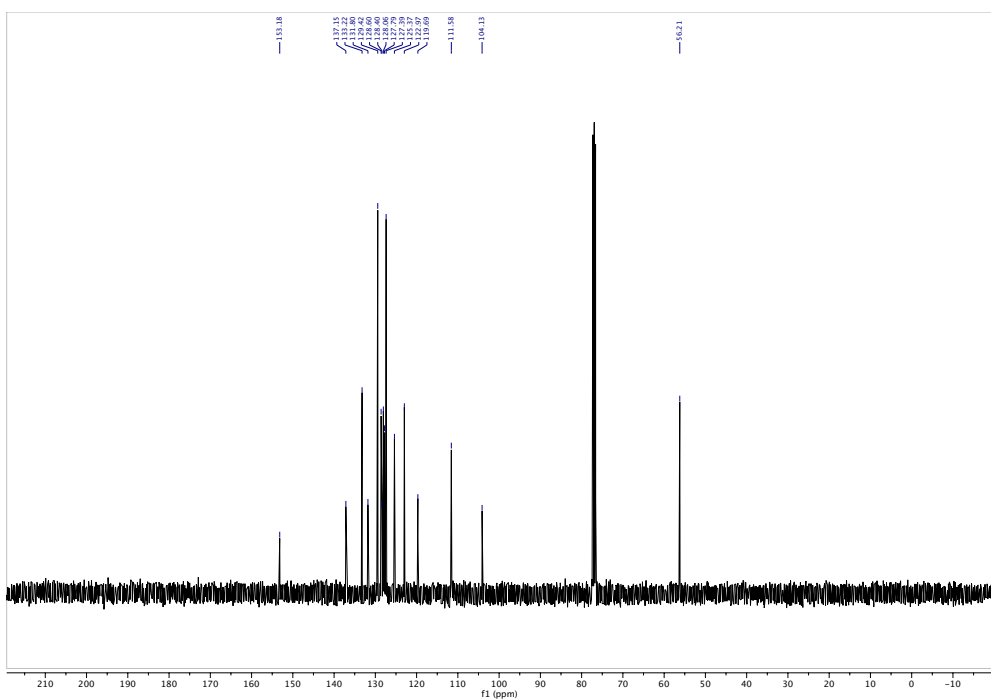


Figure A. 80. ¹³C NMR spectrum of 23da

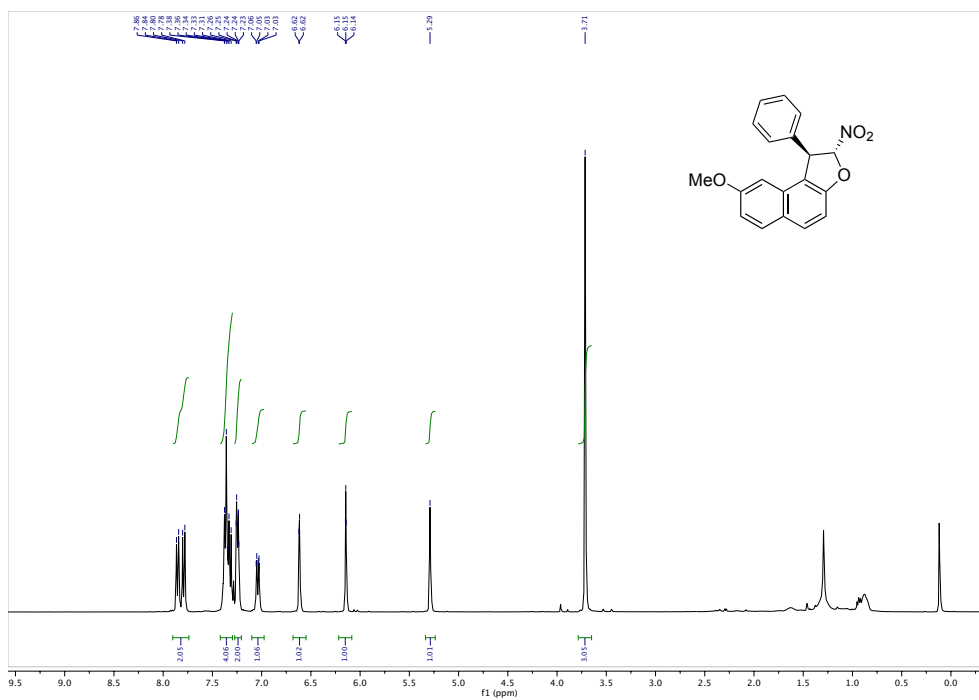
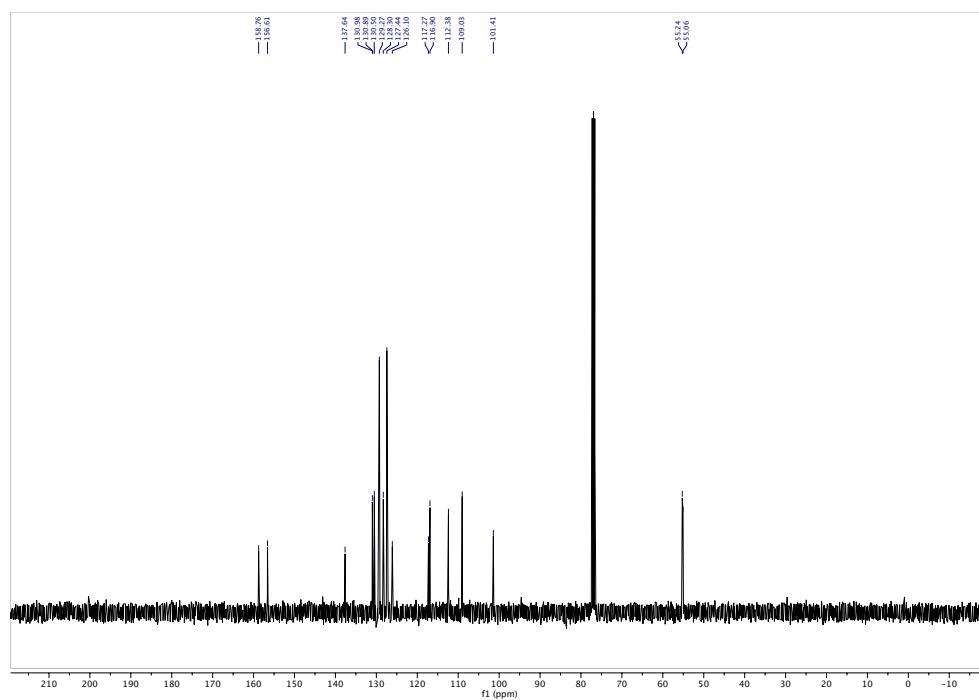
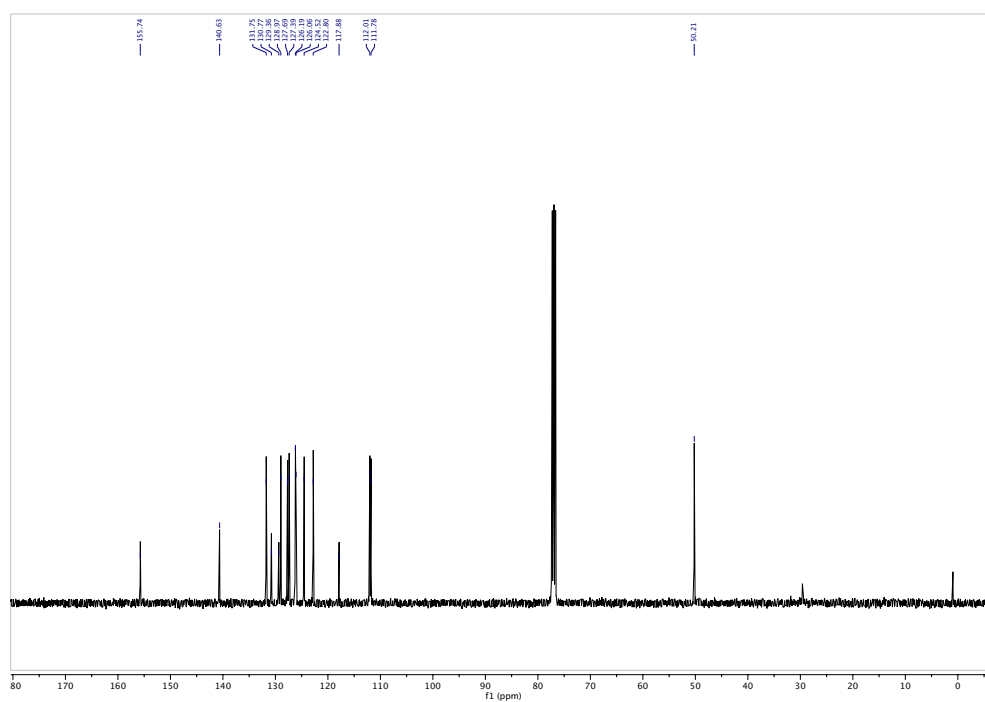
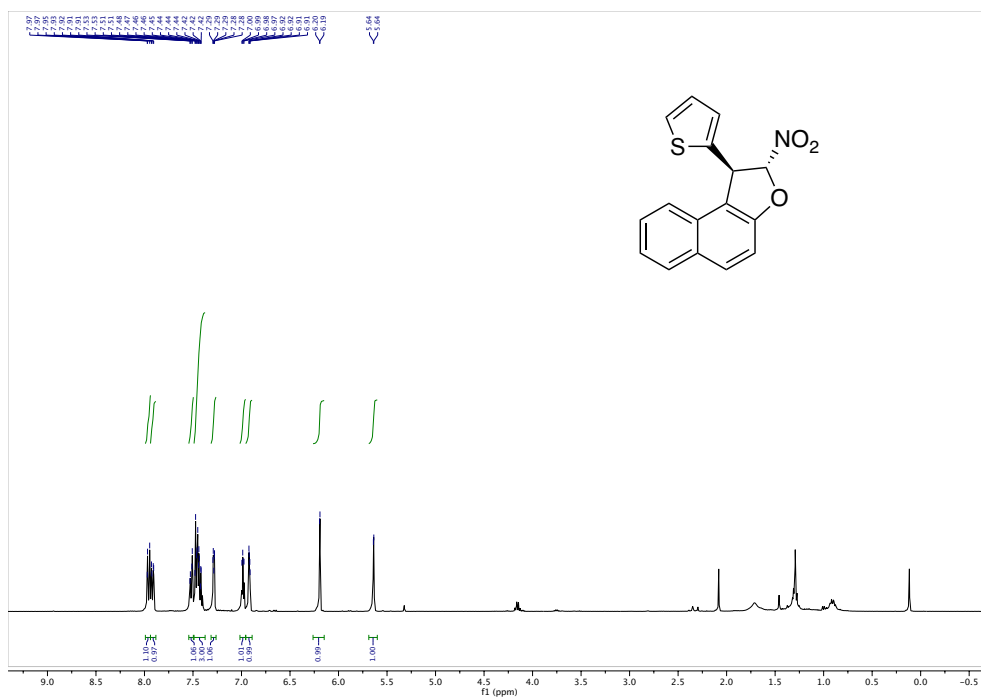


Figure A. 81. ¹H NMR spectrum of 23ea





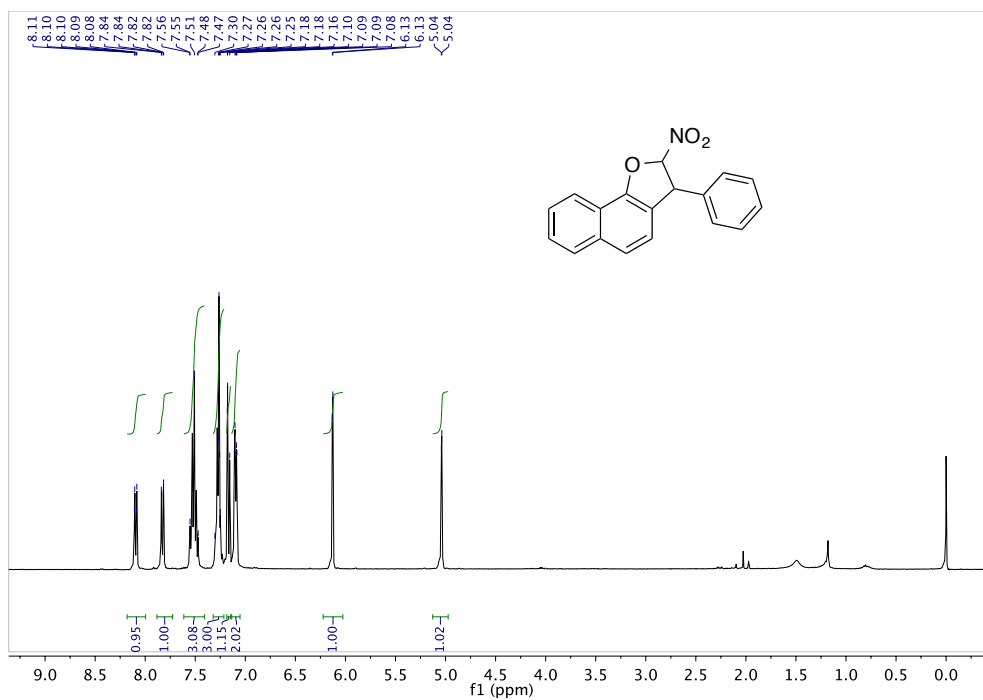


Figure A. 87. ¹H NMR spectrum of 60aa

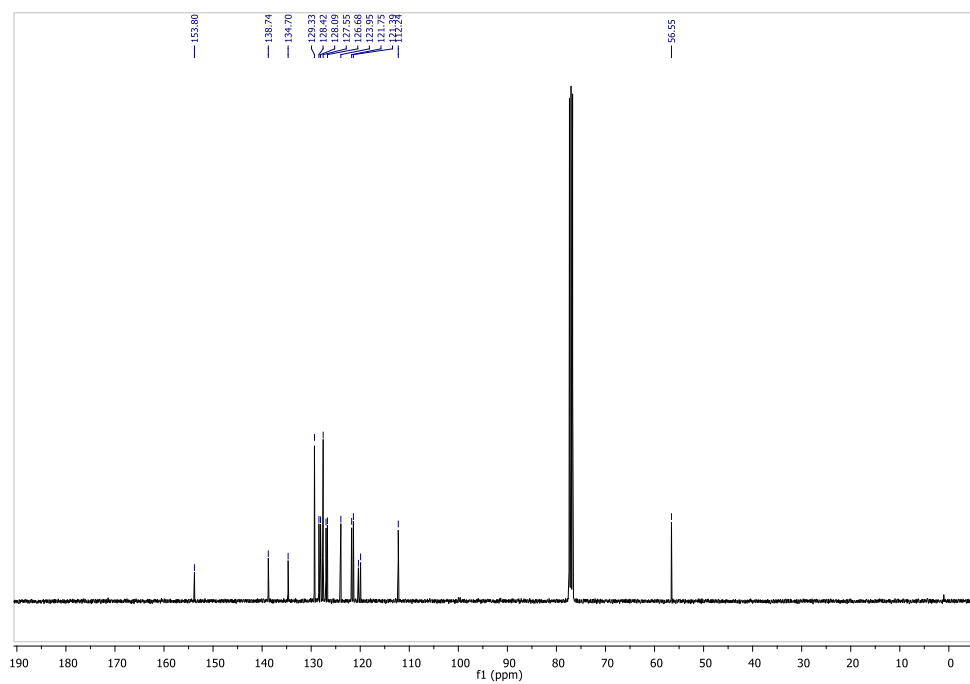


Figure A. 88. ¹³C NMR spectrum of 60aa

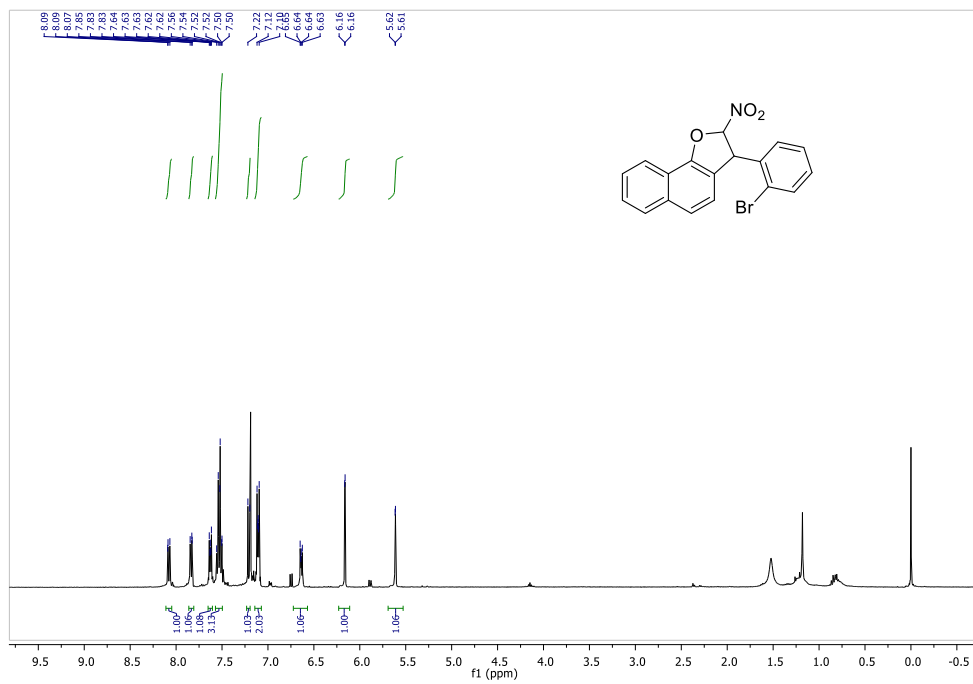


Figure A. 89. ¹H NMR spectrum of 60ab

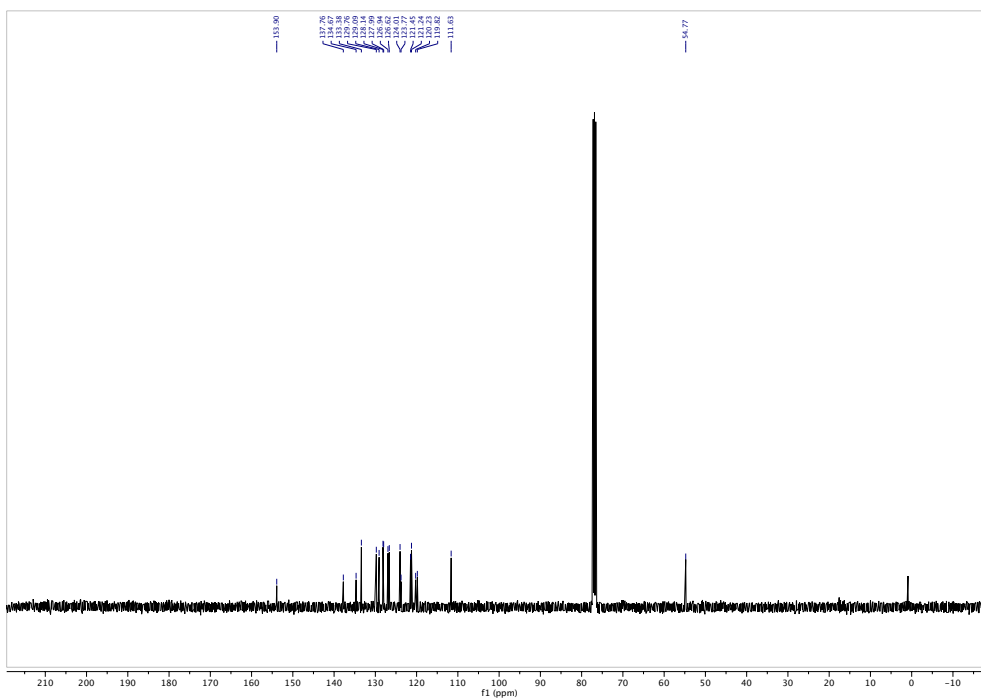


Figure A. 90. ¹³C NMR spectrum of 60ab

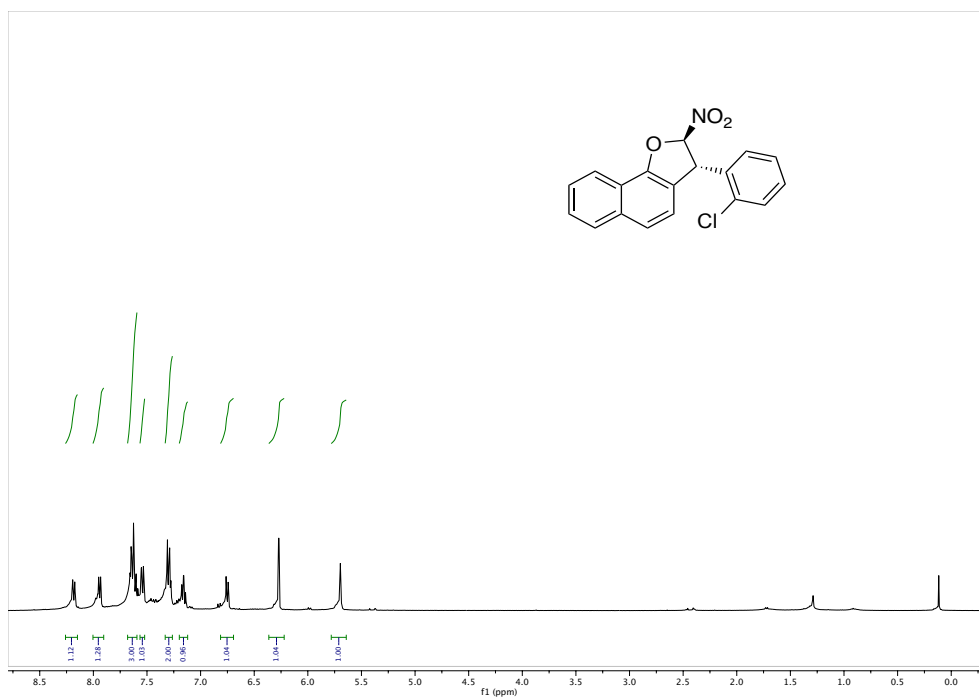


Figure A. 91. ¹H NMR spectrum of 60ac

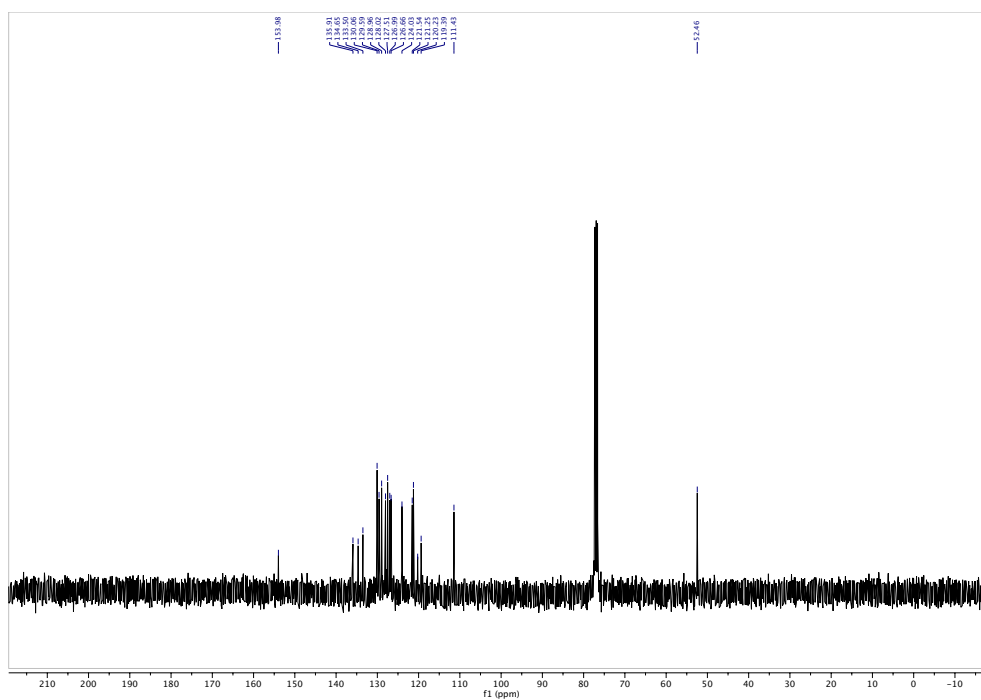


Figure A. 92. ¹³C NMR spectrum of 60ac

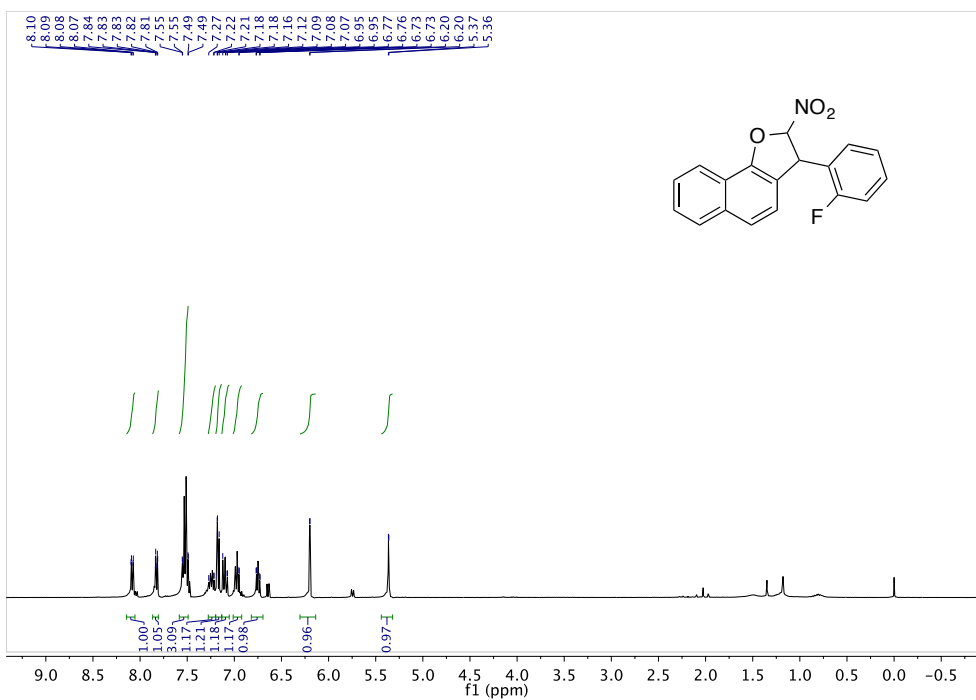


Figure A. 93. ¹H NMR spectrum of 60ad

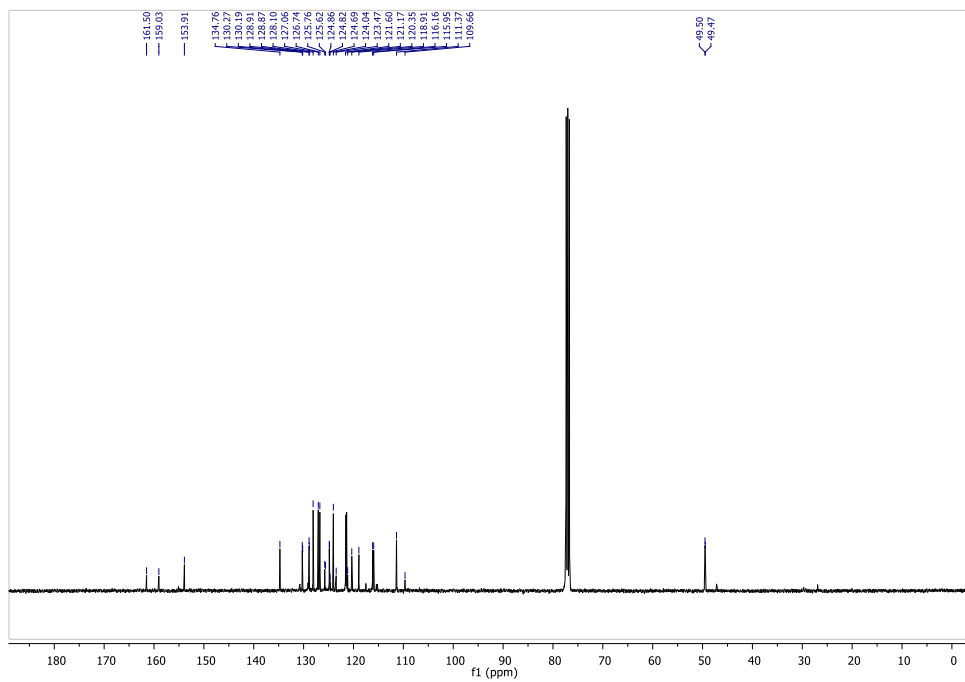


Figure A. 94. ¹³C NMR spectrum of 60ad

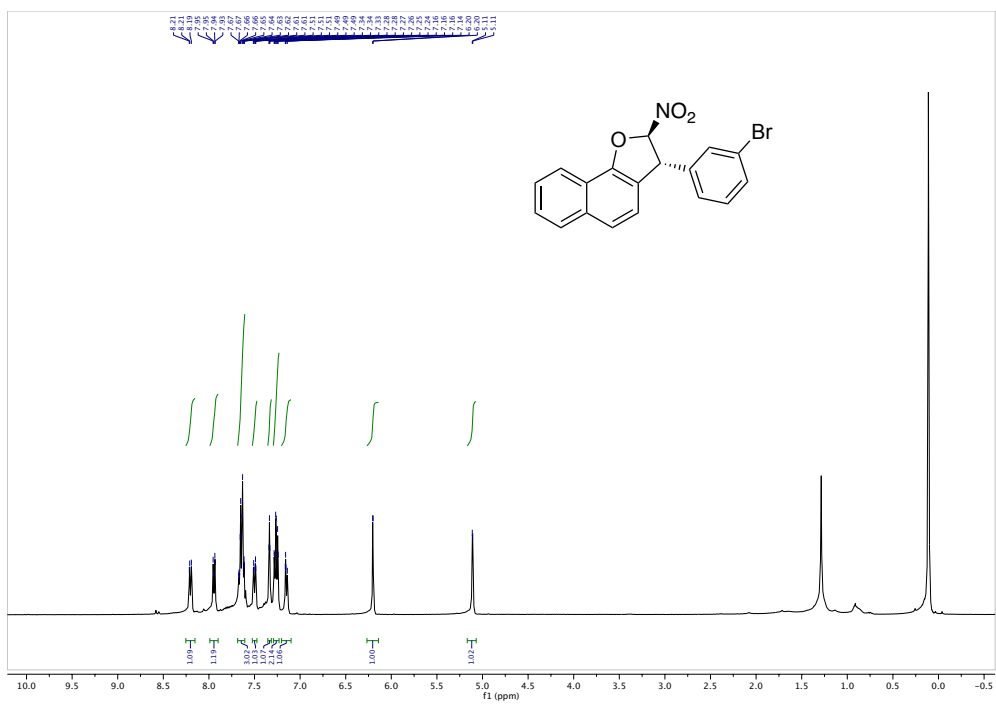


Figure A. 95. ¹H NMR spectrum of 60ae

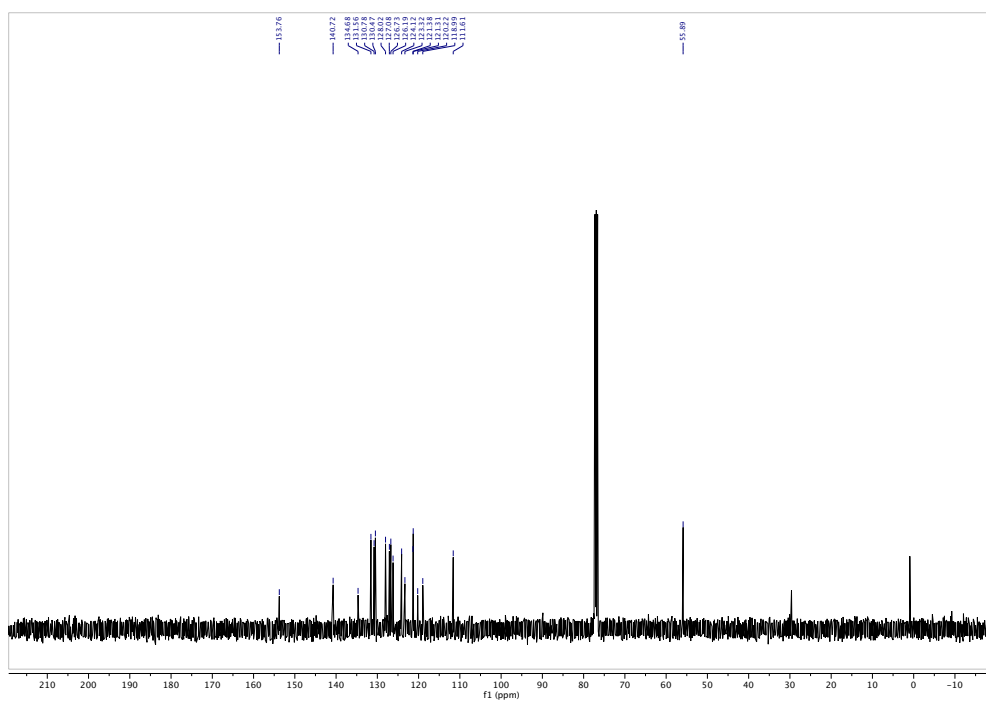


Figure A. 96. ¹³C NMR spectrum of 60ae

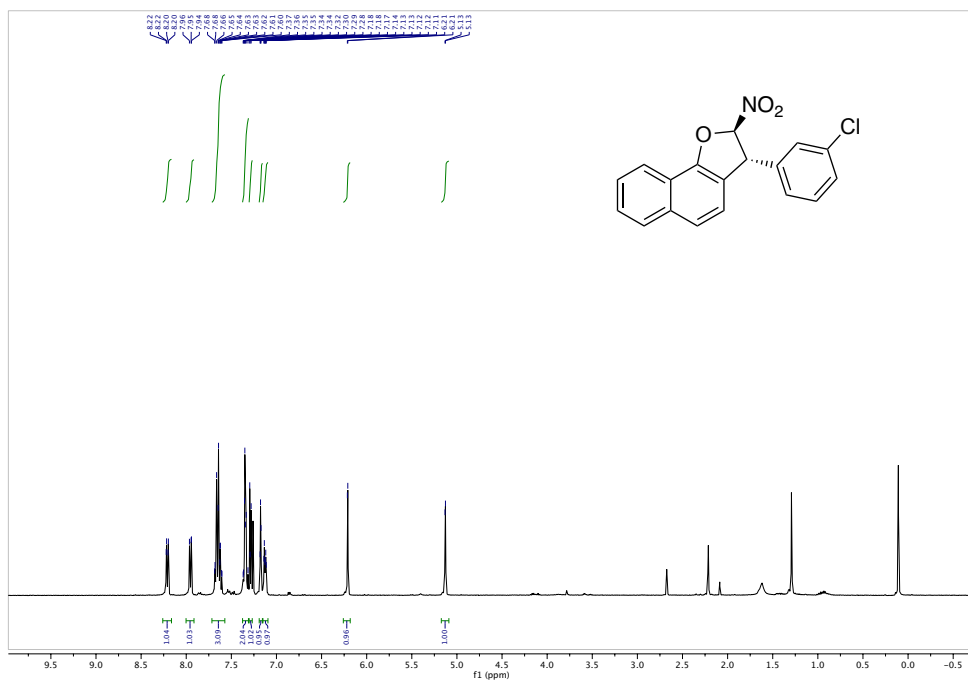


Figure A. 97. ¹H NMR spectrum of 60af

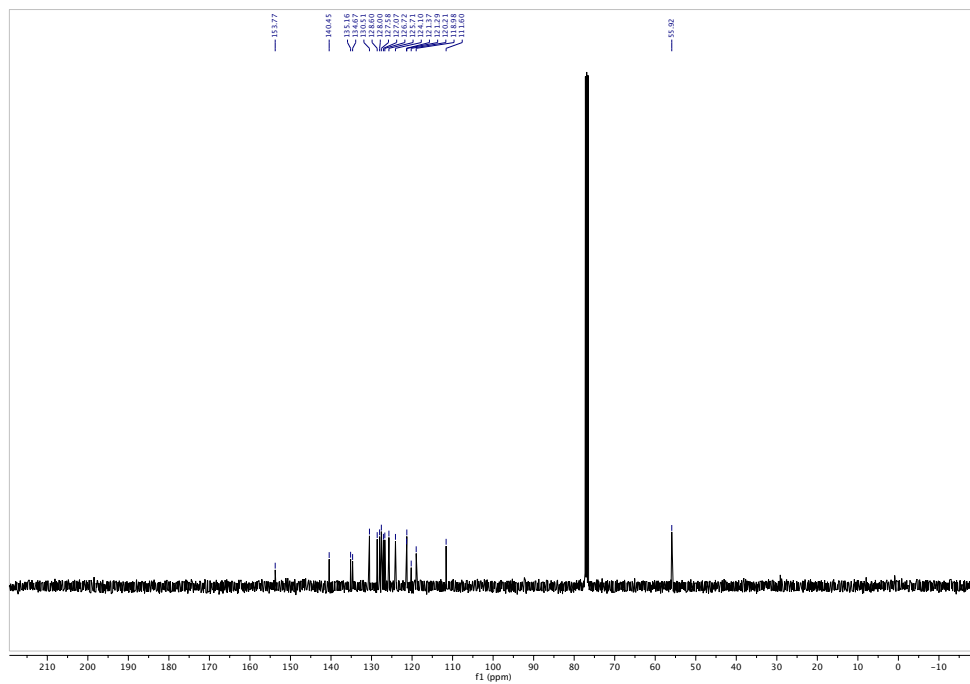


Figure A. 98. ¹³C NMR spectrum of 60af

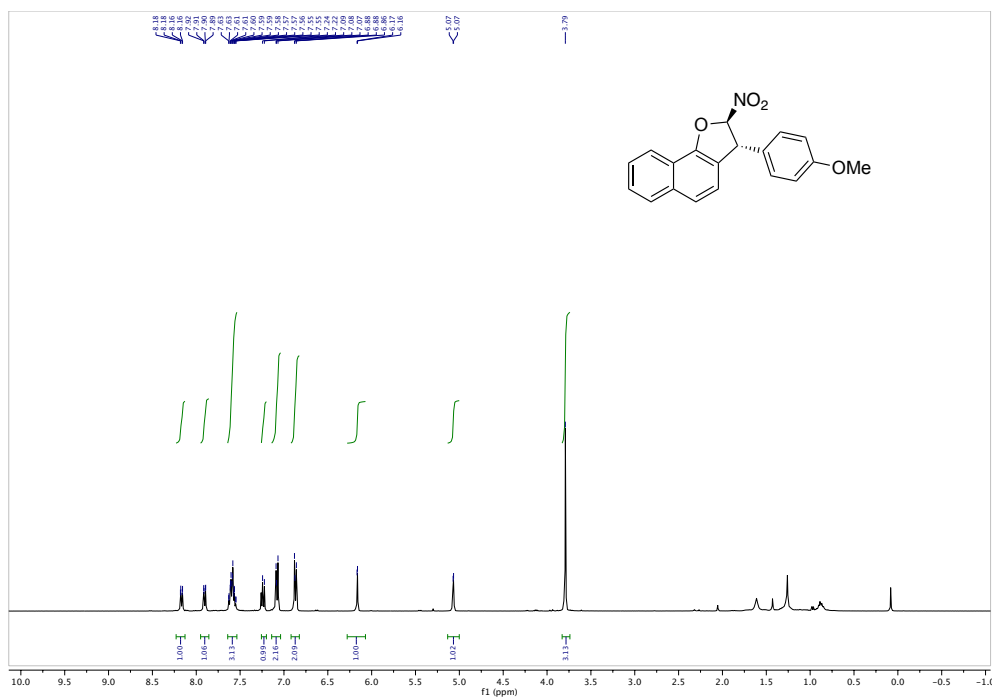


Figure A. 99. ¹H NMR spectrum of 60ag

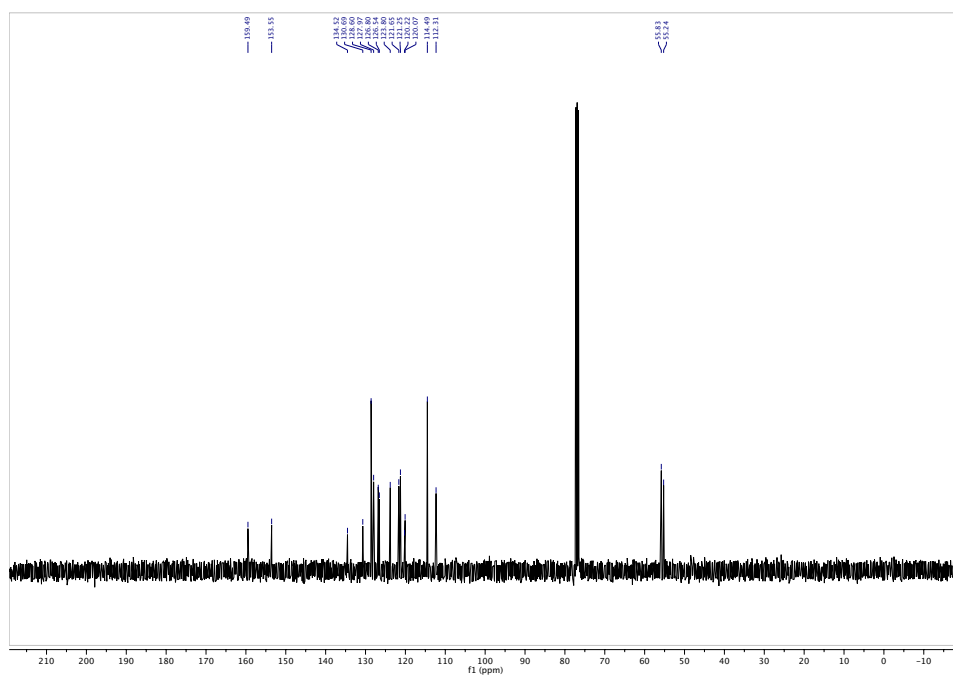
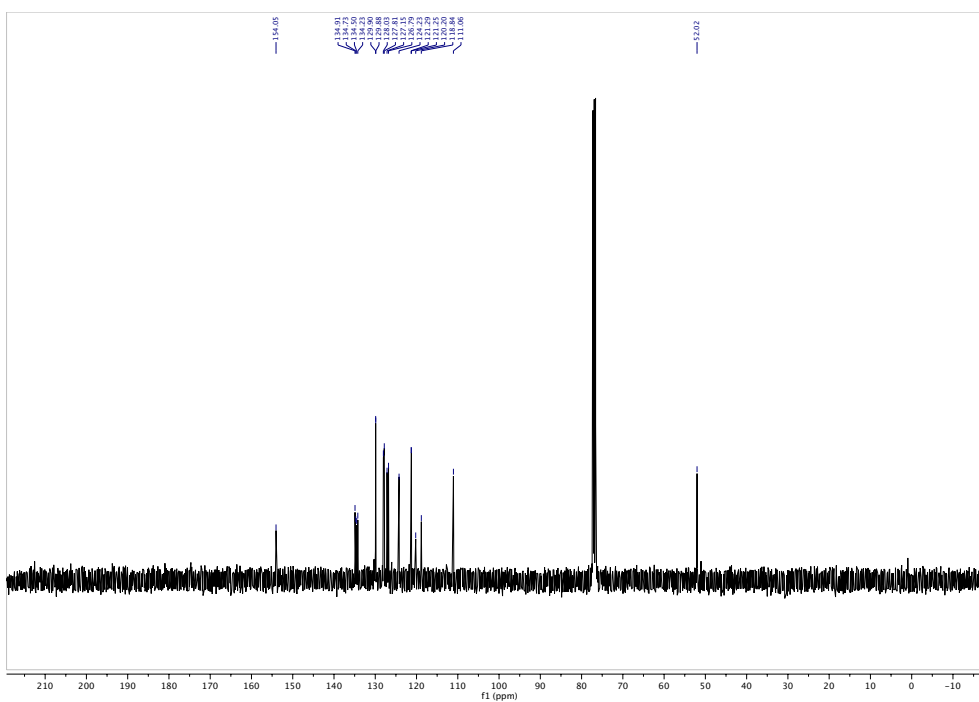
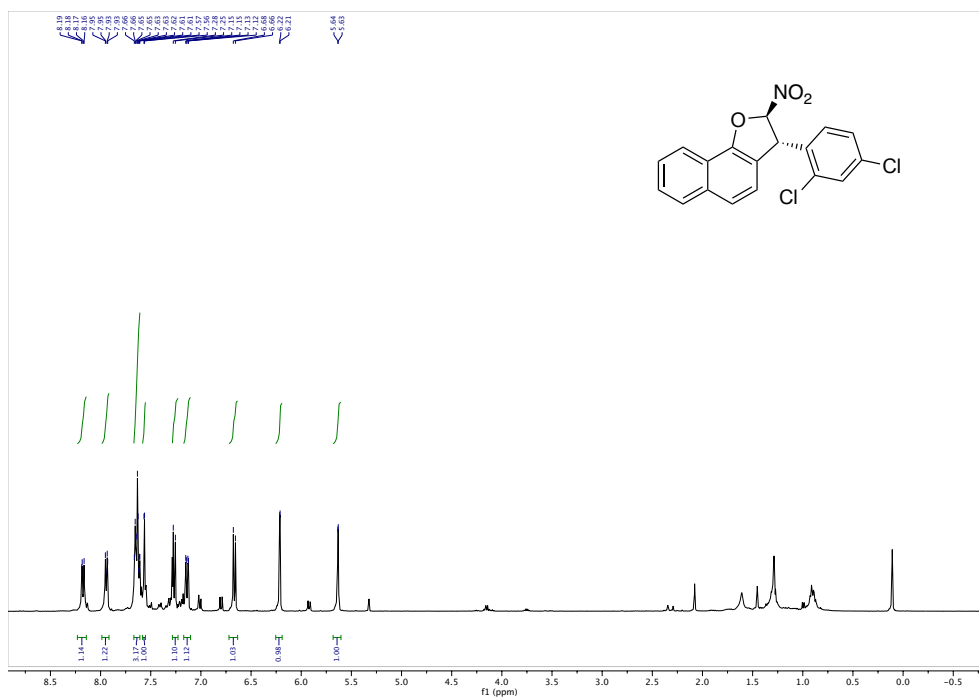


Figure A. 100. ¹³C NMR spectrum of 60ag



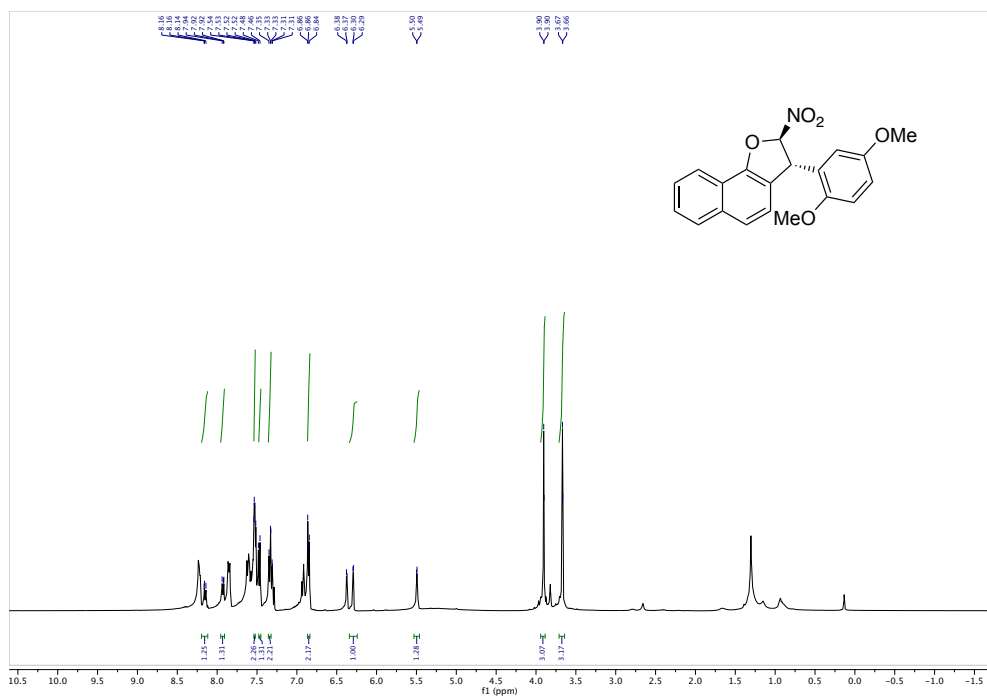


Figure A. 103. ¹H NMR spectrum of 60ai

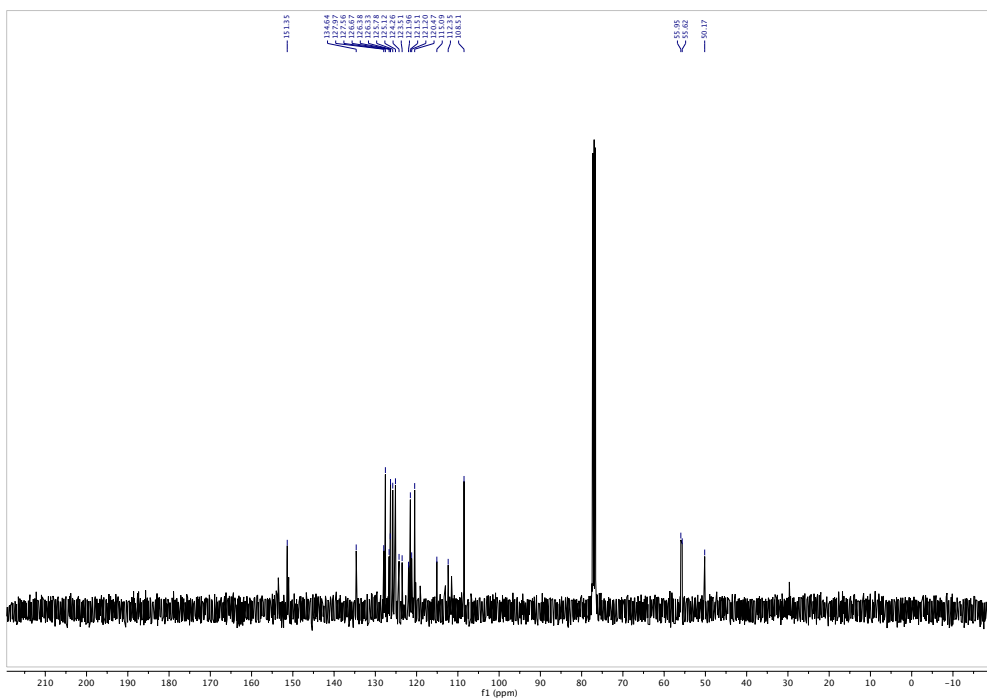


Figure A. 104. ¹³C NMR spectrum of 60ai

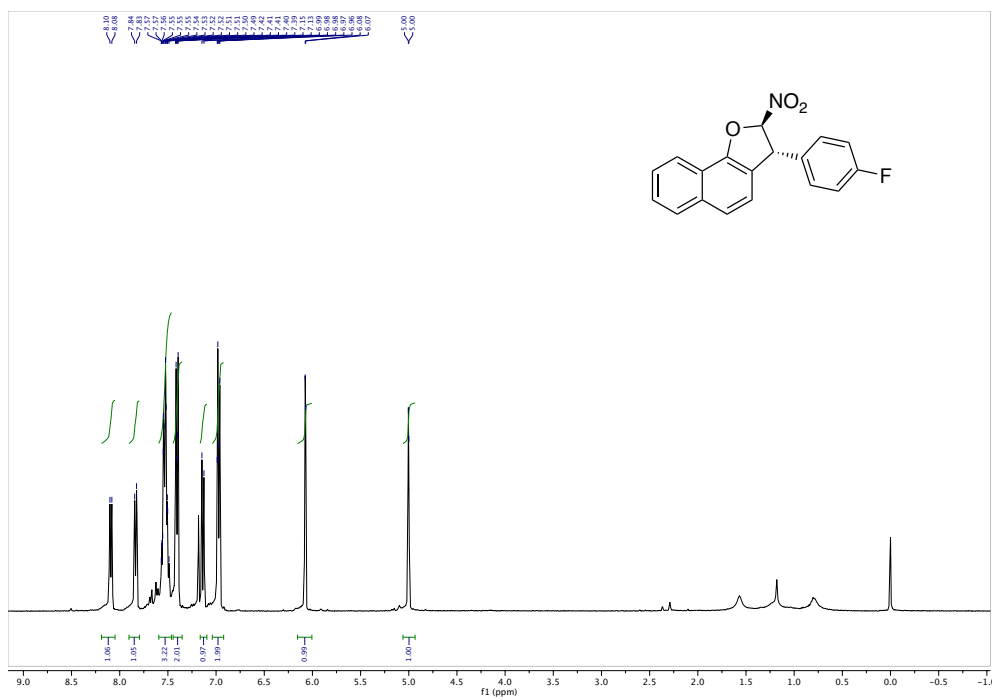


Figure A. 105. ¹H NMR spectrum of 60aj

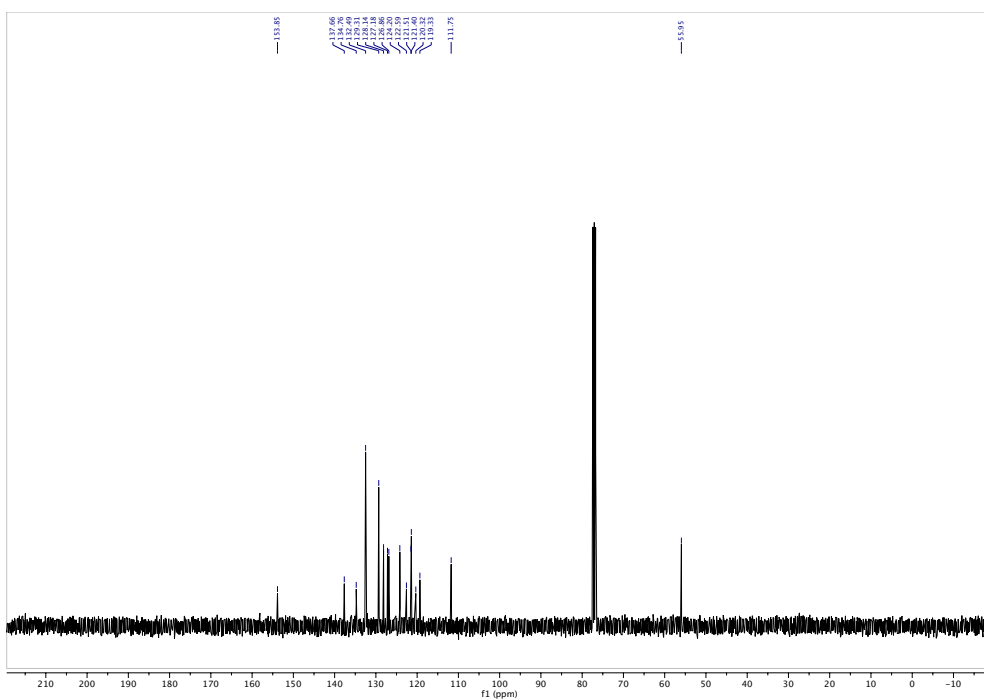
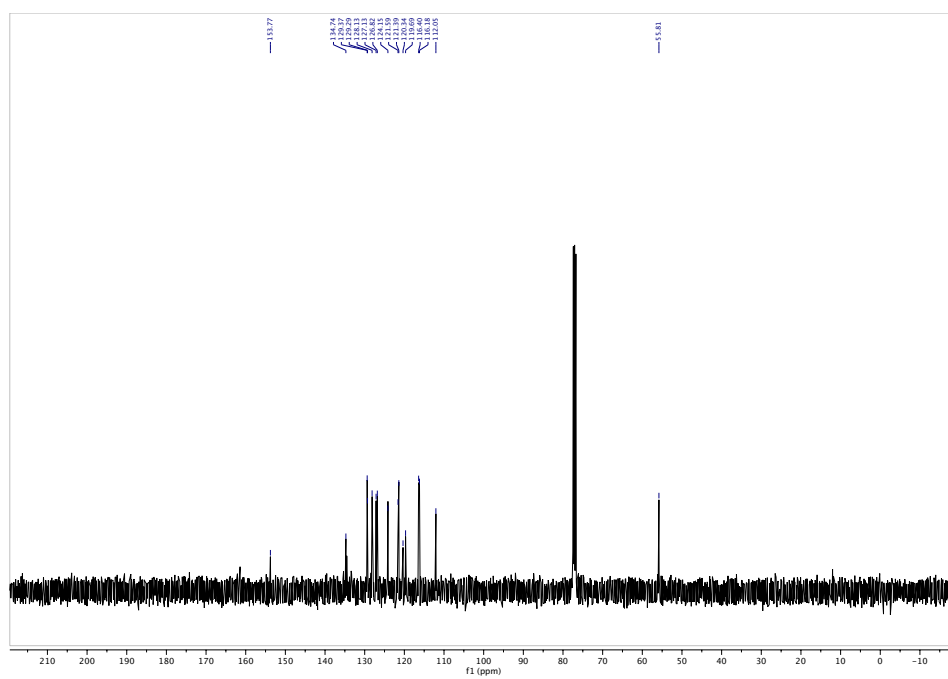
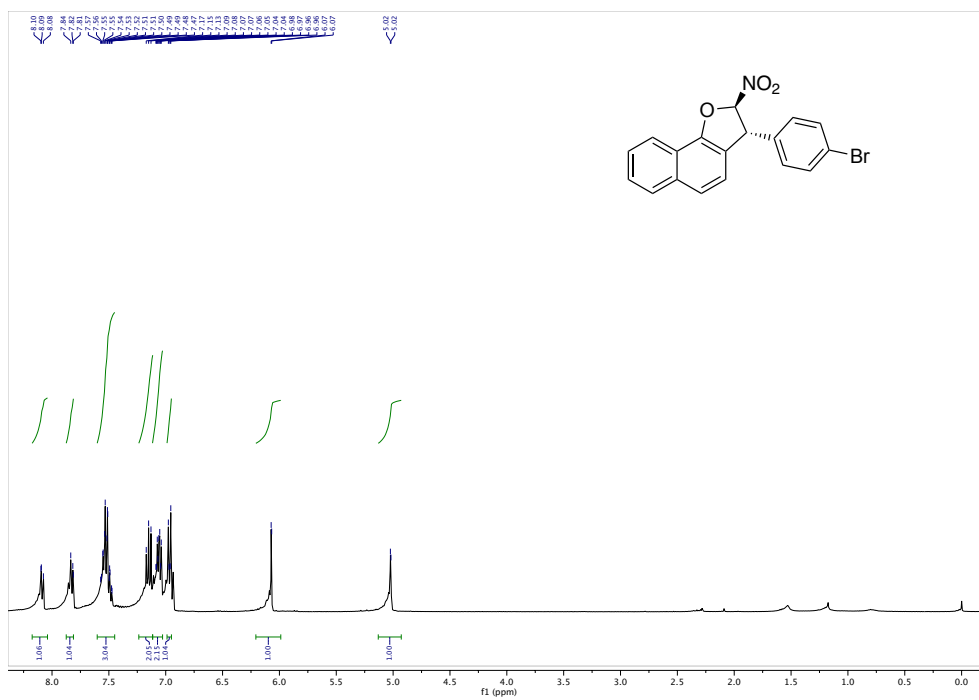


Figure A. 106. ¹³C NMR spectrum of 60aj



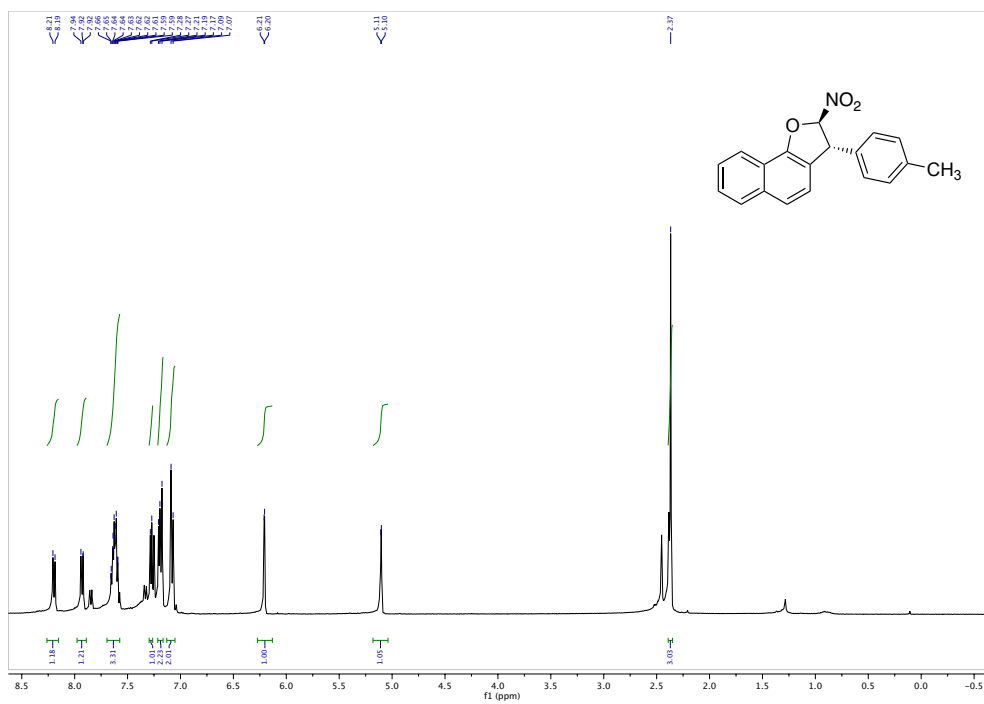


Figure A. 109. ¹H NMR spectrum of 60al

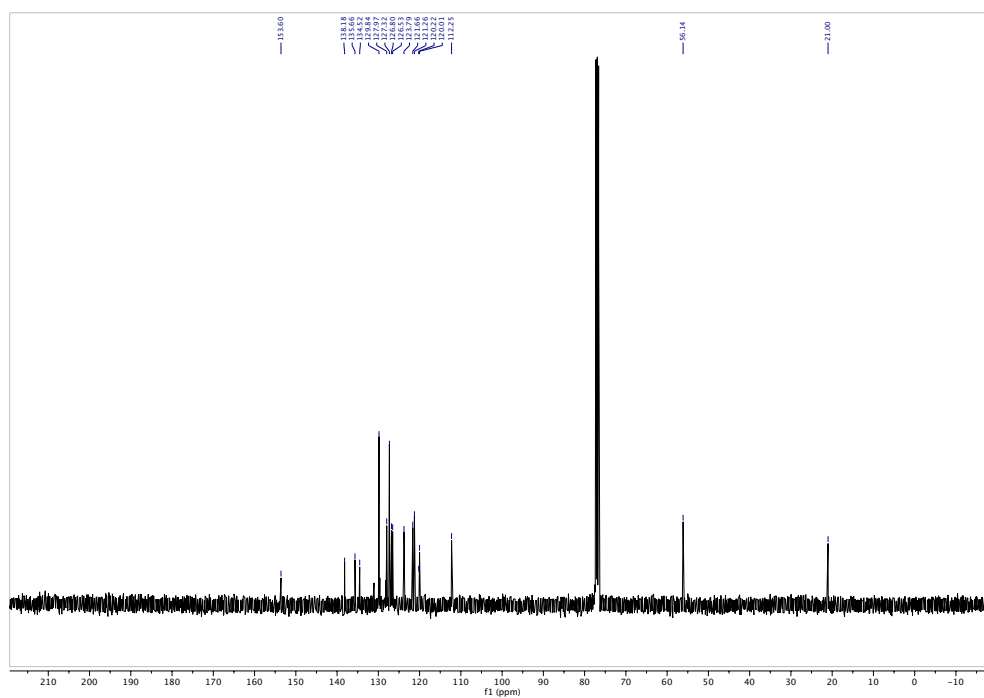


Figure A. 110. ¹³C NMR spectrum of 60al

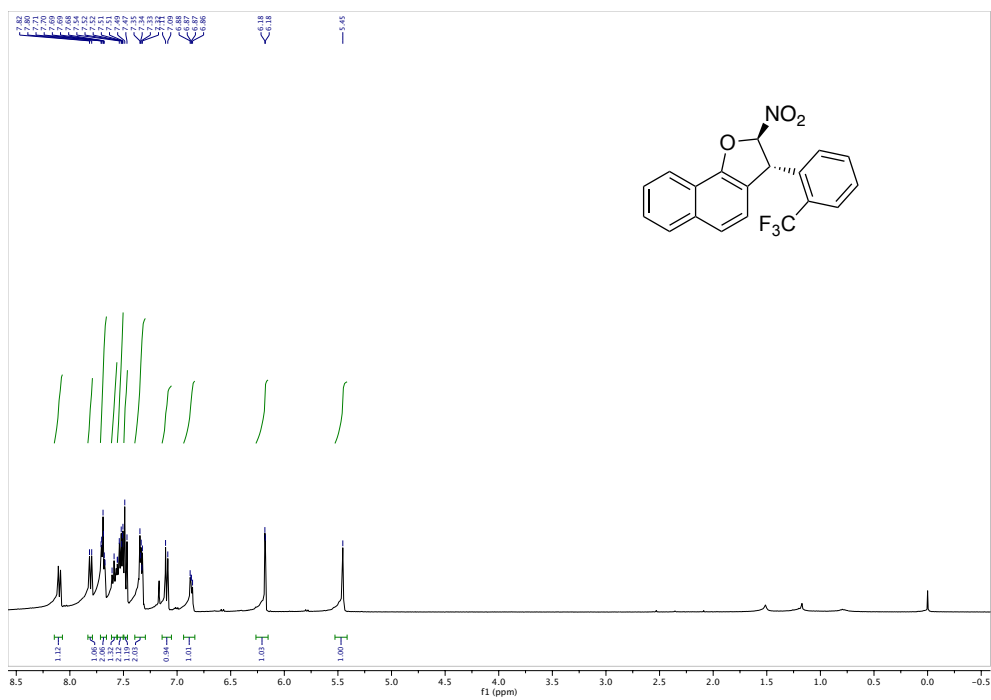


Figure A. 111. ¹H NMR spectrum of 60an

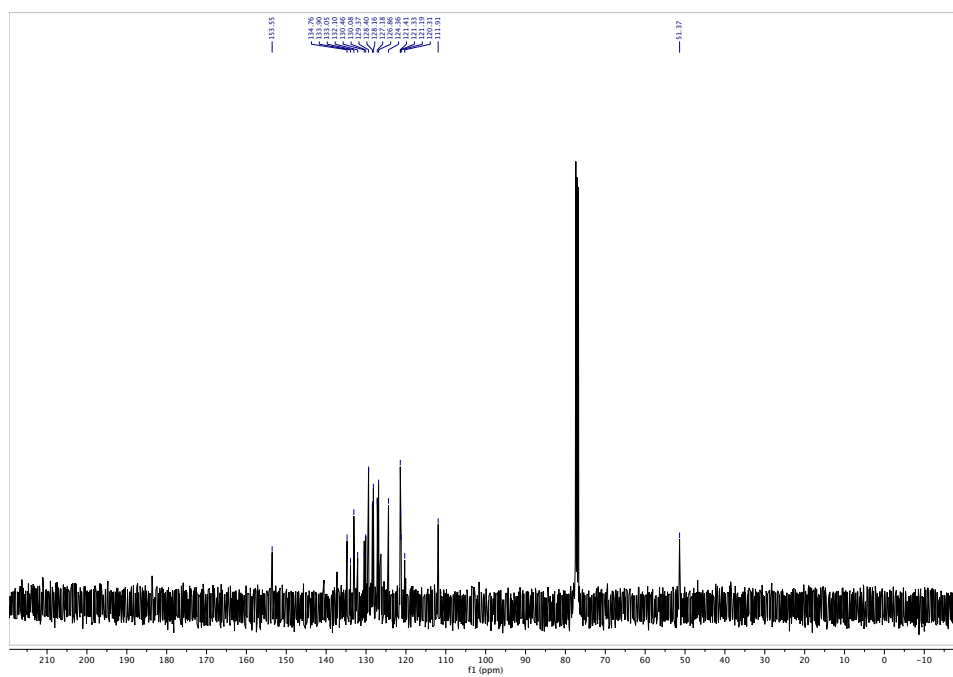


Figure A. 112. ¹³C NMR spectrum of 60an

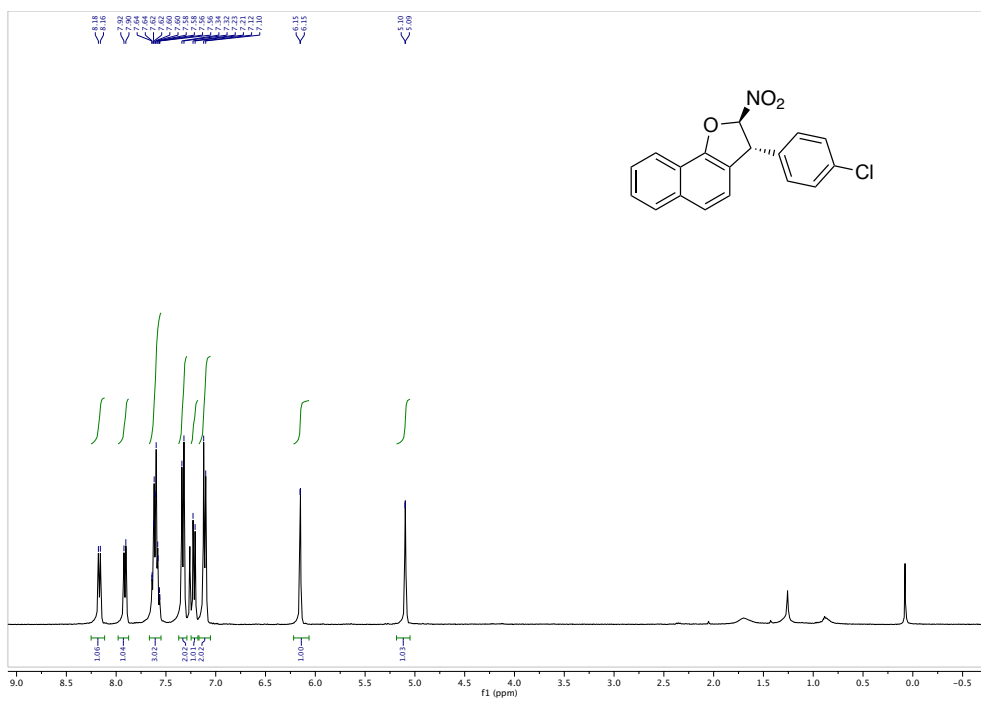


Figure A. 113. ¹H NMR spectrum of 60ao

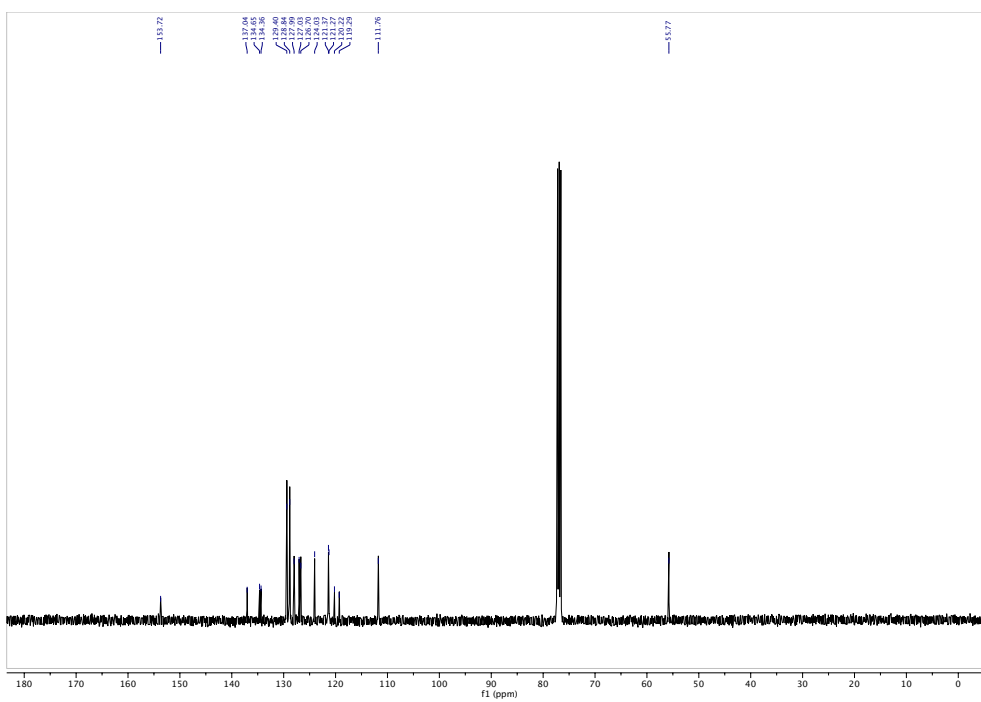
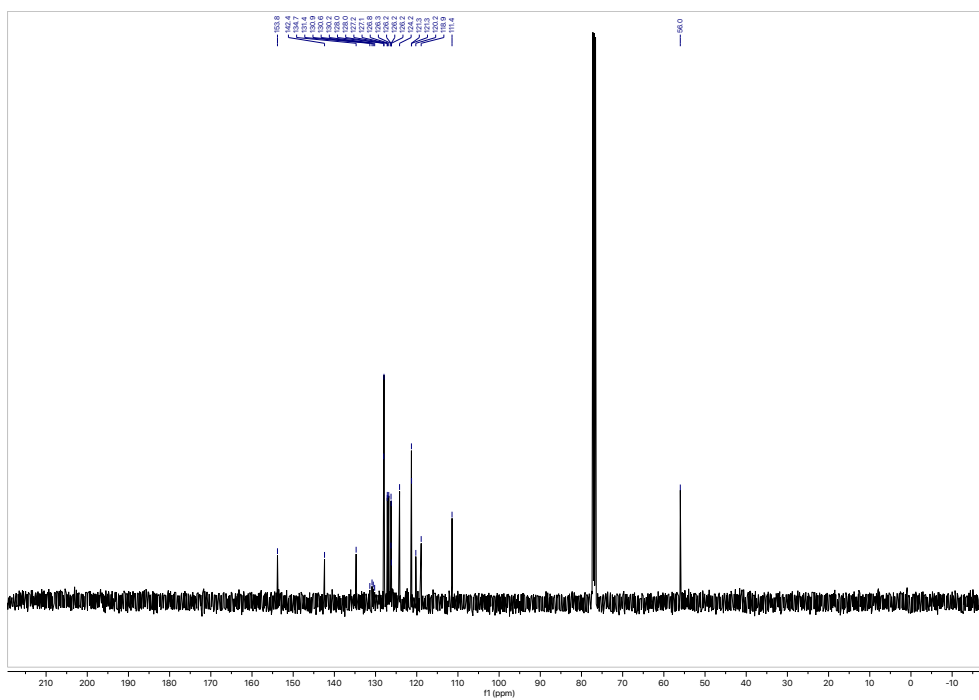
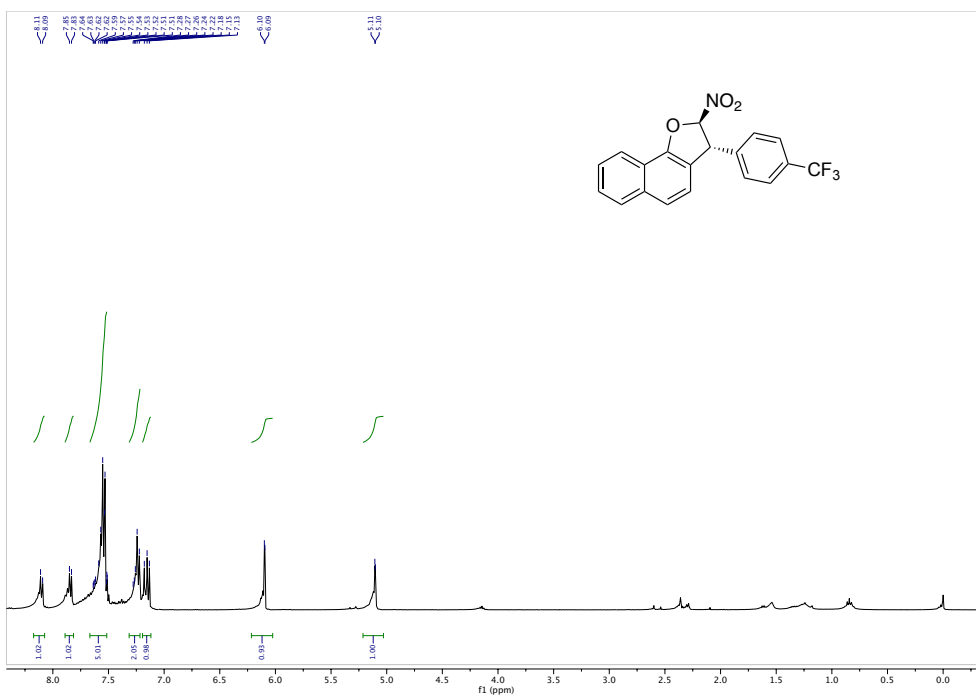


Figure A. 114. ¹³C NMR spectrum of 60ao



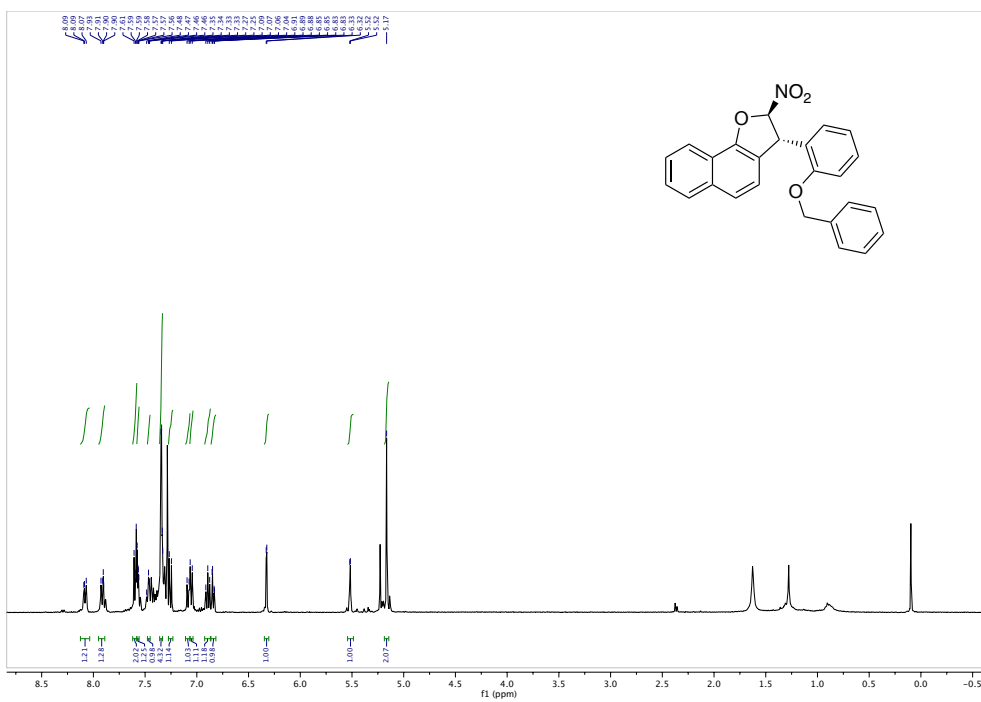


Figure A. 117. ¹H NMR spectrum of 60aq

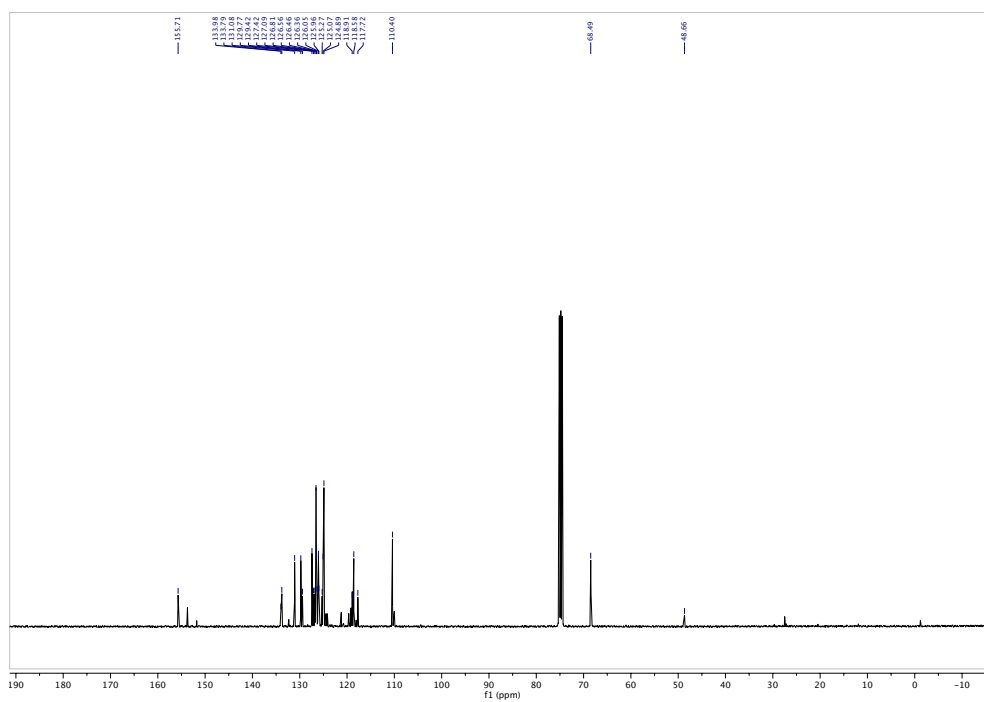
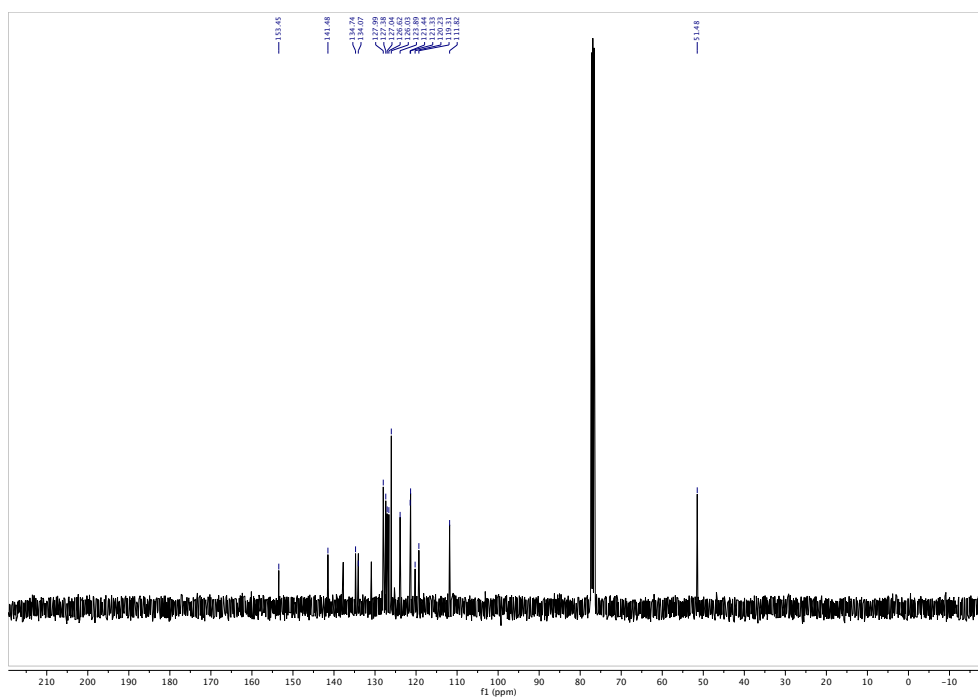
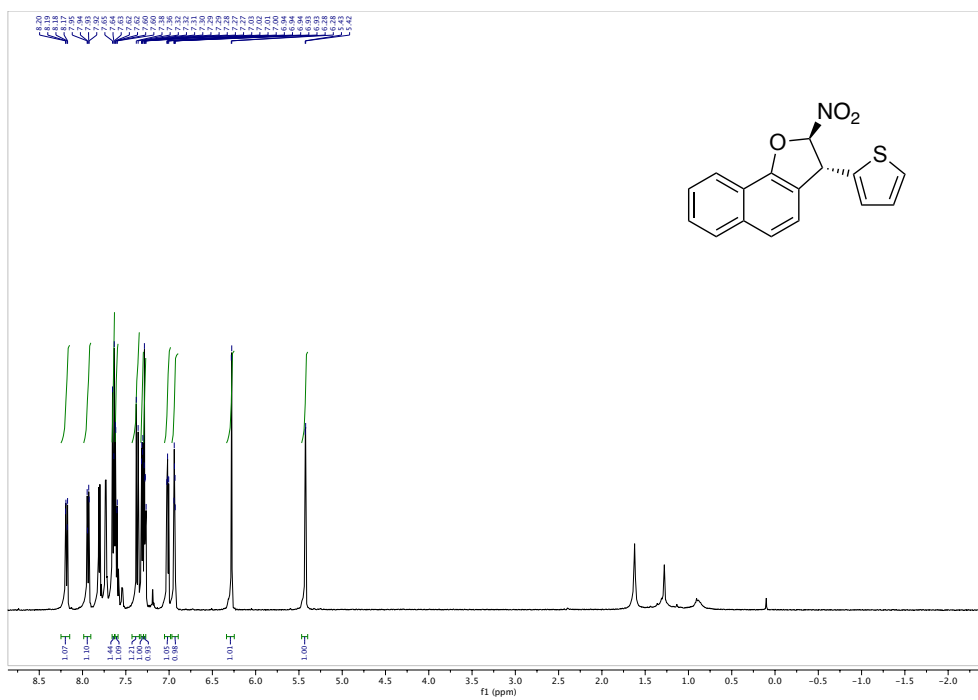


Figure A. 118. ¹³C NMR spectrum of 60aq



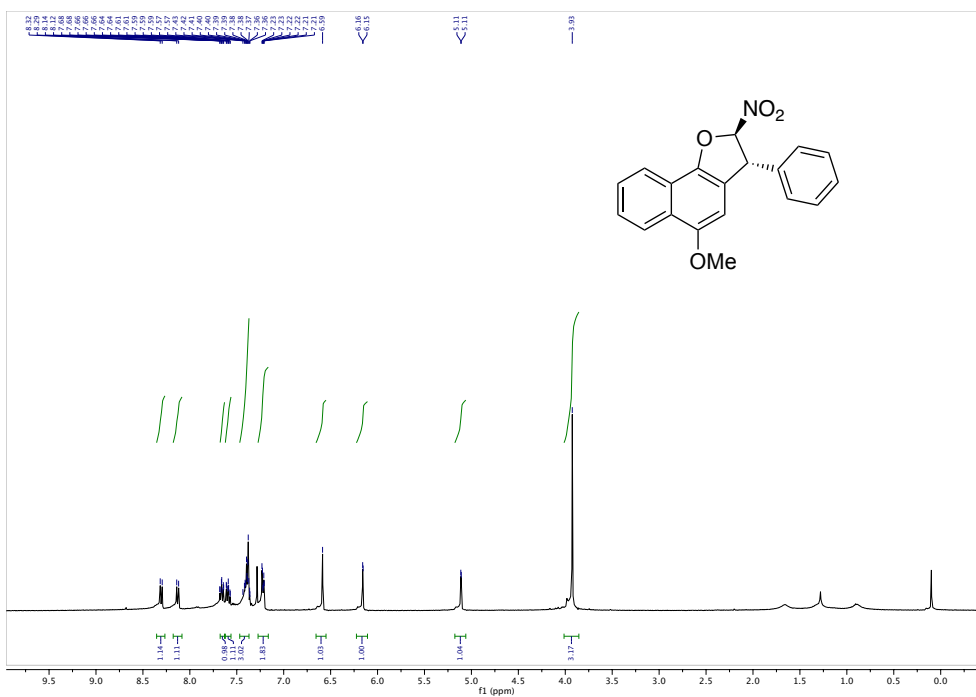


Figure A. 121. ¹H NMR spectrum of 60ba

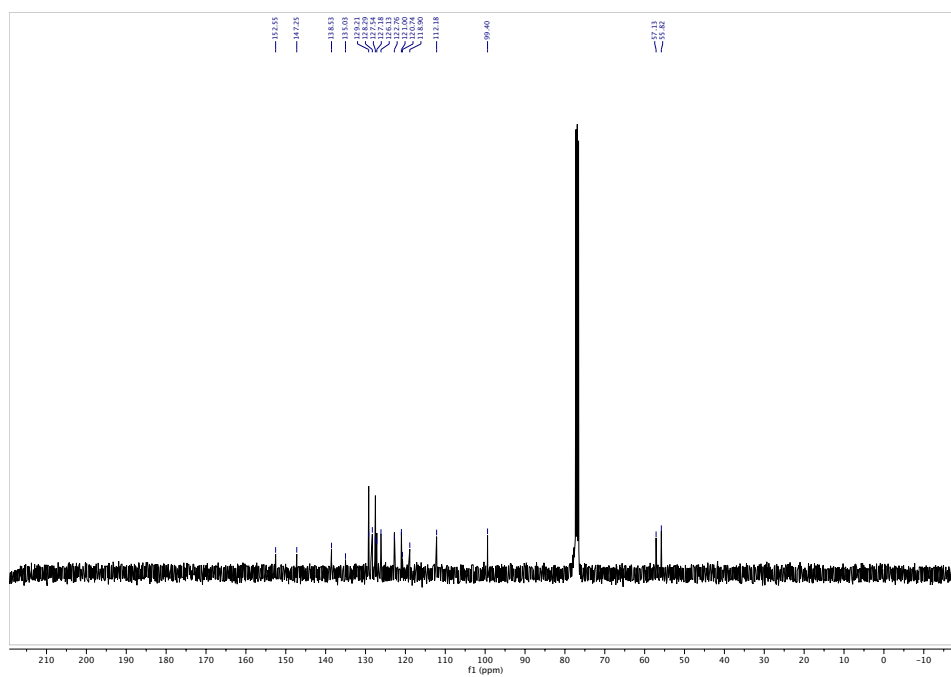


Figure A. 122. ¹³C NMR spectrum of 60ba

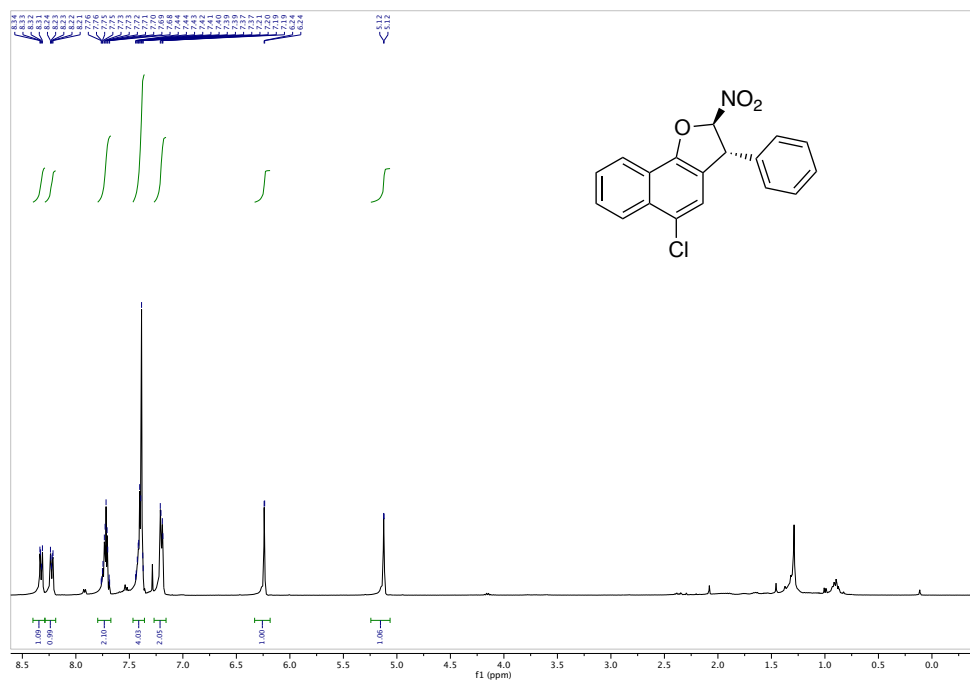


Figure A. 123. ^1H NMR spectrum of 60ca

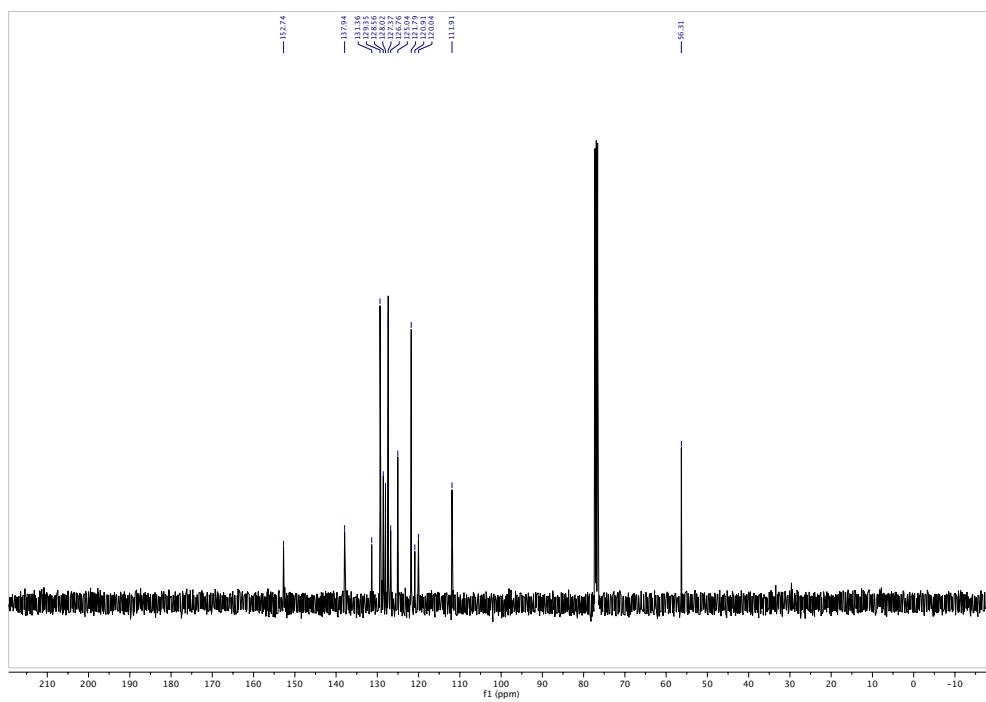


Figure A. 124. ^{13}C NMR spectrum of 60ca

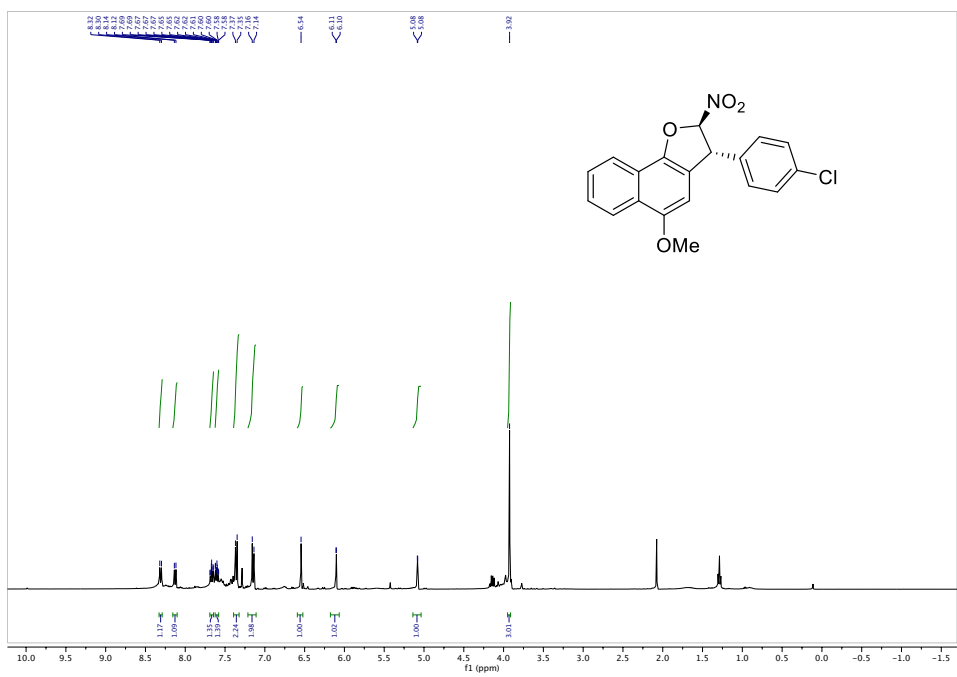


Figure A. 127. ^1H NMR spectrum of 60bo

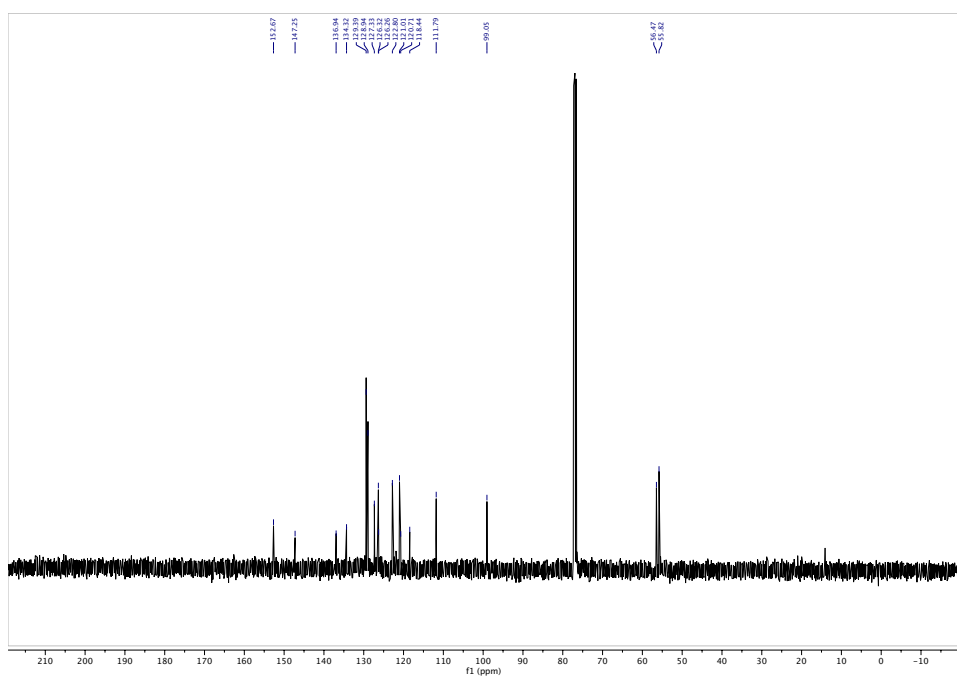


Figure A. 128. ^{13}C NMR spectrum of 60bo

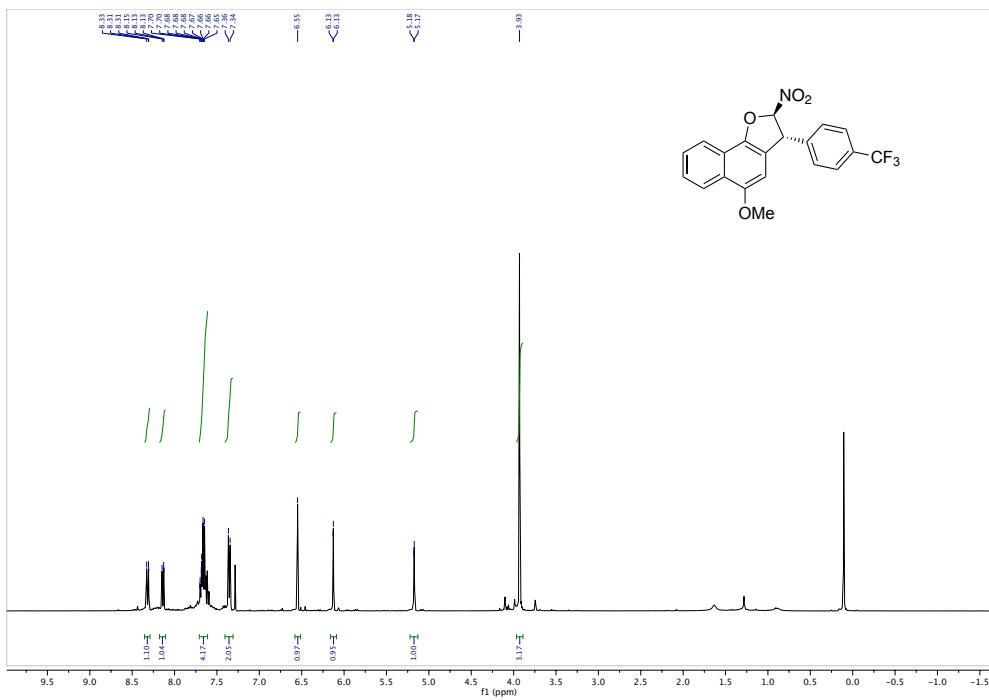


Figure A. 129. ¹H NMR spectrum of 60bp

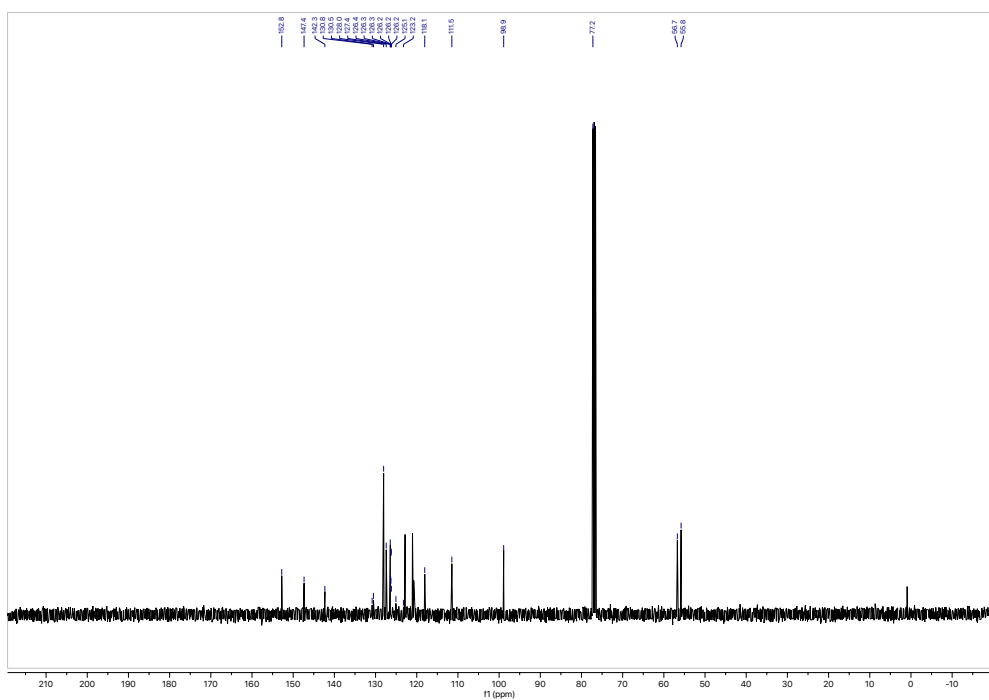


Figure A. 130. ¹³C NMR spectrum of 60bp

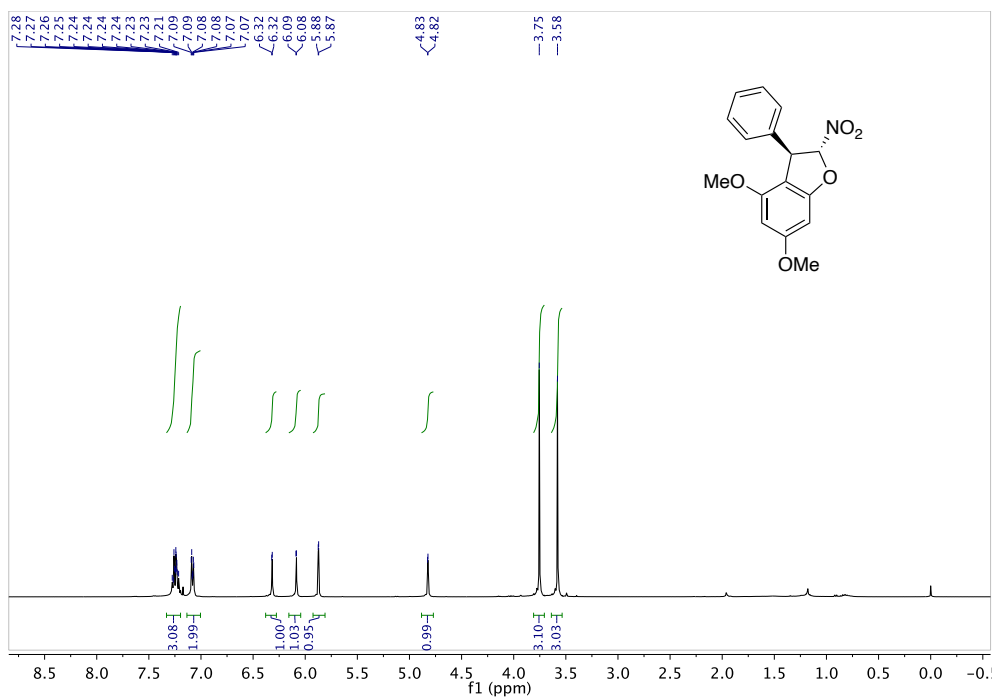


Figure A. 131. ^1H NMR spectrum of **62ba**

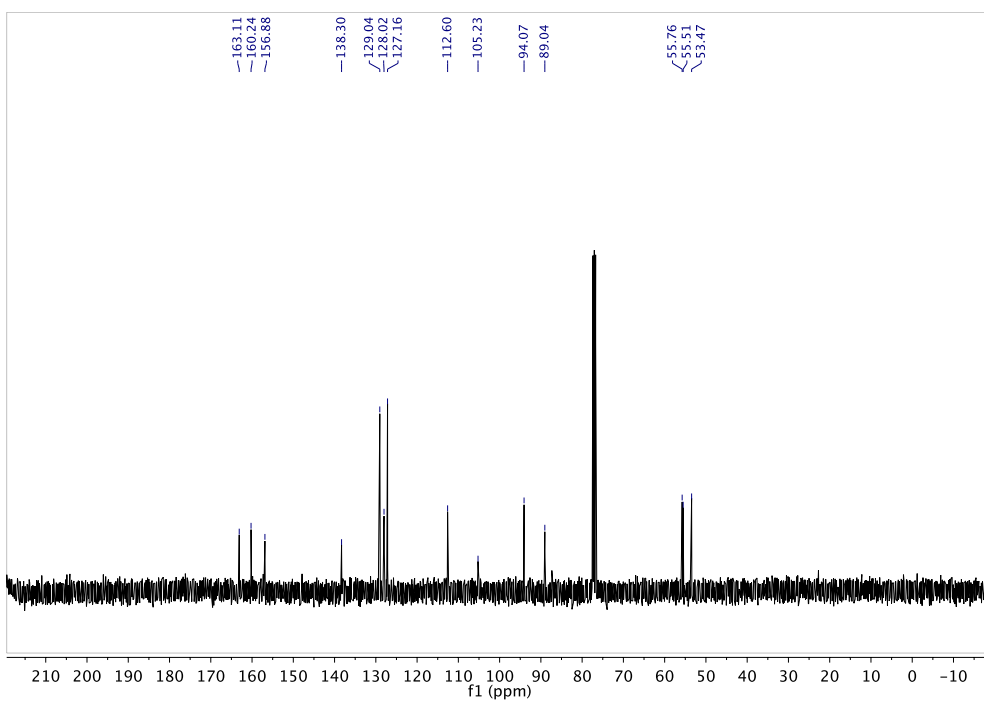
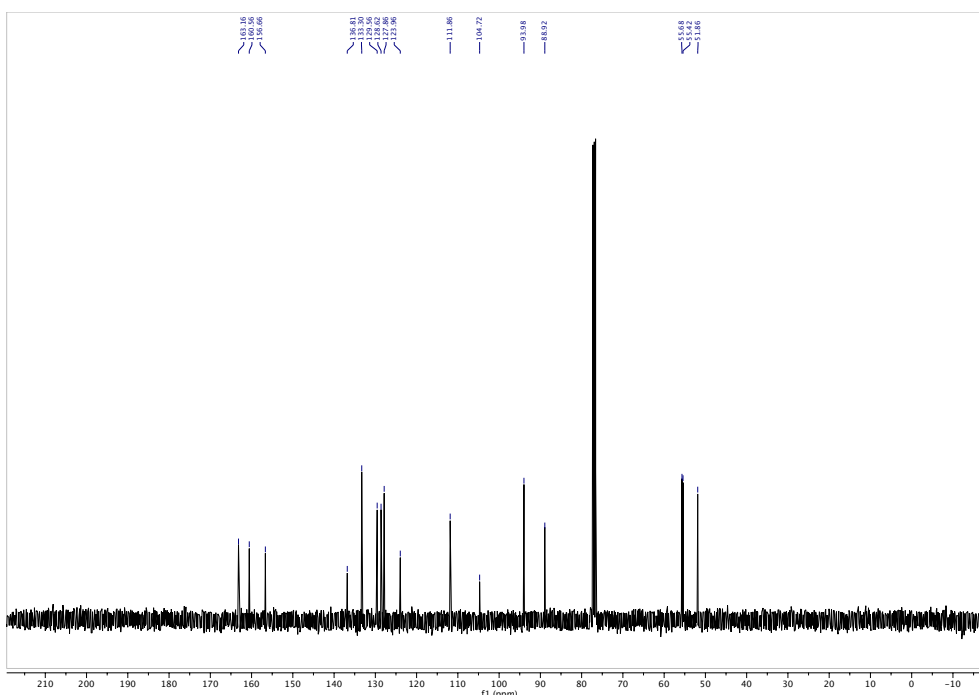
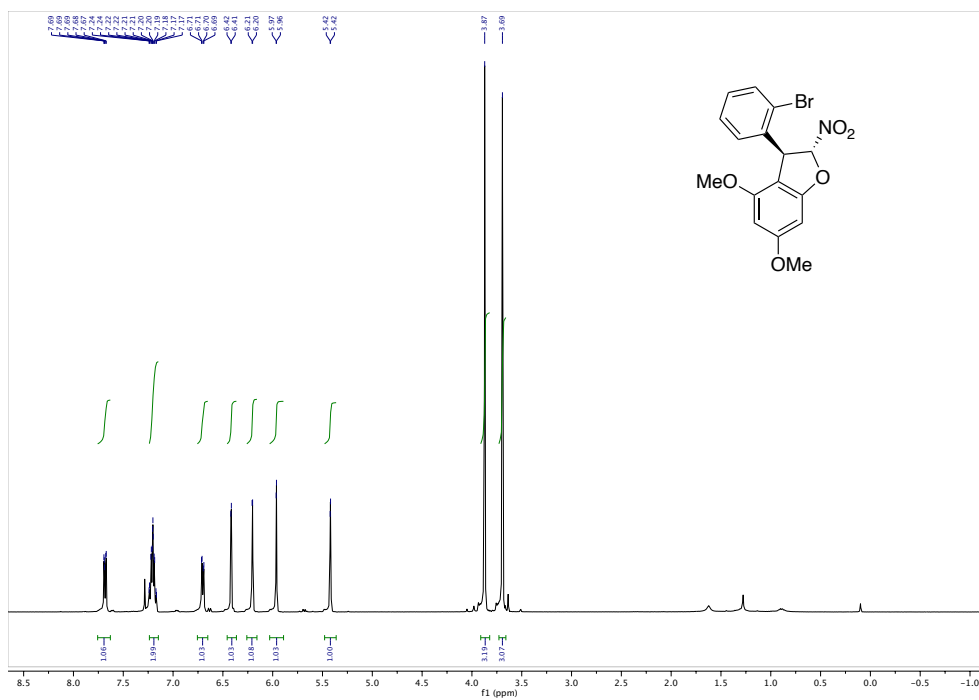


Figure A. 132. ^{13}C NMR spectrum of **62ba**



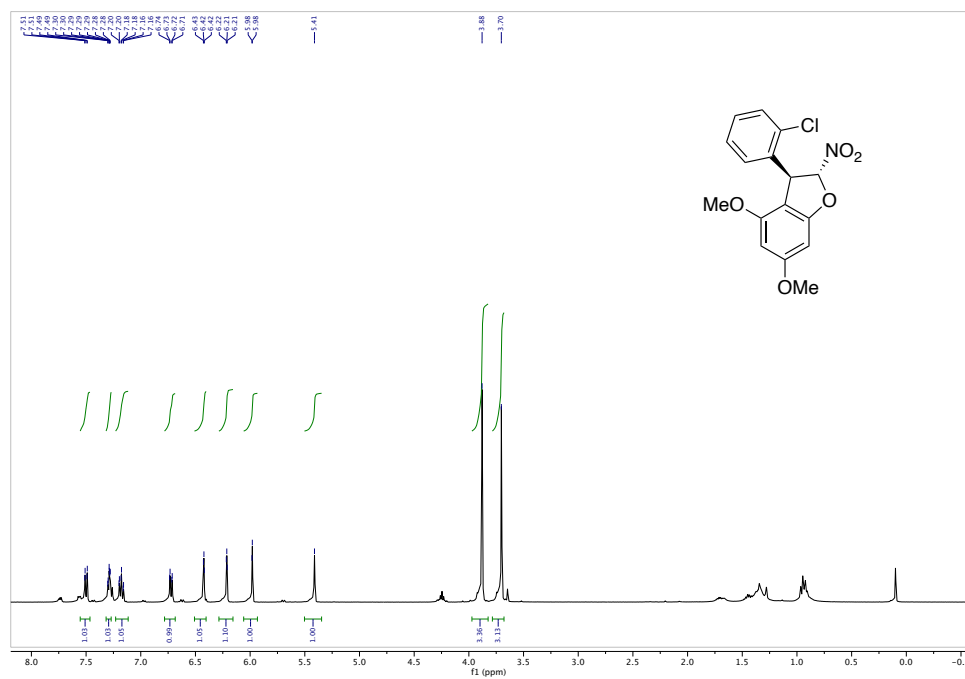


Figure A. 135. ¹H NMR spectrum of 62bc

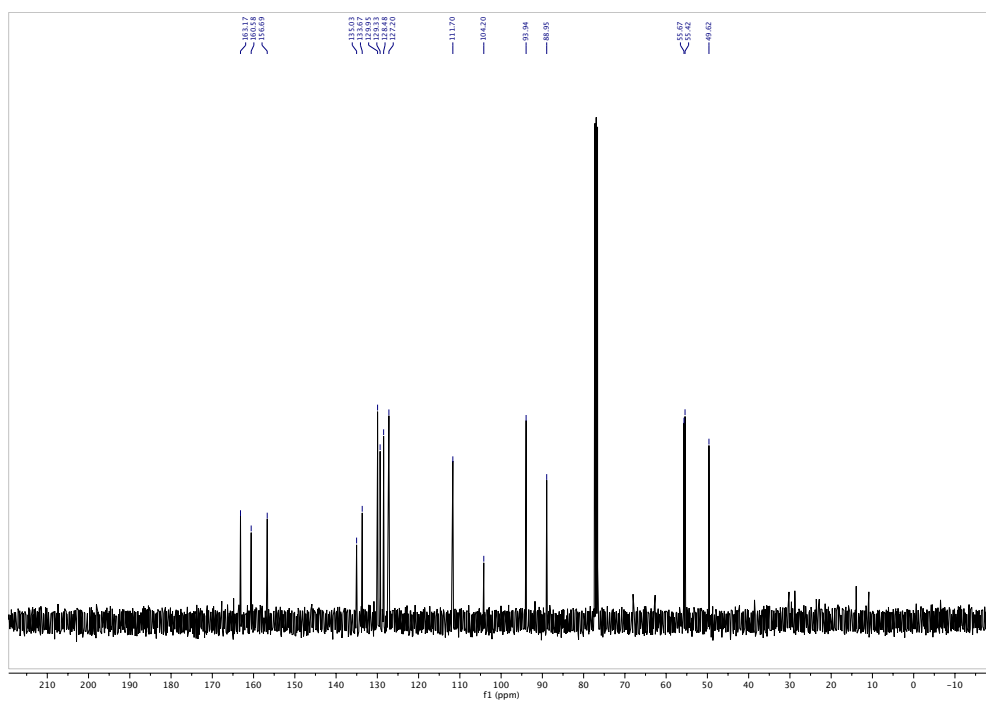


Figure A. 136. ¹³C NMR spectrum of 62bc

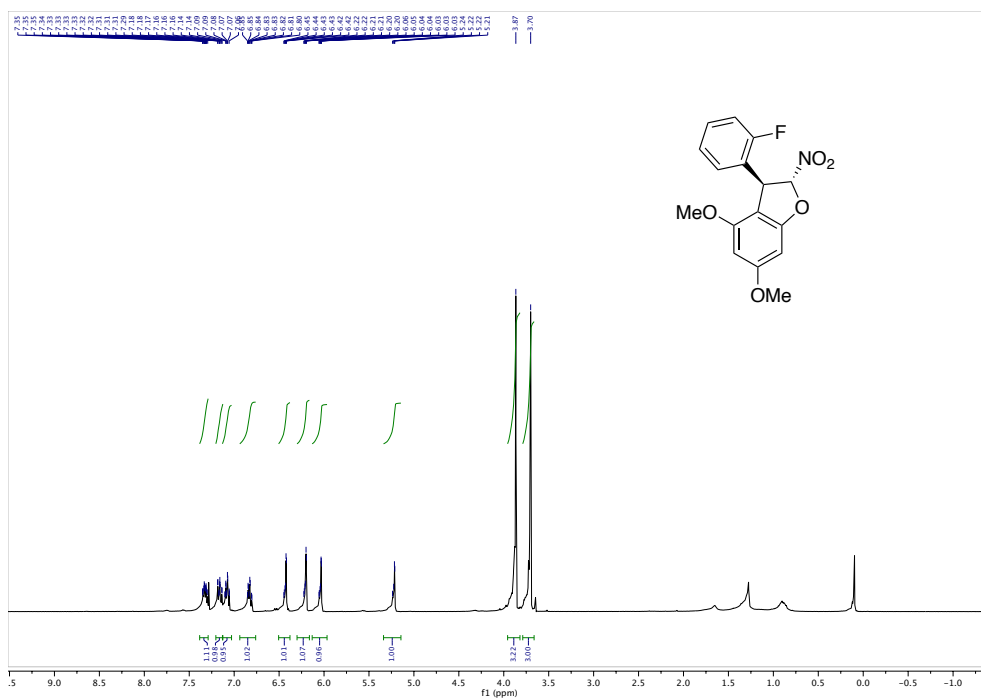


Figure A. 137. ¹H NMR spectrum of 62bd

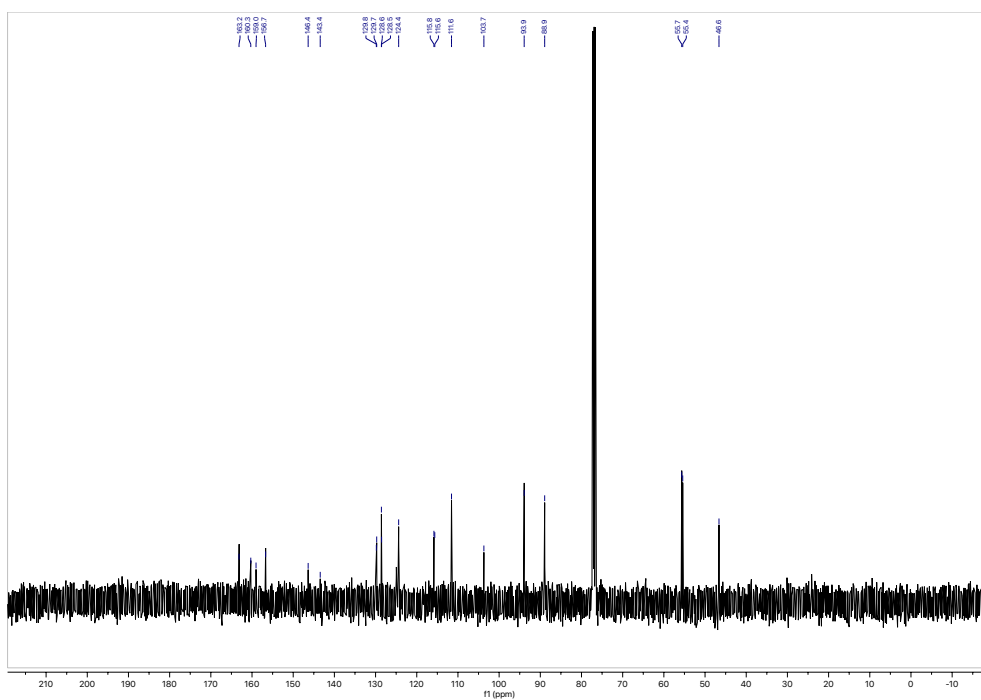
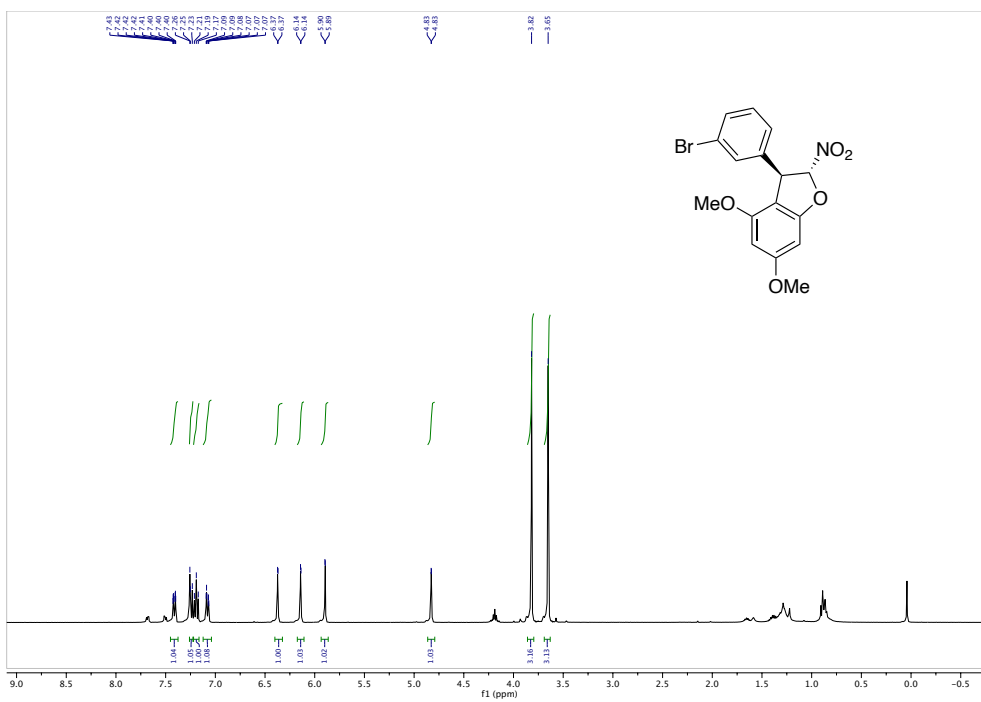


Figure A. 138. ¹³C NMR spectrum of 62bd



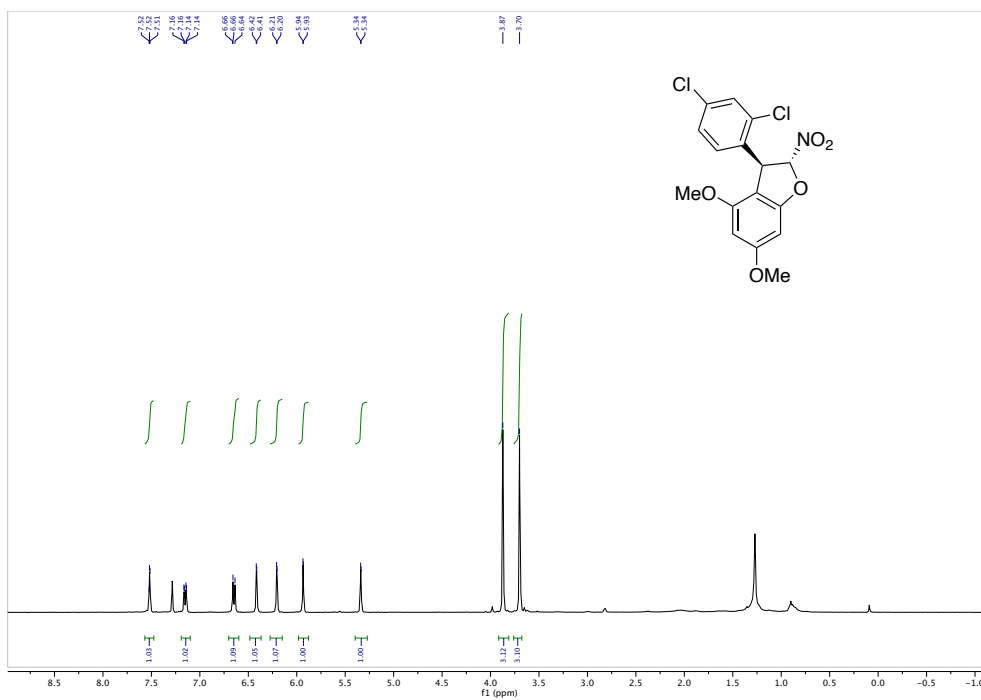


Figure A. 141. ¹H NMR spectrum of 62bh

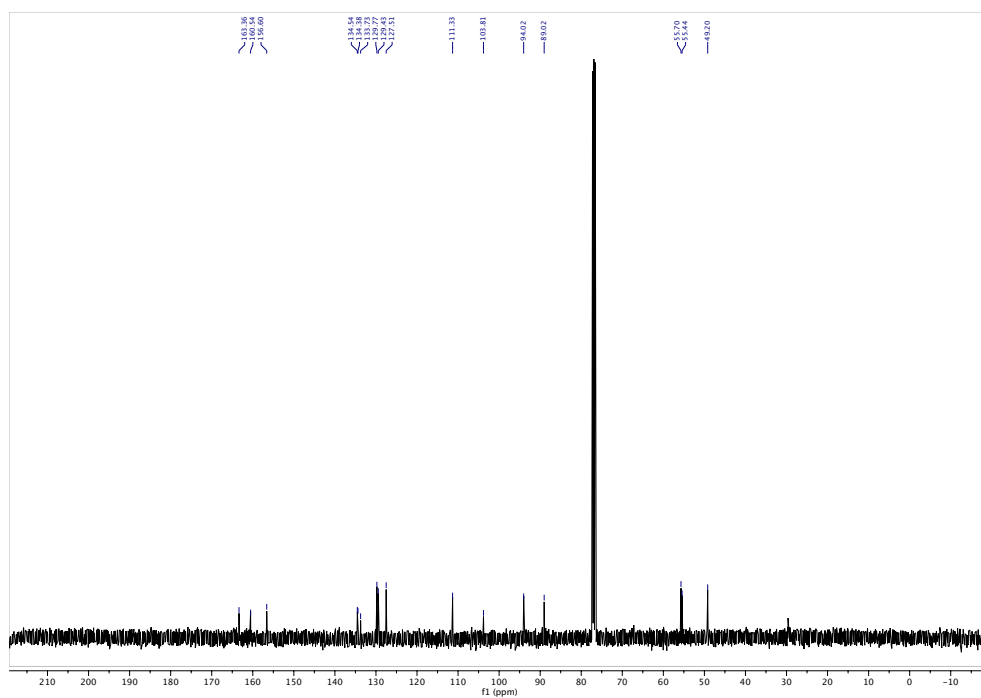
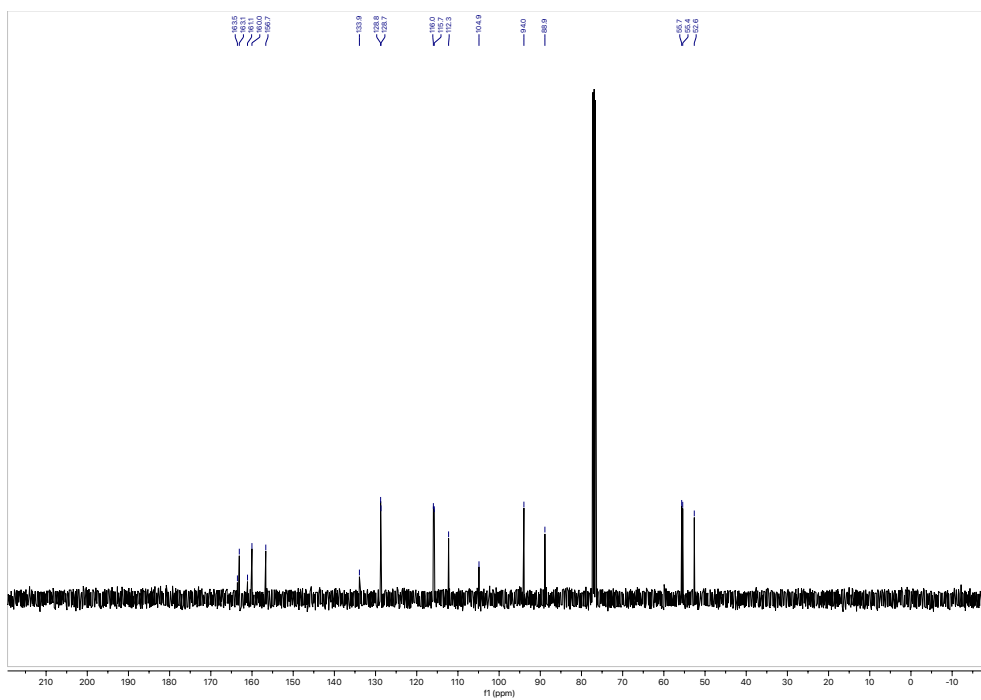
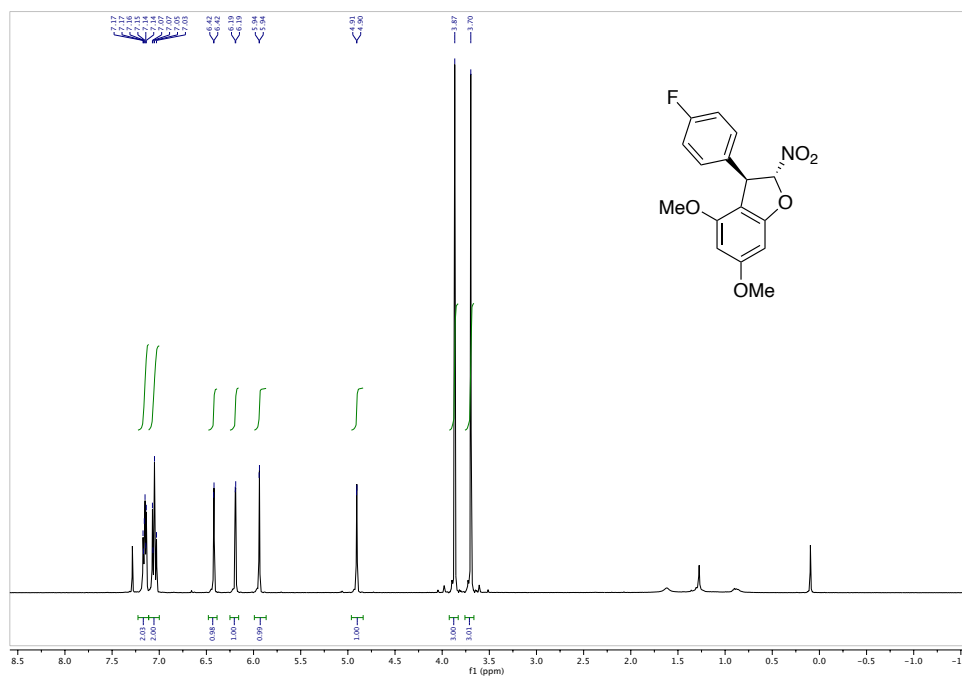


Figure A. 142. ¹³C NMR spectrum of 62bh



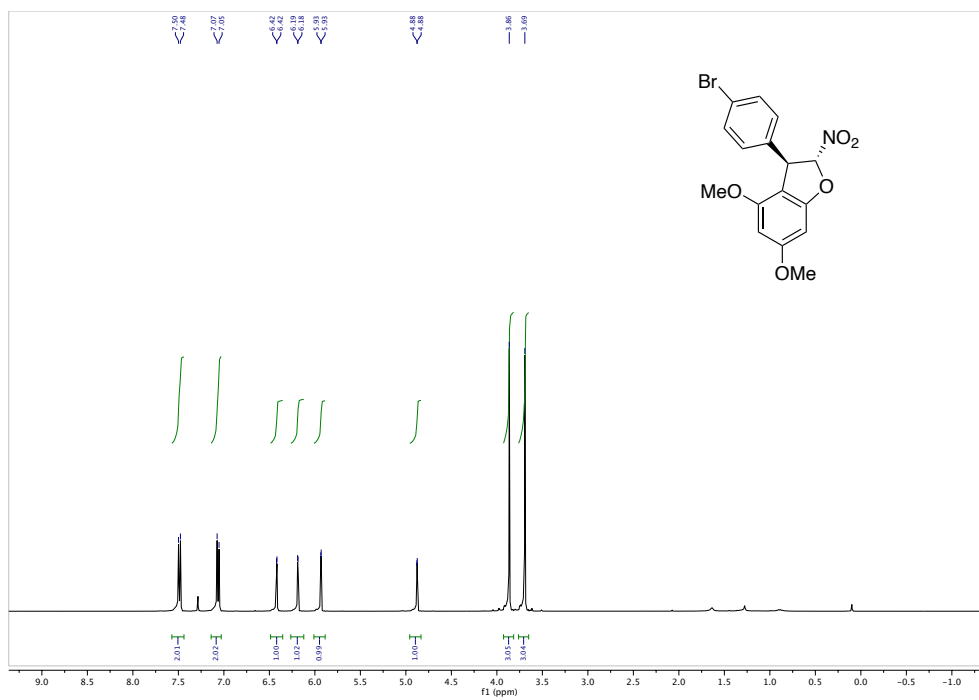


Figure A. 145. ^1H NMR spectrum of **62bk**

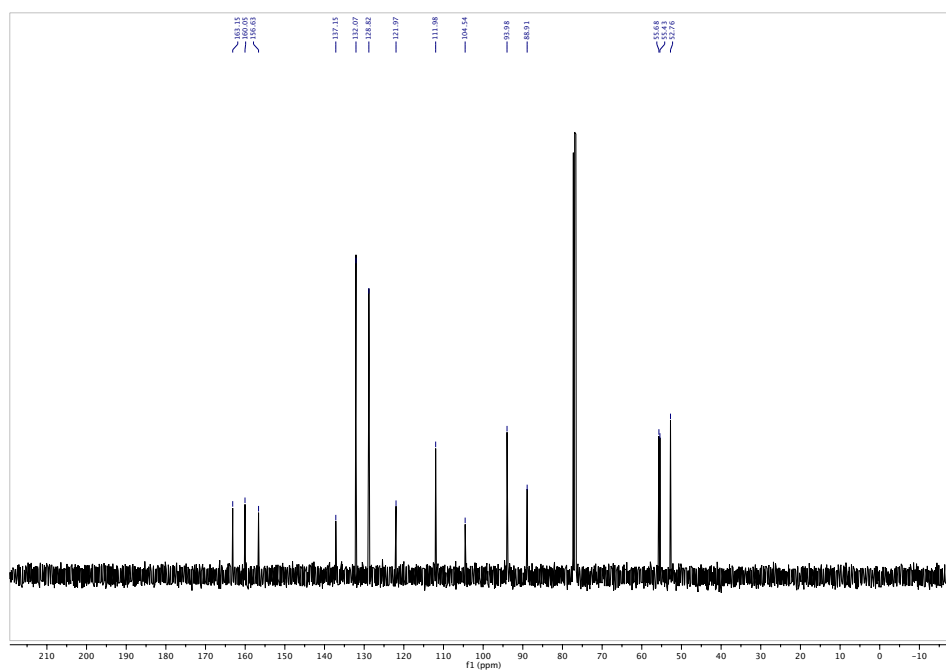


Figure A. 146. ^{13}C NMR spectrum of **62bk**

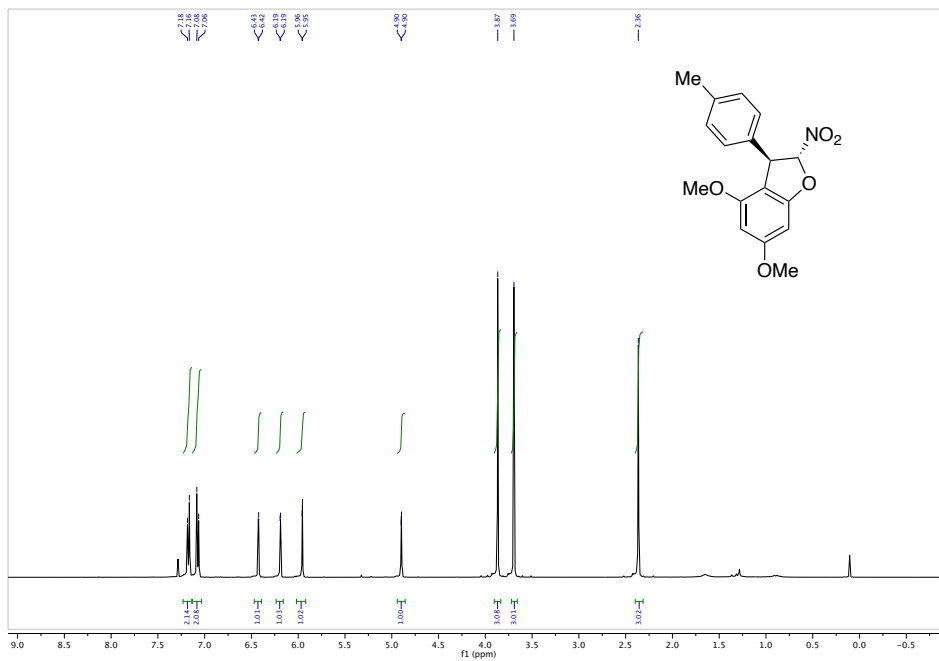


Figure A. 147. ¹H NMR spectrum of 62bl

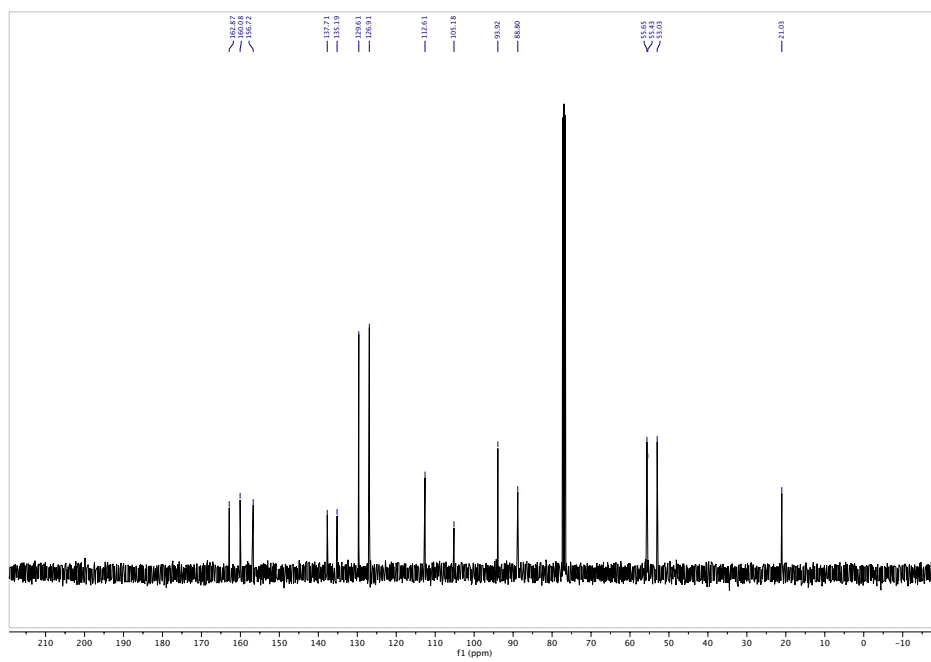
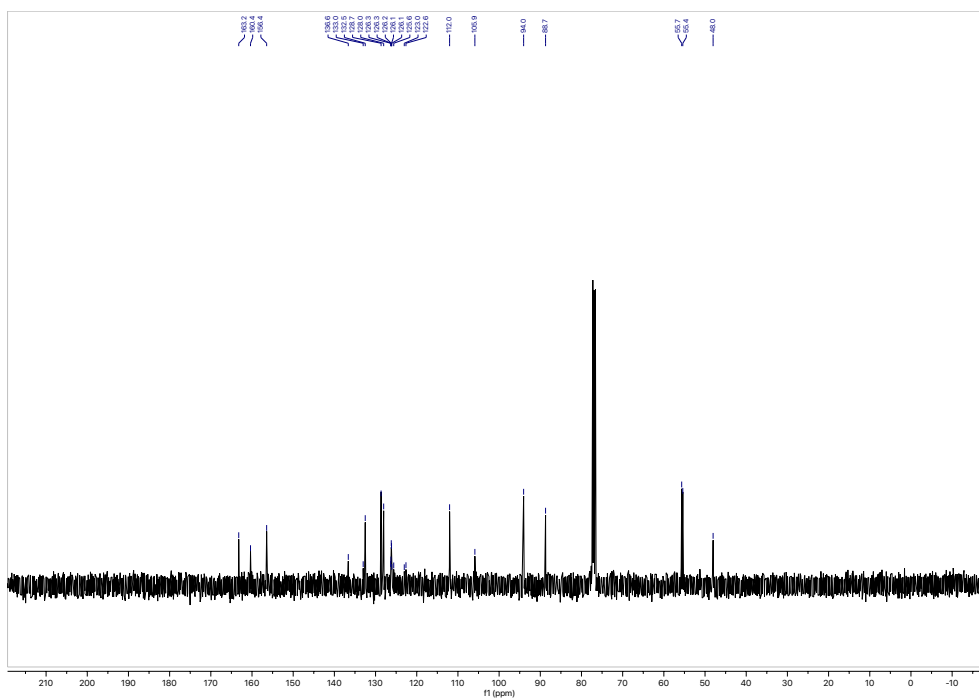
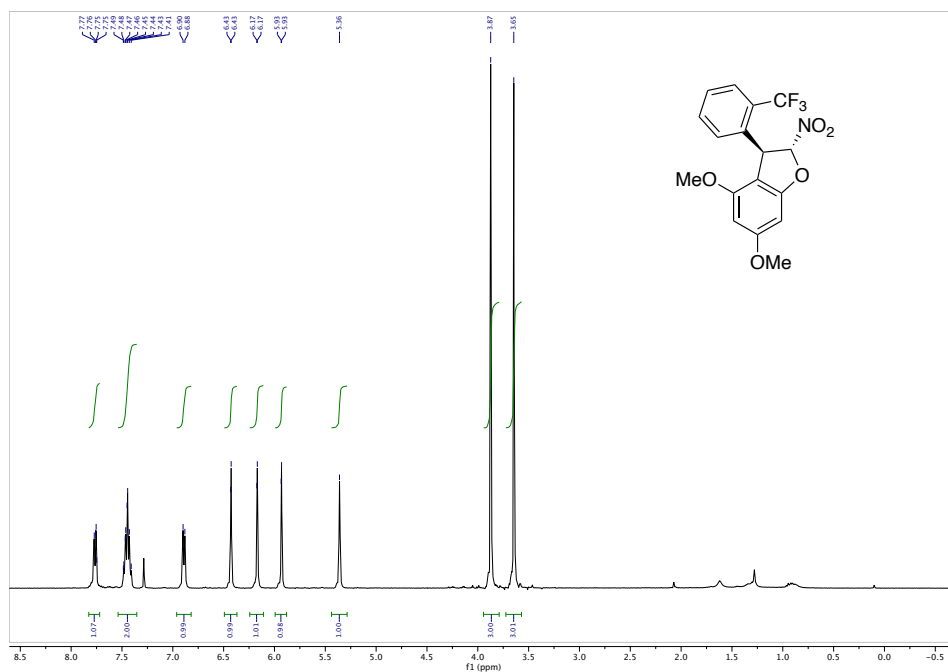


Figure A. 148. ¹³C NMR spectrum of 62bl



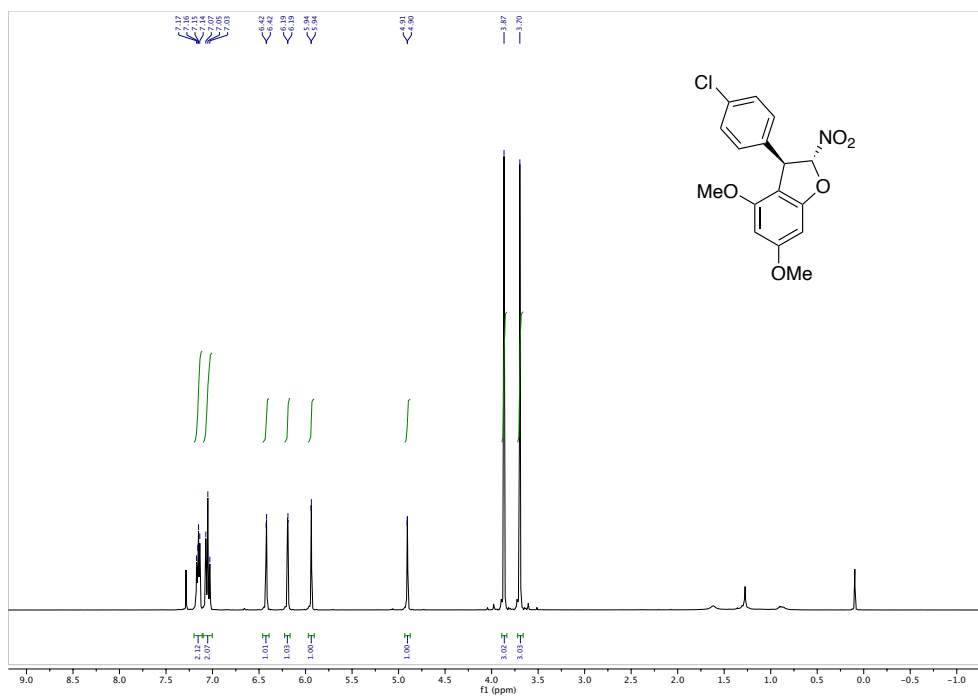


Figure A. 151. ¹H NMR spectrum of **62bo**

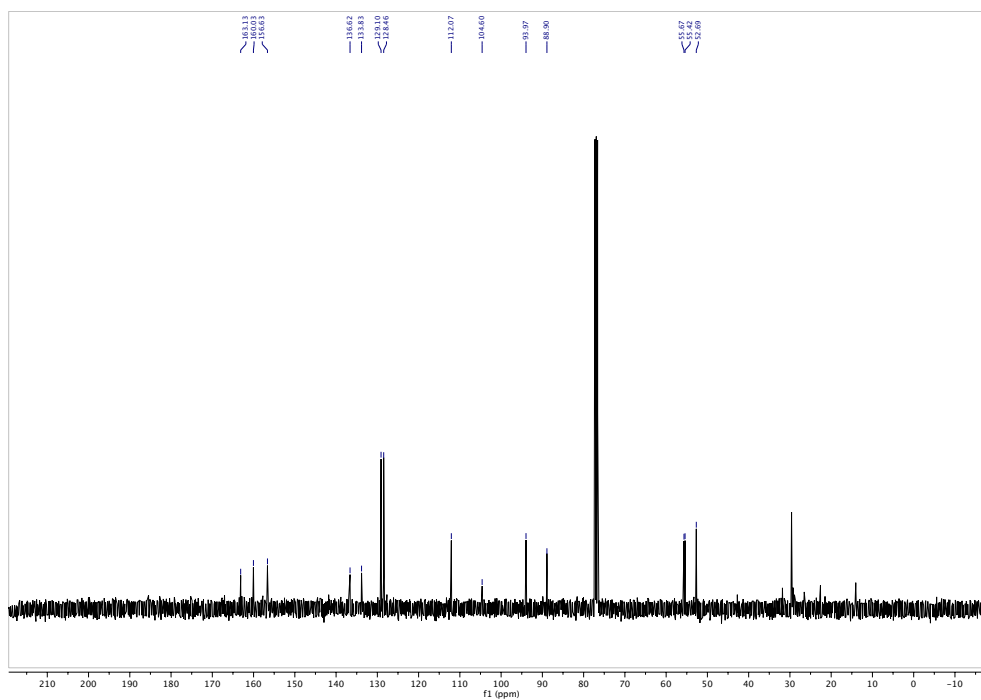


Figure A. 152. ¹³C NMR spectrum of **62bo**

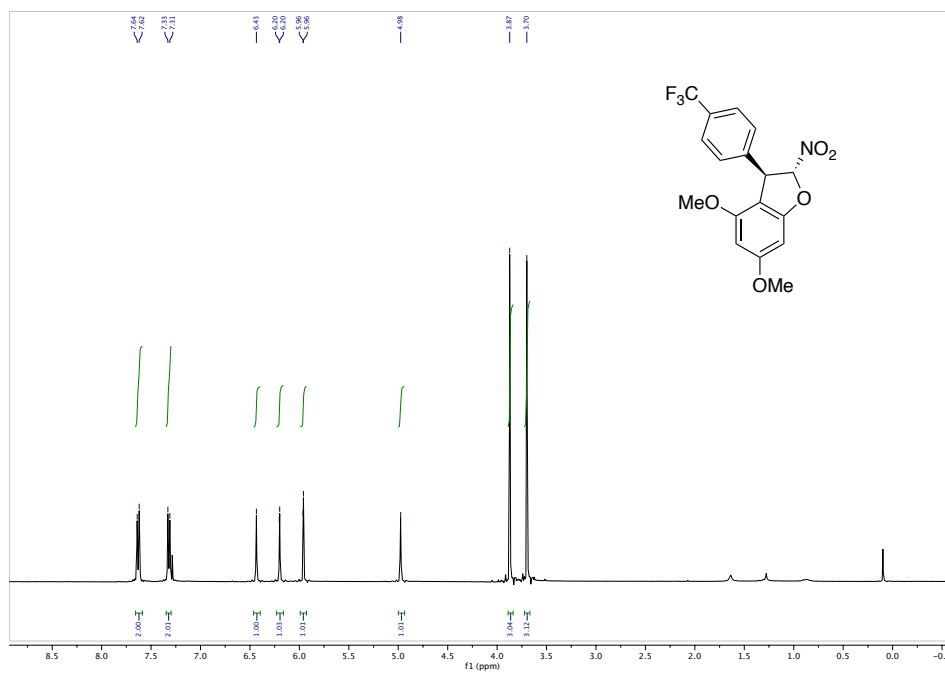


Figure A. 153. ¹H NMR spectrum of 62bp

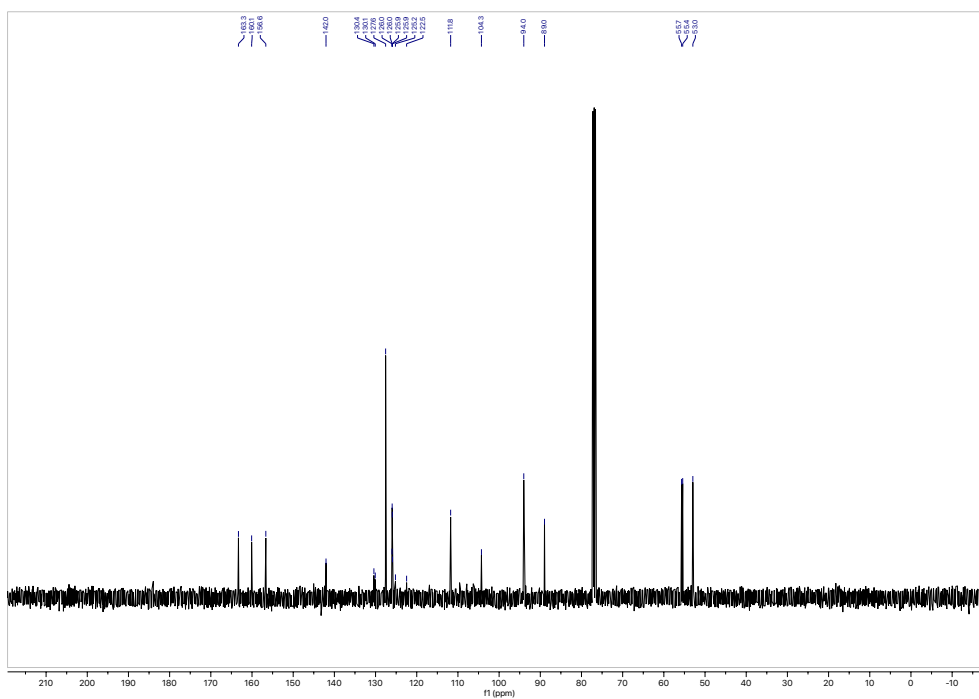


Figure A. 154. ¹³C NMR spectrum of 62bp

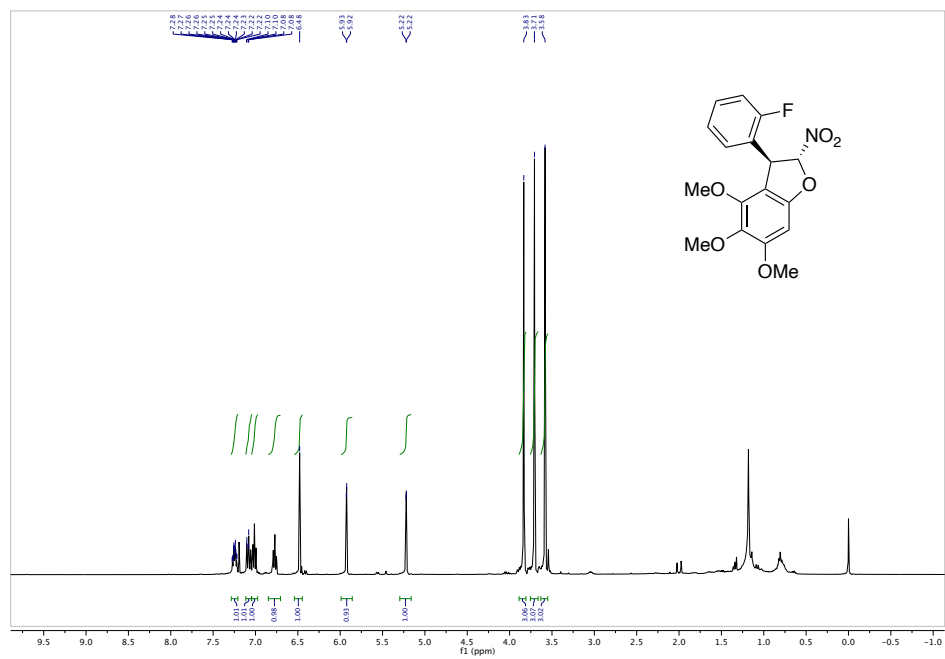


Figure A. 161. ¹H NMR spectrum of 62cd

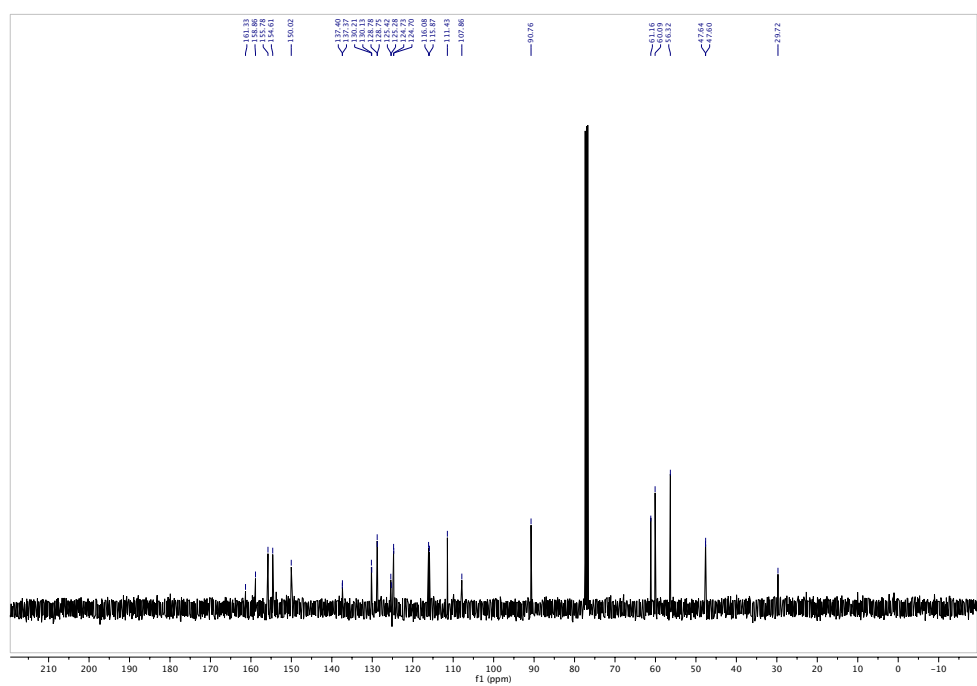
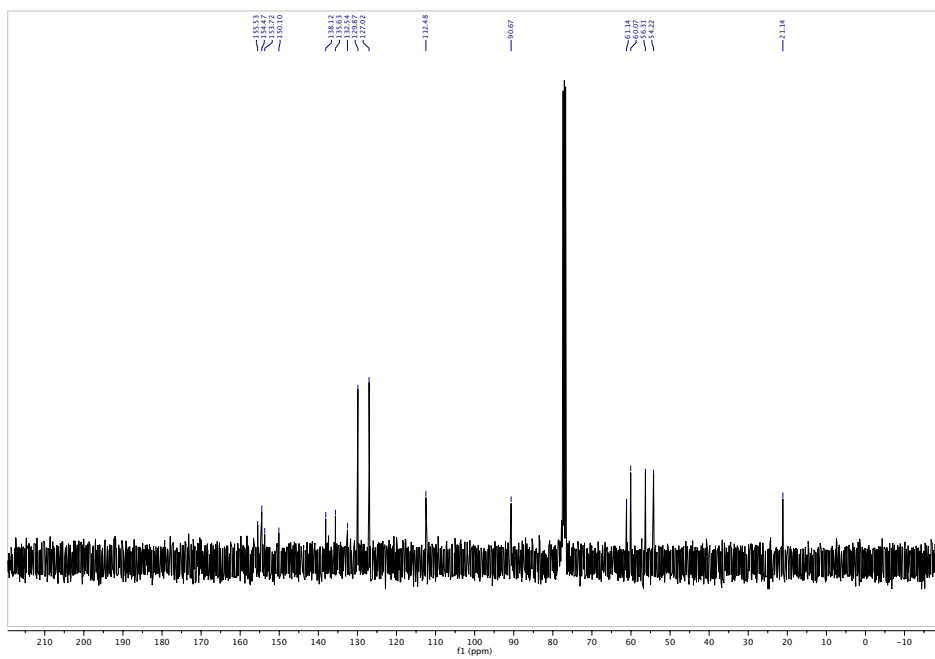
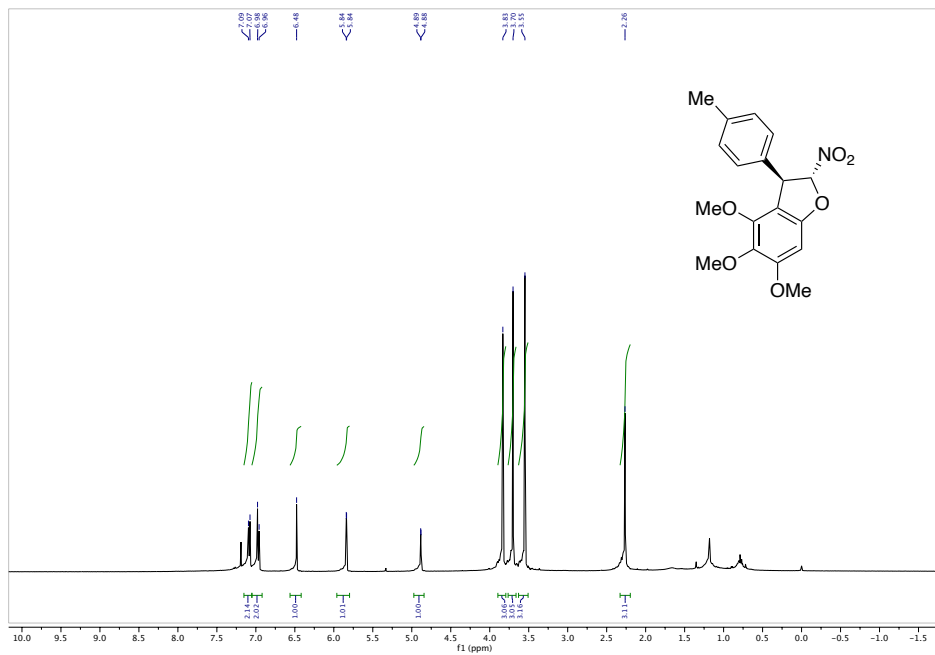


Figure A. 162. ¹³C NMR spectrum of 62cd



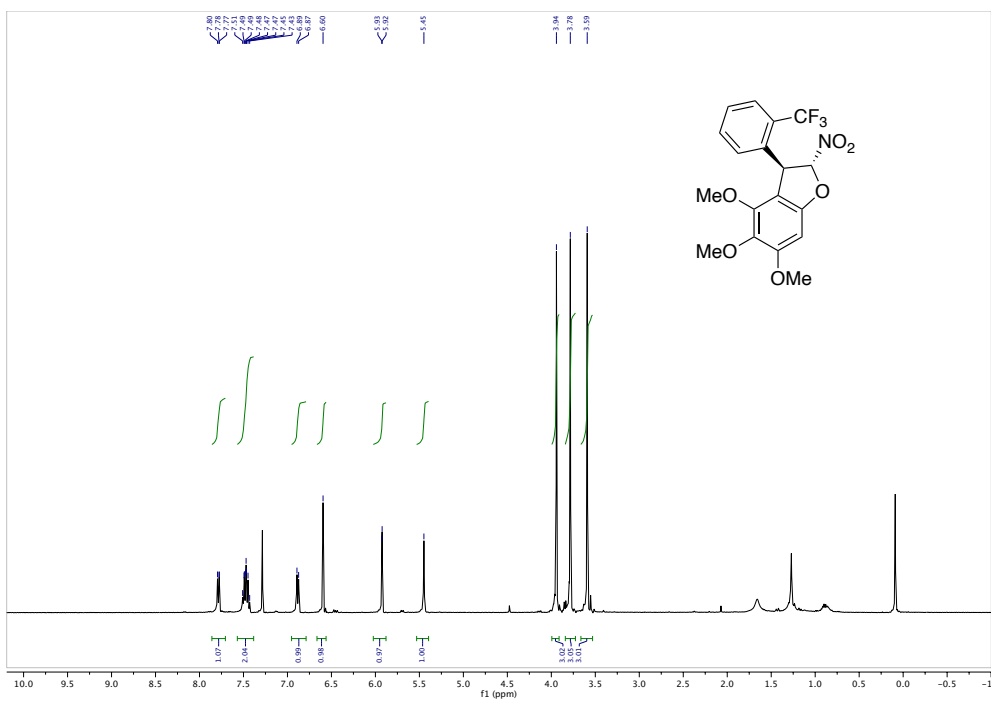


Figure A. 165. ¹H NMR spectrum of 62cn

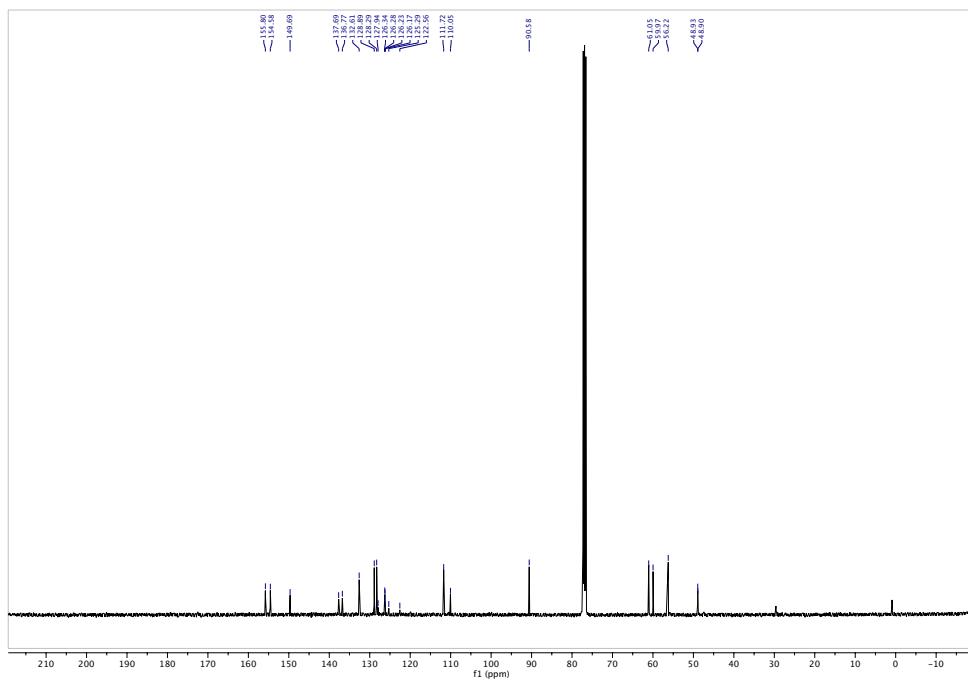


Figure A. 166. ¹³C NMR spectrum of 62cn

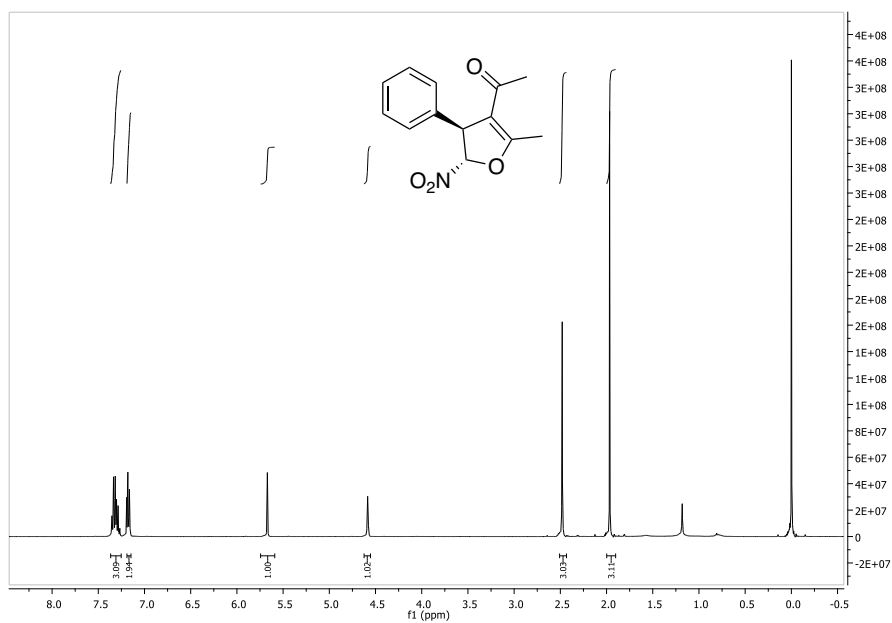


Figure A. 167. ^1H NMR spectrum of **64aa**

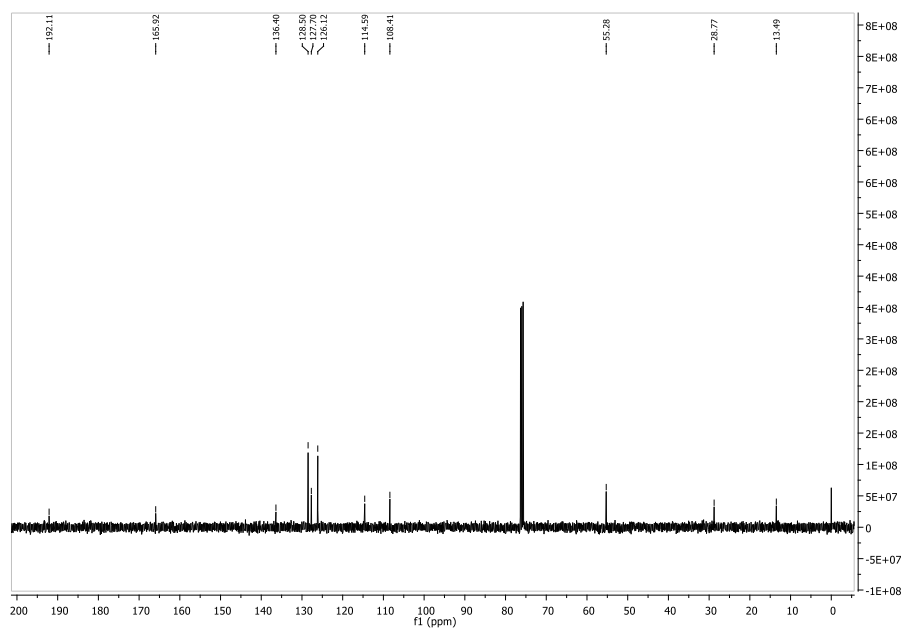


Figure A. 168. ^{13}C NMR spectrum of **64aa**

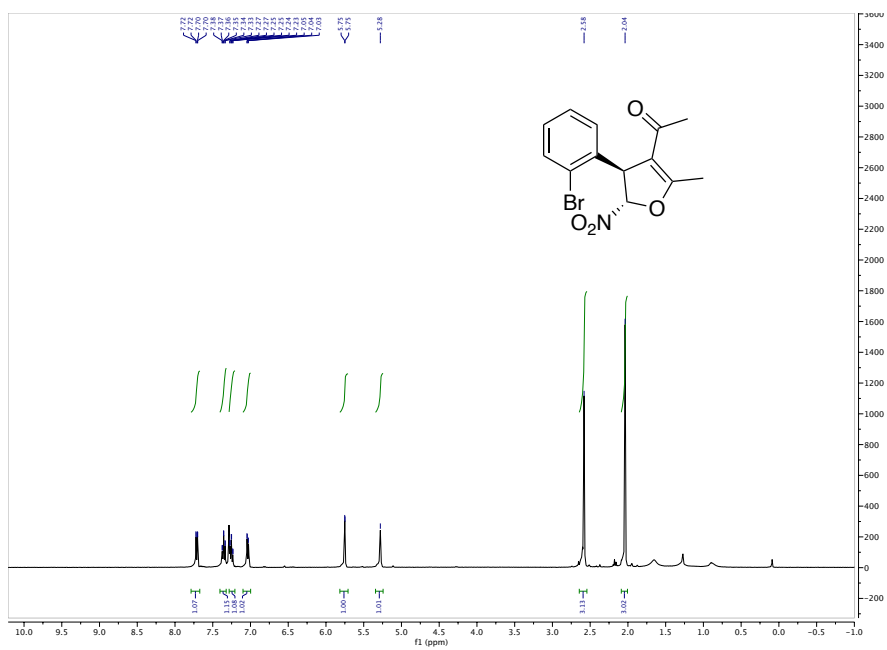


Figure A. 169. ¹H NMR spectrum of 64ab

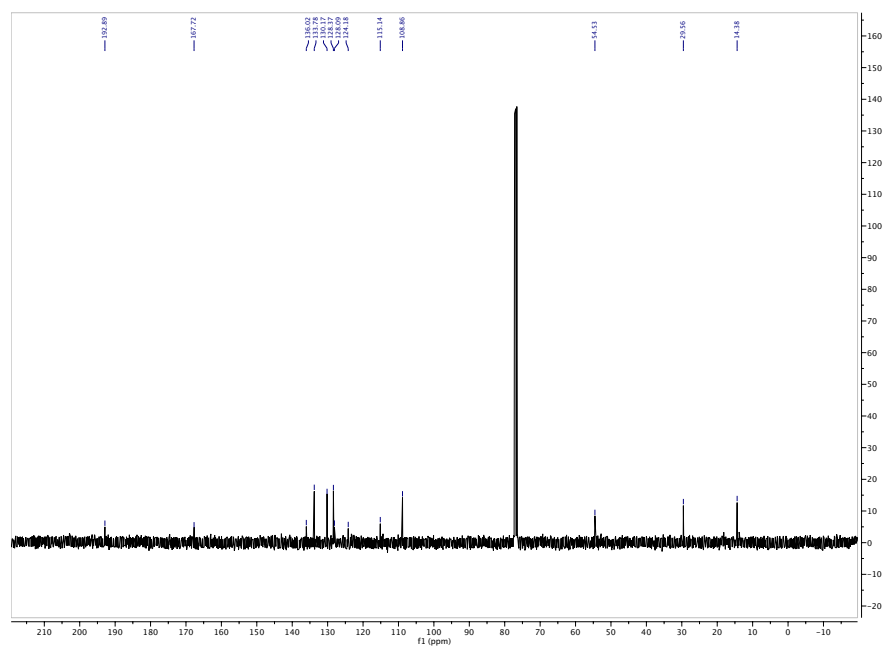


Figure A. 170. ¹³C NMR spectrum of 64ab

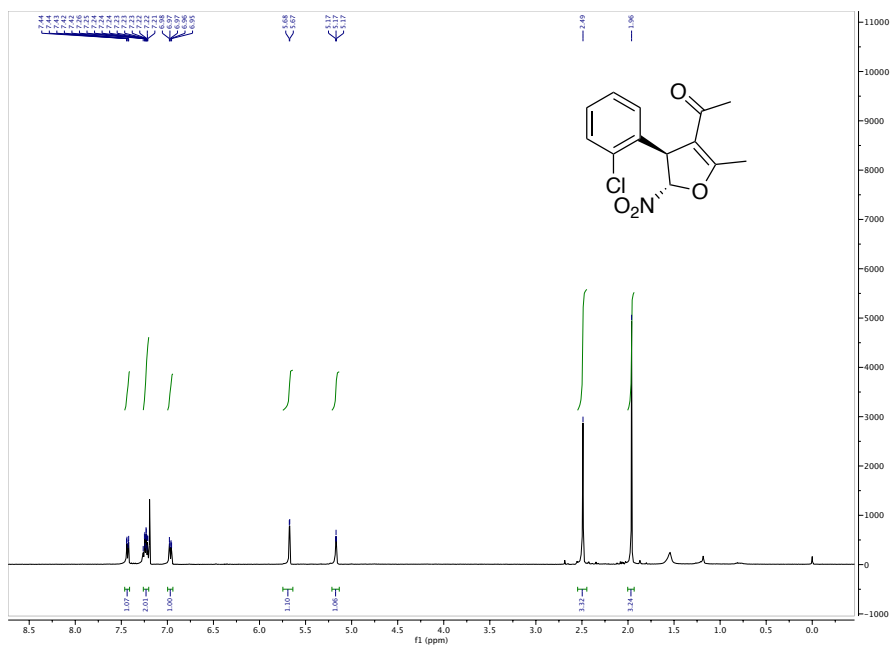


Figure A. 171. ^1H NMR spectrum of **64ac**

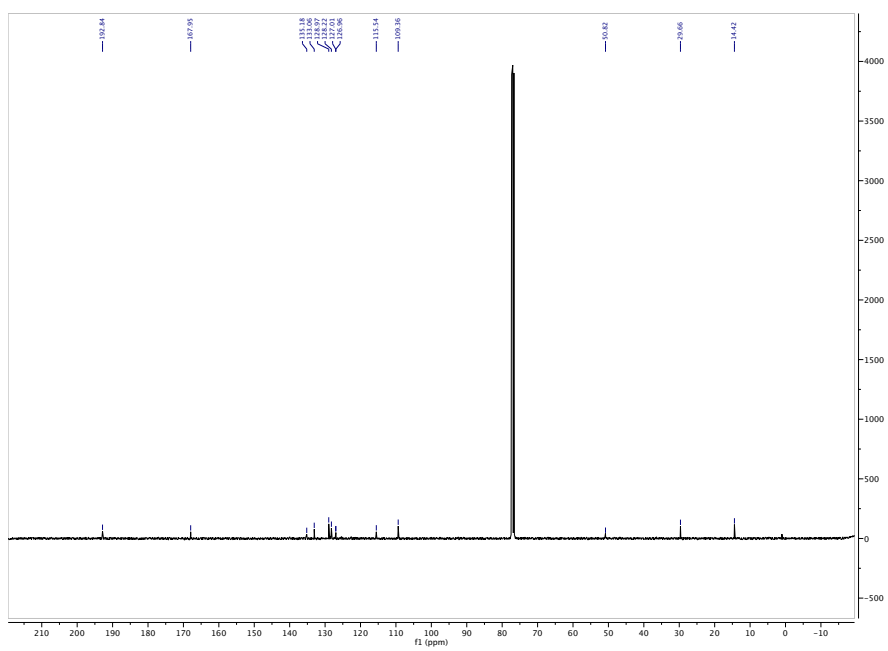


Figure A. 172. ^{13}C NMR spectrum of **64ac**

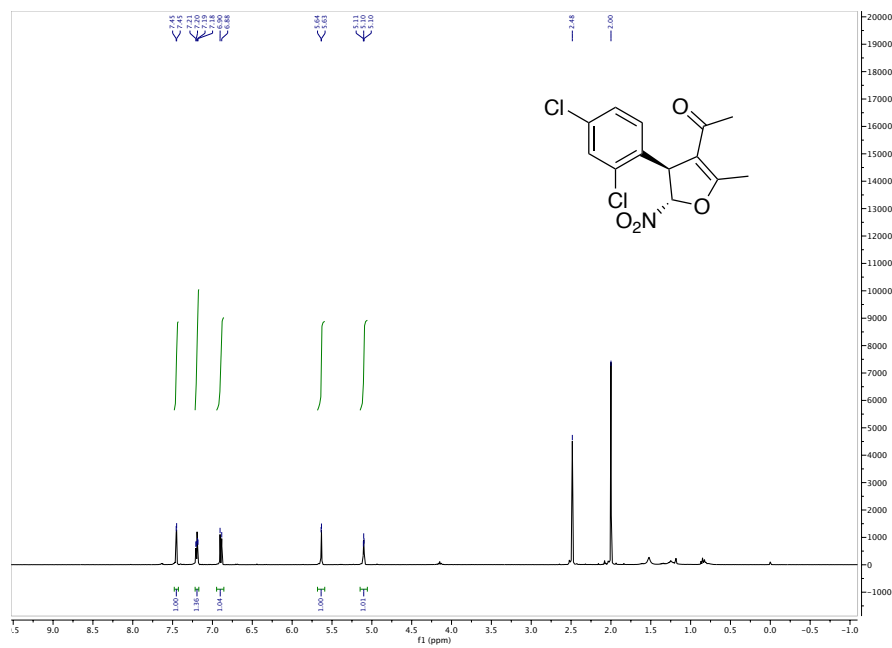


Figure A. 173. ^1H NMR spectrum of **64ah**

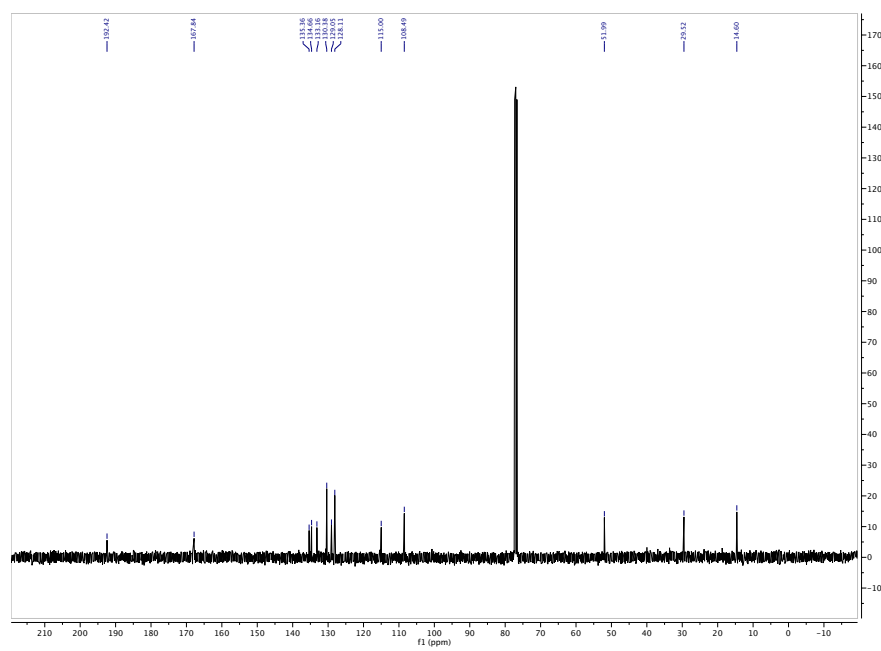


Figure A. 174. ^{13}C NMR spectrum of **64ah**

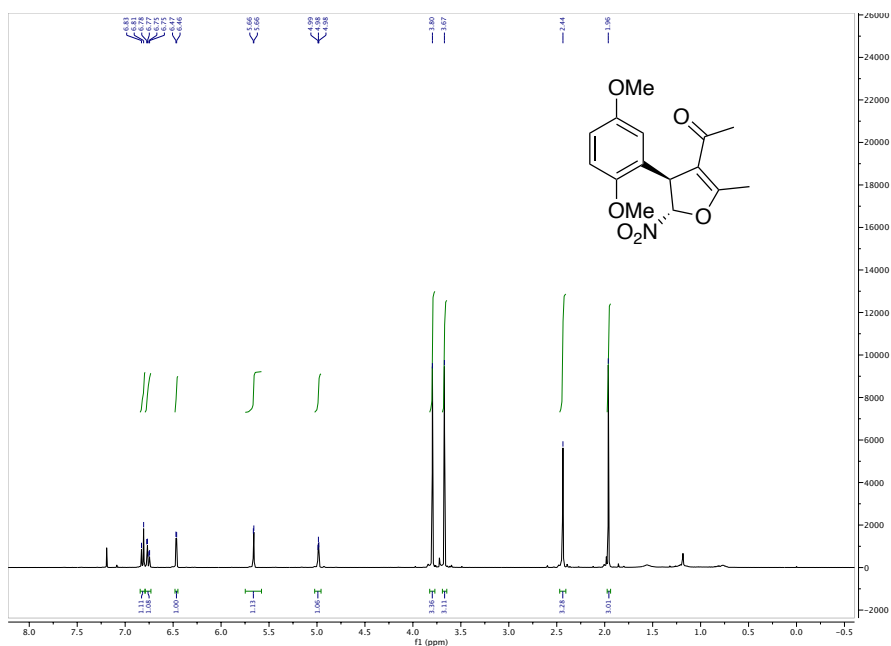


Figure A. 175. ^1H NMR spectrum of 64ai

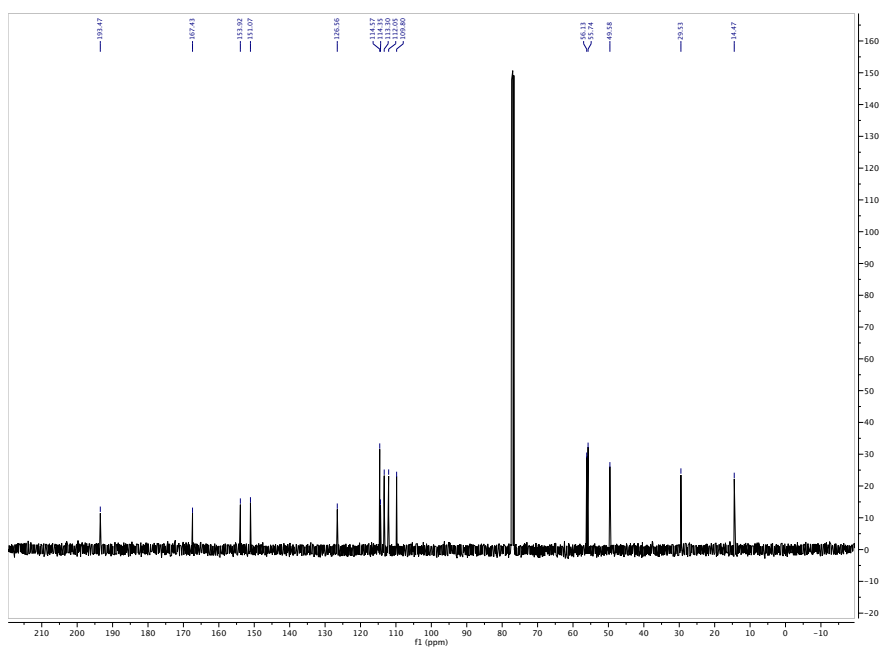
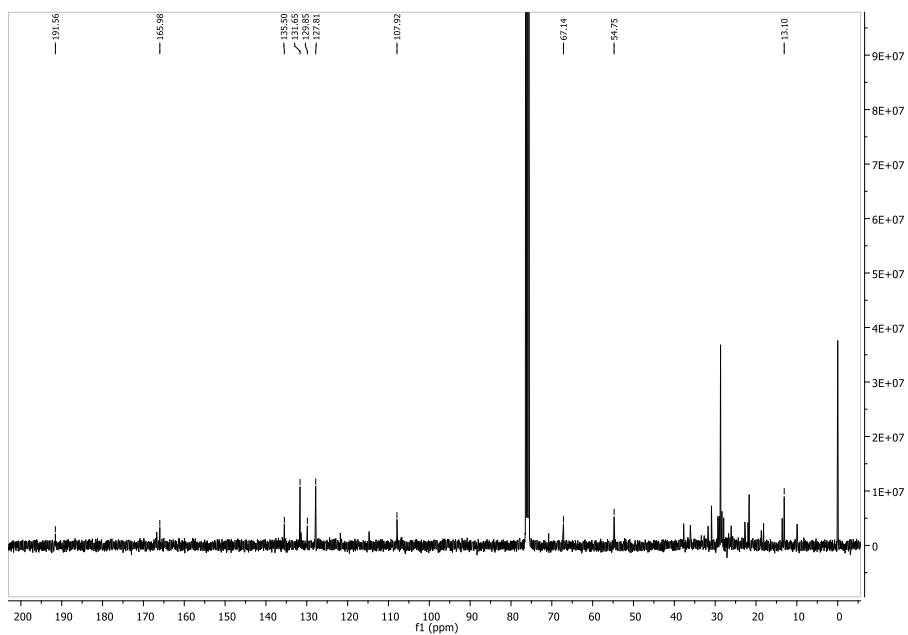
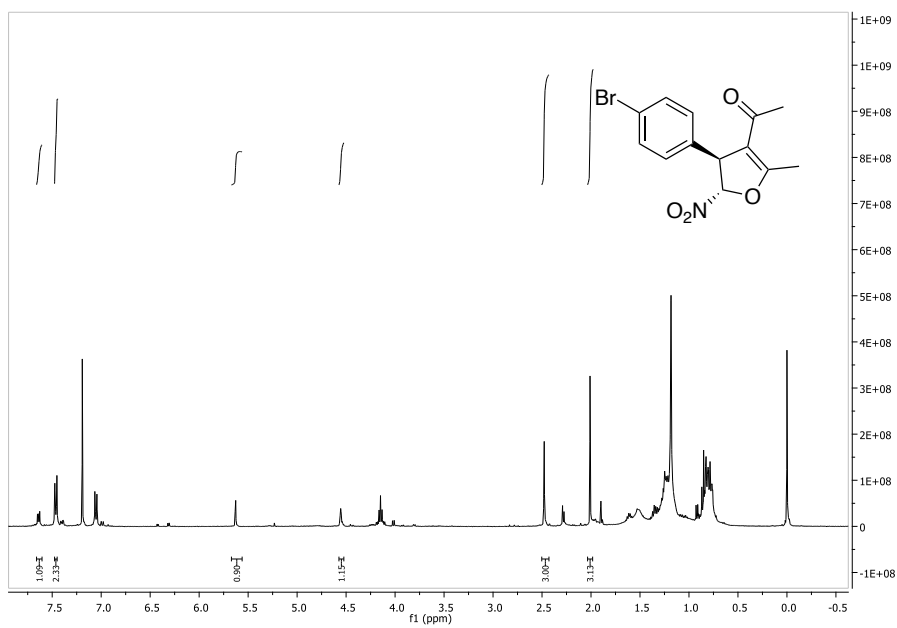


Figure A. 176. ^{13}C NMR spectrum of 64ai



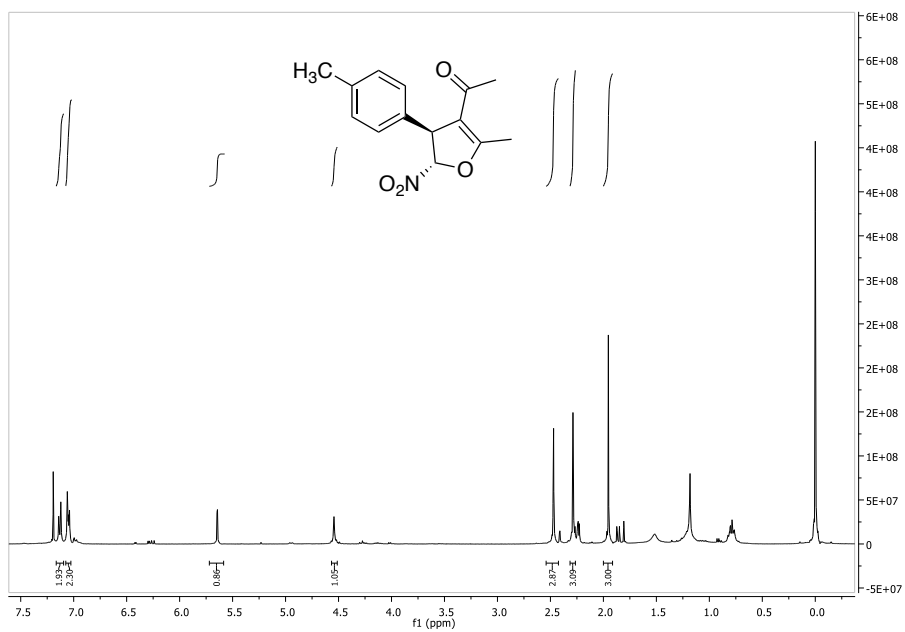


Figure A. 179. ¹H NMR spectrum of 64al

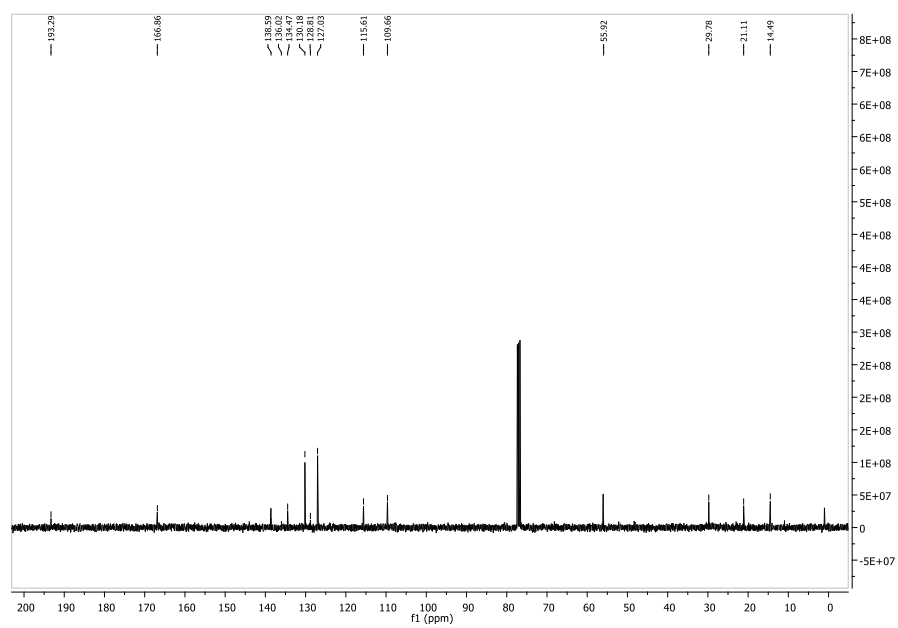
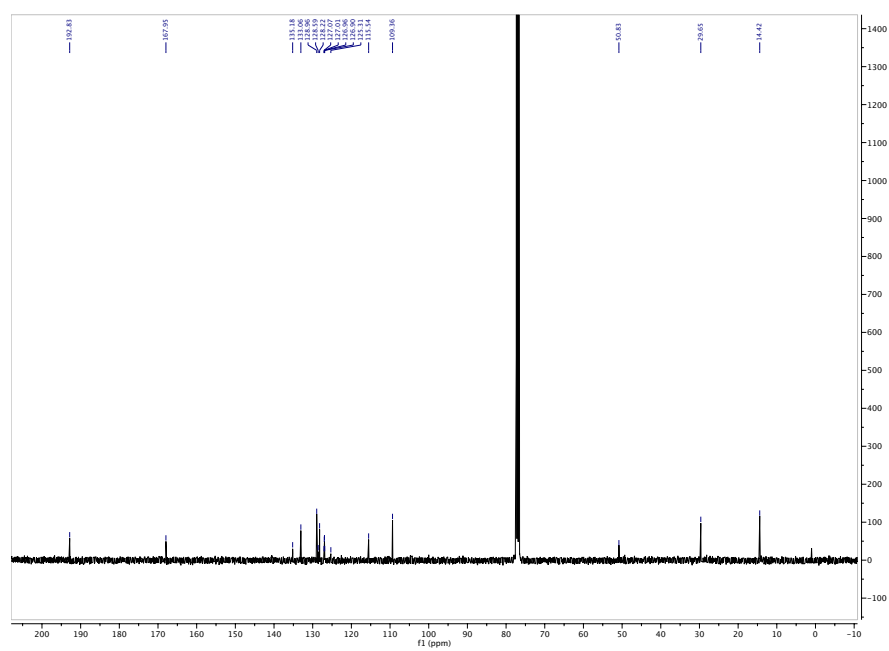
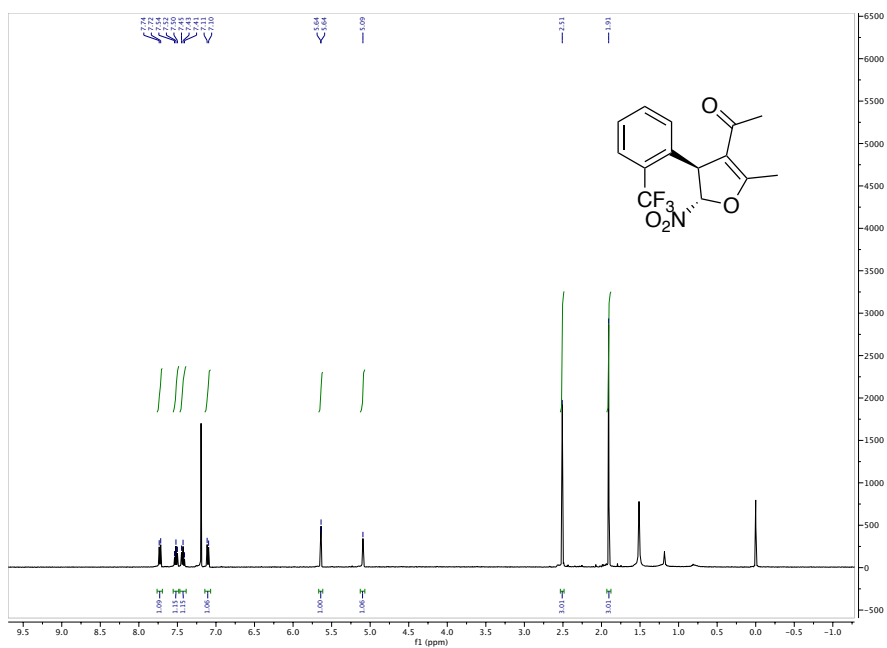


Figure A. 180. ¹³C NMR spectrum of 64al



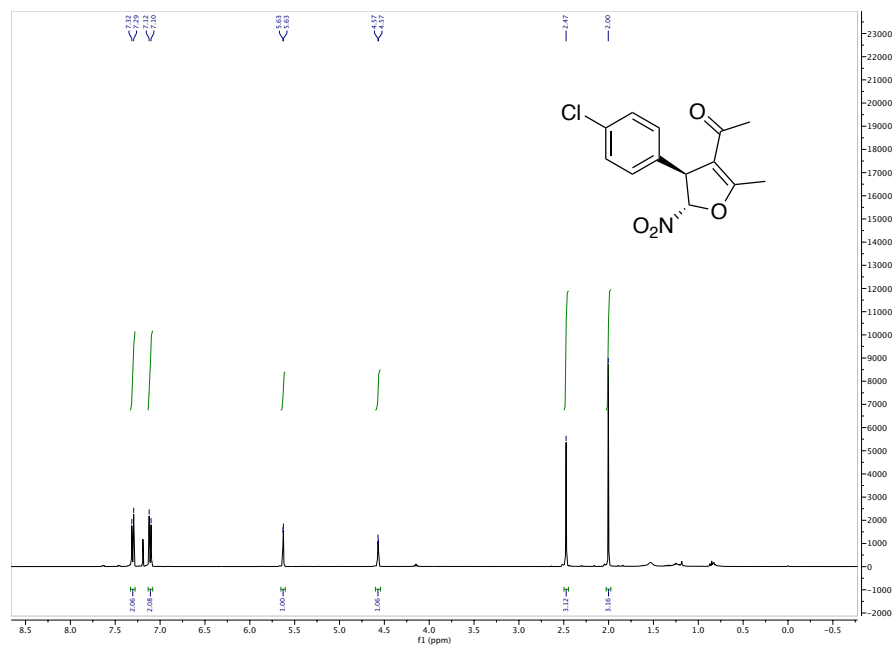


Figure A. 183. ^1H NMR spectrum of **64ao**

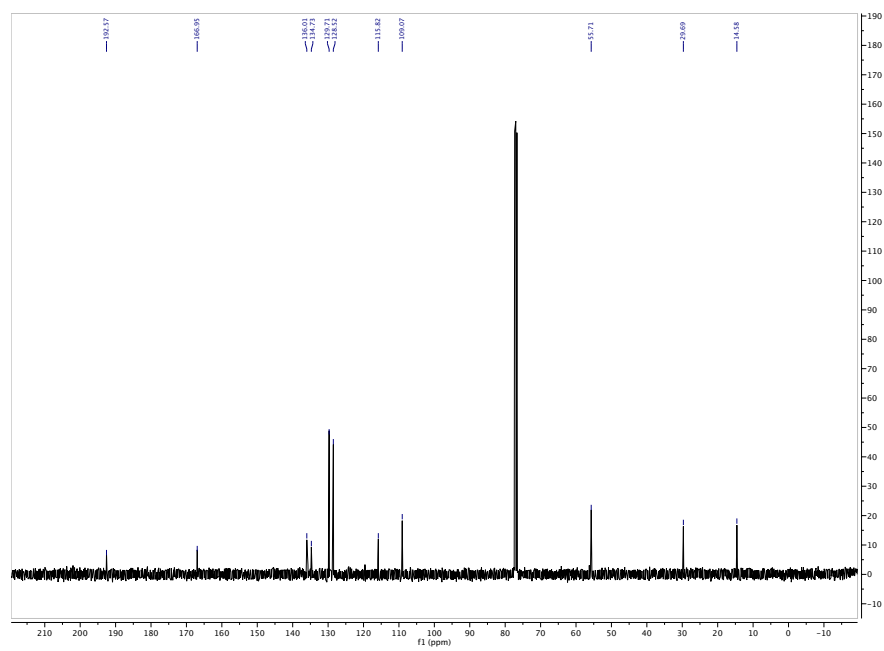


Figure A. 184. ^{13}C NMR spectrum of **64ao**

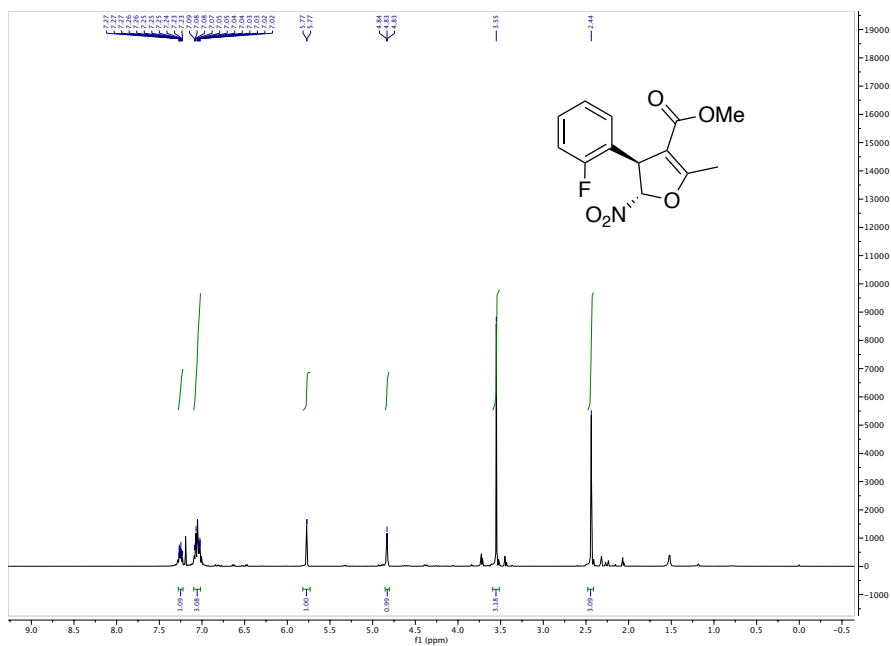


Figure A. 185. ^1H NMR spectrum of 64bd

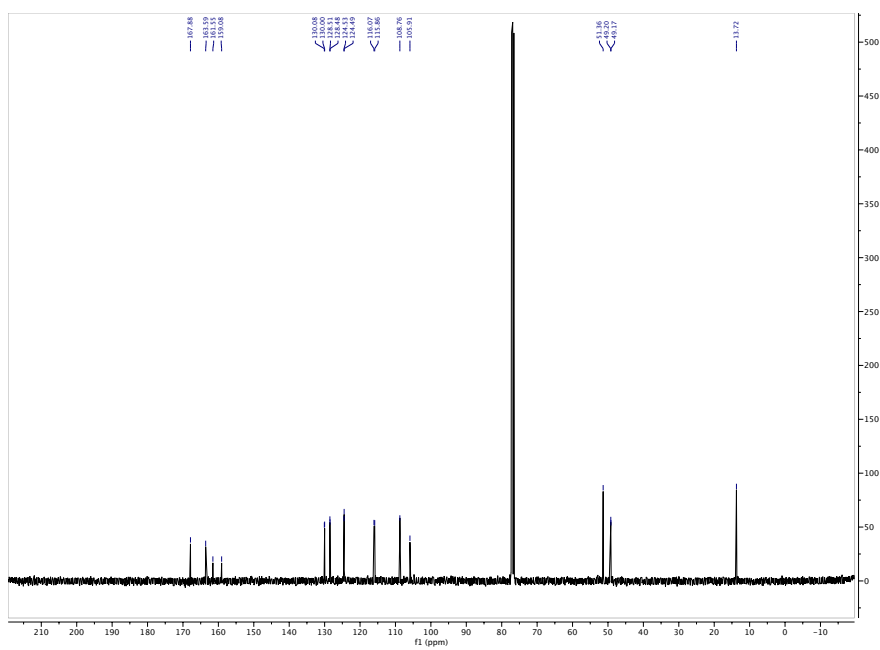


Figure A. 186. ^{13}C NMR spectrum of 64bd

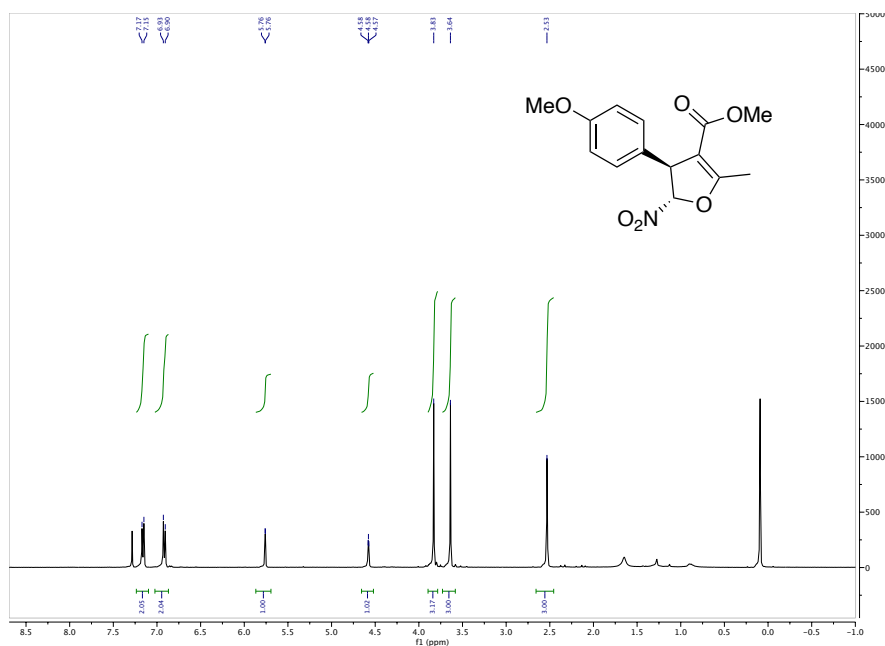


Figure A. 187. ^1H NMR spectrum of 64bg

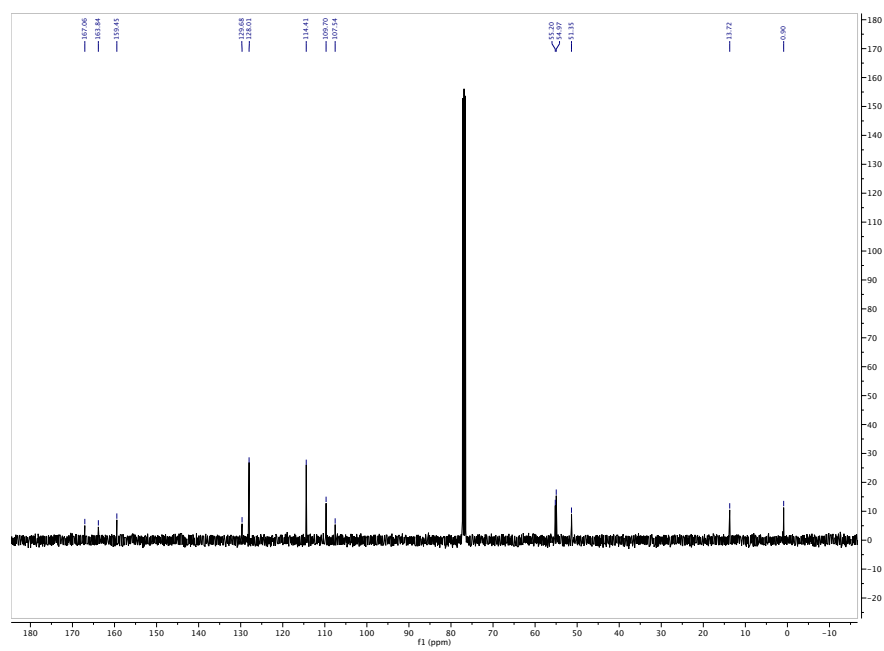
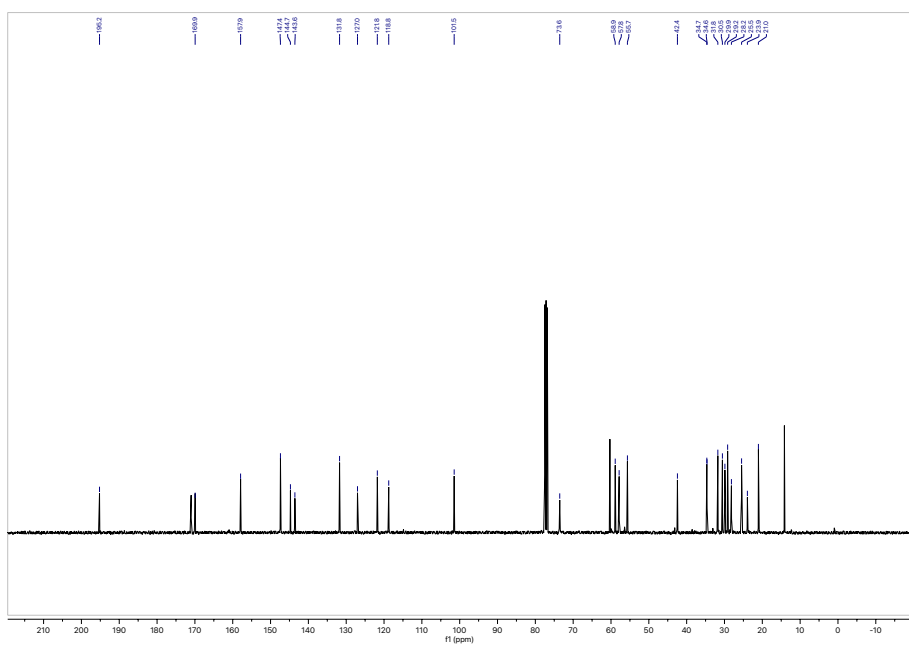
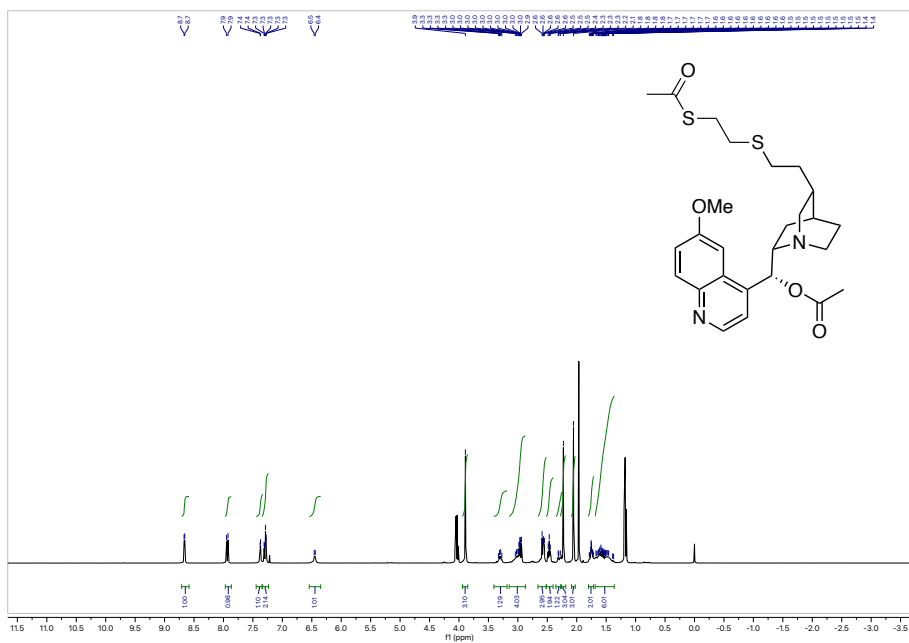
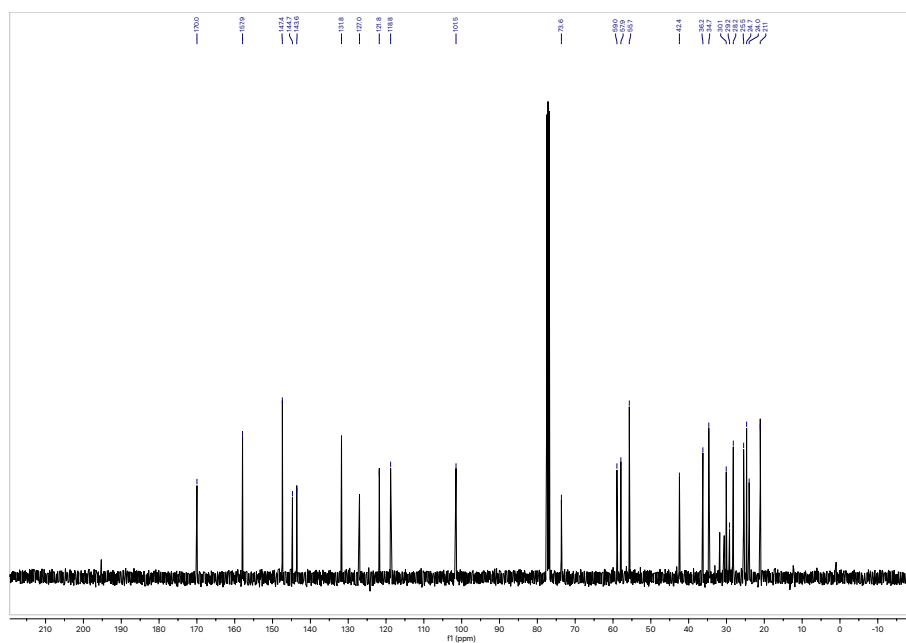
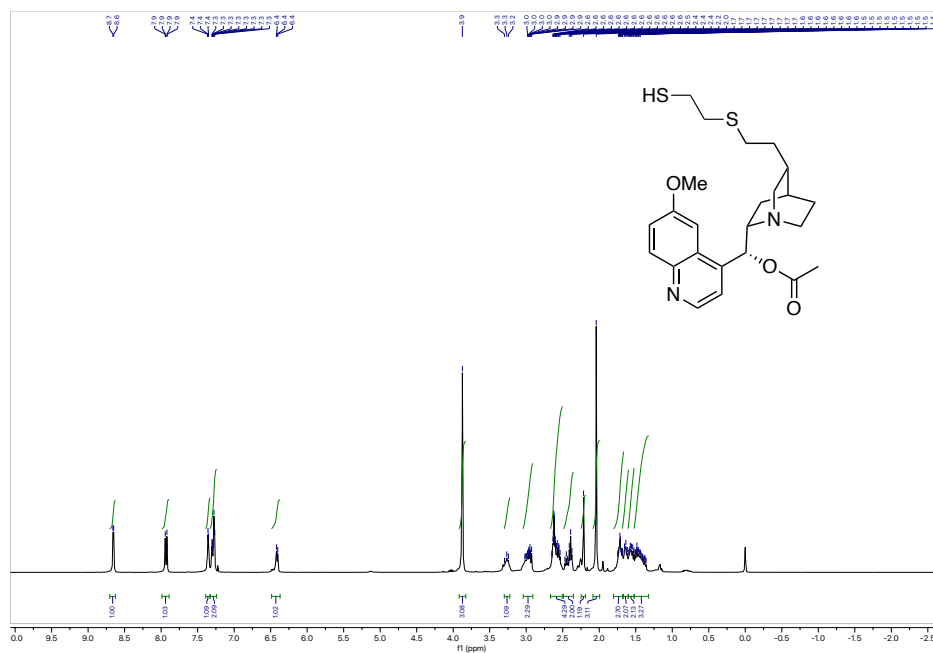


Figure A. 188. ^{13}C NMR spectrum of 64bg





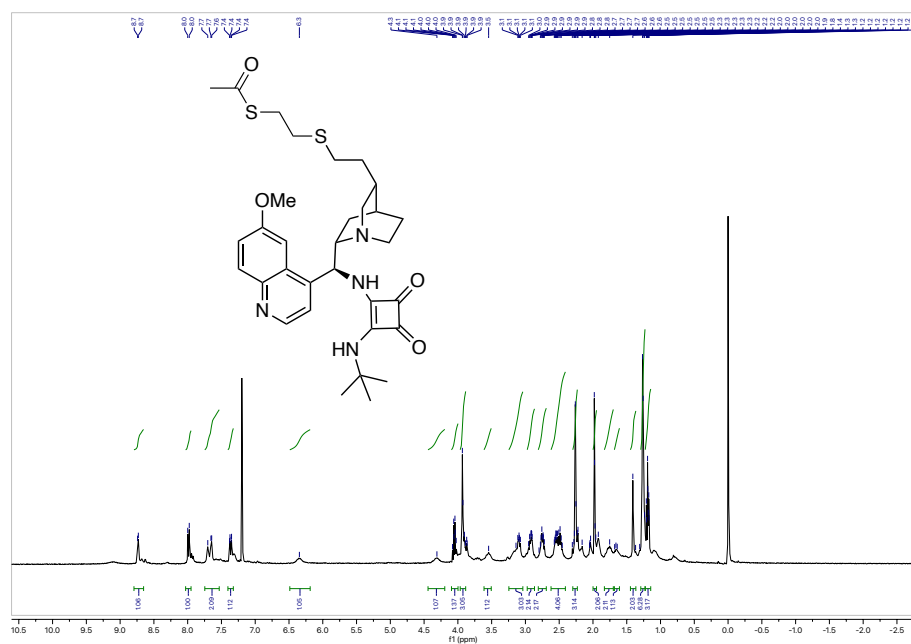


Figure A. 195. ¹H NMR spectrum of crude **69**

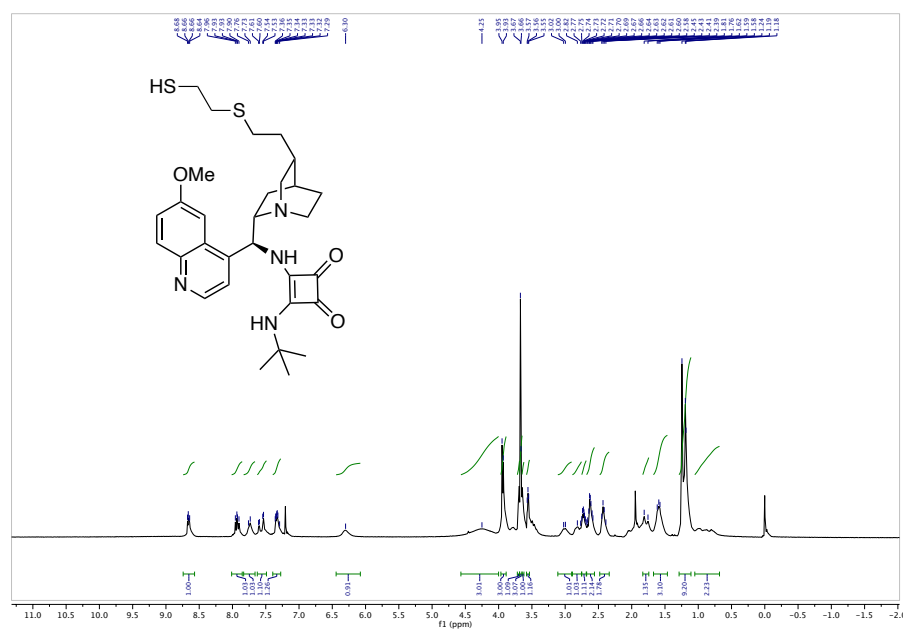


Figure A. 196. ¹H NMR spectrum of **70**

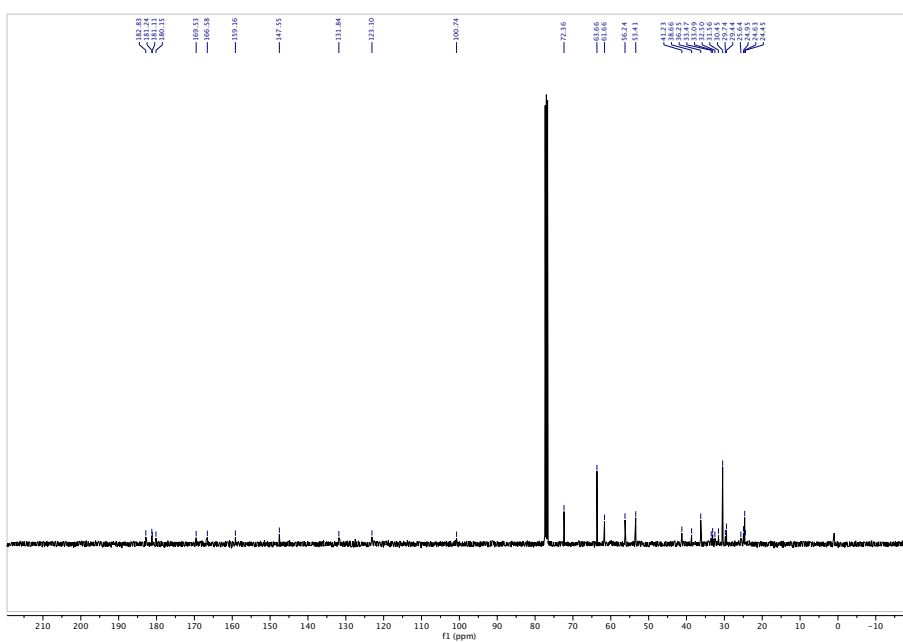


Figure A. 197. ^{13}C NMR spectrum of 70

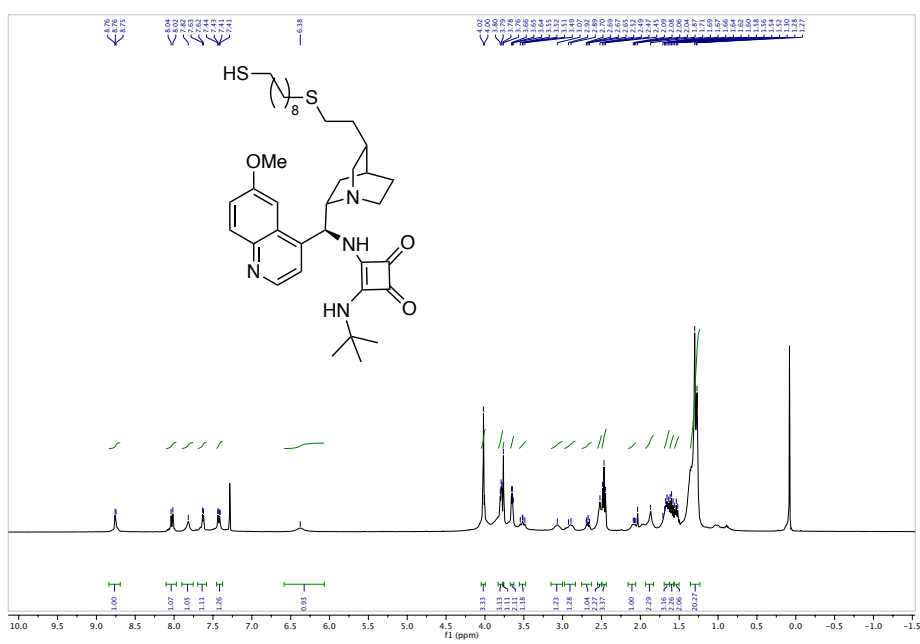


Figure A. 198. ^1H NMR spectrum of 71

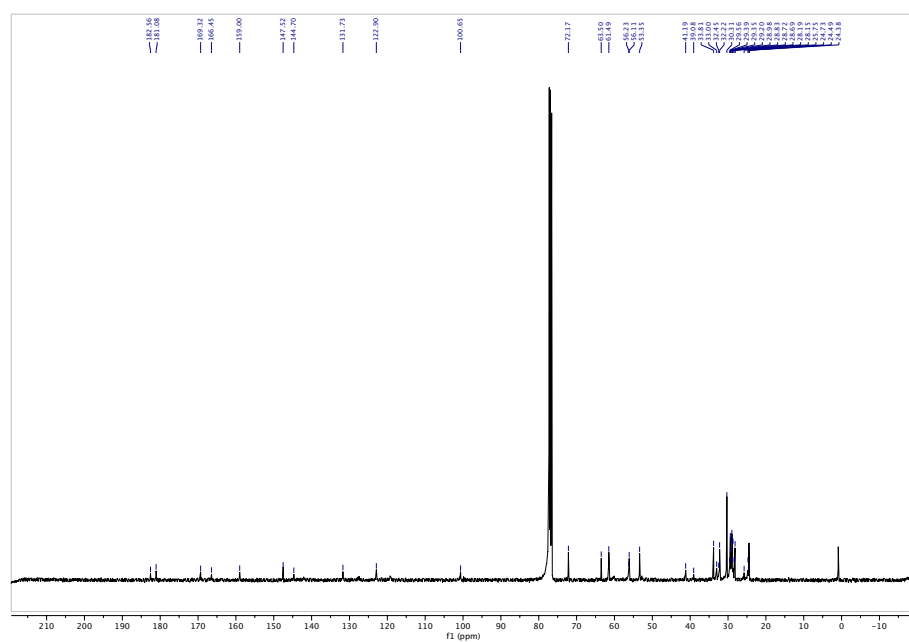


Figure A. 199. ^{13}C NMR spectrum of 71

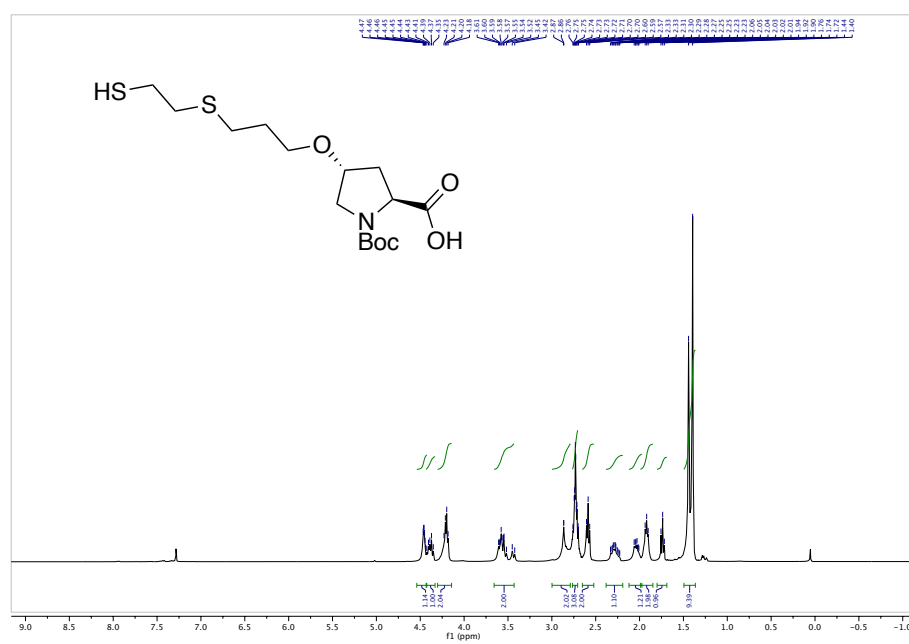


Figure A. 200. ^1H NMR spectrum of 77

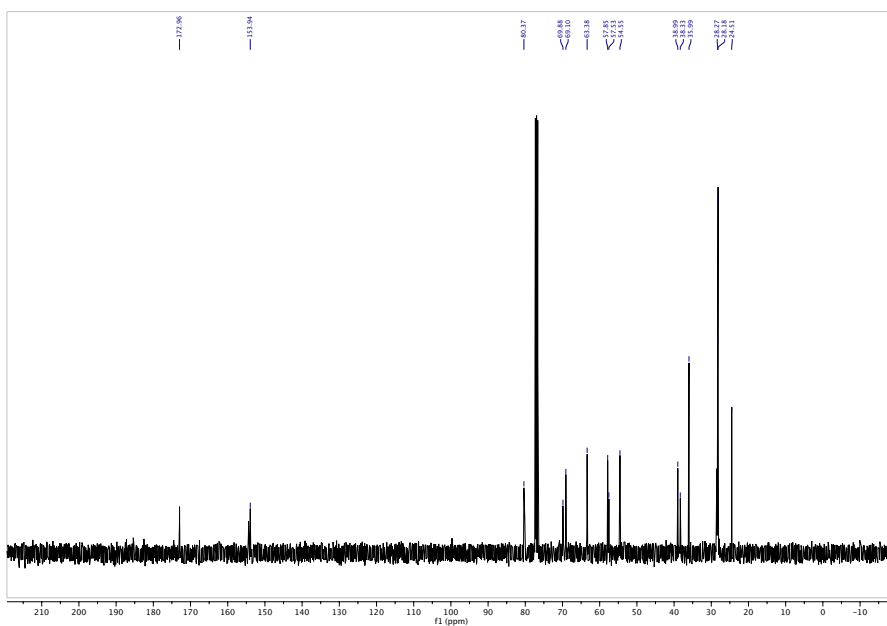


Figure A. 201. ^{13}C NMR spectrum of 77

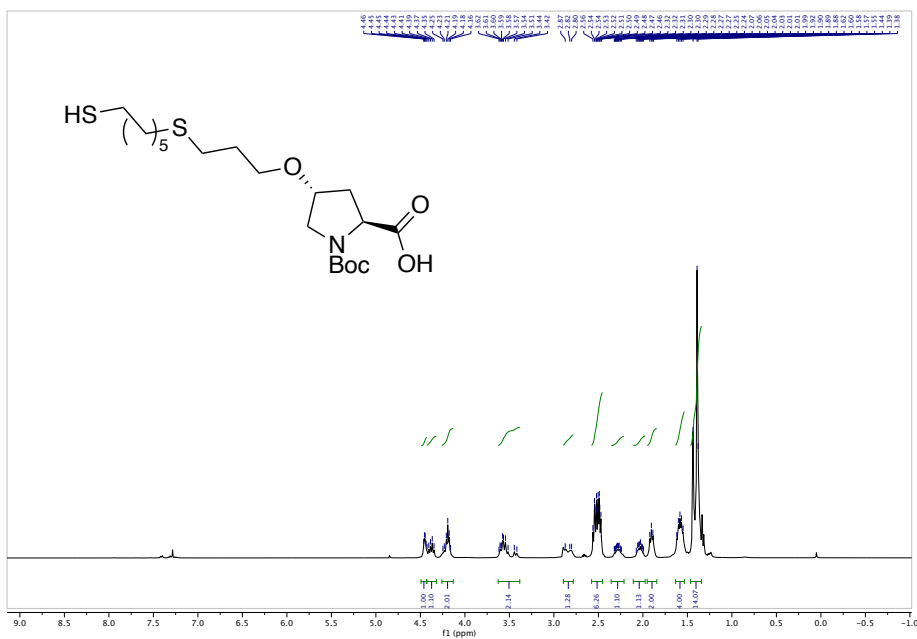


Figure A. 202. ^1H NMR spectrum of 78

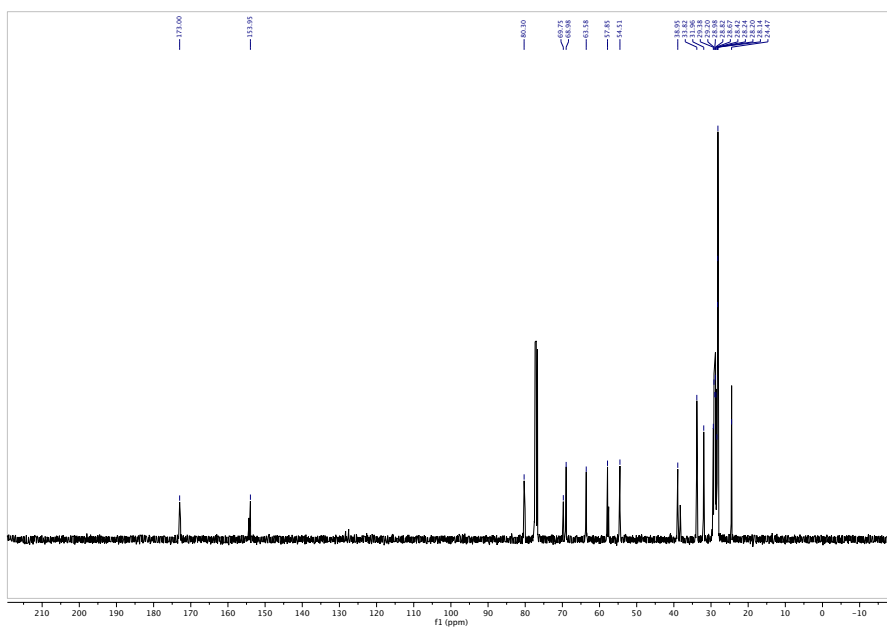


Figure A. 205. ^{13}C NMR spectrum of **79**

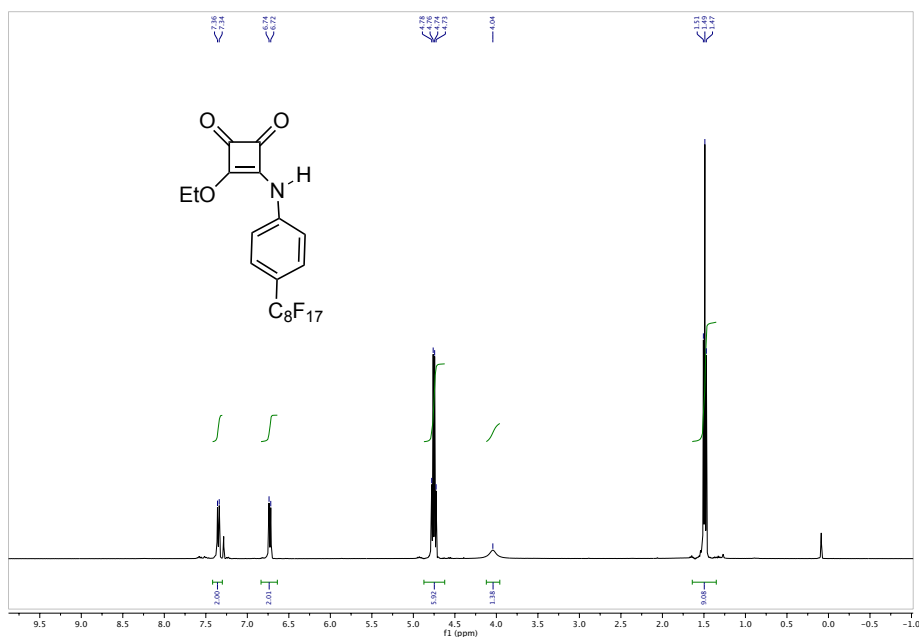


Figure A. 206. ^1H NMR spectrum of crude **82**

B. HPLC CHROMATOGRAMS

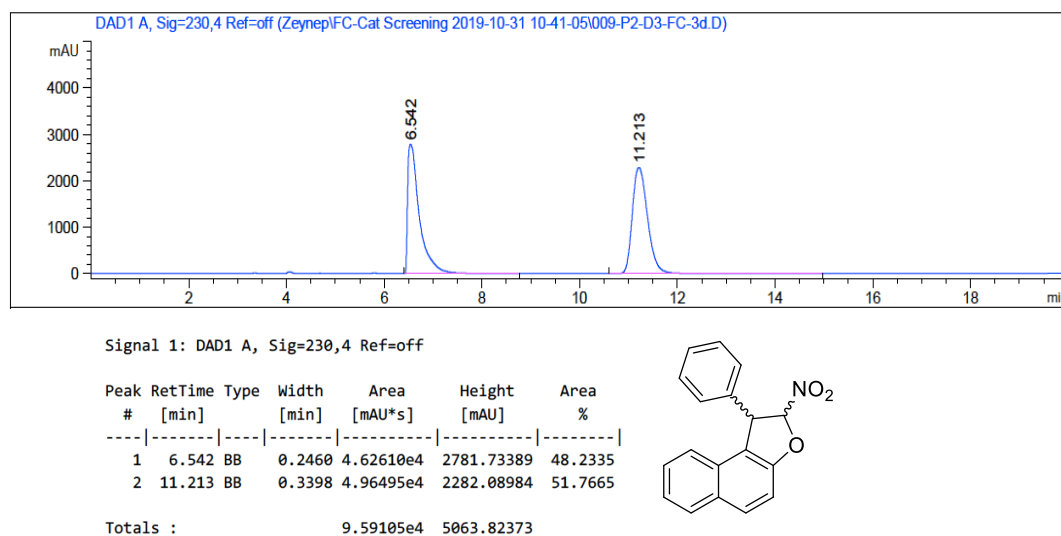


Figure B. 1. HPLC Chromatogram of *rac*-23aa

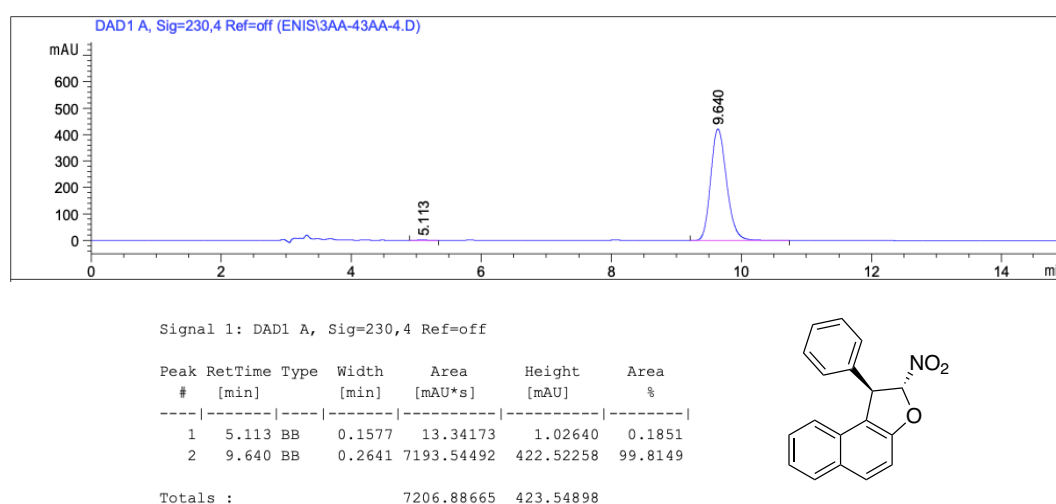
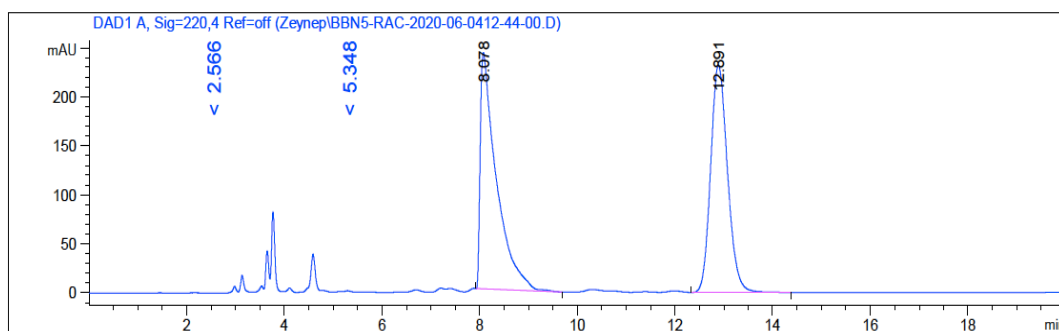


Figure B. 2. HPLC Chromatogram of enantiomerically enriched 23aa



Signal 1: DAD1 A, Sig=220,4 Ref=off

Peak #	RetTime [min]	Type	Width [min]	Area [mAU*s]	Height [mAU]	Area %
1	8.078	BB	0.3132	5549.79883	240.94987	49.9056
2	12.891	BB	0.3709	5570.78760	231.81160	50.0944

Totals : 1.11206e4 472.76147

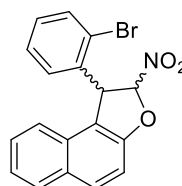
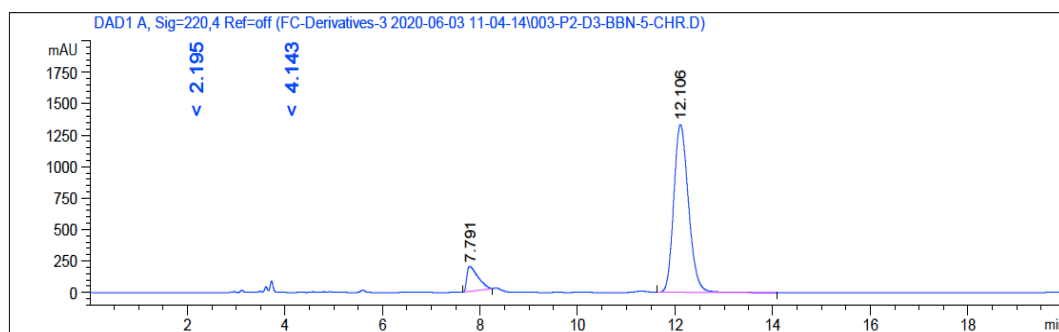


Figure B. 3. HPLC Chromatogram of *rac*-23ab



Signal 1: DAD1 A, Sig=220,4 Ref=off

Peak #	RetTime [min]	Type	Width [min]	Area [mAU*s]	Height [mAU]	Area %
1	7.791	BB	0.2281	3123.76978	200.08533	10.0436
2	12.106	BB	0.3241	2.79783e4	1334.38647	89.9564

Totals : 3.11021e4 1534.47180

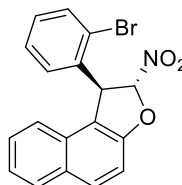
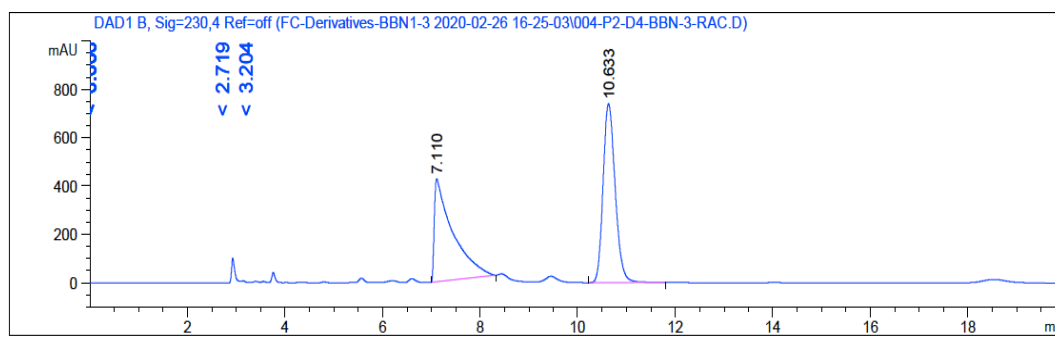


Figure B. 4. HPLC Chromatogram of enantiomerically enriched 23ab



Signal 2: DAD1 B, Sig=230,4 Ref=off

Peak #	RetTime [min]	Type	Width [min]	Area [mAU*s]	Height [mAU]	Area %
1	7.110	BB	0.3404	1.11715e4	426.71237	46.7351
2	10.633	BB	0.2661	1.27323e4	740.61688	53.2649

Totals : 2.39038e4 1167.32925

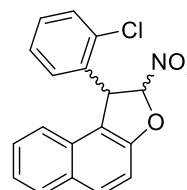
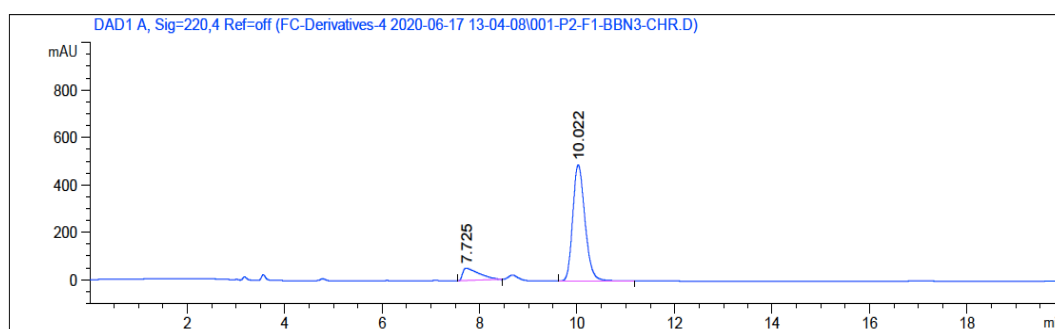


Figure B. 5. HPLC Chromatogram of *rac*-23ac



Signal 1: DAD1 A, Sig=220,4 Ref=off

Peak #	RetTime [min]	Type	Width [min]	Area [mAU*s]	Height [mAU]	Area %
1	7.725	BB	0.3192	1211.03247	51.62929	12.4422
2	10.022	BB	0.2695	8522.25684	489.85028	87.5578

Totals : 9733.28931 541.47957

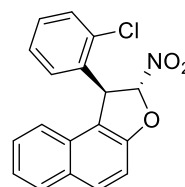


Figure B. 6. HPLC Chromatogram of enantiomerically enriched 23ac

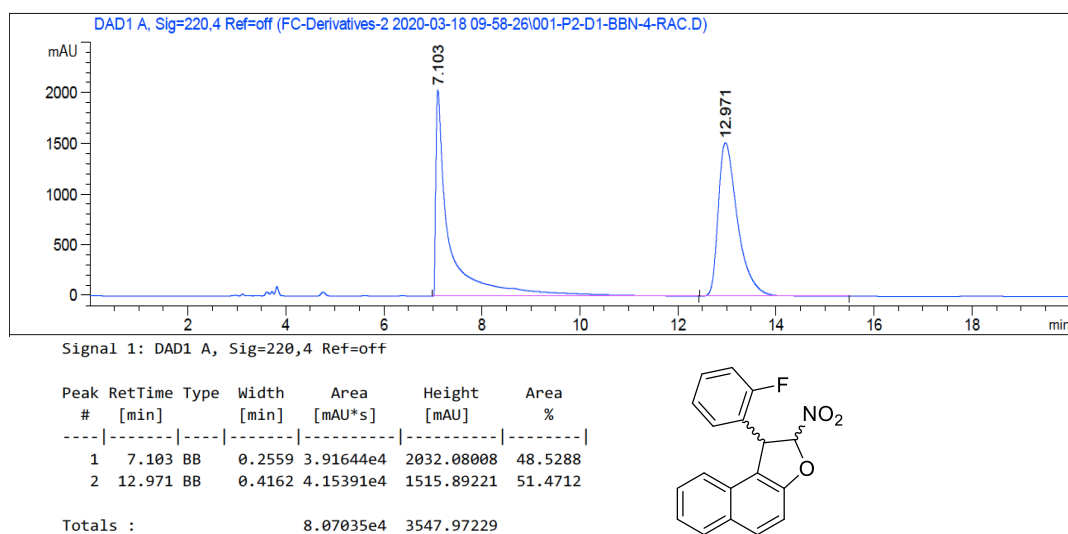


Figure B. 7. HPLC Chromatogram of *rac*-23ad

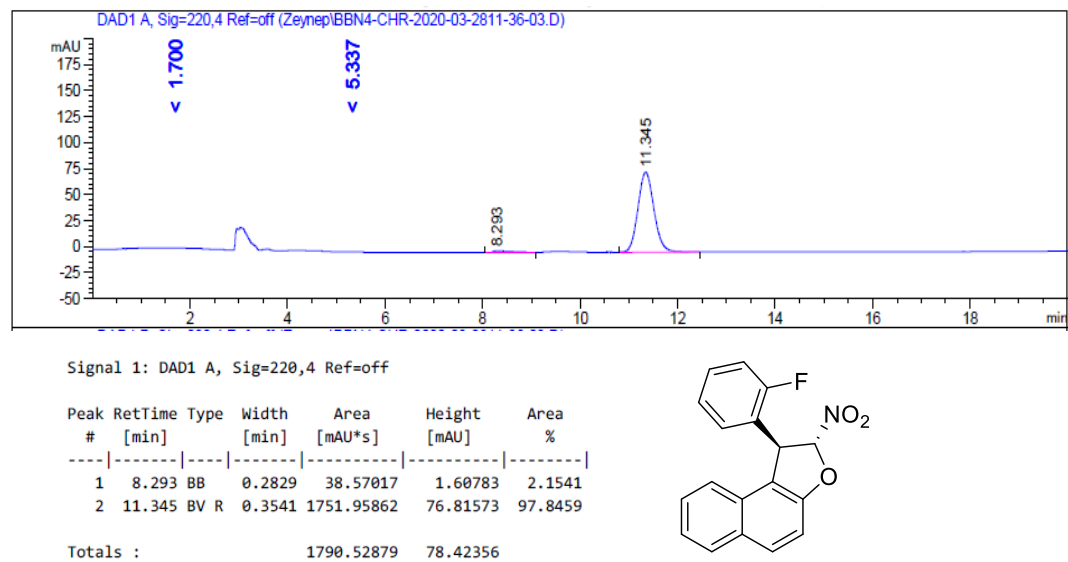


Figure B. 8. HPLC Chromatogram of enantiomerically enriched 23ad

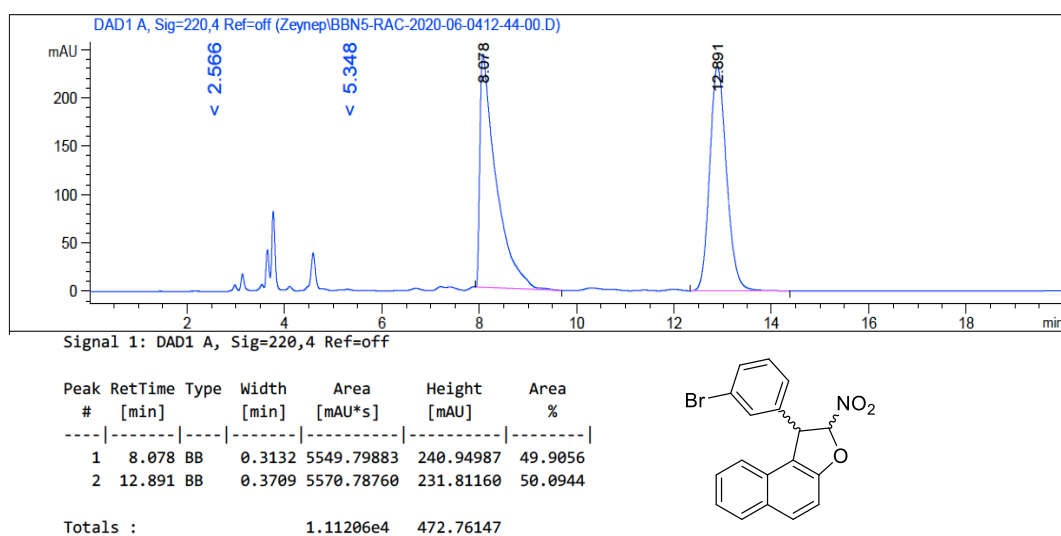


Figure B. 9. HPLC Chromatogram of *rac*-**23ae**

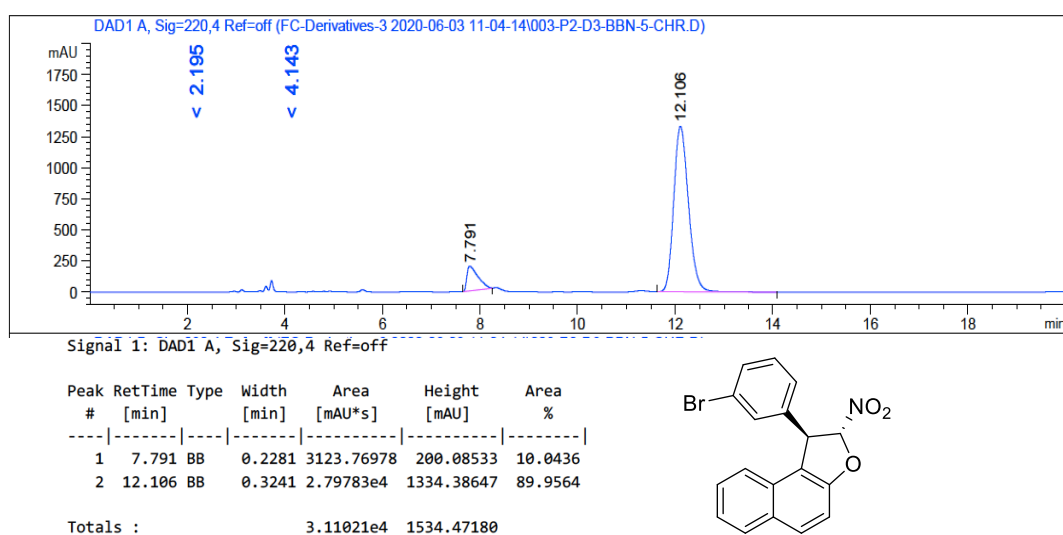
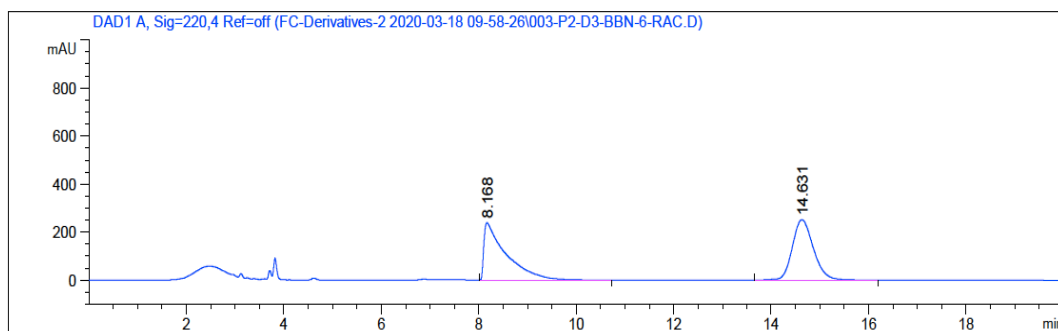


Figure B. 10. HPLC Chromatogram of enantiomerically enriched **23ae**



Signal 1: DAD1 A, Sig=220,4 Ref=off

Peak #	RetTime [min]	Type	Width [min]	Area [mAU*s]	Height [mAU]	Area %
1	8.168	BB	0.4123	7525.23145	239.04436	49.8143
2	14.631	BB	0.4583	7581.32324	251.78191	50.1857

Totals : 1.51066e4 490.82626

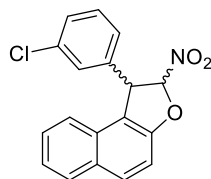
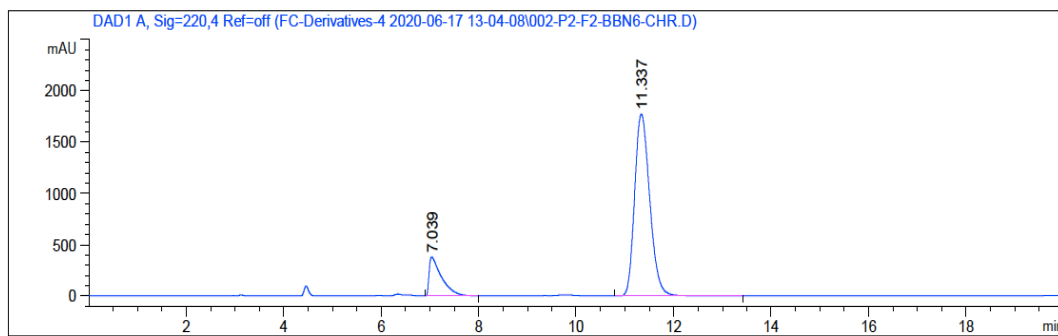


Figure B. 11. HPLC Chromatogram of *rac*-23af



Signal 1: DAD1 A, Sig=220,4 Ref=off

Peak #	RetTime [min]	Type	Width [min]	Area [mAU*s]	Height [mAU]	Area %
1	7.039	BB	0.2477	6686.58350	379.22177	14.8663
2	11.337	BB	0.3349	3.82917e4	1773.75171	85.1337

Totals : 4.49783e4 2152.97348

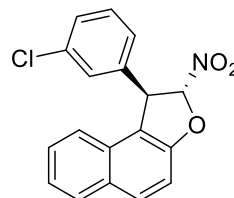
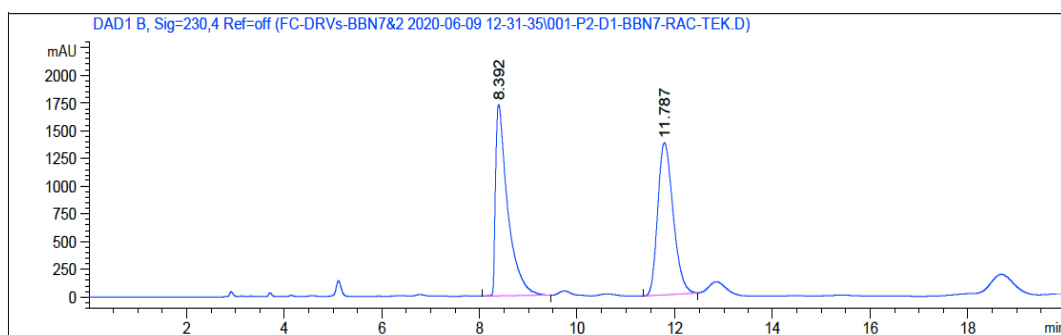


Figure B. 12. HPLC Chromatogram of enantiomerically enriched 23af



Peak #	RetTime [min]	Type	Width [min]	Area [mAU*s]	Height [mAU]	Area %
1	8.392	BB	0.2486	2.99118e4	1726.99353	49.8559
2	11.787	BB	0.3407	3.00847e4	1372.63574	50.1441

Totals : 5.99966e4 3099.62927

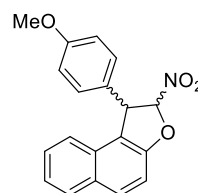
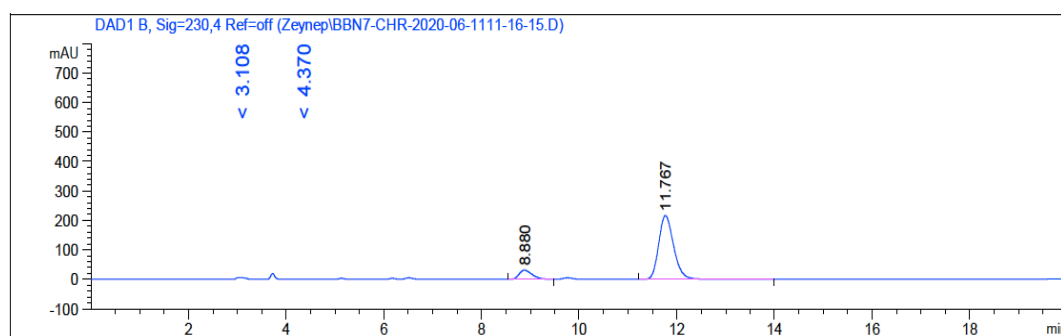


Figure B. 13. HPLC Chromatogram of *rac*-23ag



Peak #	RetTime [min]	Type	Width [min]	Area [mAU*s]	Height [mAU]	Area %
1	8.880	BB	0.2851	573.76807	31.12714	11.0766
2	11.767	BB	0.3282	4606.22021	216.50133	88.9234

Totals : 5179.98828 247.62847

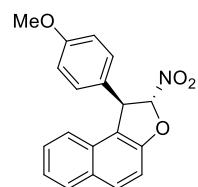


Figure B. 14. HPLC Chromatogram of enantiomerically enriched 23ag

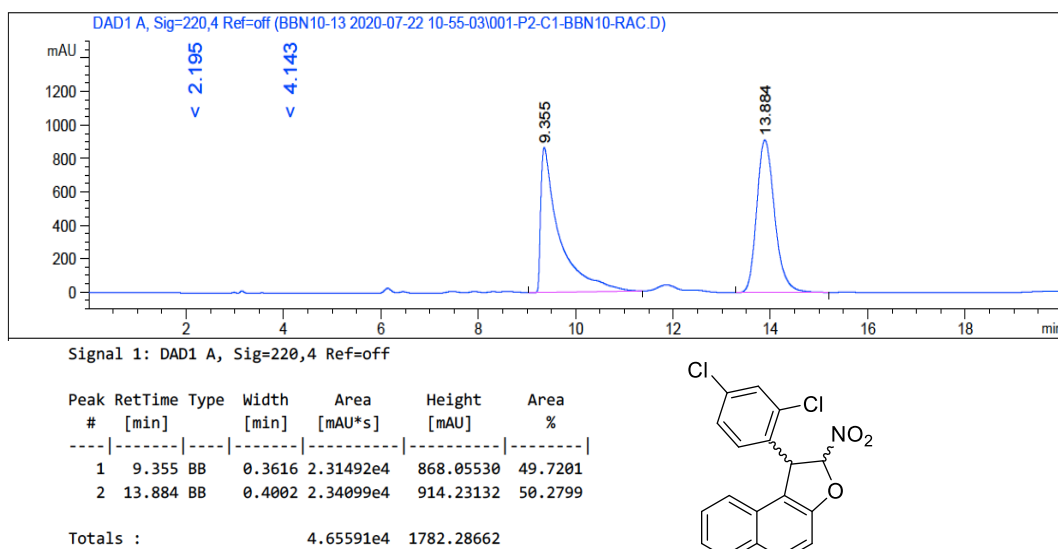


Figure B. 15. HPLC Chromatogram of *rac*-23ah

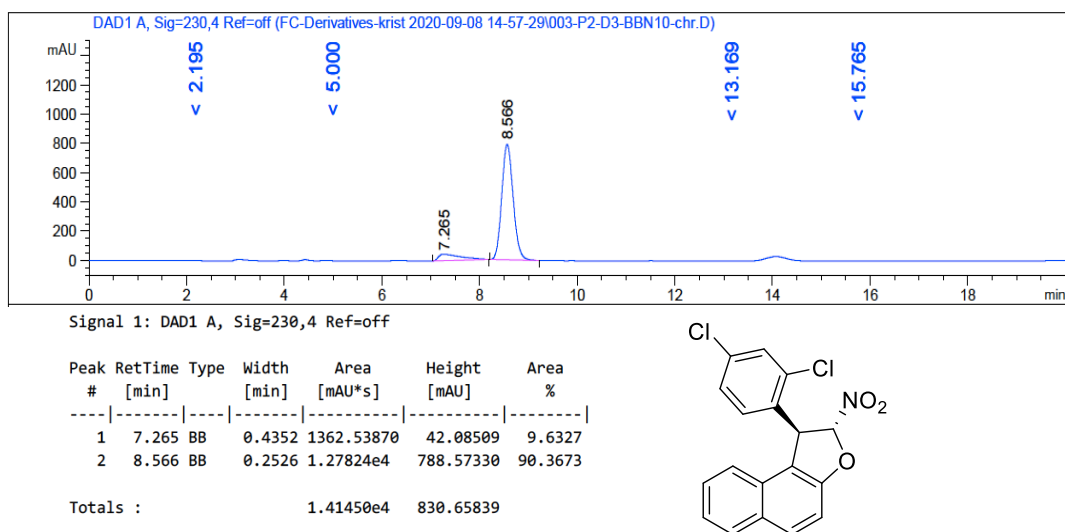


Figure B. 16. HPLC Chromatogram of enantiomerically enriched 23ah

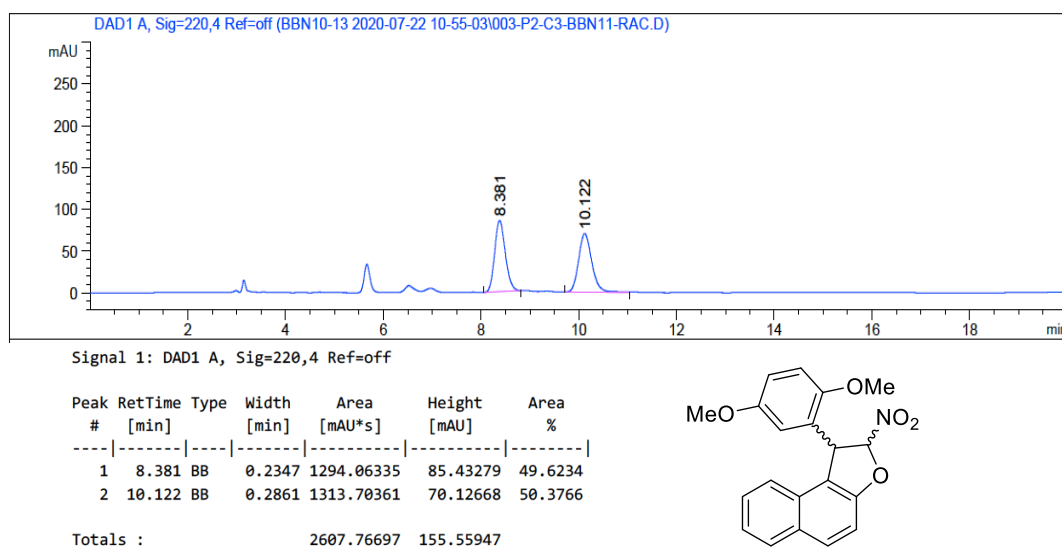


Figure B. 17. HPLC Chromatogram of *rac*-**23ai**

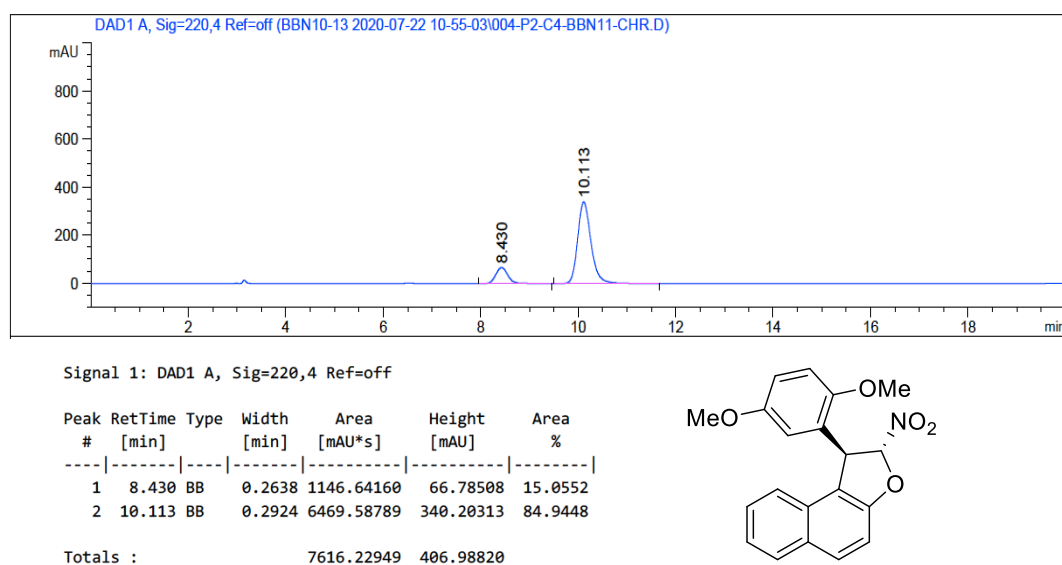
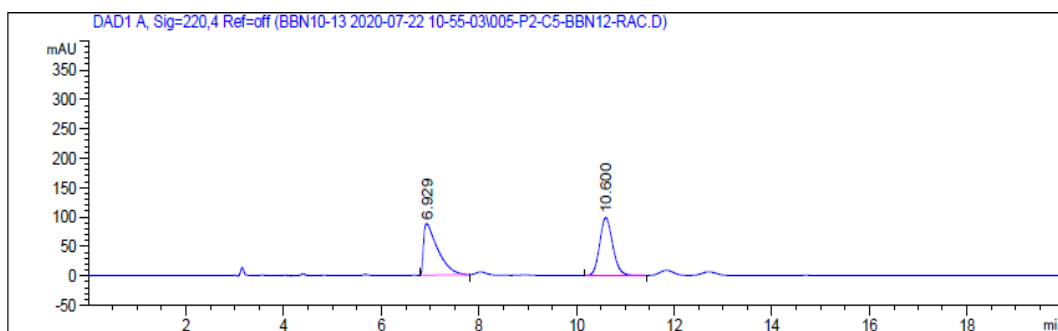


Figure B. 18. HPLC Chromatogram of enantiomerically enriched **23ai**



Signal 1: DAD1 A, Sig=220,4 Ref=off

Peak #	RetTime [min]	Type	Width [min]	Area [mAU*s]	Height [mAU]	Area %
1	7.060	BB	0.2490	405.47305	23.42256	0.9207
2	10.396	BB	0.2938	4.36365e4	2326.57471	99.0793

Totals : 4.40419e4 2349.99727

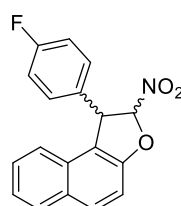
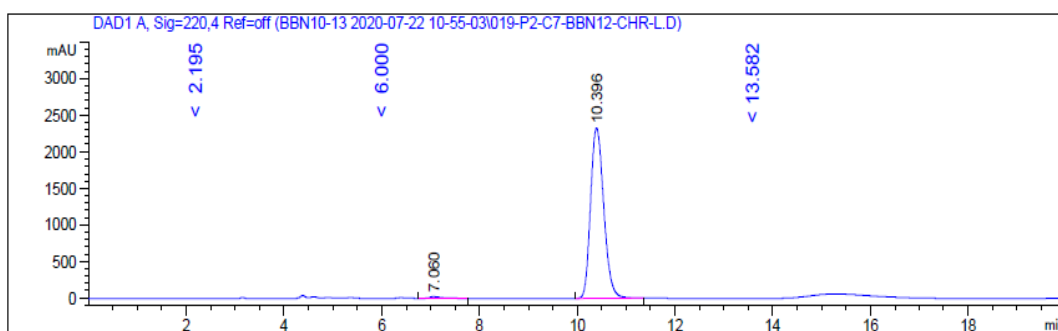


Figure B. 19. HPLC Chromatogram of *rac*-23aj



Signal 1: DAD1 A, Sig=220,4 Ref=off

Peak #	RetTime [min]	Type	Width [min]	Area [mAU*s]	Height [mAU]	Area %
1	7.060	BB	0.2490	405.47305	23.42256	0.9207
2	10.396	BB	0.2938	4.36365e4	2326.57471	99.0793

Totals : 4.40419e4 2349.99727

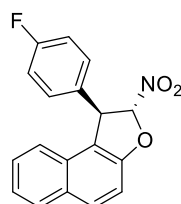
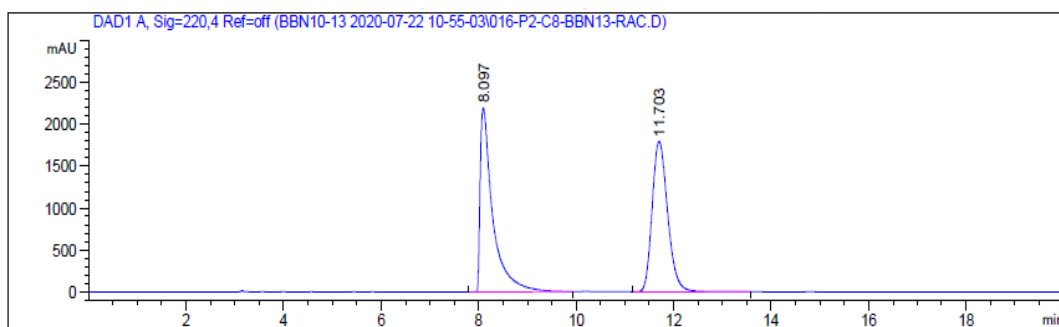


Figure B. 20. HPLC Chromatogram of enantiomerically enriched 23aj



Signal 1: DAD1 A, Sig=220,4 Ref=off

Peak #	RetTime [min]	Type	Width [min]	Area [mAU*s]	Height [mAU]	Area %
1	8.097	BB	0.2570	3.94062e4	2194.71460	49.7513
2	11.703	BBA	0.3421	3.98003e4	1795.50232	50.2487

Totals : 7.92065e4 3990.21692

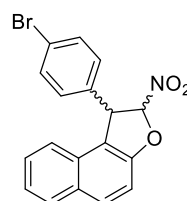
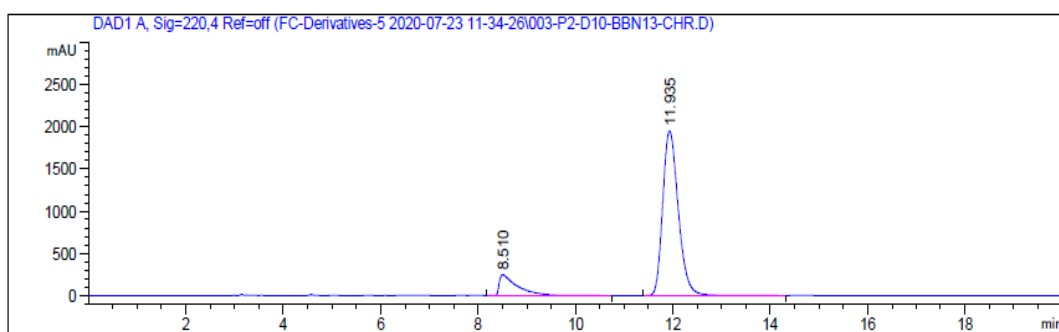


Figure B. 21. HPLC Chromatogram of *rac*-23ak



Signal 1: DAD1 A, Sig=220,4 Ref=off

Peak #	RetTime [min]	Type	Width [min]	Area [mAU*s]	Height [mAU]	Area %
1	8.510	BB	0.3595	6398.27637	245.98050	12.8552
2	11.935	BB	0.3441	4.33737e4	1949.58447	87.1448

Totals : 4.97719e4 2195.56497

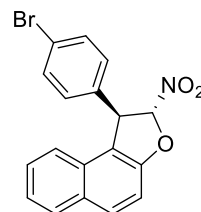


Figure B. 22. HPLC Chromatogram of enantiomerically enriched 23ak

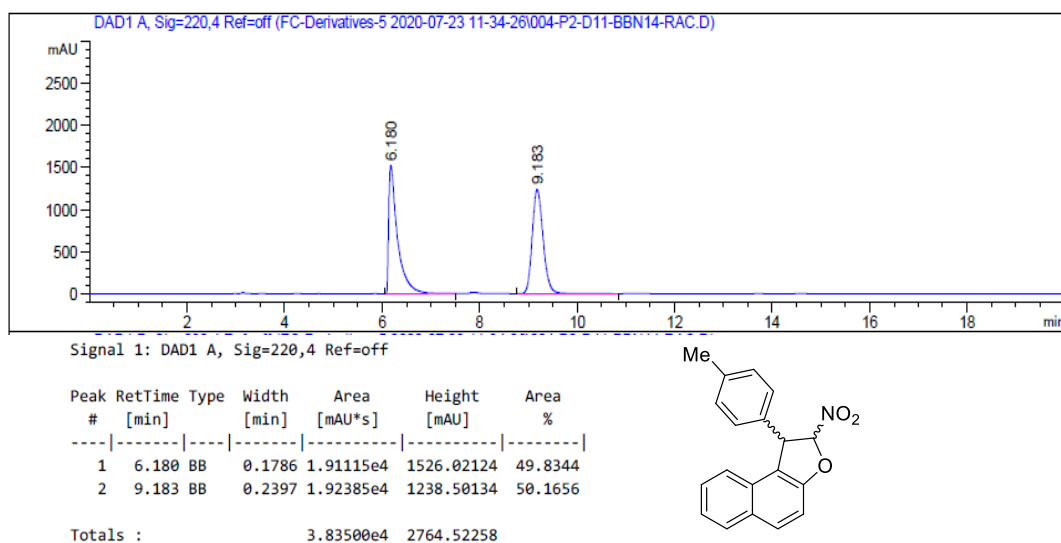


Figure B. 23. HPLC Chromatogram of *rac*-23al

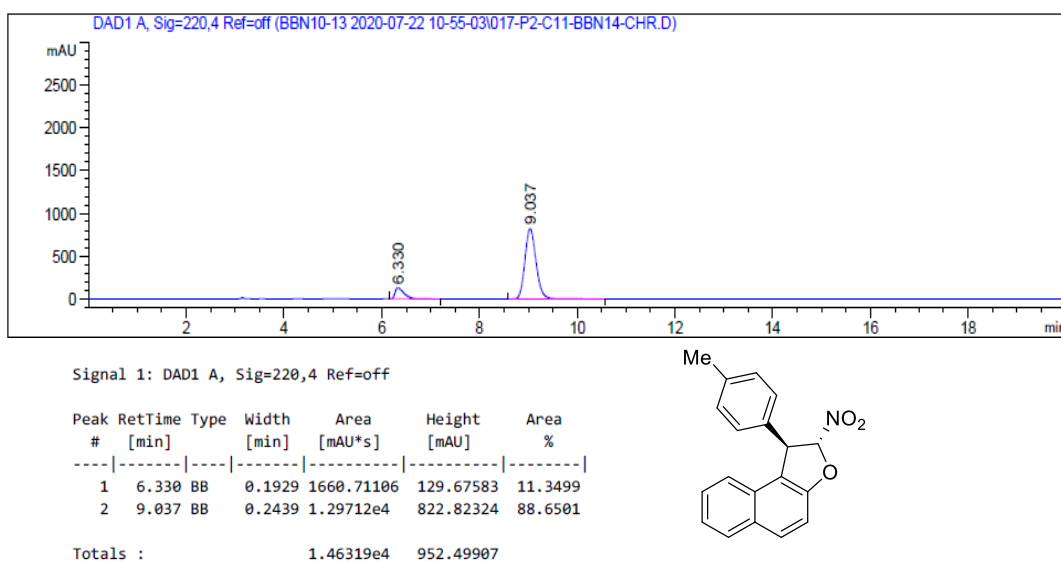


Figure B. 24. HPLC Chromatogram of enantiomerically enriched 23al

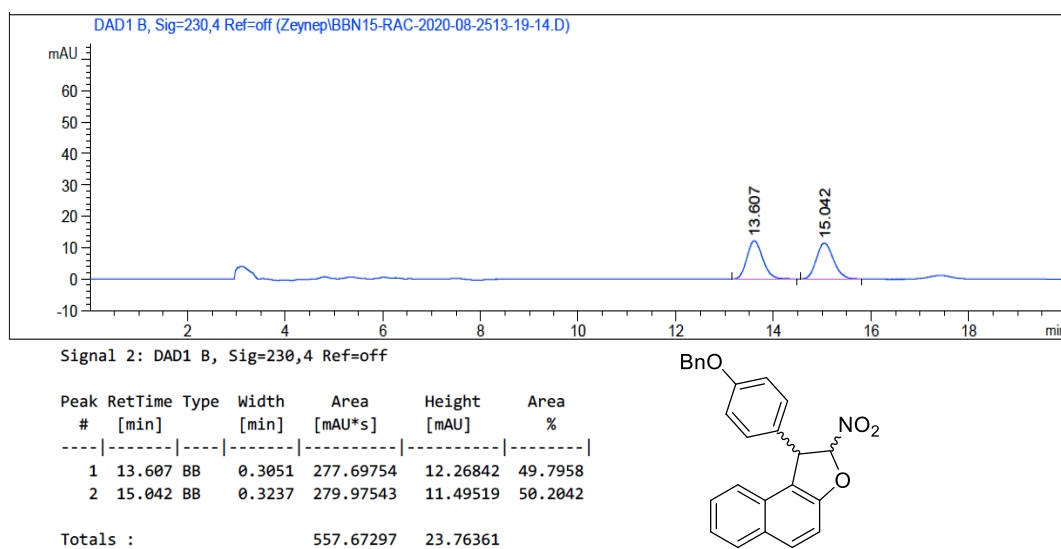


Figure B. 25. HPLC Chromatogram of *rac*-**23am**

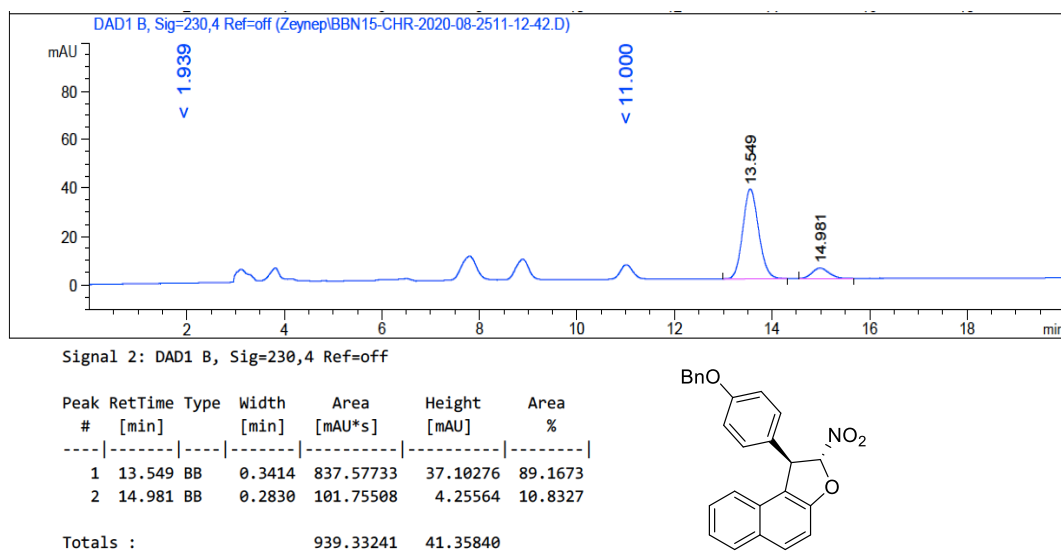
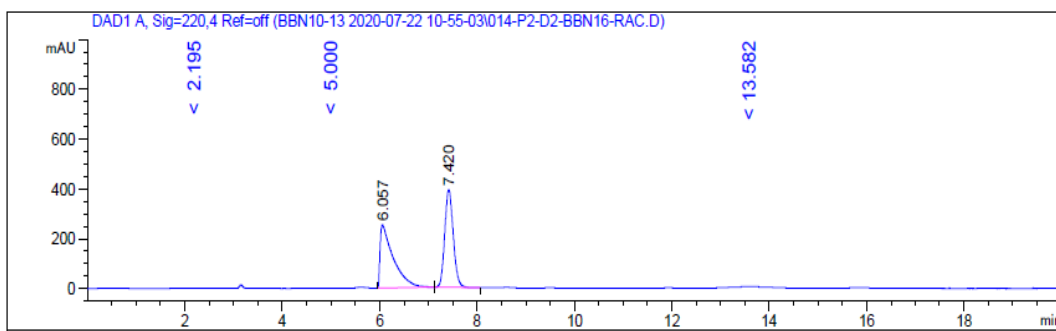


Figure B. 26. HPLC Chromatogram of enantiomerically enriched **23am**



Signal 1: DAD1 A, Sig=220,4 Ref=off

Peak #	RetTime [min]	Type	Width [min]	Area [mAU*s]	Height [mAU]	Area %
1	6.057	BB	0.2569	4760.25342	253.71597	49.9884
2	7.420	BB	0.1876	4762.46680	392.33853	50.0116

Totals : 9522.72021 646.05450

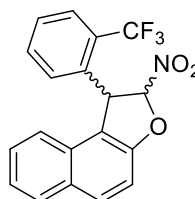
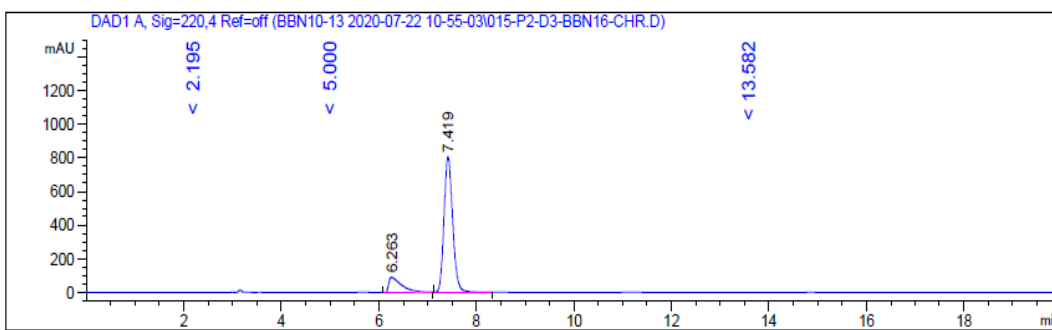


Figure B. 27. HPLC Chromatogram of *rac*-23an



Signal 1: DAD1 A, Sig=220,4 Ref=off

Peak #	RetTime [min]	Type	Width [min]	Area [mAU*s]	Height [mAU]	Area %
1	6.263	BB	0.2577	1630.26660	89.42544	14.1104
2	7.419	BB	0.1903	9923.40527	804.86676	85.8896

Totals : 1.15537e4 894.29220

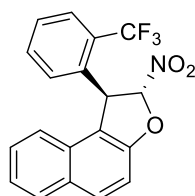
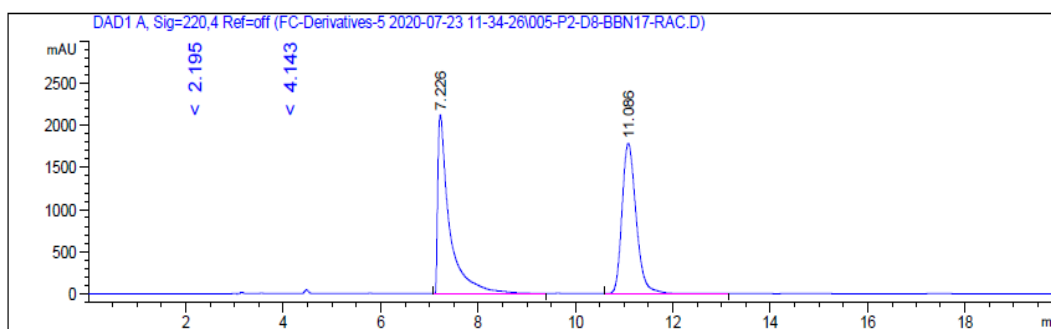


Figure B. 28. HPLC Chromatogram of enantiomerically enriched 23an



Signal 1: DAD1 A, Sig=220,4 Ref=off

Peak #	RetTime [min]	Type	Width [min]	Area [mAU*s]	Height [mAU]	Area %
1	7.226	BB	0.2357	3.56521e4	2120.31543	49.7601
2	11.086	BB	0.3115	3.59959e4	1783.54602	50.2399

Totals : 7.16480e4 3903.86145

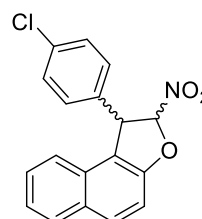
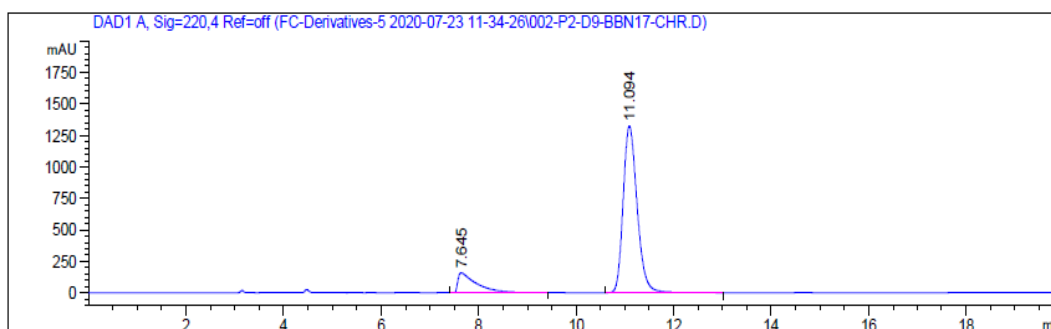


Figure B. 29. HPLC Chromatogram of *rac*-23ao



Signal 1: DAD1 A, Sig=220,4 Ref=off

Peak #	RetTime [min]	Type	Width [min]	Area [mAU*s]	Height [mAU]	Area %
1	7.645	BB	0.3546	4083.95459	156.41397	13.4126
2	11.094	BB	0.3067	2.63647e4	1324.75745	86.5874

Totals : 3.04486e4 1481.17142

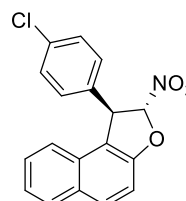


Figure B. 30. HPLC Chromatogram of enantiomerically enriched 23ao

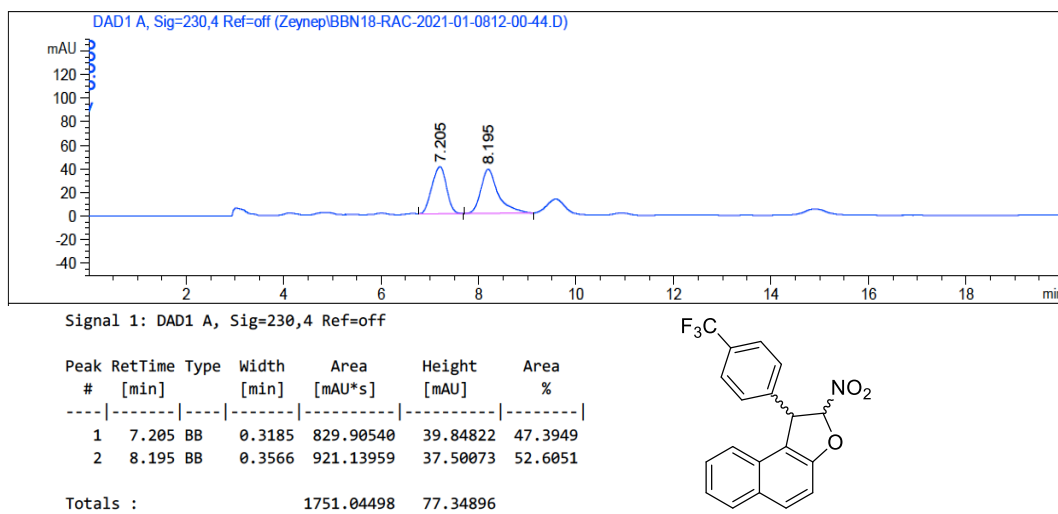


Figure B. 31. HPLC Chromatogram of *rac*-**23ap**

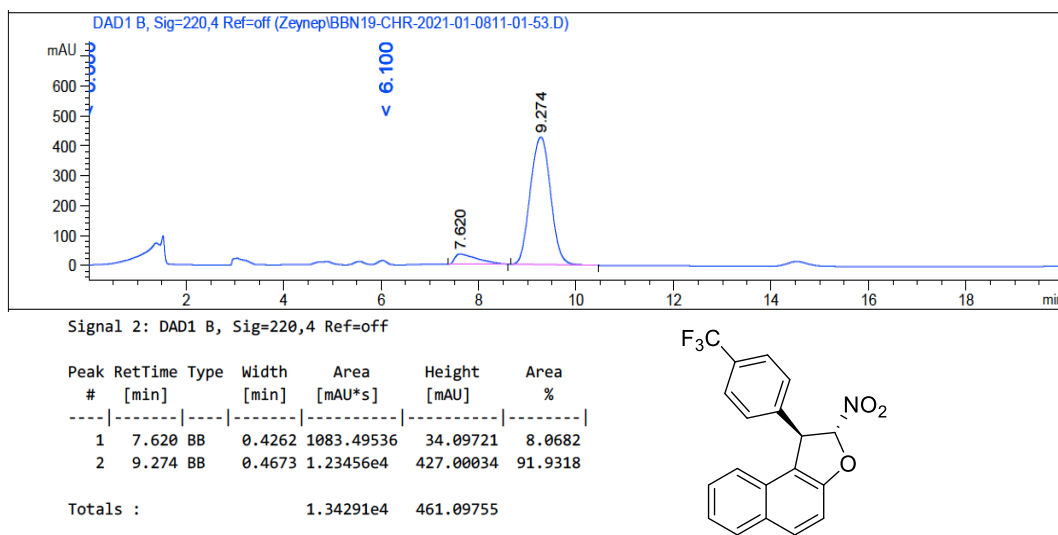
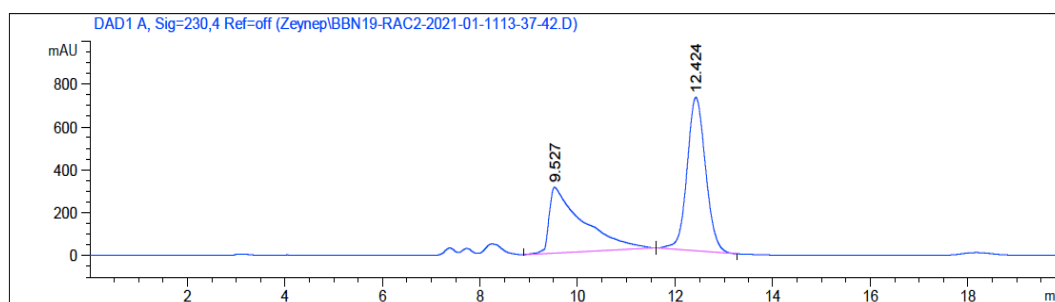


Figure B. 32. HPLC Chromatogram of enantiomerically enriched **23ap**



Signal 1: DAD1 A, Sig=230,4 Ref=off

Peak #	RetTime [min]	Type	Width [min]	Area [mAU*s]	Height [mAU]	Area %
1	9.527	BB	0.6261	1.46844e4	307.50040	43.6712
2	12.424	BB	0.4085	1.89406e4	717.36469	56.3288

Totals : 3.36250e4 1024.86508

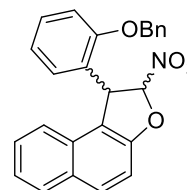
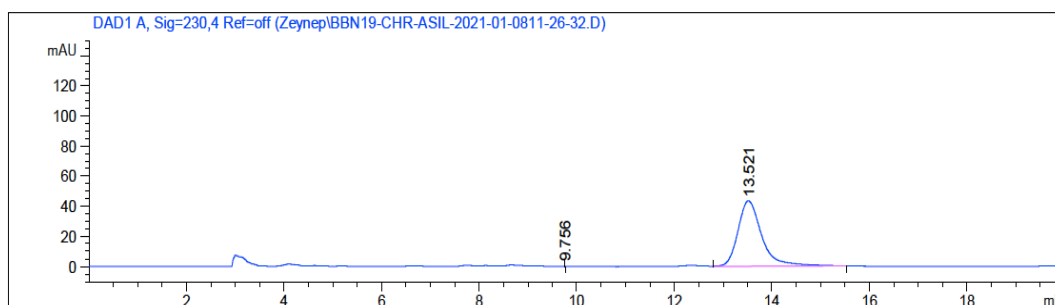


Figure B. 33. HPLC Chromatogram of *rac*-23aq



Signal 1: DAD1 A, Sig=230,4 Ref=off

Peak #	RetTime [min]	Type	Width [min]	Area [mAU*s]	Height [mAU]	Area %
1	9.756	BB	8.17e-3	4.86374e-3	1.00017e-2	3.319e-4
2	13.521	BB	0.4862	1465.55066	43.42572	99.9997

Totals : 1465.55552 43.43572

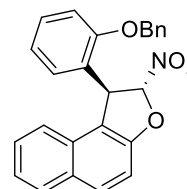
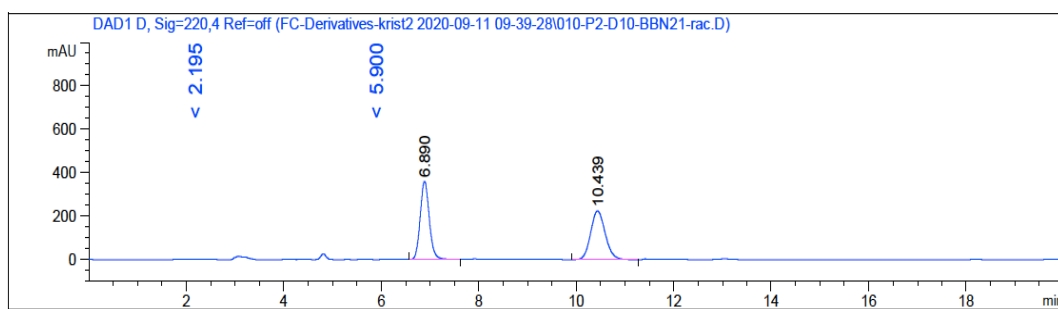


Figure B. 34. HPLC Chromatogram of enantiomerically enriched 23aq



Signal 4: DAD1 D, Sig=220,4 Ref=off

Peak #	RetTime [min]	Type	Width [min]	Area [mAU*s]	Height [mAU]	Area %
1	6.890	BB	0.1995	4655.89404	359.82172	49.9554
2	10.439	BB	0.3200	4664.21436	224.43681	50.0446

Totals : 9320.10840 584.25853

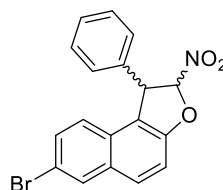
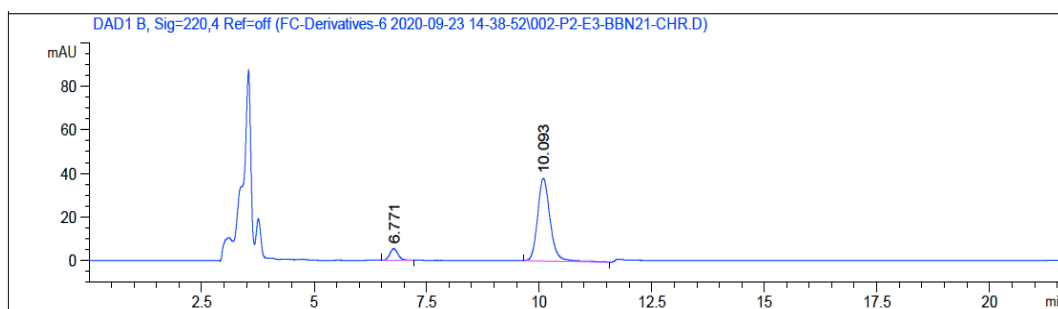


Figure B. 35. HPLC Chromatogram of *rac*-23ba



Signal 2: DAD1 B, Sig=220,4 Ref=off

Peak #	RetTime [min]	Type	Width [min]	Area [mAU*s]	Height [mAU]	Area %
1	6.771	BB	0.1823	67.35754	5.33542	8.4367
2	10.093	BB	0.2891	731.03137	37.89564	91.5633

Totals : 798.38892 43.23106

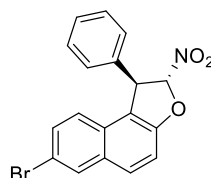


Figure B. 36. HPLC Chromatogram of enantiomerically enriched 23ba

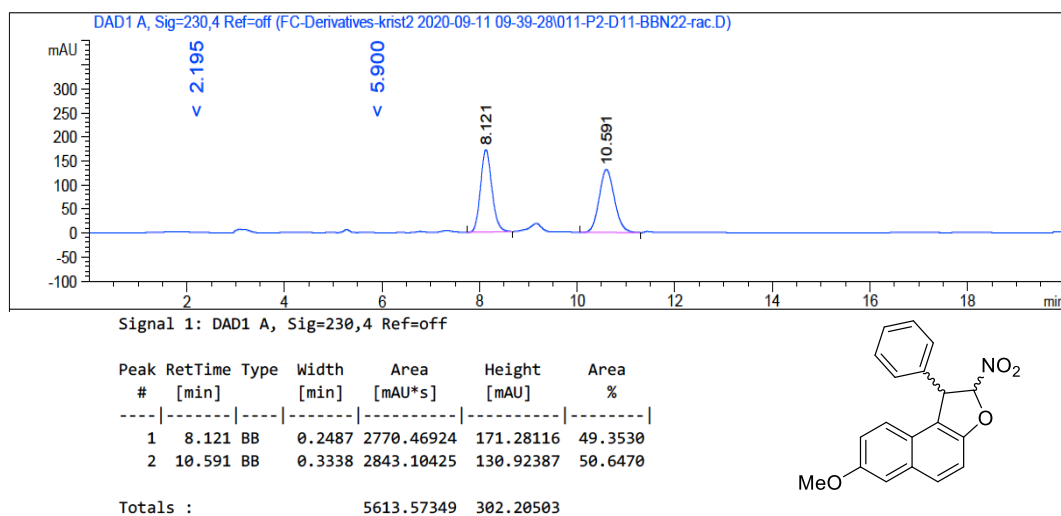


Figure B. 37. HPLC Chromatogram of *rac*-23ca

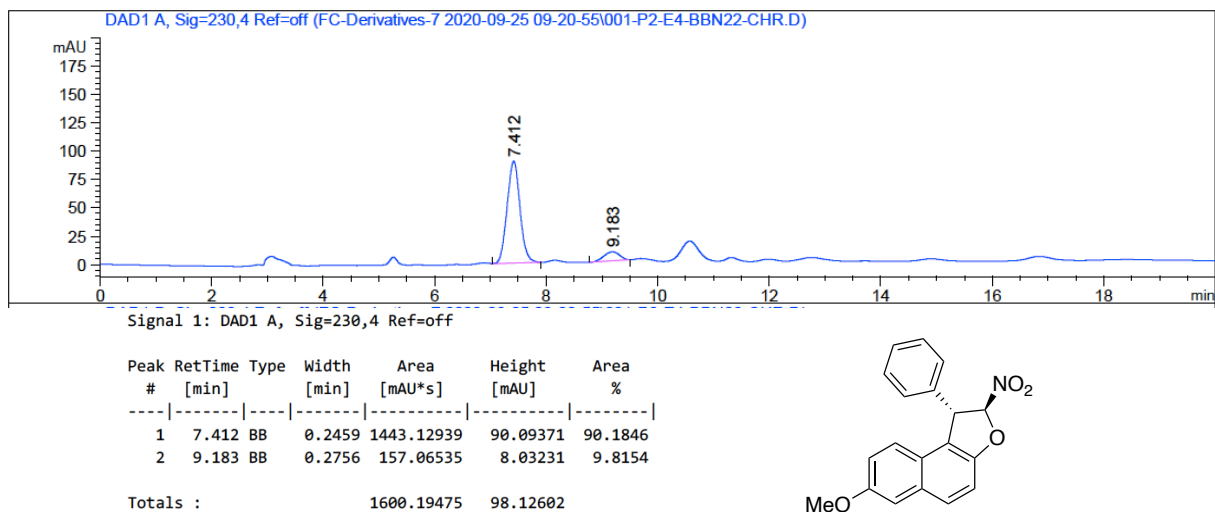


Figure B. 38. HPLC Chromatogram of enantiomerically enriched 23ca

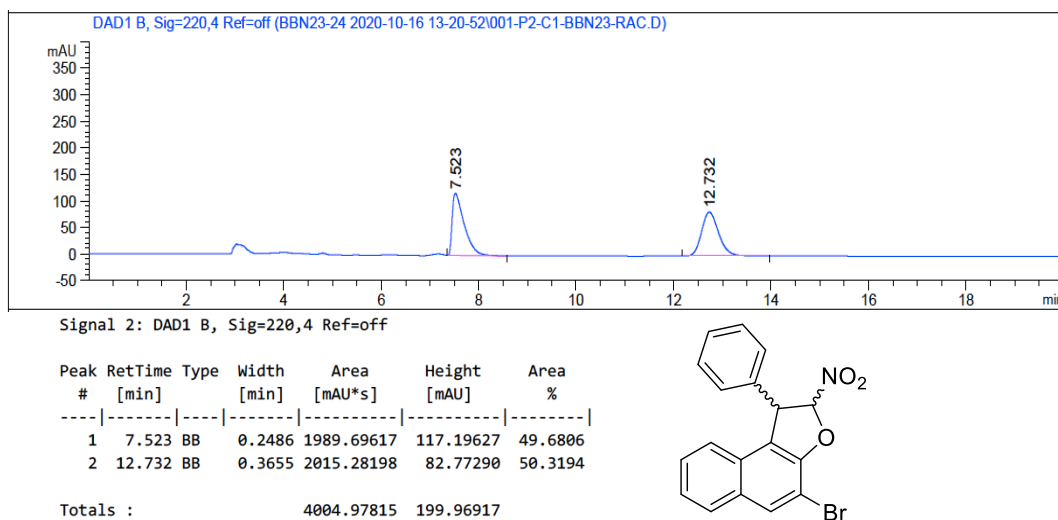


Figure B. 39. HPLC Chromatogram of *rac*-23da

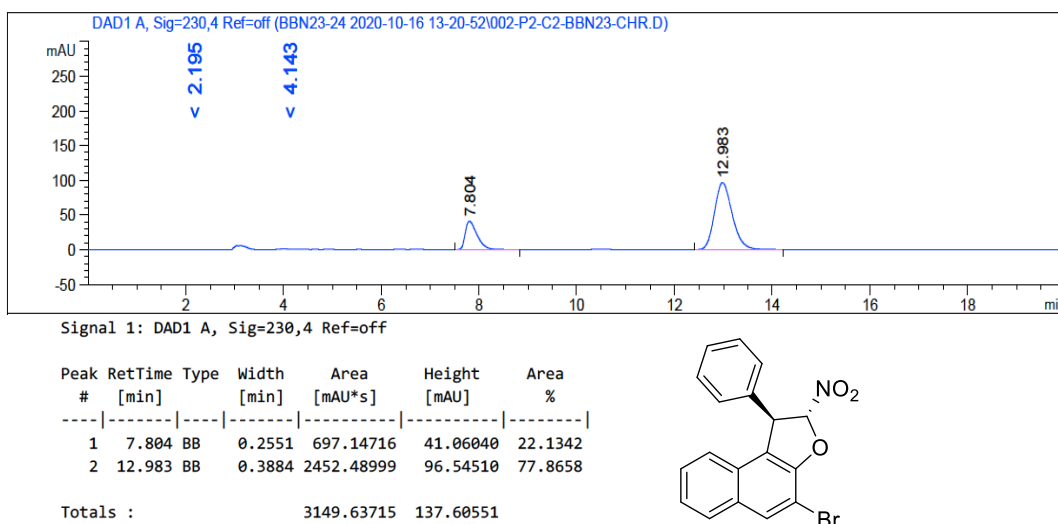


Figure B. 40. HPLC Chromatogram of enantiomerically enriched 23da

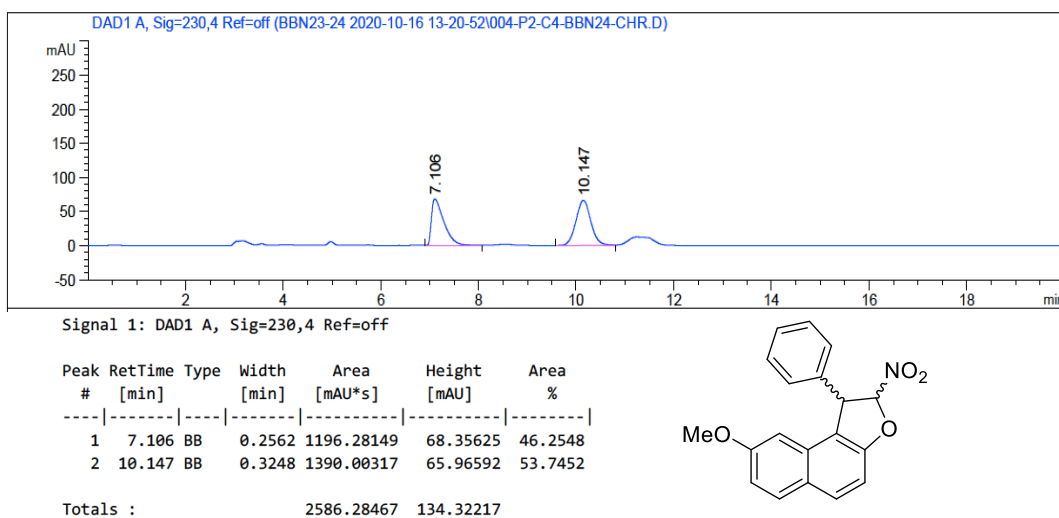


Figure B. 41. HPLC Chromatogram of *rac*-23ea

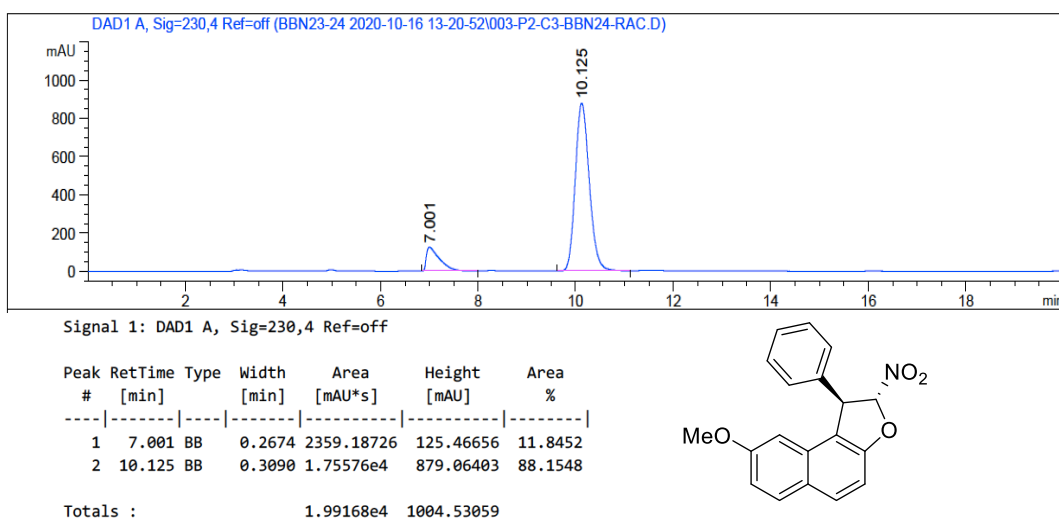


Figure B. 42. HPLC Chromatogram of enantiomerically enriched 23ea

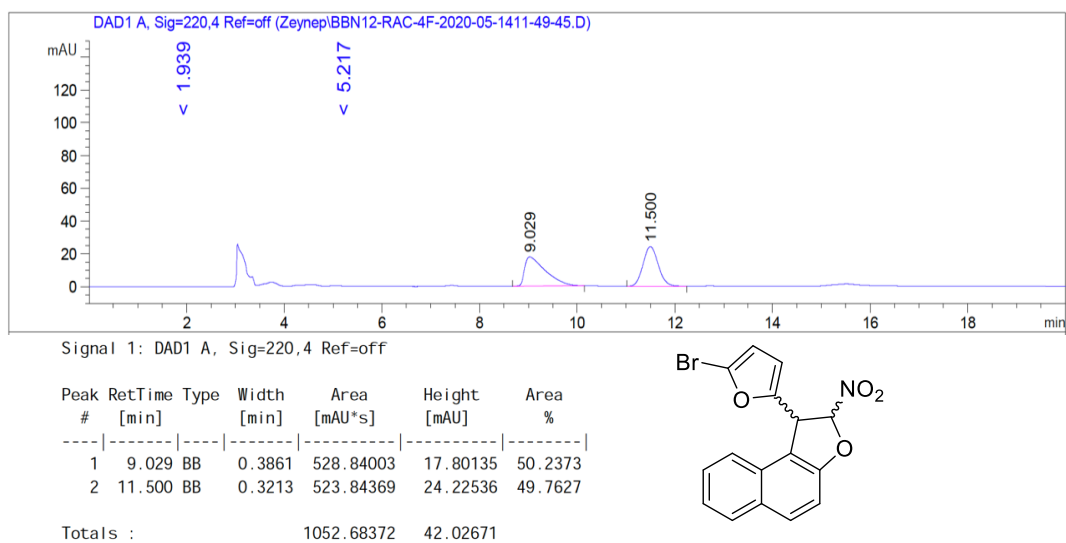


Figure B. 43. HPLC Chromatogram of *rac*-**23as**

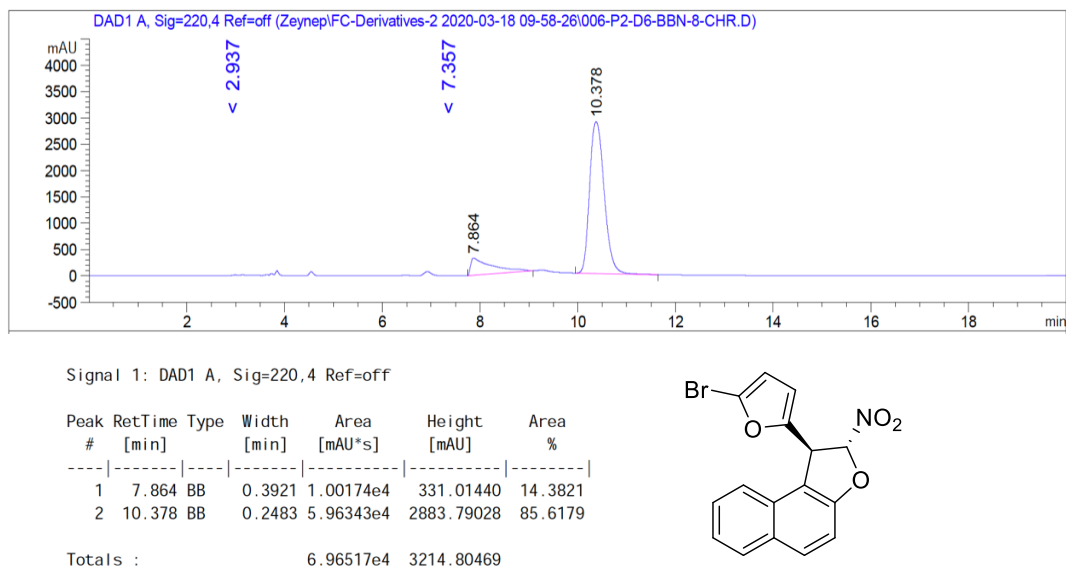


Figure B. 44. HPLC Chromatogram of enantiomerically enriched **23as**

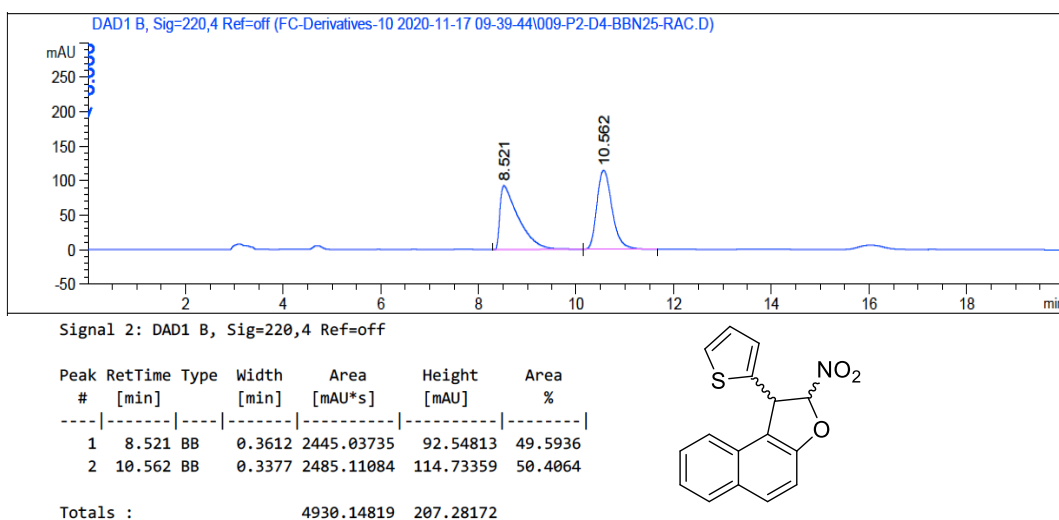


Figure B. 45. HPLC Chromatogram of *rac*-23at

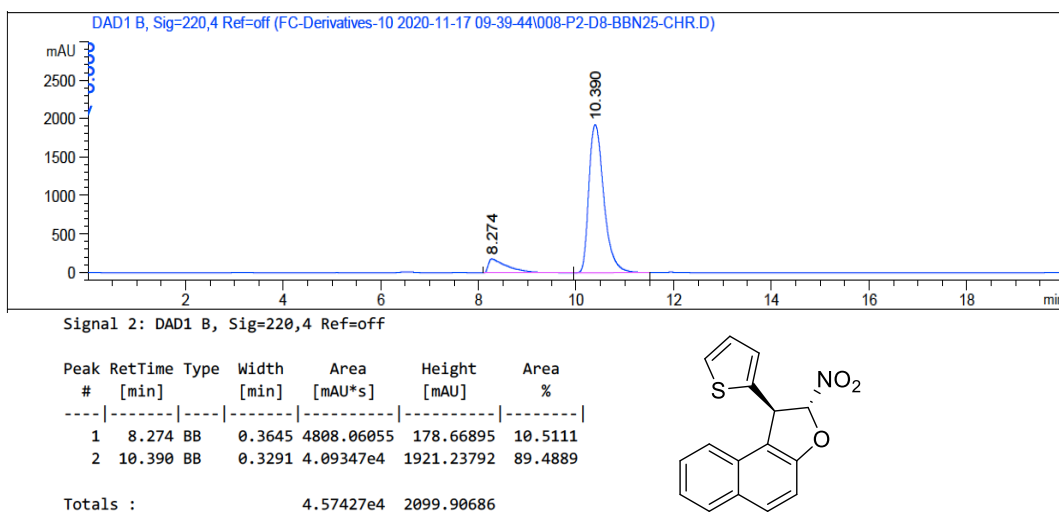


Figure B. 46. HPLC Chromatogram of enantiomerically enriched 23at

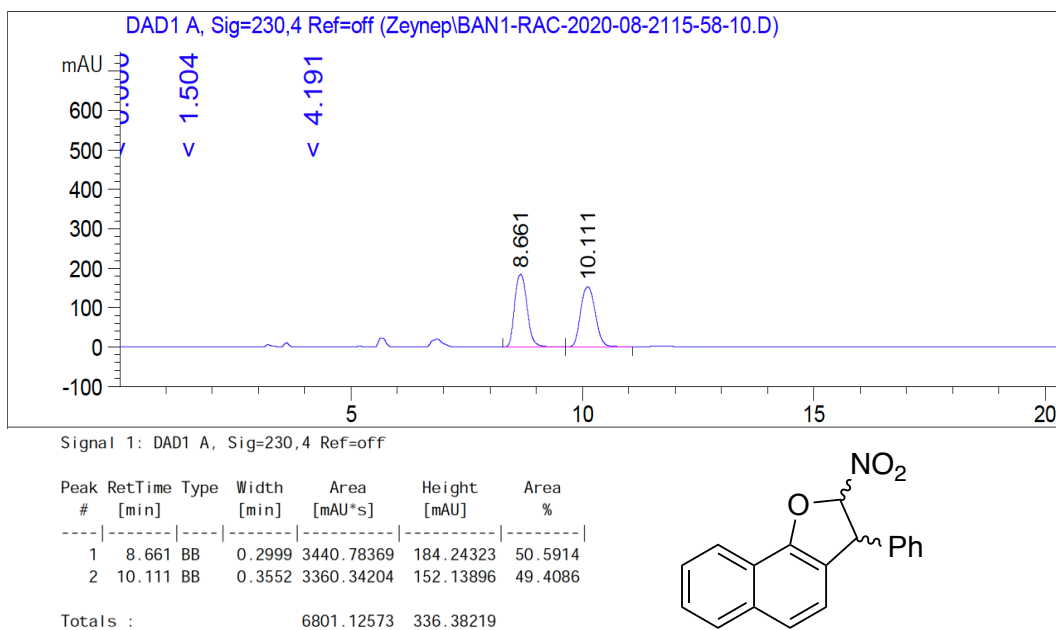


Figure B. 47. HPLC Chromatogram of *rac*-60aa

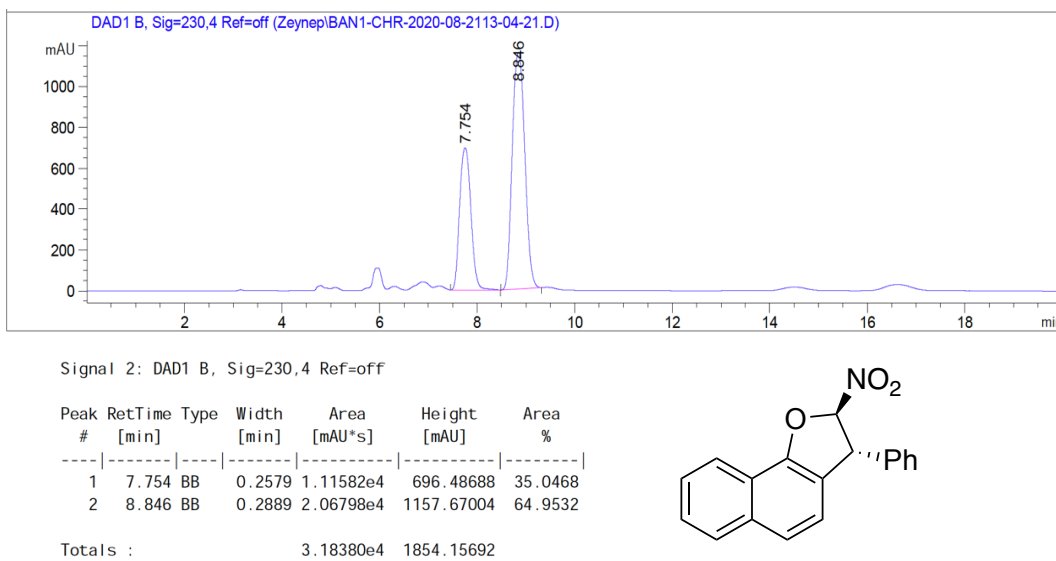
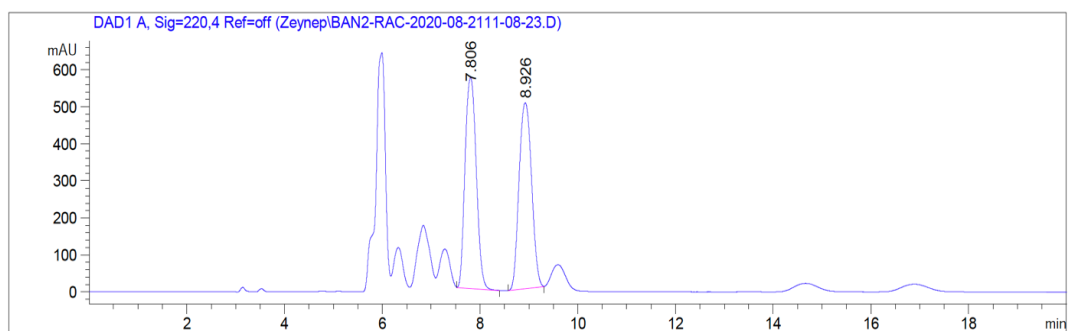


Figure B. 48. HPLC Chromatogram of enantiomerically enriched 60aa



Signal 1: DAD1 A, Sig=220,4 Ref=off

Peak #	RetTime [min]	Type	Width [min]	Area [mAU*s]	Height [mAU]	Area %
1	7.806	BB	0.2566	9060.45117	569.51318	50.2938
2	8.926	BB	0.2882	8954.59082	502.86749	49.7062

Totals : 1.80150e4 1072.38068

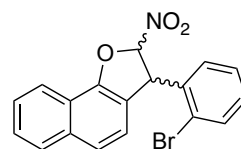
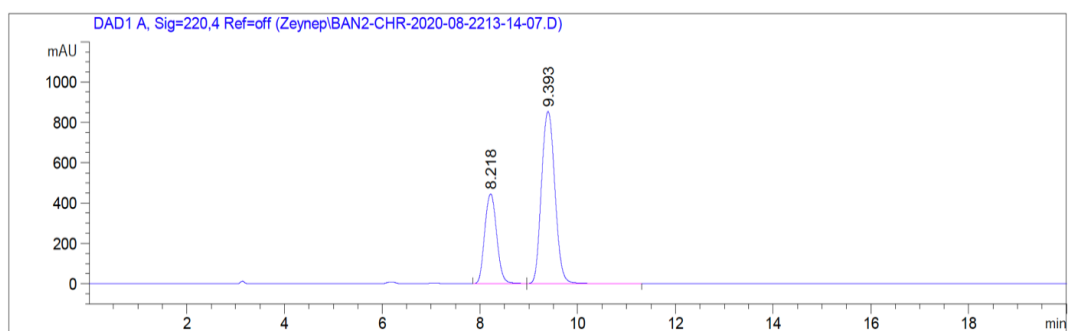


Figure B. 49. HPLC Chromatogram of *rac*-**60ab**



Signal 1: DAD1 A, Sig=220,4 Ref=off

Peak #	RetTime [min]	Type	Width [min]	Area [mAU*s]	Height [mAU]	Area %
1	8.218	BB	0.2721	7542.64355	444.28271	31.6078
2	9.393	BB	0.3052	1.63206e4	853.21423	68.3922

Totals : 2.38633e4 1297.49695

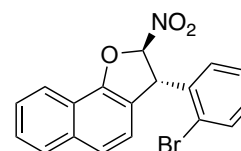


Figure B. 50. HPLC Chromatogram of enantiomerically enriched **60ab**

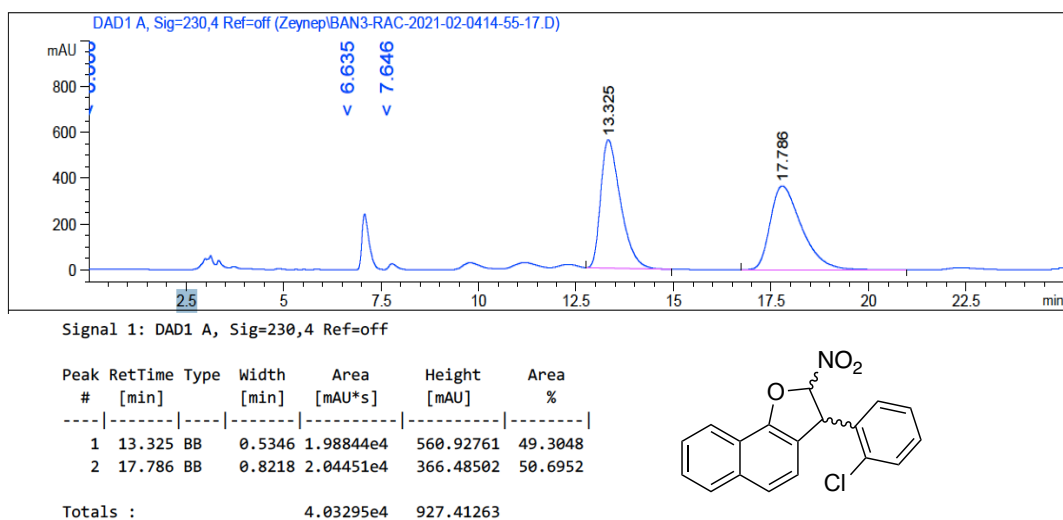


Figure B. 51. HPLC Chromatogram of *rac*-60ac

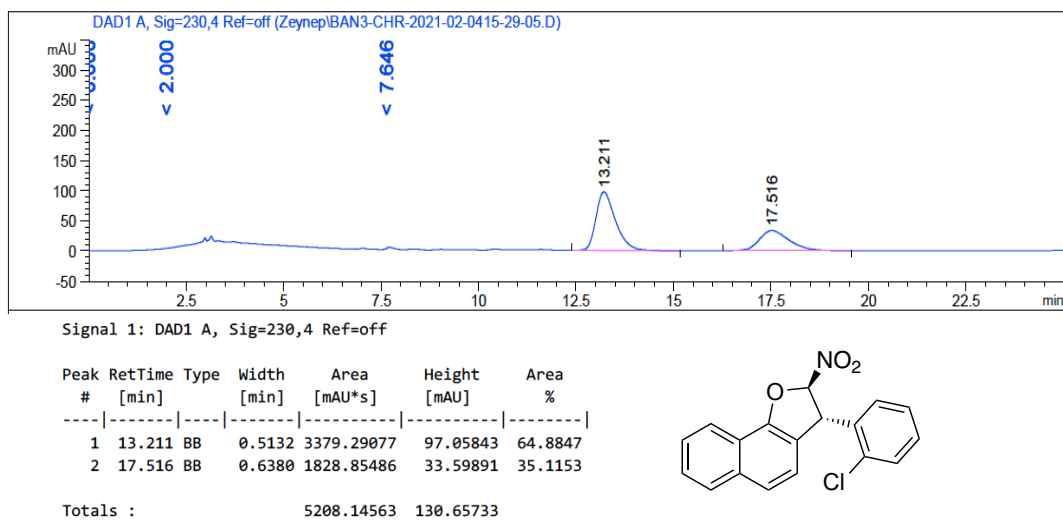


Figure B. 52. HPLC Chromatogram of enantiomerically enriched 60ac

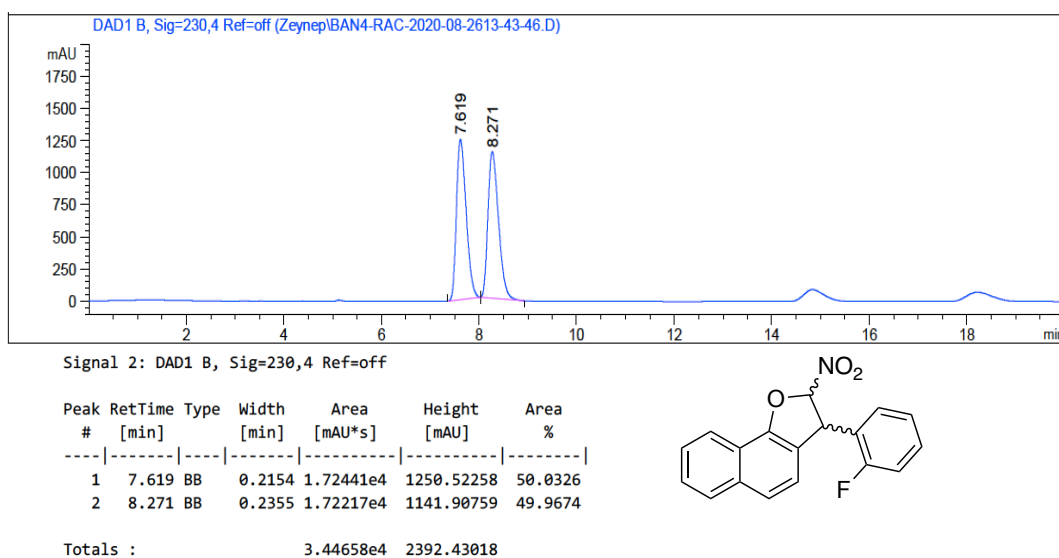


Figure B. 53. HPLC Chromatogram of *rac*-60ad

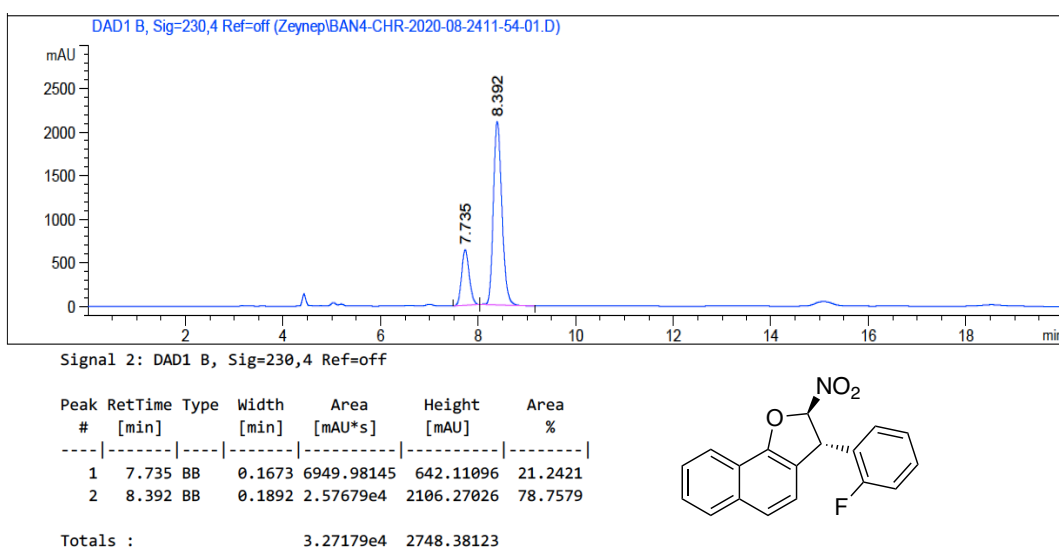


Figure B. 54. HPLC Chromatogram of enantiomerically enriched 60ad

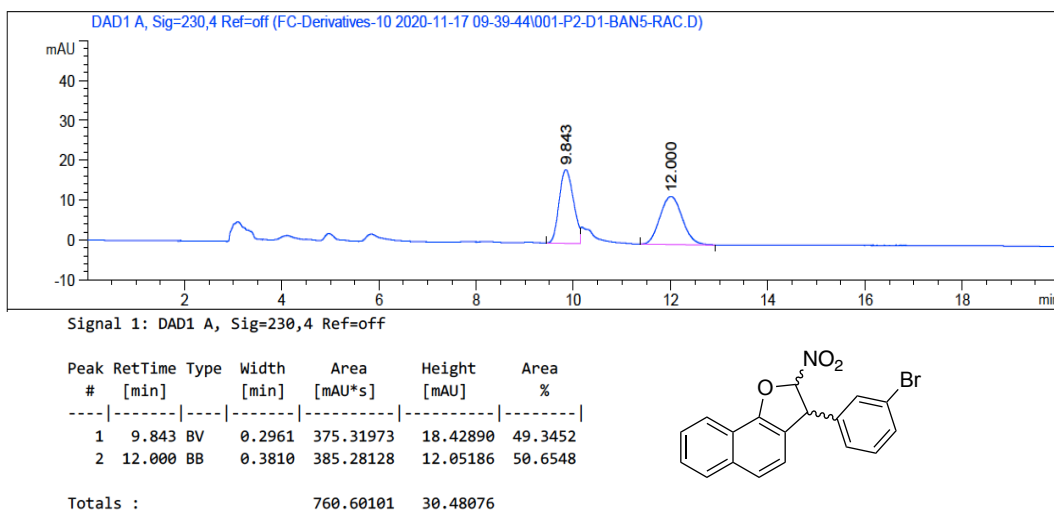


Figure B. 55. HPLC Chromatogram of *rac*-60ae

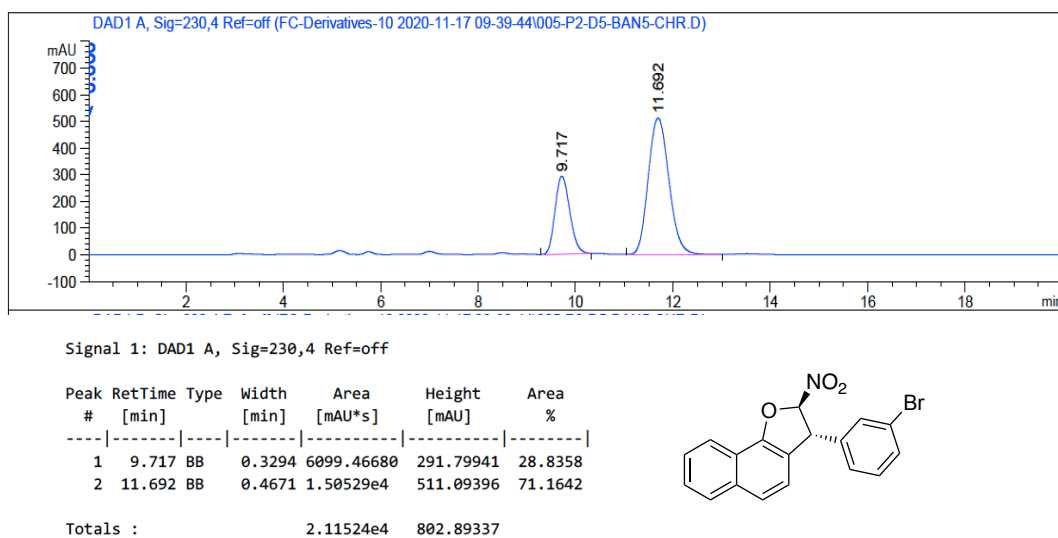
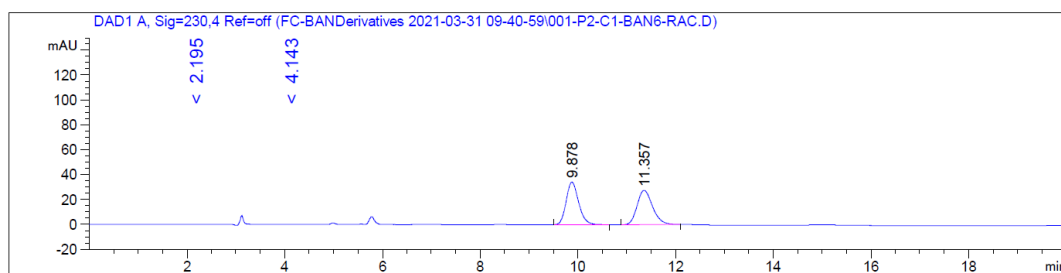


Figure B. 56. HPLC Chromatogram of enantiomerically enriched 60ae



Signal 1: DAD1 A, Sig=230,4 Ref=off

Peak #	RetTime [min]	Type	Width [min]	Area [mAU*s]	Height [mAU]	Area %
1	9.878	BB	0.2715	610.63129	34.24431	50.2428
2	11.357	BB	0.3281	604.72882	27.60069	49.7572

Totals : 1215.36011 61.84500

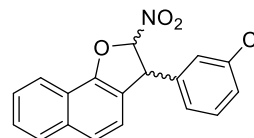
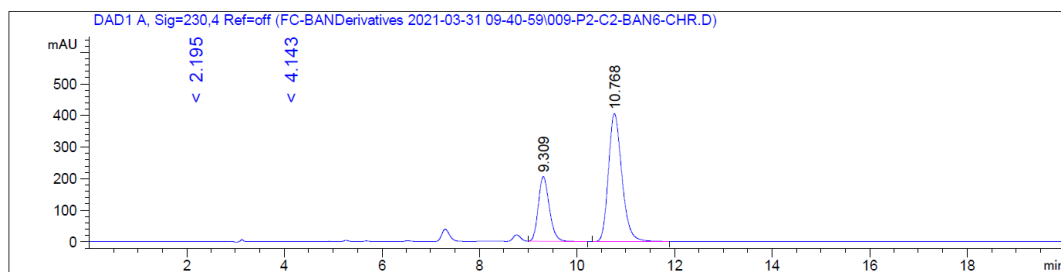


Figure B. 57. HPLC Chromatogram of *rac*-60af



Signal 1: DAD1 A, Sig=230,4 Ref=off

Peak #	RetTime [min]	Type	Width [min]	Area [mAU*s]	Height [mAU]	Area %
1	9.309	BB	0.2416	3217.16846	205.03041	29.2376
2	10.768	BB	0.2943	7786.36914	405.04269	70.7624

Totals : 1.10035e4 610.07310

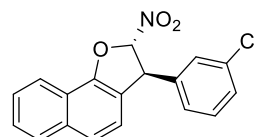
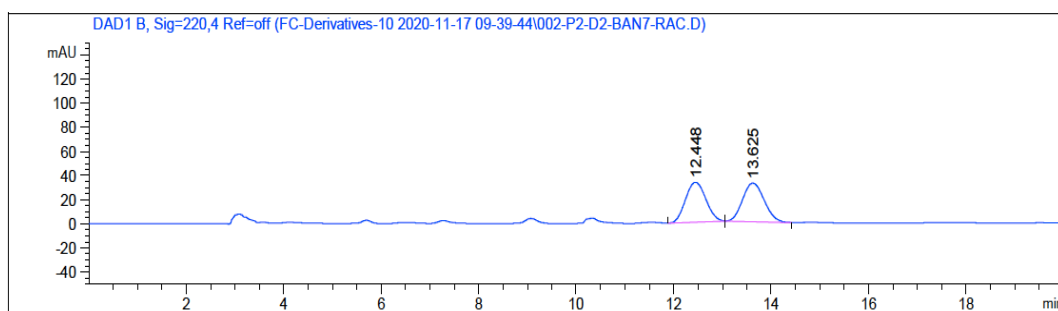
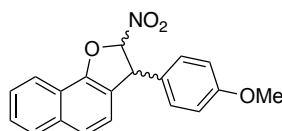


Figure B. 58. HPLC Chromatogram of enantiomerically enriched 60af



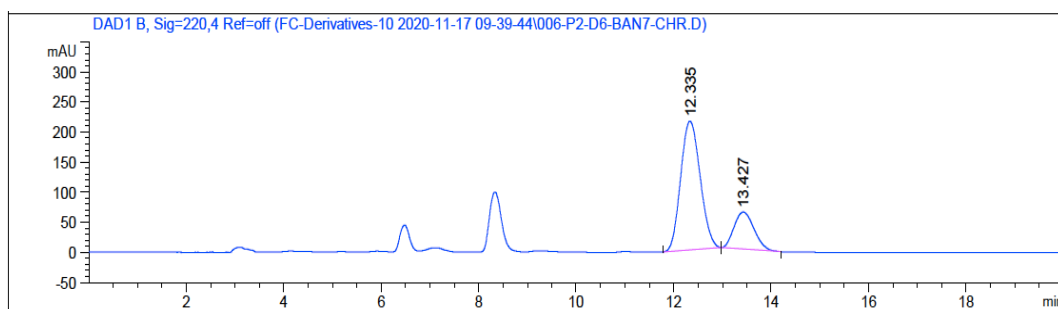
Signal 2: DAD1 B, Sig=220,4 Ref=off

Peak #	RetTime [min]	Type	Width [min]	Area [mAU*s]	Height [mAU]	Area %
1	12.448	BB	0.4308	958.39624	33.10403	49.4568
2	13.625	BB	0.4347	979.44794	31.94721	50.5432



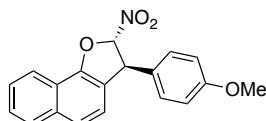
Totals : 1937.84418 65.05124

Figure B. 59. HPLC Chromatogram of *rac*-60ag



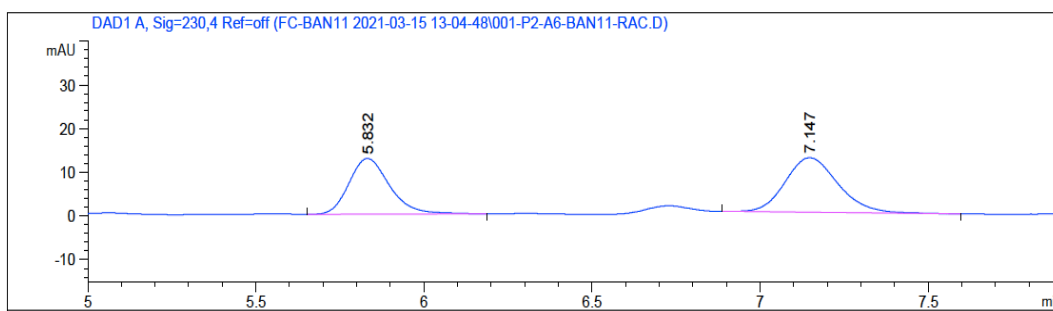
Signal 2: DAD1 B, Sig=220,4 Ref=off

Peak #	RetTime [min]	Type	Width [min]	Area [mAU*s]	Height [mAU]	Area %
1	12.335	BB	0.4390	5964.82764	214.46858	77.1381
2	13.427	BB	0.4364	1767.83167	61.67824	22.8619



Totals : 7732.65930 276.14682

Figure B. 60. HPLC Chromatogram of enantiomerically enriched 60ag



Signal 1: DAD1 A, Sig=230,4 Ref=off

Peak #	RetTime [min]	Type	Width [min]	Area [mAU*s]	Height [mAU]	Area %
1	5.832	BB	0.1281	107.09370	12.73930	43.8405
2	7.147	BB	0.1699	137.18663	12.51423	56.1595

Totals : 244.28033 25.25353

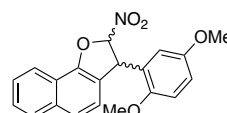
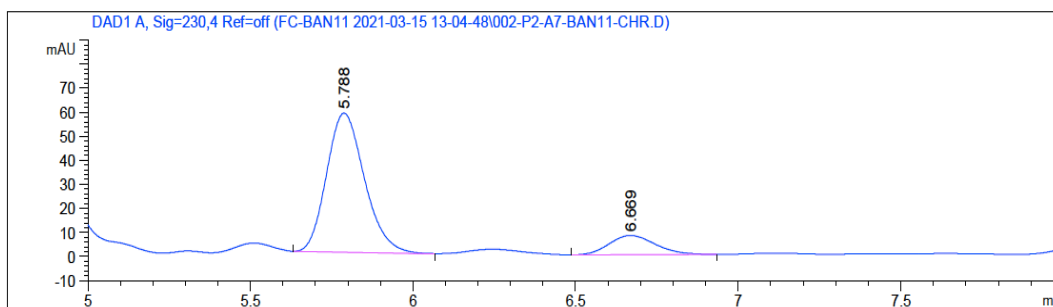


Figure B. 61. HPLC Chromatogram of *rac*-60ai



Signal 1: DAD1 A, Sig=230,4 Ref=off

Peak #	RetTime [min]	Type	Width [min]	Area [mAU*s]	Height [mAU]	Area %
1	5.788	BB	0.1249	468.25839	57.84938	85.5362
2	6.669	BB	0.1536	79.18076	8.02901	14.4638

Totals : 547.43915 65.87839

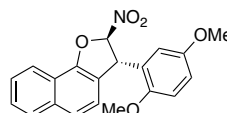
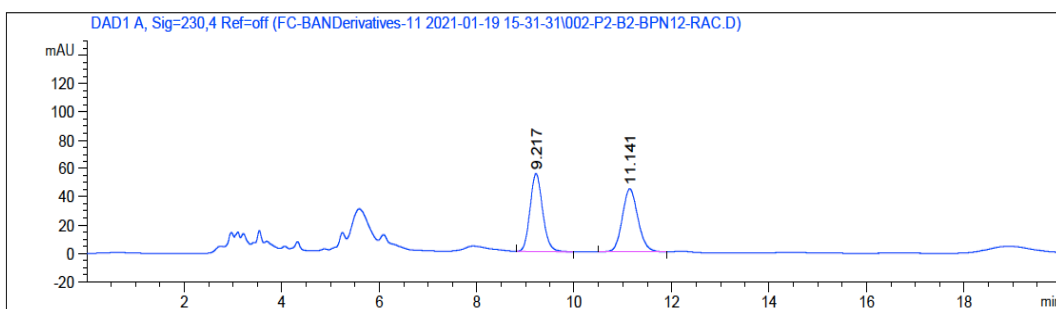
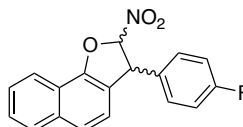


Figure B. 62. HPLC Chromatogram of enantiomerically enriched 60ai



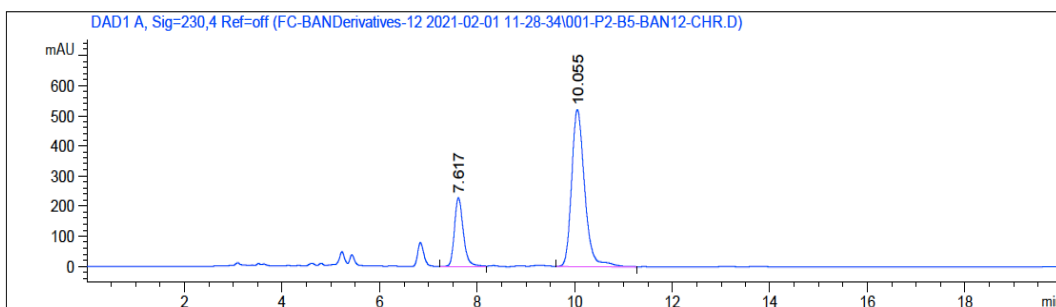
Signal 1: DAD1 A, Sig=230,4 Ref=off

Peak #	RetTime [min]	Type	Width [min]	Area [mAU*s]	Height [mAU]	Area %
1	9.217	BB	0.2758	988.29150	55.08474	49.8250
2	11.141	BB	0.3376	995.23395	44.47607	50.1750



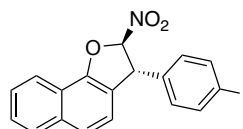
Totals : 1983.52545 99.56081

Figure B. 63. HPLC Chromatogram of *rac*-60aj



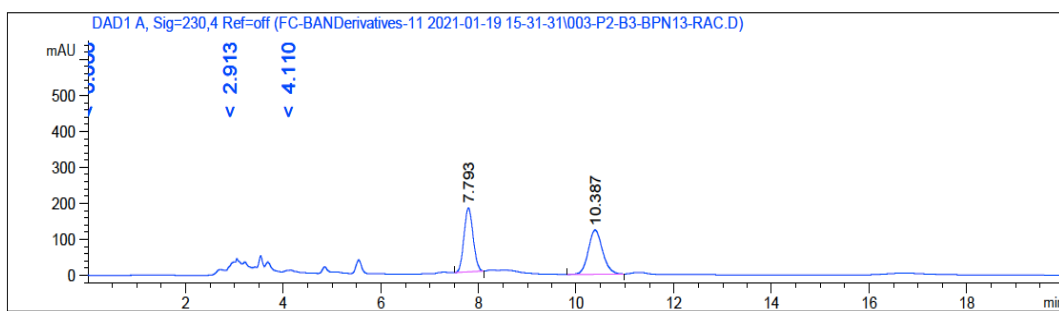
Signal 1: DAD1 A, Sig=230,4 Ref=off

Peak #	RetTime [min]	Type	Width [min]	Area [mAU*s]	Height [mAU]	Area %
1	7.617	BB	0.1925	2867.28809	228.31921	22.8689
2	10.055	BB	0.2835	9670.64746	519.98010	77.1311



Totals : 1.25379e4 748.29932

Figure B. 64. HPLC Chromatogram of enantiomerically enriched 60aj



Peak #	RetTime [min]	Type	Width [min]	Area [mAU*s]	Height [mAU]	Area %
1	7.793	BB	0.2025	2314.80347	178.21861	48.3277
2	10.387	BB	0.3111	2474.99902	122.84268	51.6723

Totals : 4789.80249 301.06129

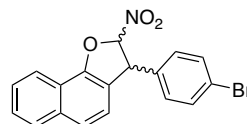
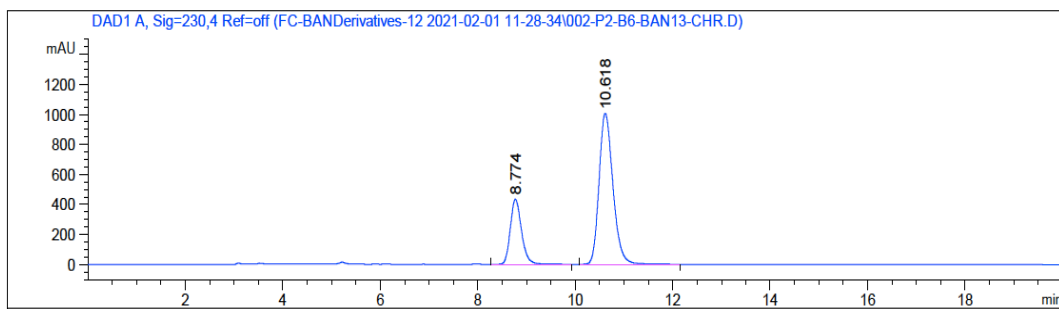


Figure B. 65. HPLC Chromatogram of *rac*-60ak



Peak #	RetTime [min]	Type	Width [min]	Area [mAU*s]	Height [mAU]	Area %
1	8.774	BB	0.2475	6943.76514	433.25980	25.8391
2	10.618	BB	0.3056	1.99294e4	1006.05664	74.1609

Totals : 2.68731e4 1439.31644

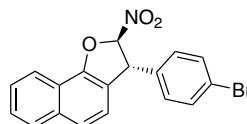
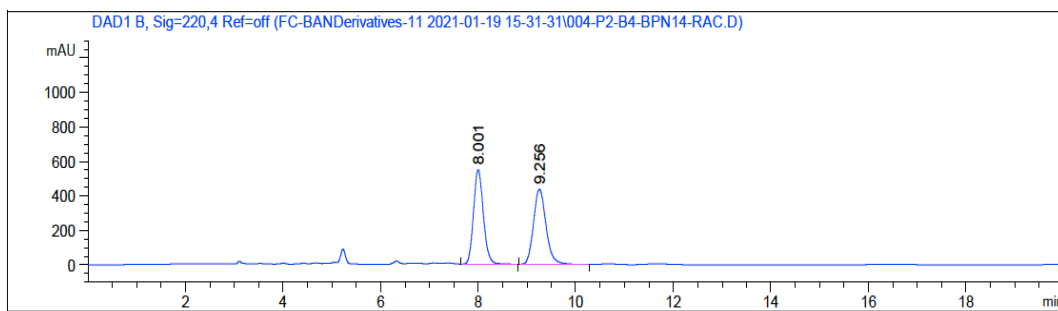
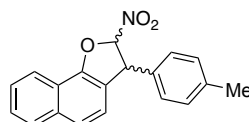


Figure B. 66. HPLC Chromatogram of enantiomerically enriched 60ak



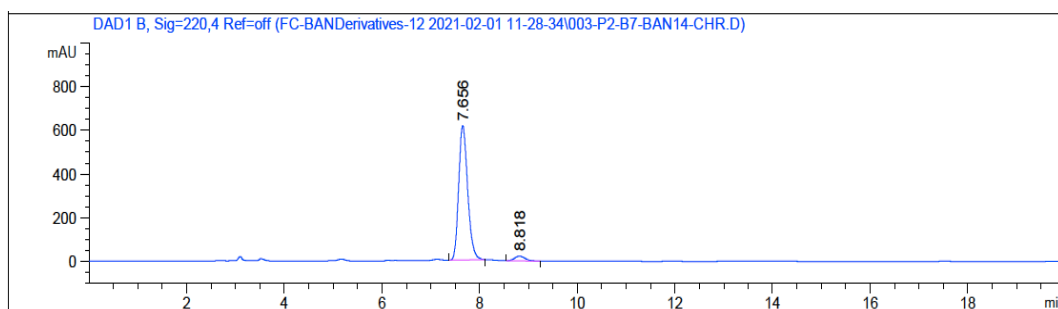
Signal 2: DAD1 B, Sig=220,4 Ref=off

Peak #	RetTime [min]	Type	Width [min]	Area [mAU*s]	Height [mAU]	Area %
1	8.001	BB	0.2172	7724.16748	548.84528	49.7023
2	9.256	BB	0.2738	7816.70313	437.71967	50.2977



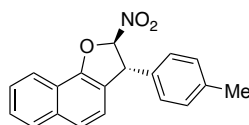
Totals : 1.55409e4 986.56494

Figure B. 67. HPLC Chromatogram of *rac*-60al



Signal 2: DAD1 B, Sig=220,4 Ref=off

Peak #	RetTime [min]	Type	Width [min]	Area [mAU*s]	Height [mAU]	Area %
1	7.656	BB	0.1978	7858.03760	614.18860	96.0137
2	8.818	BB	0.2280	326.24658	21.81530	3.9863



Totals : 8184.28418 636.00389

Figure B. 68. HPLC Chromatogram of enantiomerically enriched 60al

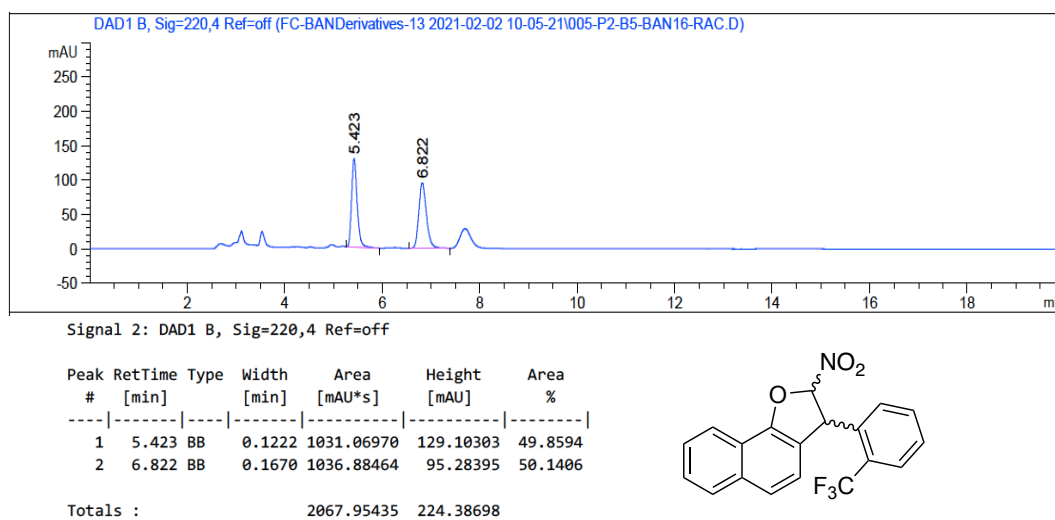


Figure B. 69. HPLC Chromatogram of *rac*-60an

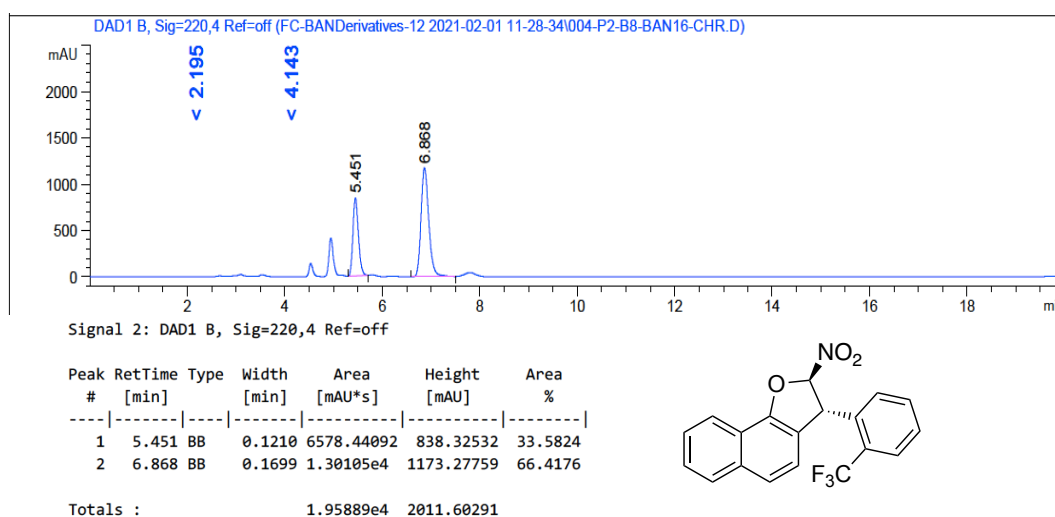


Figure B. 70. HPLC Chromatogram of enantiomerically enriched 60an

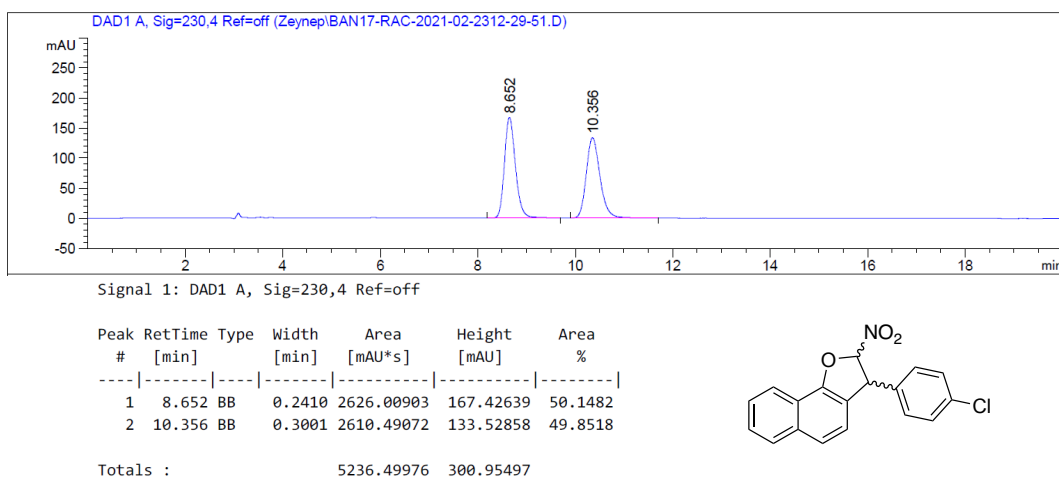


Figure B. 71. HPLC Chromatogram of *rac*-60ao

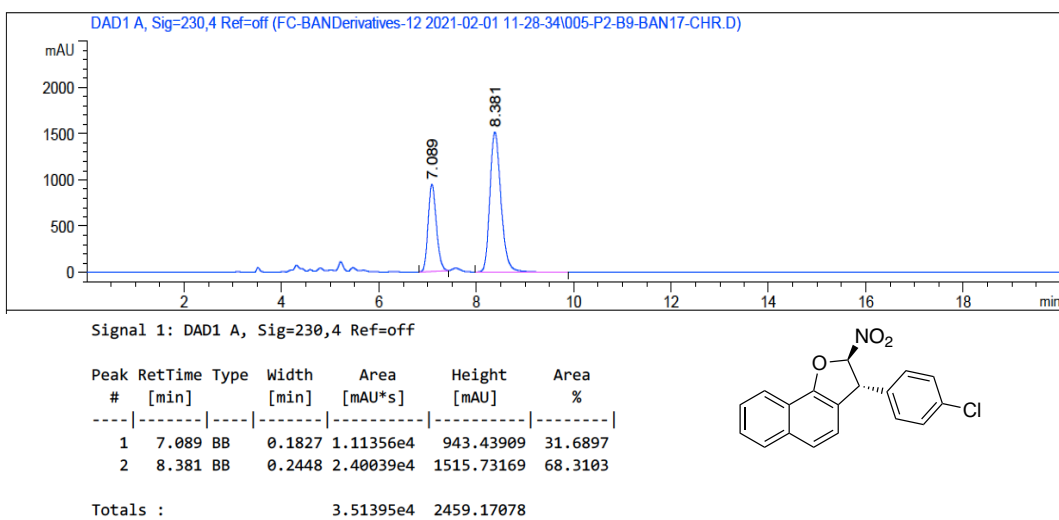


Figure B. 72. HPLC Chromatogram of enantiomerically enriched 60ao

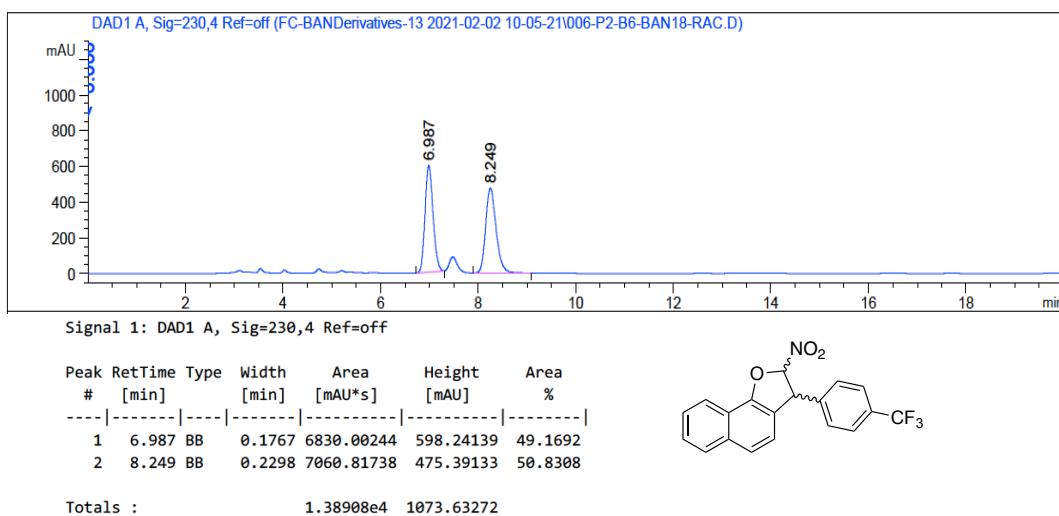


Figure B. 73. HPLC Chromatogram of *rac*-60ap

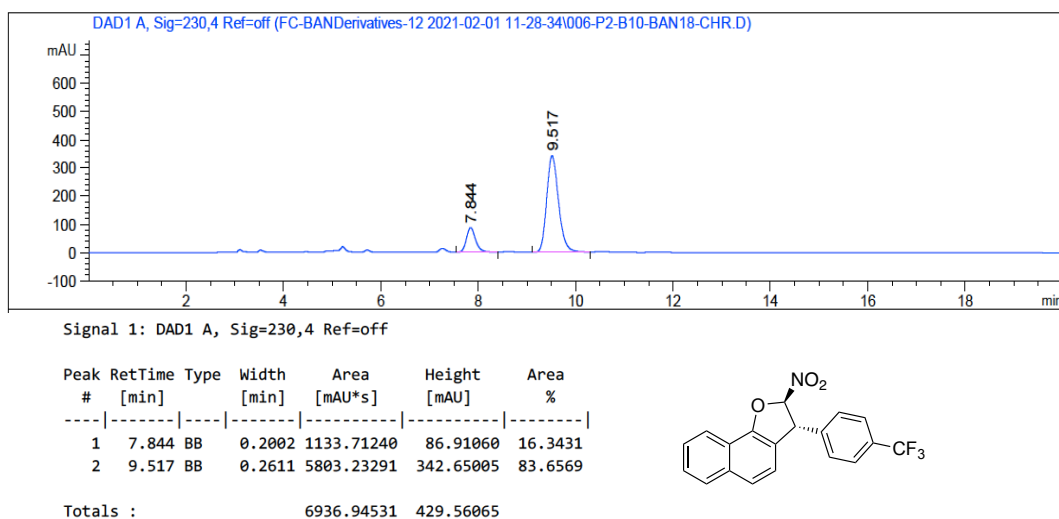


Figure B. 74. HPLC Chromatogram of enantiomerically enriched 60ap

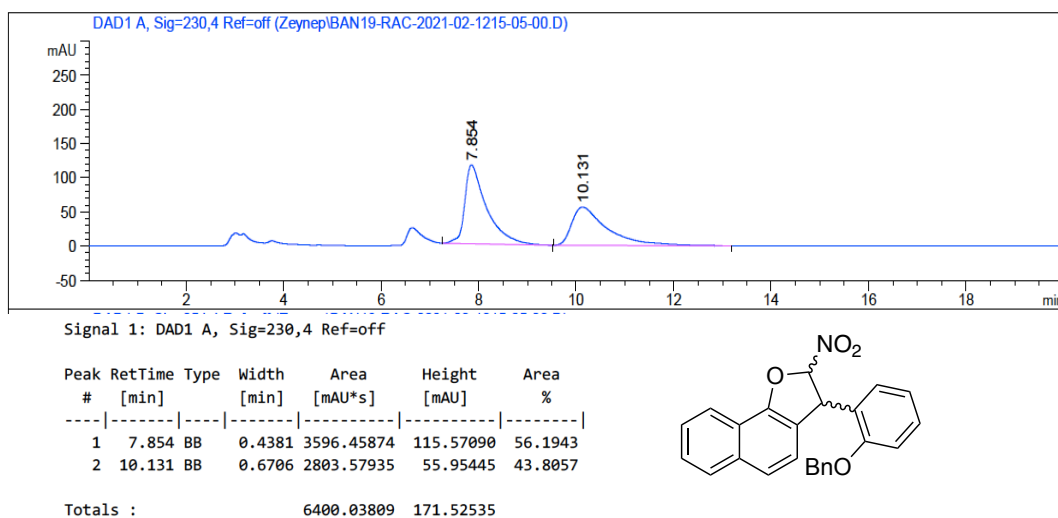


Figure B. 75. HPLC Chromatogram of *rac*-60aq

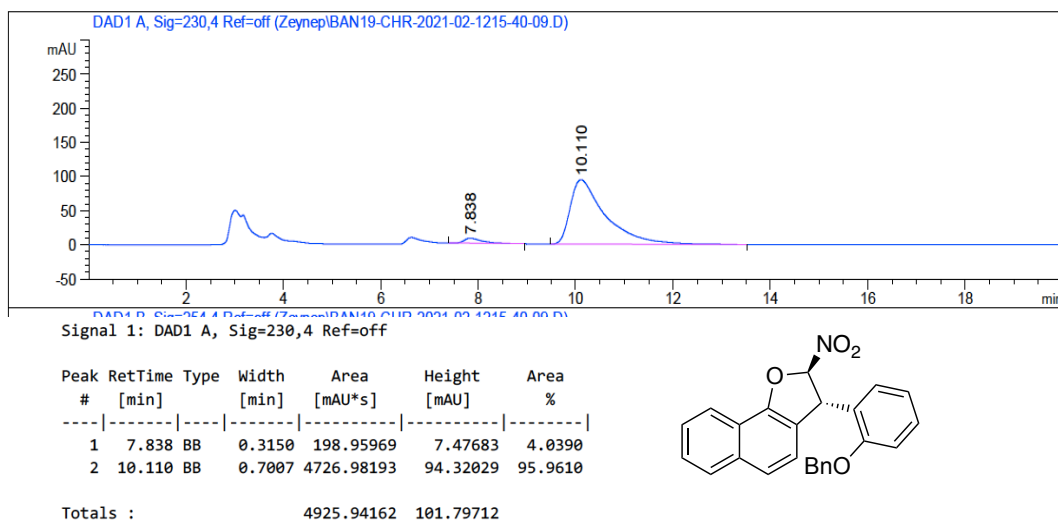


Figure B. 76. HPLC Chromatogram of enantiomerically enriched 60aq

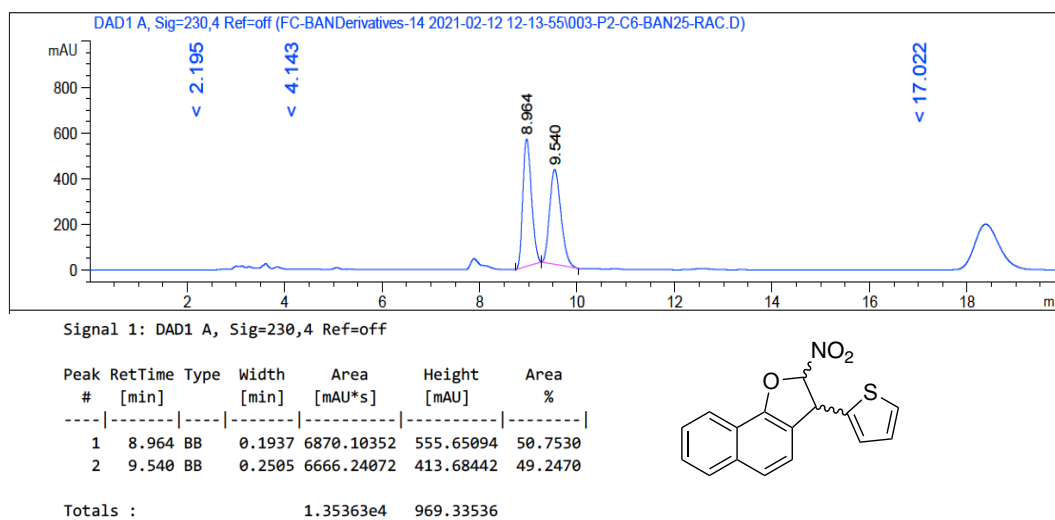


Figure B. 77. HPLC Chromatogram of *rac*-60at

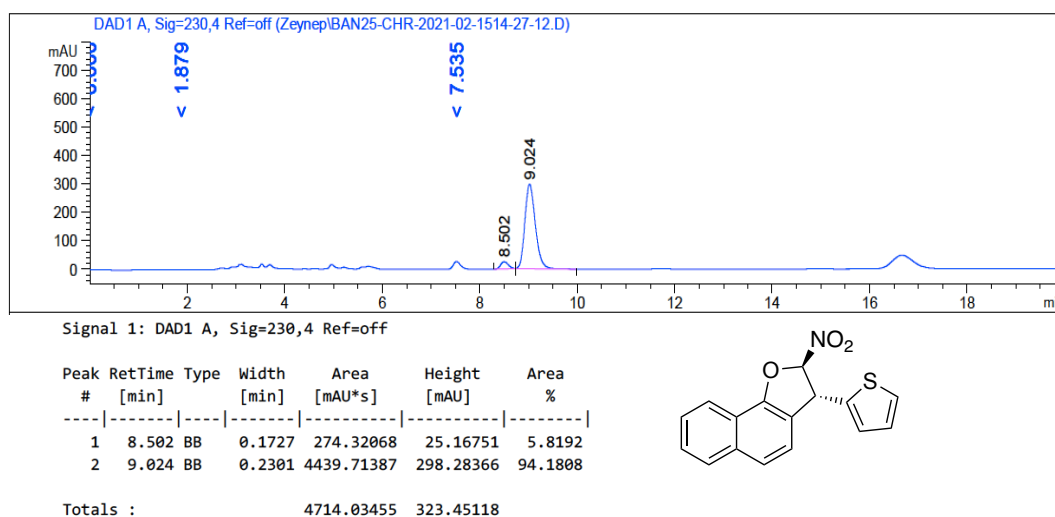


Figure B. 78. HPLC Chromatogram of enantiomerically enriched 60at

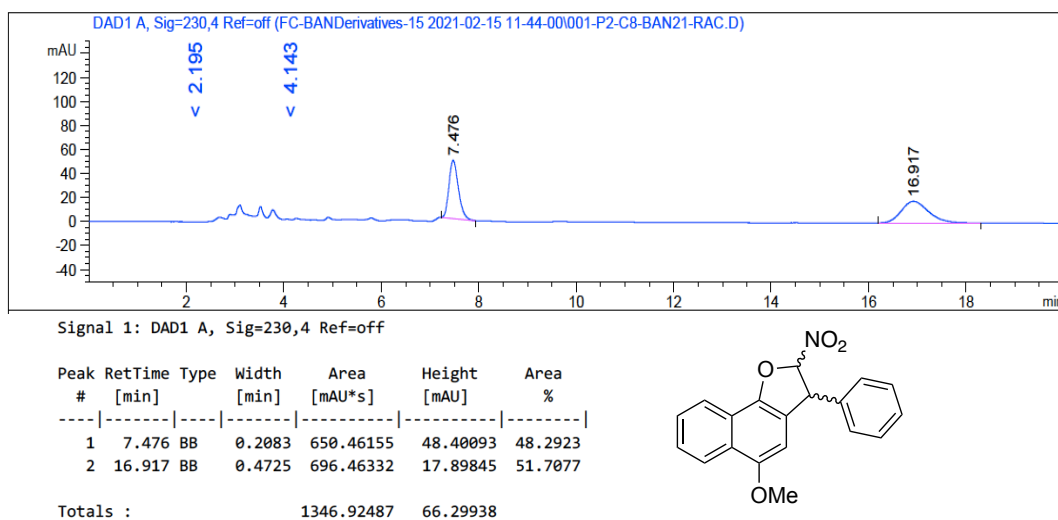


Figure B. 79. HPLC Chromatogram of *rac*-60ba

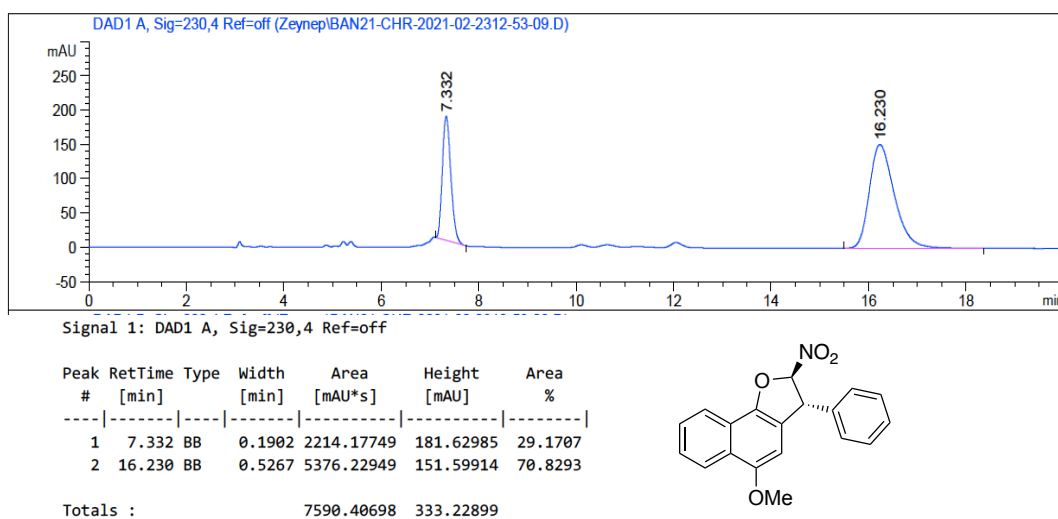


Figure B. 80. HPLC Chromatogram of enantiomerically enriched 60ba

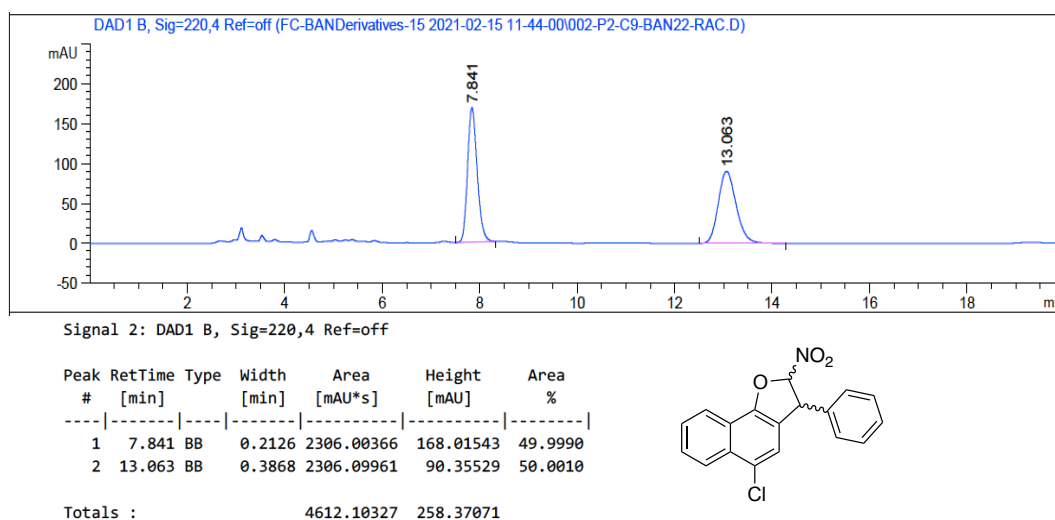


Figure B. 81. HPLC Chromatogram of *rac*-60ca

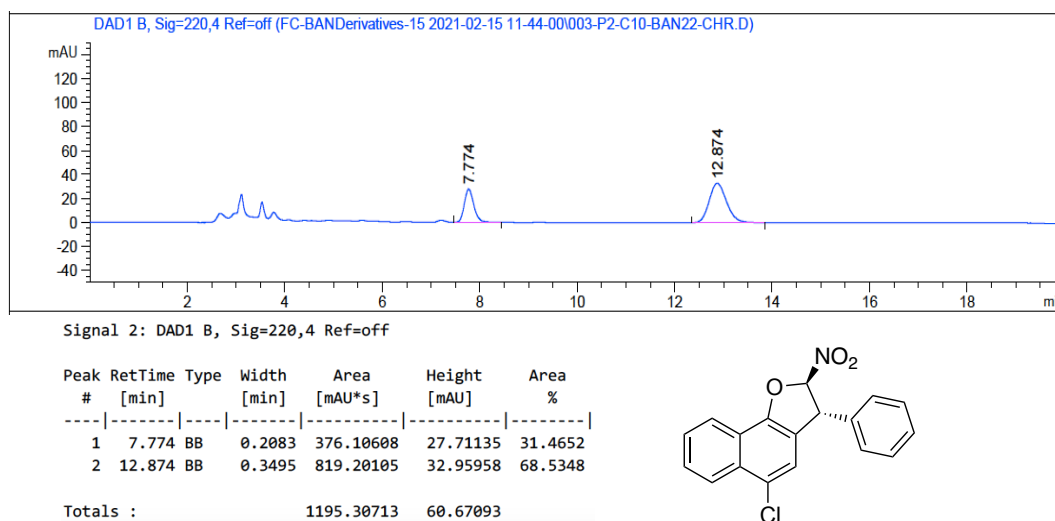
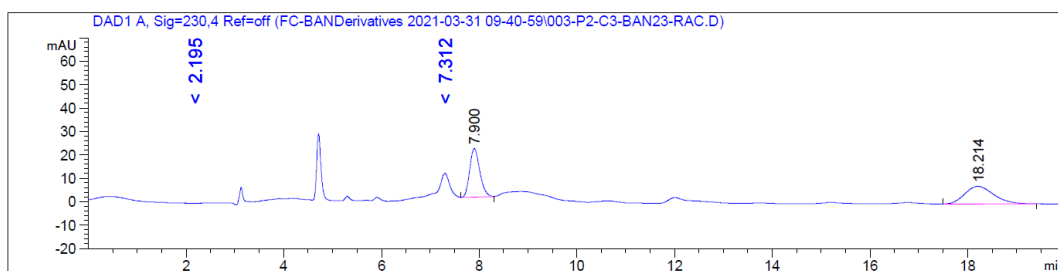


Figure B. 82. HPLC Chromatogram of enantiomerically enriched 60ca



Signal 1: DAD1 A, Sig=230,4 Ref=off

Peak #	RetTime [min]	Type	Width [min]	Area [mAU*s]	Height [mAU]	Area %
1	7.900	BB	0.2198	295.81659	20.63182	48.4999
2	18.214	BB	0.4873	314.11606	7.56765	51.5001

Totals : 609.93265 28.19947

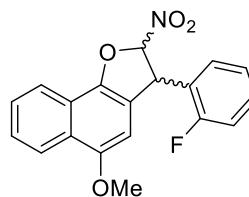
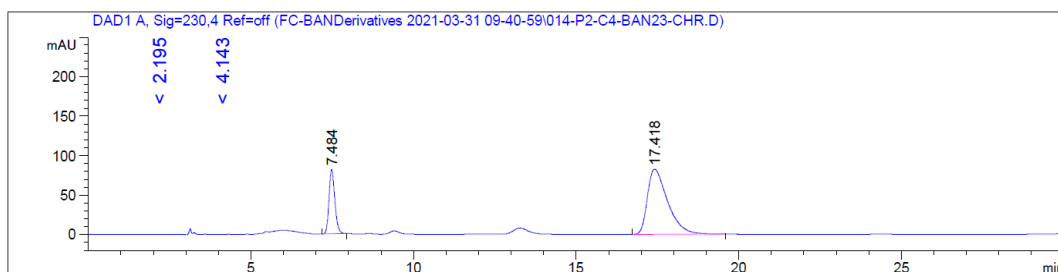


Figure B. 83. HPLC Chromatogram of *rac*-60bd



Signal 1: DAD1 A, Sig=230,4 Ref=off

Peak #	RetTime [min]	Type	Width [min]	Area [mAU*s]	Height [mAU]	Area %
1	7.484	BB	0.1923	1012.28729	81.30235	22.2135
2	17.418	BB	0.6118	3544.79102	82.32577	77.7865

Totals : 4557.07831 163.62812

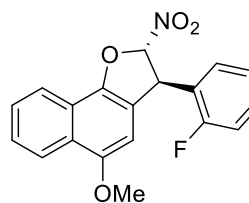
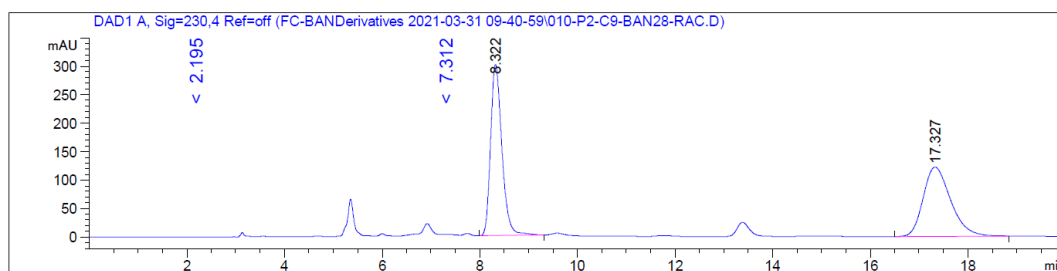


Figure B. 84. HPLC Chromatogram of enantiomerically enriched 60bd



Signal 1: DAD1 A, Sig=230,4 Ref=off

Peak #	RetTime [min]	Type	Width [min]	Area [mAU*s]	Height [mAU]	Area %
1	8.322	BB	0.2467	4853.46533	300.83029	50.5886
2	17.327	BB	0.5659	4740.51563	121.57528	49.4114

Totals : 9593.98096 422.40557

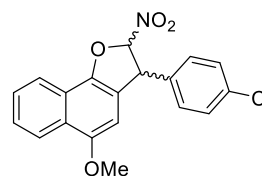
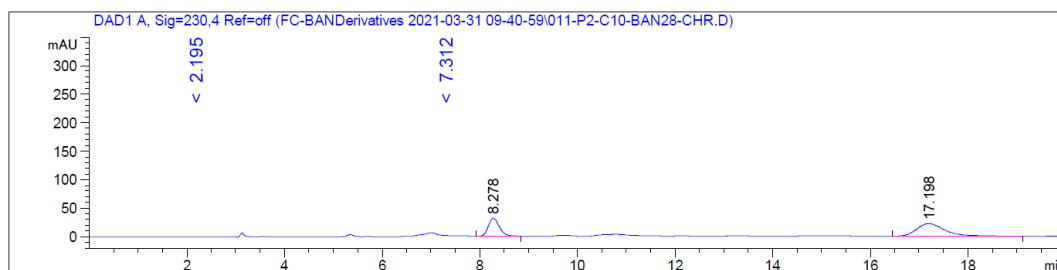


Figure B. 85. HPLC Chromatogram of *rac*-60bo



Signal 1: DAD1 A, Sig=230,4 Ref=off

Peak #	RetTime [min]	Type	Width [min]	Area [mAU*s]	Height [mAU]	Area %
1	8.278	BB	0.2428	497.23761	31.65311	35.1733
2	17.198	BB	0.4989	916.44342	22.23352	64.8267

Totals : 1413.68103 53.88663

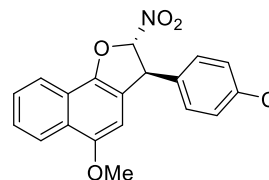
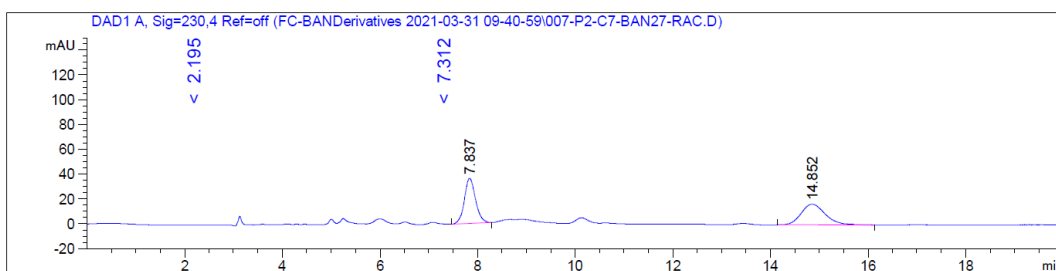


Figure B. 86. HPLC Chromatogram of enantiomerically enriched 60bo



Signal 1: DAD1 A, Sig=230,4 Ref=off

Peak #	RetTime [min]	Type	Width [min]	Area [mAU*s]	Height [mAU]	Area %
1	7.837	BB	0.2396	577.73303	36.51975	50.1613
2	14.852	BB	0.4128	574.01794	16.75250	49.8387

Totals : 1151.75098 53.27225

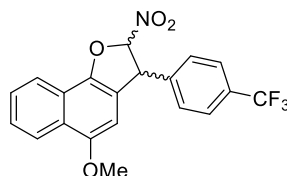
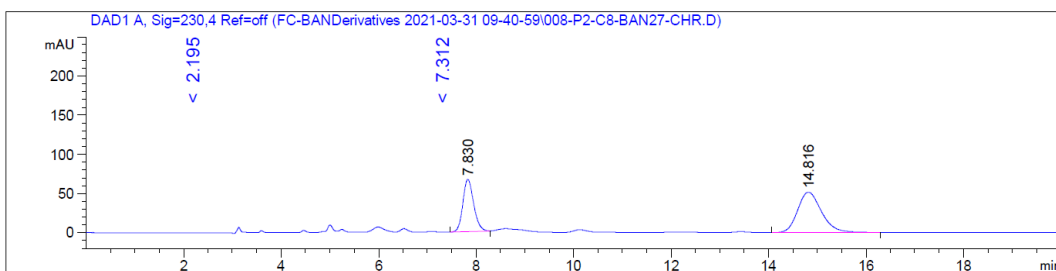


Figure B. 87. HPLC Chromatogram of *rac*-60bp



Signal 1: DAD1 A, Sig=230,4 Ref=off

Peak #	RetTime [min]	Type	Width [min]	Area [mAU*s]	Height [mAU]	Area %
1	7.830	BB	0.2355	1024.18689	66.74113	37.0607
2	14.816	BB	0.4994	1739.34924	51.44859	62.9393

Totals : 2763.53613 118.18972

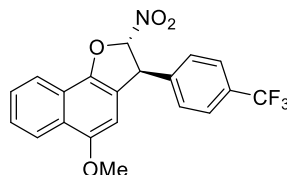
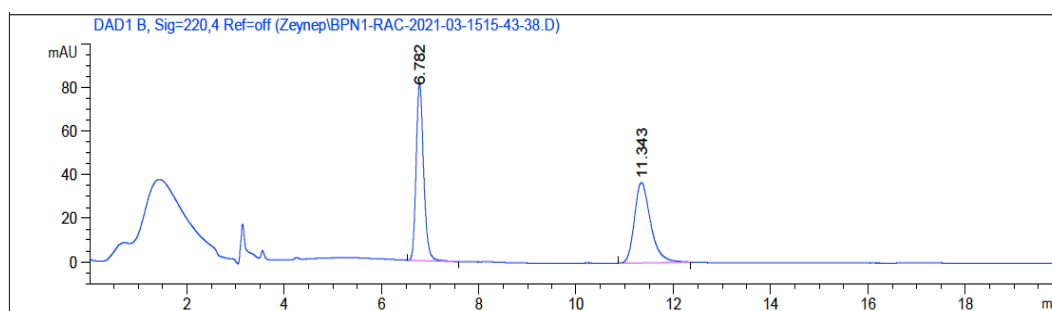


Figure B. 88. HPLC Chromatogram of enantiomerically enriched 60bp



Signal 2: DAD1 B, Sig=220,4 Ref=off

Peak #	RetTime [min]	Type	Width [min]	Area [mAU*s]	Height [mAU]	Area %
1	6.782	BB	0.1621	868.26794	81.62653	50.6133
2	11.343	BB	0.3424	847.22534	36.76473	49.3867

Totals : 1715.49329 118.39126

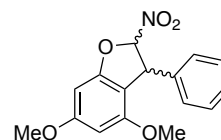
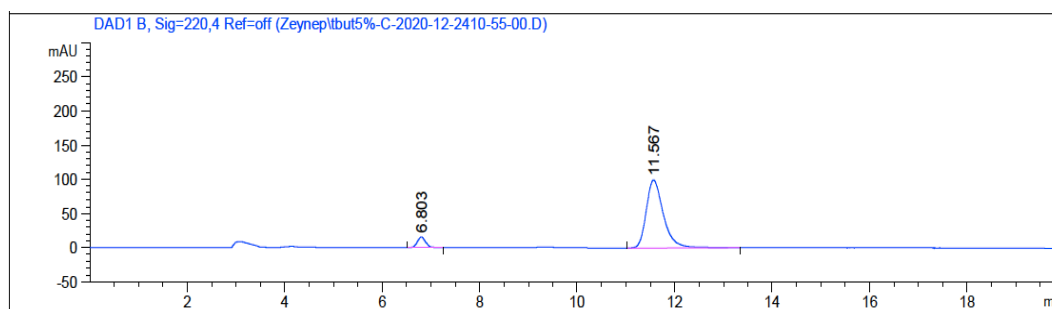


Figure B. 89. HPLC Chromatogram of *rac*-62ba



Signal 2: DAD1 B, Sig=220,4 Ref=off

Peak #	RetTime [min]	Type	Width [min]	Area [mAU*s]	Height [mAU]	Area %
1	6.803	BB	0.1851	187.36650	15.59834	7.1463
2	11.567	BB	0.3700	2434.48633	99.32394	92.8537

Totals : 2621.85283 114.92228

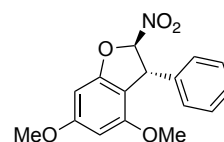


Figure B. 90. HPLC Chromatogram of enantiomerically enriched 62ba

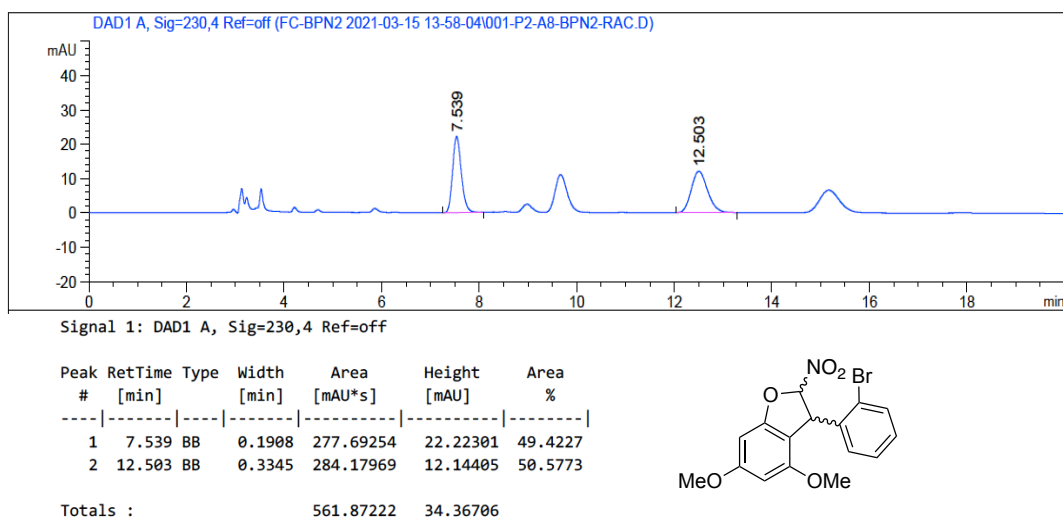


Figure B. 91. HPLC Chromatogram of *rac*-62bb

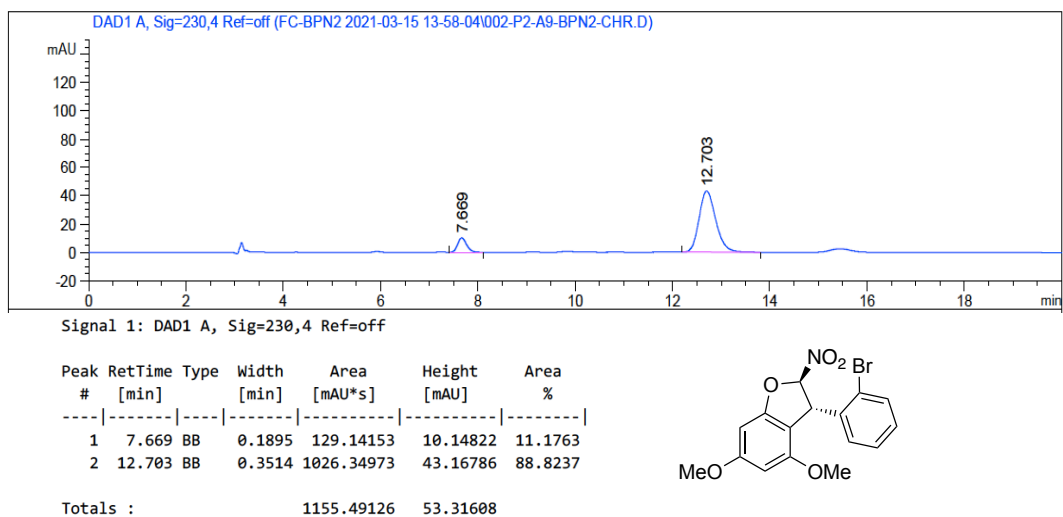
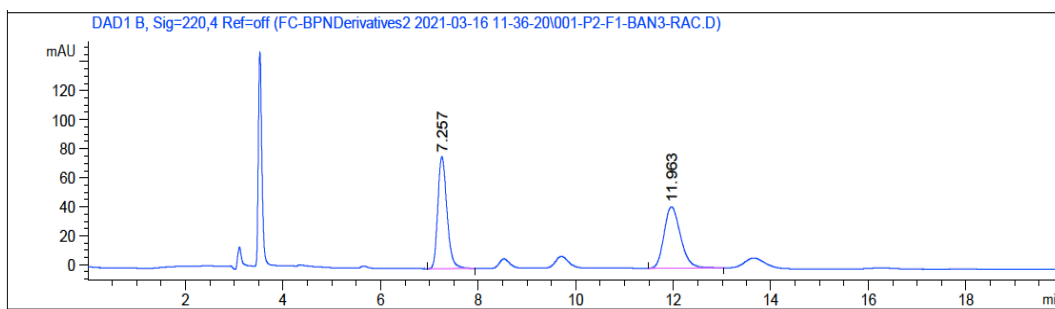


Figure B. 92. HPLC Chromatogram of enantiomerically enriched 62bb



Signal 2: DAD1 B, Sig=220,4 Ref=off

Peak #	RetTime [min]	Type	Width [min]	Area [mAU*s]	Height [mAU]	Area %
1	7.257	BB	0.2023	1002.45917	77.28426	50.3909
2	11.963	BB	0.3508	986.90698	42.28127	49.6091

Totals : 1989.36615 119.56553

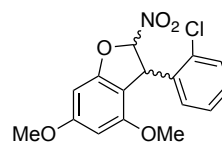
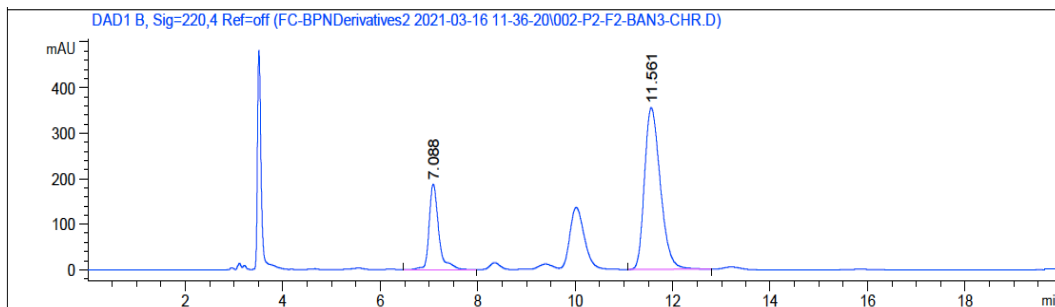


Figure B. 93. HPLC Chromatogram of *rac*-62bc



Signal 2: DAD1 B, Sig=220,4 Ref=off

Peak #	RetTime [min]	Type	Width [min]	Area [mAU*s]	Height [mAU]	Area %
1	7.088	BB	0.2060	2547.66724	187.52373	24.1239
2	11.561	BB	0.3510	8013.10156	354.74139	75.8761

Totals : 1.05608e4 542.26512

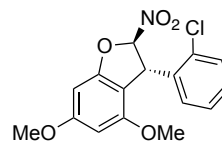


Figure B. 94. HPLC Chromatogram of enantiomerically enriched 62bc

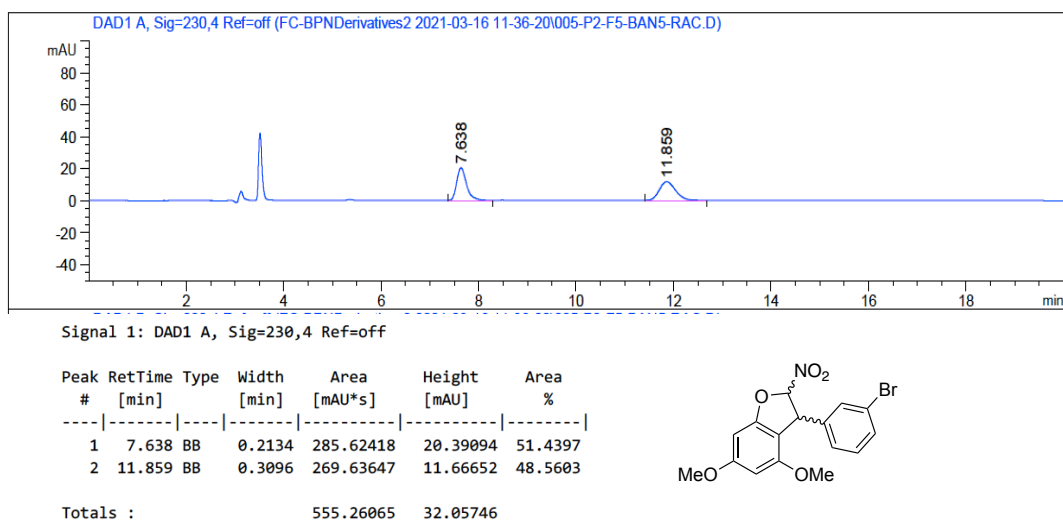


Figure B. 95. HPLC Chromatogram of *rac*-62be

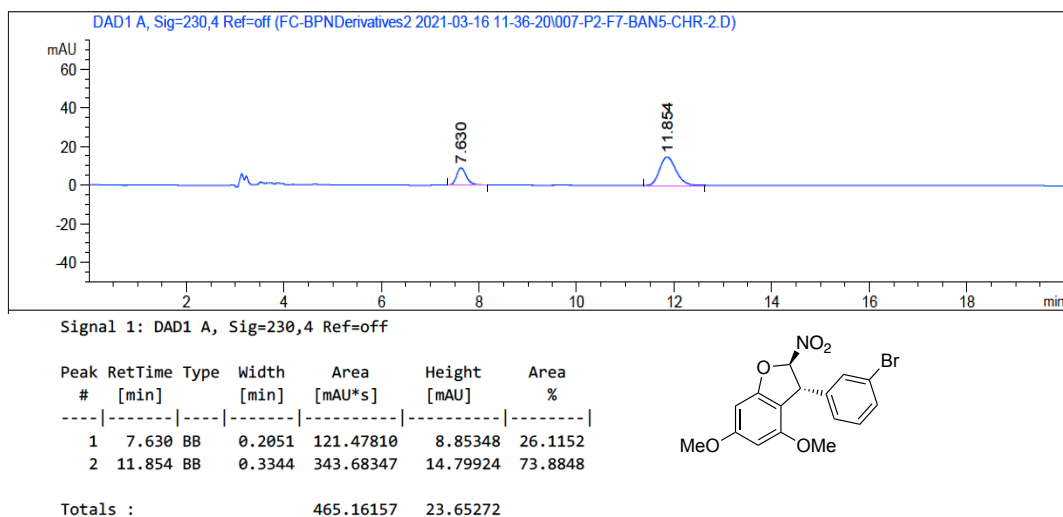


Figure B. 96. HPLC Chromatogram of enantiomerically enriched 62be

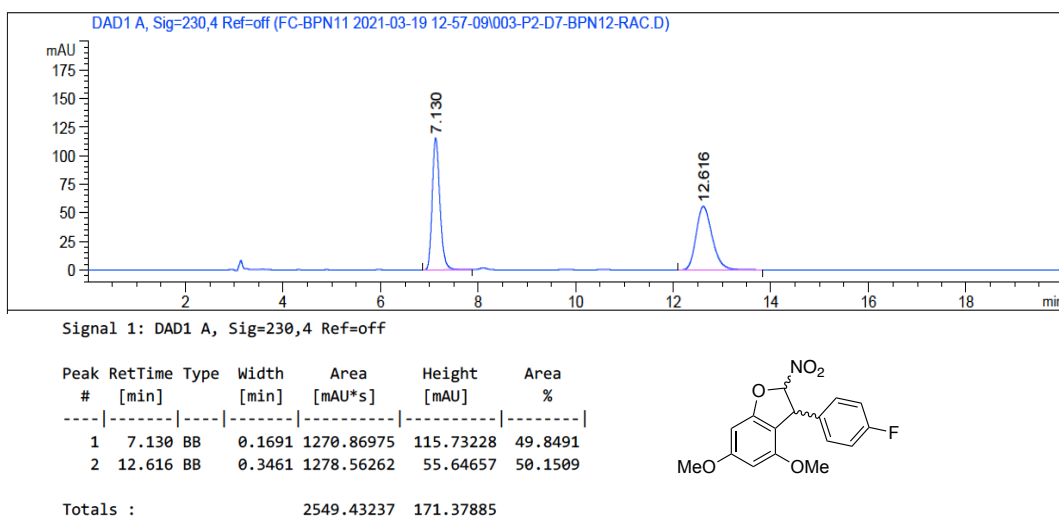


Figure B. 97. HPLC Chromatogram of *rac*-62bj

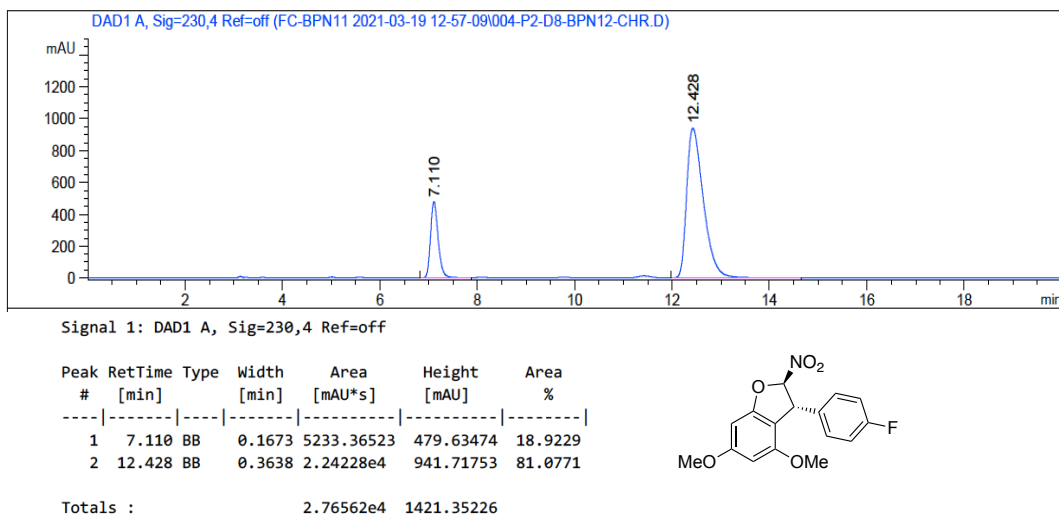


Figure B. 98. HPLC Chromatogram of enantiomerically enriched 62bj

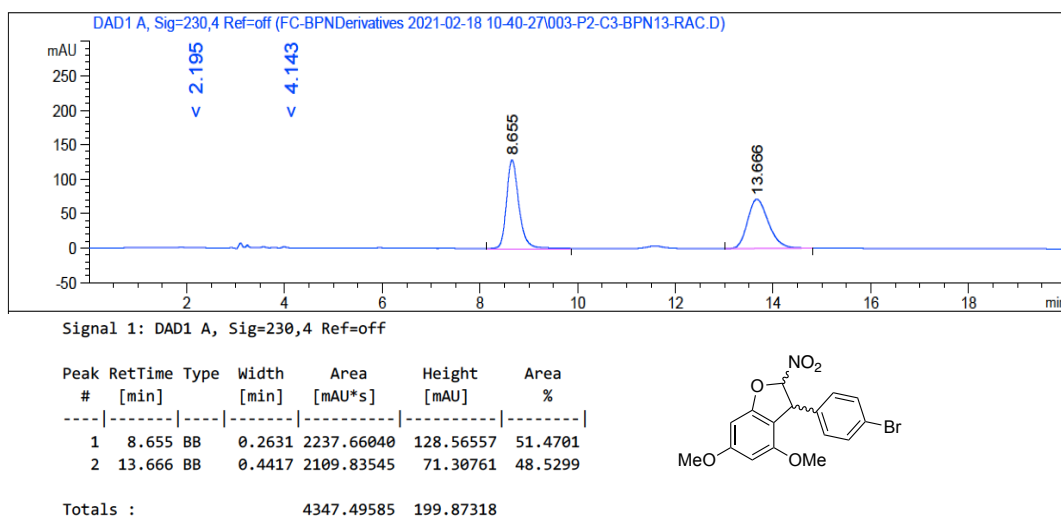


Figure B. 99. HPLC Chromatogram of *rac*-62bk

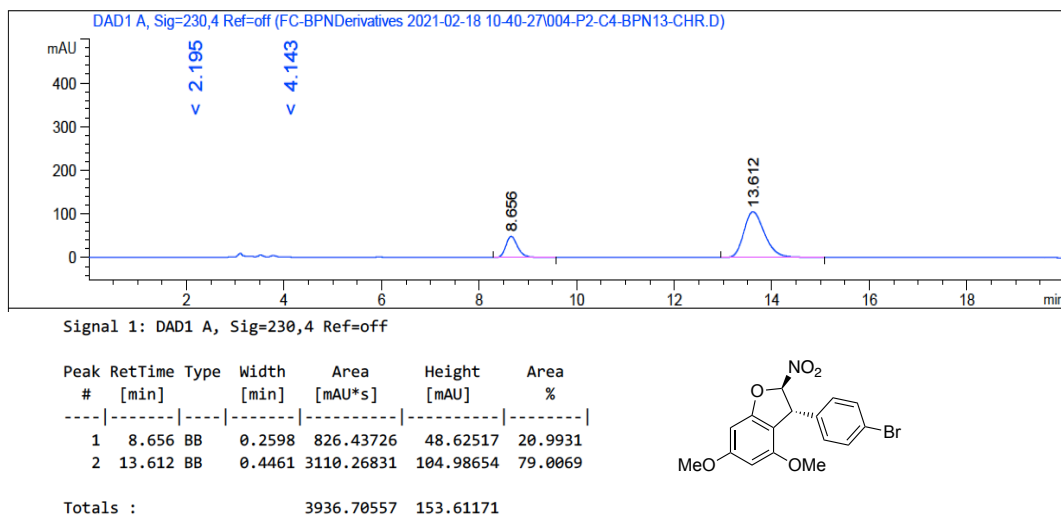
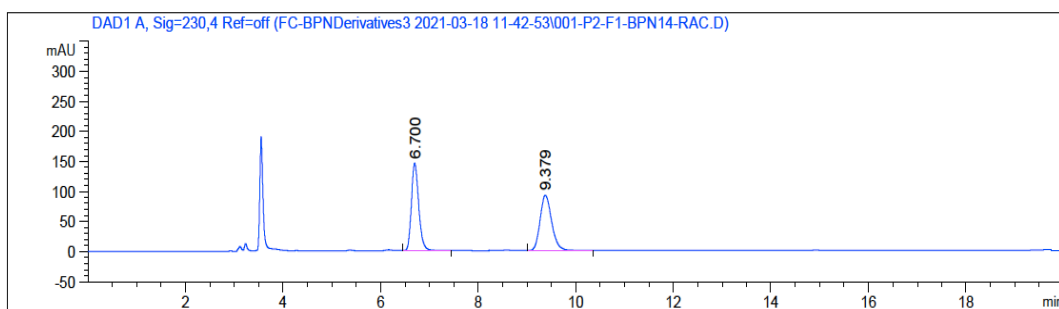


Figure B. 100. HPLC Chromatogram of enantiomerically enriched 62bk



Signal 1: DAD1 A, Sig=230,4 Ref=off

Peak #	RetTime [min]	Type	Width [min]	Area [mAU*s]	Height [mAU]	Area %
1	6.700	BB	0.1601	1520.83167	145.86447	49.8240
2	9.379	BB	0.2550	1531.57483	92.35042	50.1760

Totals : 3052.40649 238.21489

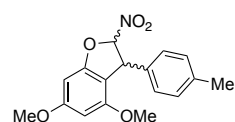
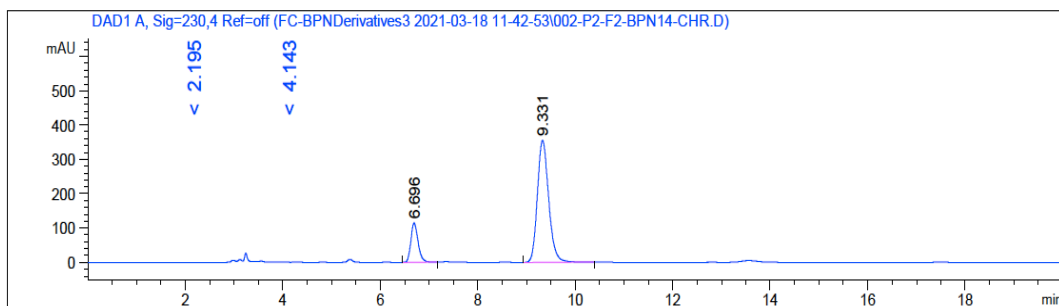


Figure B. 101. HPLC Chromatogram of *rac*-62bl



Signal 1: DAD1 A, Sig=230,4 Ref=off

Peak #	RetTime [min]	Type	Width [min]	Area [mAU*s]	Height [mAU]	Area %
1	6.696	BB	0.1575	1174.40479	114.61213	17.0151
2	9.331	BB	0.2490	5727.74219	355.49948	82.9849

Totals : 6902.14697 470.11161

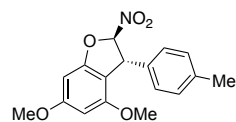


Figure B. 102. HPLC Chromatogram of enantiomerically enriched 62bl

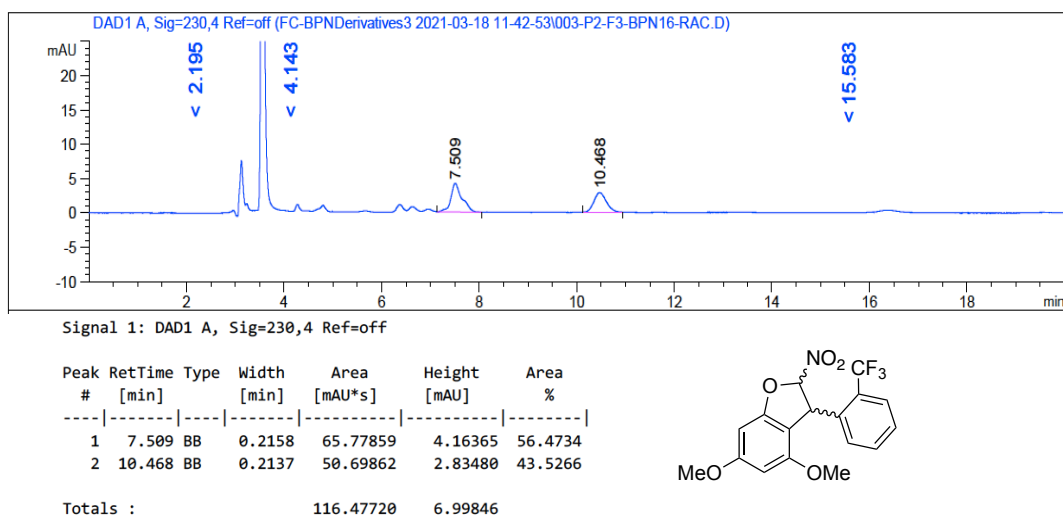


Figure B. 103. HPLC Chromatogram of *rac*-62bn

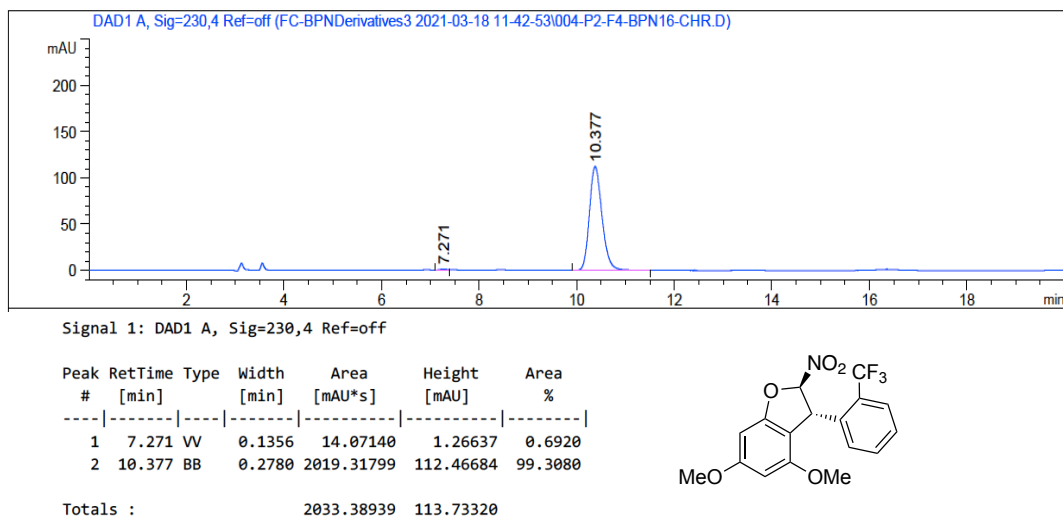
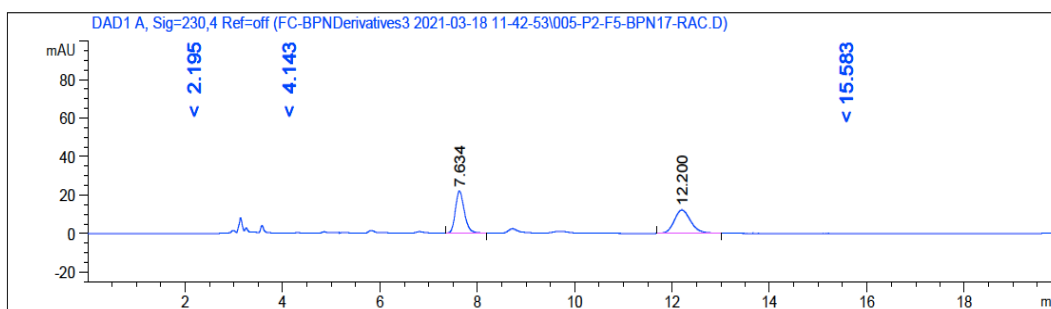


Figure B. 104. HPLC Chromatogram of enantiomerically enriched 62bn



Signal 1: DAD1 A, Sig=230,4 Ref=off

Peak #	RetTime [min]	Type	Width [min]	Area [mAU*s]	Height [mAU]	Area %
1	7.634	BB	0.1949	277.39871	21.80475	49.6951
2	12.200	BB	0.3265	280.80316	12.11201	50.3049

Totals : 558.20187 33.91676

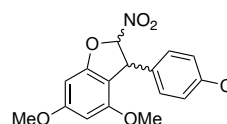
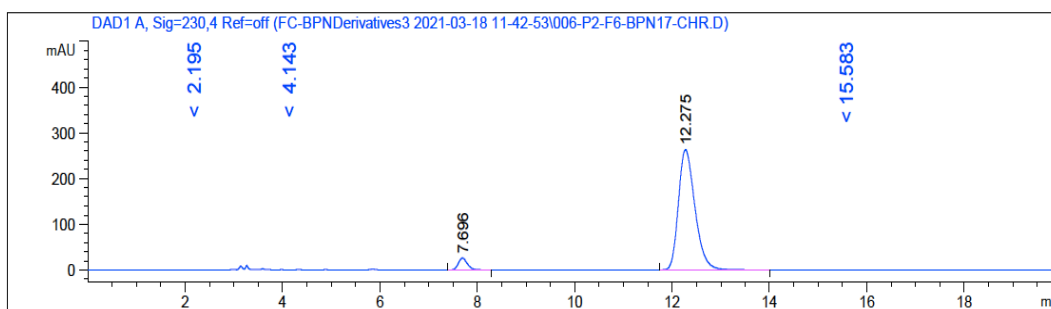


Figure B. 105. HPLC Chromatogram of *rac*-62bo



Signal 1: DAD1 A, Sig=230,4 Ref=off

Peak #	RetTime [min]	Type	Width [min]	Area [mAU*s]	Height [mAU]	Area %
1	7.696	BB	0.1983	340.15976	26.05102	5.1930
2	12.275	BB	0.3621	6210.17041	262.91376	94.8070

Totals : 6550.33017 288.96478

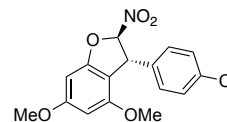
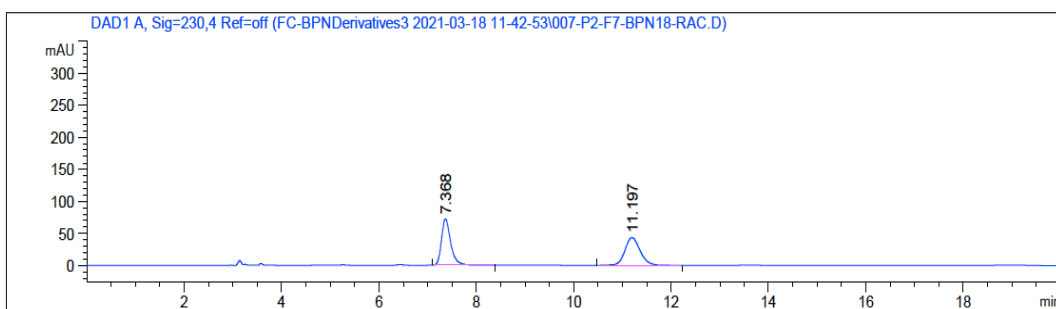
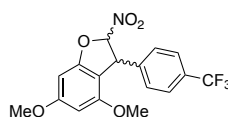


Figure B. 106. HPLC Chromatogram of enantiomerically enriched 62bo



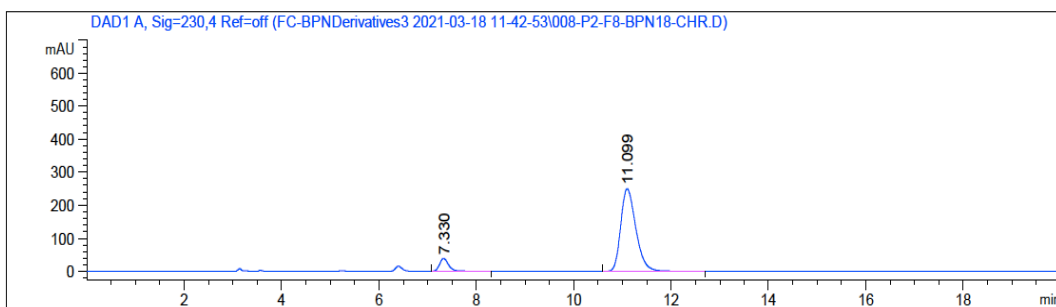
Signal 1: DAD1 A, Sig=230,4 Ref=off

Peak #	RetTime [min]	Type	Width [min]	Area [mAU*s]	Height [mAU]	Area %
1	7.368	BB	0.1998	956.61566	72.31126	50.1208
2	11.197	BB	0.3263	952.00629	43.41694	49.8792



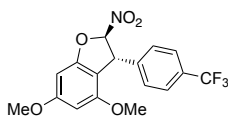
Totals : 1908.62195 115.72821

Figure B. 107. HPLC Chromatogram of *rac*-62bp



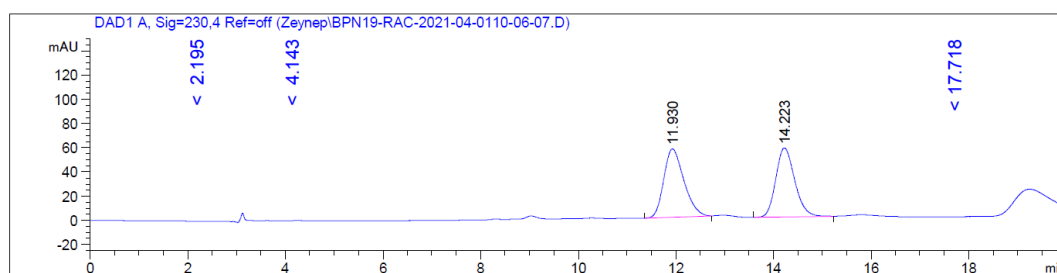
Signal 1: DAD1 A, Sig=230,4 Ref=off

Peak #	RetTime [min]	Type	Width [min]	Area [mAU*s]	Height [mAU]	Area %
1	7.330	BB	0.1946	487.95377	38.31649	8.3015
2	11.099	BB	0.3307	5389.96924	249.87657	91.6985



Totals : 5877.92300 288.19306

Figure B. 108. HPLC Chromatogram of enantiomerically enriched 62bp



Signal 1: DAD1 A, Sig=230,4 Ref=off

Peak #	RetTime [min]	Type	Width [min]	Area [mAU*s]	Height [mAU]	Area %
1	11.930	BB	0.4239	1609.78625	56.40965	51.1660
2	14.223	BB	0.4056	1536.41528	57.06903	48.8340

Totals : 3146.20154 113.47868

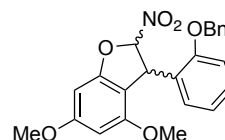
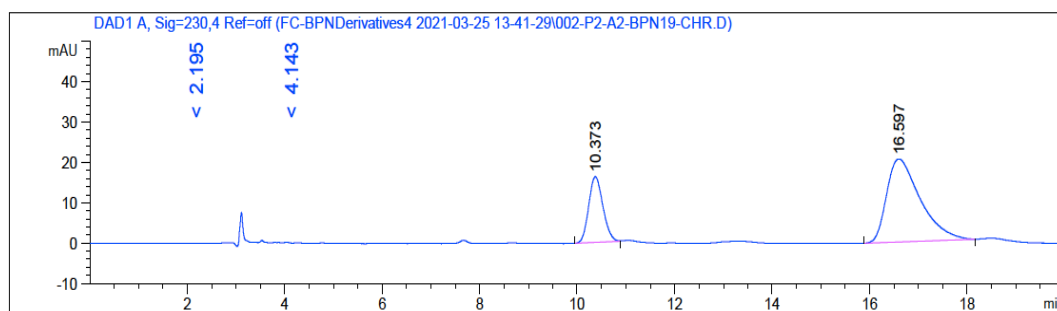


Figure B. 109. HPLC Chromatogram of *rac*-62bq



Signal 1: DAD1 A, Sig=230,4 Ref=off

Peak #	RetTime [min]	Type	Width [min]	Area [mAU*s]	Height [mAU]	Area %
1	10.373	BB	0.2929	329.37225	16.28723	25.0545
2	16.597	BB	0.5679	985.24915	20.60301	74.9455

Totals : 1314.62140 36.89024

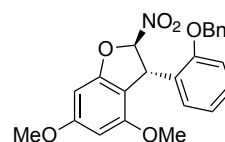


Figure B. 110. HPLC Chromatogram of enantiomerically enriched 62bq

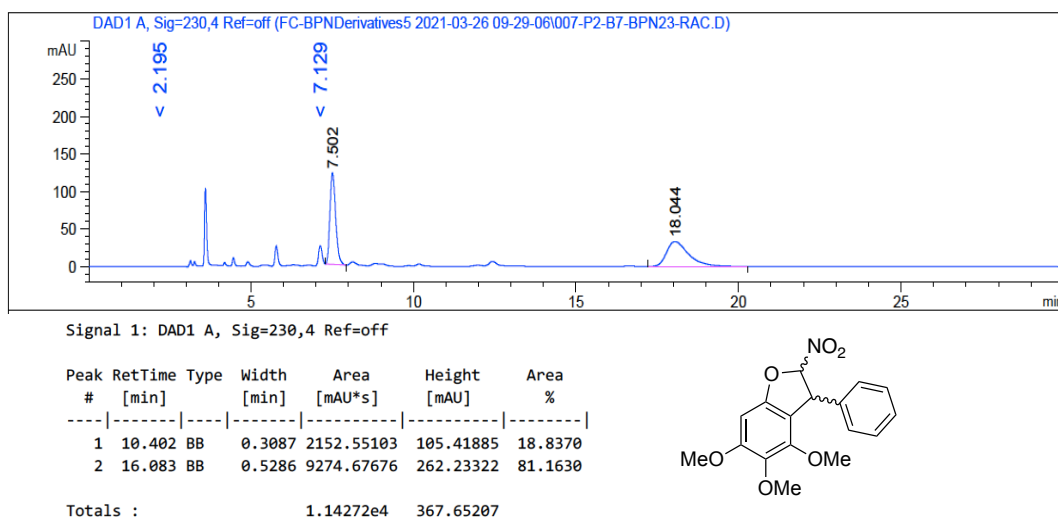


Figure B. 111. HPLC Chromatogram of *rac*-62ca

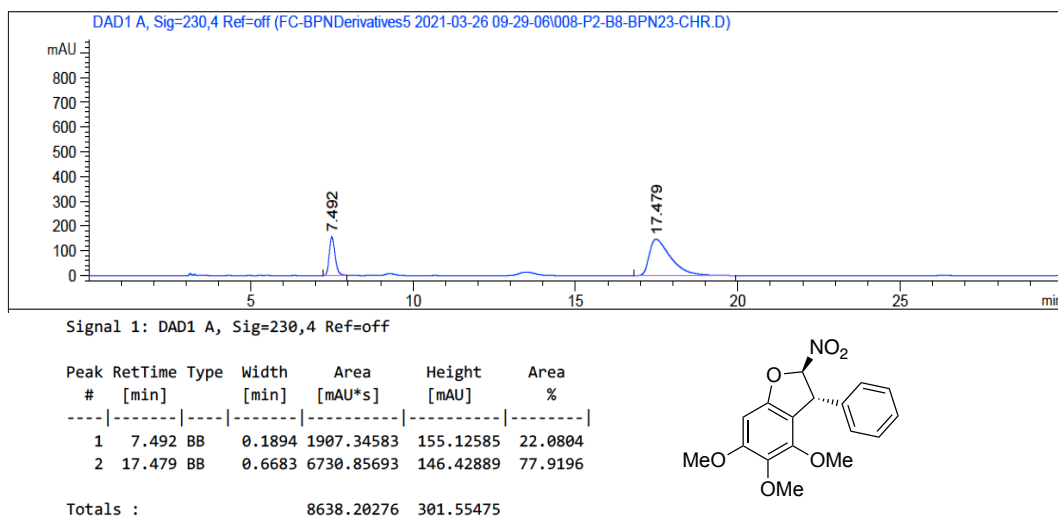


Figure B. 112. HPLC Chromatogram of enantiomerically enriched 62ca

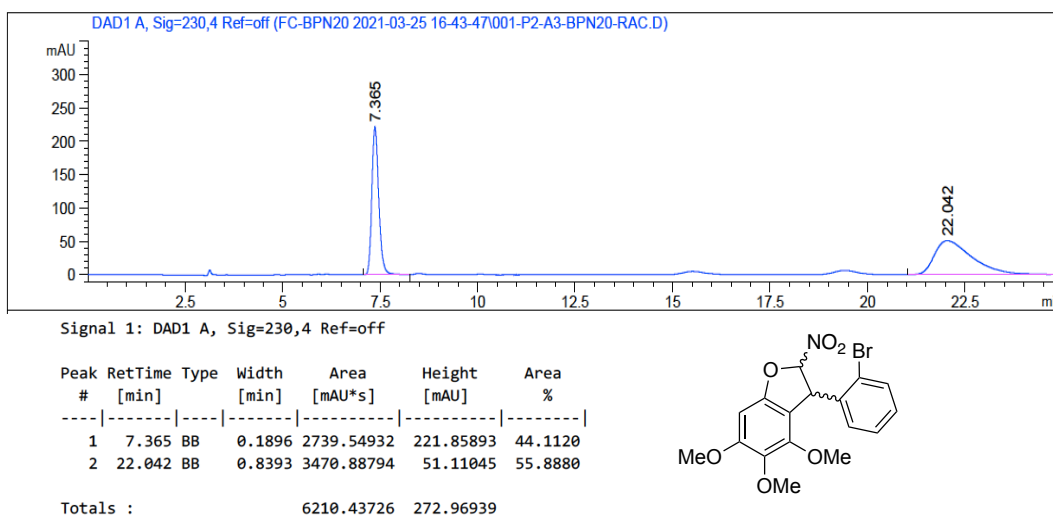


Figure B. 113. HPLC Chromatogram of *rac*-62cb

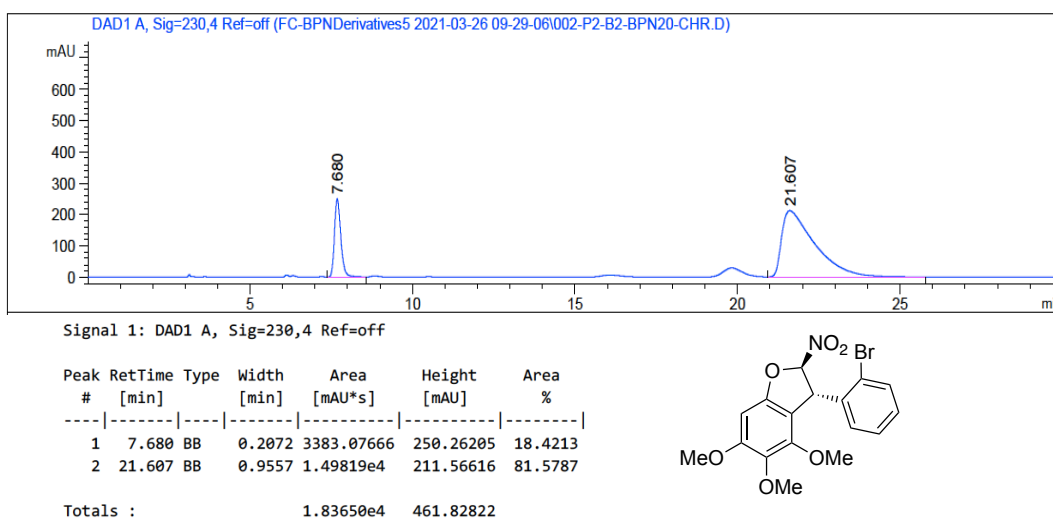


Figure B. 114. HPLC Chromatogram of enantiomerically enriched 62cb

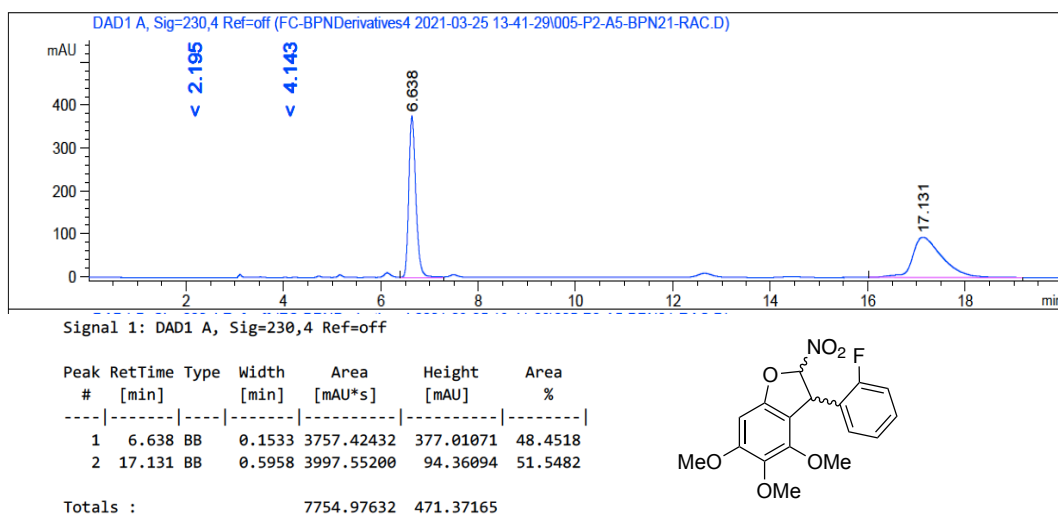


Figure B. 115. HPLC Chromatogram of *rac*-62cd

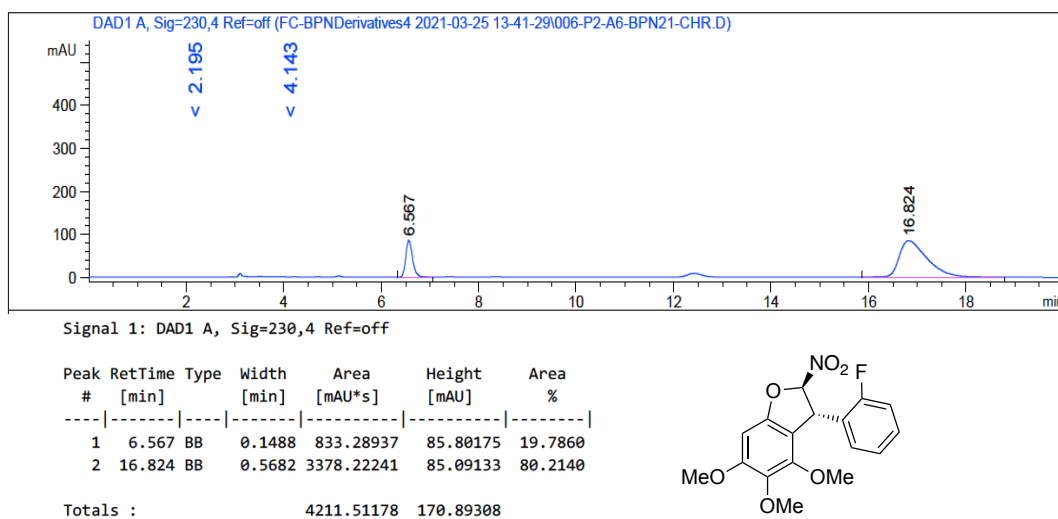
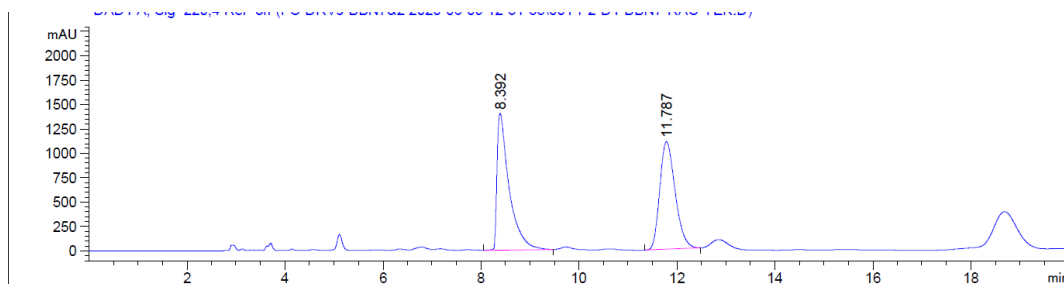


Figure B. 116. HPLC Chromatogram of enantiomerically enriched 62cd



Signal 1: DAD1 A, Sig=220,4 Ref=off

Peak #	RetTime [min]	Type	Width [min]	Area [mAU*s]	Height [mAU]	Area %
1	8.392	BB	0.2469	2.41130e4	1403.73376	50.0034
2	11.787	BB	0.3377	2.41098e4	1104.18604	49.9966

Totals : 4.82228e4 2507.91980

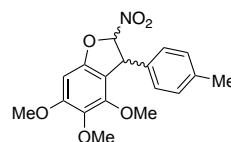
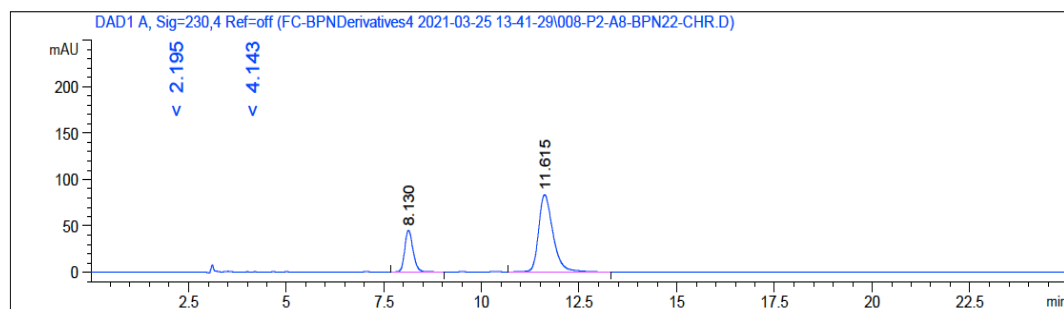


Figure B. 117. HPLC Chromatogram of *rac*-62cl



Signal 1: DAD1 A, Sig=230,4 Ref=off

Peak #	RetTime [min]	Type	Width [min]	Area [mAU*s]	Height [mAU]	Area %
1	8.130	BV R	0.2271	669.75208	45.15308	23.8583
2	11.615	BB	0.3868	2137.45581	83.31550	76.1417

Totals : 2807.20789 128.46857

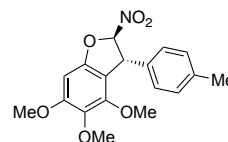


Figure B. 118. HPLC Chromatogram of enantiomerically enriched 62cl

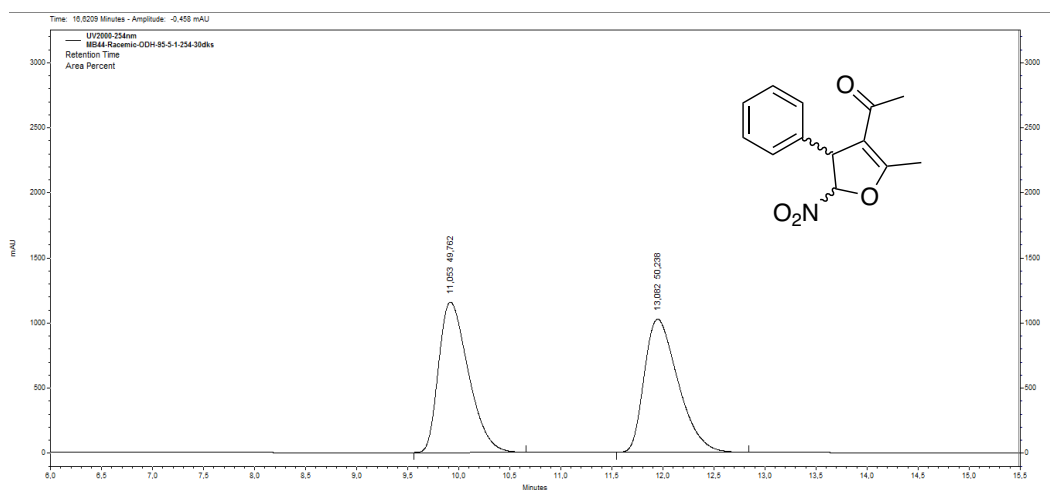


Figure B. 119. HPLC Chromatogram of *rac*-64aa

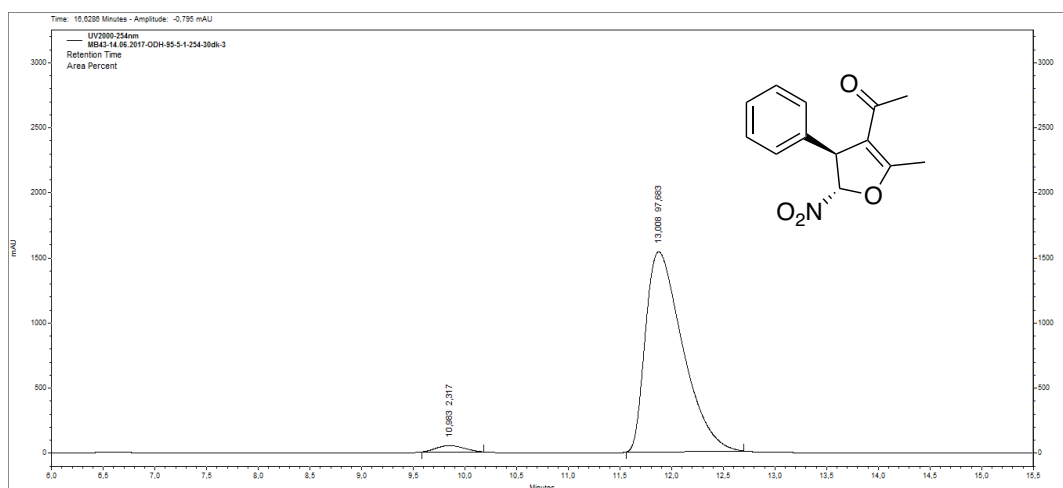


Figure B. 120. HPLC Chromatogram of enantiomerically enriched 64aa

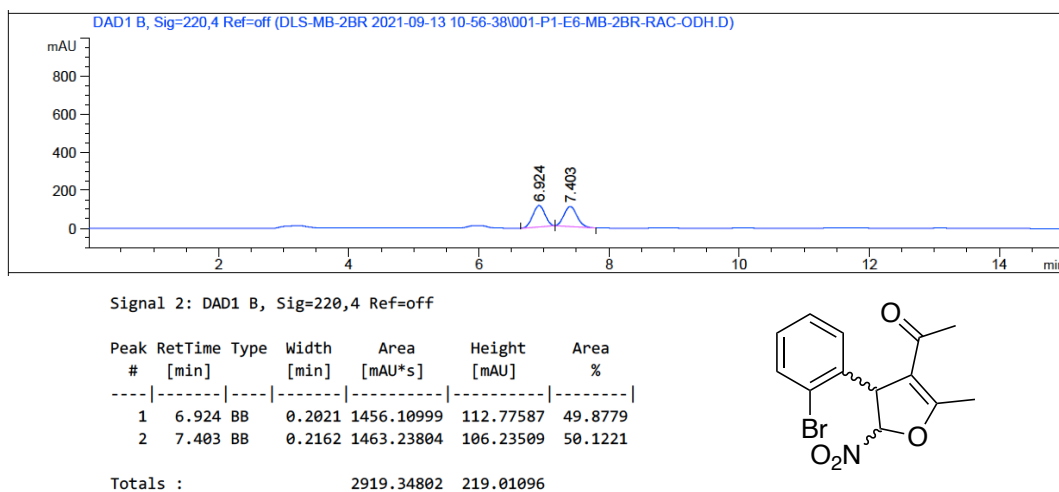


Figure B. 121. HPLC Chromatogram of *rac*-64ab

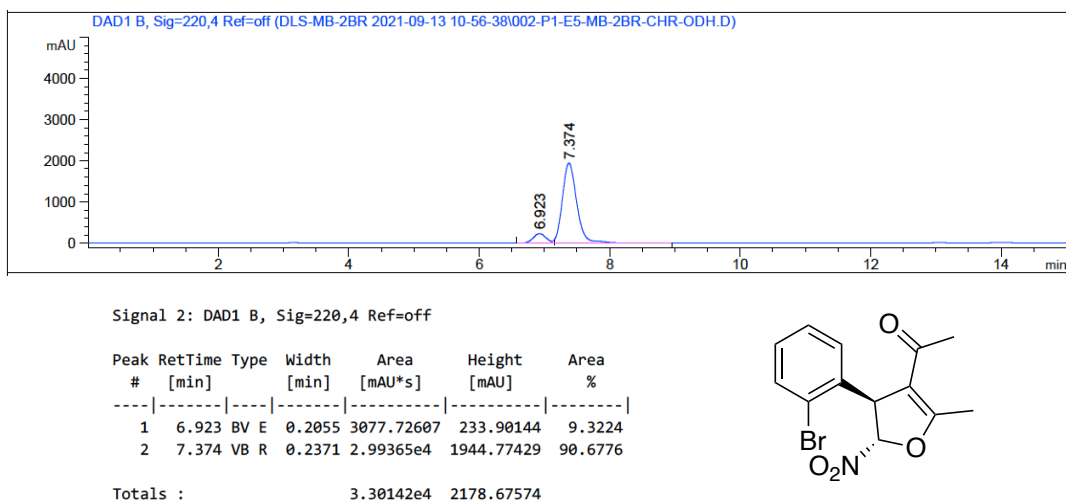
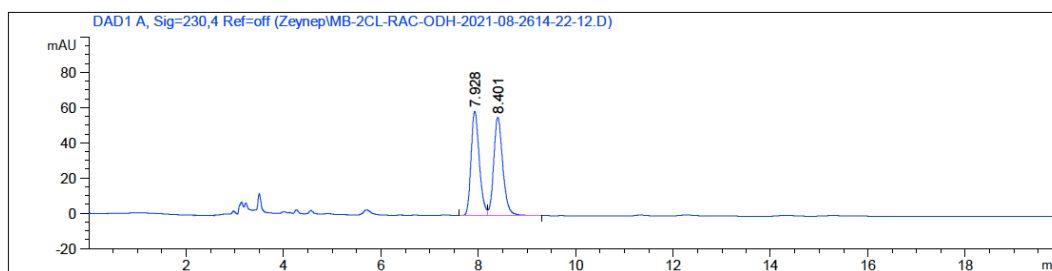


Figure B. 122. HPLC Chromatogram of enantiomerically enriched 64ab



Signal 1: DAD1 A, Sig=230,4 Ref=off

Peak #	RetTime [min]	Type	Width [min]	Area [mAU*s]	Height [mAU]	Area %
1	7.928	BV	0.1808	699.05145	59.17958	48.9920
2	8.401	VB	0.2002	727.81763	55.80560	51.0080

Totals : 1426.86908 114.98518

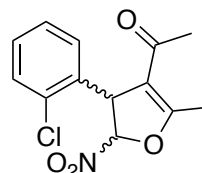
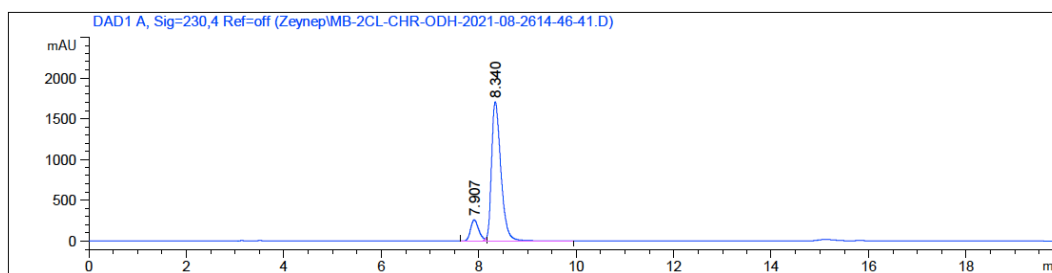


Figure B. 123. HPLC Chromatogram of *rac*-64ac



Signal 1: DAD1 A, Sig=230,4 Ref=off

Peak #	RetTime [min]	Type	Width [min]	Area [mAU*s]	Height [mAU]	Area %
1	7.907	BV E	0.1784	2986.86621	259.20132	11.6023
2	8.340	VB R	0.2047	2.27570e4	1704.90503	88.3977

Totals : 2.57438e4 1964.10635

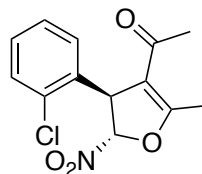


Figure B. 124. HPLC Chromatogram of enantiomerically enriched 64ac

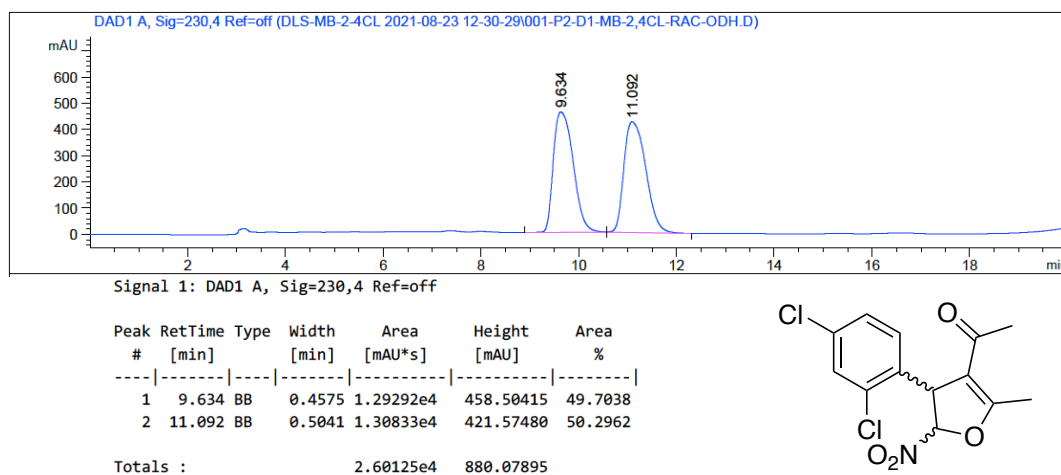


Figure B. 125. HPLC Chromatogram of *rac*-64ah

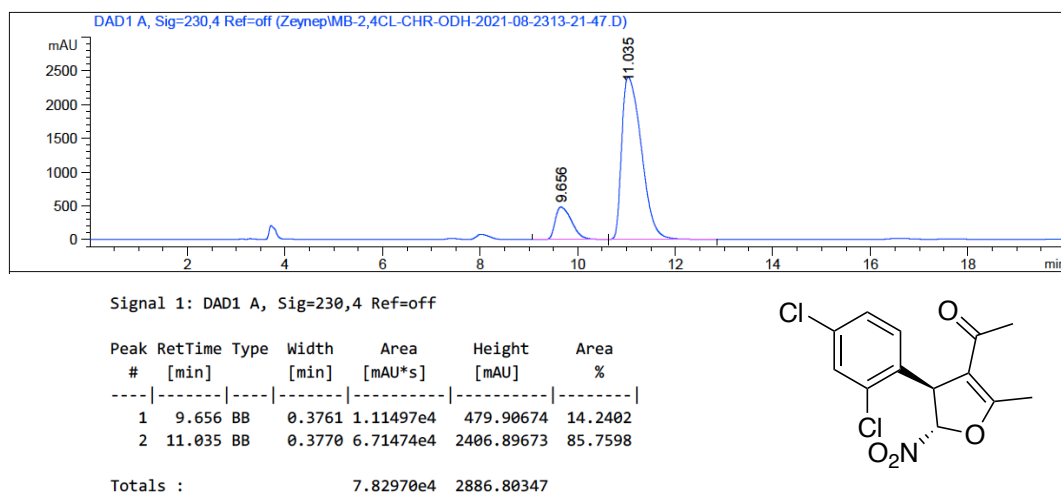


Figure B. 126. HPLC Chromatogram of enantiomerically enriched 64ah

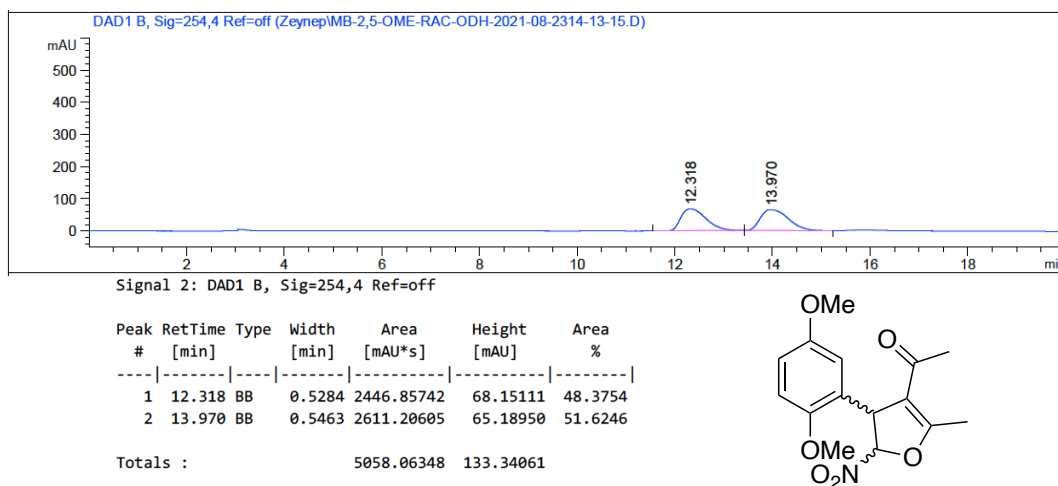


Figure B. 127. HPLC Chromatogram of *rac*-64ai

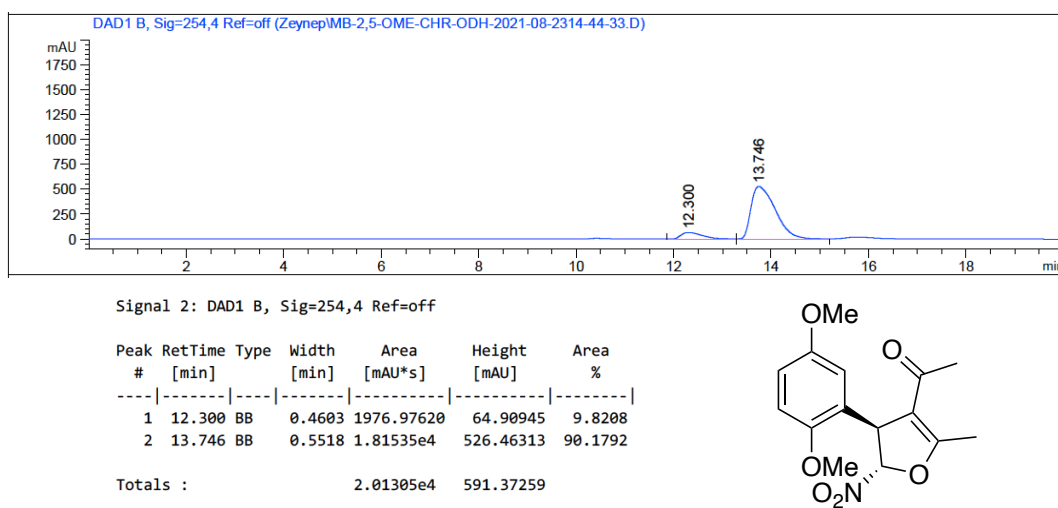


Figure B. 128. HPLC Chromatogram of enantiomerically enriched 64ai

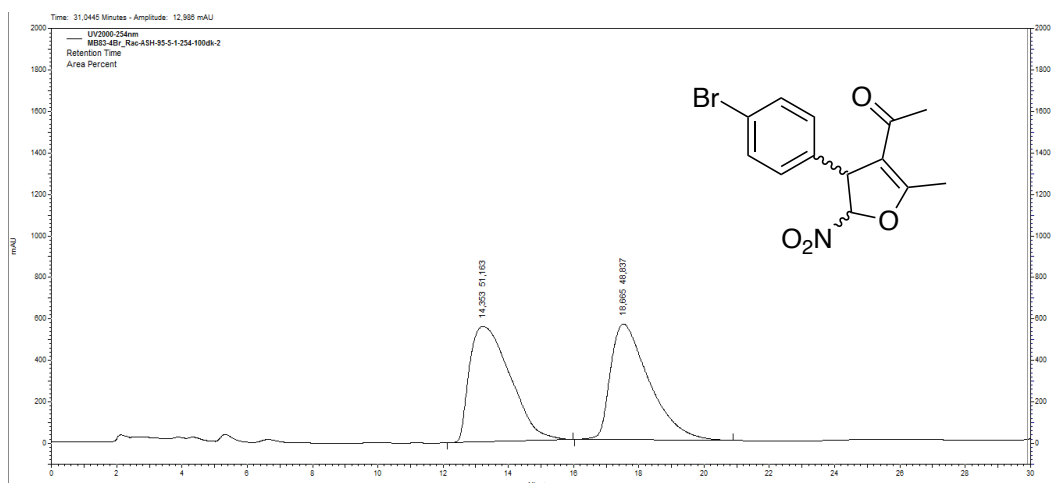


Figure B. 129. HPLC Chromatogram of *rac*-64ak

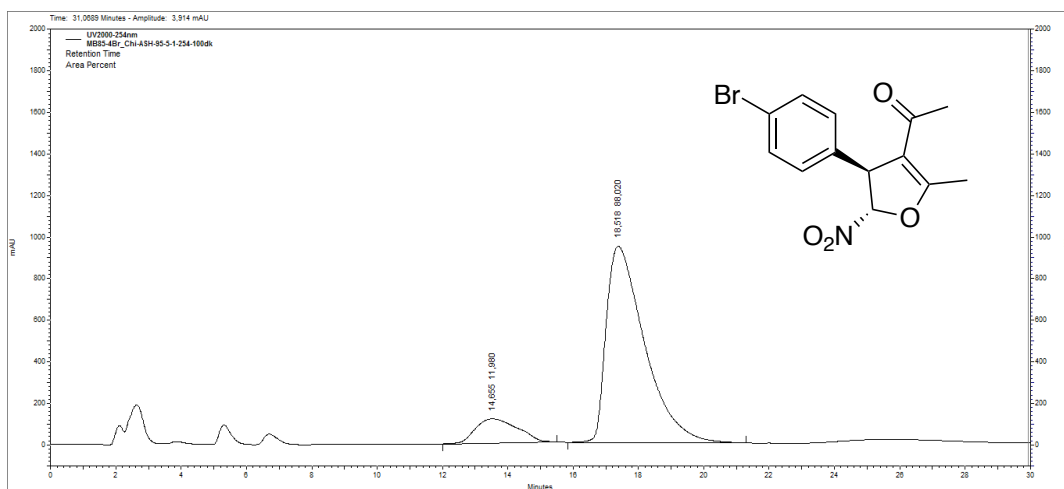


Figure B. 130. HPLC Chromatogram of enantiomerically enriched 64ak

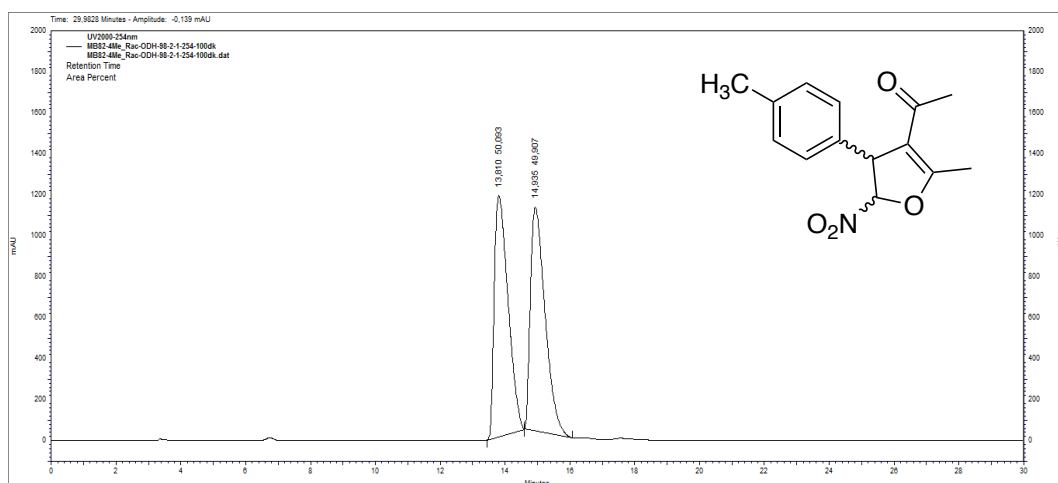


Figure B. 131. HPLC Chromatogram of *rac*-64a

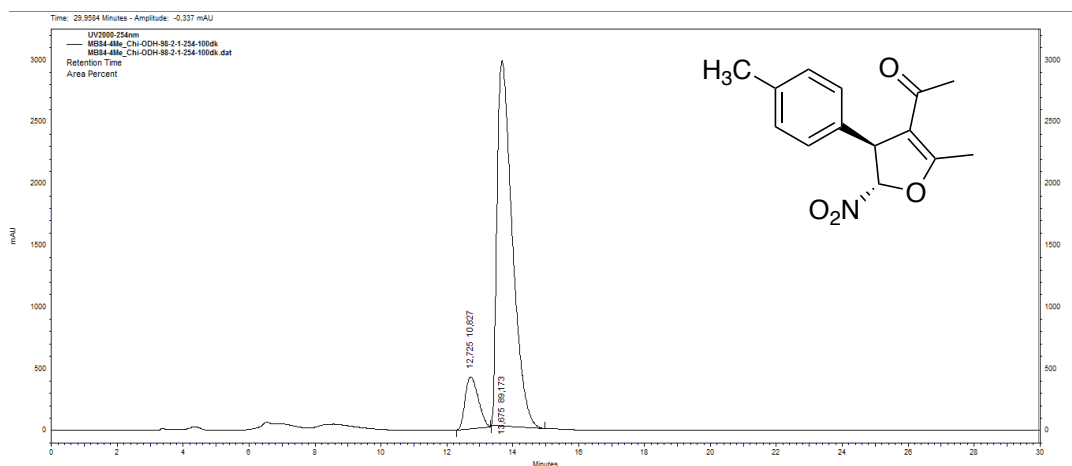
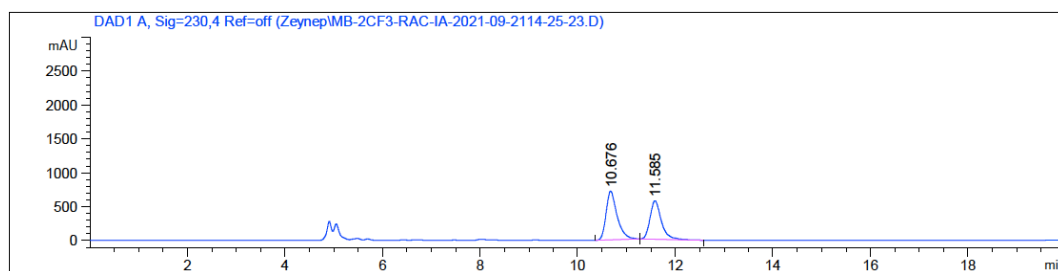


Figure B. 132. HPLC Chromatogram of enantiomerically enriched 64a



Signal 1: DAD1 A, Sig=230,4 Ref=off

Peak #	RetTime [min]	Type	Width [min]	Area [mAU*s]	Height [mAU]	Area %
1	10.676	BB	0.2331	1.13124e4	718.91040	55.1621
2	11.585	BB	0.2443	9195.13477	568.27295	44.8379

Totals : 2.05075e4 1287.18335

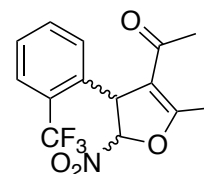
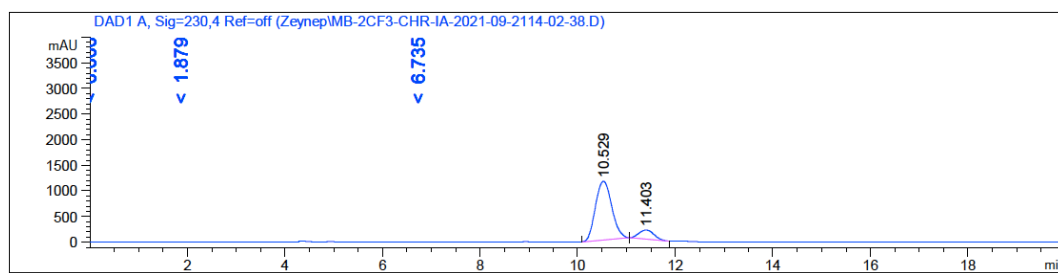


Figure B. 133. HPLC Chromatogram of *rac*-64an



Signal 1: DAD1 A, Sig=230,4 Ref=off

Peak #	RetTime [min]	Type	Width [min]	Area [mAU*s]	Height [mAU]	Area %
1	10.529	BB	0.3704	2.66403e4	1147.29211	87.4757
2	11.403	BB	0.3440	3814.21533	179.10402	12.5243

Totals : 3.04545e4 1326.39613

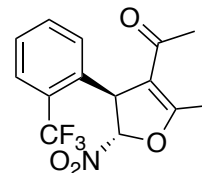


Figure B. 134. HPLC Chromatogram of enantiomerically enriched 64an

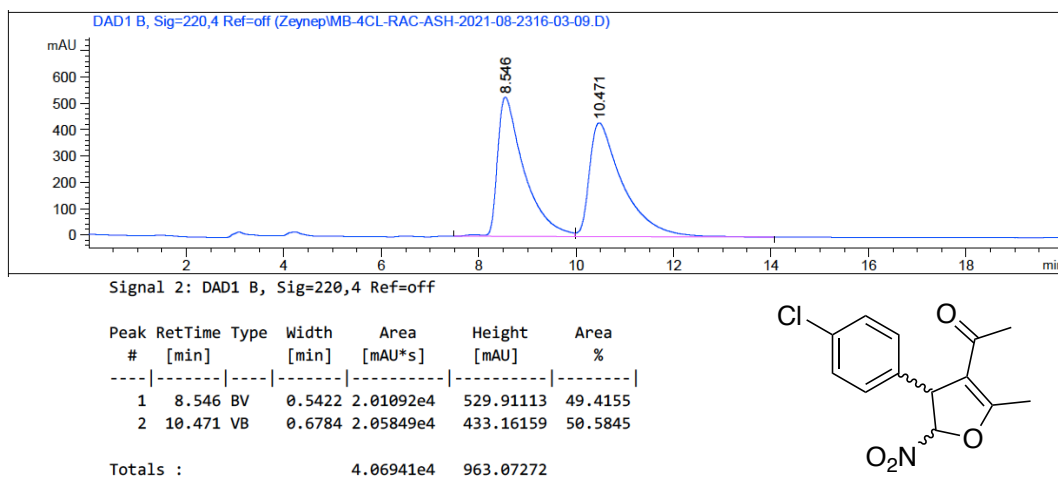


Figure B. 135. HPLC Chromatogram of *rac*-64ao

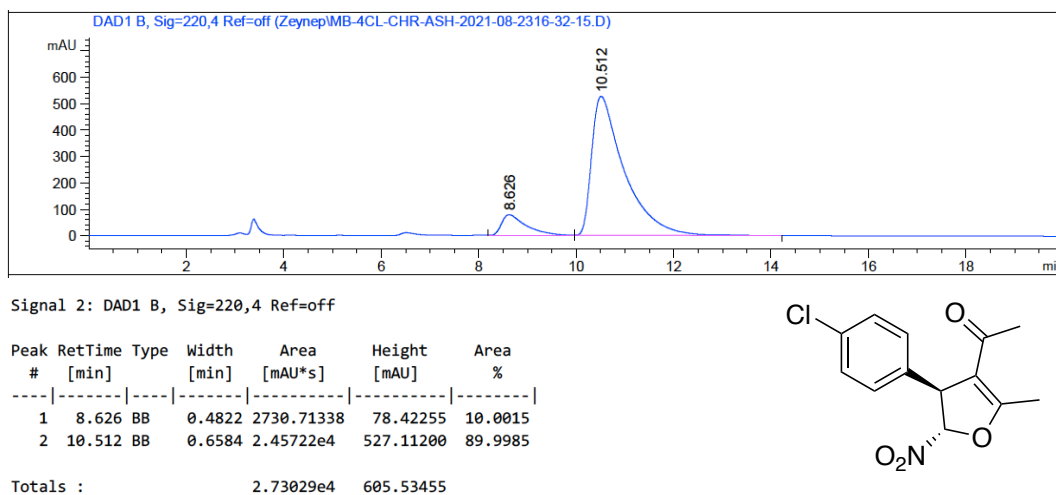


Figure B. 136. HPLC Chromatogram of enantiomerically enriched 64ao

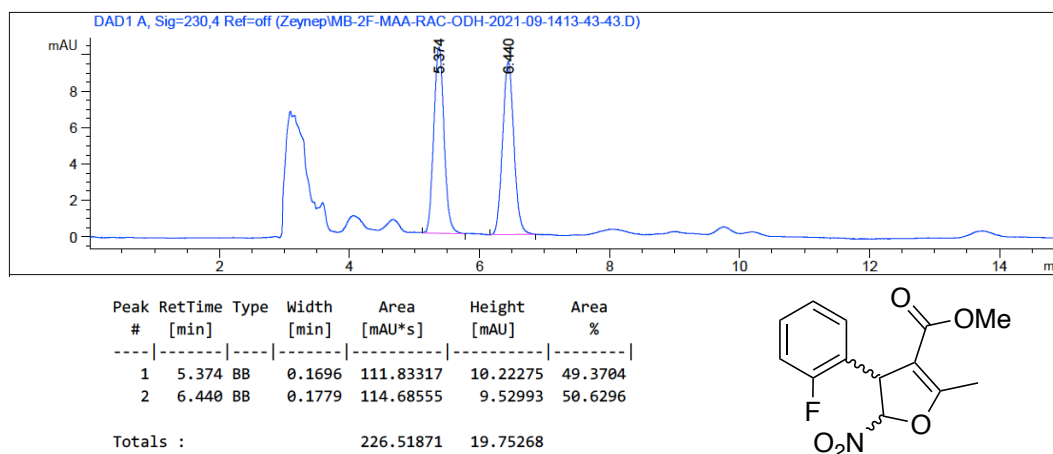


Figure B. 137. HPLC Chromatogram of *rac*-64bd

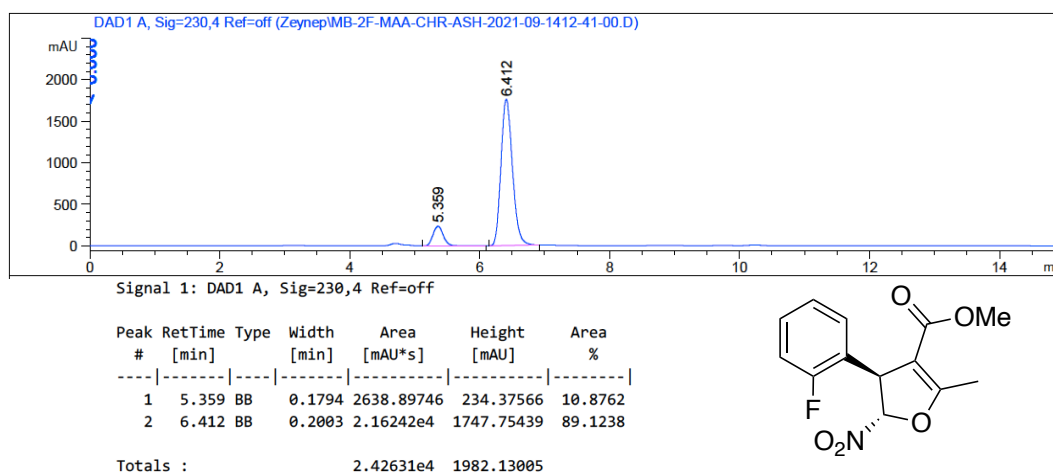


Figure B. 138. HPLC Chromatogram of enantiomerically enriched 64bd

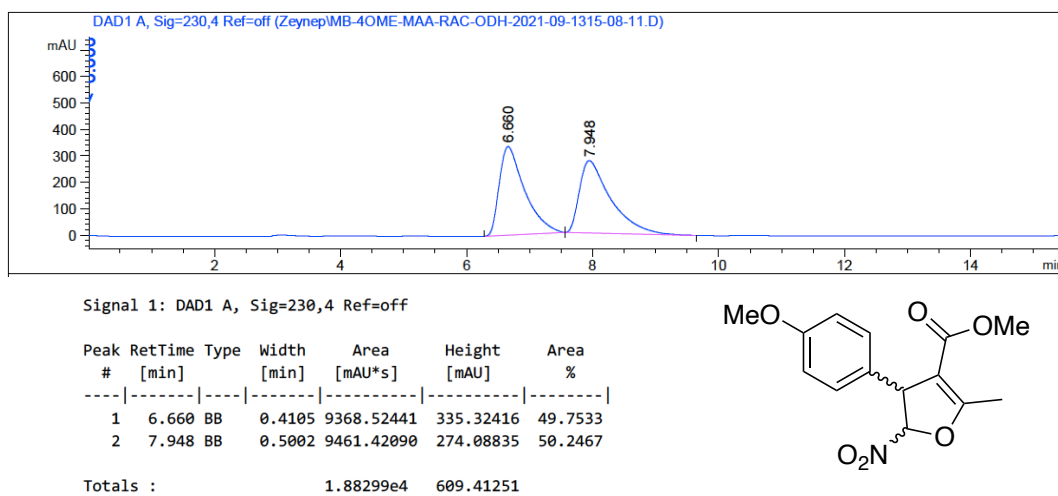


Figure B. 139. HPLC Chromatogram of *rac*-**64bg**

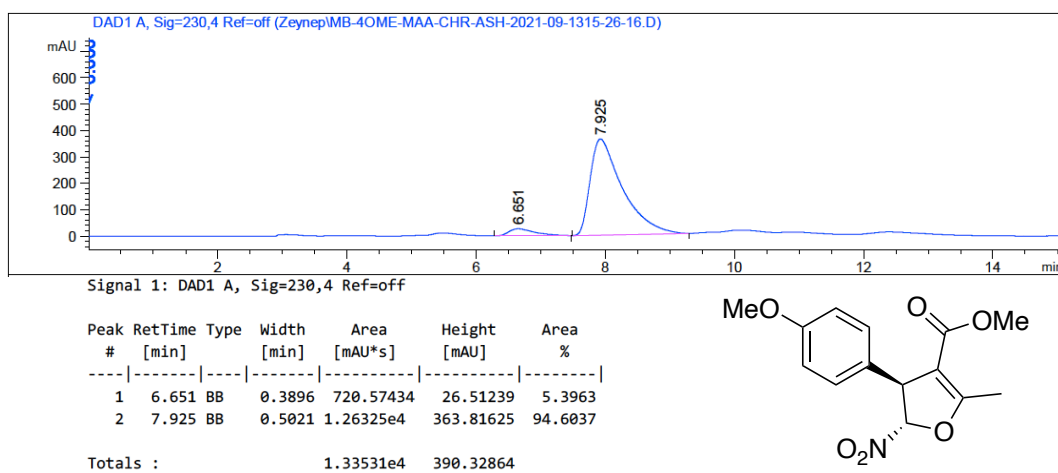


Figure B. 140. HPLC Chromatogram of enantiomerically enriched **64bg**

C. COMPUTATIONAL DATA

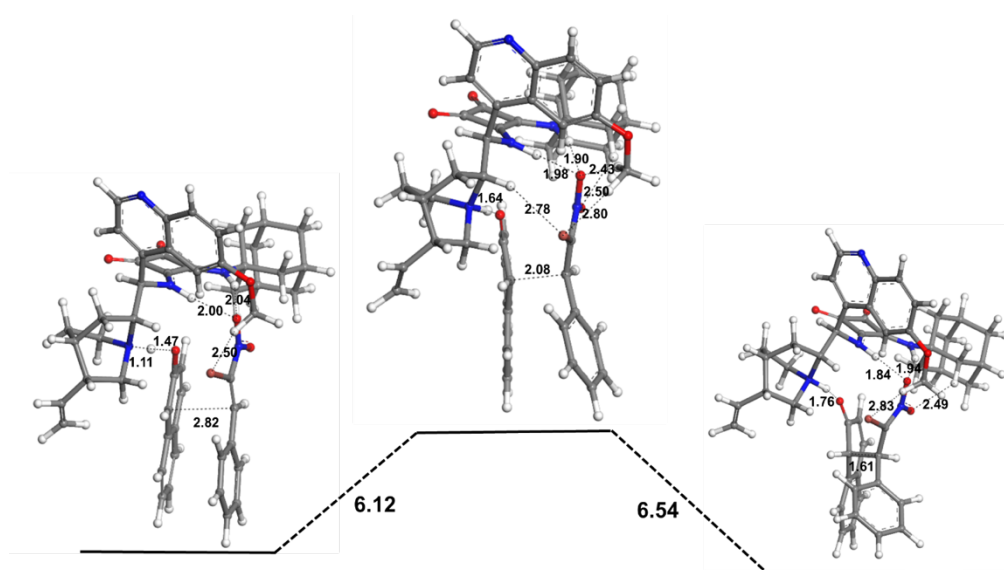


Figure C. 1. Reactant, transition state (TS1) and product of the reaction between bromonitroalkene derivative and β -naphthol coordinated with the active site of the catalyst **19c** where two amine groups of the catalyst coordinated by two oxygens of the nitro group

Atomic coordinates TS1

N	-2.01117300	-0.10744700	-0.54633500
C	-2.70590100	-1.29591800	-1.02033000
C	-4.13558400	-1.41114300	-0.50402000
C	-4.51622200	-1.45114100	0.87399000
C	-3.60940100	-1.38834800	1.97248900
C	-4.09370200	-1.37128000	3.27098100
O	-3.34202300	-1.27074800	4.39472000
C	-1.92513000	-1.22571600	4.25770400
C	-5.48961900	-1.45597100	3.52681600

C	-5.92601900	-1.52870400	1.14176400
N	-6.88386300	-1.57999700	0.17439900
C	-6.48745200	-1.52670600	-1.08070700
C	-5.13303100	-1.43137400	-1.45997800
C	-1.86493200	-2.56631800	-0.80083600
C	-2.51528000	-3.85589900	-1.36071000
C	-1.67455700	-4.40268900	-2.52592300
C	-0.28696900	-4.83957400	-1.98246200
C	0.57012000	-5.42438700	-3.07887600
C	1.74178300	-4.98974900	-3.54249600
C	0.31609800	-3.63513900	-1.22766200
N	-0.51309200	-2.40604600	-1.47015400
C	-0.62276600	-2.17659400	-2.95898800
C	-1.49071800	-3.29009100	-3.57086000
C	-1.95531400	0.98483700	-1.32732200
C	-1.58808300	2.33366600	-1.11753800
C	-1.84328400	2.65654100	-2.56090900
C	-2.23315400	1.19286400	-2.74833400
O	-2.57707700	0.45354500	-3.67445200
O	-1.73799900	3.64461300	-3.27004600
N	-1.19370000	2.98168200	-0.02558400
C	-0.75805000	4.38631500	0.03236200

C	-1.87924000	5.33013200	-0.44836500
C	-1.41284000	6.79300400	-0.32154500
C	-0.15525600	7.00450200	-1.18612900
C	0.96937900	6.07195400	-0.69840800
C	0.50765000	4.60894100	-0.82314900
C	-0.43411200	4.70245700	1.50497900
C	0.03366000	6.16291300	1.63537000
C	1.29380500	6.37774900	0.77565400
H	-1.60087100	-0.05061900	0.38704800
H	-2.54337200	-1.32567800	1.80142300
H	-1.60222300	-0.39749800	3.61903300
H	-1.54984000	-2.16616900	3.84231400
H	-1.53377900	-1.09305800	5.26736700
H	-5.81713300	-1.44611800	4.56112700
H	-7.26337500	-1.55332400	-1.84389700
H	-4.87721300	-1.35255300	-2.51273900
H	-1.63170800	-2.67088300	0.25841600
H	-3.52883900	-3.63809700	-1.70540100
H	-2.60361900	-4.60423500	-0.56703100
H	-2.17996000	-5.26386100	-2.97263900
H	-0.46785500	-5.63911100	-1.25201000
H	0.13202900	-6.31190700	-3.53680700

H	2.25806400	-4.11689500	-3.15240900
H	2.24525900	-5.50974000	-4.35180500
H	1.32865000	-3.38639300	-1.54432700
H	0.33891100	-3.78944600	-0.15084800
H	0.40266500	-2.19447200	-3.32979900
H	-1.02695500	-1.18088900	-3.13031400
H	-1.00760300	-3.67928200	-4.46989300
H	-2.46590400	-2.89082200	-3.86681400
H	-0.95158100	2.39479700	0.77561900
C	-1.08351900	7.10494500	1.14967500
H	-2.77609000	5.15813500	0.16087600
H	-2.12877500	5.10410300	-1.48893000
H	-2.21497100	7.45548400	-0.67011100
H	0.17069800	8.05158000	-1.12433700
H	-0.38541300	6.79484100	-2.23843800
H	1.86629000	6.22130400	-1.31319600
H	1.28983800	3.92453100	-0.47708700
H	0.27907200	4.37059900	-1.86810300
H	0.33949400	4.01301800	1.86036700
H	-1.33206200	4.53550100	2.11514400
H	0.26414200	6.37171100	2.68762300
H	2.10351100	5.72369600	1.12550200

H	1.64455400	7.41345100	0.87830300
H	-1.97986900	6.97785200	1.77145700
H	-0.76411700	8.15081800	1.25178300
C	-6.37545400	-1.53911900	2.49006300
H	-7.44521200	-1.60108900	2.65945800
C	6.87744200	-1.08154900	-0.93505400
C	7.22605500	0.20736200	-1.36873800
C	6.23267000	1.14421900	-1.61070600
C	4.87538800	0.82113000	-1.42022800
C	4.52297600	-0.47885500	-0.96080800
C	5.54622900	-1.41800500	-0.73386500
C	3.82631400	1.76238800	-1.72387700
C	2.51023200	1.44220700	-1.61660100
C	2.09874200	0.12522300	-1.17262200
C	3.12978400	-0.77149400	-0.68212400
O	0.87616600	-0.18249500	-1.12266500
H	0.01152300	-1.56991500	-1.08710800
H	7.65254200	-1.81943000	-0.74930500
H	8.26950200	0.46754800	-1.52003400
H	6.49074100	2.14094400	-1.95974500
H	5.28446100	-2.41087600	-0.38173400
H	4.11726700	2.74999400	-2.07468700

H	1.72388000	2.13954300	-1.88017600
H	2.84597600	-1.81850700	-0.60889000
C	6.08769200	-1.55984800	2.92264500
C	5.93480900	-2.94436500	2.97974300
C	4.75623800	-3.52512200	2.50503900
C	3.73576700	-2.73192300	1.98631100
C	3.86975200	-1.33421600	1.93736300
C	5.06897400	-0.76711200	2.39808400
C	2.87186300	-0.40682500	1.35292900
C	1.47980400	-0.42510500	1.62539000
N	0.74520900	0.72556500	1.53158900
Br	0.49028600	-2.01157600	1.92691800
O	-0.52137900	0.72178900	1.74354500
O	1.34179500	1.80198300	1.27029200
H	7.00346900	-1.09434700	3.27465600
H	6.72808200	-3.56768000	3.38197400
H	4.63204500	-4.60401500	2.53367900
H	2.83689300	-3.20342900	1.61249000
H	5.20241900	0.30876500	2.33530200
H	3.22181100	0.61988800	1.32922900
H	-2.81082300	-1.15684400	-2.09731200

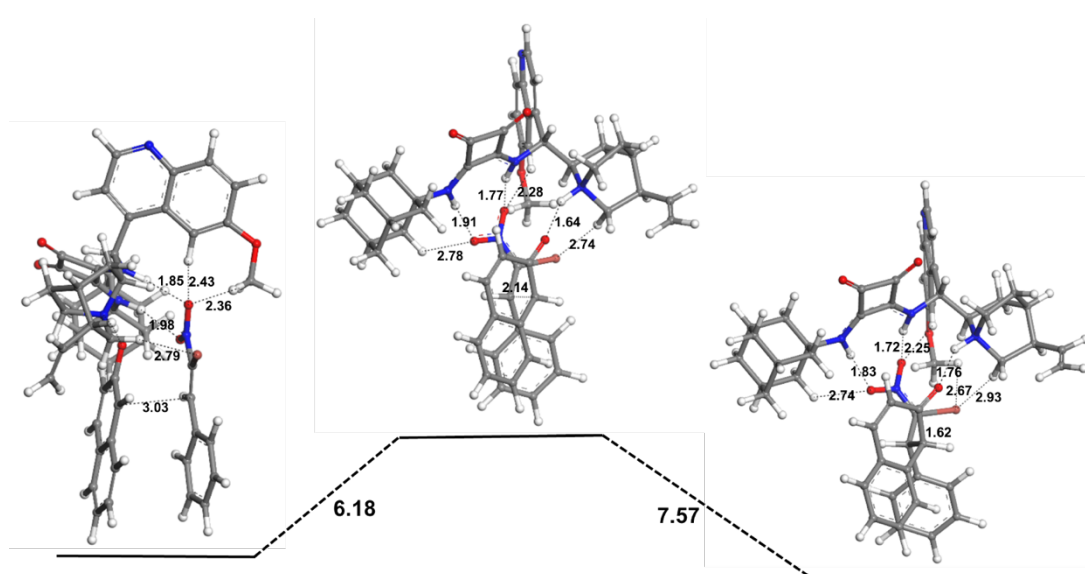


Figure C. 2. Reactant, transition state (TS2) and product of the reaction between bromonitroalkene derivative and β -naphthol coordinated with the active site of the catalyst where two amine groups of the catalyst coordinated by single oxygen of the nitro group

Atomic coordinates for TS2

N	1.85573500	1.16290900	0.35062400
C	3.14494100	0.62261300	0.77357600
C	4.33085300	1.10838300	-0.05846000
C	4.68968200	0.65770300	-1.36746700

C	3.96430700	-0.30800100	-2.11818300
C	4.41050400	-0.70016100	-3.36896600
O	3.79622600	-1.61277800	-4.16326200
C	2.63658500	-2.26013900	-3.64576500
C	5.59421400	-0.14362500	-3.92372000
C	5.87404500	1.23356400	-1.94241800
N	6.63014600	2.18665800	-1.32942800
C	6.24011900	2.60062200	-0.14068500
C	5.10971500	2.08789000	0.52917300
C	3.01454800	-0.89786300	0.95255200
C	4.32999500	-1.60410200	1.35166300
C	4.18378500	-2.21343300	2.75438700
C	3.08164100	-3.30737500	2.71567100
C	2.95891700	-3.99633300	4.05339500
C	1.91528700	-4.02657700	4.88209500
C	1.78994800	-2.65820200	2.17480700
N	1.98738000	-1.17164100	2.03787900
C	2.36759500	-0.60117700	3.37872800
C	3.78115100	-1.10079300	3.73876700
C	1.38907400	2.29503100	0.89731600
C	0.27404800	3.12487600	0.64248200
C	0.69470200	4.07485700	1.72553400

C	1.82871600	3.09956200	2.04108200
O	2.70627200	2.97015000	2.89645100
O	0.29773600	5.14549200	2.15499900
N	-0.72604000	3.01007800	-0.22843200
C	-1.83326200	3.96445800	-0.40547700
C	-1.30549000	5.31439800	-0.93485900
C	-2.48635200	6.27149500	-1.18428500
C	-3.24407100	6.50345400	0.13653300
C	-3.77907900	5.15958400	0.66604800
C	-2.59587800	4.20581200	0.91499300
C	-2.79592000	3.34929900	-1.43838700
C	-3.97423400	4.30534700	-1.69015300
C	-4.73288200	4.53826900	-0.37035400
H	1.42024800	0.77048700	-0.49396700
H	3.03202200	-0.69760900	-1.74007800
H	1.84092100	-1.54469600	-3.42320300
H	2.87806100	-2.81053500	-2.72927700
H	2.31314300	-2.95895900	-4.41827900
H	5.90669300	-0.48233700	-4.90611900
H	6.84472600	3.37160500	0.33408700
H	4.84490800	2.47546900	1.50878900
H	2.56419100	-1.34418400	0.06580900

H	5.15184400	-0.88299100	1.34487200
H	4.57610900	-2.37556000	0.61595500
H	5.13296600	-2.66083800	3.06326800
H	3.41206800	-4.06360100	1.99131700
H	3.87134400	-4.51188400	4.35555500
H	0.96453800	-3.54645100	4.66796100
H	1.97382200	-4.55502400	5.82888100
H	0.92558600	-2.78482500	2.82298500
H	1.50044200	-3.02147300	1.19007200
H	1.61096300	-0.96508300	4.07557600
H	2.29356500	0.48566500	3.33779800
H	3.78653500	-1.47302700	4.76556500
H	4.50217200	-0.27955600	3.68064800
H	-0.78795900	2.13263100	-0.75216900
C	-3.44060000	5.64948900	-2.22090200
H	-0.74553400	5.14205500	-1.86283300
H	-0.61507400	5.74344400	-0.20035700
H	-2.10109600	7.22660600	-1.56208900
H	-4.07621700	7.20136800	-0.02591700
H	-2.57567100	6.95847500	0.87818600
H	-4.31251900	5.32144500	1.61108700
H	-2.95514600	3.24585200	1.30064900

H	-1.91573300	4.63487000	1.65566400
H	-3.15618900	2.38157800	-1.06805400
H	-2.25353500	3.15620400	-2.37315000
H	-4.64733200	3.85530700	-2.43034900
H	-5.13189500	3.58621700	0.00596800
H	-5.58988500	5.20291600	-0.54186600
H	-2.91526300	5.49555200	-3.17287600
H	-4.27725700	6.33222000	-2.41972200
C	6.29844900	0.80023400	-3.22804900
H	7.19853300	1.25026300	-3.63332600
C	-6.36258200	-2.76622600	1.18368000
C	-6.88771900	-1.47593300	1.36655300
C	-6.02946000	-0.39308500	1.47760700
C	-4.63403800	-0.56902100	1.40008300
C	-4.10119100	-1.87343800	1.19310500
C	-4.99205300	-2.96163100	1.09892500
C	-3.72555900	0.53458700	1.57074800
C	-2.37464400	0.37902500	1.54862900
C	-1.78331100	-0.92872300	1.34399500
C	-2.67361300	-2.02848100	1.03664200
O	-0.53591500	-1.12056800	1.34315800
H	1.05658100	-0.79564500	1.73955900

H	-7.03279900	-3.61731400	1.10364000
H	-7.96203400	-1.32911200	1.42802600
H	-6.42447300	0.60787800	1.63382400
H	-4.59279800	-3.95956200	0.94794300
H	-4.15709300	1.51782700	1.74250200
H	-1.70111900	1.21527600	1.69875800
H	-2.24652100	-3.01773700	1.16851000
C	-5.15247000	-4.21481900	-2.36409400
C	-4.73076500	-5.50788700	-2.05867700
C	-3.49936300	-5.69845200	-1.42534100
C	-2.69100100	-4.61033100	-1.10856600
C	-3.09632700	-3.30226100	-1.42621500
C	-4.34704200	-3.12460200	-2.04021100
C	-2.33907100	-2.08171300	-1.07970400
C	-0.95651800	-1.88318500	-1.28862600
N	-0.46040700	-0.61288000	-1.39956000
Br	0.34122000	-3.25905600	-1.28078600
O	0.77551400	-0.41213300	-1.63639900
O	-1.26188200	0.36368500	-1.29697400
H	-6.11327900	-4.04999500	-2.84262000
H	-5.35766200	-6.36078900	-2.30201300
H	-3.16930400	-6.70132000	-1.16962500

H	-1.74816800	-4.77554100	-0.60380000
H	-4.68908600	-2.11763100	-2.25992900
H	-2.88592800	-1.16631700	-1.27886600
H	3.33064900	1.05080200	1.75795300

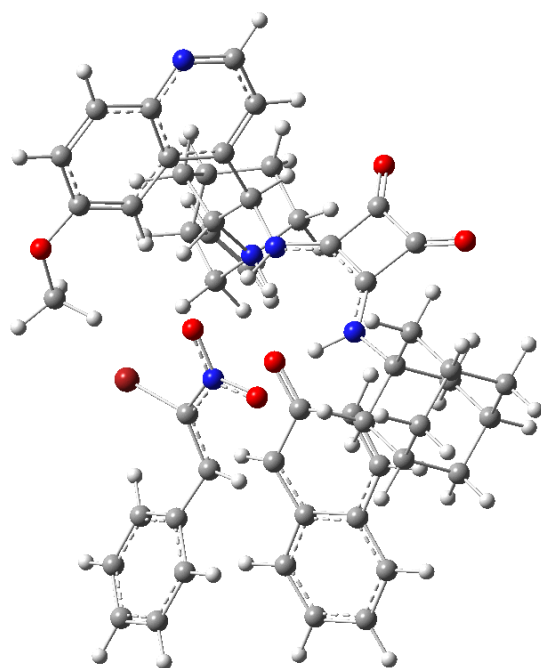


Figure C. 3. Transition State 1

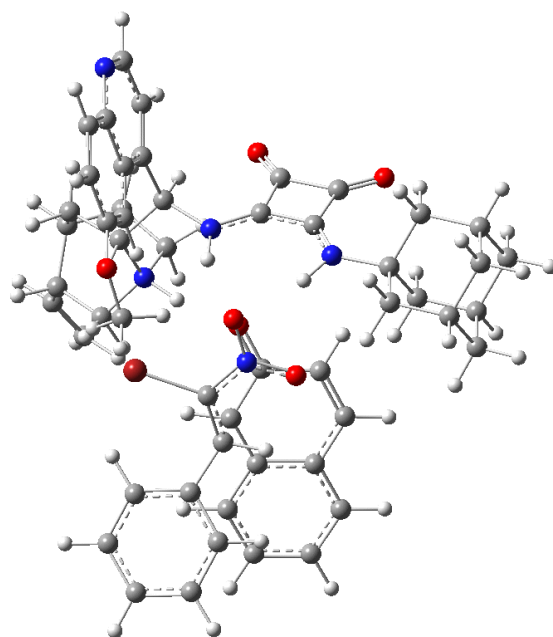


Figure C. 4. Transition State 2

D. X-RAY CRYSTALLOGRAPHY

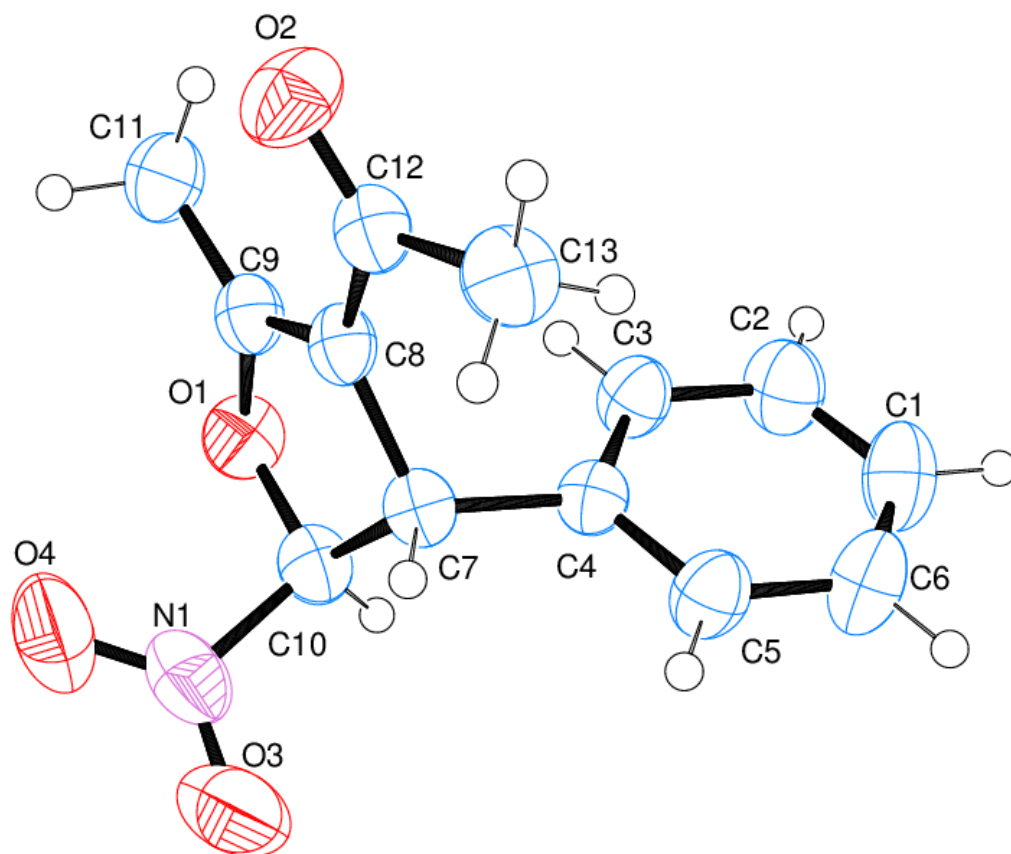


Figure D. 1. Ortep diagram of **64aa**, thermal ellipsoids are shown at the 50% probability level

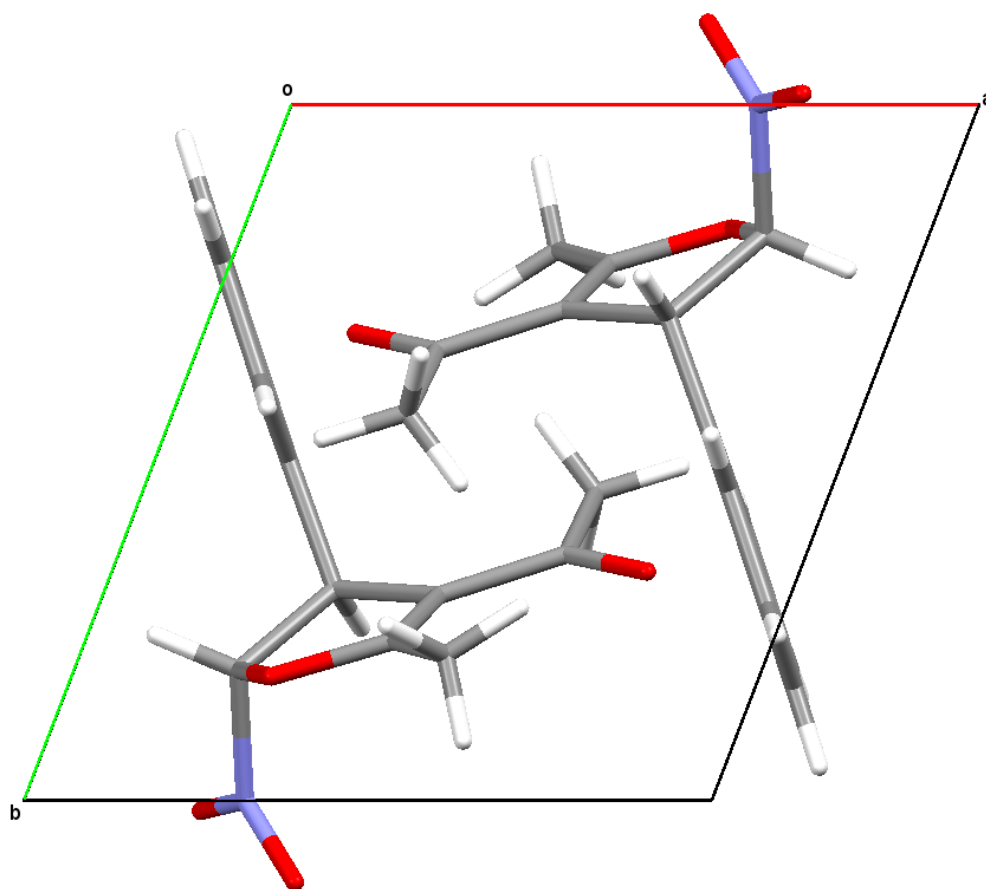


Figure D. 2. Crystal packing of **64aa** projected onto the *ab* plane

Experimental details

Chemical formula	$C_{13}H_{13}NO_4$
M_r	247.24
D_{calc} (g cm^{-3})	1.314
Crystal system, space group	Triclinic, <i>P</i> -1
Temperature (K)	293(2)

a, b, c (Å)	7.4498(3), 8.4498(4), 11.1317(8)
α, β, γ (°)	107.098(8), 91.985(7), 109.401(8)
V (Å ³)	624.89(8)
Z	2
Radiation type	Mo $K\alpha$
μ (mm ⁻¹)	0.10
No. of measured reflections	16255

$R[F^2 > 2\sigma(F^2)], wR(F^2), 0.049, 0.137, 1.03$
 S

No. of reflections	3088
No. of parameters	165
H-atom treatment	H-atom parameters constrained
$\Delta\rho_{\max}, \Delta\rho_{\min}$ (e Å ⁻³)	0.25, -0.28

Computer programs: *SHELXS* (Sheldrick, 2008), *SHELXL2018/3* (Sheldrick, 2018), *Olex2* (Dolomanov et al., 2009).

Table 1 Selected geometric parameters (Å, °) for **64aa**

O1—C9	1.3838(16)	O3—N1	1.215(2)
-------	------------	-------	----------

O1—C10	1.3976(17)	O4—N1	1.199(2)
O2—C12	1.2206(18)	N1—C10	1.539(2)
C10—O1—C9	107.88(10)	C11—C9—C8	133.53(13)
O4—N1—O3	124.41(17)	N1—C10—O1	108.82(12)
C10—N1—O3	115.46(14)	C7—C10—O1	107.59(11)
C10—N1—O4	120.09(16)	C7—C10—N1	108.01(11)
C8—C9—O1	112.41(12)	C8—C12—O2	121.50(13)
C11—C9—O1	113.99(12)	C13—C12—O2	120.79(13)
C7—C4—C5—C6	-178.3(1)	C7—C8—C12—O2	-174.1(1)
O3—N1—C10—O1	169.3(2)	C9—C8—C12—C13	-173.0(1)
O4—N1—C10—C7	103.5(2)	C7—C8—C9—C11	-172.0(2)
C4—C7—C10—O1	-101.8(1)		

CURRICULUM VITAE

PERSONAL INFORMATION

Surname, Name: Susam, Zeynep Dilşad

EDUCATION

Degree	Institution	Year of Graduation
MS	METU Chemistry	2015
BS	METU Chemistry	2012
High School	Yuvacık Atayurt Private School, Kocaeli	2007

FOREIGN LANGUAGES

Advanced English, Beginner Spanish

PUBLICATIONS

Susam, Z. D.; Özcan, B. D.; Kurtkaya, E.; Yıldırım, E.; Tanyeli C. *Org. Biomol. Chem.*, **2022**, *20*, 8725-8740.

Susam, Z. D.; Bozdemir, M.; Gündoğdu, G.; Tanyeli C. *New J. Chem.* **2022**, *46*, 599-606.

Susam, Z. D.; Tanyeli C. *Asian J. Org. Chem.* **2021**, *10*, 1251-1266.

Susam, D.; Tanyeli C. *New J. Chem.* **2017**, *41*, 3555-3561.